Design and Synthesis of Rhodamine-6G Based Highly Selective Fluorescent Probes for The Metal Ion Sensing

THESIS SUBMITTED FOR THE

DEGREE OF DOCTOR OF PHILOSOPHY (SCIENCE)

OF

JADAVPUR UNIVERSITY

2022

By

DIPANKAR DAS

DEPARTMENT OF CHEMISTRY

JADAVPUR UNIVERSITY

KOLKATA -700032

INDIA

Prof. Mahammad Ali, Professor
Department of Chemistry
Jadavpur University

Kolkata-700032, India
Email:m_ali2062@yahoo.com
Mobile: +91-9433249716

CERTIFICATE FROM THE SUPERVISOR

This is to certify that the thesis entitled **"Design and Synthesis of Rhodamine-6G Based Highly Selective Fluorescent Probes for The Metal Ion Sensing"** Submitted by Sri **Dipankar Das** who got his name registered on **22/06/2017 (Index No.- 48 / 17/ Chem. / 25)** for the award of **Ph.D.** (**Science**) degree of Jadavpur University, is absolutely based upon his own work under the supervision of **Prof. Mahammad Ali** and that neither this thesis nor any part of it has been submitted for either any degree / diploma or any other academic award anywhere before.

Date- 28/03/2022

Mahammad Ali.

Prof. Mahammad Ali

Professor of Chemistry
Department of Chemistry
Jadavpur University
Kolkata-700032

Dr. Mahammad Ali
Professor
Department of Chemistry
Jadavpur University
Kolkata-700 032


Dedicated to My Beloved
Parents, Wife and
Daughters

Acknowledgements

I would like to express my sincere gratitude to my supervisor **Prof. Mahammad Ali** for his continuous support in doing research and Ph.D. related all the works.His proper guidance,long patience and motivation have helped me to complete my research work and writing of this thesis.I have got an oppotunity to spent long time with him in my research life and to learn many things.

It is my pleasure to express my sincere gratitude to Prof. Swapan Kumar Bhattacharya, Head of the Department of Chemistry & Prof. Subenoy Chakraborty, Dean of Science and Dr. Atiskumar Chattopadhyay, Principal Secretary, Faculty of Science,Jadavpur University, Kolkata-700 032 for their kind cooperation. I am also grateful to Prof. Chittaranjan Sinha, Prof. Sujoy Baitalik, Prof Jnan Prakash Naskar, Department of Chemistry, Jadavpur University for giving me their laboratory access and instrumental facilities whenever needed.I want to thank to all my respected teachers of the chemistry department of Jadavpur University who taught me and made me eligible to pursue my Ph.D. work. I wish to thank registration section and Ph.D.section of the Jadavpur University for their cooperation to complete the official works needed related to Ph.D.

I would like to thank my research laboratory mates Dr. Rabiul Alam, Mihir Sasmal, Debjani Maiti, Ananya Dutta,Rousunara Khatun, Dolan Moni, Dr.Surajit Biswas, Dr.Arpan Dutta, Dr.Mainak Debnath, Dr. Tarun Mistri, Dr. Malay Dolai, Dr. Luna Paul, Dr. Arindam Giri, Dr.Rahul Bhowmik, Dr. Abu Saleh Musha Islam, Hasan Mahammad, Habib Ali Molla for their constant support.

I must thank my Collaborators Dr.Keya Chowdhuri and Atul katarkar, CSIR-Indian Institute of Chemical Biology, Kolkata-700032, India for their kind cooperation.

I gratefully acknowledge DST for financial support to carry out the research work.

I would like to thank Rev. Dr. Dominic Savio,Principal and Bertram Da'Silva,Vice Principal, St. Xavier's College(Autonomous),Kolkata for their kind attitude and coperation to complete my research work.I would like to thank Department of Higher Education, Govt. of West Bengal for granting me leave to complete my thesis work.

I would like to thank my departmental as well as non departmental colleagues (of St. Xavier's College) who have given me constant mental support,encouragement and cooperation in various ways.

Last but not the least,I am grateful to my mother Tulshi Rani Das and father Ramgopal Das for their sacrifices to overcome family liabilities that helped me to carry out and to complete my research work throughout my academic journey. I want to thank my wife Kakali Das and my two little daughters Trimanjaree Das and Dipmanjaree Das for their love and prayers for me at the point of crucial stages of my research work and for the journey to complete my Ph.D. thesis.

Dipankar Das.

Department of Chemistry
Jadavpur University
Kolkata– 700 032, India.

Dipankar Das

28/03/2022

Preface

The work presented in the thesis entitled **''Design and Synthesis of Rhodamine-6G Based Highly Selective Fluorescent Probes for The Metal Ion Sensing"** have been carried out in the Department of Chemistry, Jadavpur University, Kolkata.

In this thesis I have incorporated my research work. I have developed some new and simple fluorescent molecular probes which are extremely sensitive, highly selective , bio-compatible and reusabile with minium toxicity for the recognition of cations in pure and mixed organo-aqueous medium. Different spectroscopic techniques like ^{1}H NMR, Mass, UV−Vis, FTIR have been utilized to characterize the probes and their metal complexes.

Thesis consists of five chapters which are summarized below-

Chapter-1 focuses on brief introduction of chemosensing method and its need for the detection of biologically important and toxic metal ions fluorometrically over conventional methods. Discussion on different chemosensing pathways with mechanism through diagrammatic presentation is given here. How to design and how to develop a suitable and efficient chemosensor are also explained in this chapter. Literature survey on different molecular probes for the recognition of metal ions like Aluminium, Chromium, Iron, Zinc,Cupper Mercury,Lead,Cadmium,Gold based on Rhodamine -6G moiety as a core part of the chemosensing ligand are discussed here. A very brief overview of the present work is highlighted.

Chapter-2 presents synthesis of a new rhodamine-6G based chemosensor (**L^1**) and its characterisation through spectroscopic studies and by single-crystal X-ray crystallographic study. Excellent sensitivity of **L^1** for Fe^{3+}, Al^{3+} and Cr^{3+} showing absorbance at 530 nm and emission at 558 nm with large enhancement of the fluorescence intensity for Fe^{3+} (41-fold), Al^{3+} (31-fold) and Cr^{3+} (26-fold) in H_2O/CH_3CN (4: 1, v/v, pH 7.2) are explained here by graphical presentation. The K_f-values are evaluated and reported as 9.4×10^3 M^{-1} (Fe^{3+}), 1.34×10^4 M^{-1} (Al^{3+}) and 8.7×10^3 M^{-1} (Cr^{3+}). Quantum yields of **L^1** and metal complexes are calculated and reported. Caculation of LODs for Fe^{3+}, Al^{3+} and Cr^{3+} (1.28, 1.34 and 2.28 μM respectively) is shown.

Phenomenon of fluorescence quenching of [Fe^{3+}–**L^1**] complex by cyanide ion has been presented.Construction of advanced level molecular logic devices using different inputs (2 and 4 inputs) as advanced level logic gates and memory devices are described.

Chapter-3 describes the synthesis, characterisation and photophysical studies of rhodamine-6G based chemosensor,**L^2**. Selective recognition of Hg^{2+} and Al^{3+} ions by **L^2** in the presence of all other biologically relevant and toxic heavy metal ions are presented graphically and explained.Formation constants are evaluated as: $K_f = (1.01\pm0.01)\times104\ M^{-1}$ for Hg^{2+} and $K_f=(1.45\pm 0.02)\times104\ M^{-1}$ for Al^{3+}.The calculation of detection limit (47 nM) for Hg^{2+} along with cell permeability and negligible cytotoxicity are discussed here . SEM study reveals rod-like microstructure of **L^2** in water, which changes to a porous microstructure in the presence of Hg^{2+}. In this chapter it has been shown that how fluorescence quenching of Al^{3+} complex occurs on increasing the SDS concentration, while a ~33-fold enhancement of fluorescence intensity of [**L^2-Hg^{2+}**] complex in the presence of SDS . FI increases and reaches to maximum at ~7 mM of SDS in pre-micellar concentrations and beyond the critical micellar concentration (CMC) fluorescence intensity decreases gradually with further increase in [SDS] up to 28 mM is shown and explained.

Chapter-4 presents synthesis, characterisation and photophysical studies of rhodamine-6G based chemosensor,**L^3**.Its excellent selectivity and sensitivity through **CHEF** based recognition of trivalent metal ions M^{3+} (M= Fe, Al, and Cr) over other metal ions are presented graphically and explained succesfully. Prominent enhancement in absorbance at 528nm and fluorescence emission at 558 nm for Fe^{3+} (669 fold), Al^{3+} (653 fold) and Cr^{3+} (667 fold) upon addition of these metal ions into the probe in H_2O/CH_3CN (7:3, v/v, pH 7.2) are presented. Calculation of K_d values of the complexes 1.94 x 10^{-5} M^{-1} (Fe^{3+}); 3.15 x 10^{-5} M^{-1}(Al^{3+}) ; 2.26 x 10^{-5} M^{-1}(Cr^{3+}) are given here. Quantum yields of **L^3**, [**L^3**—M^{3+}] complexes and calculation of LOD's for Fe^{3+}(2.57 μM), Al^{3+} (0.78 μM), Cr^{3+} (0.47 μM), are shown here. Quenching of fluorescence intensity of [Fe^{3+}-**L^3]** complex by cyanide ion is shown here . Advanced level molecular logic gates using different inputs (2 and 4 input) and memory device have been constructed.

Chapter-5 presents synthesis and characterization of a novel rhodamine-6G based chromo and fluorogenic "OFF-ON" biocompatible chemosensor, **L^4 .** Excellent selectivity of **L^4** for Fe^{3+} ion in pure aqueous medium over other metal ions and prominent enhancement of fluorescence

intensity at 551 nm upon addition of Fe^{3+} into the probe in H_2O (pH 7.2, 10 mM HEPES buffer) have been explained and presented. The formation constant, K_f = (1.16 ± 0.04) x 10^4 M^{-1} for the 1:1 stoichiometric binding between **L^4** and Fe^{3+} , Quantum yields of **L^4 (** 0.013), [**L^4**-Fe^{3+}] complex (0.523) and LOD of **L^4** for Fe^{3+} (4.184 μM) were calculated and reported.Quenching of fluorescence emission of [**Fe^{3+}- L^4]** complex by cyanide ion has been described in this chapter.

Dipankar Das.

Department of Chemistry
Jadavpur University
Kolkata– 700 032, India.

Dipankar Das

28/03/2022

List of Abbreviations

AAS	Atomic Absorbtion Spectrometry
FAAS	Flame Furnance Atomic Absorption Spectroscopy
ICP-ES	Inductively Coupled Plasma Emission
ICP-MS	Inductively Coupled Mass Spectrometry
ICP-OES	Inductively Coupled Plasma Optical Emission Spectrometry
NAA	Neutron Activation Analysis
TXRF	Total Reflection X-Ray Fluorimetry
τ	Fluorescence Lifetime
$\Delta\overline{\nu}$	Stokes shift
Φ	Quantum yield
CHEQ	Chelation Enhancement of Quenching
CHEF	Chelation Enhancement of Fluorescence
PES	Plasma Emission Spectroscopy
MLCT	Metal–Ligand Charge Transfer
ILCT	Intra–Ligand Charge Transfer
PET	Photo-induced Electron Transfer
ICT	Intramolecular Charge Transfer
PCT	Photo-induced Charge Transfer
TICT	Twisted Intramolecular Charge Transfer
FRET	Fluorescence Resonance Energy Transfer
ESIPT	Excited-State Intramolecular Proton Transfer
AIE	Aggregation-induced emission
HOMO	Highest Occupied Molecular Orbital
LUMO	Lowest Unoccupied Molecular Orbital
HEPES	4-(2-Hydroxyethyl)piperazine-1-ethanesulfonic acid
DFT	Density functional theory
LOD	Limit of detection
MeCN	Acetonitrile
MeOH	Methanol
NaOH	Sodium hydroxide
KBr	Potassium bromide
DCM	Dichloromethane
DMF/dmf	Dimethyl formamide
H_2O	Water
DMSO/dmso	Di-methyl sulfoxide
CD_3OD	Methanol-d4
Et_3N	Triethylamine

K_2CO_3	Potassium carbonate
mL	Milliliter
μM	Micro molar
μL	Micro liter
nM	Nano molar
mM	Mili Molar
fM	Femto molar
K_a	Binding constant/Association constant
K_{ass}	Association constant
K_d	Dissociation constant
K_f /K_f'	Formations constant
ex	Excitation
em	Emission
λ	Wavelength
λ_{max}	Wavelength of maximum absorption
Λ_{em}	Wavelength of maximum emission
HeLa	Human epithelial carcinoma cell
HepG2	Human hepatocellular liver carcinoma cells
PBS	Phosphate-buffered saline
MTT	3-(4,5-di methylthiazol-2-yl)-2,5 diphenyltetrazolium bromide
%T	Percentage of Transmittance
FBS	Fetal Bovine Serum
EDTA	Ethylenediaminetetraacetic acid
Na_2H_2EDTA	Disodium EDTAdihydrate
CMC	Critical miceller concentration
SDS	Sodium dodecyl sulphate
DAPI	4',6-diamidino-2-phenylindole
LOD	Limit of detection
MS	Mass spectroscopy
NMR	Nuclear magnetic resonance
FT-IR	Fourier transform Infrared
HRMS	High-resolution mass spectrometry
ESI-MS^+	Electrospray ionization mass spectrometry
HPLC	High-performance liquid chromatography
FI /F.I	Fluorescence Intensity
NIR	Near-infrared
FE	Fluorescence Enhancement
EJ	Lung cancer cell
Tris–HCl	Tris (hydroxymethyl) aminomethane hydrochloride
UV	Ultraviolet
Vis	Visible

h	Hours
TMS	Tetramethylsilane
CH_2Cl_2	dichloromethane
$SOCl_2$	Thionyl chloride
$CDCl_3$	Chloroform-d
DMSO-d_6	Deuterated Dimethyl sulfoxide
LiCl	Lithium chloride
ATP	Adenosine triphosphate
Pi	Phosphate - Wikipedia
PPi	Pyrophosphate
MHz	Megahertz
f	Oscillator strength
°	degree
Å	Angstrom
eV	Electron volt

CONTENTS

CHAPTER -1

Inroduction

CHAPTER-2

A differentially selective probe for trivalent chemosensor upon single excitation with cell imaging application: potential applications in combinatorial logic circuit and memory devices

CHAPTER-3

A rhodamine-based fluorescent sensor for rapid detection of Hg^{2+} exhibiting aggregation induced enhancement of emission (AIEE) in aqueous surfactant medium

CHAPTER-4

Rhodamine 6G-based efficient chemosensor for trivalent metal ions (Al^{3+}, Cr^{3+} and Fe^{3+}) upon single excitation with applications in combinational logic circuits and memory devices

CHAPTER-5

A novel and highly selective "turn-on" rhodamine-6G based chromo and fluorogenic sensor for the detection of Fe^{3+} in aqueous medium with potential applications for INHIBIT logic gate and memory devices

Introduction

Title

"Design and Synthesis of Rhodamine-6G Based Highly Selective Fluorescent Probes for The Metal Ion Sensing"

CHAPTER-1

1. General Introduction

Fluorescent chemosensors are described as "compounds containing a binding site, a fluorophore unit, and there must be an appliance for communication between these two sites".[1]

A chemosensor is a molecular device which is utilized to detect a species (ionic/molecular) called an analyte through a noticieable change in absorbance/fluorescence.[2-5] The main logic behind the chemosensing is primarily based on host-guest chemistry[6,7] where the presence of a guest (analyte) at the host site (fluorophore unit) creates a recognizable change in spectroscopic property that can be monitored in practice for most of the chemosensors either by colorimetrically or by observing luminescence, using fluorescence spectroscopy.[8]

Innovative investigations which were carried out for the design and development a fluorescent chemosensor at late 1970s and next decades, where crown ethers and aza-crown ethers or any suitable ligand framework were linked to fluorophore unit.[9-13] These chemosensors selectively or somewhere specifically identifies metal ions by exhibiting a significant ehancement in intensity of the fluorescence signals. Biosensors are synthetic compounds[14] having a biological receptor such as antibodies, aptamers etc. The ability to recognise a particular analyte under diversified environmental conditions is really a very beautiful event for a real-world condition which is critical for a number of applications including an extensive range of medical, scientific and security lands. Truly speaking, chemists achieved success through decades after decades genune efforts for developing suitable detection method for cations,[5,9] anions,[3,4] small organic molecules[1,2] and biological macromolecules including peptides [10,11] and also for the detection of bacteria in food[15]and in human body.[16]

1.1 Role of Metal Ions in Biological System

It is very hard to believe '*life without metals'*. Metals were historically familiar from the era of Mesopotamians, Greeks and Romans.[17] Progress of Human Civilization is based on understading and proper utilization of metals like iron(Fe), copper(Cu), silver(Ag), lead(Pb), gold(Au), tin(Sn), aluminum (Al), calcium(Ca), magnesium (Mg) and mercury(Hg) which are mostly available in the form of ores/minerals from nature and extracted from these natural and

anthropogenic sources[18](Figure-1.1). With the advancement of civilization, the needs of metals are increased in various industries to fulfill the demand of the society. At the same time, the disposal of waste from manufacturing unit causes the environmental hazard.[19]

For the maintenance of the lifespan of living organisms including plants, animals and humans the presence of metal ions is of fundamental requirements without which a growth disorder, severe malfunction, carcinogenesis or death may occur. Many cellular functions like (i) intra and inter cellular communications, (ii) maintaining electrical charges and osmotic pressure, (iii) photosynthesis and electron transfer processes, (iv) the maintenance of pairing, stacking and the stability of nucleotide bases, and also (v) the regulation of DNA transcription essentially require the presence of specific metal ion(s). Moreover, in the proper functioning of nerve cells, muscle cells, the brain and the heart, the transport of oxygen and in many other biological processes significant contributions of metal ions are well recognized.

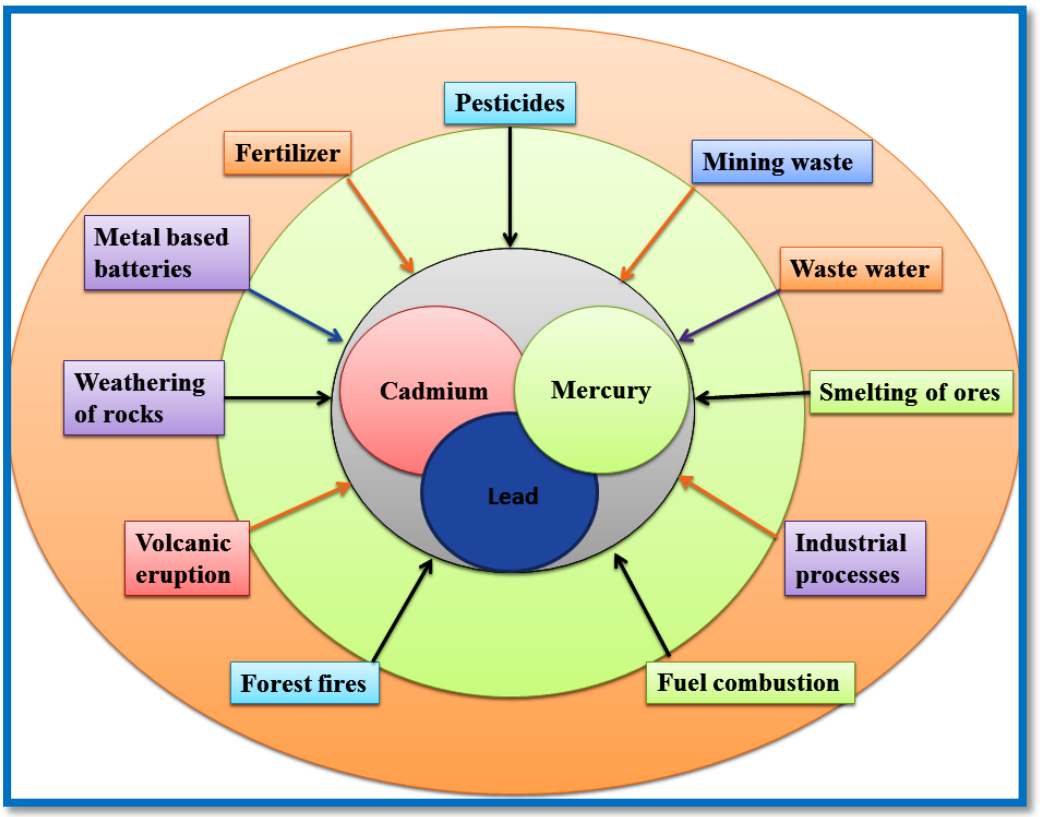

Figure-1.1: **Schematic presentation of various sources of cadmium, mercury and lead.**

(Adopted from review article: Science of theTotal Environment, 615, **2018**,476**)**

Some metals like Fe, Cu, Zn, Co, Mo etc are very much essential for the growth and some are needed to maintain the human health. On the otherhand, some metals like Hg, Pb, Cd, Cr, and As are detrimental. From food, water and polluted air inhalation many toxic metals may accumulate within the body of human and animals which may create several serious harmful effects in human life through the destruction of several enzymatic reactions.

Intra and inter cellular ion transport through channel mainly depends on the concentration gradients of spectroscopically inert alkali metal ions like sodium, potassium and calcium ions.[20] This imparts role for the transmission of nerve impulses within the brain and from it to other part of a human body. Calcium ion accelerates the clotting of blood. Calcium ions also plays key role in muscle contraction. Ca^{2+} binds to the actin filament which is the bind to myosin head in order to control a muscle contraction.[21]

The presence of one or more metal ion(s), like Fe, Zn and Cu etc, essential for the proper functioning of metallo-enzymes in living organisms including human. Iron has several vital functions in the body serving as a carrier of oxygen to the tissues from the lungs by red blood cell haemoglobin,[22,23] as a transport medium for electrons within cells, and as an integrated part of important enzyme systems in various tissues. Iron deficiency is the most common nutrition deficiency and diagnosed as anemia[25,26] and causes inadequate oxygen supply to the cell results many symptoms like weakness, hair loss irritability, impaired immune function etc. The myoglobin is an iron-containing oxygen storage protein in the muscles with similar in structure to haemoglobin but has only one heme unit and one globin chain. Zinc-finger proteins are involved in gene expression of various proteins where zinc is either bound to two cysteine and two histidine residues or to cysteine ligands only. Zn is a cofactor for many enzymes and involved in metabolism of proteins, lipids, carbohydrate. It also takes part in protein synthesis, DNA transcription, insulin pursuit and in the function of a liver.[27,28] Zn deficiency causes diarrhea, pneumonia in children's, memory impairment, impotence and mental lethargy.[29-31] Zinc(II) is a redox silent metal ion, however, it is believed that the interaction of RNS with cysteine displaces zinc from the protein, resulting in abrogation of activity.

Cu is involved in various metabolic reactions.[32,33] Cu deficiency causes gastrointestinal problems, low birth weight of a new born and it may cause genetic disorder resulting fatal

impact.[34,35] Magnesium consisting enzymes regulates nerve function, blood glucose level and blood pressure.[36,24,37]

So far we have discussed the importance of some heavy metals for the maintenance of human metabolism but their presence above the optimum level may cause adverse health effect (**Figure-1.2**). This adversity comes from complexation tendency of the metal ions with the biological ligands containing nitrogen, sulfur and oxygen atom. Structure of the protein changes through the cleavage of hydrogen bonding due to such type of complex formation and then enzyme activity is inhibited. Chromium deficiency can cause glucose intolerance and insulin resistance in patients.[38,39] can cause lung damage and cancer, aluminum is associated with Alzheimer's and Parkinson's diseases. Lead and mercury can cause joint diseases, ailments of the kidney's, circulatory system, central nervous system, reproductive system and causes many serious disorder in childrens.[40-42] Cadmium is one of the hazardous heavy metal for human health.[43] Long time exposure causes kidney damage and hypertension carcinogen,[44] it also causes infertility, cardiovascular abnormality and osteotoxicity.[45-47]

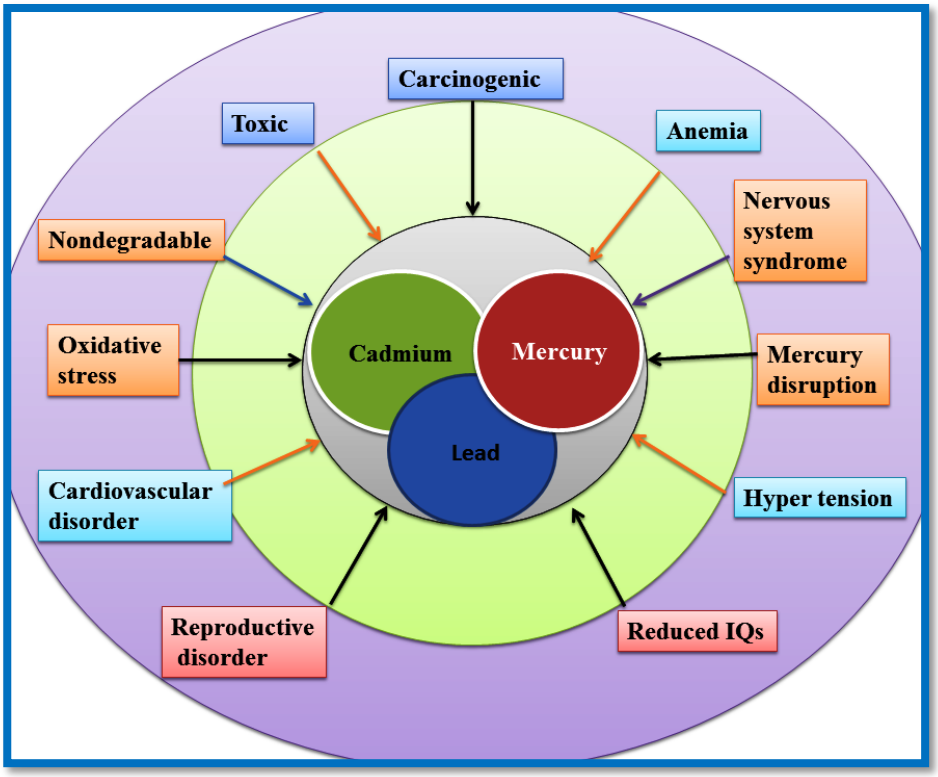

Figure-1.2: Schematic presentation of major health hazards of cadmium, mercury and lead. (Adopted from review article: Science of theTotal Environment, 615, **2018**, 476**)**

For particular and sometimes specific metal ion detection, design and synthesis of fluorescent chemosensor now-a-days receiving a huge attention in the field of chemical (molecular) sensor.[8, 48-54]

Due to sigificance of the metal cations in several biological processes vis-a-vis their toxicity and adverse effect it is very much essential to detect and measure their concentrations in environmental, chemical and biological samples for this purpose many excellent research work reported.[5-8]

1.2 Analytical Tools for Detection and Estimation of Several Metal Ions

Various instrumental methods may be applied to detect and to estimate the concentration level of certain heavy metals in a variety of environmental, biological and chemical samples. The mostly used techniques are Atomic Absorption Spectrometry (AAS), Atomic Emission/Fluorescence spectrometry (AES/AFS), Inductively Coupled Plasma Mass Spectrometry (ICP-MS); Inductively Coupled Plasma Optical Emission Spectrometry (ICP-OES); Neutron Activation Analysis (NAA), X-ray Fluorescence (XRF).

1.2.1 Atomic Absorption Spectrometry (AAS)

This kind of spectroscopy is based on absorption of radiation by a sample having atoms. When ultraviolet and visible light is allowed to pass through a medium containing mono-atomic sample such as Hg(g), Na(g) etc. it results absorption of certain frequencies of light. Absorption causes excitation of the species which results promotion of one or more electron to higher energy electronic levels. For example, sodium vapour shows two closely spaced sharp absorption peak in visible region of a spectrum at 589 and 589.6 nm due to the two separate excitation from 3S to two 3P states.Atomic absorption spectroscopy is a quantitative method for analysis of many elements.[55] This technique measures the concentration of these elements by passing radiation of certain wavelength emitted by a source usually hollow cathode lamp (HCL) and atomizers are mostly used in this method are flame, graphite furnace.(**Figure-1.3**)

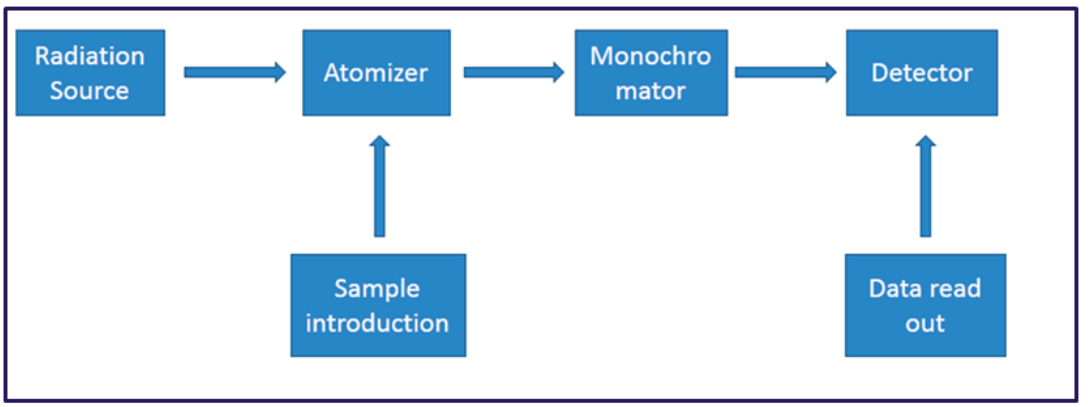

Figure-1.3: Schematic diagram of an atomic absorption spectrometry.

Cold vapor atomic absorption spectrometry (CVAAS) is a flame less technique employed at room temperature for Hg detection by the consumpsion of radiation at 253.7nm by Hg vapor. In this method Hg ion (Hg^{+} and Hg^{2+}) is first reduced to its elemental state by $NaBH_4$ or $SnCl_2$ then mercury vapor goes through a cell kept in the spectrophotometer driven by argon gas.[56]

1.2.2 Flame Atomic Absorption Spectrometry (FAAS)

This is an appropriate technique for the determination of metals with high precession at ppm level. FAAS was applied successfully for the detection of heavy metals in variety of matrices. Arsenic(As), Zirconium(Zr) like elements cannot be detected by this method because of their high atomisation energy. [57]

1.2.3 Graphite Furnace Atomic Absorption Spectroscopy (GFAAS), is a suitable atomization technique to be used to measure for a specific analyte concentrations with a permeable limit by parts per billion (ppb) level.[58]

1.2.4 Atomic Emission Fluorescence Spectroscopy (AES and AFS) are another kind of techniques where atoms are promoted to excited electronic state and then the atoms subsequently emit radiation when they come back to their ground state. Particular element emits radiation of certain wavelength which is then detected by spectrophotometer. From the spectral line wavelength, elements can be identified and from the lines intnensity number of atoms of that element can be determined.[55] However, atomic absorption is the mostly used technique as compared to AES and AFS.

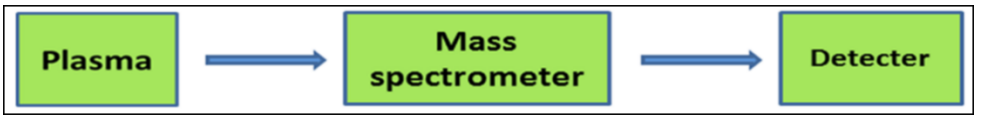

Figure-1.4: Schematic presentation of plasma emission spectroscopy.

1.2.5 Plasma Emission Spectroscopy (PES) is a type of emission spectroscopy where exciting media is the plasma at a very high temperature (7000-10000K) (**Figure-1.4**). This temperature causes the cleavage of all types of molecular bonds and results in the formation of free atoms and ions, which emits their characteristic light and gives spectra.[59-61]

1.2.6 Inductively Coupled Plasma-Mass spectrometry (ICP-MS) is a good quantitative method for estimnatinng a multi-element system of broad range of elements. This method utilises argon plasma as a source to disitnegrate the sample to ions or atoms. Then the ions come out from the plasma and then goes into the mass spectrometer, then isolated accordingly.[60] ICP-MS used for the analysis of selected trace elements such as Cu, Zn, Mn, Cd and Se in acceptable herbal medicines in various dosage forms.[62]

1.2.7 Inductively Coupled Plasma-Optical Emission Spectrometry (ICP-OES) is a spectroscopic method ivolvinng unprompted emissions of photons from atoms of trace elements of various type of sample which are excited by a radiofrequency (RF) radiation. Sample is normally incorporated to the plasma in the liquid form. Quantitative estimations of As, Cu, Zn, Cd and Pd present in soft drink sample are conducted by ICP-OES.[63]

.1.2.8 X-ray Fluorescence Spectroscopy (XRFS) is a non-destructive analysis technique employed for the elemental rannge of sodium to uranium in many matrices. This method requires minimum sample preparation effort and it uses X-ray radiation as source.[64] In this process X-ray contains sufficient energy to eject the electrons from the atoms inner shell and pushes the atom to an unstable state. So the electrons try to return to its inner shells releasing characteristic X-rays. This process of emission is called XRF.

Although such methods are sensitive to the metal ions over a wide-range and low detection limit but many of them are complicated, time consuming and costly too and not suitable in the common laboratories. So simple and less expensive methods are very much needed which not only detect the metal ions but also estimate their concentration present in industrial,

environmental and biological samples. Among them the optical detection involving change in fluorescence intensity is the satisfactory method due to it's high sensitivity and simplicity.[5,65] Hence, substantial efforts are being made to develop and to improve a very much functional tool for *in vitro* and *in vivo* recognisation of many biologically key metal ions.[5, 65-67]

1.3 Introduction to Spectroscopy: UV and Fluorescence Spectroscopy

Our god given eyes are the best detector for the different colour in the nature with absolute resolution. This detectability of band width through eyes is restricted to visible region from the entire range of electromagnetic radiation. Spectroscopes are developed to study the interaction between electromagnetic radiations with the matter (**Figure-1.5**).

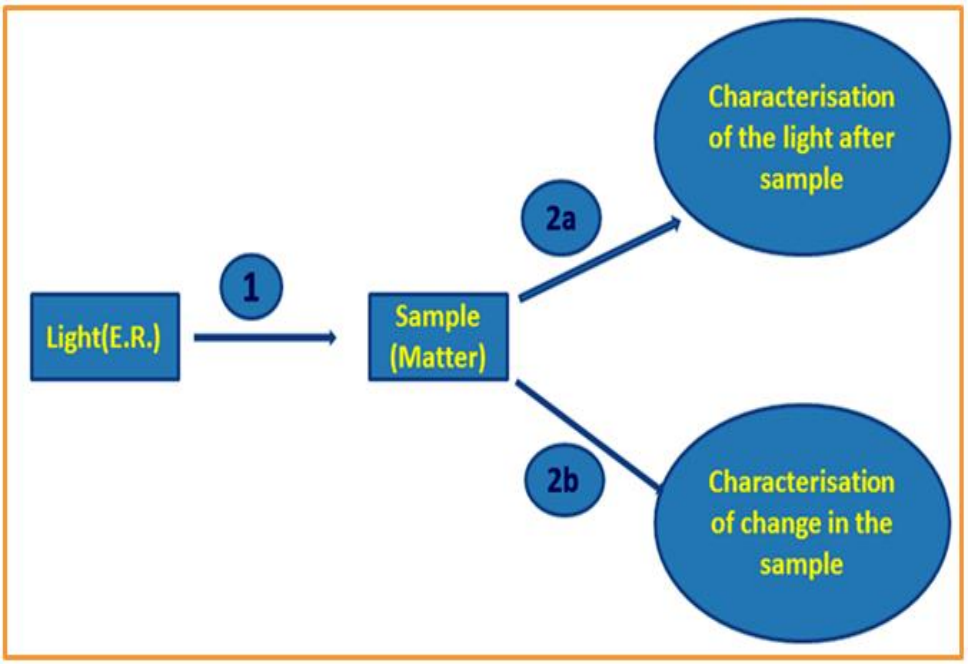

Figure-1.5: Schematic presentation of light and matter interaction.

19th century, field of spectroscopy accomplished an era of prononucned advancement with successful application for the analysis of compounds. Physicist G. R. Kirchhoff, chemist R. W. Bunsen cosntructed spectroscope and set the foundation for the broad application of spectroscopic technique in science and technology with their works "Chemical Analysis through Spectral Observations". Establishment of the structure of a species can be achieved from the

results of spectroscopic experiment and for the interpretation of experimental results from spectroscopic studies needs theoretical models. In spectroscopy there is interaction between electromagnetic radiation and matter.[68]

Basic idea involves: i) Excitation ii) Detection.

We are familiar with two kinds of spectra known as *continuous spectra* and *line spectra*.[69,70] With the help of an emission and absorption spectra of a species a lots of information can be gathered about them. The basic difference between continuous and line spectra is that first one contains all the wavelengths of a certain range and other one a selective wavelength. So the presence and absence of the lines in the spectrum makes the difference between them. The terms absorption and emission signifies how much light absorbed and emitted by a matter after interaction with the light. The emitted light is usually changed from the incident light-which is measured by spectroscopy.

1.3.1 Absorption Spectroscopy

Absorption spectroscopy is a technique that measures the intensity of absorbed radiation, at a particular frequency or wavelength, following interaction with matter. The type of transition that an analyte undergoes changes with the change of photons energy. In case of IR spectroscopy, the absorption of relatively low energy IR radiation results in the vibrational energy levels of a chemical bond within that molecule. The higher energy photons will excite the valence electrons to promote to an excited state. The known absorption spectroscopies are Infrared (IR), Atomic absorption, Raman, Ultraviolet-Visible (UV-VIS), Electron spin resonance (ESR), Nuclear magnetic resonance (NMR) and X-ray absorption.[71-75]

1.3.1.1 Electronic Spectroscopy

Every moment we can see many colorful things around us from morning to night. The cause of various colours of different things is due to an electronic spectroscopy in the visible region. The UV spectroscopy is an electronic spectroscopy as it is associated with transfer of an electron from lower to higher energy levels. UV spectroscopy is a type of absorption spectroscopy where a molecule absorbs electromagnetic radiation in the range of 200-400nm. Normally, the preferred transition takes place from HOMO to LUMO. For many molecules S orbital involved in sigma

bond formation and orbitals containing lone pair of electrons are low energy orbitals whereas p orbitals and anti-bonding orbitals are higher energy orbitals. Some important transitions with increasing energies are: **$n\rightarrow\pi^*$, $\pi\rightarrow\pi^*$, $n\rightarrow\sigma^*$ and $\sigma\rightarrow\sigma^*$**.

According the Beer-Lambert law (2.5), absorption of radiation depends on: (i) intensity of the incident beam. (ii) path length. (iii) concentration of absorbing ...Beer-Lambert law is expressed as, **$A = \log (I_0/I) = \varepsilon cl$**

Where, A = absorbance, I_0 = intensity of light incident upon sample cell, I = intensity of light leaving sample cell, C = molar concentration of solute, L = length of sample cell (cm.), ε = molar absorptivity.Transmittance is the alternative way to describe the amount of light absorption. Transmittance (*T*) is the ratio of the intensity of transmitted radiation to incident radiation and expressed as $\%T = [I/Io] \times 100$

The equation used for the measurement of binding/equilibrium constant is

$$A_{obs} = (A_0 + A_\infty K [G]_T) / (1 + K [G]_T). \quad (1)$$

Where, A_{obs} = absorbance, A_0 = free receptor absorbance, A_∞ = absorbance induced in presence of an anionic guest, $[G]_T$ = total guest concentration, and K = host-guest entity binding constant.

1.3.1.2 Infrared Spectroscopy

Infrared spectroscopy utilises electromagnetic radiation of infrared region (mid-IR: 4000-400 cm^{-1}, total spans 12820 to 33cm^{-1}) to know the molecular structure (nature of the functional groups like –OH, NH_2, C=C, CO-CH_3, C=O, C≡N, etc and bonds C-H, C-D etc.). Vibrational transitions occur in the presence of IR light and the energies of the IR absorptions are related to the bond strength in molecules and the masses of the connected atoms. Historically, infrared spectra have been represented as percent of transmittance(%T) versus either the wavenumber(ν) or the wavelength(λ). The use of wavenumbers (in cm^{-1}), is standard. By convention, the wavenumbers are plotted in decreasing order from left to right.

1.3.1.3 Magnetic Resonance Spectroscopy

Magnetic resonance is of two types **i)** NMR (Nuclear Magnetic Resonance) and ii) NQR (Nuclear Quadrupole Resonance) (a zero field NMR). NMR is associated with nucleus having non-zero spin (I ≠0) resulting to be resonance active. NMR & NQR refer to resonance from

nuclei having I = ½ & I > ½. (I, is the spin of the nucleus). When kept in a magnetic field, NMR active nuclei (I ≠0, such as ^{1}H or ^{13}C) absorbs radiation of radio frequency region and at a particular frequency resonance of nuclei occurs. NMR spectroscopy is a powerful tool for structure elucidation of a compound by knowing number and position of the signals (chemical shift), intensity of the signals and the splitting pattern of the signals (number of peaks within a signal). Mostly we deal with ^{1}H and ^{13}C nuclei but nuclei like ^{11}B, ^{19}F, ^{31}P, and ^{195}Pt gives a lot information about the molecular structure. Today research in chemistry is unthinkable without NMR.

1.3.1.4 Electron Paramagnetic Resonance (EPR)

Electron paramagnetic resonance (EPR) or electron spin resonance (ESR) spectroscopy is used to study a chemical entity containing one or more free electron(s) in organic or inorganic complexes having a transition metal ion.

EPR is actually similar to NMR but in EPR electronic spin is the key factor whereas in case of NMR it is the nuclear spin. EPR is only applicable for molecules or ions with unpaired spins.

1.3.2 Fluorescence Spectroscopy

Fluorescence is a radiative emission process that takes place when the excited molecule relaxed by releasing energy to the environment. In this spectroscopy normally light passes through the sample containing fluorophore, then sample solution absorbs the incident light that causes fluorescence from the sample. Analysis of the fluorescence intensity is the key part of this spectroscopy.

Nicolas Monardes, Spanish physician and botanist, first documented their observation that a strange blue glow was coming from the water kept in a cup which is made of a specific wood (Ligirium nephiticiem) and termed the phenomenon as fluorescence in the year 1565. In 1845 John Herschel first recorded the fluorescence emission spectrum for quinine. In the late 19th century George Stokes developed a technique for observing many colored filters for excitation and emission beam and also reported that emission wavelength is longer than excitation- known as Stokes law.

Fluoresce spectroscopy is a result of three stage process i) **Stage-1**: Energy is supplied to the fluorophore from an external source like incandescent lamp or a laser to elevate molecules from ground state to an excited electronic singlet state with several vibrational levels ii) **Stage-2** or Excited state life time: The existence of molecular excited state is in nano second time scale and within this very short time fluorophore a conformational change takes place and also subjected to various interactions with the environment. One important process is energy of S_1^v is partially dissipated producing a relaxed S_1 from where fluorescence emission obtained. **Stage-3**: Fluorophore molecule emits energy to return in its ground state. The energy stored in the excited molecule may be released in several pathways. When it comes back to its ground state, S_0, from the lowest vibrational level of S_1 with the emission of light – known as fluorescence. The energy of emitted photon is lesser than the excitation energy due to dissipation of some energy in the excited state (**Figure-1.6**). This emission of photon results fluorescence emission spectrum. Loss of fluorescence occurs due to the interaction of the fluorophore molecule with the other molecules present in the system, known as fluorescence quenching.

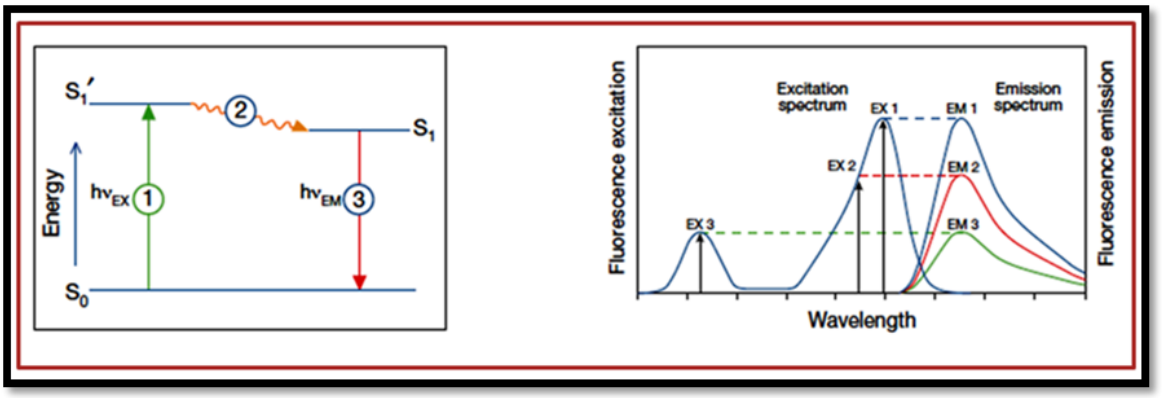

Figure-1.6: Excitation of the fluorophore molecule at three different wavelengths does not changes the fluorescence spectrum profile but variation occurs in the fluorescence intensity. (Image taken from Wikipedia**).**

Fluorescence is the emission of light from that matter at higher wavelength after absorption of light at a particular wavelength. So, fluorescence spectrum consists of excitation as well as emission spectrum. These spectrums are called fluorescence fingerprint or signature. Two

compounds can't have same fluorescence fingerprint; this principle makes the fluorometry an analytical technique with specificity. Fluorometry measures the intensity of the emitted light.

Fluorophore, a fluorescent molecule, known as fluorescent probes plays an important role in fluorescence spectroscopy. Fluorescent probes are of three different type i) intrinsic probe, ii) extrinsic covalently bound probe and iii) extrinsic associating probe. Although intrinsic probes are ideal but they are very rare e.g. tryptophan in protein.

1.3.2.1 Stokes shift

The gap between absorption maxima and emission maxima of a fluorophore is known as Stokes shift, Spectral shift to lower energy i.e. higher wavelength, is referred to as stokes shift, expressed in wavenumber (**Figure-1.7**). For both fluorescence and Raman spectroscopy stokes shift is the salient phenomenon. It is named after the name of physicist George G. Stokes to honour his contribution to this field. G.G. Stokes studied extensively the properties fluorescence in mid 19th century that how fluorescent light changes with respect to the incident light. He recorded his observations in 1852 "*On the change of the refrangrability of light*", in the Royal Society of London. In his work he stated that "*There is one law relating to internal dispersion (Fluorescence) which appears to be universal, namely, that when the refrangibility of light is changed by dispersion it is always lowered (shifted to longer wavelength)*". The term fluorescence was first chosen by Stokes.[76,77]

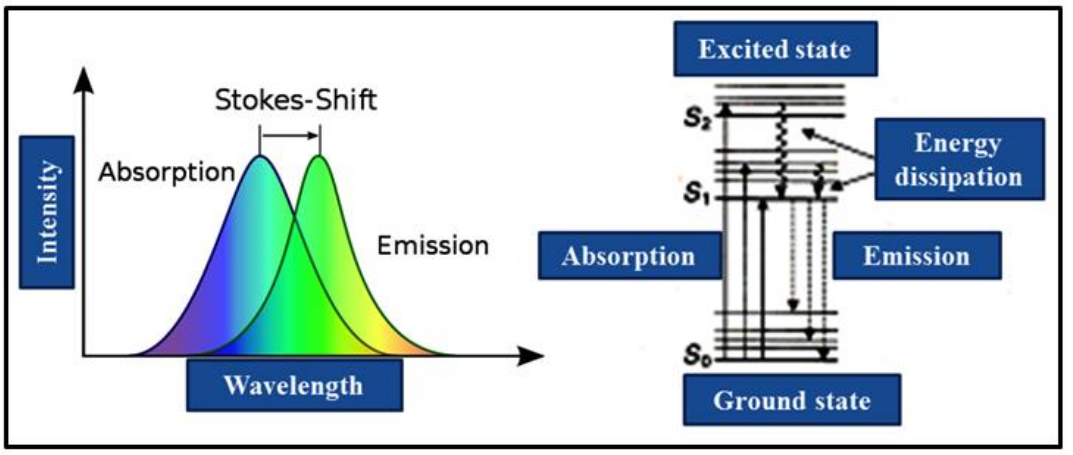

Figure-1.7: Diagram showing shift of a band: Stokes shift. (Image taken from wikipedia and then modified).

1.3.2.2 Time-Domain Lifetime Measurement

It is the time period that a fluorophore stays in the excited state before coming back to its ground state by releasing a photon is called fluorescence lifetime. It is an inherent phenomenon of fluorescent probe and widely used to study biomolecules, micro environment and their molecular association. In the excited state there may occur conformational changes, molecular interaction, rotatation and diffusion to the environment. The population of the excited state decays with time due to non-radiative processes and fluorescence emission and it is described by the differential equation as

$I_t = I_0\, e^{(-t/T)}$.

where I_t is the intensity at time t, I_0 is a normalization term (the pre-exponential factor) and τ is the lifetime.

$dn(t)/dt = -(k_r + k_{nr}).n.(t)$

Where, $n(t)$= Number of excited state molecules at time t following excitation.

k_r = Radative rate constant.

k_{nr} = Non-radiative rate constant.

This results in an exponential decay of the excited state given by the following equation

$n(t) = n_o \exp(-t/\tau)$

Where, τ is the fluorescence lifetime of the molecule.

$T = (k_r + k_{nr})^{-1}$.

The natural or radiative lifetime of the fluorophore is defined as $\tau_0 = k_r^{-1}$.

The intensity of the fluorescence decay as the function of time in a uniform population of molecules excited by pulse of light can be described by the following equation.

$$I(t) = I_0 e^{-(t/\tau)}$$

Where, $I(t)$ is the fluorescence intensity at time t.

Always triplet state life time is greater than the singlet state one. If $\boldsymbol{\tau_S}$ is the lifetime of excited state S_1, it is given by-

$$\tau_S = \frac{1}{Kr^S + K_{nr}^S}$$

Where, k_r^S is rate constant for radiative deactivation from S_1 to S_0 with fluorescence emission and k^S_{nr} is rate constant for non-radiative deactivation, i.e. sum of rate constant for internal

conversion and rate constant for inter system crossing. If the only way of de-excitation from S_1 to S_0 was fluorescence emission, the lifetime would be $1/K^s_r$ this is called the radiative life time and denoted by $\boldsymbol{\tau_s}$.[76,78]

1.3.3.3 Fluorescence Quantum Yields

The quantum efficiency (Φ_f) is an indication of the efficiency of the fluorescence process relative to all other probable ways for relaxation. Quantum yield is the number of emitted photon relative to the number of absorbed photon A quantum efficiency (Φ_f) = 0.9 implies that process is highly efficient whereas Φ_f = 0 means no molecular fluorescence. Fluorescence quantum yields were measured by the relative comparison procedure by using a reference compound in specified solvent. The quantum yield of a fluorophore varies with the change in pH, concentration, and solvent polarity**.** The quantum yield can be calculated using the equation given below-

$$\boldsymbol{\Phi_f = \Phi_{f'} (I_{sample}/I_{std}) (A_{std}/A_{sample}) (\eta^2_{sample}/\eta^2_{std})}$$

Where, $\boldsymbol{\Phi_{f'}}$ = Quantum yield of the reference compound,

I_{sample} and I_{std} are the integrated emission intensities; A_{sample} and A_{std} are the absorbance at the excitation wavelength, and η^2_{sample} and η^2_{std} are the respective refractive indices.[76,78]

1.3.3.4 Factors Affecting Fluorescence

The fluorescence intensity is related to both the exciting light and concentration of the fluorescent material. Structure of the fluorescent material plays an important role such as:

(a) Substituents: A molecule containing electron donating groups like OH, OMe, NH_2, NHMe, NMe_2, F etc. enhances the fluorescence intensity by increasing the transition probability to the excited singlet state from the ground singlet state. Whereas electron withdrawing group like NO_2, COOH, Cl, Br, etc. reduces or quenches the fluorescence intensity completely.

(b) **Molecular rigidity**: A molecule with rigid structure is more favoured for fluorescence. Molecular rigidity reduces the probability of non-radiative processes that makes suitable for strong fluorescence. For example, rhodamine, fluorescein and eosin are strongly fluorescent due to their more rigid structure whereas phenolphthalein is fluorescent.

c) Polarity of the solvent: Solvent containing heavy atoms or other such type of atoms reduces the fluorescence intensity.

c) Changes in pH: The fluorescence is more associated with π to π* state rather than n-π* state, first one possesses short average life period and this compete with the other deactivation process. For each compound certain pH range is effective for showing strong fluorescence. For example, rhodamine-6G exhibit strong fluorescent at the pH range 4 to7.4.

1.3.3.5 Fate of Excited State Molecules: Photochemical and Photophysical Processes

The photochemistry of a species arises when a molecule is being irradiated by means of photon. Molecule in its excited state contains higher energy that makes this state less stable so it must lose some energy. There are different pathways: i) Chemical process ii) Physical process(**Figure-1.8**) (emission of radiation or thermal relaxation) by which it can release some of its energy.[79]

Figure-1.8: Possible de-excitation pathways of excited molecule.

1.4 Physical Processes and Fluorescence

The photochemical promotions of the molecules mostly take place due to transition from S_o to S_1 or S_2 state; as promotion from S_o to triplet (T_1) state is "forbidden". In liquid and solid phase these higher states usually drop to S_1 state through a process called energy cascade. Initially excitation populates higher vibrational levels of S_1, after that it comes down to lowest vibrational energy level of S_1. S_1 is an important excited singlet state.[80] Variety of physical and chemical processes occurs from S_1. The physical pathways are shown in a Jablonski diagram (**Figure-1.9**). This diagram is named after the name **Alexander Jablonski.**

a) **Vibrational Cascade (VC)**

When a molecule is excited photochemically and it reaches to some higher energy level of either S_1 or S_2 state does not remain for long time so it loses its energy by giving to environment and come down to its lowest vibrational level of S_1or S_2, such energy release process in the form of heat is called vibrational cascade.

b) **Internal Conversion(IC)**

Decay of the molecule from from S_2 to S_1 or S_3 to S_1 is known as internal conversion and this process is nonradiative, shown in the diagram by wavy bond, by which it gives up energy to the envioronment.

c) **Inter System Crossing (ISC**)

If the singlet state is long lived, then S_1 to T_1 conversion occurs by a process called intersystem crossing. Benzophenone has 100% ISC efficiency. This process is a slow process because it is a spin forbidden process. As singlet state energy is higher than triplet state; this energy must be given up. One way is that molecule goes from S_1 state to higher vibrational level of T_1 state and then it cascades down (10^{-12}) to its lowest vibrational level.[81]

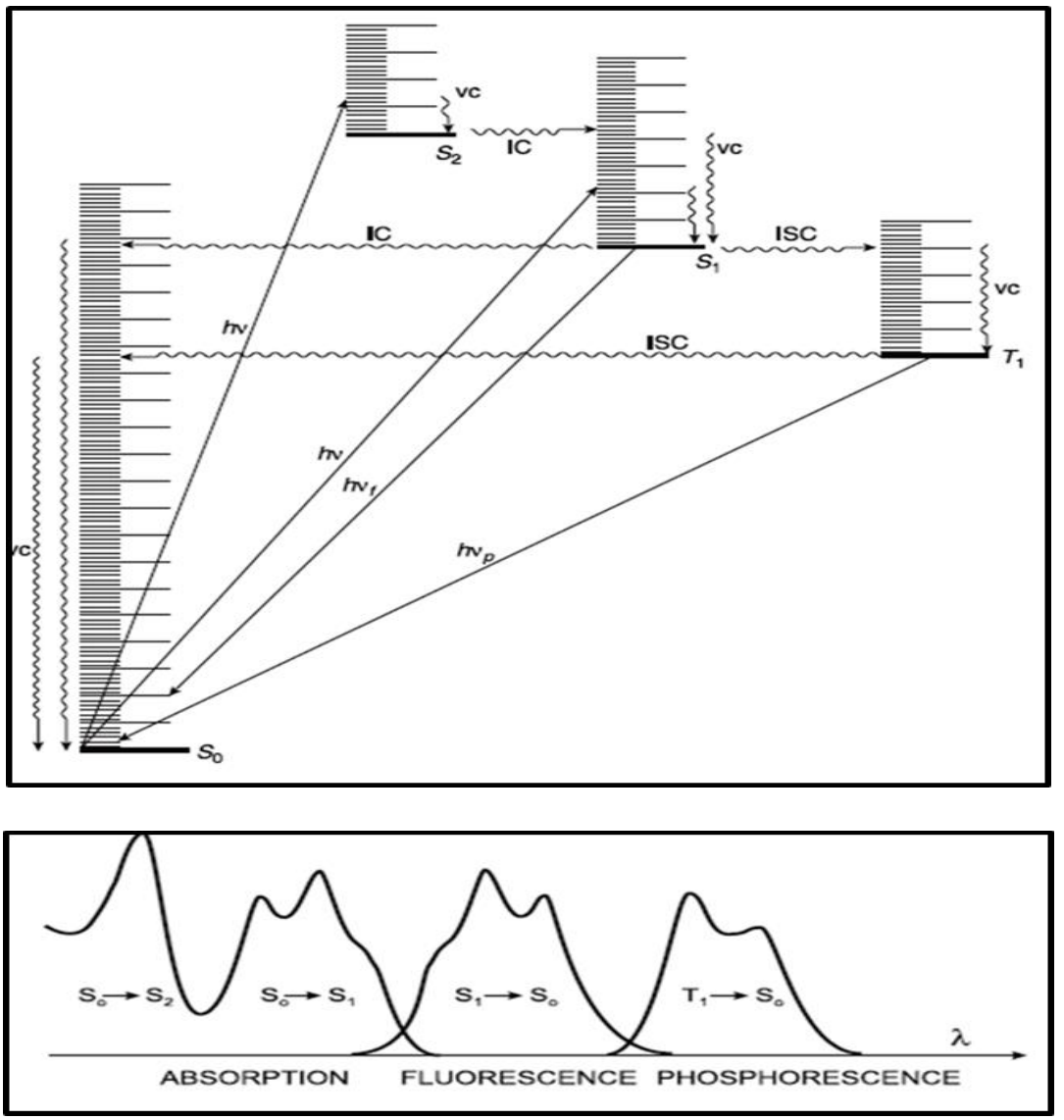

Figure-1.9: Jablonski diagram for different energy levels and transitions (Image taken from "Advanced Organic Chemistry-Jerry March"**).**

d) **Fluorescence**

A molecule in the S_1 state may return to some low vibrational level to the So, (V_2, V_3, V_4 but not to V_o) state by giving up energy in the form of light. This radiative process is called fluorescence, generally happens within 10^{-9} sec. This path is not very common for small molecules like diatomic molecules and rigid molecules. Fluorescence is very weak or undetectable for most of the compounds. The compound which shows fluorescence for those

fluorescence emission spectra usually the approximate mirror images of their absorption spectra. This mirror image relationship nature is due the fact that during fluorescence emission molecules drops from the lowest vibrational level of S_1 to various levels of So. Whereas during absorption it occurs from lowest vibrational level of So to various levels of S_1. The only one peak which is common that results from transition between the lowest vibrational levels of the two states, is called 0-0 peak. In solution 0-0 peak may be non-coincidental due to difference of solvation. Because of the possibility of fluorescence, any chemical reactions of the S_1 state must take place very fast, or fluorescence will occur before they can happen.

e) **Phosphorescence**

A molecule from T_1 state may come back to the S_0 state by releasing heat (intersystem crossing) or by releasing light. This light emission is called Phosphorescence.[82,83] Both the process of intersystem crossing and phosphorescence are slow (10^{-3} to 10^{-1}) this indicates longer lifetime of T_1 state (life time of $S_1 = 10^{-9}$ to 10^{-15}sec); life time of $T_1 = 10^{-5}$ to 10^{-3} sec).

Transition	**Time scale (sec.)**	**Phenomenon**	**Radiative process?**
Absorption	10^{-15}	$\mathbf{S_o + h\gamma \rightarrow S_1^v}$	Yes
Internal conversion	10^{-13} to 10^{-11}	$\mathbf{S_1 \rightarrow S_o}$ **+ heat**	No
Vibrational relaxation	10^{-13} to 10^{-11}	$\mathbf{S_1^v \rightarrow S_1}$ **+ heat**	No
Intersystem crossing	10^{-3} to 10^{-1}	$\mathbf{T_1 \rightarrow S_o}$ **+ heat Or** $\mathbf{S_1 \rightarrow T_1^v}$	No
Phosphorescence	10^{-3} to 10^{1}	$\mathbf{T_1 \rightarrow S_o + h\gamma}$	Yes
Fluorescence	10^{-9}	$\mathbf{S_1 \rightarrow S_o + h\gamma}$	Yes

Table-1.1: Tabular form of different photophysical processes and their time scale.

1.5 Design of Fluorescent Molecular Sensor and Basic Principle

1.5.1 Chemical Sensors

Commonly used terms in the area of fluorescence are fluorescent molecular sensor, fluorescent sensor, fluorescent chemosensor, luminescent sensor, luminescent sensor molecules, fluorescent optical sensor etc. There is a sharp difference between analyte responsive moiety and optical sensing device. In the former case fluorophore creates a singal by changing the fluorescence intensity in the presence of an analyte (**Figure-1.10**). Another important term in the field of fluorescence is chemosensor which is also completely different from biosensors. There is no specific and universal definition of a chemical sensor, so there is debate in scientific community over the time. One of the defition is that *"chemical sensors are miniautorized devices which can deliver real-time and on-line information in the presence of a specific analyte"*.[84] It is also defined as *"A chemical sensor is a molecule of abiotic origin that signals the presence of mater or energy- A.W. Czarnick,*[78] So it can be said that it is a measurement device that convert physical and chemical properties of an analyte into a measurable signal and intensity depends on analyte concentration.

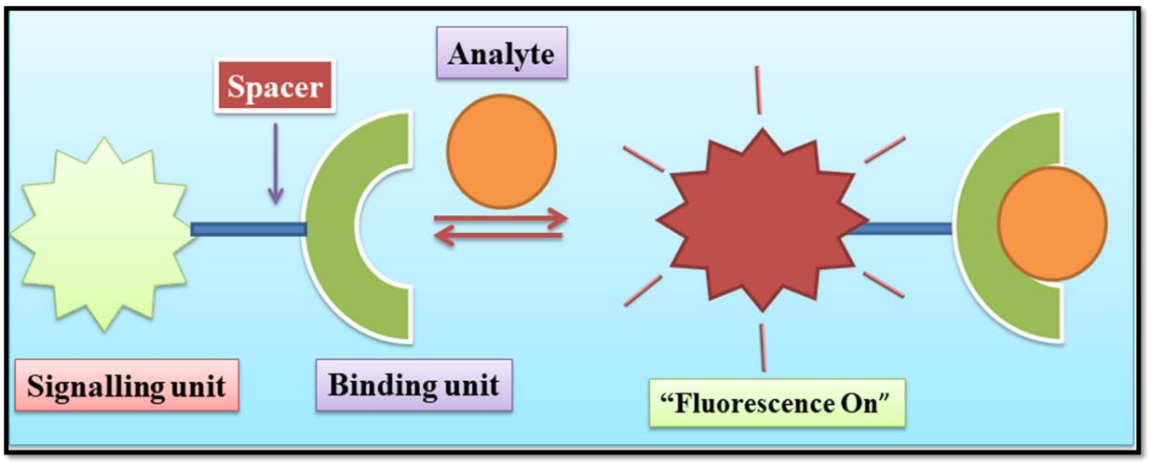

Figure-1.10: Schematic presentation of complex formation with change in optical properties through binding of an analyte (guest) by a chemosensor (host).

A Chemical sensor can determine the detectable presence, concentration and the quantity of a particular analyte. Both the sensitivity and selectivity are the most important aspects of a chemosensor and these are affected by the phase, dimensional and temporal effect of the analyte, which may be present in the form of gas, liquid or solid in various dimensional scale.Chemical sensing application requires existence of two basic components as chemical recognition system, called receptor (host) that binds with analytes(guest) selectively and reversibly and a transducer component[85,86].On the other hand, biosensor is a molecular device of biotic origin that indicates the presence of matter or energy.

1.5.2 Basic Principles and Types of Chemosensors

To design a fruitful chemosensor it must have three essential components (**Figure-1.11**)

i) A chemical receptor which can bind precisely and efficiently with an analyte of our interest.

ii) A signalling unit or fluorophore unit known as transducer which should contains an chromophoric group which converts binding phenomenon or recognition event, takes place at the site of a receptor, into a measurable fluorescence change and converting into a useful information.

iii) Spacer between the receptor and signalling unit.

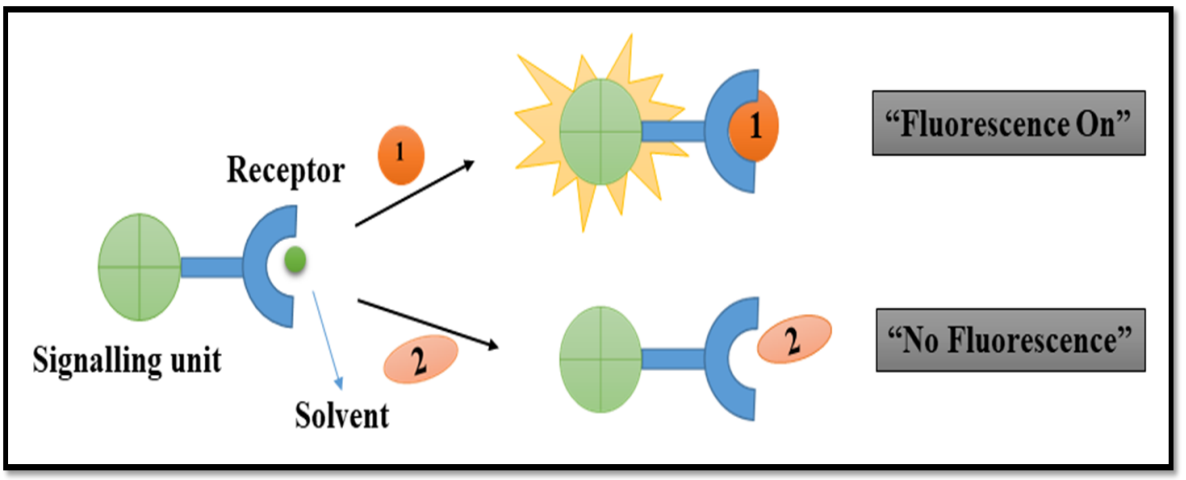

Figure-1.11: Schematic presentation showing binding of an analyte (guest) by a chemosensor (host), with change in optical properties of the complex.

Three separate approaches which were mainly used by many research groups for chemosensing are-

i) Binding site-signalling approach

ii) Displacement approach

iii) Chemodosimeter approach

Two parts namely binding site and signalling subunit are linked through a covalent bond [**Figure-1.12a**]**.** Three types of signalling events may occur:

(a) The interaction between receptor and analyte influences the electronic characteristic of the signalling unit and produces a sensing event.

(b) In the displacement method[87-89](**Figure-1.12b**) receptor site and signalling unit together form a molecular ensemble although they are not connected by the covalent bond.

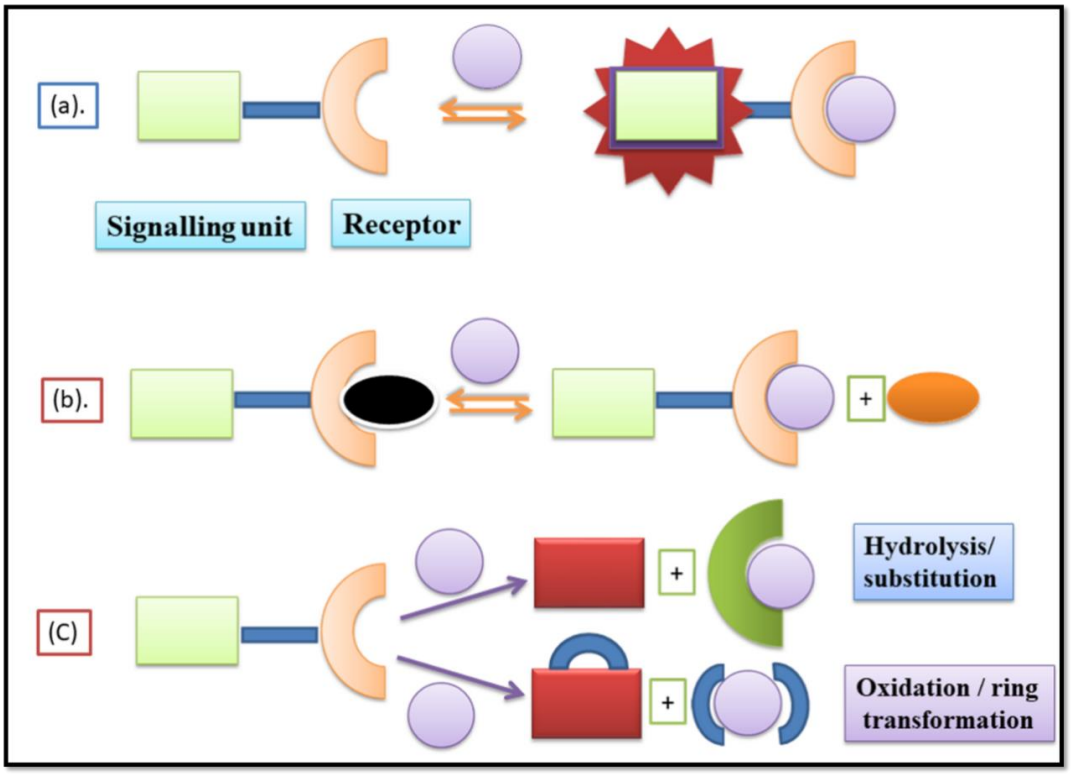

Figure-1.12: Schematic presentation of chemosensing events through a) binding site signalling approach b) displacement and c) chemodosimeter approach.

(Adopted from Critical Review: Analyst, **2015**, 140, 7082**)**

(c) Appearence of certain guest in the solution containing that molecular ensemble results a displacement reaction where signalling subunit is released upon coordination of the analyte with the binding site and causes sensing phenomenon which is commonly termed as chemodosimeter approach.[90-95]

Chemosensors are molecules of an abiotic origin which can communicate with the sample to produce a measurable signal within a very short time. The host-guest coordination event is the basic principle of chemosensing. So, the reaction between receptor and analyte accompanying a change in signal may be reversible (**Figure-1.13**) [96,97-104]

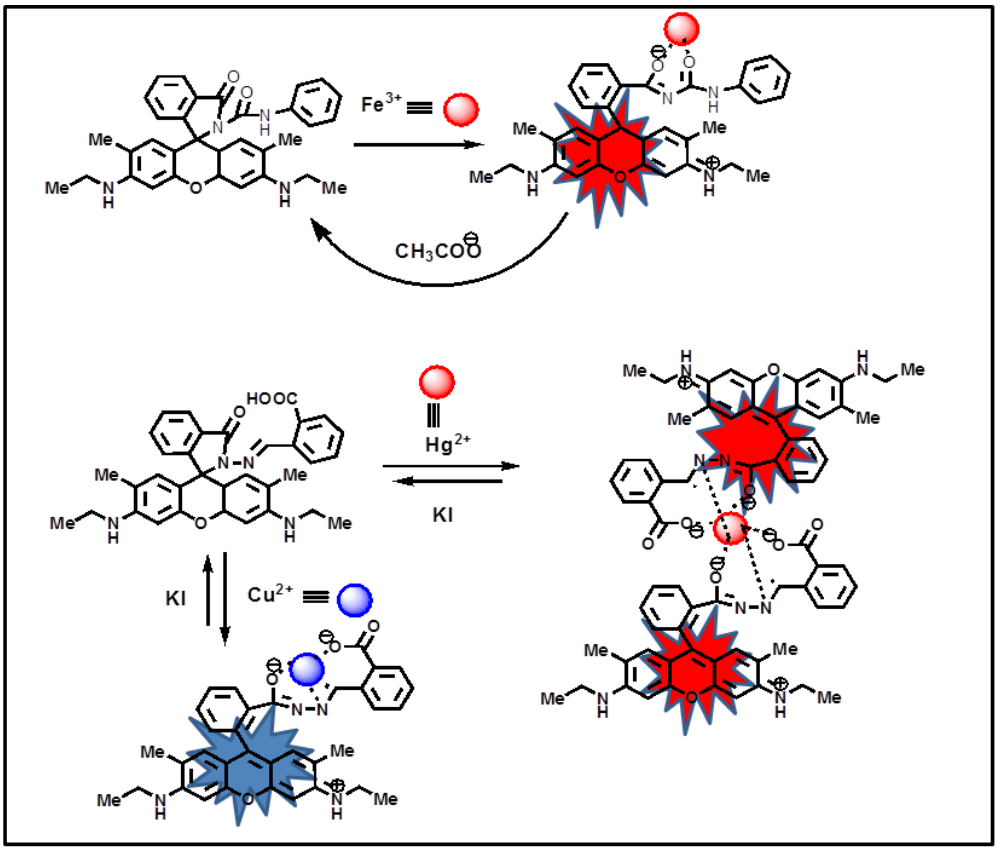

Figure-1.13: Examples of Various types of fluorescent Chemosensor (Reversible).

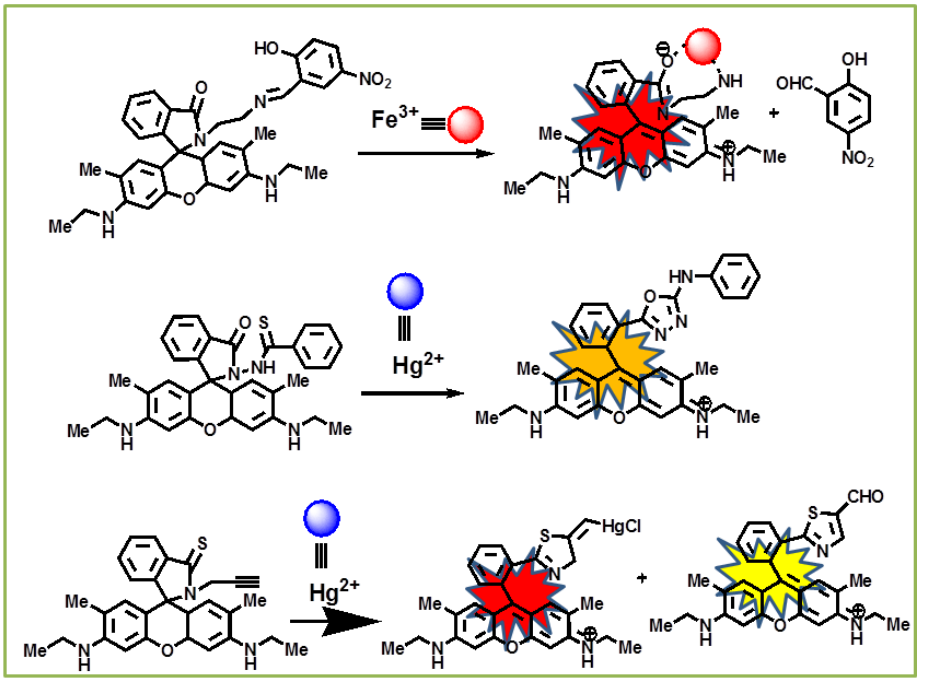

Figure-1.14: Examples of Various types of fluorescent Off-On Chemodosimeter (Irreversible).

Optical sensors further can be classified into two categories-

i) Chromogenic chemosensors and

ii) Fluorogenic chemosensors [105,106]

i) Chromogenic chemosensors: For such chemosensors the binding site receives the guest analyte in such a manner that signalling unit shows the colorchange in the visible region. Development of chromogenic chemosensors is getting importance and appreciated since naked eye detection gives qualitative information about a species without performing any spectroscopic studies.

ii) Fluorogenic chemosensors: The luminescence method of chemosensing is the emission of radiation from an excited state of the molecule. Depending on the way of excitation various terms like chemoluminescence,[107] electroluminescence,[108] radioluminescence,[109] sonoluminescence[110] etc are commonly used. Luminescence[76] phenomenon is of two types:
one is fluorescence when emission takes place from an excited state of a molecule in the same spin multiplicity and when it takes place from changed spin multiplicity it is known as phosphorescence.[76]

1.6 Various Mechanistic Pathways for Fluorescence Signaling in Rhodamine Systems

Various fluorophores are able to show the fluorescence and in some cases the intensities are changed in the presence of a cationic species for a particular fluorophore. The important mechanisms which are responsible for showing such kind of analyte specific fluorescence responses are:

(i) Photo-induced electron transfer (PET) [111,112]

(ii) Intramolecular charge transfer (ICT) [113,114]

(iii) Energy transfer (ET)[76]

(iv) Aggregation Induced Emission (AIE)[139]

1.6.1 Photo-induced Electron Transfer (PET)

This method is a most significant and frequently seen mechanism for fluorogenic chemosensor, so it is broadly used for the cation and anion sensing. It is discussed before that the phenomenon of fluorescence occurs only when electrons from the excited singlet state of the fluorophore molecule goes to the ground singlet state by releasing excess energy as radiation. So relaxation of an electron from LUMO to HOMO is the cause of fluorescence. When electron is transferred from ionophore HOMO to the the excited fluorophore HOMO through space, that blocks the transfer of an excited electron of fluorophore present in the LUMO to HOMO of that fluorophore resulting fluorescence quenching; and this is possible only when the energy level of the ionophore is laying in between the HOMO and LUMO of the fluorophore. This fluorescence quenching process is known as photo-induced electron transfer (PET) [76,115-117] resulting non radiative energy dissipation.

When ionophore binds with a target metal ion through coordination energy of the ionophore HOMO decreases to such an extent that it lies below the HOMO of the fluorophore. Under such a condition electron transfer from ionophore HOMO to fluorophore LUMO can no longer takes place. So, fluorescence takes place (**Figure-1.15**). As this fluorescence is enhanced due to

chelation with the metal ion so it is called as *chelation enhanced fluorescence* (CHEF) effect (**Figure-1.16**).[118]

In an alternative PET mechanism can takes place when metal ion LUMO is laying in between HOMO and LUMO of the fluorophore, here fluorophore LUMO act as an electron donor to the LUMO of metal ion. Hence, the excitation of the fluorophore in the complex, followed by deactivation through non-radiative pathway to LUMO of the transition metal ions results the quenching of fluorescence .[115]

Generally, electron transfer to or from a fluorophore in the excited singlet state causes radical D-A ion pair formation and the system reaches to the ground state via recombination of the charge. The efficiency of PET quenching depends on van der Waals contact via collision (dynamic quenching) and due to the formation of p-staked complexes (static quenching) which also depends on the spatial distance between the fluorophore and ionophore i.e. between donor and acceptor.[119,120] Theoretically electron transfer can be described as coupling of molecular orbitals through a tunnelling, super exchange or hopping process.

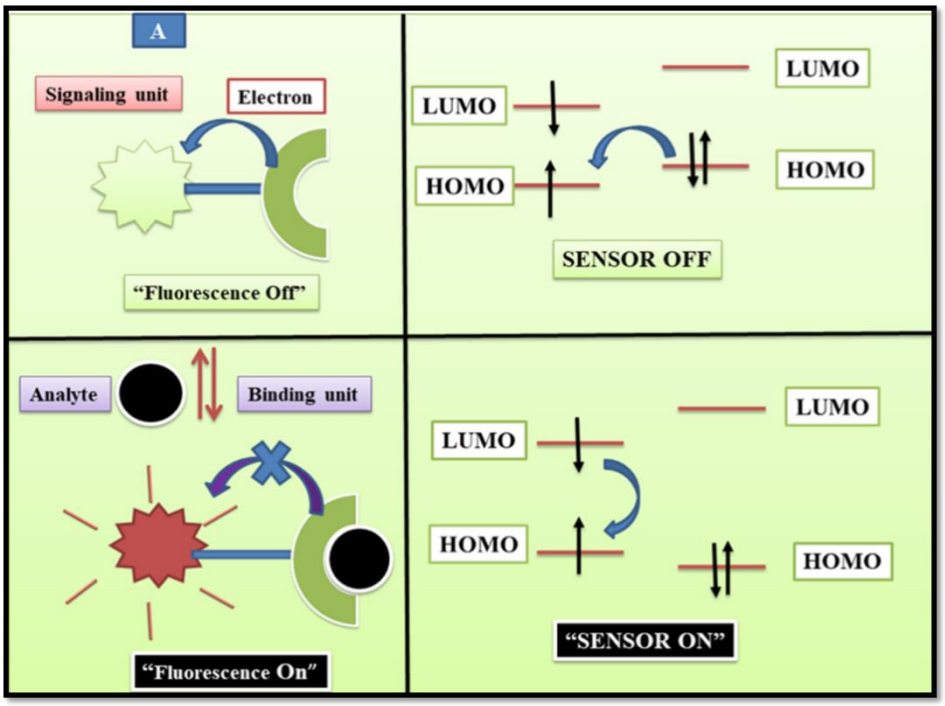

Figure-1.15: Cation recognition through fluorescent PET sensors (A) through reductive electron transfer mechanism.

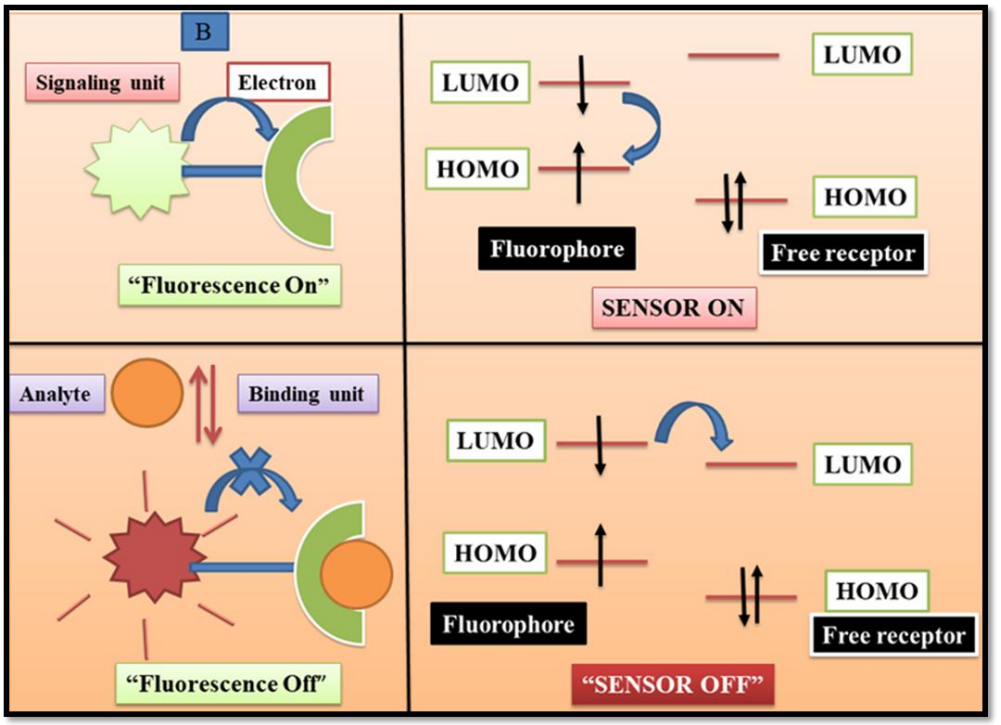

Figure-1.16: Cation recognition through fluorescent PET sensors (B) through oxidative electron transfer mechanism.

With the help of PET mechanism spectral characteristics of fluorescein derivatives have been studied extensively. For **PET-1** (Reductive-PET) electron transfer in the excited from an aromatic amino group to rhodamine fluorophore moiety causes low fluorescence quantum yield. After complexation with Hg^{2+} the PET process is conquered and strong fluorescence enhancement occurs. **Figure-1.17** depicts development of an **OFF-ON** type of Hg^{2+} selective fluorescent chemosensor.[121] On the other hand, **PET-2** ligand (Oxidative PET**)** showed strong fluorescence quenching due to complexation with Cu^{2+} and Hg^{2+} that was ascribed to electron transfer from naphthyl fluorophore to Hg^{2+} in the complex (**Figure-1.17**).[122] An **ON-OFF** type chemosensor based on variety PET mechanism as ON-OFF type chemosensor was built. According to this principle, many fluoroionophores have been designed by altering the fluorophore and/or changing the binding motif. [123,124]

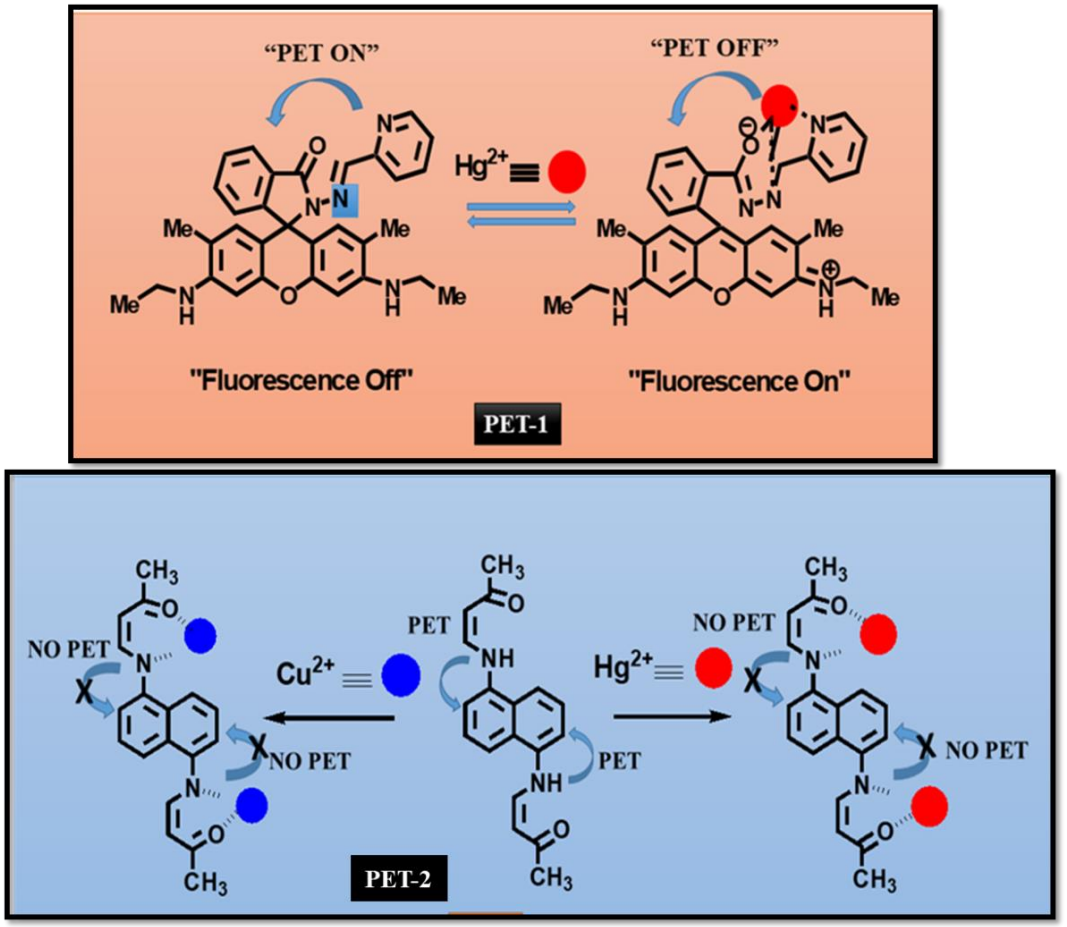

Figure-1.17: Example PET-1 type OFF-ON sensor for Cu^{2+} and PET-2 Type "ON-OFF" sensor for Hg^{2+}.

1.6.2 Intramolecular Charge Transfer (ICT)

Intramolecular charge transfer is another kind of fluorescence enhancing mechanism that causes the shift of an emission band either towards longer wavelength or towards shorter wavelength referred as red shift and blue shift, respectively. Like PET mechanism there is no spacer between receptor and fluorophore in the ICT based probes. In this types of probes receptor unit remains in conjugation with the fluorophore via π framework. One end of these probes must be electron rich that will act as donor moiety and other end should be electronically poor, that will act as acceptor. When such type of system is photo excited electronic reorganization occurs in the excited state that induces change in the dipolar character. This triggers the internal charge transfer from donor to acceptor known as ICT. When an analyte binds with the receptor either

negative or positive interaction may take place which results a change in emission and absorption spectra.[125]

If the receptor unit of the probes is an electron donor then binding with the cationic species reduces the electron donation ability of the receptor through conjugation and there by HOMO–LUMO energy gap increases and hence absorption band shifted towards shorter wavelength, blue shift occurs. Photophysical change also takes place. The electron donating group which becomes positively charged in the excited state so binding with the cation destabilizes the excited. So, energy gap increases that results blue shift in the emission spectrum (**Fig.-1.18-B**). For example, after coordination with **Hg^{2+}** of the donor moiety electron donation ability of the N atom of thia-oxa-aza macrocycle to BODIPY decreases so blue shift occurs in the absorption spectra (**Figure-1.19A**).[126] In the presence of cation large blue shift takes place meanwhile little blue shift of the fluorescence was seen. Such nature of PCT chemosensors has been developed for the detection of metal ions selectively. [127,128]

When receptor act as an acceptor and cation come in closer interaction with the acceptor group then electron pulling character increases so then conjugation between receptor and acceptor enhances as a result HOMO-LUMO energy gap decreases and results bathochromic shift of the spectral band.When binding of the cation with the electron acceptor receptor occurs then excited state is stabilized more than ground state and hence decreased HOMO-LUMO energy gap and results red shift in the emission spectrum (**Figure-1.18A**). Various compounds can be designed on the basis of ICT mechanism.

In the absence of Cu^{2+} BENZPYR (**Figure-1.19B**) exhibits absorption band at 297 nm and 419 nm but after the addition of Cu^{2+} these absorption bands gradually vanished and new absorption band at 503 nm appeared. The generation of a new peak at 503 nm obtained due to intraligand charge charge transition and d-d transition. BENZPYR showed an emission peak at 536 nm but after the addition Cu^{2+}. This emission peak experienced a red shift from 536 to 572 nm on coordination of Cu^{2+}. This principle is greatly exploited in colorimetric and fluorescent detection of metal ions.[129]

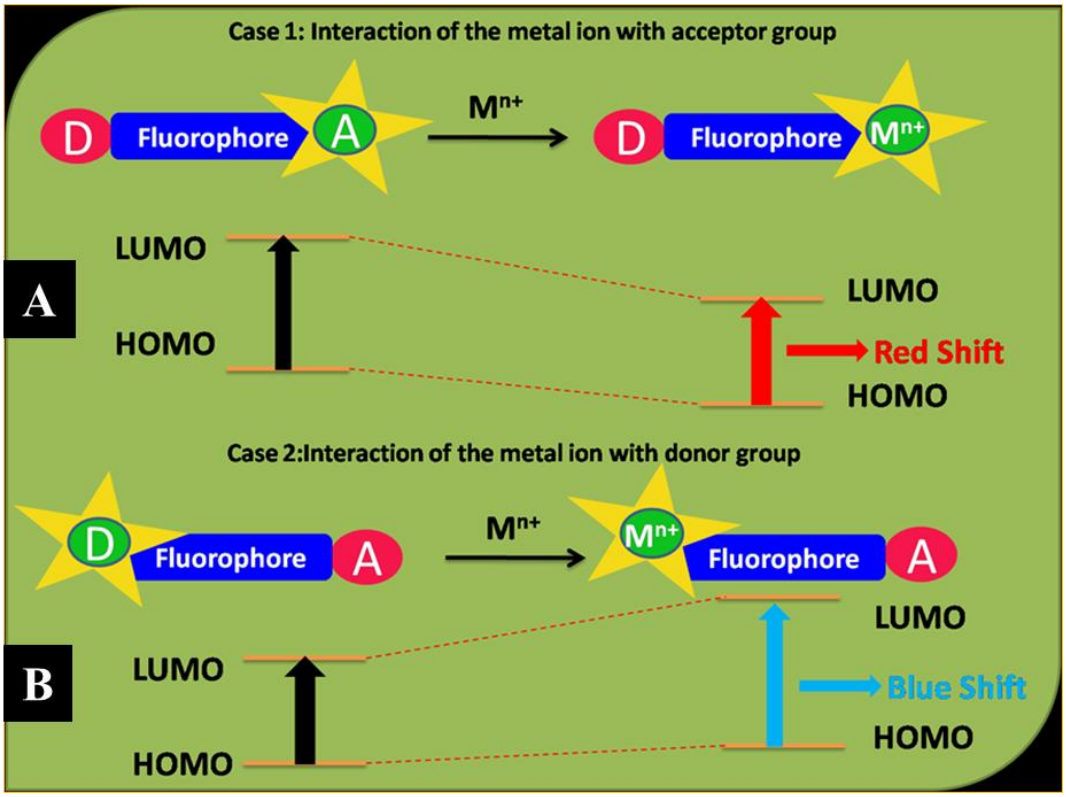

Figure-1.18: Schematic presentation of intramolecular charge transfer showing red shift and blue shift. (Adopted from: Biosensors **2015**, 5, 337**)**

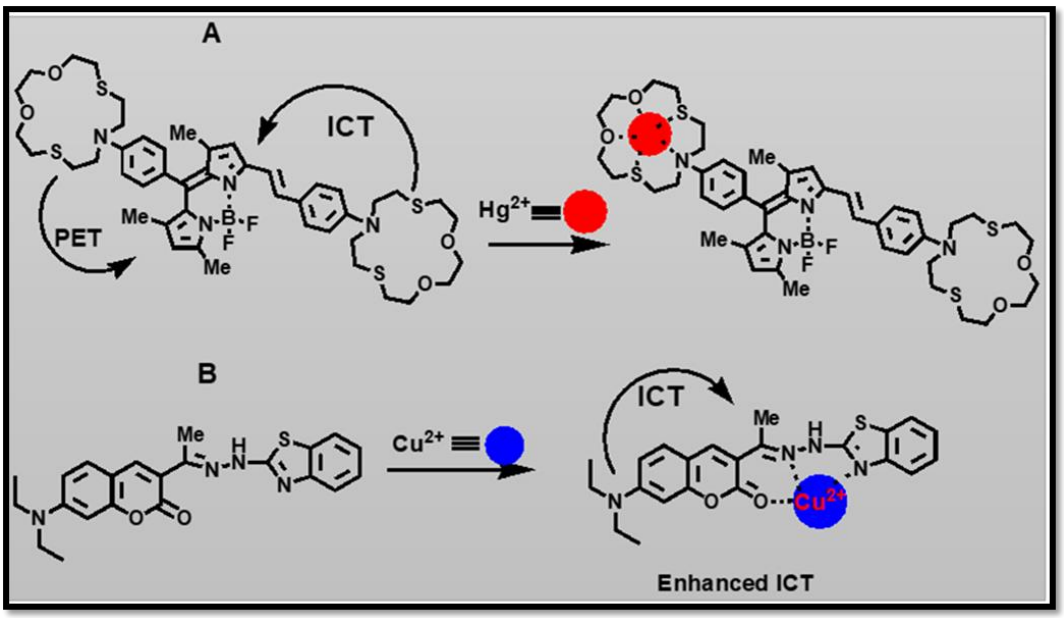

Figure-1.19: Structures of the compound showing ICT resulting red shift and blue shift.

Depending on the nature of the receptor moiety same compound may show different spectral behavior with the same analyte. For example, two BODIPY dye shows similar type spectra but shift in opposite direction on protonation. One of the dye consist of electron donating N, N-substituted aniline moiety (C) whereas another contains electron withdrawing pyridine moiety (D). So, these two compounds show opposite shift on protonation in the spectrum (**Figure-1.20**). Rhodamine derivative[130] (**Figure-1.20, E**) in the presence of Hg^{2+} changes siprocycle to open ring form and results significant enhancement of the absorption and emission intensities. The maximum absorption at 300 nm is due to intraligand π–π* charge-transfer (ICT) transition. After the addition of Hg^{2+} to the ligand in CH_3CN-Aqueous HEPES buffer solution (1 mM, pH 7.2; 1:1, v/v), a new absorption band appears at 531nm with change in colour from colourless to bright pink and luminescence intensity at 557 nm is enhanced on excitation at 500 nm.

Probes which show intramolecular charge transfer (ICT) from donor to receptor via π bridge framework are also known as "push- pull" systems (D-π-A system).

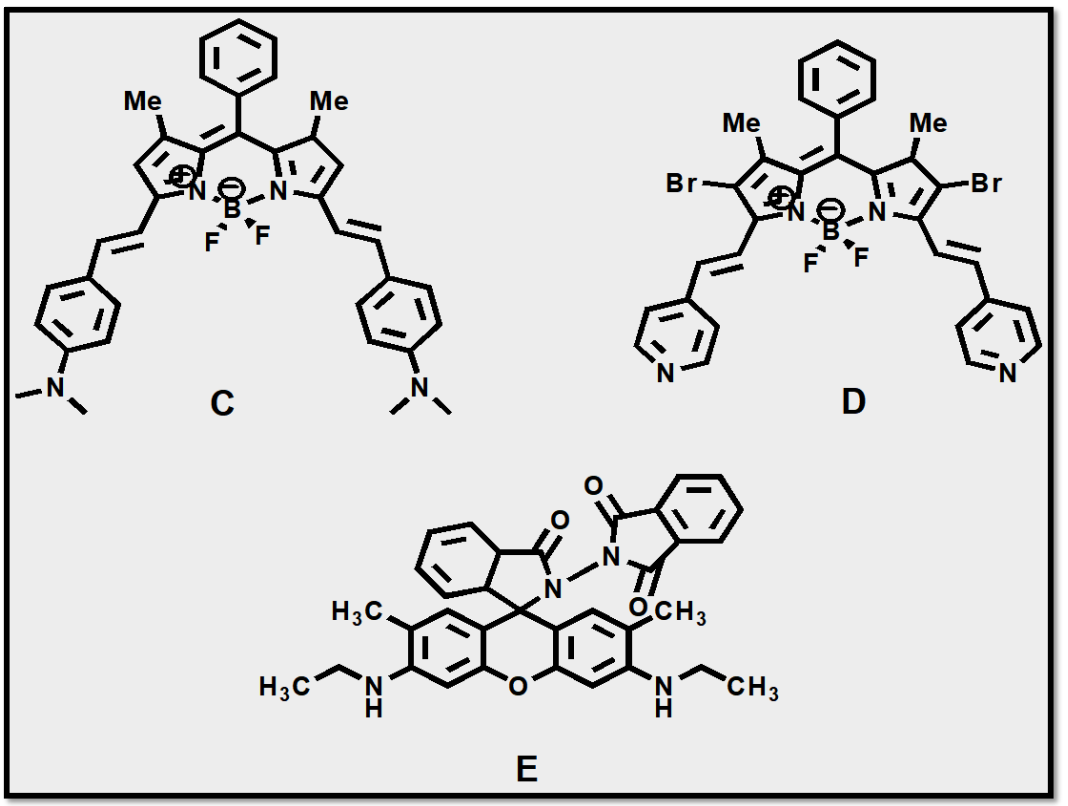

Figure-1.20: Structures of the two similar BODIPY and rhodamine shows ICT resulting red shift and blue shift.

1.6.3 Energy Transfer (ET)

The process of energy transfer is another way of fluorescence signal producing mechanism. Based on the interactive distance between the energy donor and acceptor in a multiple probe (chromophoric) system, the process of energy transfer can be classified into two types one is electronic energy transfer (EET) or dexter energy transfer (DET) and another is fluorescence resonance energy transfer (FRET) (**Figure-1.21**).In this mechanism energy emitted from a donor (D) is taken to excite the acceptor molecule that means donor fluorophore absorbs light at shorter wavelength and acceptor fluorophore receives light of longer wavelength. If the interacting donor and acceptor positioned within the distance of 10Å then energy transfer takes place through DET process and when the gap from donor to acceptor ranges from 10 to 100Å then FRET occurs. However, for an efficient FRET to occur there must be overlap between the emission spectrum of donor and absorption spectrum of an acceptor. These two types of energy transfer are the processes familiar as Dexter and Forster type energy transfer.

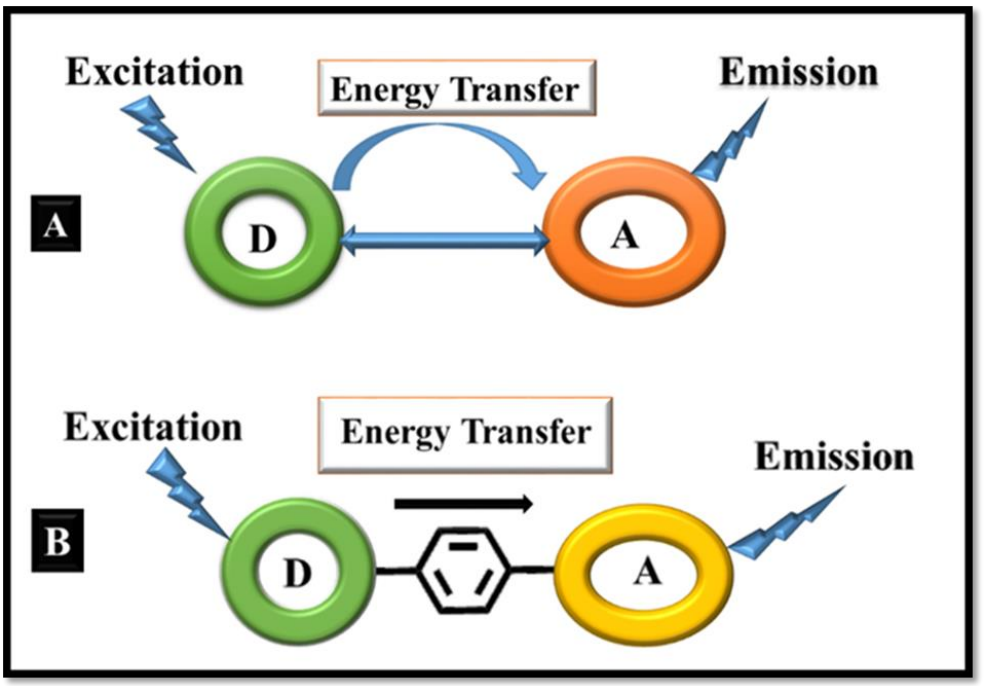

Figure-1.21: Schematic representation of energy transfer through-space (A) and through bond energy transfers (B).

(Adopted from Critical Review: Analyst, **2014**,139, 543**)**

1.6.3.1 Forster Resonance Energy Transfer (FRET)

Most of the fluorescent dye has very little stokes shift. If stokes shift of a single fluorescent probe is inadequate for a specific use, then multi-chromophoric systems are used to transfer the energy between the two probes. When an excited state donor (D) transfer its energy spatially to the closest ground state of an acceptor (A) molecule via a non-radiative pathway then the acceptor molecule shows fluorescence -this phenomenon is known as fluorescence resonance energy transfer (FRET) also known as forster resonance energy transfer (FRET)(**Figure-1.22A**).

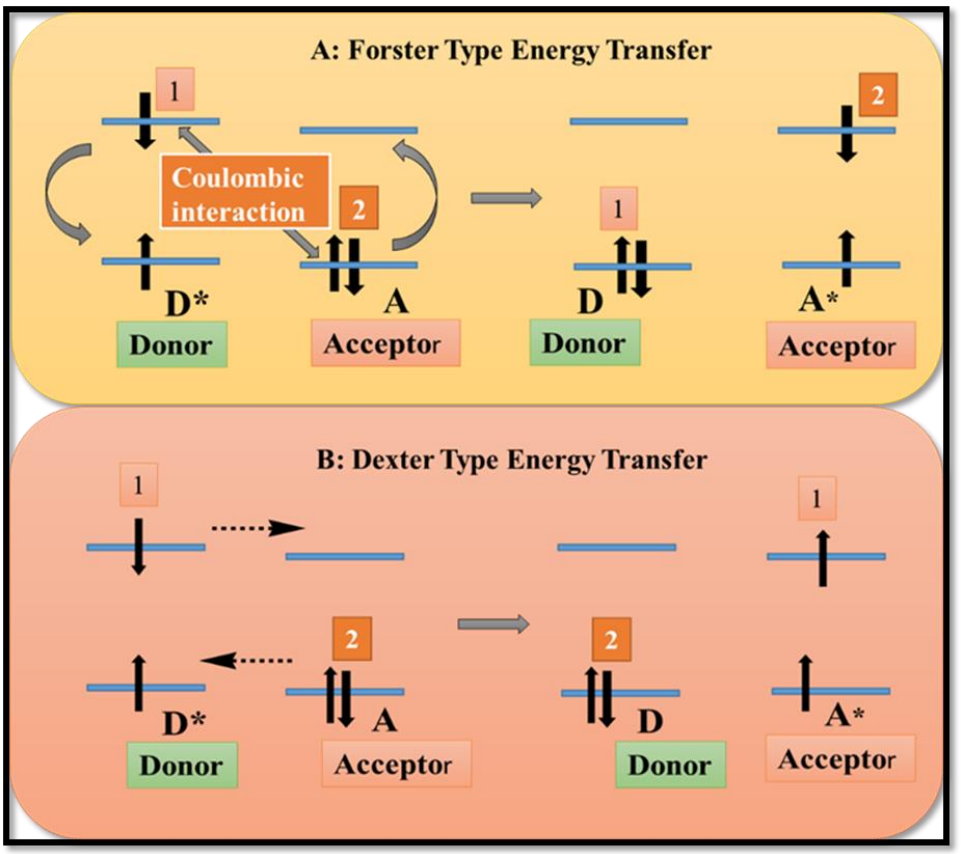

Figure-1.22: Energy transfer mechanism: (A) Förster type and (B) Dexter type.

Donor (D) and acceptor (A) molecule are not necessarily connected by conjugation, linked by a molecular framework. The FRET process is independent on orbital interaction among the donor probes and acceptor probe. So relatively large distance (10 to 100 Å) between them may admit this kind of transfer of energy. In this process an electron is promoted from HOMO to LUMO of acceptor molecule after receiving energy that released from LUMO of the donor during

relaxation to its HOMO. There must be an absorption and emission spectral overlap of the acceptor and donor chromophoric group. For an efficient FRET process relative orientation and the distance between the two probes (D and A) imparts a very important role. [131,132] FRET efficiency of a system can be determined either by steady state approach or by time resolved approach.[133] Major problems of this method is the self-absorption and causes lowering of the quantum yield. Use of very dilute solution lowers the self-absorption.[133] FRET efficiency using steady state approach can be formulated as follows.

$E = 1 - (\Phi_{DA}/\Phi_D)$

Where, Φ_{DA}, Φ_D are the quantum yields of the donor molecule in the presence and in the absence of acceptor molecule respectively.

FRET efficiency of a system can be calculated more accurately by using time resolved approach. If decay of emission is a single exponential then FRET can be expressed as [134]

$E = \tau_D * k_{FRET} / (1 + \tau_D * k_{FRET})$

$k_{FRET} = 1/\tau_{DA} - 1/\tau_D$

Where, τ_{DA} and τ_D are the excited state decay time of the donor molecule in the presence and in the absence of acceptor molecule respectively.

In recent days resercher's are using this mechanism to construct a fluorescent probe for chemosensing of the metal ions. [135] in the presence of metal ion two fluorophore comes closer to each other to effect FRET. It is clearly demonstrated in **Figure-1.23**. So, by exciting the donor moiety the emission spectra of acceptor can be detected.

For the first case, the emission spectra of the fluorophore are recorded when the donor fluorophore excited because FRET is averted due to large distance between two fluorophores. But, binding with the metal ion, the gap between the donor and acceptor fluorophores decreases and then FRET occurs. In this way excitation the donor fluorophoric moiety makes possible to record emission spectra of acceptor fluorophoric moiety(**Figure-1.23**).[135]

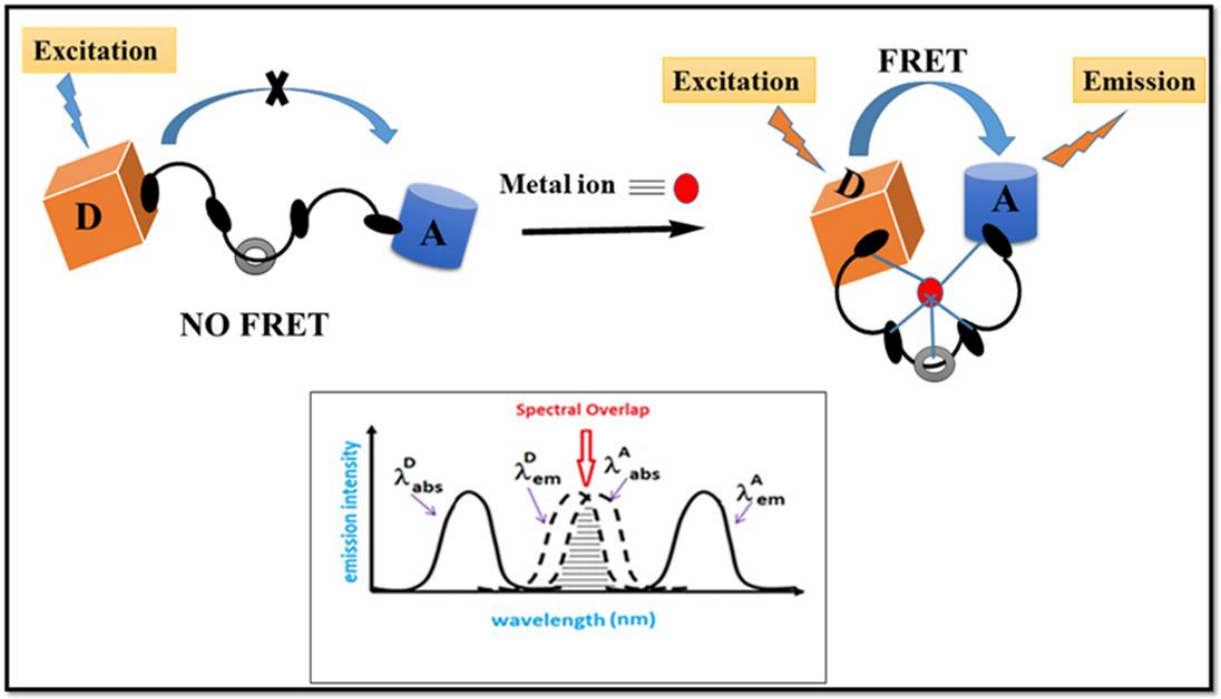

Figure-1.23: The Schematic representation of analyte (metal ion) triggered FRET mechanism along with the spectraral overlap of Donor and Acceptor moiety.

(Adopted from Critical Review: Analyst, **2014**,139, 543)

1.6.3.2 Dexter Type Energy Transfer (DET)

There should be an orbital interaction either directly or by bridge to occur energy transfer from one fluorophore to another in this method. It happens when donor and acceptor are connected by a conjugated linker, this process is also known as through bond energy transfer (TBET) (**Figure-1.21B**). Electron exchange takes place within HOMO and LUMO of donor and acceptor in this energy transfer process (**Figure-1.22B**). As interaction between the orbitals is the necessary condition so the fluorophores must be close enough. Rate constant for energy transfer exponentially falls with distance.

K_{ET}= K.J exp. (-2R_{DA}/ L)

Where, K is the orbital interaction and J represents integral overlap of donor emission and acceptor absorption, R_{DA} is the distance between donor and acceptor, L is the van der Waals radii. TBET processes are familiar for the construction of models usable in biological systems. Use of this mechanism for the fluorogenic detection of the metal ion is not so much developed.

From the above discussion it is clear that modulation of various key points such as orientation of the fluorophore ion pair, separation between them, and spectral overlap region can influence the energy transfer ability and to conceptualize for the recognition of metal ions.[135]

As given in **Figure-1.24(1)**, selective binding with Cu^{2+} persuade the ring-opening of rhodamine fluorophore, leads to spectral overlap of naphthalimide and rhodamine.[136] Thereafter, energy transfer took place, that is evident from fluorescence quenching of dansyl moiety and fluorescence uplift of rhodamine takes place shown in **Figure-1.24(2).**[137]

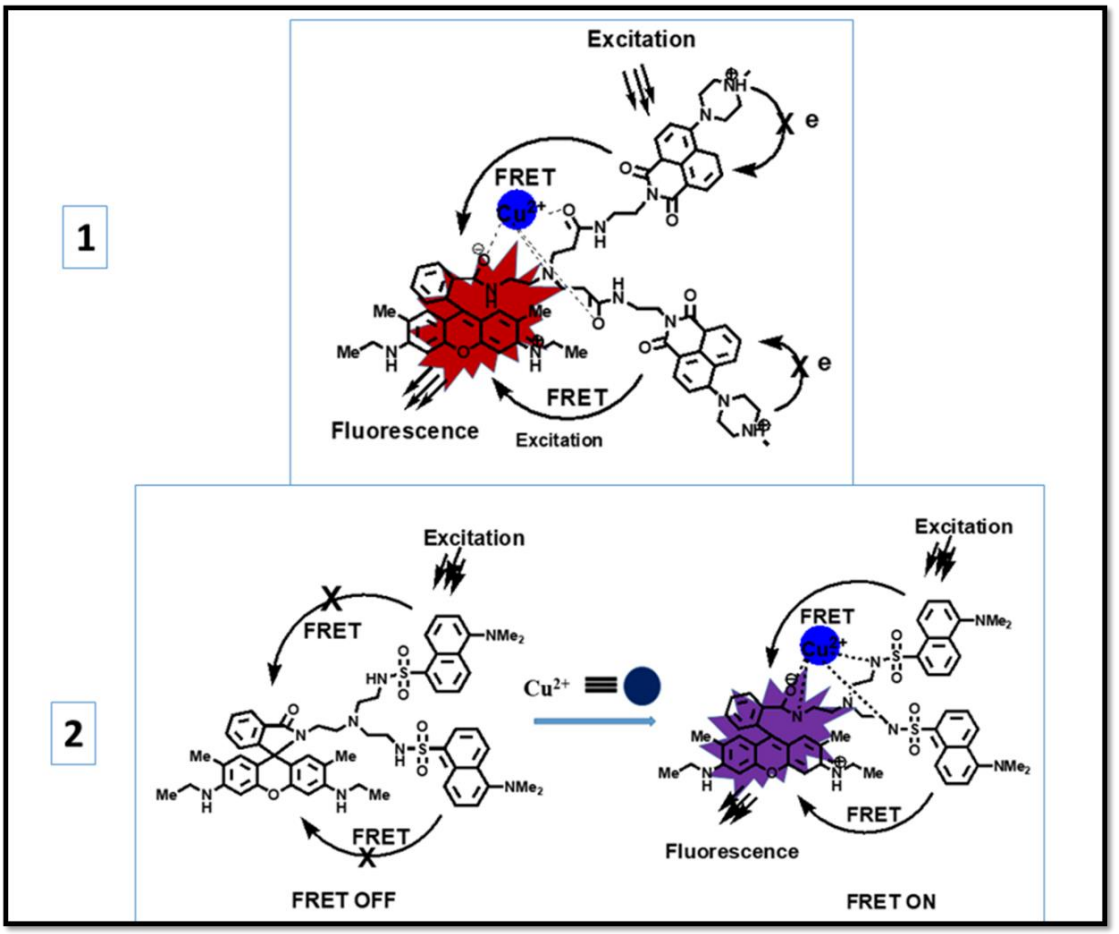

Figure-1.24: Structures of the chemosensor based on FRET

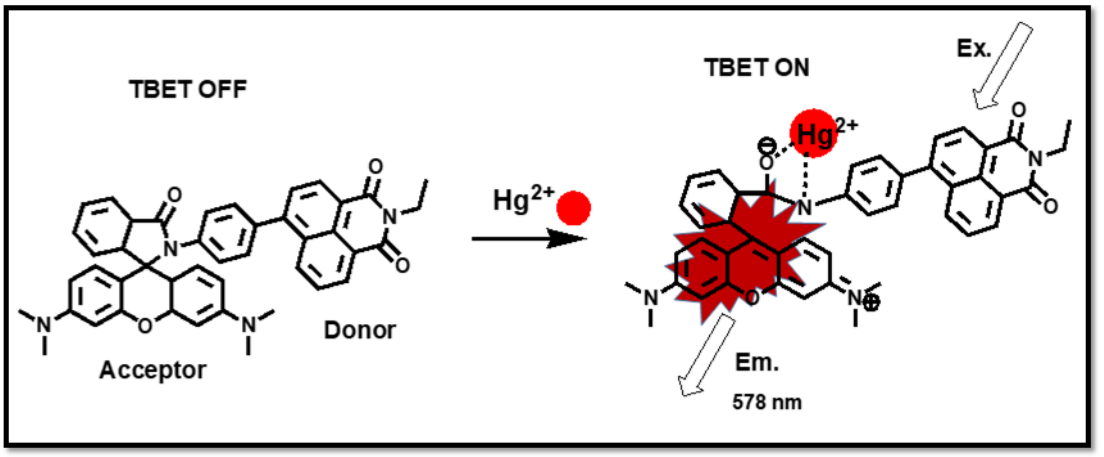

Figure-1.25: Structures of the Hg^{2+}-chemosensor based on TBET.

Naphthalimide-adjoined rhodamine-fluorophore where **TBET** mechanism applied for the specific detection of Hg^{2+} ions in combined aqueous media (**Figure-1.25**).[138]

Apart from the above mentioned processes for fluorocent chemical sensor design for cations, another two modern pathwayshave been introduced for the same purpose of designing cation recognitions and they are mentioned bellow.

1.6.4 Aggregation Induced Emission (AIE)

When the fluorescence emission of organic fluorophore is quenched due to aggregation of the fluorophoric moiety this effect is called aggregation caused quenching(ACQ). To suppress the ACQ effect branched chain, bulky cyclic chain is attached to the fluorophoric unit. Conventional fluorescent probes for example rhodamine, fluorescein and cyanine shows fluorescence efficiently in dilute solution but in the concentrated solution an aggregation and hence quenching of fluorescence occurs. There are some organic fluorophores some are non-fluorescent in dilute solution but shows fluorescence in their aggregated form[139]. This is known as Aggregation Induced Emision (AIE). This AIE fluorescence was first reported in 2001 since then various hypothesis like restriction of intramolecular motion (RIM), j-aggregates, excimer formation, excited state proton transfer (ESIPT) and inhibition of TICT process have been suggested for the AIE mechanism. Among various hypothesis restricted intramolecular motion mechanism is proved experimentally. PDHA molecule in the solution state due to rotation of

dihydroanthracene backbone consumes excitation energy and shows no emission in the dilute condition but in the aggregated form intramolecular rotation is constricted and fluorescence emission occurs. Based on the RIM mechanism many AIEgens reported such as tetraphenylethene (TPE), quinoline-malononitrile (QM), as tetraphenylpyrazine, cyanostilbene, distrylanthracene (DSA). In the figure given below represents the various way of "Turn-On" sensing phenomenon based on AIE process (**Figure-1.26**) and few specific examples of AIE based chemosensors (**Figure-1.27**).

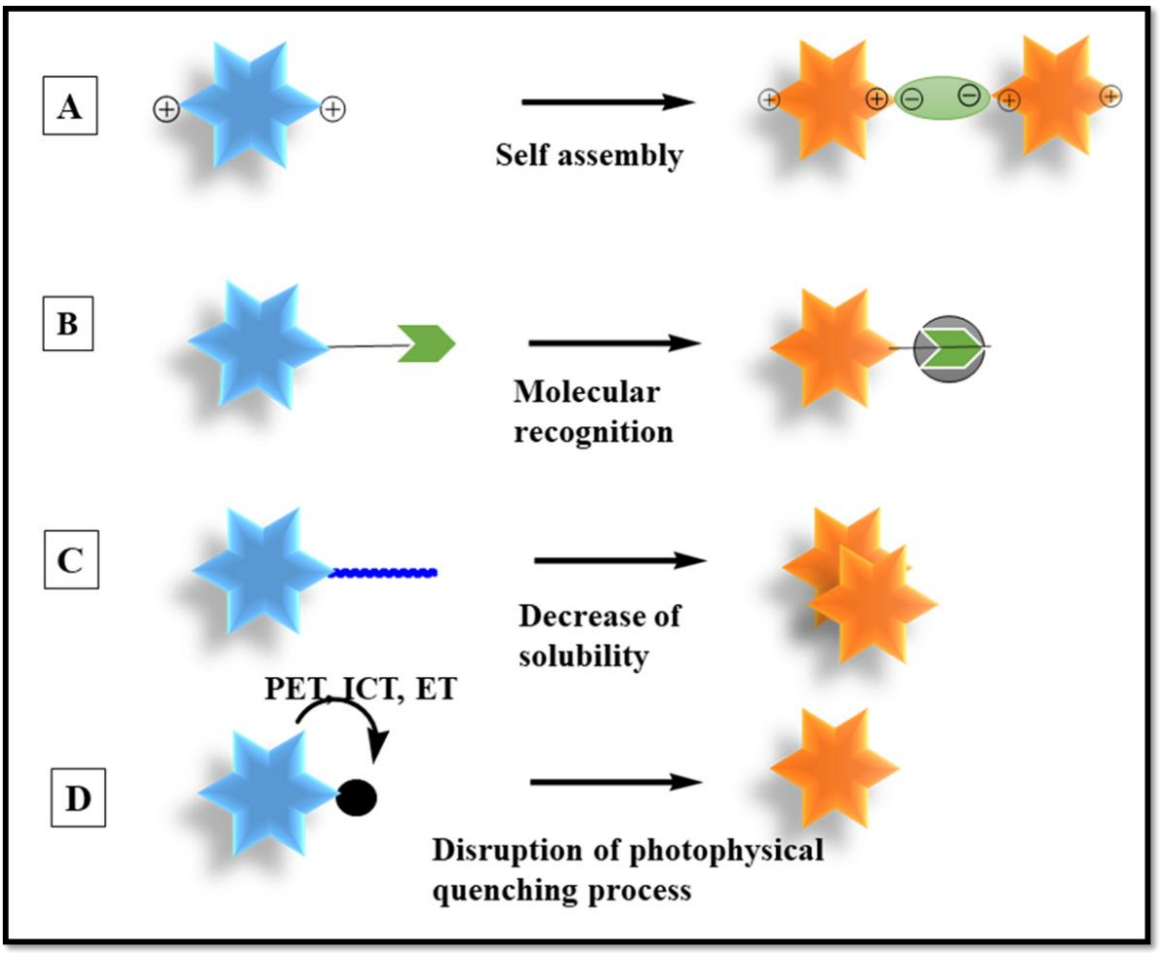

Figure-1.26: Schematic presentation of principles of AIE sensors: (A) aggregates formation through self-assembly; (B) selective binding with analyte to confind intramolecular motion; (C) solubility decrease leading to aggregate formation; (D) quenching of photophysical processes due to disruption.

(Image adopted from: ACS Sens. **2017**, 2, 1382)

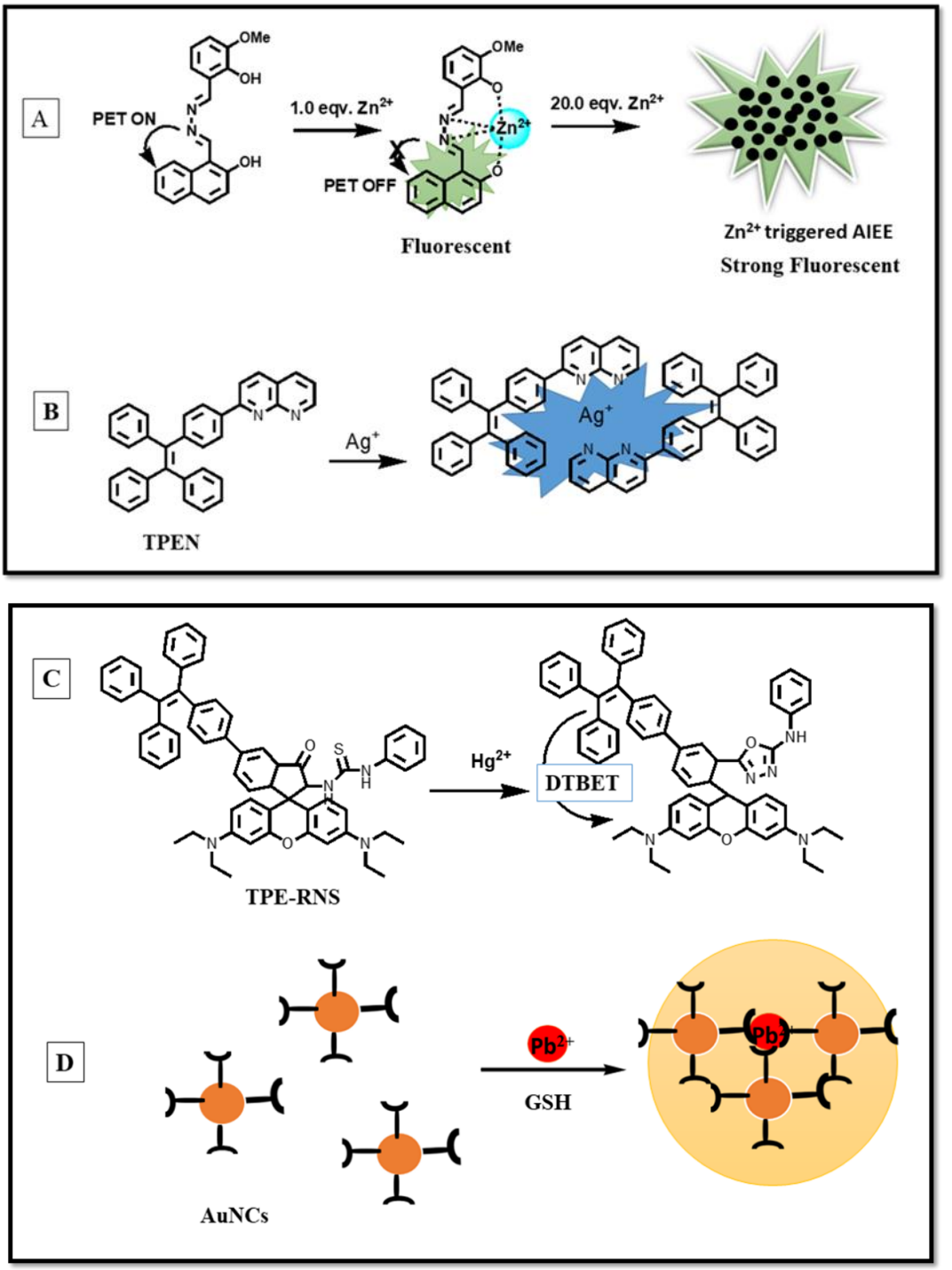

Figure-1.27: (A) Schematic presentation of AIE based Zn^{2+} sensor. (B)Scematic resentation of complexation between TPEN and Ag^{+} and followed by fluorescence due to constrain of intramolecular motion (C) Presentation of ratiometric chemosensing of Hg^{2+} via DTBET. (D) Schematic presentation of Pb^{2+} triggered aggregation of GSH-AuNCs and fluorescence emission.

1.7 Introduction to Rhodamine Chemistry

For the sensing and recognition of various cations in the biological and environmental sample fluorescence technique in conjunction with a suitable probe is a very good approach due to its rapidness and sophisticated instrumentation. This fluorometric method involving proper fluorescent probes is highly sensitive and non-destructive, it can provide us the presence and quantity of a species in analytical samples. Selection of fluorophore for a particular chemosensing event must satisfy the following requirements:

i) longer absorption and emission wavelengths of the fluorophores.
ii) Solubility of fluorohore in broad range of environments in so that this probe can be used for all types of samples.
iii) Stability of a fluorophore under experimental condition.
iv) Access of that fluorophore by synthetic means from readily available starting material.

Various fluorophores are known; such as zwitter ionic (BODIPY, squaraines, cyanine dyes), xanthene group (rhodamine and fluorescein, eosin Y and pyronine Y), 1,8-naphthalimide, coumarin, Thioflavin T, luminol, nitrobenzofuran, 8-aminoquinoline, 8-hydroxy quinolone, acridine, pyrene etc.[140-148]

Xanthene group fluorophore i.e. rhodamine and fluorescein are very much preferable to be used as fluorescent probe because of their excellent photostability, high quantum yield, high extinction coefficient and long emission wavelength. The basic moiety of a xanthene group chromophore is given in **Figure-1.28**.

Noelting and Dziewonsky first synthesized rhodamine in 1905 and after that this compound has been used widely in the field of research and as fluorescent marker in biologoical studies.[149,150] In 1997 use of rhodamine B derivatives and their ring opening phenomenon received a focus of organic chemist.[151] Rhodamines are used as laser dyes, [152] pigments and as fluorescent probes for the characterization of polymer nanoparticles surface,[153] lipid membranes fluidity, detection of polymer-bioconjugates[154,155]oligonucleotides absorption on latexes, structure and dynamics study of micelles,[156-158] imaging in living cells.[159]

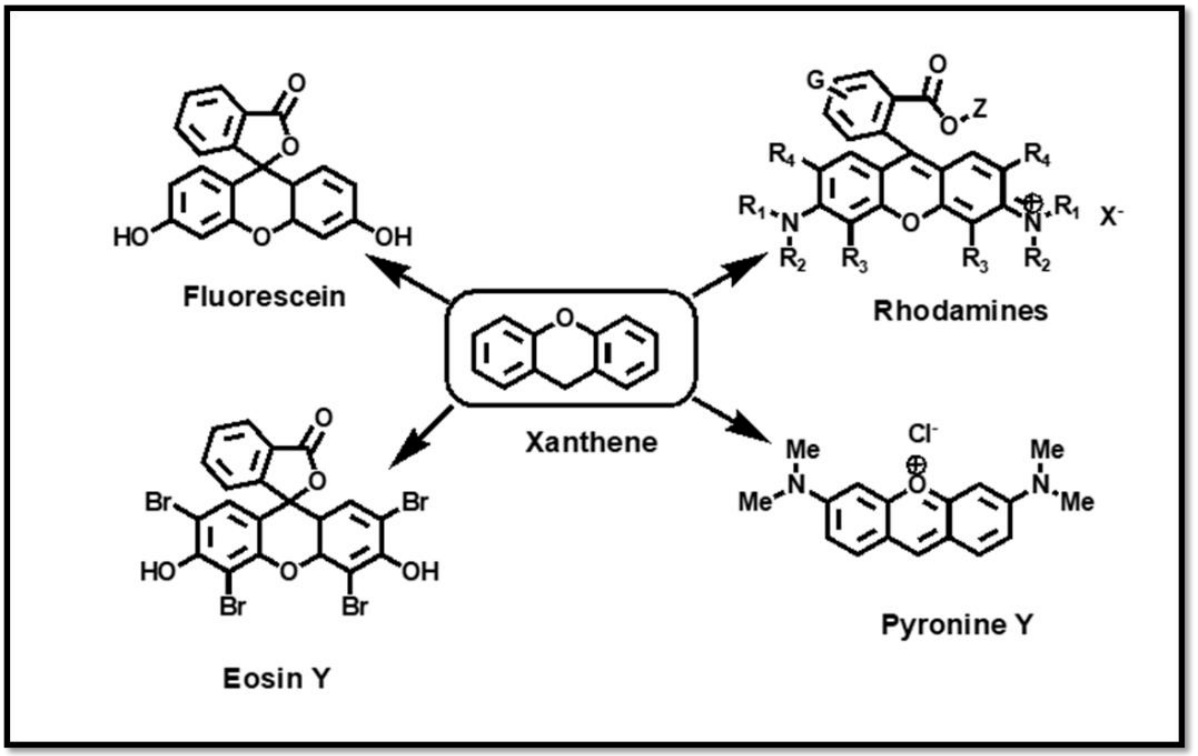

Figure-1.28: Structures of xanthene group fluorophores.

Rhodamine 6G is another widely used red-orange colored powder dye which is soluble in MeOH it has high quantum yield (0.95) and its absorption maxima is about 530 nm and its emission wavelength is greater than 550 nm both are in the visible region that makes this probe more advantageous in nacked eye colour change.

Most of the rhodamine 6G derivatives are colourless and non-fluorescent in its ring closed form but gives a strong fluorescence emission and orange-pink colour in the ring open form. Rhodamine derivatives shows red colour in acidic solution due to spirolactam ring opening; similarly, a rhodamine 6G derivative also exhibit a colour change in the presence of a metal ion.

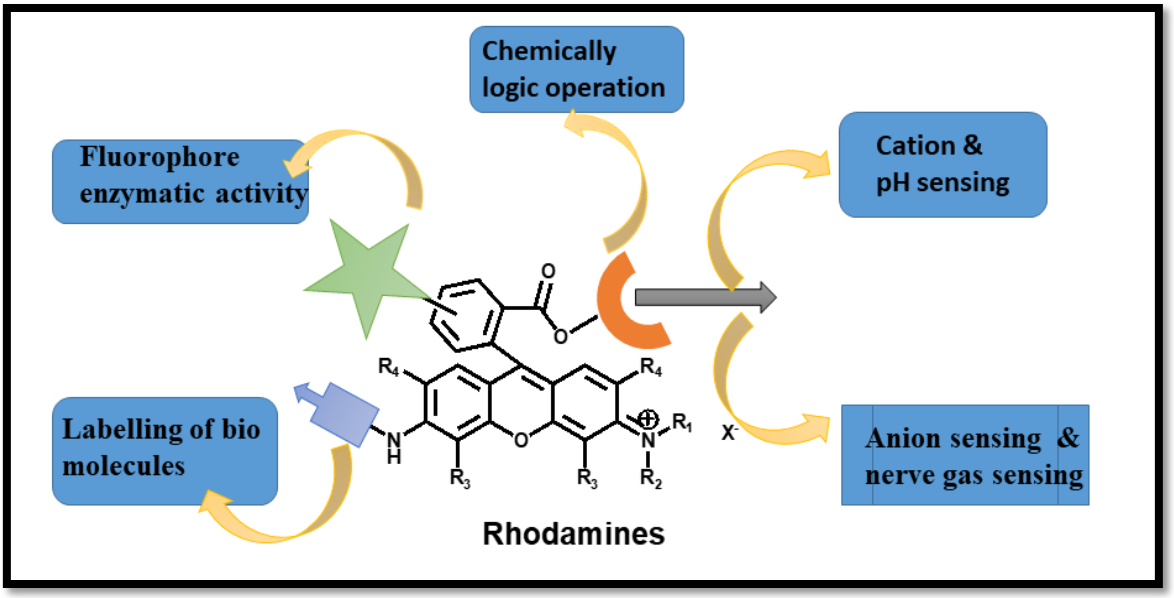

Figure-1.29: Schematic presentation of various aplications of rhodamine derivatives.

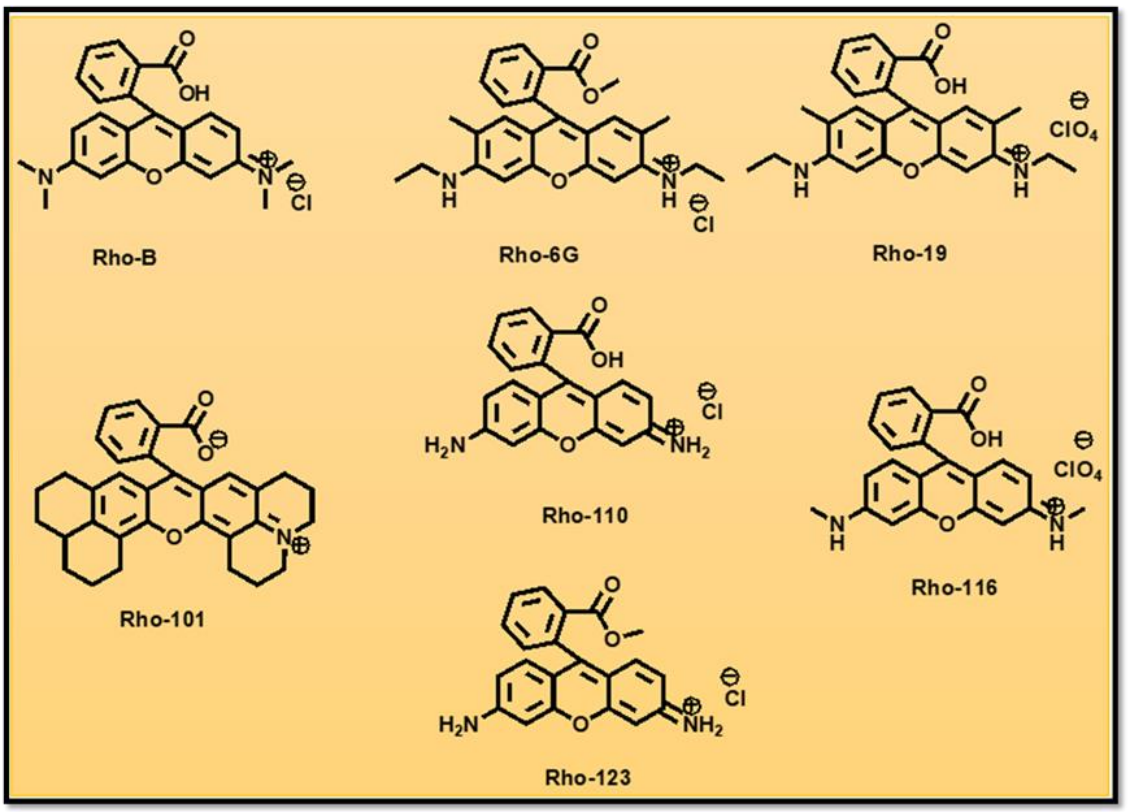

Figure-1.30: Commercially available various rhodamine moieties.

Rhodamine derivatives has been used as molecular switches, for surface modification of a virus and extensively used as chemosensors *in vitro* or *in vivo* for the recognition of metal ions, anions, nerve gas, thiols etc. Recently, fluorescent labelling of biomolecules and development of logic gate devices using rhodamine spotlighting the usefulness of rhodamine derivatives for that application.[160-162] Many important applications of rhodamine moiety is shown in the following schematic view(**Figure-1.29**). Let see the commercially available various Rhodamines moieties at a glance in **Figure-1.30**.[162]

Due to many advantages of rhodamine 6G fluorescent dye it is selected as fluorophore unit to design and synthesis of suitable turn-on chemosensor for cations. Among many commercially available rhodamine dyes rhodamine 6G dye is less expensive and its derivative can be prepared very easily and moreover the most of the rhodamine 6G (Rho 6G) derivatives are crystalline and so it is the added advantage for further processing.

1.7.1 Chemosensing Mechanism of Rhodamine 6G in the Presence of Cationic Analytes

Chemosensing event of rhodamine 6G is different from other fluorophore although xanthene group fluorophores shows same kind of mechanism. The spirolactam ring closed form of rhodamine is colourless and non-fluorescent but when this ring opens up due to the coordination with a certain metal ion it becomes reddish pink colour in most of the cases and it becomes highly fluorescent and so this chemosensing can be classified as "Turn-On" fluorescence (**Figure-1.31**).

This spirolactam ring opening phenomenon of Rho-6G may be reversible or irreversible in the presence of an external analyte. When it is reversible then rhodamine derivative can built up its ring form after removal of that coordinated metal ion in the presence of quenching species and so then have reusable advantages with respect to irreversible one.

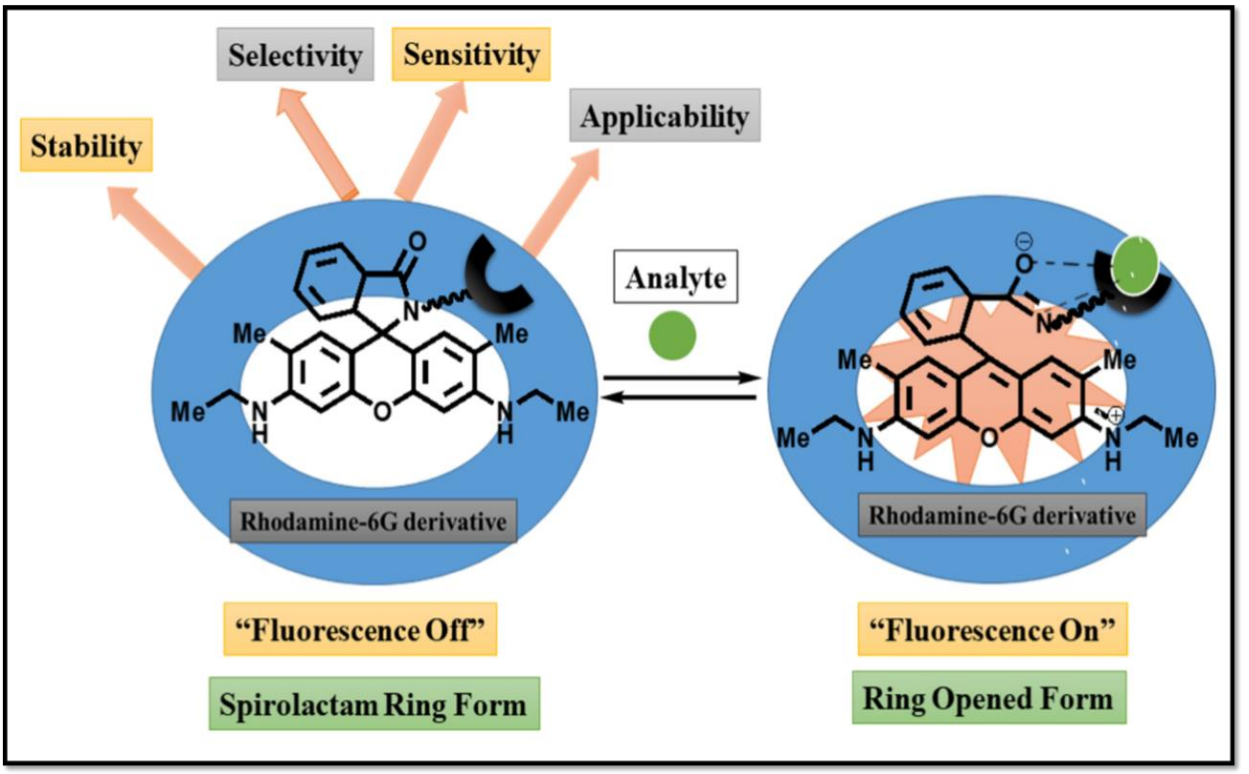

Figure-1.31: Schematic presentation of chemosensing event of Rho-6G in the presence of metal ion.

Because of all the above-mentioned advantages, rhodamine 6G derivatives are designed for the recognition of a specific metal ions. In general, such changes could be achieved upon reversible as well as irreversible reaction with an appropriate metal ion (**Figure-1.31**). But the design of reversible **chemosensor** of rhodamine 6G derivative is **desirable** because of the **re-usable advantage** of such sensing platform with respect to irreversible one.

1.8 Brief Literature Survey on Rhodamine-6G Based Molecular Chemosensors for Cations

1.8.1 Brief Literature Survey on Al^{3+} Chemosensors

Aluminium is a non-essential element for living systems. Accumulation of excess Al causes neurodegenerative disease like Alzheimer's, Parkinson's and also causes many health hazards such as anemia, encephalopathy, cardiotoxicity, gastrio-intenstinal disease. Acidic soils are polluted due to the toxic effect of aluminium and largely hampers crop performance in acidic soils. Hence detection of aluminium is essential and there is a need to design a specific and sensitive fluorescent probe for Al^{3+} in combined aqueous solution.

Lee and coworkers reported rhodamine attached carbon dots (C-dots) as a ratiometric probe $\mathbf{L^1}$ afor the detection of Al^{3+} in aqueous solution based on FRET mechanism. In the presence of Al^{3+}chelation occurs and results spirolactam ring opening and probe showed increased fluorescence intensity due to transfer of energy from C-dots to rhodamine upon excitation **(Figure-1.32)**. The C-dots-rhodamine 6G showed many fold enhanced fluorescence intensity in the presence of Al^{3+} only when excitation occurs at 350 nm (absorption wavelength of C-dots) instead of 526 nm (absorption maximum of rhodamine moiety). In addition, a paper strip soaked with C-dots-rhodamine 6G ensemble can detect Al^{3+} ion.[163] The LOD was found to be $3.5x10^{-5}$M insolution and from paper strip method it is $3.89x10^{-5}$.

Ali et al. developed a rhodamine 6G based bio friendly chromo-fluorosensor $\mathbf{L^2}$ for Al^{3+}which is a three input and output combinatorial intelligence molecular device for information processing **(Figure-1.33).** It shows a fluorogenic behaviour towards Al^{3+} but chromogenic towards Cu^{2+}. It was used to devise as key-pad-logic function based on the fluorescence response. It performes as a Boolean function that shortens the complications of chemically direct intelligent device. Fluorometric titration of this probe with Al^{3+} solution in methanol aqueous HEPES buffer solution (7:3) results K_d = (6.07- 0.12)10^{-6}M which is comparable with the K_d values obtained from absorption studies. This probe can work under physiological condition. No cell cytotoxity was found for HepG2 and HCT116 cells upto 100 µM of probe.[164]

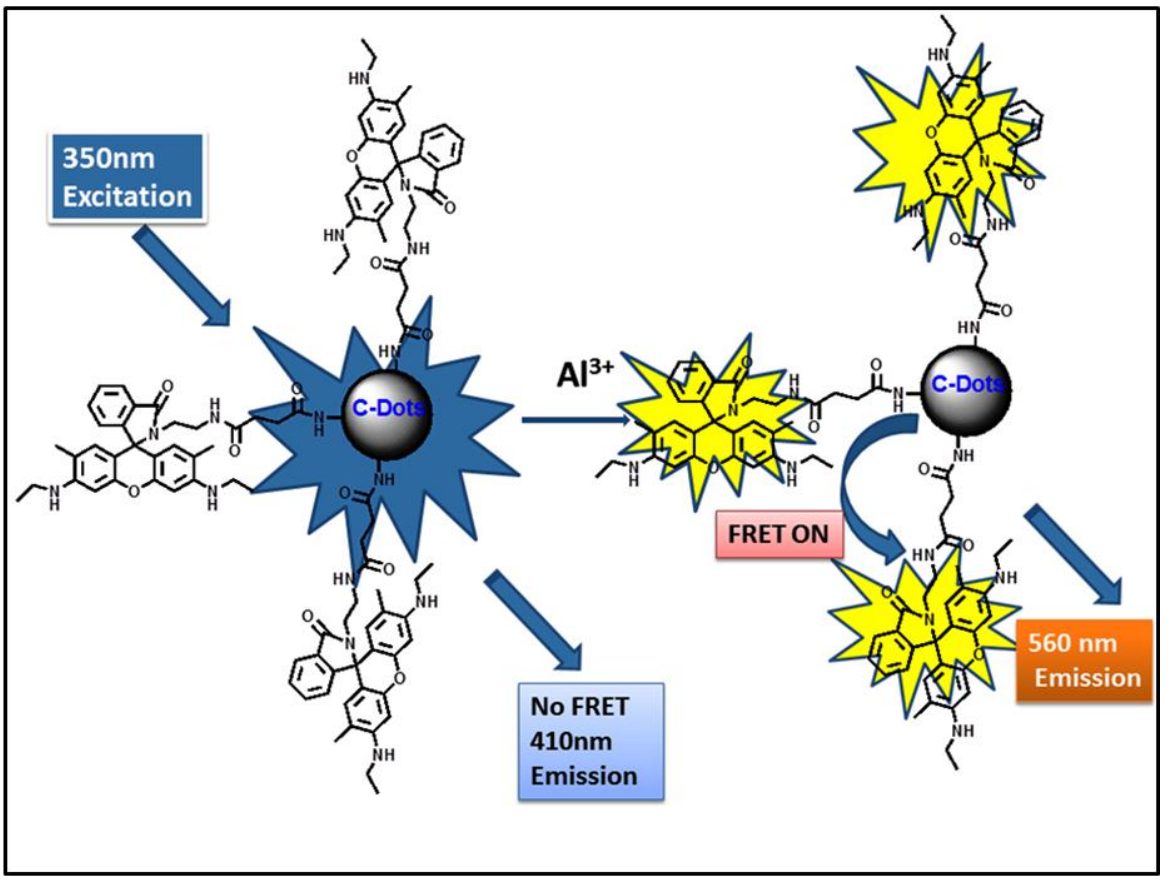

Figure-1.32: Structure of ratiomatric probe L^1.

Roy's group reported Rhodamine-6G-N-lactam ethylenediamine based proble $\mathbf{L^3}$ with its single crystal structure, for the selective detection of Al^{3+}. They recorded both absorption and emission spectra of this ligand **(Figure-1.33)** in 20 mM HEPES buffer at pH=7.4 H_2O/MeOH (1:4, v/v). Various physical parameters like life time 2.61 and 0.76), quantum yields (0.0011 and 0.6618), radiative rate constants ($4.21x10^5$ and $1.15x10^9$) and non-radiative rate constants ($0.38x10^9$ and $1.65x10^9$) for the ligand $\mathbf{L^3}$ and its complex with Al^{3+} were determined. They reported LOD of Al^{3+} as 2.86 nM. At low pH it is fluorescent but in the pH range 5.0 to 9.0 it can work well. The reversibility of the probe tested by succesive addition of Al^{3+} and AsO_4^{3-}.[165]

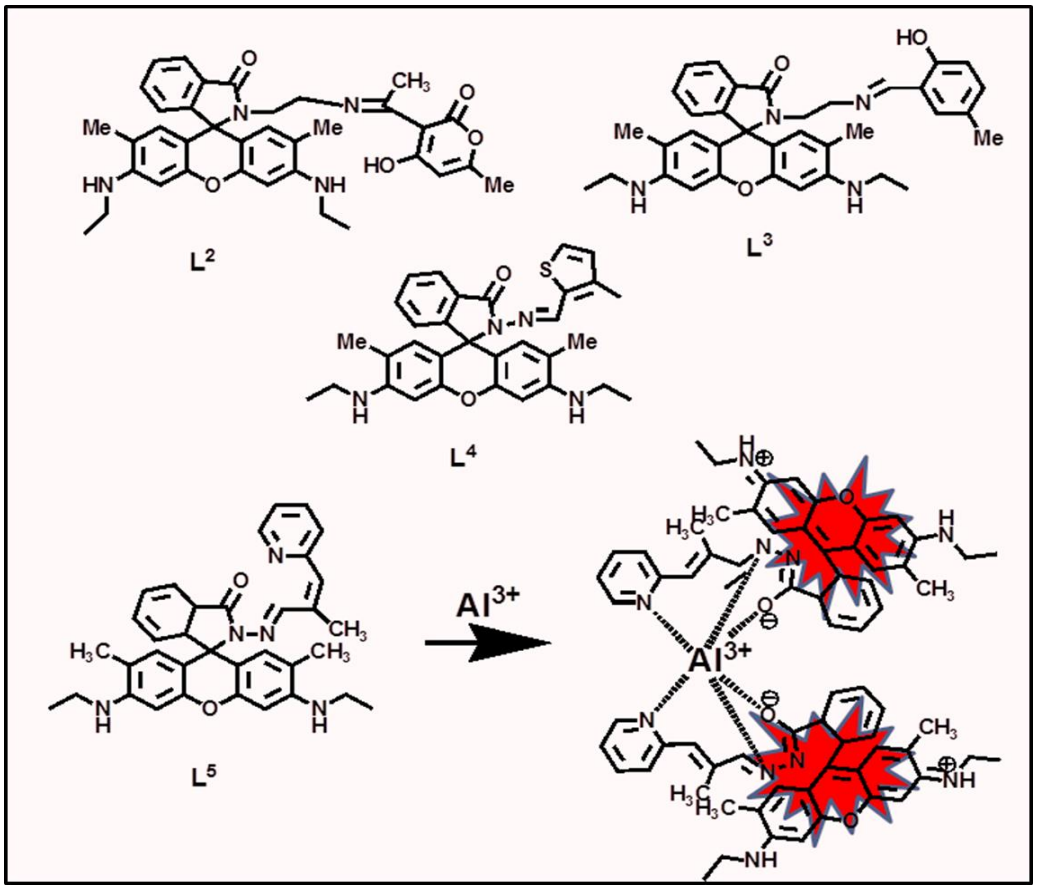

Figure-1.33: Structures of the chemosensors (L^2-L^5) for Al^{3+}.

A highly sensitive and selective rhodamine-6G based fluorescent chemosensor **L^4** for Al^{3+} detection in a mixed aqueous medium was reported by **Qing Xu** et el. This ligand **L^4 (Figure-1.33)** shows a significant increase in absorption at 530 nm in UV-Vis spectroscopy and emission at 555 nm in the fluorescence spectroscopy (λ_{ex} = 350 nm) in the presence of Al^{3+}. Increase in fluorescence intensity at 555 nm shows a good linearity (0.99613) with respect to Al^{3+} concentration of the range 5-15 µM and formation constant for 1:1, **L^4** to Al^{3+} binding was determined to be $4.73x10^4\ M^{-1}$. Detection limit for Al^{3+} was estimated as $4.58x\ 10^{-6}$.[166]

Young-A son et.al. developed a new colorimetric and fluorogenic probe, **L^5** (**Figure-1.33**), which is a very sensitive and selective for the detection of Al^{3+} in a mixed acetonitrile and DMSO solvent. They declared existence of equilibrium between siprolactam ring open and closed form corresponds to "ON and OFF" state. The LOD of Al^{3+} was calculated as 8.5nM. Job's method recommends a 2:1 binding mode for ligand and metal. This chemosensor was

improved by blending with polyurethane electrospun nanofibreswhich enables it to detect Al^{3+} in mixed aqueous medium which also could recognize Al^{3+} onsite in live sample. This blended nano-fibres shows reversibility with EDTA.[167]

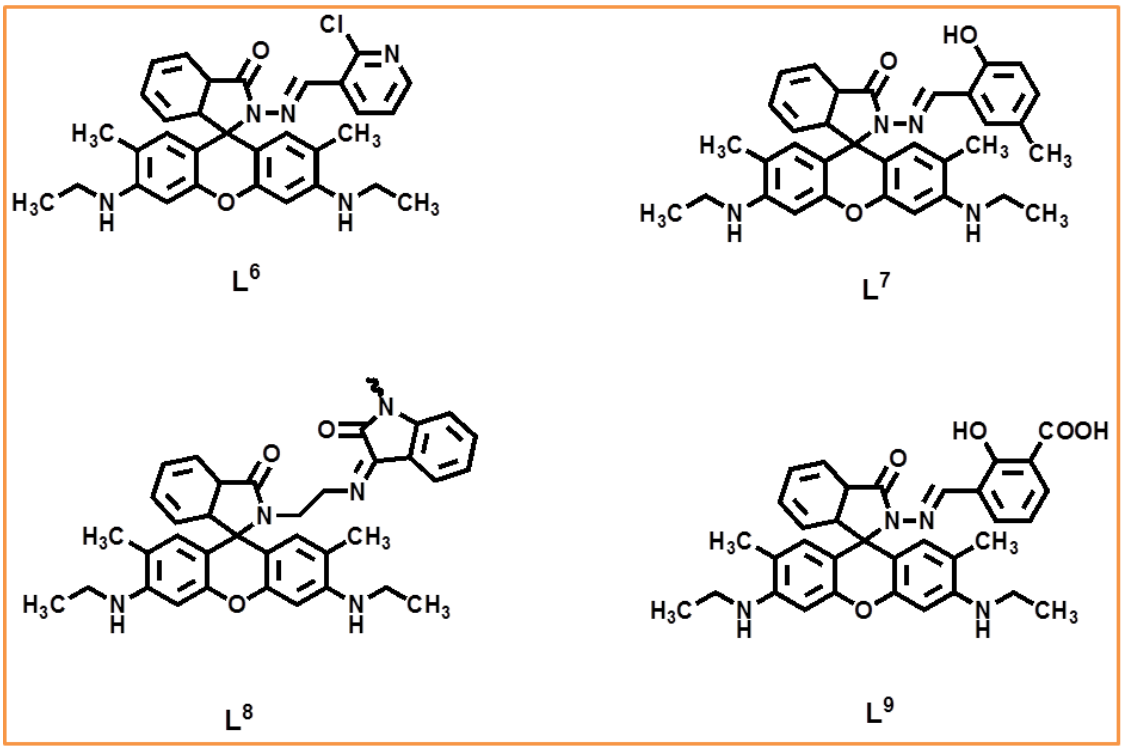

Figure-1.34: Structures of the chemosensors (L^6-L^9) for Al^{3+}.

Young-A Son et al. reported a rhodamine 6G-2-chloronicotinaldehyde based "OFF-ON" chemosensor **L^6 (Figure-1.34)** for the detection of Al^{3+} in the presence of other cations. In the presence of Al^{3+} **L^6** shows enhancement of absorption intensity at 528 nm. The fluorescence intensity was enhanced by 800 fold at 553 nm upon excitation at 528 nm in acetonitrile. Jobs plot and NMR studies confirms that 1:1 binding between **L^6** and Al^{3+} occurs during complexation. This group reported LOD as 4.28 nM M and formation constant $5.71x10^5$ M^{-1}. Reversibility and reusability of the probe was established through experiment performed with azide ion solution added to **L^6**-Al^{3+} solution containing a paper strip, which results a change in colour from pale pink to colourless again. When it is modified to polymer based PEGDMA- **L^6** probe it performs as a reversible sensor for Al^{3+} in presence of azide ion.[168]

A rhodamine 6G based chemosensor **L^7** (**Figure-1.34**) was reported by **Young-A Son** et al for the recognition of Al^{3+} in aqueous medium. A new band appears at 528 nm in UV-Vis spectroscopy whereas an emission band appears at 560 nm upon addition of Al^{3+} to **L^7** in acetonitrile. The A 2:1 liagnd: metal stoichiometry was found in the the jobs plot and LCMS techniques. Fluorescence intensity of the ligand showed a linearity with the Al^{3+} concentration having correlation coefficient of 0.991 and from the slope of that plot LOD was calculated as 0.27 nM. A visible colour change was observed for **L^7** thin film after immersing in water containing Al^{3+}.[169]

Rhodamine 6G-isatin based chemosensor **L^8** (**Figure-1.34**) was found to detect Al^{3+} in mixed acetonitrile-water (7:3, v/v, pH=7.2) solvent over other cations except Ga^{3+} as reported by **Goswami's** group. Probe **L^8** exhibited a colourimetric as well as fluorogenic "OFF-ON" type chemosensory behaviour in the presence of Al^{3+}.The **L^8**-Al^{3+} complex discriminates ppi over other anions in aqueous solution. During complexation metal ligand stoichiometry was found to be 1:1 from job's plot. The formation constant was calculated to be $2.51x10^4 M^{-1}$ and $8x10^4$ M^{-1} by UV-Vis and fluorometric methods respectively.[170]

Zang et al. developed Rhodamine 6G based chemosensor **L^9** (**Figure-1.34**) for Al^{3+} which works in aqueous solution with high sensitivity. From HRMS and job's plot binding stoichiometry between **L^9** and Al^{3+} was found to be 2:1. The formation constant for the complexation between probe and Al^{3+} was estimated to be $3.14x10^5$ M^{-1} from Benesi-Hildebrand plot. This is used as bio imaging agent for the identification of Al^{3+} in living cells.[171]

1.8.2 Brief Literature Survey on Cr^{3+} Chemosensors

Chromium (III) is a vital nutrient for human beings, its deficiency influences metabolism of glucose and lipids, and causes diabetes, cardiovascular disease and disorder in nervous system. When chromium concentration exceeds from optimum level it then binds with cellular components and inhibit DNA transcription and relication. So, development of cost efficient fluorescent chemosensor for the detection of Cr^{3+} is an important target to the researcher.

Kaur's group reported rhodamine 6G tagged thiourea and urea derivatives $\mathbf{L^{10}}$ and $\mathbf{L^{11}}$ **(Figure-1.35)** respectively from there they developed corresponding nanoparticles $\mathbf{L^{10}}$-NP, $\mathbf{L^{11}}$-NP of which $\mathbf{L^{10}}$-NP, was selective chemosensor for Cr^{3+} but it was observed that $\mathbf{L^{11}}$-NP was silent towards Cr^{3+}.The complex, $\mathbf{L^{10}}$-NP-Cr^{3+} was found to be used for the recognition of anionic species like organophosphates, pesticides etc. This complex can also be employed for the selective detection of azinphos-methyl among various organophosphates pesticides (OP) through "ON-OFF" mechanism via cation displacement strategy. The LOD of azinphos-methyl OP was found to be 1.73 nM. The $\mathbf{L^{10}}$-NP-Cr^{3+} complex showed very good applicability in the detection of Cr^{3+} in the tap water and river water samples.[172]

D. Nataraj et al. synthesized gold nano particle which is capped with Rhodamine 6G, a cost effective chemosensor for detection of Cr^{3+} in water sample. Aqueous solution of Rd-6G-NP produces absorption and emission bands at 525 nm and 551 nm, respectively along with the observable change from pale pink to green on addition of Cr^{3+} solution. Formation constant with Cr^{3+} was found to be 1.345×10^4 M^{-1} and LOD of Cr^{3+} was calculated to be 9.28µM, these parameters indicates the excellent selectivity towards fluorescence quencher over other transition cations. The probe having 90% cell viability can detect Cr^{3+} in breast cancer cell of human (HeLa).[173]

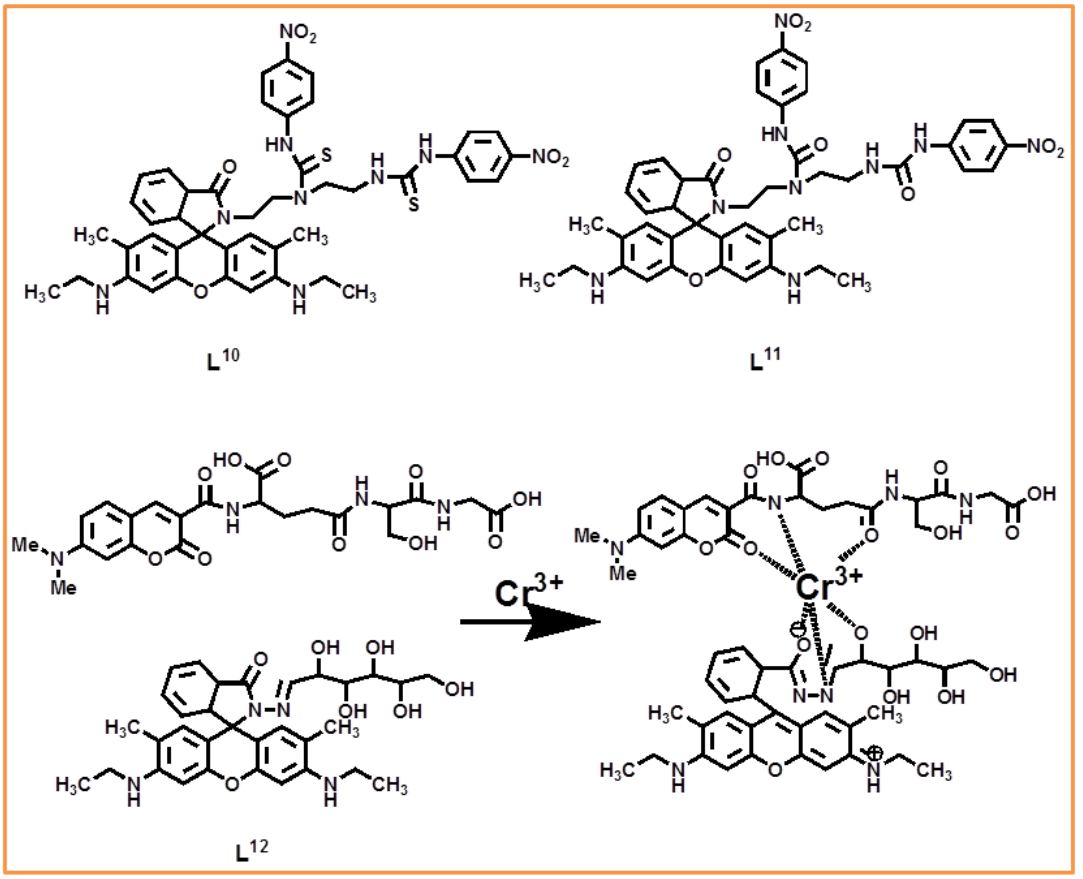

Figure-1.35: Structures of the chemosensors (L^{10}-L^{12}) for Cr^{3+}.

Duan et al. reported ratiometric chemosensor **L^{12} (Figure-1.35)** based on FRET mechanism for the recognition of Cr^{3+} in aqueous medium utilising glutathione and glucose as receptors along with the rhodamine-6G and coumarin moiety as signalling units. In the presence of only one receptor either glutathione or glucose separately the probe shows high sensitivity but poor selectivity but in the presence of both it shows excellent selectivity over other cations and high sensitivity with the detection limit less than 0.1ppm. Free receptor CG1 shows emission at 475 nm due to coumarin unit but in the presence of Cr^{3+} quenching of fluorescence occurs. Receptor shows little enhancement of fluorescence intensity at 555 nm in the presence of Cr^{3+}. When both the CG1 and RH1 combined together shows a strong enhancement of fluorescence intensity at 550 nm upon excitation at 450 nm due to FRET. This probe has been utilised for the biomedical research and for studying biological activity of Cr^{3+} in living systems.[174]

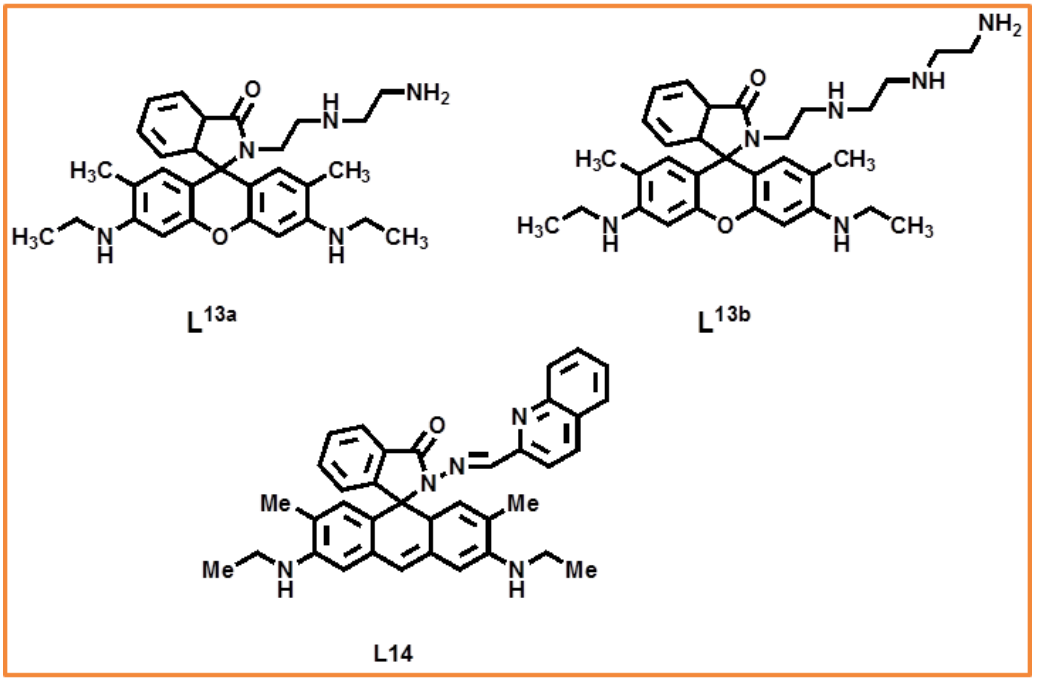

Figure-1.36: Structures of the chemosensors (L^{13}-L^{14}) for Cr^{3+}.

Liu et al. reported rhodamine-6G based "OFF-ON" chemosensors **L^{13a} and L^{13b}(Figure-1.36)** for the selective detection of Fe^{3+} and Cr^{3+} in 100% aqueous medium at biological pH. Fluorescence intensity of the probes **L^{13a}** and **L^{13b}** increases at 552 nm by 22 fold and 61 fold upon addition of Fe^{3+} and Cr^{3+}solution, respectively. From the jobs plot binding stoichiometries of **L^{13a}** and Fe^{3+} and **L^{13b}** and Cr^{3+} were determined to be 2:1 and 1:1, respectively. The formation constants of **L^{13a}** and **L^{13b}** with Fe^{3+} and Cr^{3+} were calculated to be 6428 M^{-1} and 41600 M^{-1} respectively.[175]

Das and Ghosh developed rhodamine 6G based chemosensor **L^{14} (Figure-1.36)** which was structurally characterized by single crystal X-ray diffraction. It was found to recognize Cr^{3+} and Hg^{2+} in physiological condition with cell imaging applications. In the presence of both Cr^{3+} and Hg^{2+} the probe shows a visual change in colour from colourless to pink. In HEPES buffer (acetonitrile-water, 3:2, v/v, pH=7.3) this probe showed the appearance of a strong absorption band at 530 nm and emission band at 555 nm upon excitation at 500 nm due to the opening of spirolactum ring in presence of Cr^{3+} and Hg^{2+} only. The 1:1 Binding equivalency of the probe **L^{14}** towards Cr^{3+} and Hg^{2+} was confirmed from B-H plot and Job's plot . The formation constants were found to be 3.11x 10^3 $M^{-1}$and 2.0x 10^3 $M^{-1}$and LODs were calculated to be 10.72 ppm and

5.6 ppm for Hg^{2+} and Cr^{3+}respectively. It was found that on addition of KI to the $\mathbf{L^{14}}$-Hg^{2+} complex absorption and emission band disappear due to removal of Hg^{2+} as HgI_2 and then further addition of Cr^{3+} to the same mixture again bands appeared. This probe is used for detection of Cr^{3+} selectively in the samples in the presence of I^-. This probe is used in bio-imaging of breast cancer cell MCF7.[176]

1.8.3 Brief Literature Survey on Fe^{3+} Chemosensors

Iron is an essential component of our diet and imparts oxygen carrying capacity in haemoglobin, low oxygen supply causes anaemia, diabetes, liver damage and cancer and it has vital role in many enzymes of human body. A key role in metabolism is also performed by iron. Its deficiency causes damage to nucleic acids, proteins and lipids causing diseases like Alzheimer's and Parkinson's.

Hava Ozay et al. developed a hexapodal ligand $\mathbf{L^{15}}$ **(Figure-1.37) -** an excellent "OFF-ON" chemosensor for the recognition of Fe^{3+} in various samples over other cations and anions. This ligand was prepared from hexaazide-substituted phosphazene and rhodamine-6G derivative. Sensing characteristics of $\mathbf{L^{15}}$ was studied from UV-Vis and fluorescence spectroscopy. Stoichiometry in the complex between $\mathbf{L^{15}}$ andFe^{3+} was found to be 1:3 from Jobs plot. The LOD of $\mathbf{L^{15}}$ for Fe^{3+} detection was calculated to be 4.8 µM. The reversible nature of this probe $\mathbf{L^{15}}$ was tested with ethylenediamine (EDA). According to this group fluorescence intensity of the complex quenched after the addition of EDA due to exchange of ions from complex to EDA.[177]

Ozay et al. reported reusable hydrogel sensor derived from sensor $\mathbf{L^{16}}$ **(Figure-1.37)** for the detection of Fe^{3+} in DMSO-water (1:9, v/v, pH 7.4). An absorption peak appeared at 532 nm and emission peak at 555 nm along with the nacked eye observation colourless to pink-orange when Fe^{3+} is added to the solution containing $\mathbf{L^{16}}$. Formation of 1:1 complex was confirmed from Job's plot. This group also prepared a cross-linked hydrogel through polymerisation of $\mathbf{L^{16}}$ monomer with AAM and HEMA. These hydrogels were used as nacked-eye chemosensor for Fe^{3+} ions in aqeous medium. The detection limit of the hydrogel was estimated to be 0.1ppm.[178]

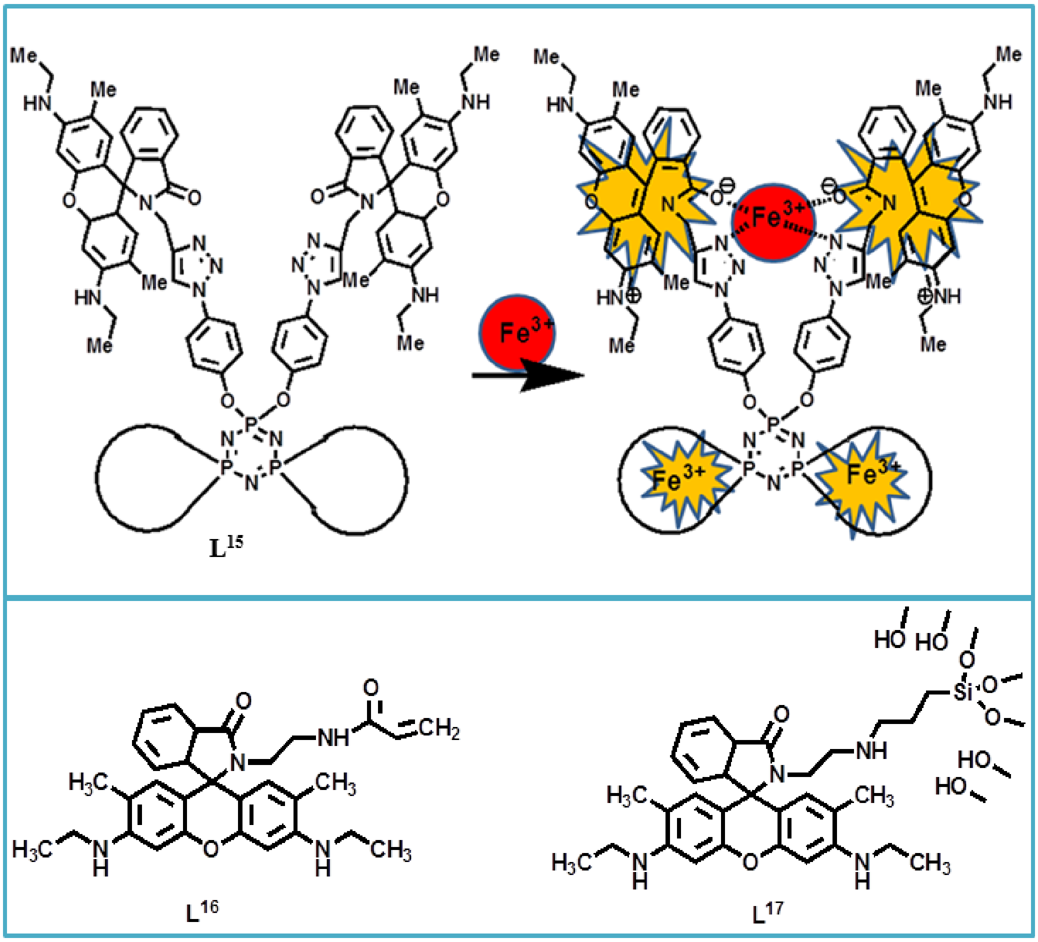

Figure-1.37: Structures of the chemosensors (L^{15}-L^{17}) for the detection of Fe^{3+}.

Young-A Son et al. developed a rhodamine 6G scaffold silica particle $\mathbf{L^{17}}$ (**Figure-1.37**), which are covalently attached onto the mesoporous silica forming organic-inorganic hybrid fluorescent chemosensor. RSSP shows 80-fold boost of the fluorescence intensity at 552 nm with a greenish yellow colour through "OFF-ON" manner upon addition of Fe^{3+} over other metal ions. B-H plot results a linear relationship with R=0.99 and association constant was calculated to be $8.46x10^3M^{-1}$. RSSP -Fe^{3+} complex becomes non-fluorescent in the presence of EDTA but again its intensity was found to be increased after adding Fe^{3+} to the same mixture confirming the reversible narture of the binding phenomenon between RSSP and Fe^{3+}. Fluorescence image was taken successfully from HeLa cell indicating non toxicity of RSSP towards cell confirming the applicability of this sensor for biological samples.[179]

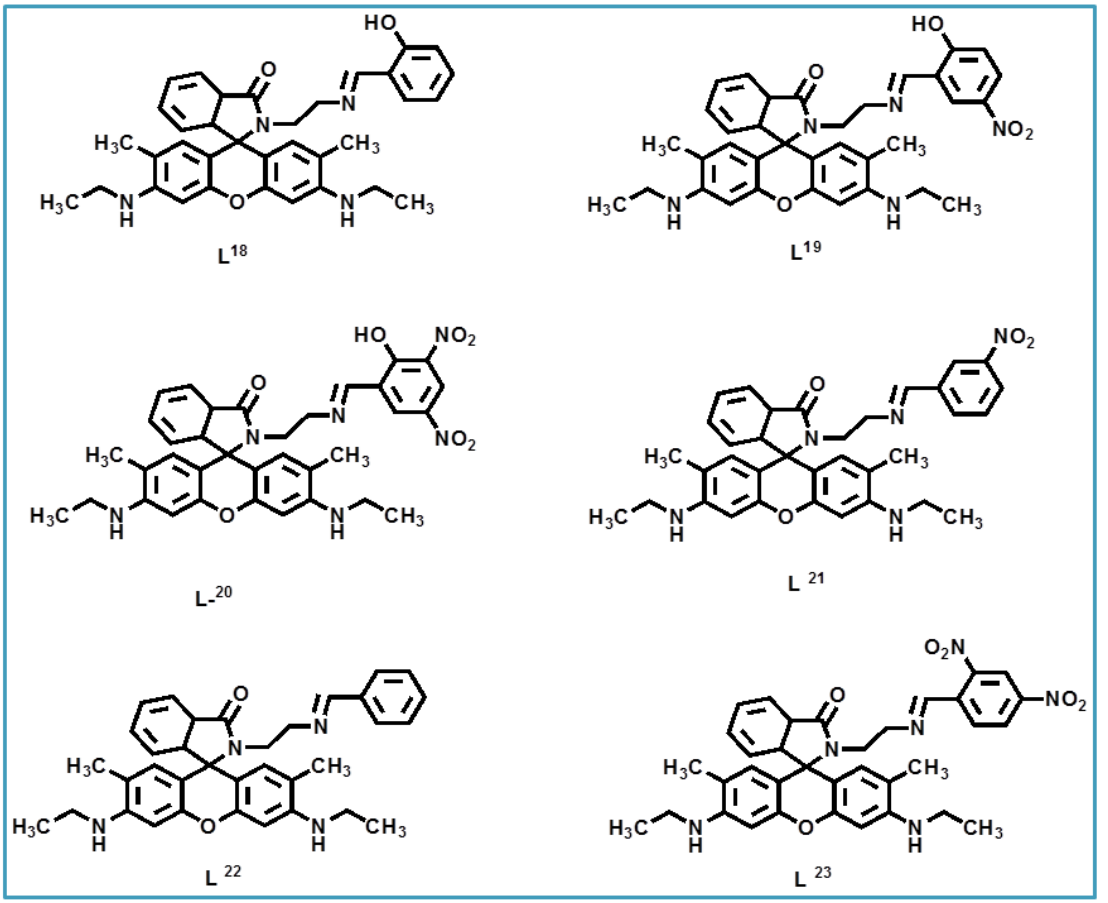

Figure-1.38: Structures of the chemosensors (L^{18}-L^{23}) for Fe^{3+}.

Lee, Kang and **Kim's** group reported rhodamine-6G based fluorescent probes **L^{18}-L^{23} (Figure-1.38)** for the detection of Fe^{3+} in presence or absence of other metal ions in biological systems. Probes **L^{18}-L^{23}** showed a fluorescence change in the presence of Fe^{3+} accompanied with the hydrolysis of the Schiff base. Spectroscopic studies were performed with **L^{18}-L^{23}** in aqueous solution (CH_3CN: H_2O, 5:95). Absorption and emission band appeared at 526 nm and 551nm for **L^{22}** and band became prominent with increase in Fe^{3+} concentration but in the presence of other biological metal ions fluorescence intensity remains almost unhanged. They observed usefulness of these probes for imaging of Fe^{3+} in theloaded HepG2 cell.[180]

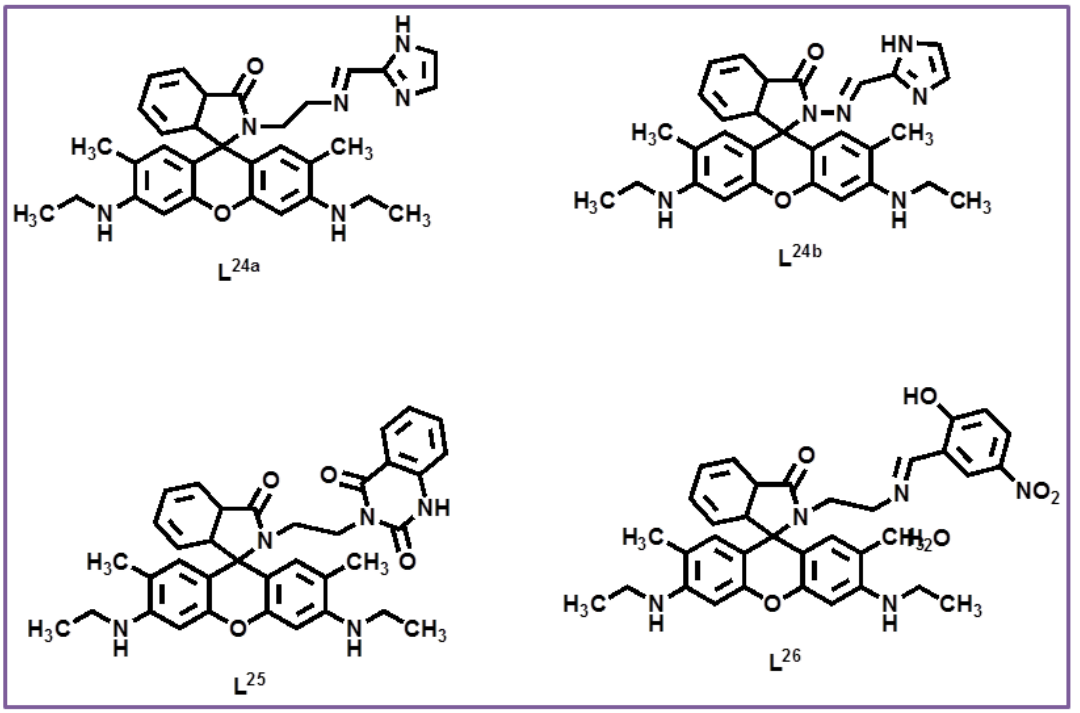

Figure-1.39: Structures of the chemosensors (L^{24}-L^{26}) for Fe^{3+}.

Chellappa et al. prepared rhodamine 6G based probes $\mathbf{L^{24a}}$ and $\mathbf{L^{24b}}$ **(Figure-1.39)** for chromo and fluorogenic sensing of Fe^{3+} in aqueous-PBS buffer (DMSO: H_2O, 2:8, pH=7.4) over other cations. The colour of the solution containing these probes changed from colourless to pink-red in the presence of Fe^{3+} ion. During fluorometric titration a strong emission band appeared at 553 nm and increase in intensity of the band continues till the saturation comes at 1.1 equivalent of metal ions. The LOD's of $\mathbf{L^{24a}}$ and $\mathbf{L^{24b}}$ were evaluated as $6.6x10^{-8}$ M^{-1} and $4.45x10^{-8}$ M^{-1}respectively.The association constants of L^{24a} and L^{24b} towards Fe^{3+} were determined to be $6.74x10^4$ M^{-1} and $3.964x10^4$ M^{-1} respectively. This probe is almost non-fluorescent in the pH range 5 to 9 that makes the ligand usefulness in the physiological condition and for imaging of Fe^{3+} in living cell.[181]

Wei-Na Wu and **Qing Xu** et al reported $\mathbf{L^{25}}$ **(Figure-1.39)** which has been prepared from rhodamine-6G ethylenediamine and methyl 2-isothiocyanatobenzoate. $\mathbf{L^{25}}$ is very much selective and sensitive towards Fe^{3+} in biological condition. This ligand also displayed a visual change in colour from colourless to yellow in the presence of Fe^{3+} ion. This probe showed a appearance of a broad absorbance band at 380 nm and an emission band at 555 nm with increase in

Fe^{3+}concentration in 10 mM HEPES buffer (pH=7.4) and intensity change was linear with the concentration of Fe^{3+}. Binding stoichiometry of $\mathbf{L^{25}}$ with Fe^{3+} found to be 1:1 from job's plot. Quantum yield of $\mathbf{L^{25}}$ for five equivalent Fe^{3+} found to be 0.69 in ethanol. The detection limit for Fe^{3+} was found to be 4.11µM. This probe was used successfully for Fe^{3+} monitoring in glioma cell line U251.This group also reported single crystal structures of $\mathbf{L^{25}}$ with Ag^{+} and Hg^{2+}.[182]

Kim et al. reported fluorescent chemosensor $\mathbf{L^{26}}$ **(Figure-1.39)** for the *in vitro* detection of Fe^{3+} selectively in the presence of other metal ions. Complexation of Fe^{3+} with $\mathbf{L^{26}}$ was found to be irreversible as the opening of the spirolactam ring is accompanied with the hydrolysis of imine linkage. Gradual addition of Fe^{3+} into the solution of $\mathbf{L^{26}}$ (H_2O: CH_3CN, 95:5) results in appearance of an absorption band at 526 nm and a fluorescence band at 551nm and the detection limit of $\mathbf{L^{26}}$ for Fe^{3+} was calculated to be 0.1µM. Chemodosimeter $\mathbf{L^{26}}$ was used for the recognition of intracellular Fe^{3+} in hepatocytes.[183]

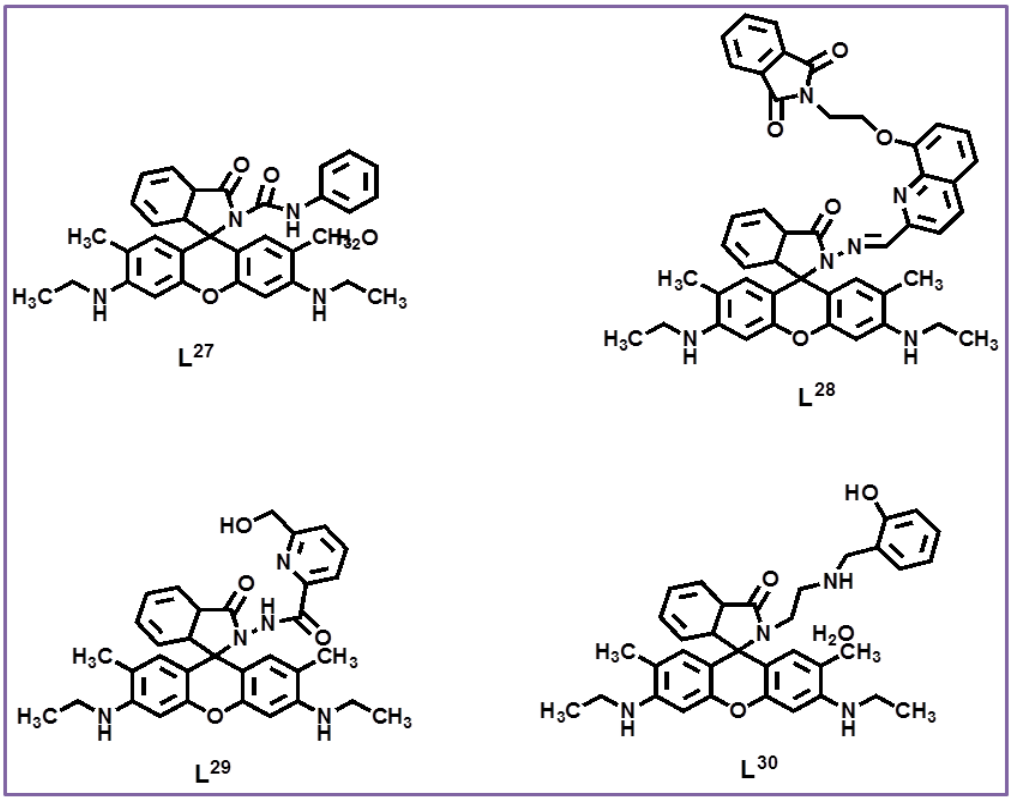

Figure-1.40: Structures of the chemosensors (L^{27}-L^{30}) for Fe^{3+}.

A novel chromogenic and fluorogenic chemosensor **L**^{27} **(Figure-1.40)** based on rhodamine-6G phenyl urea was developed by **Qiang Hu** et al. for the detection of Fe^{3+} in aqueous medium. **L**^{27}-Fe^{3+} complex was further used to detect acetate ion in aqueous medium. In the absence of Fe^{3+} ion **L**^{27} exhibited a weak band at 500 nm but in the presence of Fe^{3+} a prominent absorption band at 530 nm and an emission band at 556 nm were appeared with remarkable increase in intensity in H_2O-CH_3CN (1:1, v/v). The fluorescence quantum yield was calculated to be 0.86. pH study revealed that **L**^{27} showed a very strong sensitivity in the pH range 5.2 to 7.1. From the jobs plot the binding stoichiometry for the reaction between Fe^{3+} and **L**^{27} was evaluated to be 1:1.[184]

Xi and **Zeng** et al. developed "OFF-ON" fluorescent chemosensor **L**^{28} **(Figure-1.40)** for the detection Fe^{3+} ion in aqueous medium. **L**^{28} showed selectivity towards Fe^{3+} in the presence other toxic metal ions and other metal ions in living organism. **L**^{28} showed a remarkable enhancement of an absorption band intensity at 532 nm and emission band at 559 nm with 189-fold enhancement in an aqueous ethanol (7:3, v/v) solution. The formation constant for Fe^{3+} was calculated to be $1.1x10^6$ $M^{-1}$and stoichiometric ratio was observed to be 1:1 from Job's plot. **L**^{28} could act as chemosensor for Fe^{3+} in living cells.[185]

Goswami and **Mondal** group reported CHEF induced colorimetric and fluorogenic highly selective and sensitive sensor **L**^{29} for Fe^{3+}. This group reported the crystal structure of **L**^{29} **(Figure-1.40)**. It showed specificity over other transition metal ions and heavy metal ions having colourimetric change from colourless to pink in presence of Fe^{3+} ion. A 23-fold enhancement of fluorescence intensity was noticed at 550 nm in the presence of Fe^{3+} along with greenish yellow nacked eye fluorescence at pH=7.2. The formation constant was calculated to be 5.55×10^{-7} M and 1:1 stoichiometric ratio was confirmed from Job's plot. Reversibility and reusability of **L**^{29} for the detection of Fe^{3+} was established with EDTA fluorometrically.[186]

Peng's group reported a chemosensor **L**^{30} **(Figure-1.40)** for the fluorometric detection of Fe^{3+} selectively. The association constant estimated to be (K_a) of $1.1\times10^4M^{-1}$ in ethanolic medium. But this probe sufferes from selectivity problem as it is interfered by the presence of Ni^{2+}, Co^{2+}, Mg^{2+} and Ba^{2+}.[187]

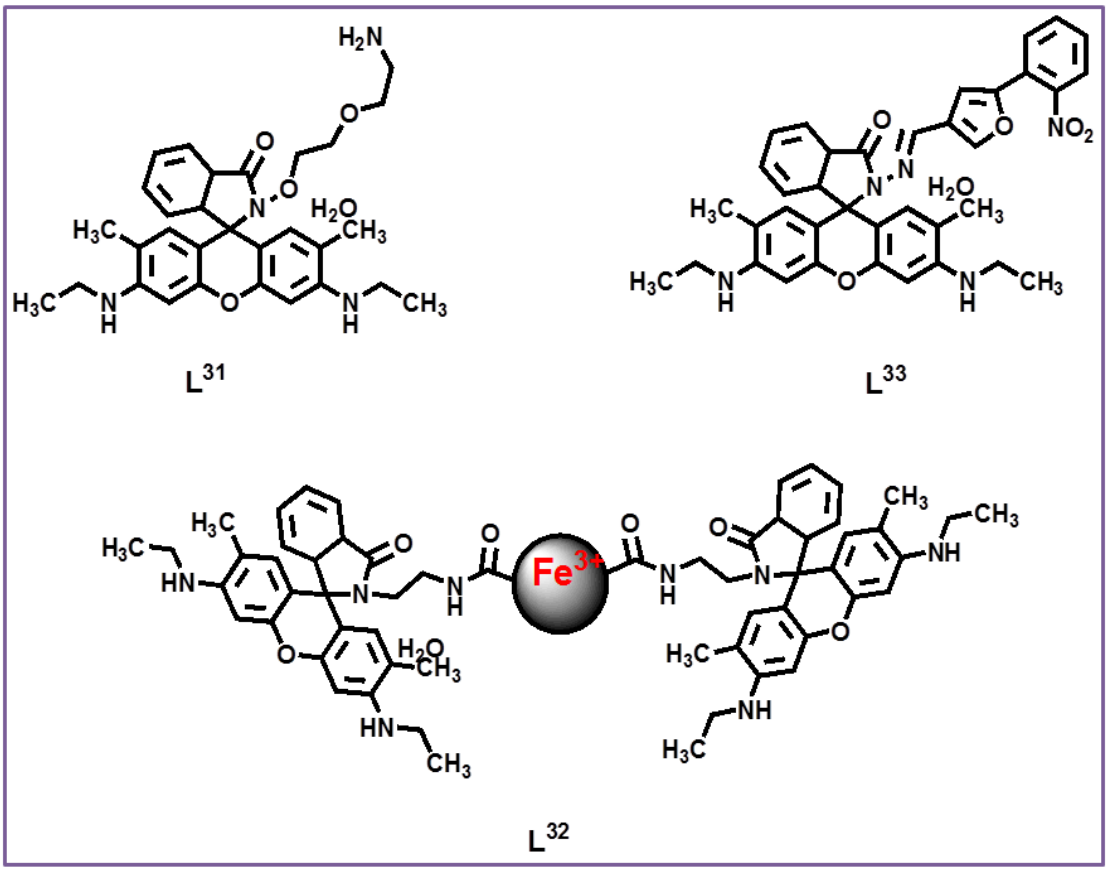

Figure-1.41: Structures of the chemosensors (L^{31}-L^{33}) for Fe^{3+}.

Tae et. al. synthesized rhodamine-6G based chemosensor $\mathbf{L^{31}}$ (**Figure-1.41**) that has a flexible bis-aminoxy (diethylene glycol) multidentate binding site for the detection of Fe^{3+} ions in aqueous medium over other cations. Formation constant was calculated to be K_a=8.0 x10^4 M^{-1} in H_2O-DMSO (99:1, v/v) medium.[188]

Jiang et al. reported a very sensitive and specific fluorescent nano-sensor $\mathbf{L^{32}}$ **(Figure-1.41)** for detecting Fe^{3+} in aqueous medium. In $\mathbf{L^{32}}$ rhodamine moiety covalently attached to the surface of C-dots. It worked on FRET mechanism where energy is transferred from C-dots to rhodamine moiety. The emission spectrum of C-dots showed a wide overlap with the emission band of rhodamine showing FRET process. $\mathbf{L^{32}}$ showed a strong emission band at 550 nm with yellow fluorescence and absorption band at 530 nm and detection was studied at physiological pH to avoid effect of acidity in rhodamine ring opening.[189]

Ali et al reported rhodamine 6G based "OFF-ON" chemosensor **L^{33} (Figure-1.41)** for the selective detection of Fe^{3+} over other biologically important and toxic metal ion and this group showed an interaction between **L^{33}**-Fe^{3+} complex and DNA. **L^{33}** showed a gradual upgrade of the emission band at 556 nm in the presence of Fe^{3+} in HEPES buffer at pH=7.2. The binding constant was calculated as $1.72x10^{4}M^{-1}$ and the detection limit for Fe^{3+} was evaluated to be 0.17µM. The interaction between DNA and complex was monitored with the outcome of hypochromic shift of the emission band of the complex in the presence of increasing concentration of DNA.[190]

1.8.4 Brief Literature Survey on Cu^{2+} Chemosensors

Among the transition metals copper is the third most abundant and it has a very crucial role in environmental and ecological system. However, above the optimum cellular concentration it can cause oxidative stress, neurological disorder like Alzheimer's and Parkinson's disease. Since Cu^{2+} is an efficient fluorescence quencher, due to its paramagnetic nature, the the turn-ON fluorescence sensor for Cu^{2+} ion is very less frequent. Hence it is a very challenging task to design efficient turn-ON fluorescence sensors for the detection Cu^{2+} in biological and environmental sample selectively.

Zang et al. reported "OFF-ON" colorimetric and highly sensitive fluorescent probe **L^{34} (Figure 1.42)** for the detection of Cu^{2+} selectively. This group also reported the single crystal X-ray structure of **L^{34}**. This probe changes its colour from colourless to pink in the presence of Cu^{2+}. An absorption band appeared at 528 nm and strong emission band at 559 nm with 200-fold increase fluorescence intensity upon addition of Cu^{2+} to **L^{34}** in DMF-Water (95:5) Stoichiometric ratio between Cu^{2+} and **L^{34}** in the complex was estimated to be 1:1 from Job's plot. The formation constant was calculated from absorption titration data as $2.439x10^{4}$ M^{-1}. Detection limit was calculated to be $9.12x10^{-7}$ M[191]

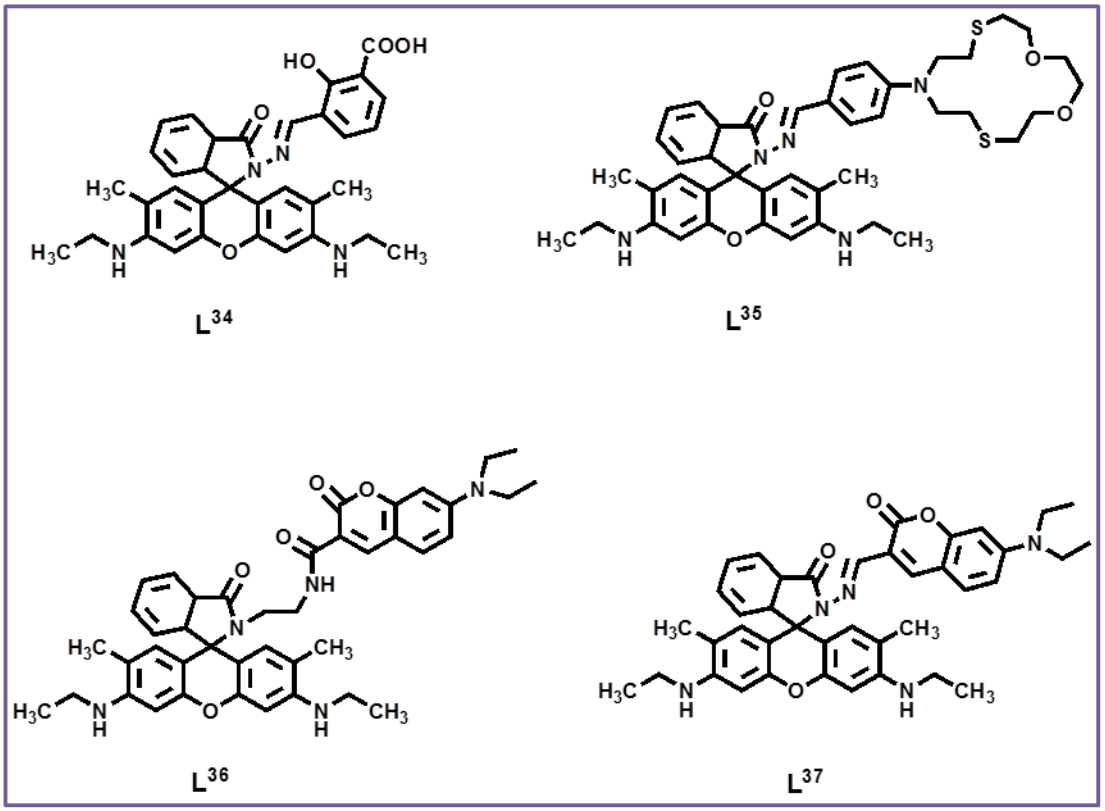

Figure-1.42: Structures of the chemosensors (L^{34}-L^{37}) for Cu^{2+}.

Mironenko et al. developed a rhodamine-6G based novel probe $\mathbf{L^{35}}$ (**Figure-1.42**) for the recognition of Au^{3+} through fluorometric sensing and Cu^{2+} through colorimetric response. Spectroscopic studies showed the development of absorption band at 520 nm for Au^{3+} and at 527 nm for Cu^{2+} and emission band at 555 nm in 10 mM HEPES buffer (CH_3CN: H_2O, 1:1, pH=7.0). Detection limit was calculated to be $5x10^{-7}$M and $2x10^{-6}$M for Cu^{2+} and Au^{3+} respectively. Binding stoichiometries were estimated to be 1:2 for Cu: $\mathbf{L^{35}}$ and 2:1 for Au:$\mathbf{L^{35}}$ from the Job's plot.[192]

Duan et al. reported a ratiometric fluorescent chemosensor $\mathbf{L^{36}}$ and $\mathbf{L^{37}}$ (**Figure-1.42**) for Cu^{2+} and Hg^{2+} based on FRET mechanism. In this probe coumarin act as donor and a rhodamine act as acceptor and it showed an excellent sensitivity and selectivity towards Cu^{2+}. $\mathbf{L^{36}}$ showed anabsorption band at 525 nm in the presence of $\mathbf{Cu^{2+}}$and $\mathbf{L^{37}}$ at 530 nm in the presence of Hg^{2+} respectively with change in colour from yellow to pink. The linear curve fitting method revealed a 2:1 binding ratio for $\mathbf{L^{36}}$ and Cu^{2+}. The association constant for $\mathbf{L^{36}}$ was found to be $2.66x10^{12}$.

A strong emission band appeared at 460 nm for coumarin, an energy donor, for **L**[36]. FRET efficiency was calculated as 90%.[193]

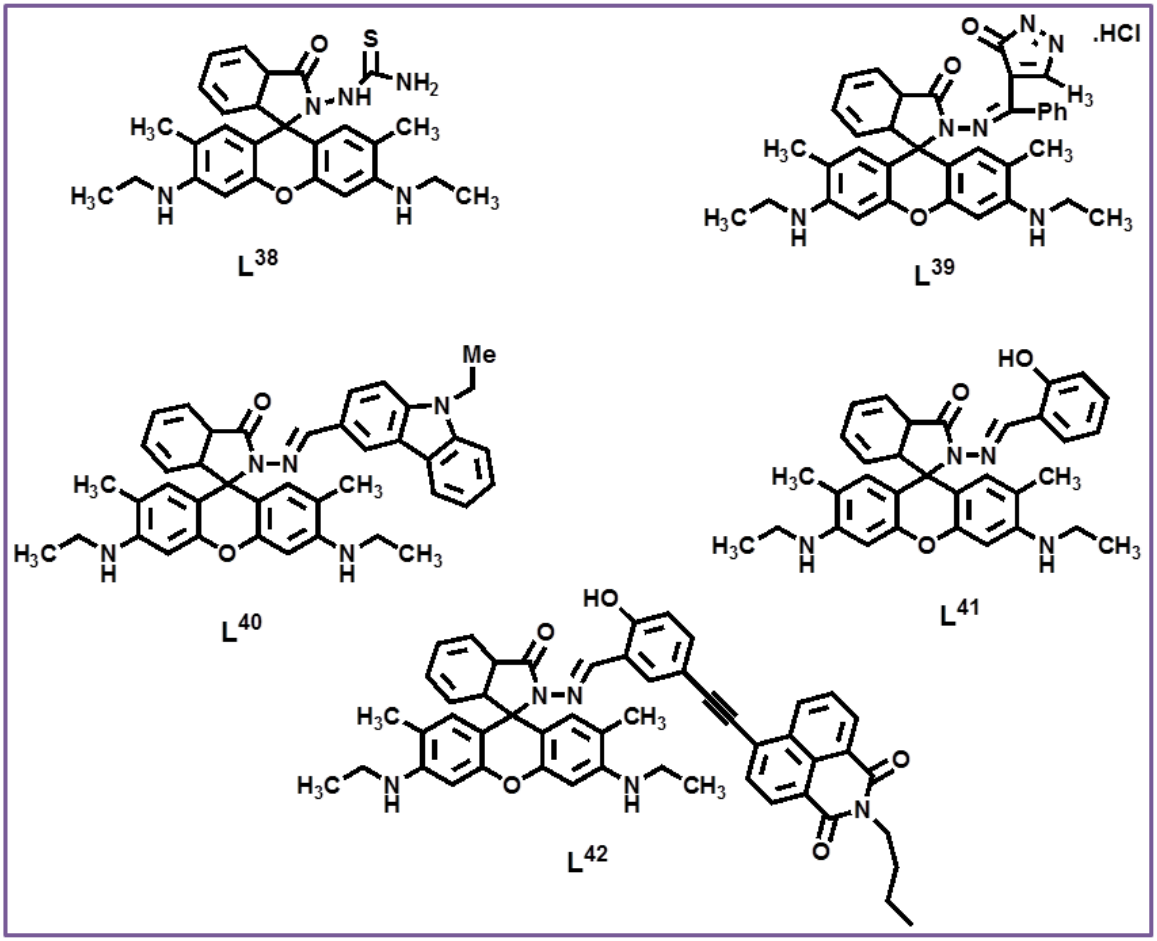

Figure-1.43: Structures of the chemosensors (L[38]-L[42]) for the detection of Cu^{2+}.

Zeng et al. synthesized a rhodamine-6G based fluorogenic and colorimetric "Turn-On" chemodosimeter **L**[38]**(Figure-1.43)** for the detection of Cu^{2+} selectively in aqueous medium over other trace metal ions and biologically important cations. In presence of Cu^{2+}, **L**[38] showed a gradual increase in absorption band at 529nm and an enhanced emission band at 554nm in Tris-HCl buffer (CH_3CN: H_2O,1:1) at pH =7.2. It's sensitivity below 2ppb.The fluorescence image of EJ cells with Cu^{2+} was done successfully.[194]

Wang et al. developed a turn-on fluorescent chemosensor **L**[39] **(Figure-1.43)** for Cu^{2+}. **L**[39]showed a high selectivity towards Cu^{2+} over other toxic and biological relevant metal ions. It exhibited a strong absorption band at 523 nm and emission band at 557nm with 250 times enhanced

fluorescence in MeCN. **L[39]** containing solution was changed from colorless to purple. Binding constant was measured as $3.34x10^4M^{-1}$. **L[39]**-Cu^{2+} complex crystal structure confirmed the ring opened form which was claimed to be the main cause of giving high fluorescence intensity. The LOD's evaluated as 2.5 µM for Cu^{2+} and the binding stoichiometry was found to be 1:1 from Job's plot.[195]

Young-A Son developed a rhodamine 6G scaffold **L[40]** containing carbazole unit (**Figure-1.43**) for identifyingof Cu^{2+} and Ce^{4+} in aqueous solution. **L[40]** behaved as fluorescent chemosensor for Cu^{2+} and chemodosimeter for Ce^{4+}. **L[40]** showed a Cu^{2+} induced chelation enhanced fluorescence with spirolactm ring opening. This could act through bond energy transfer (TBET) mechanism resulting a highly sensitive chemodosimeter for Ce^{4+}. Spectroscopic studies revealed that a new absorption band appeared at 531nm and emission band at 552nm for both Cu^{2+} and Ce^{4+} in mixed aqueous medium (water-acetonitrile, 1:1, v/v) medium. **L[40]** showed 120-fold fluorescence intensity enhancement by Cu^{2+} and 250 fold in presence of Ce^{4+} with yellowish green and green colour change respectively. The LOD for Cu^{2+} was calculated to be $1.176x10^4M$ and the formation constant was estimated to be1 $3.9x10^{-8}M^{-1}$. The LOD for Ce^{4+} was calculated to be $2.396x10^6\ M^{-1}$ and the formation constant was estimated to be $11.49x10^{-3}M^{-1}$.[196]

Tong et al prepared **L[41]** **(Figure-1.43)** chemosensor which displayed only colorimetric "turn-on" responses for Cu^{2+}. **L[43]** showed enhancement of emission intensity at 550 nm on addition of Cu^{2+} in aqueous ethanol solution [50% (v/v) with 10 mM neutral acetate buffer (pH 7.0)].[197]

Kim and co-workers developed a new rhodamine-6G-based reversible chemosensors **L[42]** with N-butyl-1,8-naphthalimide group (**Figure-1.43**), which gives colorimetric and fluorogenic "turn-ON" changes at 550 nm via spirolactam ring opening mechanism towards Cu^{2+} in CH_3CN-HEPES buffer (0.02 M; pH 7.4; 5:5, v/v). Association constant (K_a) was calculated to be 0.52×10^4 for L^{42}-Cu^{2+} complex. But exceptional ratiometric fluorescence enhancement was observed toward Zn^{2+} via intramolecular charge transfer (ICT) pathway. So, it is not a selective chemosensor rather a dual sensor.[198]

Tanget al. reported a highly sensitive fluorescent chemosensor **L[43]** (**Figure-1.44**) for the selective detection Cu^{2+} in an aqueous phase (20 mM PBS, pH=7.4) with a small dissociation

constant (K_d) value of 0.1 μM for the Cu^{2+} complex with the probe. This "OFF-ON" type fluorescence change after addition of Cu^{2+} was also successfully applied in bioimaging.[199]

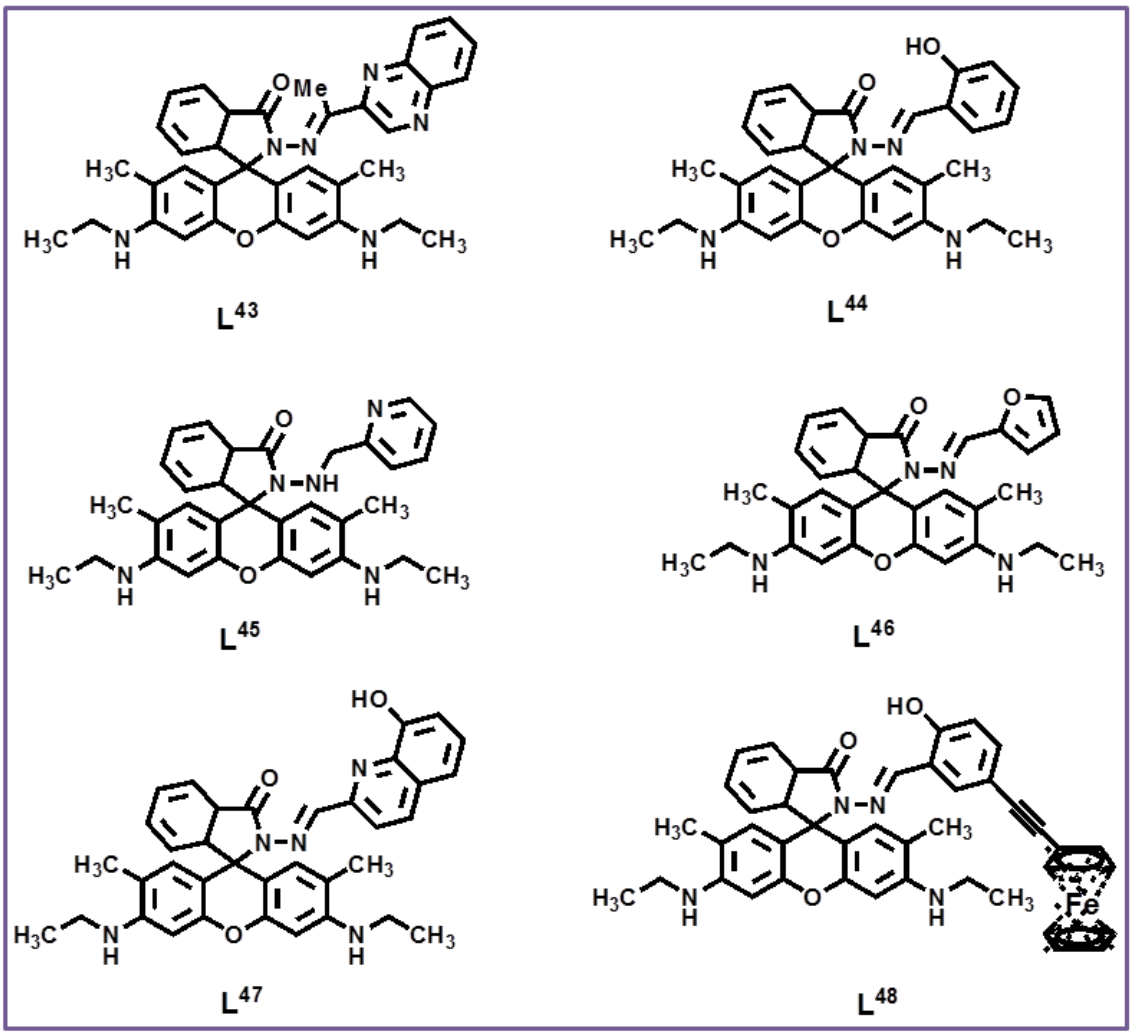

Figure-1.44: Structures of the chemosensors (L^{43}-L^{48}) for Cu^{2+}.

Zeng's group reported a chemosensor **L^{44} (Figure-1.44)** which produces a selective turn-ON fluorescence response towards Cu^{2+} in HEPES buffer (20 mM, pH 7.0) containing 50% (v/v) CH_3CN with its potential bioimaging application in SPC-A-1 (lung cancer) cells.[200]

Zhang et. al. also reported a chemosensor **L^{45}** (Figure-1.44) for the fluorometric detection of Cu^{2+} with a dissociation constant estimated to be 8.0x 10^{-7} M^{-1} in buffered aqueous solution (Tris-HCl, pH 7.1, water-ethanol, 8:2, v/v) system. The reported chemosensor is used for the estimation of Cu^{2+} in river water samples and for cell imaging applications.[201]

The chemosensor **L**[46] (**Figure-1.44**) was also reported by **Zhang's** group which was found to selectively bind with Cu^{2+} ion in 1:1 stoichimetric ratio over other cations present in aqueous media. In the presence of Cu^{2+}, **L**[46] produced a strong absorption band at 529 nm and an emission band at 552 nm with the 32-fold enhancement in intensity in water-acetonitrile (1:1, v /v). Association constant was assesed to be 8.9 x 10^3 M^{-1}. Experiments done with living cells indicates that chemosensor is cell viable and used successfully to detect intracellular Cu^{2+} ion.[202]

Long's group repoted a chemosensor **L**[47] **(Figure-1.44)** which exhibits a dynamic response range for Cu^{2+} from 2×10^{-7} to 5×10^{-5}M in Tris–HCl/EtOH (7:3, v/v, PH=7.4). In addition, this turn-on fluorescent enhancement was also applied in cell imaging.[203]

Yao et al. synthesised a ferrocene unit containing rhodamine-6G based chemosensor **L**[48] (**Figure-1.44**). Sonogashira coupling reaction was involved to introduce ferrocenyl moiety into the rhodamine fluorophore. A new absorption peak at 530 nm and an emission peak at 554 nm were developed after gradual addition of Cu^{2+} in ethanol-water (1 :1, v/v, pH=7.0). Due to the high affinity of Cu^{2+} towards **L**[48] provides good selectivity and high sensitivity to Cu^{2+} without interference from other cations. The detection limit 6.96×10^{-7} M was obtained from fluorescence titration data, and corresponding formation constant was calculated to be 1.52×10^6 M^{-1} from absorbance titration data. It was observed that after interaction with Cu^{2+} a configurational change occurred which influences the electron density within ferrocene group. Detection limit for Cu^{2+} was calculated as 3 μM and a 1:1 binding stoichiometry was found from the Job's plot. It was prosperouslly applied in fluorescence imaging for Cu^{2+} in HeLa cells due to its good solubility and biocompatibility.[204]

Yoon *et. al.* developed a pyrene embedded rhodamine-6G based ratiometric "OFF-ON" based nacked eye chemosensor **L**[49] **(Figure-1.45)**. This probe **L**[49] showed ratiometric fluorescence enhancement due to chelation with visual colour change in the presence of Cu^{2+} and displayed a fantastic selectivity in the presence of other cations. **L**[49] showed a clear enhancement of emission intensity at 575nm with a iso-emission point at 558 nm in acetonitrile-HEPES buffer (4:6, v/v, pH=7.4). The 1:1 Stoichiometry of **L**[49]-Cu^{2+} was evident from Job's plot. Formation constant was calculated to be $2.5x10^4M^{-1}$ using absorption titration data. Reversibility of the complexation was examined by EDTA.[205]

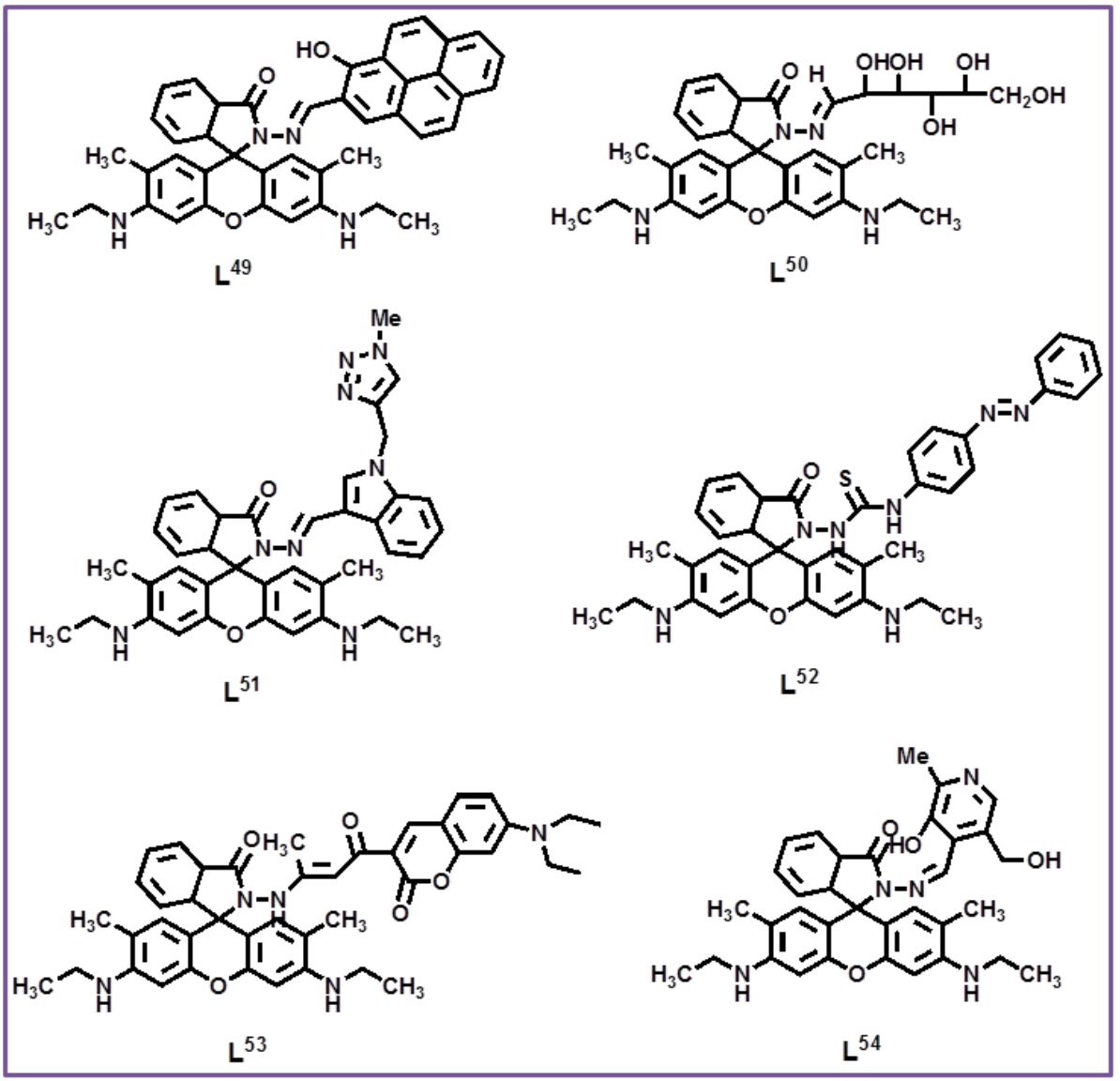

Figure-1.45: Structures of the chemosensors (L^{49}-L^{54}) for Cu^{2+}.

Yuguo Du reported a turn-ON fluorescent chemosensor **L^{50} (Figure-1.45)** for the detection of Cu^{2+}r in aqueous medium with excellent selectivity. **L^{50}** also showed a nacked eye colour change at the concentration level of 3μM and limit of detection was calculated to be 12μgL^{-1}. **L^{50}** also showed an enhancement fluorescence intensity at 560 nm (λ_{ex}520 nm) in water-acetonitrile (4:1). The reversible sensing behavour of the probe was tested by EDTA.[206]

Thennarasu et al reported a chemosensor **L^{51} (Figure-1.45)** which is a rhodamine-indole conjugate for the detection of Cu^{2+} at sub-micromolar level in aqueous phase at biological pH and in living cellswith a measurable interference by Fe^{3+} and Ni^{2+} in non-aqueous medium but in

aqueous phase only by Fe^{3+}. **L^{51}** gives an absorption band at 525 nm with 69, 274 and 652-fold enhancement in fluorescence intensity in the presence of Ni^{2+}, Fe^{3+} and Cu^{2+} respectively. LODof Cu^{2+} was calculated to be $3x10^{-8}$ M.[207]

Yang et al synthesised a novel fluorogenic and and colourimetric chemosensor **L^{52} (Figure-1.45)** for the detection of Cu^{2+} over other cations. Based on "Host-Guest" chemistry magnetic fluorescent nanoparticle was constructed from azobenzene containing rhodaminw-6G and cyclodextrin modified $Fe_3O_4@SiO_2$. Nano particle modified **L^{52}** showed a visual colour change to yellow green in the presence of Cu^{2+} during fluorometric titration and light yellow to pink in absorption studies. This inclusion complex magnetic nanoparticles (IFIC MNPs) showed an emission peak at 555 nm in the presence of Cu^{2+} in water-acetonitrile (1:1, v/v, pH=7.2). The detection limit was found to be $2.5x10^{-7}$ mol/L.[208]

Wang and coworkers developed a rhodamine 6G and coumarin containing a novel chemosensor **L^{53} (Figure-1.45)** for the detection of Cu^{2+} and Hg^{2+}.Chemosensor **L^{53}**, a colourimetric and ratiometric probe exhibited a very strong sensitivity and high selectivity towards Cu^{2+} in neutral aqueous solution, however, it showed strong sensitivity for Hg^{2+} at pH=10.0. Metal ligand binding and then spirolactam ring opening was confirmed from absorption and emission studies. An enhanced absorption band at 520 nm and emission band at 550 nm appeared due to the incremental addition of $Cu^{2+}$to **L^{53}** in CH_3CN/H_2O (9:1,v/v, pH=7.4). LOD for Cu^{2+} was estimated to be 6.88µM. Fluorescence band was shifted to 490 nm in the presence of Hg^{2+} in CH_3CN/H_2O (9:1, v/vpH=10.0). LOD for Hg^{2+} was 2.96 µM and the binding ratio of **L^{53}** and Hg^{2+} was found to be 1:1 and the binding constant with Hg^{2+} evaluated to be $3.34x10^4M^{-1}$ from emission data using B-H plot. This probe was applied as chemosensor in tracking intracellular Cu^{2+} in Hela cell .[209]

Zhang et al synthesised a rhodamine 6G based chemosensor **L^{54} (Figure-1.45)** for the rapid recognition of Cu^{2+} in aqueous medium. Fluorescence intensity of **L^{54}** greatly enhanced 36 fold in presence of Cu^{2+} along with naked eye colour change to pink. The probe showed a remarkable enhancement in absorption intensity at 529 nm and emission intensity at 573 nm in Tris-HCl buffer solution (pH=7.2). The detection limit of Cu^{2+} was calculated to be 3.9 $x10^{-7}$mol/L and the binding stoichiometry was evaluated to be 1:1 from Job's plot.[210]

1.8.5 Brief Literature Survey on Hg^{2+} Chemosensors

Mercury is a very toxic metal and its contamination results a very serious environmental concern. Due to its high level of toxicity, it can damage DNA and disrupts central nervous system and endocrine, various cognitive and motor disorder can cause Minemata disesese. So its detection by fluorometric method is a great deal of attraction for the scientist in the recent years.

Lin et al. reported a chemosensor $\mathbf{L^{55}}$ (**Figure-1.46**) consisting of a sulfur atom and an alkenyl moiety for the selective detection of Hg^{2+} in PBS buffer at pH=7.0. Due to the thiophilic character of mercury ions, the receptor having S atom furnished a suitable binding site for Hg^{2+}. A remarkable enhancement of fluorescence intensity (1000-fold) at 561 nm was observed after incremental addition of Hg^{2+} in 25mM PBS buffer at pH=7.0. The stoichiometry of binding between $\mathbf{L^{55}}$ and Hg^{2+} as determined from Job's plot was 1:1 and abinding constant 2.5 x 10^{-5}M. The probe showed excellent sensitivity towards Hg^{2+} with detection limit 27.5 nM.[211]

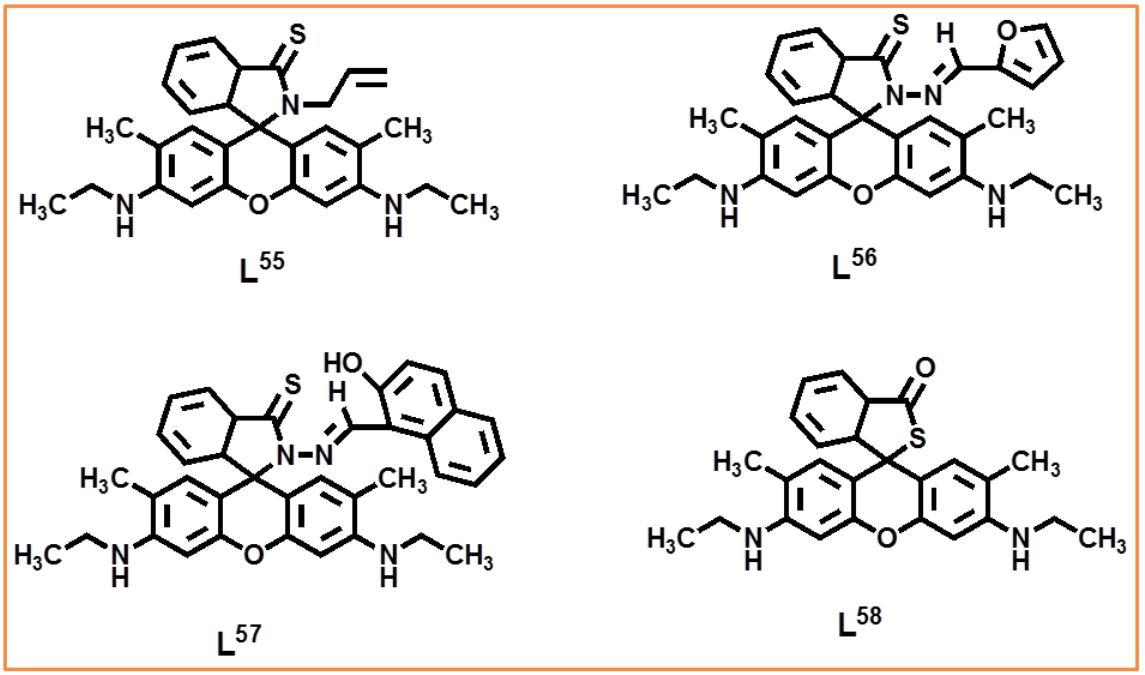

Figure-1.46: Structures of the chemosensors (L^{55}-L^{58}) containing sulfur (S) atom as one of the coordinating site for Hg^{2+} sensing.

Yang et al. developed a colourimetric fluorescent chemosensor $\mathbf{L^{56}}$ **(Figure-1.46)** containing thiospirolactam moeity for the identification of Hg^{2+} in aqueous medium. Photophysical studies

were performed to investigate the signal change upon binding with Hg^{2+} in water-DMF (1:1,v/v pH=7.0). This probe **L**[56] showed a 120-fold enhancement in fluorescence intensity at 564 nm. Binding stoichiometry between **L**[56] and Hg^{2+} was determined as 2:1 and binding constant was calculated to be $5.20x10^5M^{-1}$ from absorption titration data. The probe **L**[56] was applied for *in vivo* bioimaging in rat Schwann to confirm its usability to recognize Hg^{2+} in living cells.[212]

Li et al. developed a cell compatible novel fluorescent chemosensor **L**[57] (**Figure-1.46**) for the detection of Hg^{2+}. **L**[57] offered an excellent sensitivity and selectivity towards Hg^{2+} over other cations. This "OFF-ON" type probe successfully mimics a molecular keypad lock in the presence of Cu^{2+}. Particular sequence of inputs that means the correct password is the main reason for intense fluorescence emission at 555 nm that can be utilised to "open" the molecular keypad lock. The binding constant and binding ratio with Hg^{2+} was estimated to be $8.42x10^4\ M^{-1}$and 1:1. similarly for Cu^{2+} ion these are $1.98x10^4M^{-1}$ and 1:1 respectively. This molecular key pad lock has potential role in protecting information at the molecular scale.[213]

Yoon's reported **L**[58] chemosensor (**Figure-1.46**) bearing thiolactone moiety exhibits Hg^{2+} sensing property through spirolactam ring-opening of rhodamine 6G unit in the buffer (CH_3CN-HEPES ,1:99, v/v, pH 7.4). It is also applied to bioimaging for Hg^{2+}.[214]

He and **Duan** *et. al.* reported rhodamine based sensors and **L**[60] (**Figure-1.47**), for the recognition of Hg^{2+} in aqueous phase having thio moiety as coordinating site. Interference was observed from Cu^{2+}, Pb^{2+} and Ag^{+} for the detection of Hg^{2+} by **L**[59]; however, in the case of **L**[60] no such interference was observed. For **L**[60], metal-ligand binding ratio during complexation was found to be 1:2 from Job's plot with a formation constant (K_a= 8.18 x 10^7 M^{-2}) Probe **L**[59] also have same binding mode and higher association constant (K_a= 1.58 x 10^{13} M^{-2}).[215]

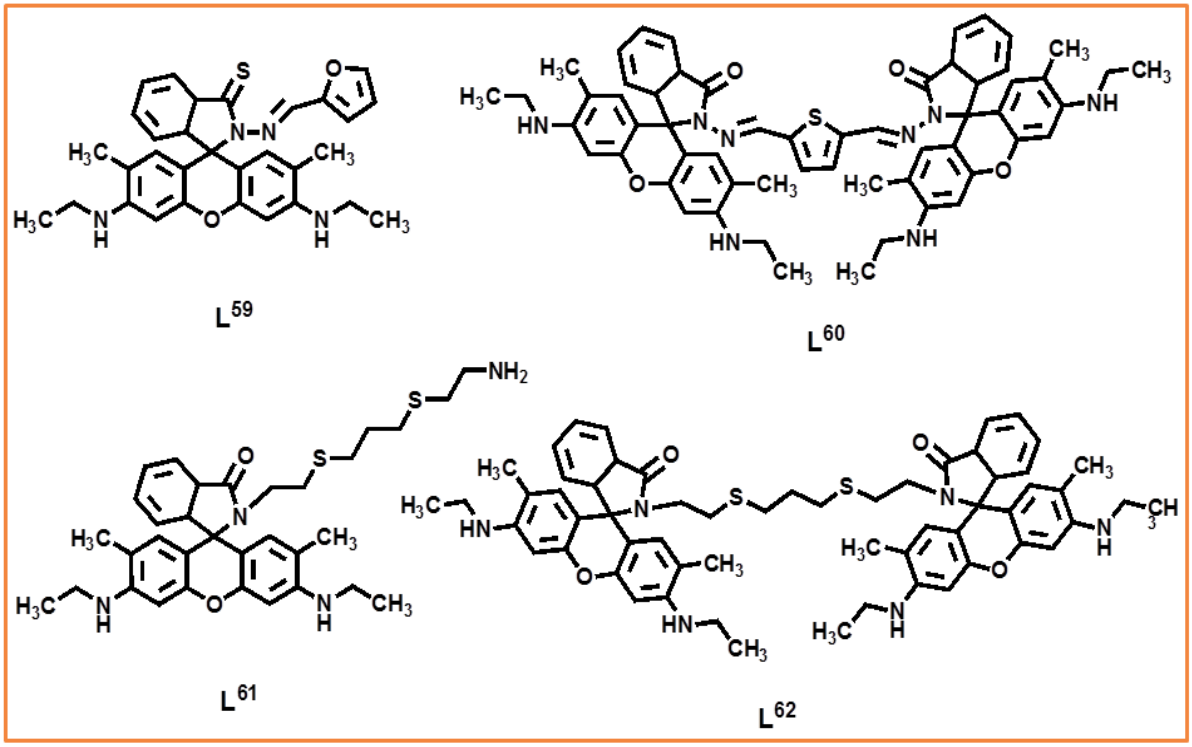

Figure-1.47: Structures of the Chemosensors (L^{59}-L^{62}) Containing "S" Atom as One of the Coordinating Site for Hg^{2+} Sensing.

Wanichacheva *et. al.* synthesised a turn-ON colorimetric and fluorometric chemosensors **L^{61}** and **L^{62}** (**Figure-1.47**) for the detection of Hg^{2+}. These sensors exhibited high sensitivity towards Hg^{2+} in the presence of other competiting cations in terms of fluororescence enhancement and naked eye colour change from colourless to pink. This research greported that the probe **L^{61}** and **L^{62}** exhibited an absorption band and emission band at 529 nm and 545 nm respectively in 5% DMSO water. The detection limit was given as 8.7 $x10^{-9}$ M and $1.5x10^{-5}$ M for **L^{61}** and **L^{62}** respectively. The binding ratio was found to be 1:1 for both the probes and the formation constant was evaluated as $1.04x10^{5}M^{-1}$ for **L^{61}**.The reversibility of the chemosensor was demonstrated with **L^{61}** by tetraethyl ammonium iodide.[216]

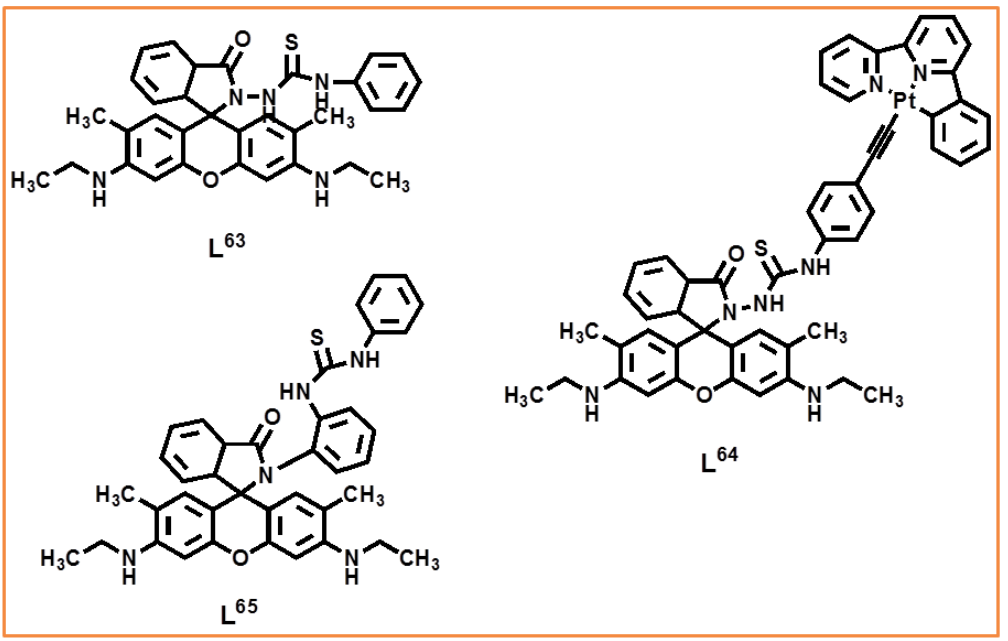

Figure-1.48: Structures of the chemosensors(L^{63}-L^{65}) containing "S" as one of the coordinating atom for Hg^{2+} sensing.

Sanchez's group reported sensing film developed from the incorporation of rhodamine-6G based derivative **L^{63}** (**Figure-1.48**) into a hydrophilic but water insoluble copolymer synthesised by radical polymerisation. This Chemodosimeter shows its sensing capability and produces strong fluorescence intensity in the presence of Hg^{2+} after immobilization of MMA-co-HEMA, copolymer containing 29.6% HEMA.This recognises Hg^{2+} at 0.9 mM to 12 nM range with LOD 0.3 mM. The applicability of this sensor was successfully demonstrated with tap and mineral water.[217]

Cho and **Kim** synthesised rhodamine-Pt (II) complex a water soluble chemosensor **L^{64}** (**Figure-1.48**) for the detection of Hg^{2+}. in water sample as well as in live cells. A visual colour change of the solution containing L^{64} was observed from light yellow to pink in presence of Hg^{2+} due to opening of xanthene ring resulting 1,3,4-oxadiazole ring formation. The chemosensor **L^{64}** exhibits a strong absorption band at 535 nm and emission band at 545 nm with 23-fold enhanced intensity in acetonitrile-HEPES buffer (20 mM,1:1, v/v, pH=7.0). The detection limit was calculated to be 4.87×10^{-8}M and Job's plot confirms the 1:1 binding ratio. This probe L^{64} was applied successfully to locate and to estimate trace amount of Hg^{2+} in live HeLa cells by two photon microscope.[218]

Yang et al. developed a colorimetric and fluorescent indicators **L**[65] (**Figure-1.48**) for Hg^{2+} detection. This probe showed selectivity towards Hg^{2+} over wide range of pH (5-10) but it remains silent towards other cations. Cytotoxicity studies revealed that probes had slight cytotoxicity, cell permeability and suitable for the Hg^{2+} detection in biological system. This probe showed its ability to detect Hg^{2+} by adsorbing on solid surface and detection of Hg^{2+} in water samples indicating promising future for the successful detection of Hg^{2+}in biological environment .[219]

Recognition of Hg^{2+} using immobilized molecular probes as chemosensors bearing Rhodamine 6G unit has been progressively developed now-a-days (**Figure-1.49**). This probe is apprehended on a solid surface or imprisoned in a porous structure, naturally preferred than using solution of that probe.

Fu and **Xie** et al. reported a rhodamine 6G based organic inorganic composite fluorescent chemosensor SiO_2@mSiO_2@Rd-6G, **L**[66] (**Figure-1.49**) immobilized on mesoporous silica microspheres for the detection Hg^{2+} in aqueous phase. The specific response of hybrid solid chemosensor **L**[58] in water is considered to be highly dense rhodamine probe. The mentioned probe showed excellent selectivity to Hg^{2+} over other competiting environmental and biologically crucial metal ions. The detection limit estimated as 0.1nM. This hybrid chemosensor was used for the detection of Hg^{2+} over a wide range of pH, it can be readily regenerated.[220]

Wang's group reported an excellent fluorescent surface sensor containing rhodamine probe **L**[67] (**Figure-1.49**) where mesoporous silica acted as support for the detection of Hg^{2+}. Water suspension of the probe was taken for absorption and emission study, where pale yellow colour of the modified silica particles changes to a red colour after addition of Hg^{2+} with enhancement of the emission signal at **550** nm. In addition to high selectivity this chemosensor showed enhanced sensitivity to Hg^{2+} as the detection limit was found to be $1.0x10^{-8}$ M in water. Excellency of this probe was checked from reversibility studies. Upon addition of TBAH fluorescence intensity was found to be vanished.[221]

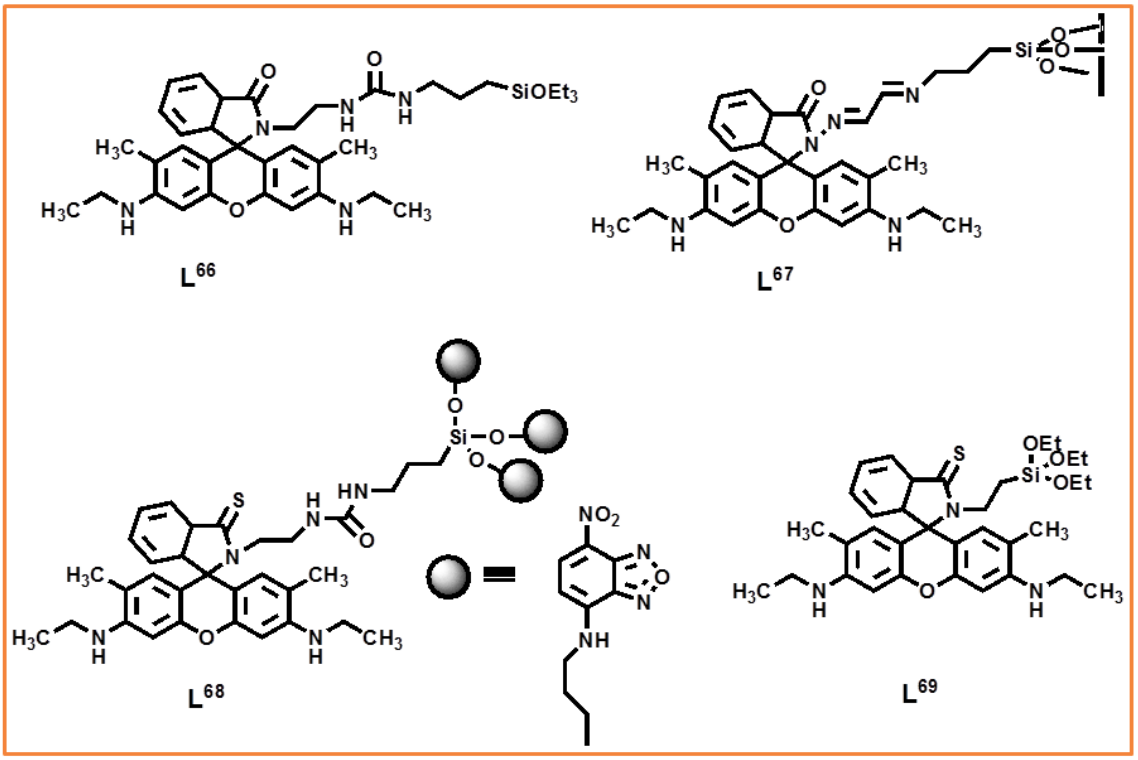

Figure-1.49: Immobilized silica based chemosensor made of rhodamine -6G moiety (L^{66}-L^{68}) for the recognition of Hg^{2+}.

Zeng and **Wu** et al. prepared a FRET-based chemosensor **L^{68}** (**Figure-1.49**), multilayered silica film on a quartz plate for the ratiometric detection of Hg^{2+} in aqueous solution. In this work they successively inserted silica functionalized donor (a nitrobenzoxadiazolyl derivative, NBD) layer, spacer layer and finally the acceptor (rhodamine) layer on the plate for binding of metal ions. This probe showed a strong emission band at 580 nm in the presence of Hg^{2+} in aqueous phase due to ring opening of the rhodamine 6G moiety. FRET based fluorescence mechanism was found to be operative in the whole event excitation wavelength at 430 nm and emission wavelength at 580 nm that proved energy transfer took place from NBD to rhodamine 6G fluorophore. Furthermore, it's detection limit is 1 mM cfor Hg^{2+} ion in aqueous phase.[222]

Chen et al. synthesised a ratiometric fluorescent chemosensor **L^{69}** (**Figure-1.49**) for the selective recognition of Hg^{2+} in aqueous medium. The detection limit was found to be 2.59 nM. In this chemosensor rhodamine-6G moiety grafted onto silica nanoparticles and strong fluorescence was observed.[223]

Liu et al. developed a fluorescent molecular probe **L^{70}** (**Figure-1.50**) for chemosensing Hg^{2+}. This probe was used successfully for cell imaging applications. The LODs was estimated to be 1.41nM in aqueous medium.[224]

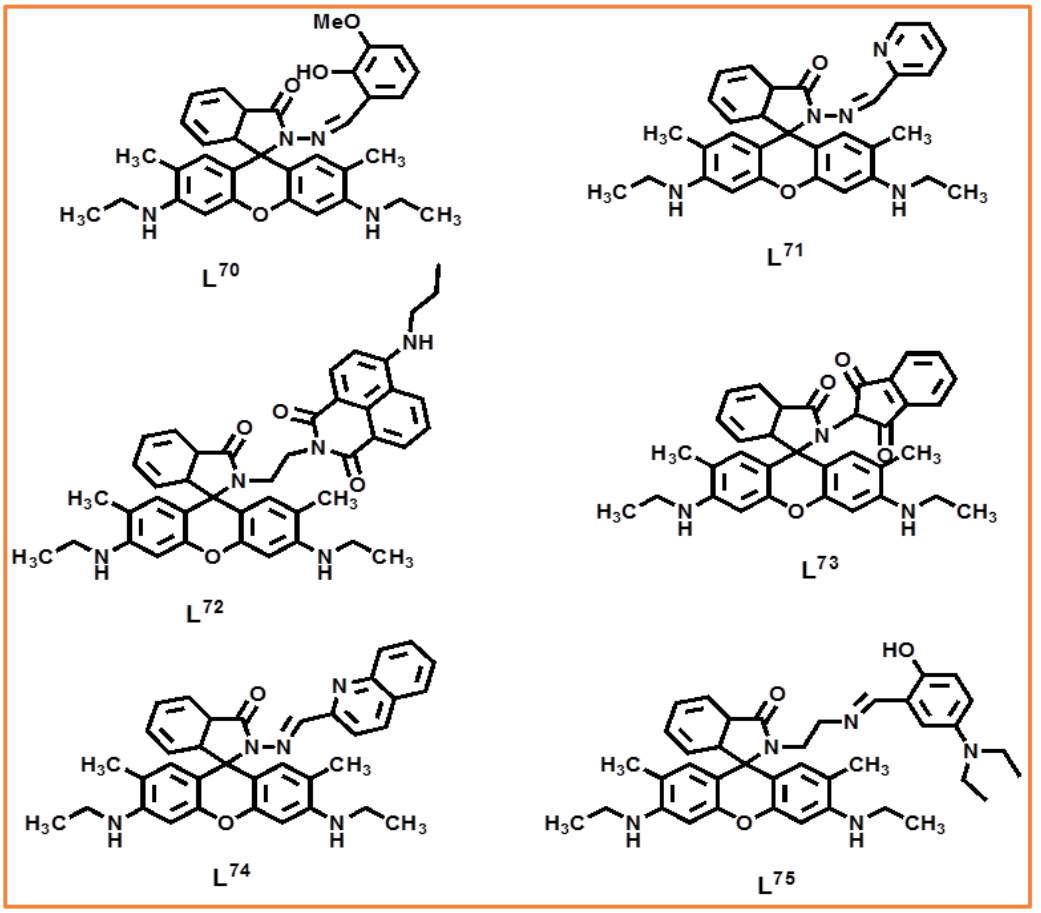

Figure-1.50: Structures of the chemosensors (L^{70}-L^{75}) containing "N, O" as coordinating atoms for Hg^{2+} sensing.

Duan et al. developed a chemosensor **L^{71}** (**Figure-1.50**) for selective detection of Hg^{2+} over other biological and environmentally important metal ions in aqueous medium. In the absence of Hg^{2+} there was very weak absorption band but after incremental addition of 2.5 equivalents a gradual built up of an absorption band appeared at 538 nm and a strong emission band observed at 560 nm along with naked eye colour change from colourless to pink. The detection limit for Hg^{2+} by this sensor was found to be in ppb level with the binding ratio 2:1 as delineated by Job's plot. The formation constant was calculated to be $2.4x10^{9}$ M^{-2}.[225]

Yao et al. prepared and reported rhodamine 6G-napthalimide based chemosensor **L**[72] (**Figure-1.50**) for the selectivedetection of Hg^{2+} in acetonitrile medium. The limit of detection was found to be 5.46 µM and the binding constant was calculated to be $4.36x10^5M^{-1}$.[226]

Das and co-workers also developed a new rhodamine-6G based chemosensor **L**[73] (**Figure-1.50**) which was found to be very much sensitive and selective towards Hg^{2+} along with the interference of Cr^{3+} in the presence of other metal ions. Binding of this probe with Hg^{2+} or Cr^{3+} results changes in their UV and fluorescence spectral pattern. The detection limit was found to be even lower than the permissibility of either [Hg^{2+}] or [Cr^{3+}] in safe drinking water according to standard U.S. EPA norms.[227]

Quang's et al. reported a rhodamine 6G -derived chemosensor **L**[74] (**Figure-1.50**) for the detection of Hg^{2+} in C_2H_5OH-H_2O solution (1/4, v/v) at pH 7.0 with an estimated formation constant 3.5×10^6 M^{-1} for the corresponding complexation process.[228]

Das and co-workers reported a new rhodamine-6G based chemosensor **L**[75] (**Figure-1.50**), functionalized with quinoline moiety, which could selectively detect Hg^{2+} with an interference from Cr^{3+} in CH_3CN-HEPES buffer (pH= 7.3). In both the cases visual change was significant to detect Hg^{2+} . Interestingly emission for quinolone was not observed due to C=N isomerization and intersystem crossing during Hg^{2+} ion detection. This probe was successfully used in imaging the human cancer cell (MCF7) for the detection of Hg^{2+} using confocal microscope.[229]

Tang and **Nandhakumar** et al. reported a novel rhodamine-6G based chemosensor **L**[76] (**Figure-1.51**), remarkably for the detection of Hg^{2+} through colorimetric and fluorometric methods in MeOH-H_2O (3:1, v/v) solution at pH 7.4. The naked eye colour change was observed only for Cu^{2+}in the same solvent mixture. In the presence of Cu^{2+} probe solution produces weak fluorescence due to quenching by paramagnetic Cu^{2+}. The binding stoichiometry was found to be 1:1 from Job's plot. The formation constants were estimated as 2.44×10^5 M^{-1} for Cu^{2+} and $3.4 \times 10^2M^{-1}$ forHg^{2+} using Benesi -Hildebrand plot.[230]

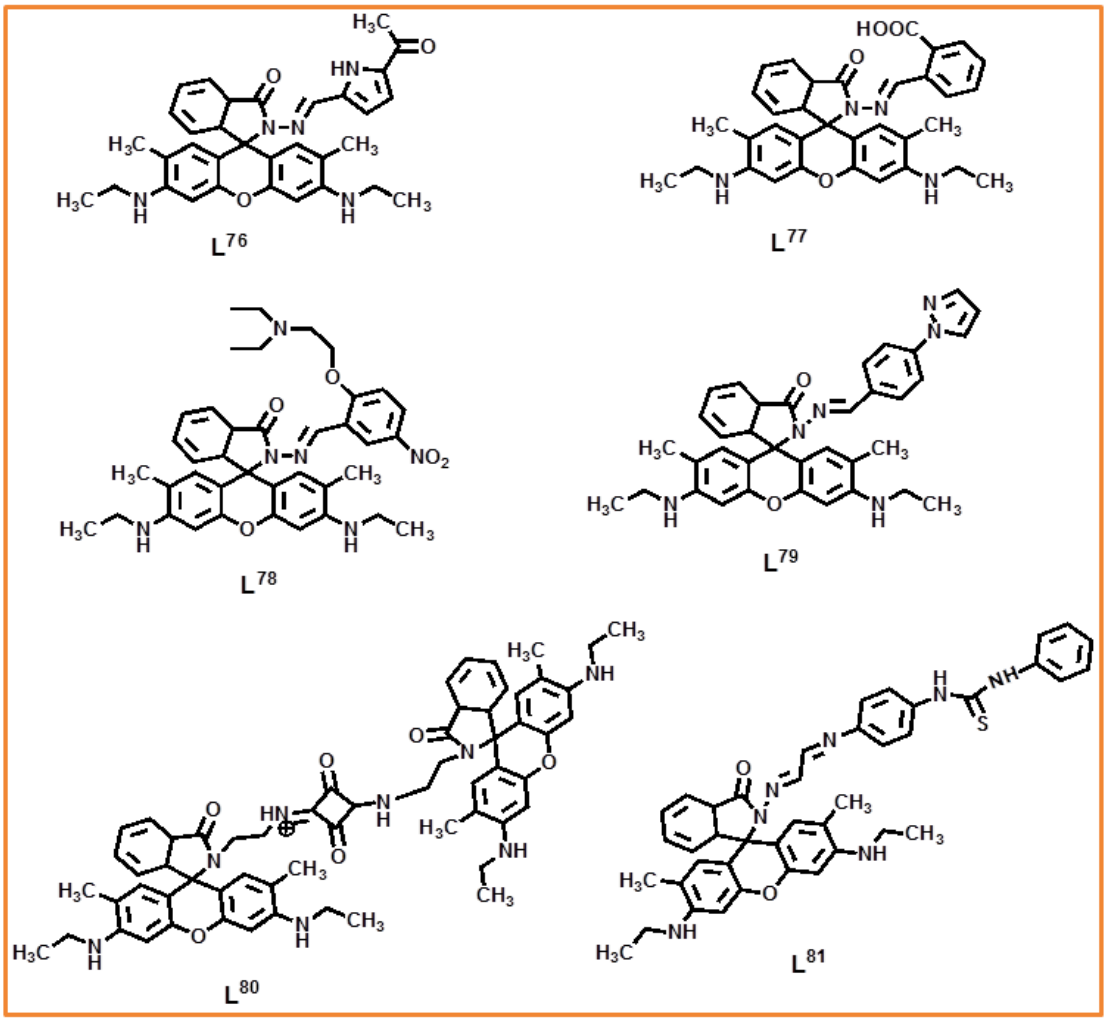

Figure-1.51: Structures of the chemosensors (L^{76}-L^{81}) containing "N, O" as coordinating atoms for Hg^{2+}sensing.

Das et al. developed a rhodamine-based chemosensor $\mathbf{L^{77}}$ (**Figure-1.51**) for the chromo-fluorogenic detection of Hg^{2+} in aqueous solution. $\mathbf{L^{77}}$ showed a colourimetric response for Cu^{2+} but change in fluorescence intensity was not observed. Whereas, other metals could not produce any change in color and fluorescence intensity under same conditions. Absorption titrations indicates that it can bind with Cu^{2+} and Hg^{2+} and forms Cu^{2+}-$\mathbf{L^{77}}$ and Hg^{2+} -$\mathbf{L^{77}}$ complexes with formation constants of 1.68 x 10^5M^{-1} and 8.0 x 10^5M^{-2} respectively in water-methanol (1:1,v/v) at pH =7.0 . $\mathbf{L^{77}}$ can be utilized to detect the Hg^{2+} using optical microscope on the cell surface of Pseudomonas putida where bacteria cell colour changed from colourless to pink after application with $\mathbf{L^{77}}$.[231]

Ali and his group developed a chemosensor **L^{78}** (**Figure-1.51**) for the detection of Hg^{2+} which exhibited asurfactant modified aggregation resulting emission enhancement. **L^{78}** recognises Hg^{2+} over other biologically important metal ions very selectively and rapidly. The detection limit was found to be 78 nM. The ligand **L^{78}** exhibited an intense 316-fold enhanced emission intensity at 553 nm (λ_{ex} 510 nm) in H_2O-CH_3CN (8:2, v/v, pH=7.2). The 1:1 binding stoichiometry was determined from Job's plot and the formation constant was calculated to be $2.39x10^4$ $M^{-1}$from absorption studies and $2.02x10^4$ M^{-1} from fluorescence studies.TEM studies showed aggregation of **L^{78}** in the presence of 9 mM SDS. The quantum yield and association constant were found to be enhanced in the presence SDS than its absence. Also the fluorescence intensity of **L^{78}** was found to enhanced by 143 fold in the presence of SDS as compared to only in the presence og Hg^{2+}.This probe **L^{78}** showed a cytoplasmic cell imaging application with negligible cell cytotoxicity.[232]

Duan et al. reported an efficient and sensitive colorimetric chemosensor **L^{79}** (**Figure-1.51**) for the detection of Hg^{2+} in water. The UV-Vis and fluorescence studies reveal that this probe selectively binds with Hg^{2+} and forms a complex resulting visual colour change from colourless to pink. A prominant emission band appeared at 575 nm upon excitation at 525 nm in DMSO-Water (1:1, v/v). The detection limit for Hg^{2+} was calculated to be $2.07x10^{-8}$M and the binding ratio was found to be 1:1 from the Job's plot.^{1}HNMR and FT-IR spectroscopic studies demonstrated a chelation enhanced fluorescence (CHEF) mechanism. Reversibility study was performed with **L^{79}** by EDA. When EDA is added to **L^{79}**-Hg^{2+} complex the fluorescence intensity was found to decreased abruptly due to demetallation.[233]

A. Son reported a novel chemosensor **L^{80}** (**Figure-1.51**) squarine-bis(rhodamine-6G) for the detection of Hg^{2+} very selectively. Sensing behaviour of this probe was tested in the presence of different cations and found to be highly selective to Hg^{2+} with "Turn-ONresponse. **L^{80}** produced an absorption peak at 527nm and emission peak at 553 nm with 200-fold enhanced fluorescence intensity in 10 µM CH_3CN solution. The binding stoichiometry between **L^{80}** and Hg^{2+} was found to be 1:1 from the Job's plot. The LOD and formation constant were calculated to be $1.69x10^{-9}$M and $9x\ 10^8M^{-1}$ respectively.[234]

A. Son et al. developed a dual fluorescent and colorimetric chemodosimeter **L^{81}**(**Figure-1.51**) by modification of thiourea derivative for the recognition of Hg^{2+}. This probe showed high

selectivity and sensitivity towards Hg^{2+} in the presence of other metal ions with the appearance of an absorption and emission band at 530 nm and 556 nm respectively in acetonitrile solvent. The fluorescence intensity was found to be enhanced by 1000 fold after the addition of 1.8 equivalent Hg^{2+}. The detection limit was reported as $4.52x10^{-7}M$ and the proposed binding stoichiometry is 1:1 from the Job's plot.[235]

Wanichacheva et al. reported [5]-helecene containing rhodamine 6G based colorimetric and fluorometric chemosensor, **L^{82} (Figure-1.52)** for Hg^{2+} detection based on FRET mechanism. In this FRET mechanism helecene acted as donor and **L^{82}**-Hg^{2+} complex as acceptor. The detection limit of **L^{82}** for the detection of Hg^{2+} was found to be 2.3ppb. The event of complexation followed by ring opening was confirmed from the visual colour change from colourless to greenish yellow and from the enhancement of the fluorescence intensity. This probe exhibited a strong absorption and emission band at 528 nm and 549 nm respectively upon excitation at 373nm in 10% aqueous acetonitrile. The excitation and emission wavelength indicate the operation of FRET process. The quantum yield was increased from 0.01 to 0.35 after addition of Hg^{2+}.The binding stoichiometry was determined from Jobs' plot as 1:1 and the formation constant was estimated to be $4.09x10^{4}M^{-1}$.[236]

Das et al. reported a FRET based chemosensor **L^{83}** (**Figure-1.52**) where resonance energy transferred takes place from dansyl unit to rhodamine 6G moiety after binding with Hg^{2+} in mixed aqueous medium. The phenomenon of FRET was evident from generation of emission band on excitation at 340 nm which was an absorption maximum of dansyl unit. The efficiency of energy transfer from dansyl unit was 83% and rate constant for the transfer of energy process was calculated to be $2.84\ x10^{8}S^{-1}$. Although the probe **L^{83}** showed very little interference by Cu^{2+}, the association constant was calculated to be $5.0\ x\ 10^{4}\ M^{-1}$ for Hg^{2+}.[237]

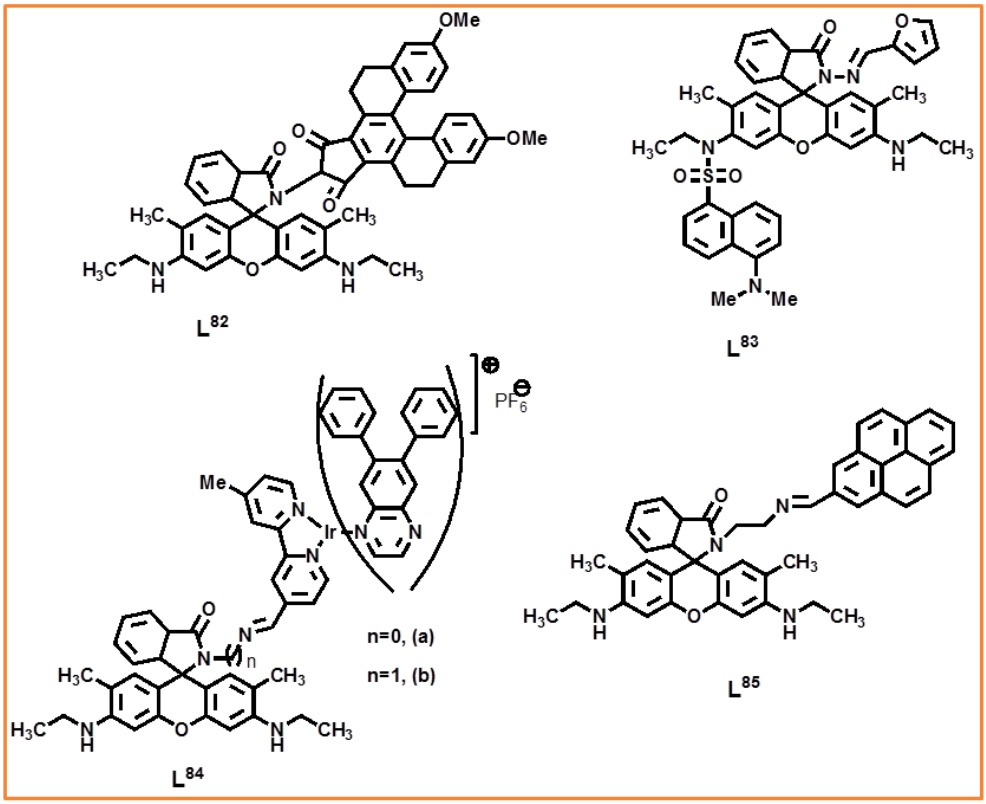

Figure-1.52: Structures of FRET based Chemosensors (L^{82}-L^{85}) equipped with Rho-6G unit for Hg^{2+}.

Wang and **Wong** recently reported afluorescent chemosensors $\mathbf{L^{84}}$ (**Figure-1.52**) (a and b), composed of rhodamine unit and a luminescent iridium (III) complex. A very weak fluorescence emission at 555 nm was observed from rhodamine unit of L^{84} (a) when excited at 365 nm. When Hg^{2+} is added to methanolic solution of $\mathbf{L^{84}}$ it results a development of an emission band of originated from iridium(III)-based MLCT at 675 nm due to the energy transfer from rhodamine to the iridium(III) luminophore. Whereas, no such change in the emission intensity of the iridium (III) luminophore in $\mathbf{L^{84}}$ (b) observed. The inefficient energy transfers in $\mathbf{L^{84}}$ (b) is due to the non-conjugated ethyl group linker between rhodamine and the iridium (III) luminophore.[238]

Ghosh and his group developed chemosensor $\mathbf{L^{85}}$ (**Figure-1.52**) composed of pyrene and rhodamine-6G moiety for the selectively detection of Hg^{2+} over other cations. Solution containing $\mathbf{L^{85}}$ shows change in colour from colorless to pink in the presence of Hg^{2+}. The UV–Vis study shows appearance of an absorption peak at 525 nm with a Ɛ value of 5.2 x 10^4 M^{-1} cm^{-1} due to opening of rhodamine spirolactam ring. It is also an example of Fluorescence Resonance

Energy Transfer (FRET) mechanism induced by Hg^{2+} resulting energy transfer from pyrene donor unit to the Rhodamine 6G acceptor unit.[239]

Duan's group developed ferrocene attached rhodamine-6G based multi-responsive chemosensors, **L**[86] and **L**[87] and **L**[88] (**Figure-1.53**) for the recognition of Hg^{2+} in aqueous medium. A 'turn-ON' response was found after binding with Hg^{2+}. Due to the presence of ferrocene unit in the ligand the binding event was monitored by the ferrocene/ ferrocenium couple potential upon binding with Hg^{2+}. Formation of the complex was evident from Job's plot and electrospray-ionization mass spectrometry (ESI-MS). The association constant was estimated to be 1.16 x 10^6 M^{-1}. The chemosensor **L**[87] bearing two fluorescent active rhodamine groups showed affinity to Hg^{2+} with an association constant of 2.8 x $10^5 M^{-1}$. The 1: 1 binding stoichiometry between ligand and Hg^{2+} was confirmed from the Job's plot. [240,241]

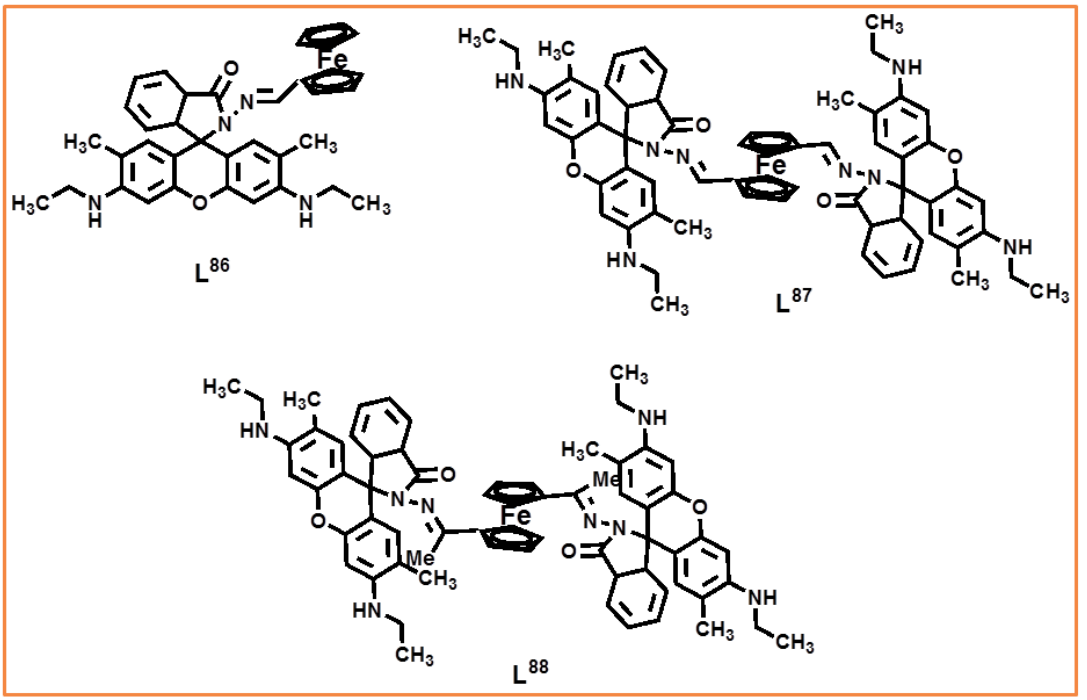

Figure-1.53: Structure of Rhodamine 6G-based chemosensors (L[86]-L[88]) having ferrocene unit for the recognition of Hg^{2+}.

1.8.6 Brief Literature Survey on Zn^{2+} Chemosensors

Zinc is essential element, obtained from shellfish, meat and diary like foods. It is needed to develop body immune power, for cell growth, cell division. During pregnancy and childhood zinc is needed for proper development. So, its detection is very much needed in biological and environmental samples. Design and synthesis of Rhodamine-6G based fluorescent chemosensors for Zn^{2+} is mentioned as follows.

Mashraqui et al. prepared a rhodamine 6G-based chromo and fluorogenic chemosensor **L^{89}** (**Figure-1.54**) which can detect Zn^{2+} at the micromolar concentrations level in the biological and environmental samples. The solution containing **L^{89}** changes from colourless to orange just after the addition of Zn^{2+} and it showed a strong emission band due to opening of spirolactam ring .[242]

Chellapa and his group reported a rhodamine 6G based" turn-on" fluorescent chemosensor **L^{90}** (**Figure-1.54**) for Zn^{2+}. This probe showed a strong absorption and emission band due to the opening of spirolactam ring in phosphate buffer solution (pH =7.54). The formation constant was calculated to be 3.43 x 10^2 M^{-1}. Zn^{2+} in Escherichia coli cells has also been well studied with this probe.[243]

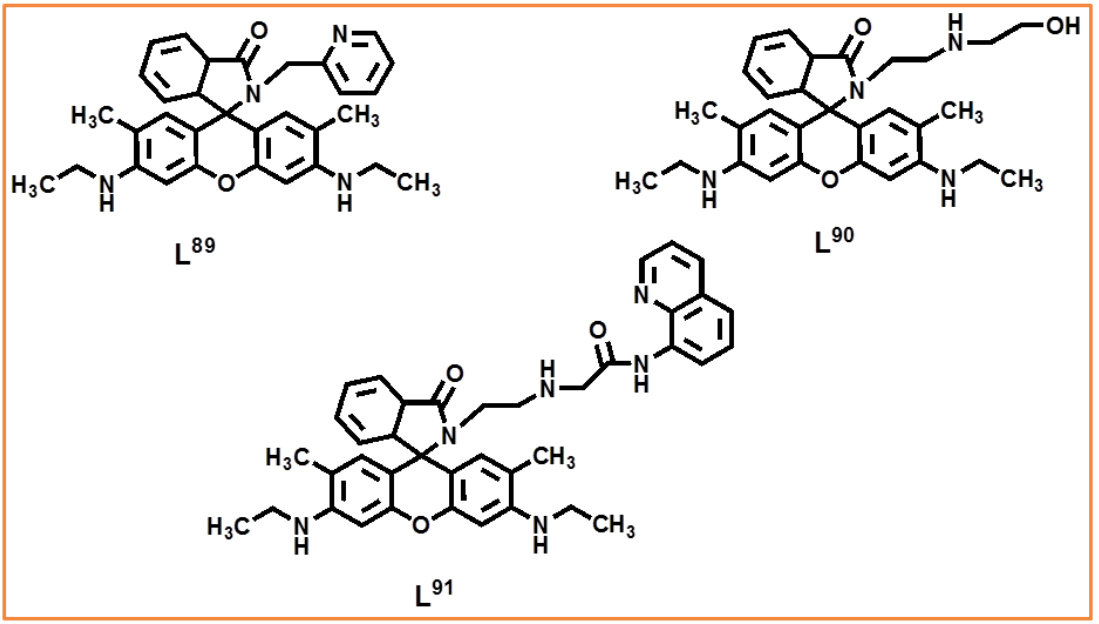

Figure-1.54: Structure of Rhodamine 6G-based chemosensors (L^{89}-L^{91}) for Zn^{2+}.

A fluorescent, colorimetric chemosensor **L^{91}** (Figure-1.54) consist of 8-aminoquinoline attached rhodamine-6G, has been developed for the recognition of Zn^{2+}. It exhibits high selectivity and sensitivity towards Zn^{2+} over other divalent and trivalent metal ions in a physiological pH range. This chemosensor showed a 1:1 binding mode between the probe and Zn^{2+} evident from Job's plot. The formation constant of **L^{91}** with Zn^{2+} was estimated to be $2.9x10^4$ M^{-1} in CH_3CN/H_2O (95:5, v/v) solution. This chemosensor is cell-permeable and biocompatible too.[244]

1.8.7 Brief Literature Survey on Ca^{2+} Chemosensors

Calcium is one of the most abundant element in our body. Many biological processes like nerve impulse transmission, muscle contraction and cardiovascular functions are assisted and controlled by calcium. Calcium is the key factor for the growth of teeth and bone and cofactor for many enzymes. Calcium deficiency causes osteopenia and osteoporosis, muscle problem, premenstrual syndrome, extreme fatigue depression and psychiatric disorders. So synthesis of highly selective fluorescent chemosensor for Ca^{2+} has drawn attraction for the researcher.

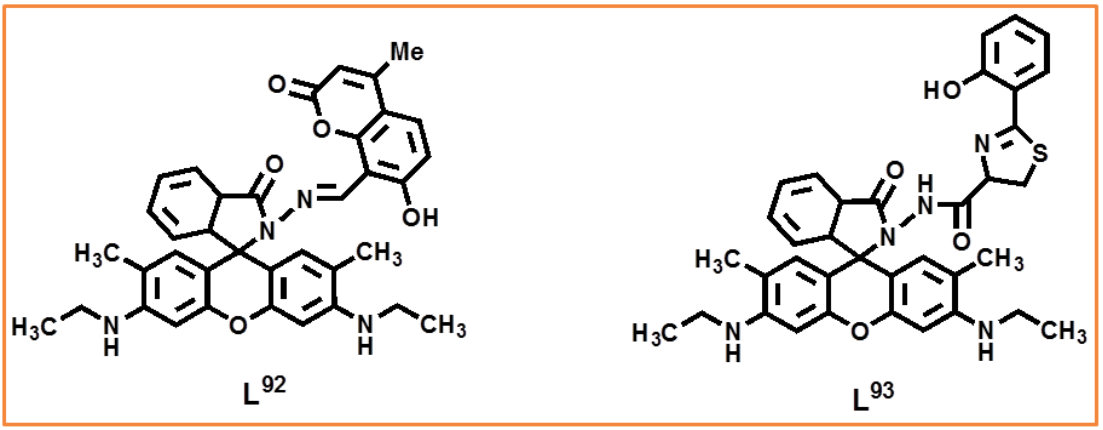

Figure-1.55: Structure of Rhodamine-6G based chemosensors (L^{92}- L^{93}) for Ca^{2+}.

Yang et al. reported a fluorescent chemosensor,7-hydroxy-4-methylcoumarincoumarin-8-carbaldehyde-rhodamine **L^{92}** (**Figure-1.55**) for the detection of Ca^{2+} through OFFON signaling mechanism. This probe **L^{92}** showed preferential binding with Ca^{2+} in the presence of other biologically important cations. The fluorescence intensity of **L^{92}** was enhanced by 64 fold after the addition of one equivalent Ca^{2+} along with the development of a strong emission band at 500

nm (λ_{ex} 419 nm). According to Yang the PET mechanism coupled with ICT process are responsible for the said fluorescence response. The binding ratio and formation constant with Ca^{2+} was estimated to be as 1:1 and $2.3x10^{7}M^{-1}$ respectively and the detection limit was evaluated as 30 ppb. The fluorescence intensity was found to quenched in the presence of Na_2EDTA indicated the reversibility of the chemosensing phenomenon.[245]

Chatterjee and his group reported a Ca^{2+} specific chemosensor **L^{93}** (**Figure-1.55**) that is used as staining agent in the Artemia living organism. A strong absorption band at 525 nm and emission band appeared at 548 nm after the addition of Ca^{2+} to 100% aqueous solution in HEPES buffer of the probe at pH=7.4. The fluorescence intensity enhancement was nearly 17 fold in the presence of Ca^{2+}. The binding stoichiometry was found to be 1:1. The interference of Cu^{2+} can be removed by L-cysteine. The detection limit calculated to be 70 nM and the formation constant was calculated as $0.3x10^{5}M^{-1}$. This fluorescent chemosensor could detect Ca^{2+} up to 5µM in the midgut region of gastrointestinal tract of the animal Artemia.[246]

1.8.8 Brief Literature Survey on Pb^{2+} Chemosensors

Pb^{2+} is very toxic and hazardous metal. This metal has adverse effect on human life like mental retardation, memory loss, anaemia and neurological disease. Its permissible limit, according to US environmental protection agency and Bureau Indian standard, is 0.05mg/L and 0.mg/L respectively. So detection of lead in various sample is a very challenging task to the scientist engaged in chemosensing field.

Bag and **Biswal** synthesised rhodamine 6G based probe as chromogenic and fluorogenic turn on chemosensor **L^{94}** and **L^{95}** for Pb^{2+} ion detection. In **L^{95}** aromatic secondary amine group attached to a bulky aromatic group (**Figure-1.56**). This bi-fluorophoric **L^{95}** probe in the presence of Pb^{2+} ions showed high selectivity and reversibility towards Pb^{2+} through conbined PET and FRET. The ratiometric fluorescence signalling pattern of **L^{95}** enable it for the detection of Pb^{2+} ion at low concentration even in the E. Coli living organism. This probe showed appearance of an absorption peak at 527 nm and emission peak at 555 nm in CH_3CN-H_2O (9.5:0.5, v/v) with an isobestic point at 515 nm. The complexation stoichiometry was found to be 1:1 (**L^{95}-Pb^{2+}**) and the association constant was found to be $2.312x10^{4}M^{-1}$ from the absorption data.[247]

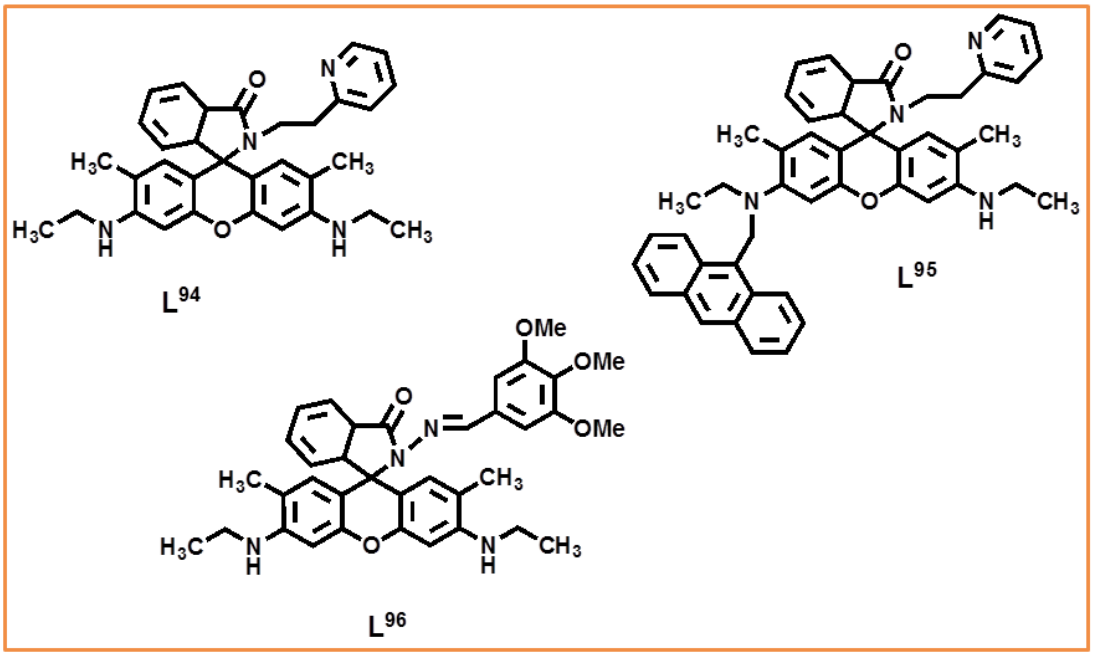

Figure-1.56: Structure of Rhodamine-6G based chemosensors (L^{94}-L^{96}) for Pb^{2+}.

Sivaraman and his group reported a rhodamine 6G based "turn-on" fluorescent chemosensor **L^{96}** (**Figure-1.56**) for the detection of Pb^{2+} in aqueous solution at nanomolar level. This probe witnessed a high selectivity and sensitivity towards Pb^{2+} with a change in colour of the solution to pink from colourless making it a naked eye detectable. An absorption band at 530 nm is the characteristic band for amide group of rhodamine and it found to be increased its intensity after the gradual addition of Pb^{2+}. In the presence of Pb^{2+} an emission band at 552 nm showed a 100-fold enhancement of fluorescence intensity after the gradual addition of 1.5 equivalent Pb^{2+}. DFT calculation exposed the observed spectral changes that took place due to internal charge transfer followed by spirolactam ring opening. Job's plot confirms the 1:1 binding stoichiometry between ligand and Pb^{2+}. The probe sensitivity demonstrated in living cells and can be used in cell imaging of Pb^{2+}.[248]

1.8.9 Brief Literature Survey on Pd^{2+} Chemosensors

Sinha and his group reported a rhodamine-6G appended turn–on fluorescent chemodosimeter $\mathbf{L^{97}}$ (**Figure-1.57**) for the detection of Pd^{2+} specifically in the presence of other cations. Chemosensing event involves Pd(II) triggered carbon-oxygen, allyl bond cleavage along with the spirolactam ring opening resulting fluorescence enhancement. This probe showed a strong absorption band at at 535nm and an emission band at 563nm with 22-fold enhancement in fluorescence intensity and in CH_3CN-water HEPES buffer (1: 4, v/v, pH =7.4). The detection limit was evaluated to be 50 nM.[249]

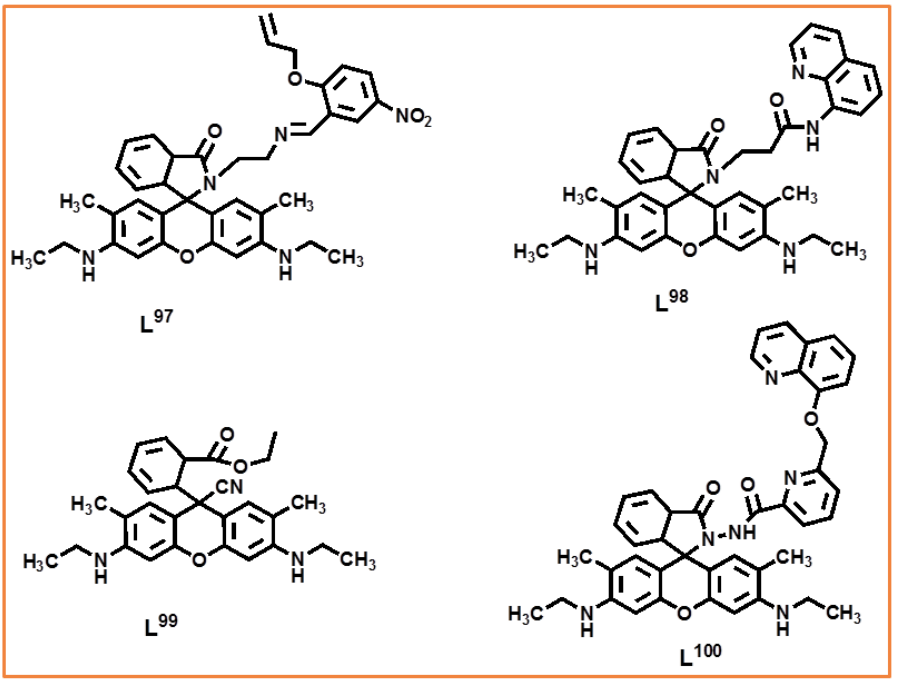

Figure-1.57: Structure of rhodamine-6G based chemosensors (L^{97}-L^{100}) for Pd^{2+}.

Goswami and his group reported "OFF-ON" colorimetric fluorescent chemosensor, $\mathbf{L^{98}}$ **(Figure-1.57)** for the selective detection of Pd^{2+}.They also reported X-ray crystal structure of $\mathbf{L^{98}}$. After addition of Pd^{2+} to the solution containing $\mathbf{L^{97}}$ an absorption band appeared at 540 nm and an emission band at 562 nm with the generation of pink colour of the solution. The binding ratio of $\mathbf{L^{98}}$ and Pd^{2+} was estimated to be 1:1 and the association constant was calculated to be $4.17x10^4M^{-1}$. The pink colour was found to be disappear after addition of S^{2-} in to the complex solution.[250]

Goswami and his group designed and synthesised a rhodamine-6G based chemosensor **L^{99}** **(Figure-1.57)** through green approach. This probe **L^{99}** showed a specific C-CN bond cleavage by the addition of Pd^{2+} followed by the development of a new colour and enhanced fluorescence intensity. In the presence of Pd^{2+} solution containing **L^{99}** produces an absorption band at 525 nm and in the presence of Pt^{2+} this band was less intensed. This probe showed an emission band at 555 nm with 22-fold enhanced intensity. The detection limit for Pd^{2+} was calculated to be 0.57μM. This chemosensing event was applied successfully for the bioimaging of Pd^{2+} in HeLa cells.[251]

Goswami and his group also synthesised a quinoline attached rhodamine-6G based fluorescent chemosensor **L^{100}** **(Figure-1.57)** for the detection of Cd^{2+} specifically in aqueous phase. A strong absorption band at 530 nm and emission band at 550 nm appeared after the addition of Cd^{2+} into the probe solution made of CH_3OH-HEPPES buffer (1:4,v/v pH=7.1). Enhancement of 14-fold in the emission intensity was observed in the presence of 2.0 equivalent of Cd^{2+}. During complexation host -guest binding stoichiometry was found to be 1:1 from the Job's plot and the association constant evaluated to be $2.38 \times 10^{-5} M^{-1}$. The LOD for Cd^{2+} was calculated to be 10^{-7} M level.[252]

1.8.10 Brief Literature Survey on $Au^{3+}$and Cd^{2+} Chemosensors

Lin et al. developed a reversible fluorescent gold chemosensor **L^{101}** (**Figure-1.58**). This gold chemosensor was prepared from the structural modification of a Cu^{2+} chemosensor. In the presence of Au^{3+} a strong emission band was appeared at 556 nm with 100 -fold enhanced fluorescence intensity in aqueous-ethanol medium (7:3, v/v) due to spirolactam ring opening. Job's plot revealed that 1:1 stoichiometric composition between the ligand and Au^{3+} and the formation constant was evaluated to be logK=5.56. The DFT calculation supports the proposed sensing mechanism. This probe was used as potential sensor for imaging Au^{3+} in the living cells.[253]

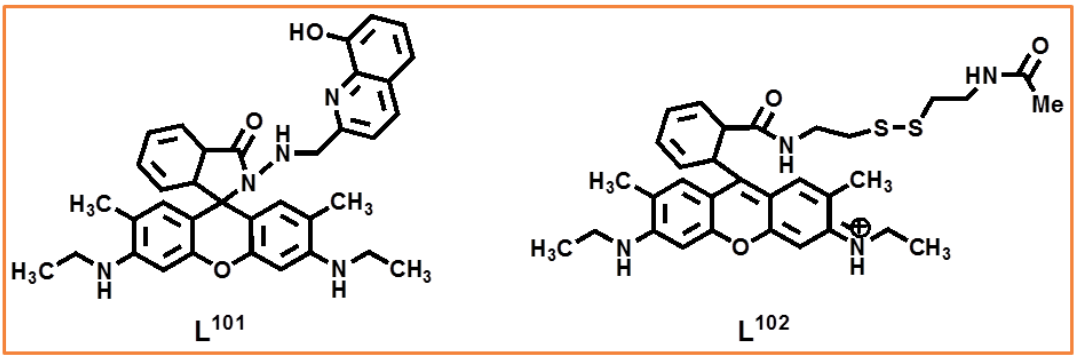

Figure-1.58: Structure of Rhodamine-6G based chemosensors (L^{101}-L^{102}) for Au^{3+}.

Mironenko et al. published a rhodamine-6G based fluorogenic chemosensor $\mathbf{L^{95}}$ (**Figure-1.58**) for the identification of Au^{3+} and Pd^{2+} in the aqueous phase. This probe after interaction with Au^{3+} and Pd^{2+}created a new product with different optical properties. Upon succesive addition of Au^{3+} and Pd^{2+} to the ligand solution separately results a decrement of the fluorescence intensity at 554nm. The detection limit for Au^{3+} and Pd^{2+} were estimated to be $2\text{-}10^{-7}$M or 0.02eqv.and $1\text{-}10^{-7}$M or 0.01 eqv. respectively. The binding ratios for Au^{3+} and Pd^{2+} with the probe was found to be 3:1 and the formation constant calculated to be $1.08\text{x}10^{8}$ and $8.35\text{x}10^{8}M^{-1}$respectively.[254]

1.9 Aim of the Thesis Works

Aim of the thesis is to present how to design and synthesize a fluorogenic probes based on rhodamine 6G framework for the selective detection of toxic and biologically relevant metal ions from different sources in aqueous and mixed aqueous medium. Conventional methods for the detection of analytes are complicated and not cost effective whereas optical detection methods which involves change in absorbance and fluorescence intensity of the probes in the presence of a particular metal ion should have the advantages like-

(i) It should be simple to apply

(ii) It should have very quick response time

(iii) It should be non-invasive in nature

(iv) It should be photo stable, cell permeable and useful for *in vitro* / *in vivo* cell imaging applications

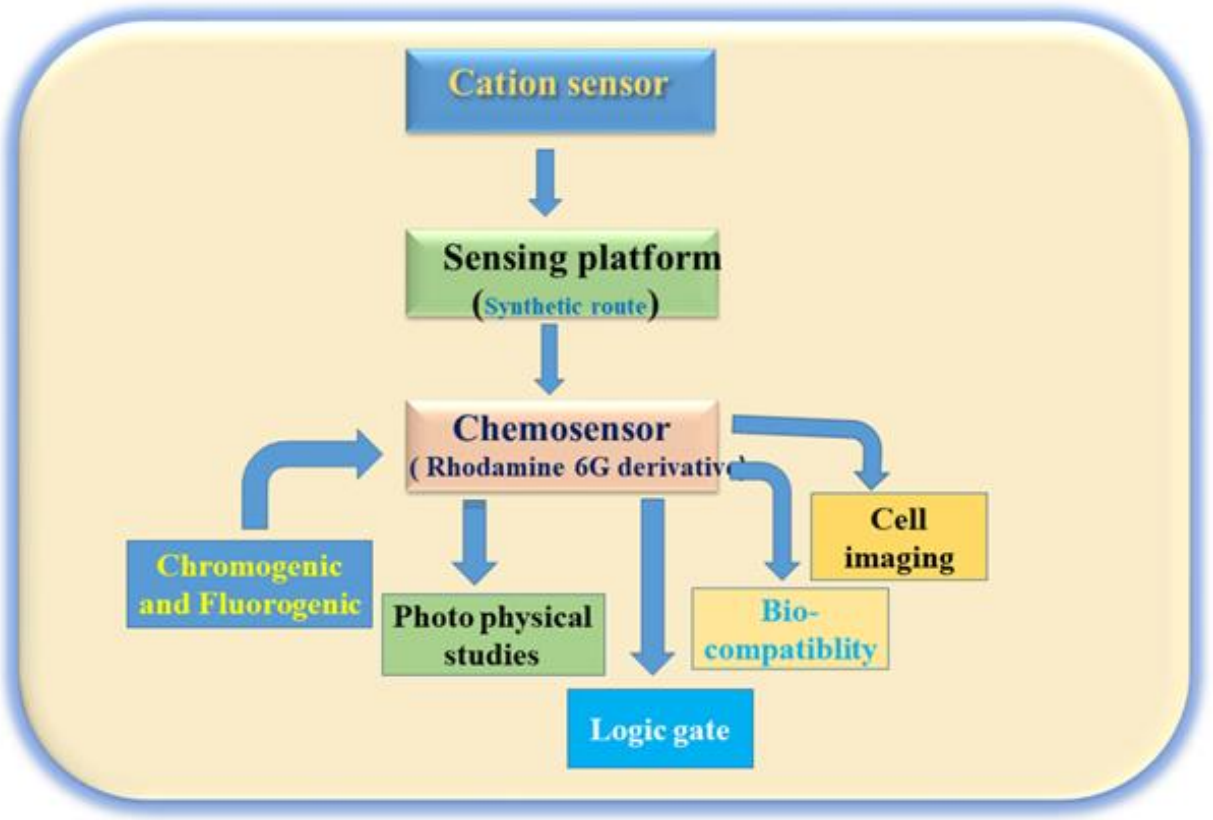

Figure-1.59: Schematic presentation of research work

So it is a good challenge to develop a portable molecular optical device. Optical sensors based on rhodamine moiety has drawn a great importance due to its excellent and exceptional photophysical properties as outlined above and so entire thesis is focused on the development of new rhodamine-6G based chemosensor for the detection and monitoring of metal ions .As quenching of fluorescence is less sensitive compared to fluorescence enhancement so "Turn-ON" fluorescent probe designing has attracted special attention to develop a chemosensor due to its reusability over chemodosimeter as it can act as irreversibly.

1.10 Present Work

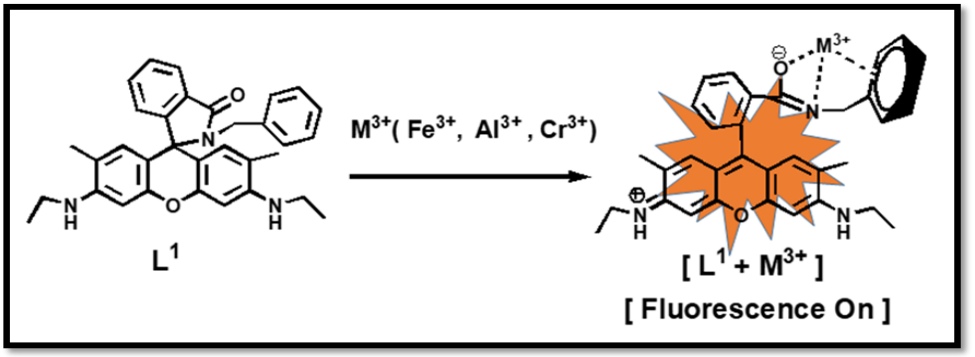

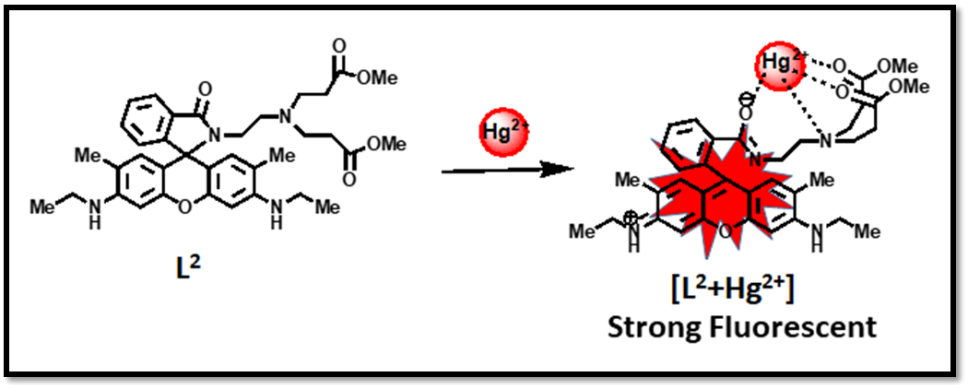

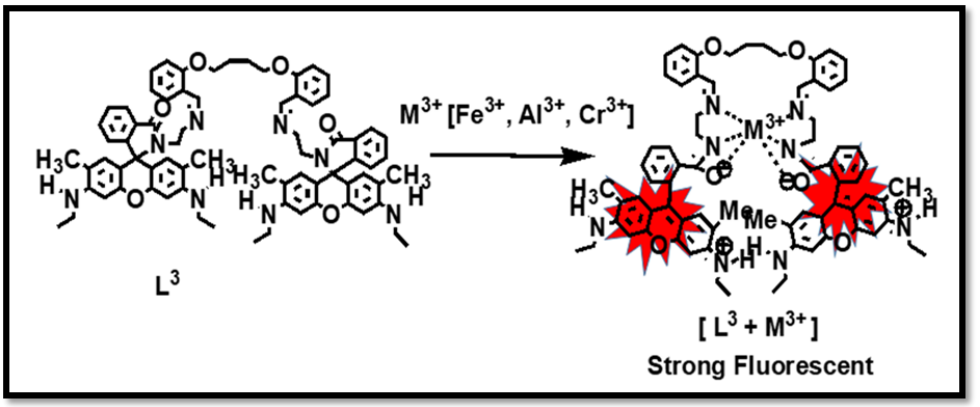

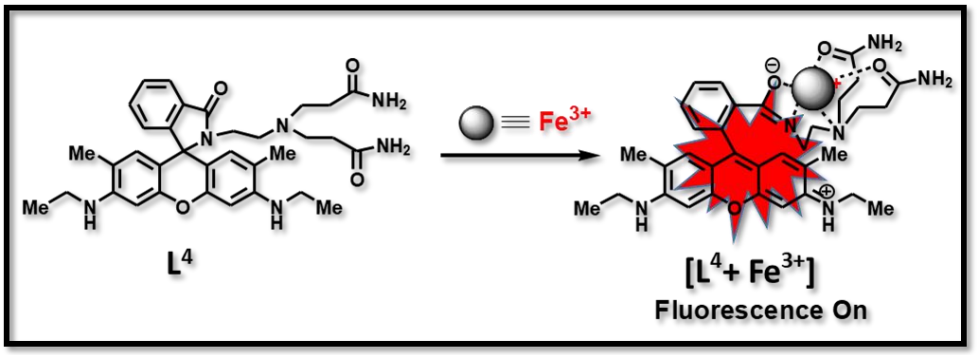

Figure-1.60: Design of target molecule and sensing of selective metal ions.

1.11 Physical Measurements

(i) ***Elemental analyses*:** Elemental analyses were carried out using a Perkin–Elmer 240 elemental analyzer.

(ii) ***FTIR spectra*:** Infrared spectra (400–4000 cm^{-1}) were recorded in the liquid state on a Nickolet Magna IR 750 series-II FTIR spectrometer.

(iii) ***^{1}H NMR and ^{13}C spectra*:** ^{1}H and ^{13}CNMR spectra were recorded in DMSO-d_6, $CDCl_3$, CH_3OD, CD_3CN on a Bruker 300 MHz NMR spectrometer using tetramethylsilane (δ = 0) as an internal standard.

(iv) ***UV-vis spectra*:** UV-vis spectra were recorded on an Agilent diode-array spectrophotometer (Model, Agilent 8453).

(v) ***Mass spectra***: ESI-MS^+ (m/z) of the ligands and corresponding metal complexes were recorded on a Waters' HRMS spectrometer (Model: QTOF Micro YA263 and XEVO G2QTof).

(vi) ***Fluorescence spectra*:** Steady-state fluorescence measurements were performed with a PTI QM-40 spectrofluorometer and Shimadzu spectro fluorometer (Model RF-5301).

(vii) ***Lifetimes measurements:*** Lifetimes were measured in Horiba–Jobin–Yvon on a Hamamatsu MCP photomultiplier (R3809) and analysed using IBH DAS6 software.

(viii) ***DFT calculations:*** Ground state electronic structure calculations of the ligand and complexes have been carried out using using Gaussian 09W software package, associated with the conductor-like polarizable continuum model (CPCM).

(ix) ***Cell imaging*****:** Cell imaging studies have been performed under fluorescence microscope. Bright field and fuorescence images of the HepG2 cells, HCT116 cells, were taken using a fuorescence microscope (Leica DM3000, Germany) with an objective lens of 40x,20x magnification.

(x) ***pH study:*** The pH of the solutions was recorded using a Systronics digital pH meter (Model 335, India) with the pH range 2–12. The pH meter was calibrated using standard buffer solutions (Acros Organics) of pH 4.0, 7.0 and 10.0.

References

1. A.W. Czarnik, "Fluorescent Chemosensors for Ion and Molecule Recognition" American Chemical Society, **1993**.
2. D. Wu, A. C. Sedgwick, T. Gunnlaugsson, E. U. Akkaya, J. Yoon, D.T. James, Chemical Society Reviews, **2017**, 46**(**23**)**, 7105.
3. B. Wang, Eric V. Anslyn. "Chemosensors: Principles, Strategies, and Applications", John Wiley & Sons. **2011**.
4. A.W. Czarnik, Accounts of Chemical Research, **1994**, 27(10), 302.
5. A.P.de Silva, H. Q.N. Gunaratne, T. Gunnlaugsson, A.J. Huxley, C.P. McCoy, J.T. Rademacher, T. E. Rice, Chemical Reviews, **1997**, 5, 1515.
6. J. M. Lehn, Angew. Chem. Int. Ed. Engl., **1988**, 27, 89.
7. D. J. Cram. Angew. Chem., Int. Ed. **1988**, 27, 1009.
8. B. Valeur, I. Leray, Coord. Chem. Rev., **2000**, 205, 3.
9. L. R Sousa, J. M. Larson, J. Am. Chem. Soc., **1977**, 99, 307.
10. J. P Konopelski, F. K. Hibert, J.M. Lehn, J.P. Desvergne, F. Fagès, A. Castellan, H. B. Laurent, J. Chem. Soc., Chem. Commun., **1985**, 433.
11. A.P. de Silva, S. A. de Silva, J. Chem. Soc., Chem. Commun., **1986**, 1709.
12. G. Grynkiewicz, M. Poenie, R. Y. Tsien, J. Biol. Chem., **1985**, 260, 3440.
13. M. E Huston, K. W Haider, A. W. Czarnik, J. Am. Chem. Soc., **1988**, 110,4460.
14. M. Mayer, A. J. Baeumner, Chem. Rev., **2019**, 119, 7996.
15. G.K. Mishra, A. Barfidokht, F. Tehrani, R.K. Mishra. Foods, **2018**, 7, 141.
16. A. Psichas, F. Riemann, F.M. Gribble, J. C. Invest., **2015**, 125, 908.

17. T. R. Gairola, B. Ware, Ancient India Bulletin of the Archaeological Survey of India,**1956**, 12, 116.

18. M. Triassi, R. Alfano, M. Illario, A. Nardone, O. Caporale. Int. J. Environ. Res. Public Health **2015**, 12, 1216.

19. S. W. Ragsdale, Chem. Rev., **2006**, 106, 8, 3317.

20. J. Zheng, M. C. Trudeau, "Hand book of ion channel", CRC Press, 1st edition, **2015**.

21. A. G. S. Györgyi, Biophys J., **1975**, 15, 707.

22. A. C. Ross, B. Caballero, R. J. Cousins, K. L. Tucker, R. G. Ziegler, "Modern Nutrition in Health and Disease", Wolters Kluwer Health Adis (ESP). 11th ed. ,**2014**.

23. J. W. Erdman, I. A. Macdonald, S. H. Zeisel, P. J. Aggett, Iron. In., **2012**, 10th ed., 506.

24. P. M. Coates, J. M. Betz, M. R. Blackman, G. M. Crag, M. Levine, J. Moss, J. D. White. Encyclopedia of Dietary Supplement", Informa healthcare, 2nd ed., **2010**, 527.

25. R. Casiday, R. Frey, "Iron Use and Storage in the Body: Ferritin and Molecular Representations". **2007** Washington University, St. Louis, MO 63130.

26. R. C. Hider, X. Kong. "Iron: Effect of overload and deficiency". Springer Science and Business Media BV, **2013**, 229.

27. J. Osredkar, N. Sustar, Journal of Clinical Toxicology, **2011**, S3, 1.

28. S. C. Burjonrappa, M. Miller, Journal of Pediatric Surgery, **2012**, 47, 760.

29. C. A. Heyneman, Ann Pharmacother., **1996**,30,186.

30. W. Maretm, H. H. Sandstead, Journal of Trace Elements in Medicine and Biology, **2006**, 20, 3.

31. M. Hambidge, The Journal of Nutrition, **2000**,130, 1344S.

32. R. Uauy, M. Olivares, M. Gonzalez, Journal of Clinical Nutrition, **1988**, 67(5), 952.

33. M. Angelova, S. Asenova, V. Nedkova, R. Koleva-Kolarova, Trakia Journal of Sciences, **2011**, 9(1), 88.

34. H. Kodama, C. Fujisawa., Metallomics, **2009**, 1(1), 42.

35. S. G. Kaler, C. J. Liew, A. Donsante, J. D. Hicks, S. Sato, J. C. Greenfield, Journal of International Medicine and Dentistry, **2010**, 33(5), 583.

36. M. Umair. M. Alfadhel. Cells, **2019**, 8, 1598.

37. A. C. Ross, B. Caballero, R. J. Cousins, K. L. Tucker, T. R. Ziegler. "Modern Nutrition in Health and Disease". 11th ed., **2012**, 159.

38. W. Mertz, Physiological Reviews, **1969**,49,163.

39. R. A. Anderson, Journal of the American College of Nutrition, **1998**, 17, 548.

40. G. Flora, D. Gupta, A. Tiwari, Interdisciplinary Toxicology, **2012**, 5(2), 47.

41. U.S. Food and Drug Administration.: U. S. Department of Health and Human Services, **2015**, 41.

42. Centers for Disease Control and Prevention (**2002**), Atlanta, GA: United States Department of Health and Human Service.

43. J. Luevano, C. A. Damodaran, Journal of environmental pathology, toxicology and oncology, **2014**, 33(3), 183.

44. M.P. Waalkes. Mutat Res. **2003**, 533(1-2), 107.

45. M. Hartmann, A. Hartwig, Carcinogenesis. **1998**, 19(4), 617.

46. B. Messner, M. Knoflach, A. Seubert, Arteriosclerosis, thrombosis, and vascular biology.**2009**, 29(9), 1392.

47. A. Engström, S. Skerving, J. Lidfeldt, A. Burgaz, T. Lundh, G. Samsioe, M. Vahter, A. Akesson, Environ Res., **2009**, 109, 188.

48. A. P. de Silva, D. B. Fox, A. J. M. Huxley and T. S. Moody, Coord.Chem. Rev., **2000**, 205, 41.

49. S. K. Kim, S. H. Lee, J. Y. Lee, J. Y. Lee, R. A. Bartsch and J. S. Kim, J. Am. Chem. Soc., **2004**, 126,16499.

50. H. N. Kim, M. H. Lee, H. J. Kim, J. S. Kim and J. Yoon, Chem. Soc.Rev., **2008**, 37, 1465.

51. D. T. Quang and J. S. Kim, Chemical Reviews, **2010**, 110, 6295.

52. X. Qian, Y. Xiao, Y. Xu, X. Guo, J. Qiana and W. Zhua, Chem. Commun., **2010**, 46, 6418.

53. Y. Zhou, Z. Xu and J. Yoon, Chem. Soc. Rev., **201**1, 40, 2222.

54. X. Chen, T. Pradhan, F. Wang, J. S. Kim, J. Yoon, Chem. Rev., **2012**, 112, 1910.

55. R.D. Beaty, J.D. Kerber, Perkin Elmer Shelton CT, **1993**, 8.

56. Z. Mester, R.E. Sturgeon. A.E. Amsterdam, Elsevier **2003**; 1033.

57. N. Eka, S. Retno, A. Rohman, Int Food Res J **2012**, 19, 937.

58. S. Gupta, P. Pandotra, A.P. Gupta, J.K. Dhar, G.R. Sharma, Y.S. Bedi, Food Chem Toxicol, **2012**,48, 2966.

59. J. R. Dean., D.J. Ando, John Wiley and Sons, **2008**, 2nd ed., 42.

60. R. J. C. Brown, M.J.T. Milton, Trends in Analytical Chemistry, **2005**,24, 266.

61. R. Barnes Trends in Analytical Chemistry, **1981**,1, 51.

62. F.L. Rasdi, N.K. A. Bakar, S. Mohamad, Int J Mol Sci., **2013**, 14, 3078.

63. M. Bıngöl, G. Yentür, Er B, A.B. Öktem, Czech Journal of Food Sciences **2010**, 28, 213.

64. B. Beckhoff, B. Kanngießer, N. Langhoff, R. Wedell, H. Wolff. Handbook of practical X-ray fluorescence analysis. Berlin, Springer **2007**.

65. J. F. Zhang, Y. Zhou, J. Yoon and J. S. Kim, Chem. Soc. Rev., **2011**, 40, 3416.

66. M. Formica, V. Fusi, L. Giorgi and M. Micheloni, Coord. Chem. Rev., **2012**, 256, 170.

67. L, Xin, Y.Z. Chen, L.Y. Niu, L.Z. Wu, C.H. Tung, Q.X. Tong, Q.Z. Yang, Org. Biomol. Chem., **2013**, 11, 3014.

68. J. G. Haub; Y. He; R. T. White, "Spectroscopic Applications of Pulsed Tunable Optical Parametric Oscillators".**2016**,17 (3rd ed.).

69. L. Bruneau, V. Jakši´, Y. Last, C.A. Pillet, *Commun. Math. Phys.*, **2016**, 344 (3), 959.

70. N. A. Sinitsyn, Y. V. Pershin, "The theory of spin noise spectroscopy: A review"cond-mat. mes-hall, **2016**.

71. D. L. Pavia, G. M. Lampman, G. S. Kriz, J.R. Vyvyan, "Introduction to Spectroscopy" 5th ed., **2015**.

72. W. Kemp, "Organic Spectroscopy" Palgrave, London,**1991**.

73. D. C. Harris, M. D. Bertolucci, Symmetry and Spectroscopy:An Introduction to Vibrational and Electronic Spectroscopy,Dover Publications; New edition ,**1989**.

74. T. H. Roos, W.J.Price, Spectrochimica Acta Part B: Atomic Spectroscopy, **1971**, 26(5), 279.

75. G. M. Barrow, Introduction to Molecular Spectroscopy, McGraw-Hill, **1962**.

76. J. R. Lakowicz, Principles of Fluorescence Spectroscopy, Plenum Press, New York. **1983**.

77. C.N. Banwell, E.M. McCash, "Fundamentals of Molecular Spectroscopy" McGraw-Hill, 4th ed., **1994**.

78. International Refereed Journal of Reviews and Research Volume 3 Issue 5 September **2015**.

79. N.J. Turro, V. Ramamurthy, W. Cherry, W. Farneth, Chem. Rev. **1978**, 78, 125.

80. A. Z. Weller, Phys. Chem. (Frankfurt am Main) 1955, 3, 238, Discuss. Faraday Soc. **1959**, 27, 28.

81. J. Kommandeur, Recl. Trav. Chim. Pays-Bas 1983, 102, 421; K.F. Freed. Acc. Chem. Res. **1978**, 11, 74.

82. a) R. Li, E.C Lim, Chem. Phys. **1972**, 57, 605; b) R. Sharf, Silbey, Chem. Phys. Lett. **1970**, 5,314; c) E.W Schlag, S. Schneider, S.F. Fischer, Annu. Rev. Phys. Chem. 1971,

22, 465, 490. d) A. J. Samanta, Am. Chem.Soc. **1991**, 113, 7427. e) R. Tanaka, Y. Kuriyama, H. Itoh, H. Sakuragi, K. Tokumaru, Chem.Lett. **1993**, 1447; f) M. Ohsaku, N. Koga, K. Morokuma. J. Chem. Soc. Perkin Trans. 2 **1993**, 71.

83. S. K Lower, M.A. El-Sayed, Chem. Rev. **1966**,66, 199.

84. National Academemis Press: Washington, DC, USA, **1995**; Chapter 6, 73.

85. P. Ripka, A. Tipek, Hand Book of Modern Sensors, 1st ed., ISTE LTD: London, **2007**, 49.

86. P. Grundler, "Chemical sensor: an introduction to scientists and engineers", 5th ed., Springer: Berlin, **2007**, 1, 1.

87. R. Martínez-Máñez, F. Sancenón, Chem. Rev., **2003**, 103, 4419.

88. Bissell, A. P. de Silva, P. H. Q. N. Gunaratne., P. L. M. Lynch, G. E. M Maguire, K. R. A. S Sandanayake, Chem. Soc. Rev., **1992**, 187.

89. S. L. Wiskur, H. Aït-Haddou, J. J. Lavigne, E. V. Anslyn, Acc. Chem. Res., **2001**, 34, 963.

90. B. Valeur, I. Leray, Coord. Chem. ReV., **2000**, 205, 3.

91. (a) M. Inouye, K. Hashimoto, K.J. Isagawa, J. Am. Chem. Soc., **1994**,116, 5517. (b) K.N. Koh, K. Araki, A. Ikeda, H. Otsuka, S.J. Shinkai, J. Am. Chem. Soc. **1996**, 118, 755.

92. A. Metzger, E.V. Anslyn, Angew. Chem., Int. Ed., **1998**, 37, 649.

93. K. Niikura, K.; Metzger, A.; Anslyn, E. V. J. Am. Chem. Soc., **1998**, 120, 8533.

94. J. J. Lavigne, E.V. Anslyn, Angew. Chem., Int. Ed., **1999**, 38, 3666.

95. S. L. Wiskur, E.V. Anslyn, E. V. J. Am. Chem. Soc., **2001**, 123, 10109.

96. M. Suresh, A. Shrivastav, S. Mishra, E.E. Suresh, A. Das, Org. Lett., **2008**, 10, 3013.

97. Z.Q. Hu, X. M. Wang, Y. C. Feng, L. Ding, M. Li, C.S. Lin, Chem. Commun., **2011**, 47, 1622.

98. Y.K. Yang, K.J. Yook, J.J. Tae, J. Am. Chem. Soc. **2005**, 127, 16760.

99. F. Song, S. Watanabe, P.E. Floreancig, K.J. Koide, J. Am. Chem.Soc., **2008**, 130, 16460.

100. V. Dujols, F. Ford, A.W. Czarnik, J. Am. Chem. Soc., **1997**, 119, 7386.

101. J.P. Desvergne, A.W. Czarnik, NATO Asi Series, Series C; Kluwer Academic Publishers: London, **1997**.

102. C. Suksai, T. Tuntulani, Chem. Soc. ReV., **2003**, 32, 192.

103. H. Tsukube, S. Shinoda, Chem. ReV., **2002**, 102, 2389.

104. L. Pu, Chem. ReV., **2004**, 104, 1687.

105. J. Wu, B. Kwon, W. Liu, Eric V. Anslyn, P. Wang, J. Seung Kim. Chem. Rev. **2015**, 115, 7893.

106. Li, X., Gao, X.; Shi, W.; Ma, H. Chem. Rev. **2014**, 114, 590.

107. A. M. García-Campaña, W. R. G. Baeyens, *Analusis*, **2000**, 28, 686–698, 2000.

108. U. Mitschke P. Bäuerle, J. Mater. Chem., **2012**, 22, 24981.

109. A. MoroñoE, R.Hodgson , Journal of Nuclear Materials , **1995**, 224(3), 216..

110. A. J. Walton, G. T. Reynolds, Sonoluminescence, **1984**, 33, 595.

111. D. C. Magri, Analyst, **2015**, 140, 7487.

112. A. P. Davis, John E. O'Brien, M. Glynn, Organic letters, **2002**, 4, 15, 2449.

113. R. Ali, S. S. Razi, R. C. Gupta, S. K. Dwivedi, A. Misra. New J.Chem., **2016**, 40, 162.

114. K. L. Diehl, E. V Anslyn, Chem. Soc. Rev. **2013**, 42, 8596.

115. K. L. Diehl, E. V. Anslyn, Chem. Soc. Rev. **2013**, 42, 8596.

116. Z. Zhou, M. Yu, H. Yang, K. Huang, F. Li, T. Yi and C. Huang, Chem. Commun., **2008**, 3387.

117. P. Thirupathi, J.Y. Park, L. N. Neupane, Y. L. N. Mallela, Kishore, Lee. Keun-Hyeung, ACS Appl. Mater. Interfaces **2015**, 7, 14243.

118. T. Gunnlaugsson, A. P. Davis, J. E. O'Brien, M. Glynn, Organic Letters, **2002**, 4, 15, 2449**.**

119. H. Liu, P. Yu, D. Du, C. He, B. Qiu, X. Chen and G. Chen, Talanta., **2010**, 81, 433.

120. L. Yang, Q. Song, K. Damit-Og and H. Cao, Sens. Actuators B, **2013**, 176, 181.

121. Metivier, I. Leray, B. Valeur, Chemistry-a Eur.opean Journal, **2004**, 10, 4480.

122. G. Bergamini, L. Boselli, P. Ceroni, P. Manca, G. Sanna and M. Pilo, Eur. J. Inorg. Chem., **2011**, 4590.

123. H. J. Jeong, Y. Li, M. H. Hyun, Bulletin of the Korean Chemical Society, **2011**, 32, 2809.

124. S.M.Cheung, W.H.Chan, Tetrahedron, **2006**, 62, 8379.

125. M. Yuan, Y. Li, J. Li, C. Li, X. Liu, J. Lv, J. Xu, H. Liu, S. Wang, and D. Zhu, Organic Letters, **2007**, 9(12), 2313.

126. W. Jiang, Q. Fu, H. Fan and W. Wang, Chem. Commun., **2008**, 259.

127. K. SaravanaMani,R. Rajamanikandan, B. Murugesapandian, R, Shankar, G. Sivaraman, M. Ilanchelian, S. P. Rajendran, Spectrochimica Acta Part A: Molecular and Biomolecular Spectroscopy, **2019**, 214, 170.

128. J. Bourson, J. Pouget, B. Valeur, Journal of Physical Chemistry, **1993**, 97, 4552.

129. Y. Zhou, Y. Xiao, S. Chi, X. Qian, Org. Lett., **2008**, 10, 633.

130. P. Mahato, S. Saha, E. Suresh, R. D. Liddo, P. P. Parnigotto, M. T. Conconi, M. K. Kesharwani, B. Ganguly and A. Das, Inorg. Chem., **2012**, 51, 1769.

131. N.J. Turo, Modern Molecular Photochemistry, **1991**.

132. T. Forster, Ann. Phys., **1948**, 2, 55.

133. T. Forster, Disc. Faraday Soc., **1959**, 27,7.

134. Y. Egawa, R. Hayashida, T. Seki, J. Anzai, Talanta, **2008**, 76, 736.

135. A. Sharma, S.G. Schulman, Introduction to Fluorescence Spectroscopy, Wiley Science, **1999**.

136. a) K. Kaur, R. Saini, A. Kumar, V. Luxami, N. Kaur, P. Singh and S. Kumar; Coordination Chemistry Rev., 2012, 256 ,1992. b) N. Kumar, V. Bhalla and M. Kumar, Analyst, **2014**, 139, 543.

137. N. I. Georgiev A. M. Asiri, A.H. Qusti, K.A. Alamryand V. B. Bojinov, Dyes Pigm., **2014**, 102, 35.

138. M. H. Lee, H. J. Kim, S. Yoon, N. Park, J. S. Kim. Organic Letters, **2008**, 10, 2, 213.

139. E. L. Quitevis, A. H. Marcus and M. D. Fayer, J. Phys. Chem.,**1993**, 97, 5762.

140. J. S. Kim, D. T. Quang, Chem. Rev. **2007**, 107, 3780.

141. E. M. Nolan, S. J. Lippard, Chem. Rev. **2008**, 108, 3443.

142. X. Chen, Y. Zhou, X. Peng, J. Yoon, Chem. Soc. Rev., **2010**,39, 2120.

143. Y. Zhou, Z. Xu, J. Yoon, Chem. Soc. Rev., **2011**, 40, 2222.

144. H. N. Kim, Z. Guo, W. Zhu, J. Yoon, H. Tian, Chem. Soc. Rev., **2011**, 40, 79.

145. Z. Xu, S.K. Kim, J. Yoon, Chem. Soc. Rev., **2010**, 39, 1457.

146. E. Noelting, K. Dziewonsky, Ber. Dtsch. Chem. Ges., **1905**, 38, 3516.

147. C. Wu , J. Wang , J. Shen , C. Zhang, Z. Wu, H. Zhou, Tetrahedron, **2017**, 73, 5715.

148. P. Madhu, P. Sivakumar, R. Sribalan, New J. Chem., **2019**,43, 14426.

149. R. P. Haugland, Handbook of Fluorescent Probes and Research Chemicals, 9th ed., **2002**.

150. F. Amat-Guerri, A. Costela, J. M. Figuera, F. Florido, R. Sastre, Chem. Phys. Lett., **1993**, 209, 352.

151. V. Dujols, F. Ford, A.W. Czarnik, J. Am. Chem. Soc., **1997**,119, 7386.

152. K. H. Drexhage, J. Res. Natl. Bur. Stand., **1976**, 80A, 421.

153. T. Fonseca, P. Relo´ gio, J. M. G. Martinho and J. P. S. Farinha, Langmuir, **2007**, 23, 5727.

154. S. T. Bogen, J. Karolin, J. G. Molotkovsky and L. B.A. Johansson, J. Chem. Soc., Faraday Trans., **1998**, 94,2435.

155. J. Nicolas, V. San Miguel, G. Mantovani and D. M. Haddleton, Chem. Commun., **2006**, 4697.

156. T. J. V. Prazeres, A. Fedorov and J. M. G. Martinho, J. Phys.Chem. B, **2004**, 108, 9032.

157. T. J. V. Prazeres, A. M. Santos and J. M. G. Martinho, Langmuir, **2004**, 20, 6834.

158. E. L. Quitevis, A. H. Marcus and M. D. Fayer, J. Phys. Chem., **1993**, 97, 5762.

159. Z. G. Zhou, M. X. Yu, H. Yang, K. W. Huang, F. Y. Li, T. Yi and C. H. uang, Chem. Commun., **2008**, 3387.

160. H. N. Kim, M. H. Lee, H. J. Kim, J. S. Kim and J. Yoon, Chem. Soc. Rev., **2008**, 37, 1465.

161. M. Beija, C. A. M. Afonso and J.M. G. Martinho, Chem. Soc. Rev., **2009**, 38, 2410.

162. X. Chen, T. Pradhan, F. Wang, J.S. Kim, and J. Yoon, Chem. Rev., **2012**, 112, 1910.

163. Y. Kim, G. Jang, T. S. Lee, ACS Appl. Mater. Interfaces, **2015**, 7, 15649.

164. T. Mistri, R. Alam, R. Bhowmick, A. Katarkar, K. Chaudhurib, M. Ali, New J.Chem., **2016**,40, 330.

165. A. Roy, R. Mukherjee, B. Dam, S. Damc, P. Roy, New J.Chem., **2018**, 42, 8415.

166. W. N. Wu, P. D. Mao, Y. Wang, X. L. Zhao, L. Jia, Z.Q. Xu Journal of Molecular Structure, **2016**, 1122, 24.

167. C. Kim, Ji-Y. Hwang, K.S. Ku, S. Angupillai, Y. A Son, Sensors and Actuators B, **2016**, 228, 259.

168. J. W. Jeong, B. A. Rao, J.Y. Lee, Ji.Y. Hwang, Y. A Son, Sensors and Actuators B, **2016**, 227, 227.

169. K.S. Ku, P. Muthukumara, S. Angupillaia, Y.A Sona, Sensors and Actuators B, **2016**, 236, 184.

170. S. Goswami, S. Paul, A. Manna RSC Adv., **2013**, 3, 10639.

171. Y. Fu, X.J. Jiang, Y.Y. Zhu, B.J. Zhou, S.Q. Zang, M.S. Tang, H.Y. Zhang, T. C. W. Maka, Dalton Trans., **2014**, 43, 12624.

172. R. Kaur, N. Kaur, Dyes and Pigments, **2017**,139, 310.

173. N. Manjubaashini, T. Daniel Thangadurai, G. Bharathib, D. Natarajan, Journal of Luminescence, **2018**,202, 282.

174. X. Hu, X. Zhang, G. He, C. He, C. Duan, Tetrahedron, **2011**,67, 1091.

175. J. Mao, L. Wang, W. Dou, X. Tang, Y. Yan, W. Liu, Oganic letters, **2007**,9, 22,4567.

176 S. Saha, P. Mahato, U. Reddy, E. Suresh, A. Chakrabarty, M. Baidya, S. K. Ghosh, A. Das, Inorg. Chem., **2012**, 51, 336.

177. R. Kagit, M. Yildirim, O. O. S. Yesilot, H. Ozay, Inorg. Chem., **2014**, 53, 2144.

178. H. Ozay, O. Ozay, Chemical Engineering Journal, **2013**,232, 364.

179. C.H. Kima, B.A. Raoa, J. Jeonga, S. Angupillaia, J.S. Choib, J.O. Namc, C.S. Leec, Y.A. Son, Sensors and Actuators B, **2016**, 224, 404.

180. M. H. Lee, H. Lee, M. J. Chang, H. S. Kim, C. Kang, J. S. Kim, Dyes and Pigments, **2016**,130, 245.

181. G. Sivaraman, V. Sathiyaraja, D. Chellappa Journal of Luminescence, **2014**,145,480.

182. Y. Wanga, H.Q. Changa, W.N. Wua, X.L. Zhaoa, Y. Yangb, Z.Q. Xua, Z.H. Xuc, L. Jiaaa, Sensors and Actuators B, **2017**, 239, 60.

183. M. H. Lee, T. V. Giap, S. H. Kim, Y. H. Lee, C. Kang, J. S. Kim, Chem. Commun., **2010**, 46, 1407.

184. Z.Q. Hu, X.M. Wang, Y.C. Feng, L. Ding, M. Li, C. Sheng, Chem. Commun., **2011**, **47**, 1622.

185 L. Huang, F. Hou, J. Cheng, P. Xi, F. Chen, D. Baib, Z. Zeng, Org. Biomol. Chem., **2012**, 10, 9634.

186. S. Goswami, S. Das, K. Aich, D. Sarkar, T. K. Mondal, C. K. Quahc, H.K. Func Dalton Trans., **2013**, 42, 15113.

187. L. Zhang, J. Fan, X. Peng, Spectrochim. Acta, Part A, **2009**,73, 398.

188. K. S. Moon, Y. K. Yang, S.H. Ji, J.S. Tae, Tetrahedron Lett.,**2010**, 51, 3290.

189. M. Deng, S. Wang, C. Liang, H. Shang, S. Jiang, RSC Adv., **2016**, 6, 26936.

190. R. Bhowmick, A. S. M. Islam, U. Saha, G. S. Kumar, M. Ali, *New J. Chem.*, **2018**, 42, 3435.

191. Y. Fu, Q.F. Tian, Y.Q. Guo, S.Q. Zang, Inorganica Chimica Acta **2014**,419, 141.

292. A. Yu. Mironenko, M.V. Tutov, A.K. Chepak P.A. Zadorozhny, S. Yu. Bratskaya, Tetrahedron, **2019**,75, 1492.

193. G. He, X. Zhang, C. He, X. Zhao, C. Duan, Tetrahedron, **2010**,66, 9762.

194. L. Huang, F.P. Hou, P. Xi, D. Bai, M. Xu, Z. Li, G. Xie, Y. Shi, H. Liu, Z. Zeng, Journal of Inorganic Biochemistry, **2011**,105,800.

195. T. Li, Y. Yang, P. Zhou, Z. Peng, J. Qin, Li Liu, Y. Wanga, Polyhedron, **2017**,128, 154.

196. J. Jeong, B. Ananda Rao, Y.A. Son, Sensors and Actuators B, **2015**, 220, 1254.

197. Y. Xiang, Z. Li, X. Chen, A. Tong, Talanta, **2008**, 74, 1148.

198. J. F. Zhang, Y. Zhou, J. Yoon, Y. Kim, S. J. Kim, J. S. Kim, Org. Lett., **2010**, 12, 3852.

199. F. Yu, W. Zhang, P. Li, Y. Xing, L. Tong, J. Ma, B. Tang, Analyst., **2009**, 134, 1826.

200. P. Xi, J. Dou, L. Huang, M. Xu, F. Chen, Y. Wu, D. Bai, W. Li, Z. Zeng, Sens. Actuators, B **2010**, 148, 337.

201. Y. Zhao, X. B. Zhang, Z.X. Han, L. Qiao, C.Y. Li, L.X. Jian, G.L. Shen and R. Q .Yu,. Anal. Chem., **2009**, 81, 7022.

202. L. Huang, X. Wang, G. Xie, P. Xi, Z. Li, M. Xu, Y. Wu, D. Bai, Z. Zeng, Dalton Trans., **2010**, 39, 7894.

203. J. Wang, L. Long, D. Xie, X. Song, Sensors and Actuators B, **2013** ,177,27.

204. Y. Fang, Y. Zhou, Q. Rui, C. Yao, Organometallics **2015**, 34, 2962.

205. Y. Zhou, F. Wang, Y. Kim, S.J. Kim, J. Yoon, *Org. Lett.* **2009**, 11, 19, 4442.

206. X. Ma, Z. Tan, G. Wei, D. Wei, Y. Du, Analyst, **20**12, 137, 1436.

207. N. R. Chereddy, S. Janakipriya, P. S. Korrapati, S. Thennarasu, A. B. Mandal Analyst, **2013**, 138, 1130.

208. Y. Zhang, Q. Li, J. Guo, Y. Li, Q. Yang, J. Du, RSC Adv., **2015**, 5, 66674

209. Z. Q. Xu, X.J. Mao, Y. Wang, W.N. Wu, P.D. Mao, X.L. Zhao, Y.C. Fan, H.J. Li RSC Adv., **2017**, 7, 42312.

210. Q. Huang, Y. T. Chen, Y. W. Ren, Z. Y. Wang, Y. X. Zhu and Y. Zhang Anal.Methods, **2018**, 10, 5731.

211. W. Lin, X. Cao, Y. Ding, L. Yuan, Q. Yu, Org. Biomol. Chem., **2010**, 8, 3618.

212. H. Wang, Y. Li, S. Xu, Y. Li, C. Zhou, X. Fei, L. Sun, C. Zhang, Y. Li, Q. Yang, X. Xu, Org. Biomol. Chem., **2011**, 9, 2850.

213. Y. Wang, Y. Huang, B. Li, L. Zhang, H. Song, H. Jianga, J. Gaoa, RSC Advances, **2011**, 1, 1294.

214. X. Chen, S.W. Nam, M. J. Jou, Y. Kim, S.J. Kim, S. Park, J. Yoon, Org. Lett., **2008**, 10, 5236.

215. W. Huang, X. Zhu, D. Wua, C. He, X. Hu, C. Duan, Dalton Trans., **2009**, 47,10457.

216. N. Wanichacheva, P. Praikaew T. Suwanich K. Sukrat: Molecular and Biomolecular Spectroscopy **2014**,118, 908.

217. F. J. Orriach-Fernández, A. M.Castillo, J. F. Fernández-Sánchez, A. M. de la Peña, A. Fernández-Gutiérreza, Anal. Methods, **2013**, 5, 6642.

218. J. F. Zhanga, C. S. Lima, B. R. Cho, J. S. Kim, Talanta **2010**,83, 658.

219. Y. Long, M.P. Yang, B.Q. Yang, Journal of Inorganic Biochemistry **2017**,172, 23.

220. X. C. Fu, J. Wu, C.G. Xie, Y. Zhonga, J. H. Liub, Anal. Methods, **2013**, 5, 2615.

221. W. Huang, D. Wu, G. Wu and Z. Wang, Dalton Trans., **2012**, 41, 2620.

222. B. Liu, F. Zeng, Y. Liu, S. Wu, Analyst, **2012**, 137, 1698.

223. L. Yang, Q. Song, K. Damit-Og and H. Cao, Sens. Actuators B, **2013**, 176, 181.

224. L. Wang, J. Yan, W. Qin, W. Liu and R. Wang, Dyes and Pigments. **2012**, 92, 1083.

225. H. Wang, Y. Li, S. Xu, Y. Li, C. Zhou, X. Fei, L. Sun, C. Zhang, Y. Li, Q. Yang X. Xu, Org. Biomol. Chem., **2011**, 9, 2850.

226. Y. Fang, Y. Zhou, J. Y. Li, Q. Q. Rui, C. Yao, Sensors and Actuators B. **2015**, 215,350.

227. P. Mahato, S. Saha, E. Suresh, R. Di Liddo, P. P. Parnigotto, M. T. Conconi, M. K. Kesharwani, B. Ganguly, A. Das, Inorg. Chem., **2012**, 51, 1769.

228. D.T. Quanga, J.S. Wub, N. D. Luyena, T. Duonga, N. D. Dana, N. C. Baoa, P. T. Quyc; Spectrochimica Acta Part A., **2011**, 78, 753.

229. S. Saha, P. Mahato, G. U. Reddy, E. Suresh, A. Chakrabarty, M. Baidya, S. K. Ghoshand, A. Das, Inorg. Chem., **2012**, 51, 336.

230. L. Tang, F. Li, M. Liu and R. Nandhakumar, Spectrochim. Acta, Part A, **2011**, 78, 1168

231. M. Suresh, A. Shrivastav, S. Mishra, E. Suresh, A. Das, Org. Lett., **2008**, 10, 3013.

232. R. Bhowmick, A. S. M. Islam, A. Katarkar, K. Chaudhurib, M. Ali, Analyst, **2016**, 141, 225.

233. G. Yang, X. Meng, S. Fang, H. Duan, L. Wang, Z. Wang, RSC Adv., **2019**, 9, 8529

234. H.S. Soa, B.A. Rao, J. Hwanga, K. Yesudas, Y.A Son, Sensors and Actuators B **2014**,202. 779.

235. J. Y. Lee, B. A. Rao, J.Y. Hwang, Y.A. Son, Sensors and Actuators B, **2015**, 220, 1070.

236. A. Petdum, W. Panchan, J. Sirirak, V. Promarak, T. Sooksimuang N. Wanichacheva, NewJ.Chem, **2018**,42, 1396.

237. M. Suresh, S. Mishra, S. K. Mishra, E. Suresh, A. K. Mandal, A. Shrivastav and A. Das, Org. Lett., **2009**, 11, 2740.

238. C. Wang and K. M.C. Wong, Inorg. Chem., **2011**, 50, 5333.

239. B. N. Ahamed, P. Ghosh, Inorganica Chimica Acta., **2011**,372,100.

240. D. Wu, W. Huang, Z. Lin, C. Duan, C. He, S. Wu and D. Wang, Inorg. Chem., **2008**, 47, 7190.

241. W. Huang, D.Y. Wu, C.Y. Duan, Inorg. Chem. Commun., **2010**, 13, 294

242. S. H. Mashraqui, T. Khan, S. Sundaram, R. Betkar, M. Chandiramani, Chem. Lett., **2009**, 38, 730.

243. G. Sivaraman, T. Anand D. Chellappa, Analyst, **2012**, 137, 5881.

244. G. Xie, Y. Shi, F. Hou, H. Liu, L. Huang, P. Xi, F. Chen, Z. Zeng, Eur. J. Inorg. Chem. **2012**, 327.

245. J. M. An, Z. Y. Yang, M.H. Yan, T. R. Li, Journal of Luminescence, **2013**,139, 79.

246. M. Raju, R. R. Nair, I.H. Raval, S. Haldar, P.B. Chatterjee, Analyst, **2015**, 140, 7799.

247. B. Biswal, B. Bag, RSC Adv., **2014**, 4, 33062.

248. O. Sunnapu, N. G. Kotla, B. Maddiboyina, S. Singaravadivel, G. Sivaraman, RSC Adv., **2016**, 6, 656.

249. A. K. Bhanja, S. Mishra, K. D. Saha, C. Sinha, Dalton Trans., **2017**, 46,9245.

250. S. Goswami, D. Sen, N. K. Das, H.K. Fun, C. K. Quah, Chem. Commun., **2011**, 47, 9101.

251. S. Goswami, A. Manna, A.K. Maity, S. Paul, A. K. Das, M. K. Das, P. Saha, C. K. Quahc H. K. Func, Dalton Trans., **2013**, 42, 12844.

252. S. Goswami, K. Aich, S. Das, A. K. Das, A. Manna, S. Halder, Analyst, **2013**, 138, 1903.

253. J. Wang, W. Lin, L. Yuan, J. Songa, W. Gao, Chem. Commun., **2011**, 47, 12506.

254. A. Y. Mironenko, M.V. Tutov, A.A. Sergeevc, Voznesenskiy, S.Yu. Bratskaya, Sensors and Actuators B, **2017**,246, 389.

A differentially selective probe for trivalent chemosensor upon single excitation with cell imaging application: potential applications in combinatorial logic circuit and memory devices

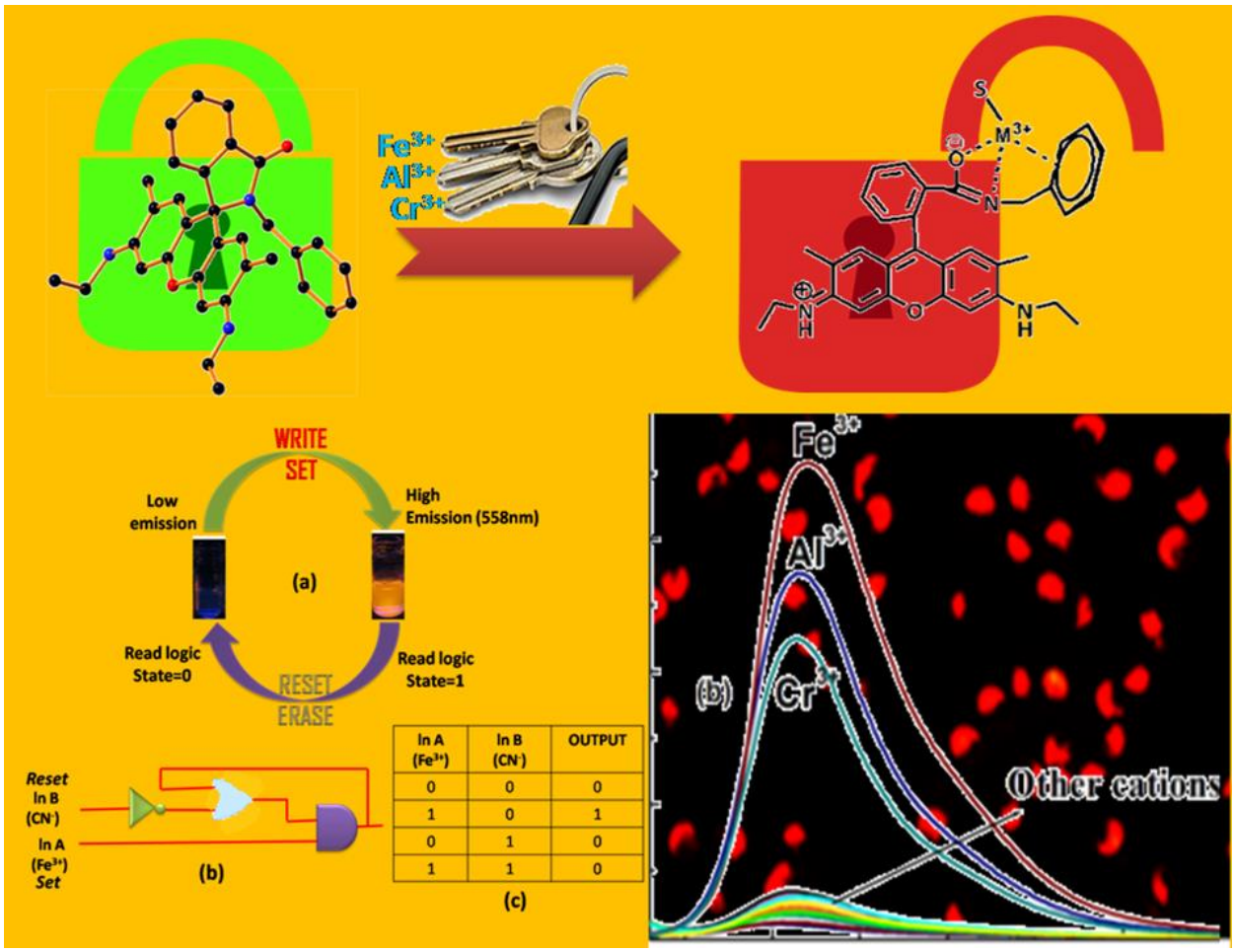

Abstract

A new rhodamine 6G-benzylamine-based sensor (**L**^{1}), having only hydrocarbon skeletons in the extended part, was synthesized and characterized by single-crystal X-ray crystallographic study. It exhibited excellent selective and sensitive recognition of trivalent metal ions M^{3+} (M = Fe, Al and Cr) over mono- and divalent and other trivalent metal ions. A large enhancement of fluorescence intensity for Fe^{3+} (41-fold), Al^{3+} (31-fold) and Cr^{3+} (26-fold) were observed upon the addition of 3 equivalents of these metal ions into the probe in H_2O/CH_3CN (4: 1, v/v, pH 7.2) with naked eye detection through prominent change in absorbance at 530 nm. The corresponding K_f-values were evaluated to be 9.4×10^3 M^{-1} (Fe^{3+}), 1.34×10^4 M^{-1} (Al^{3+}) and 8.7×10^3 M^{-1} (Cr^{3+}). Quantum yields of **L**^{1}, [**L**^{1}–Fe^{3+}], [**L**^{1}–Al^{3+}] and [**L**^{1}–Cr^{3+}] specieses in H_2O/CH_3CN (4: 1, v/v, pH 7.2) were found to be 0.012, 0.489, 0.376 and 0.310, respectively, using rhodamine-6G as standard. LODs for Fe^{3+}, Al^{3+} and Cr^{3+} were determined by 3σ methods and found to be 1.28, 1.34 and 2.28 μM, respectively. Cyanide ion scavenged Fe^{3+} from the [Fe^{3+}–**L**^{1}] complex and quenched its fluorescence via its ring-closed spirolactam form. Advanced level molecular logic gate and memory devices were constructed using 2 and 4 inputs. The large enhancement in fluorescence emission of **L**^{1} upon complexation with M^{3+} metal ions makes the probe suitable for bio-imaging of M^{3+} (M = Fe, Al and Cr) in living cells.

2.1 Introduction

With the increase in urbanization and socioeconomic advancement, unlike other pollutants like petroleum hydrocarbons and domestic and municipal litter which may visibly build up in the environment, the traces of heavy metal ions increase the toxicity level to a higher extent in the environment and also cause harmful effects on human health. Nowadays, contamination by toxic metal ions is increasing due to leather tanning, electroplating, pigments, emissions from vehicular traffic gas exhausts, energy and fuel production, intensive agriculture and sludge dumping and from mining industries.

As a result, contamination of drinking water and food, especially in developing countries, with metals is very much unsafe. So many researchers have tried to detect toxic metal ions, such as iron,[1] chromium,[2] aluminium,[3,4] lead,[5] silver,[6] cadmium,[7] zinc [8,9] and mercury,[10] in water and foods. Among these trivalent metal ions, Fe^{3+}, $Al^{3+}$and Cr^{3+} have biological as well as environmental importance.[11–24] Fe^{3+} is not only the most abundant transition metal in cellular systems but also plays an important role in many metabolic pathways, such as oxygen transport processes in tissues, nerves signal conduction, cellular growth and tissue formation.[25] On the other hand, the excess accumulation of Fe^{3+} can lead to a variety of diseases, such as cell damage and organ dysfunction through the abnormal production of reactive oxygen species (ROS),[26,27] leading to Alzheimer's, Huntington's, Parkinson's etc. diseases.[28] Moreover, disruption of iron homeostasis can lead to a number of disease, such as cancer,[29] hepatitis[30] and neurodegenerative diseases.[31]

Cr^{3+} is an effective nutrient and gives immunity power to the human body. Cr^{3+} overdose is known to inflict a negative effect on normal enzymatic activities, and the cellular structure and function causing a disturbance in glucose levels and lipid metabolism, while a deficiency of Cr^{3+} in humans can cause maturity-onset diabetes and cardiovascular disease and nervous system disorders.[32,33] The Cr^{3+} ion, present in the cytoplasm, is known to bind non-specifically to DNA at an elevated level, affecting the cellular structures and damaging the cellular components, which can lead to mutation and cancer.[34] Chromium deficiency can cause a risk of diabetes, cardiovascular diseases and nervous system disorders.[35]

Al^{3+} is the third most abundant metal in the Earth's crust and also one of the most common species of metal cations that are mostly found in the +3 oxidation state in most kinds of animal and plant tissues and in natural waters everywhere.[36–40] It has been found that aluminium accumulates in various mammalian tissues, such as the brain, bone, liver and kidney,[41,42] which causes renal failure[43] and problems associated with age.[44] Aluminium toxicity damages the central nervous system and it is surmised to play a role in neurodegenerative Alzheimer's and Parkinson's diseases. It is also responsible for intoxication in haemodialysis patients.[45] Moreover, aluminium toxicity may cause gastrointestinal problems and interference with Ca^{2+} metabolism.[46–48] Again, increasing free Al^{3+} due to acid rain and human activities in the environment and surface water is detrimental to growing plants.[49]

Various methods, such as inductively coupled plasma emission spectrometery (ICP),[50] X-ray photoelectron spectrometry (XPS) and atomic fluorescence spectroscopy (AFS) have been used

for heavy metal ion detection.[51,52] Compared with these complicated methods, optical probes are inexpensive, simple and rapid.Thus, there is an urgent need to design single fluorogenic probes, displaying changes in optical properties through a "turn-on" response that are capable of detecting the presence of Fe^{3+}, Al^{3+} and Cr^{3+} ions simultaneously and in the presence of large number of monovalent, divalent and other trivalent metal cations[53–55] in biological samples.

As Cr^{3+} and Fe^{3+} are paramagnetic in nature, they function as fluorescent quenchers,[56] which makes it a challenging task to develop a turn-on fluorescent sensor for these ions. Very few turn-on sensors for Cr^{3+} and Fe^{3+} have been reported with cell imaging applications.[57–59]

Although, Al^{3+} functions as a turn-on fluorescent sensor, due to its strong hydration in water, most of the reported dye based Al^{3+} sensors require organic solvents or mixed solvents, with very few being suitable for Al^{3+}-imaging applications.[60]

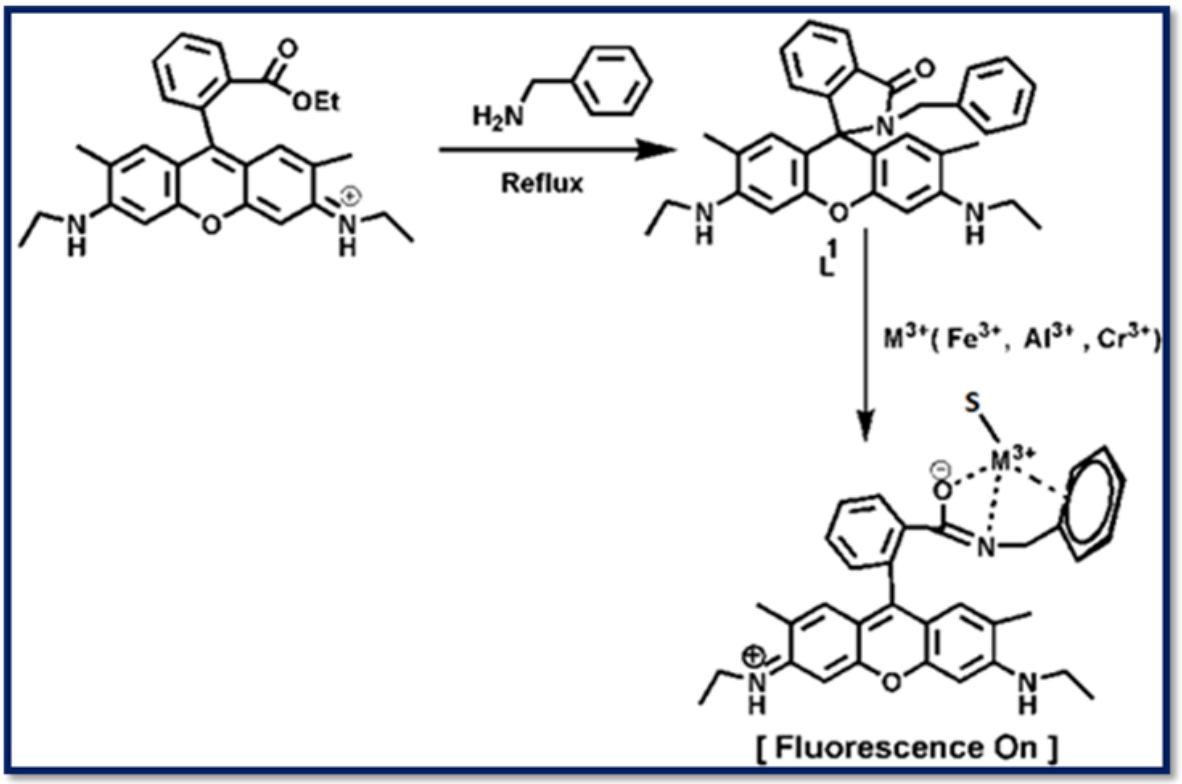

Scheme-2.1: Tentative binding mode of $\mathbf{L^1}$ with M^{3+}.

Given our interest in developing new chemosensors, we report herein a rhodamine 6G-based probe (**Scheme-2.1**), characterized by X-ray single-crystal diffraction analysis (**Figure-2.1**) and by other common spectroscopic analysis, for the detection of trivalent cations, like Fe^{3+}, Al^{3+} and Cr^{3+}, in

an aqueous medium over monovalent, divalent and other trivalent metal ions. Though there are a few[61,62] reports on trivalent sensors, where in all cases external coordinating atom(s) are present along with the basic amidic moiety of rhodamine, however, in our reported probe it is absent. Herein, we disclose a benzylamine- rhodamine-6G (**L^1**) conjugate (**Scheme-2.1**) that selectively senses these trivalent metal ions in a mostly aqueous medium (4: 1, H_2O:CH_3CN, v/v) with very high fluorescence enhancement.

2.2 Experimental Section

2.2.1 Materials and methods

All solvents used for synthesis were of reagent grade (Merck). For the spectroscopic (UV/Vis and fluorescence) studies, HPLC-grade MeCN and double-distilled water were used. Rhodamine 6G hydrochloride and metal salts, such as perchlorates of Na^+, Fe^{2+}, Co^{2+}, Ni^{2+}, Zn^{2+}, Pb^{2+}, Cd^{2+}, Hg^{2+}, Cu^{2+}, $Al(NO_3)_3{\cdot}9H_2O$, $Cr(NO_3)_3{\cdot}9H_2O$, $Fe(NO_3)_3{\cdot}9H_2O$ were purchased either from Sigma–Aldrich or Merck and used as received. All other compounds were purchased from commercial sources and used without further purification.

2.2.2 Physical measurements

^{1}H-NMR spectra were recorded in $CDCl_3$ and DMSO-d_6, on a Bruker 300 MHz NMR spectrometer using tetramethylsilane ($\delta = 0$) as an internal standard. Infrared spectra (400–4000 cm^{-1}) were recorded in the liquid state using a Nickolet Magna IR 750 series-II FTIR spectrometer. ESI-MS^+ (m/z) of the ligand and complexes were recorded on a Waters' HRMS spectrometer (Model: XEVO G2QTof). UV-Vis spectra were recorded on an Agilent diode-array spectrophotometer (Model, Agilent 8453). Steady-state fluorescence measurements were performed on a PTI QM-40 spectrofluorometer. Lifetimes were measured using a Horiba Jobin–Yvon Hamamatsu MCP photomultiplier (R3809) and data were analyzed using IBH DAS6 software. The pH of the solutions was recorded using a digital pH meter 335, calibrated using pH 4, 7 and 10 buffers in the range pH 2–12.

2.2.3 Synthesis of rhodamine 6G conjugate (L^1)

Rhodamine 6G (5.0 mmol) and benzylamine (10.0 mmol) were dissolved in EtOH and refluxed for 10 hours with continuous stirring, whereupon a white crystalline solid of the probe (**L^1**) was deposited **(**Scheme-2.1). The solid was filtered and washed several times with ethanol and dried in air (75% yield). The compound (**L^1**), was dissolved in MeOH and refluxed for 2 h with constant stirring and filtered. After 2 days, single crystals suitable for X-ray diffraction studies were obtained. ^{1}H NMR (300 MHz, DMSO-d_6) (ppm): 1.18 (t, J = 6.8 Hz, 6H (–CH_3)), 1.69 (s, 6H (–Ar–CH_3)), 2.49 (s, 2H, (–CH_2)), 3.09 (t,J = 6.3 Hz, 4H (–Ar–CH_2)), 4.96 (s, 2H, (–NH)), 5.87 (s, 2H,(–Ar–H)), 6.18 (s, 2H, (–Ar–H)), 6.85 (s, 2H, (–Ar–H)), 6.95 (d,J = 5.4 Hz, 4H (–Ar–H)), 7.48 (m, 1H,(–Ar–H)), 7.50 (m, 1H,(Ar–H)), 7.80 (m, 1H, (–Ar–H)) (Figure-2.2). ^{13}C NMR: 14.63,17.32, 37.90, 43.69, 65.08, 95.90, 104.76, 118.44, 122.84, 124.09, 126.53, 127.75, 128.39, 128.68, 130.92, 133.16, 138.07,147.90, 151.54, 153.95, 167.38 (Figure-2.3). ESI-MS$^+$ (m/z):504.26 (L^1 + H^+) (Figure-2.4). IR spectrum: 1684 cm^{-1} (–C=O),1378 cm^{-1} (–C–N) (Figure-2.5).

2.2.4 Solution preparation for UV-Vis and fluorescence studies

For both the UV-Vis and fluorescence titrations, a stock solution of 1.0 × 10^{-3} M of the probe **L^1** was prepared by dissolving 12.58 mg in 25 mL CH_3CN. Analogously, 1.0 × 10^{-3} M stock solutions of Fe^{3+}, Al^{3+} and Cr^{3+} were prepared in MeOH. A solution of 20 mM HEPES buffer (4: 1, H_2O: CH_3CN) was prepared and the pH was adjusted to 7.2 by using HCl and NaOH. For the UV-Vis spectra, a 60 μM probe was taken in a cuvette containing 2.5 mL of buffer solution and then Fe^{3+} salt solution was added incrementally starting from 0 to 240 μM in a regular interval of time, and the absorption spectra were recorded. Similar experiments were performed for Al^{3+} and Cr^{3+}. Again 2.5 ml of this buffer solution was pipetted into a cuvette to which 60 μM of the probe (**L^1**) solution was added and Fe^{3+} salt solution was then added incrementally starting from 0 to 140 μM in a regular interval of time, and the fluorescence spectra were recorded, setting the excitation wavelength at 502 nm. Similar titrations were conducted with Al^{3+} and Cr^{3+}. Path lengths of the cells used for absorption and emission studies were 1 cm. Fluorescence measurements were performed using a 2 nm × 2 nm slit width.

2.2.5 Cell culture

Human hepatocellular liver carcinoma (HepG2) cell lines (NCCS, Pune, India), were grown in DMEM supplemented with 10% FBS and antibiotics (penicillin, 100 μg ml^{-1}; streptomycin,50 μg ml^{-1}). Cells were cultured at 37 °C in a 95% air/5% CO_2 incubator.

2.2.6 Cell cytotoxicity assay

To assess if there was any cytotoxic effect of the ligand (**L^1**), a cell viability assay was performed using 3-(4,5-dimethylthiazol-2-yl)-2,5-diphenyltetra-zolium bromide (MTT).63 HepG2 cells (1 × 10^5 cells per well) were cultured in a 96-well plate with incubating at 37 °C, and were treated with increasing concentrations of **L^1** (1, 10, 20, 40, 60, 80 and 100 μM) for 24 h. After the incubation, 10 μl of MTT solution [5 mg ml^{-1}, dissolved in 1× phosphate-buffered saline (PBS)] was added to each well of the 96-well culture plate, and then incubated at 37 °C for 4 h. Media were decanted from the wells and 100 μL of 0.04 N acidic isopropyl alcohol was added into each well to solubilize the intracellular formazan crystals (blue-violet) formed, and the absorbance of the solutions was measured at 595 nm wavelength (EMax Precision Micro Plate Reader, Molecular Devices, USA). Values were calculated as the mean ± standard errors of three independent experiments. The cell viability was expressed as the optical density ratio of the treatment to control.

2.2.7 Cell-imaging study by fluorescence microscopy

HepG2 cells were cultured in a 35 × 10 mm culture dish on a coverslip for 24 h at 37 °C. The cells were treated with 10 μm solutions of **L^1**, prepared by dissolving **L^1** into the mixed solvent DMSO: water = 1: 9 (v/v) and incubated for 1 h at 37 °C. To study the complex formation of **L^1** with the three metal ions (Fe^{3+}, Cr^{3+}, Al^{3+}), HepG2 cells were pre-incubated separately with 10 μM, 20 μM and 40 μM of each of the metal ions for 60 min at 37 °C, followed by washing them twice with 1× PBS and subsequent incubation with 10 μM **L^1** for 60 min at 37 °C. Fluorescence images of HepG2 cells were taken using a fluorescence microscope (Leica DM3000, Germany) with an objective lens of 40× magnification.

2.2.8 Job's plot

This method is based on the measurement of the fluorescence of a series of solutions in which molar concentrations of the probe ($\mathbf{L^1}$) and M^{3+} vary but their sum remains constant. Here, the fluorescence of each solution was measured at 558 nm and plotted against the mole fraction of M^{3+}. The maximum fluorescence occurred at the mole ratio corresponding to the combined ratio of the two components. The composition of the complex was determined by Job's method and found to be 1: 1 with respect to $\mathbf{L^1}$ for the Fe^{3+}, Al^{3+} and Cr^{3+} complexes.

2.3 Results and Discussion

As depicted in **Scheme-2.1**, receptor $\mathbf{L^1}$ was synthesized from the reaction of rhodamine-6G with benzylamine in EtOH in reflux conditions for 10 h. The final crystallized product ($\mathbf{L^1}$) was well characterized by ^{1}H NMR (**Figure-2.2**), ^{13}C NMR (**Figure-2.3**), HRMS (**Figure-2.4**), IR (**Figure-2.5**) and a single-crystal X-ray diffraction study (**Figure-2.1**). The receptor $\mathbf{L^1}$ was found to be a very sensitive and highly selective colorimetric and fluorogenic chemosensor for trivalent metal ions, M^{3+} (M^{3+} = Fe^{3+}, Al^{3+} and Cr^{3+}), while in the absence of M^{3+}, the solution of $\mathbf{L^1}$ was colourless and very weakly fluorescent.

2.3.1 X-ray crystallography study

Single-crystal X-ray diffraction studies revealed that the compound $\mathbf{L^1}$ is crystallized in a triclinic system of space group $P1^-$ (no. 2). The crystallographic details are depicted in **Table-2.1**. A molecular view of $\mathbf{L^1}$ is shown in **Figure-2.1**, with H atoms are removed to get better clarity.

Molecular formula	$C_{33}H_{33}N_3O_2$
Formula Weight	503.62
Crystal System	Triclinic
Space group	P-1(No. 2)
a /Å	9.0397(8)

b /Å	12.5823(11)
c /Å	12.8196(11)
α /deg	86.214(2)
β/deg	73.428(2)
γ/deg	72.357(2)
V /Å^3	1331.5(2)
Z	2
D(calc) /g cm^{-3}	1.256
μ(MoK$_\alpha$) /mm^{-1}	0.079
F(000)	536
T /K	273
θ min, max /deg	2.3, 27.5
Dataset	-11: 11 ; -16: 16 ; -16: 16
Tot., Uniq. Data, R(int)	13172, 6036, 0.023
Observed data [I> 2(I)]	4637
N_{ref}, N_{par}	6036, 356
R, wR_2, S	0.0527, 0.1522, 1.05

Table-2.1: Crystallographic data and details of the structure determination.

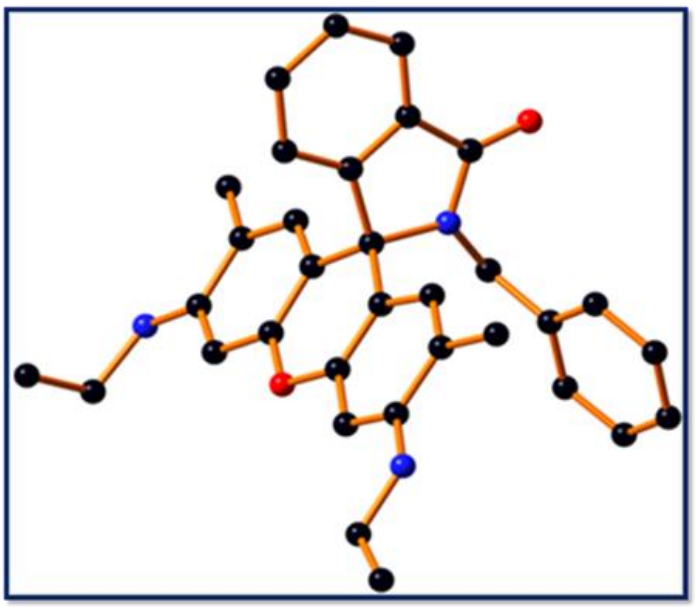

Figure-2.1: The molecular view of ligand $\mathbf{L^1}$. All H-atoms are omitted for clarity.

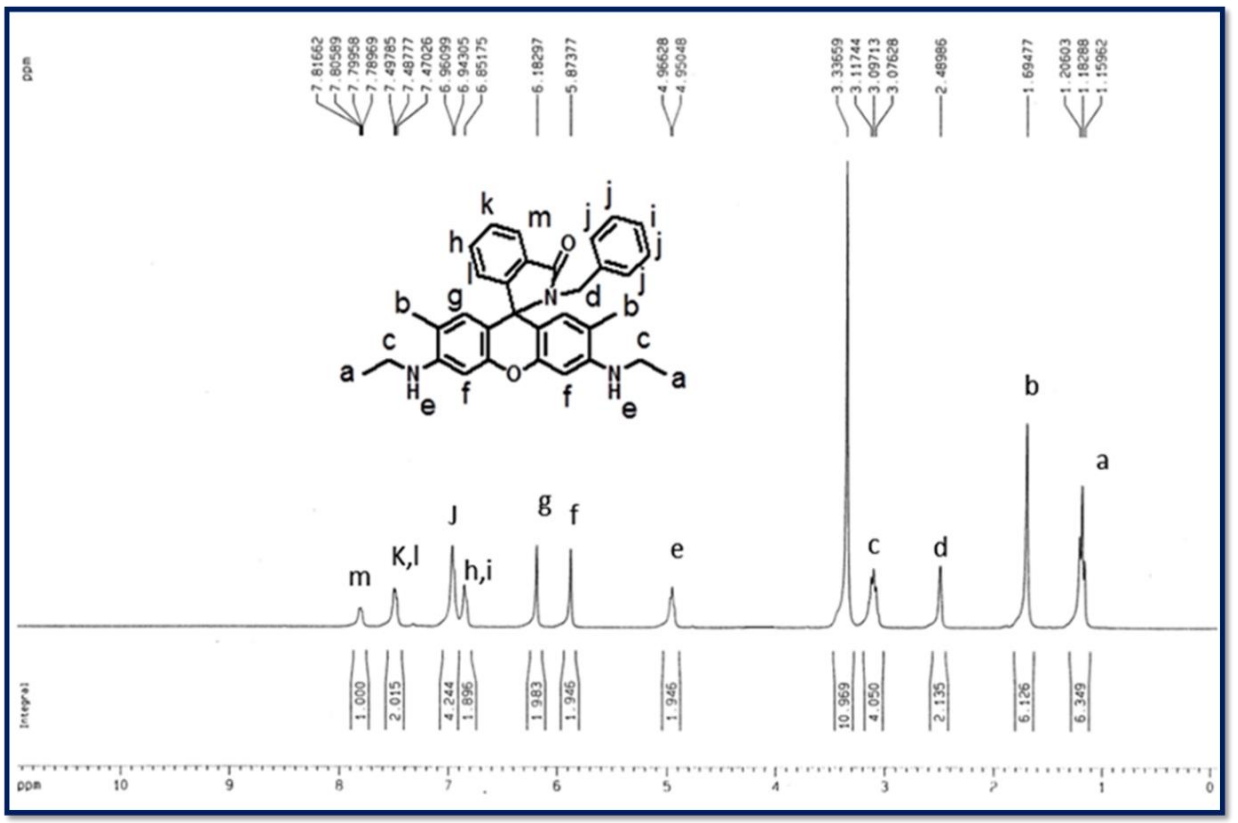

Figure-2.2: ^{1}H NMR spectrum of $\mathbf{L^1}$ in DMSO-d_6, in Bruker 300 MHz instrument.

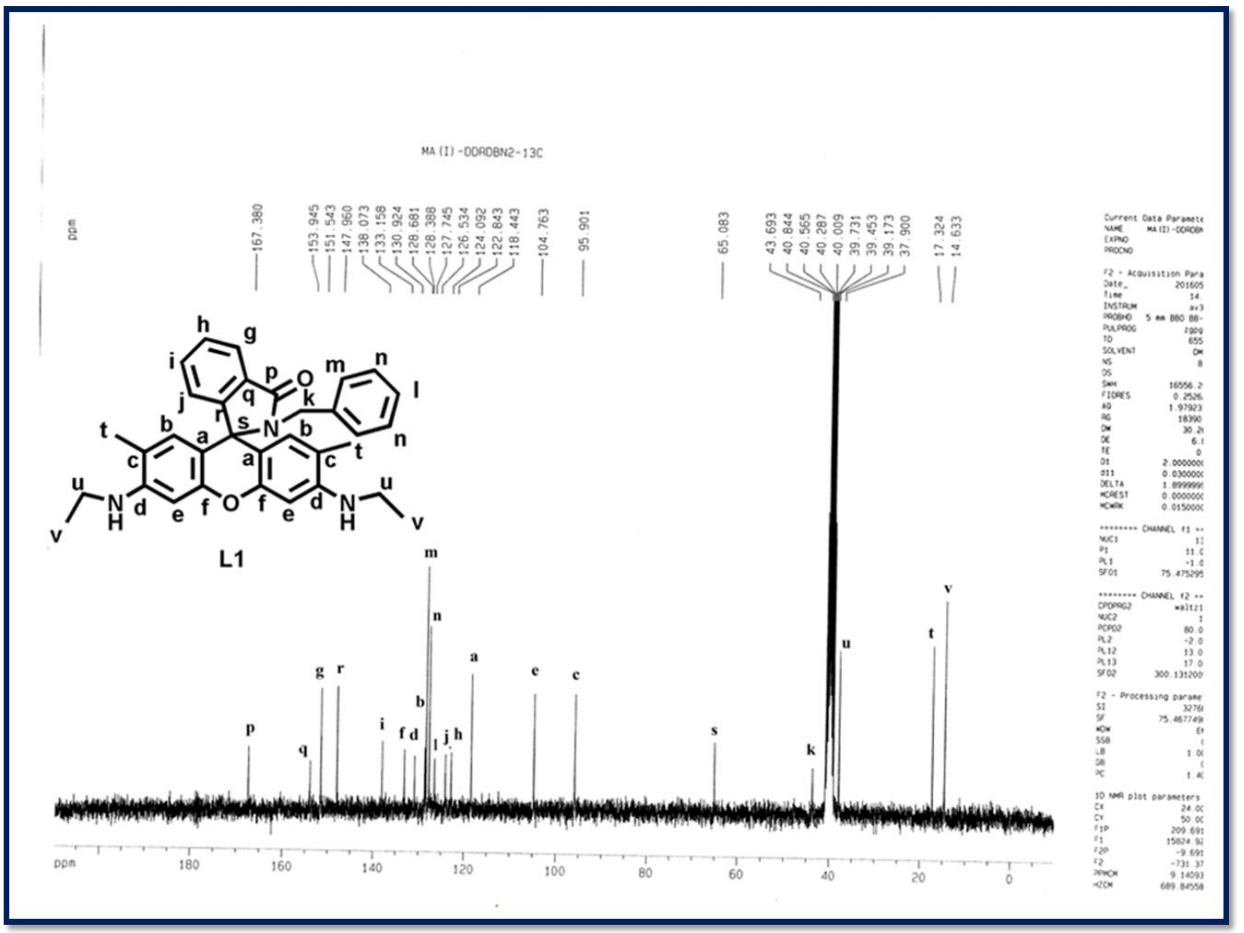

Figure-2.3: ^{13}C NMR spectrum of **L^{1}** in DMSO-d_6, in Bruker 500 MHz instrument.

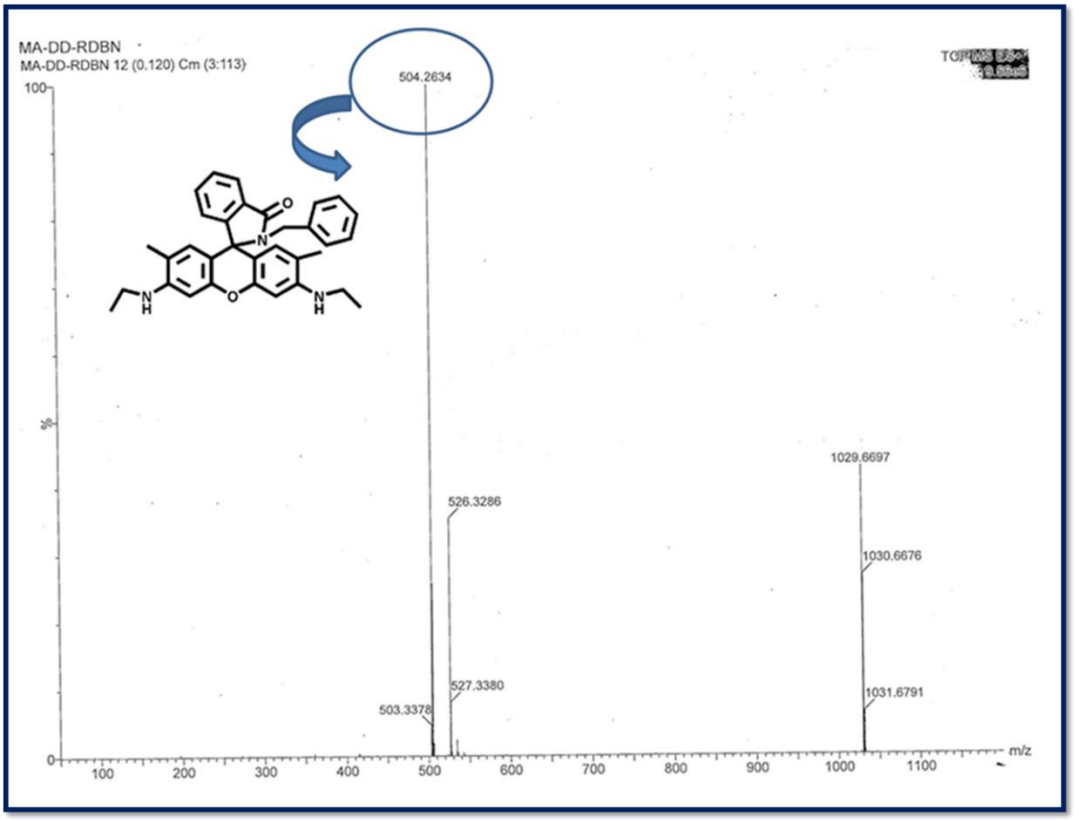

Figure-2.4: Mass spectroscopy of $\mathbf{L^1}$ in MeOH.

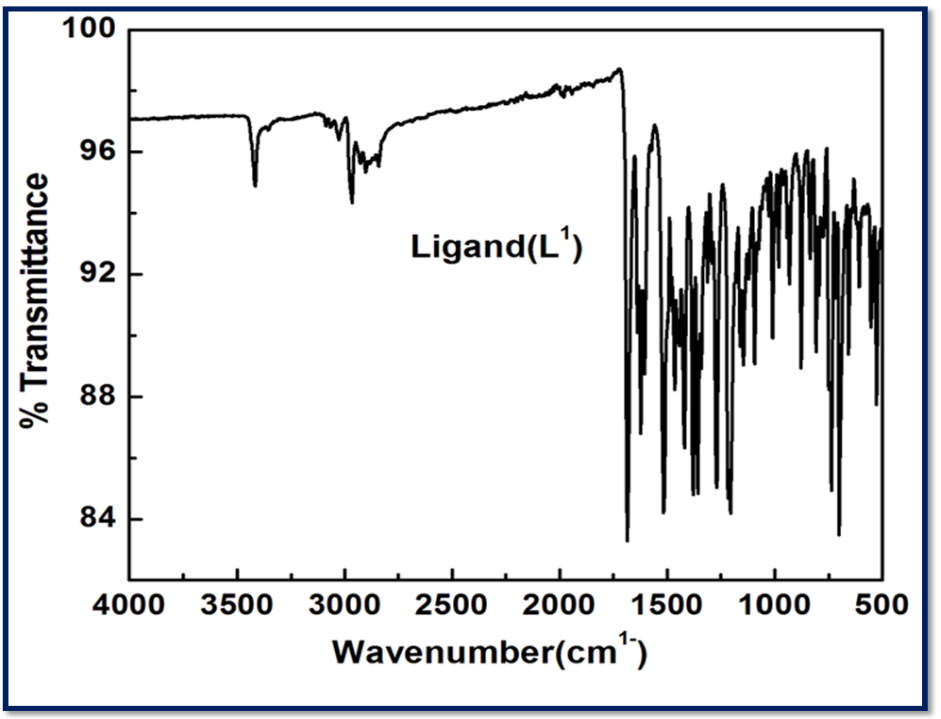

Figure-2.5: FT-IR spectrum of $\mathbf{L^1}$

2.3.2 UV-Vis Absorption studies

The UV-Vis spectrum of **L^1** (60 μM) was recorded in a mixed aqueous solvent of H_2O/CH_3CN (4: 1, v/v, pH 7.2, 20 mM HEPES buffer). The gradual addition of Fe^{3+}, Al^{3+} and Cr^{3+} individually to separate solution of **L^1** revealed that there was a development of two absorption peaks at 350 nm and 530 nm (**Figure-2.6** and **Figure-2.7, Figure-2.8**), with a sharp visual colour change of the representative solution from colourless to orange-red, whereas no such peaks appeared in the presence of monovalent, divalent or other trivalent metal ion solutions (**Figure-2.9**). Between these two peaks, the second one is very important as it exhibits a greater increase in absorbance. The appearance of this peak clearly demonstrates the opening of the spirolactam ring due to the coordination of Fe^{3+}, Al^{3+} and Cr^{3+} with the probe **L^1**. The probable coordination mode of L^1 towards M^{3+} (Fe^{3+}, Al^{3+} and Cr^{3+}) is demonstrated in **Scheme-2.1**. UV-Vis titrations were carried out by varying the concentration of trivalent metal ions Fe^{3+}, Al^{3+} and Cr^{3+} in the range 0–240 μM keeping the probe concentration fixed at 60 μM in H_2O/CH_3CN (4: 1, v/v, pH 7.2, 20 mM HEPES buffer). Plots of absorbance vs. [M^{3+}] yielded linear curves, which were analyzed by linear curve-fitting of the titration data according to eqn. **(6)** (where a, b and c have the usual meaning) under the conditions $1 \gg c \times x$ with n = 1, giving apparent association constant K_f values as 1.19×10^4 M^{-1}, 1.09×10^4 M^{-1} and $1.0^4 \times 10^4$ M^{-1} for Fe^{3+}, Al^{3+} and Cr^{3+} respectively.

$$y = (a+b*c*x^n)/(1+c*x^n) \quad \ldots\ldots\ldots\ldots \quad (6)$$

The absorbance intensity of the [**L^1**–Fe^{3+}] complex was found to be selectively quenched in the presence CN^- ion (**Figure-2.10**).

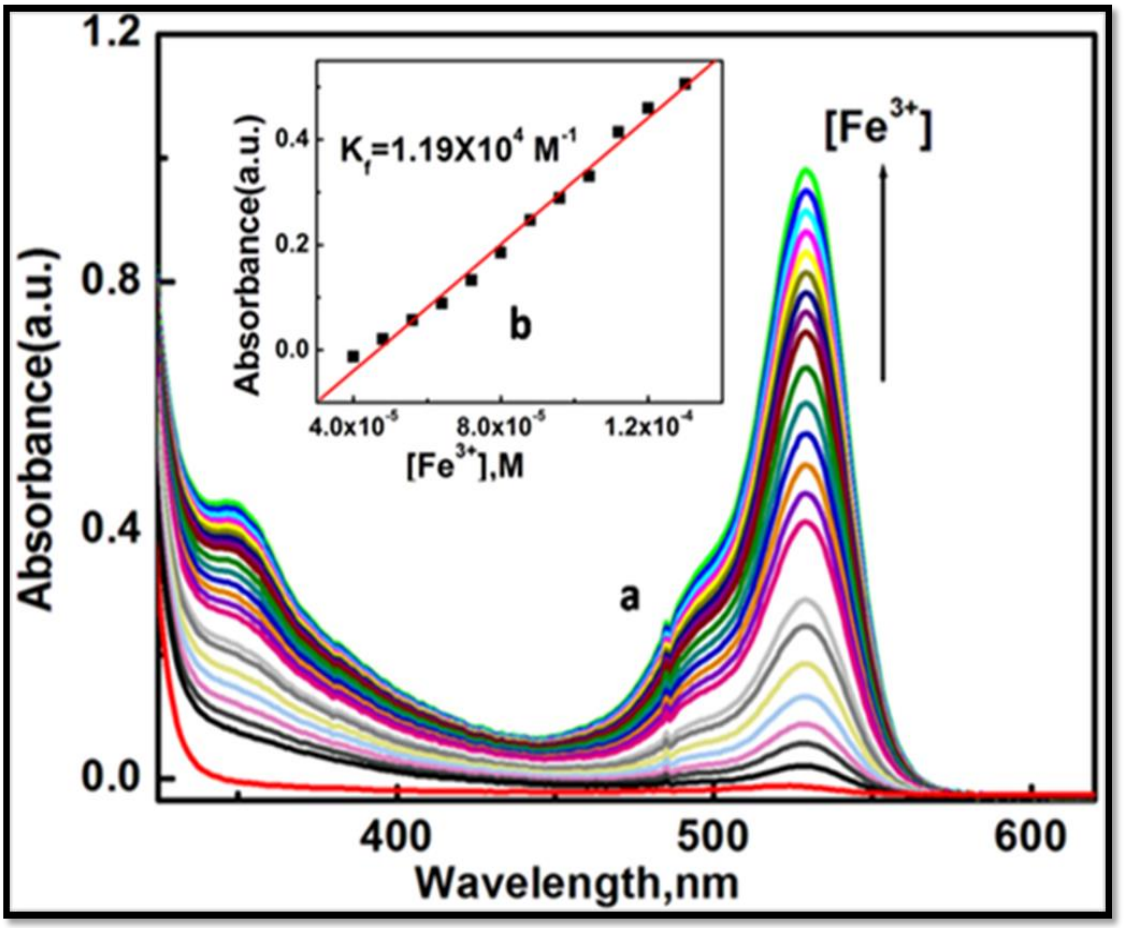

Figure-2.6: (a) UV-Vis absorption spectra of $\mathbf{L^1}$ (60 μM) in H_2O/CH_3CN (4:1, v/v, pH 7.2, 20 mM HEPES buffer) solutions with the increase in concentration of Fe^{3+}solution (0-240 μM); (b) linear fit of absorbance vs. $[Fe^{3+}]$ plot.

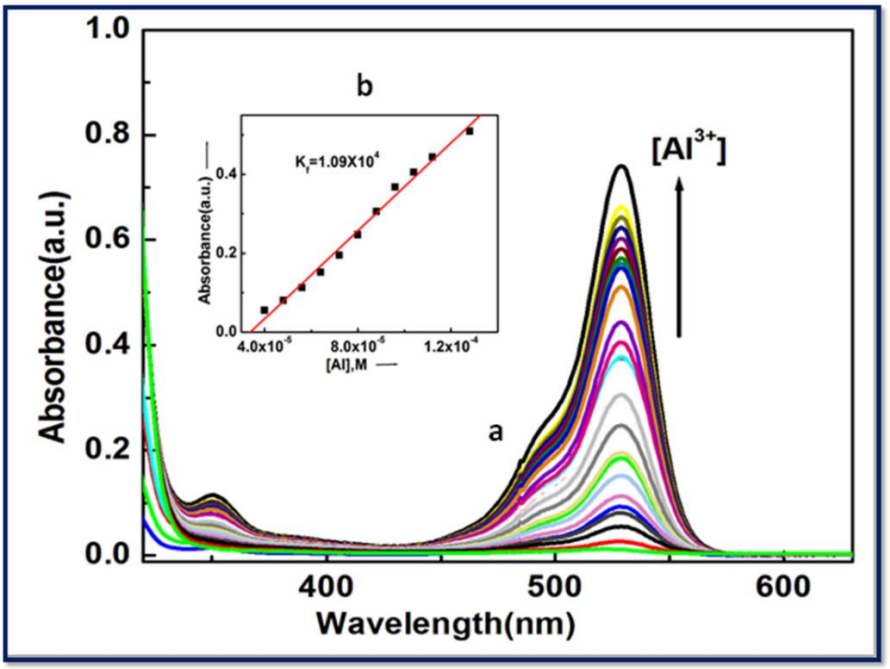

Figure-2.7: (a) UV-Vis titration of $\mathbf{L^1}$ (60 μM) in H_2O- MeCN-(4:1, v/v) in HEPES buffer at pH 7.2 by the gradual addition of Al^{3+} (0-240 μM). Inset (b) linear curve-fit of absorbance vs. $[Al^{3+}]$ plot.

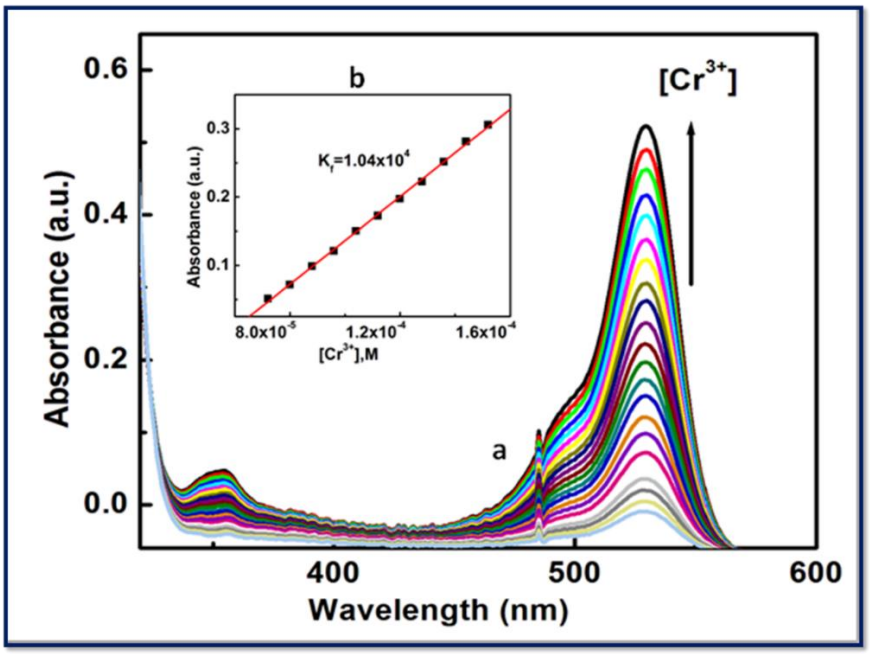

Figure-2.8: (a) UV-Vis titration of $\mathbf{L^1}$ (60 μM) in H_2O- MeCN-(4:1, v/v) in HEPES buffer at pH 7.2 by the gradual addition of Cr^{3+} (0-224 μM). Inset (b) linear curve-fit of absorbancevs. $[Cr^{3+}]$ plot.

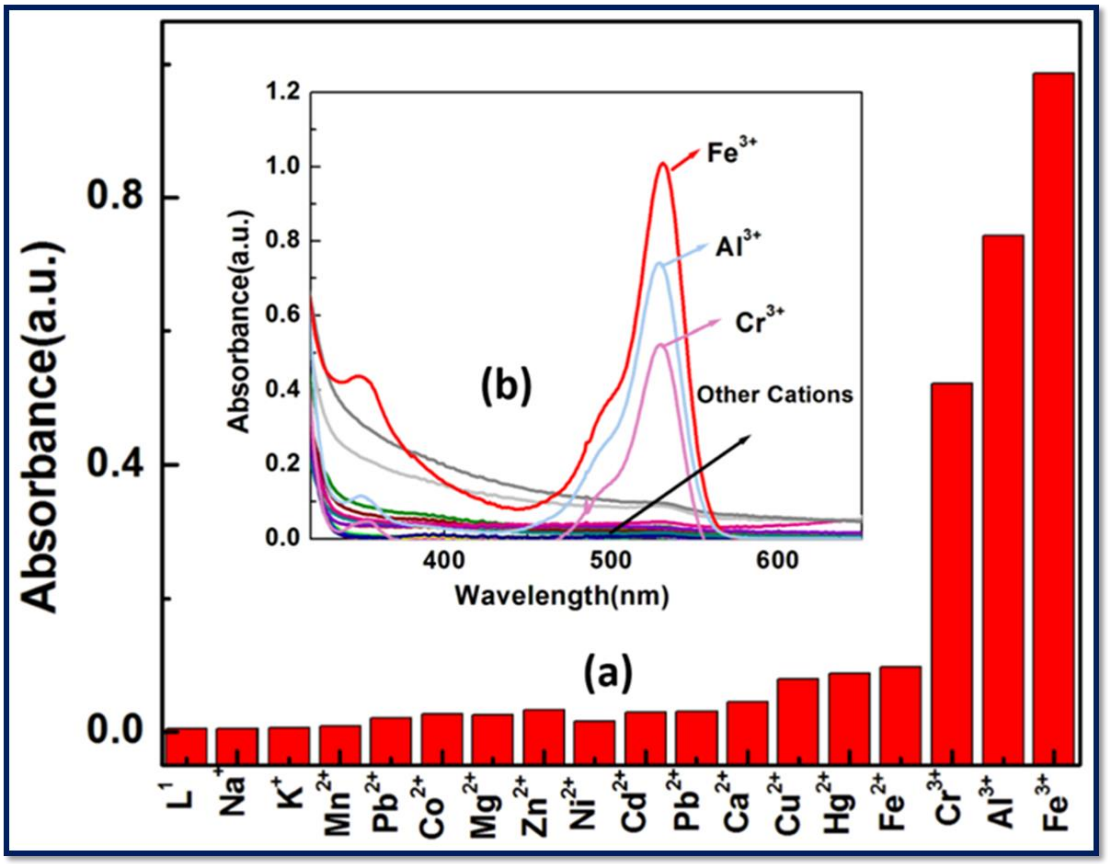

Figure-2.9: (a) UV-Vis bar diagram for the selective response of **L^1** (60 μM) towards M^{3+} (M = Fe, Al, Cr) over other di and monovalent metal ions in H_2O/CH_3CN (4:1, v/v, pH 7.2, 20 mM HEPES buffer), λ_{ex} = 502 nm, λ_{em}=558 nm); (b) UV-Vis absorbance response of **L^1** (60 μM) upon addition of 3.0 equivalents of Fe^{3+}, Al^{3+}, Cr^{3+}, Mn^{2+}, Fe^{2+}, Co^{2+}, Ni^{2+}, Cu^{2+}, Zn^{2+}, Pb^{2+}, Cd^{2+} Hg^{2+}, Na^+, K^+, Ca^{2+} and Mg^{2+}.

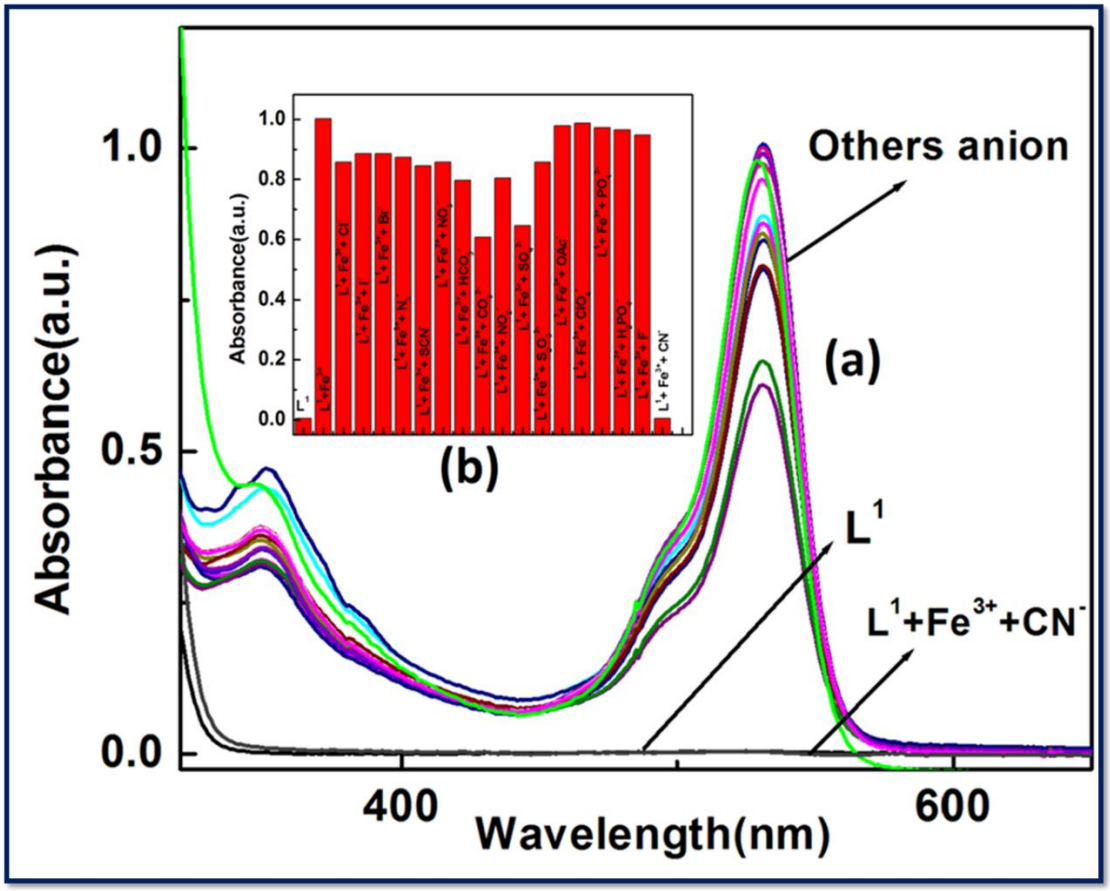

Figure-2.10: (a) UV-visible absorbance spectra of CN^- ion selectivity spectra with $\mathbf{L^1}$–Fe^{3+} complex; (b) Histogram plot of CN^-ion selectivity with $\mathbf{L^1}$-Fe^{3+} complex.

2.3.3 Fluorescence studies

The emission spectra of $\mathbf{L}^1$ and its fluorescence titration with M^{3+} (Fe^{3+}, Al^{3+} and Cr^{3+}) were performed in H_2O/CH_3CN (4: 1, v/v, pH 7.2, 20 mM HEPES buffer) with the fixed concentration of L^1 at 60 μM. A significant turn-on fluorescence response was observed in the presence of Fe^{3+}, Al^{3+} and Cr^{3+} with a fluorescent maximum at 558 nm. For example, upon gradual addition of Fe^{3+} (0–3 equivalent) to the non-fluorescent solution of $\mathbf{L^1}$, a 41-fold enhancement in fluorescence intensity at 558 nm was observed following excitation at 502 nm, which also suggests the opening of the spirolactam ring in $\mathbf{L^1}$ upon coordination to the Fe^{3+} ion [64](**Figure-2.11**). A 31-fold and 26-fold enhancement of fluorescence intensity was observed during the titration of $\mathbf{L^1}$ with Al^{3+} and

Cr^{3+} respectively (**Figure-2.12** and **Figure-2.13**). Fascinatingly, this change was also accompanied with a naked-eye colour change from colourless to orange-red after the addition of Fe^{3+}, Al^{3+} and Cr^{3+} indicating that the probe $\mathbf{L^1}$ is a highly sensitive colorimetric chemosensor for these trivalent metal cations.

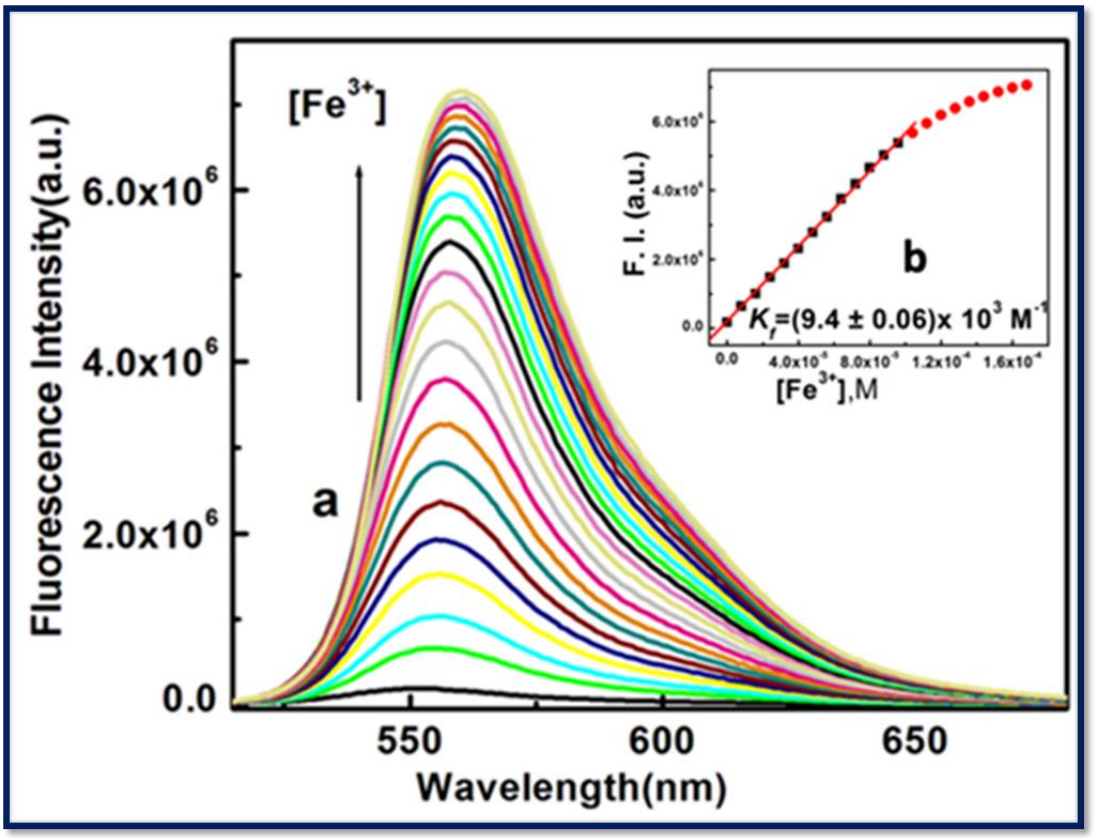

Figure-2.11: (a) Fluorescence spectra of $\mathbf{L^1}$ (60 μM) in H_2O/CH_3CN (4:1, v/v, pH 7.2, 20 mM HEPES buffer) solutions upon addition of Fe^{3+} (0-3.0 equivalent), each spectrum was taken after 3 minute of Fe^{3+}addition, λ_{ex}= 502 nm, λ_{em}= 558 nm; (b) Linear curve fitting of titration curves with K_f values.

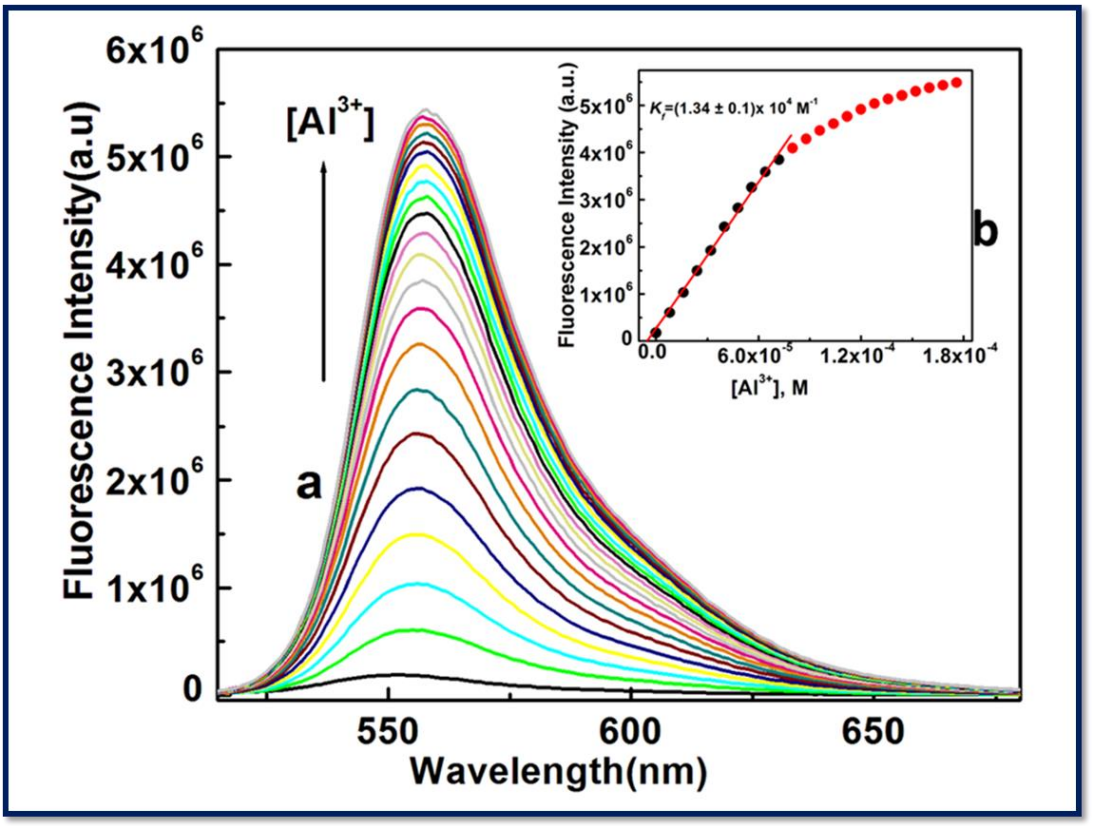

Figure-2.12: (a) Fluorescence titration of $\mathbf{L^1}$ (60 μM) in H_2O- MeCN-(4:1, v/v) in HEPES buffer at pH 7.2 by the gradual addition of Al^{3+} (0-130 μM). Inset (b), linear curve-fit of F.I vs. [Al^{3+}] plot. λ_{ex}= 502 nm, λ_{em}=558nm.

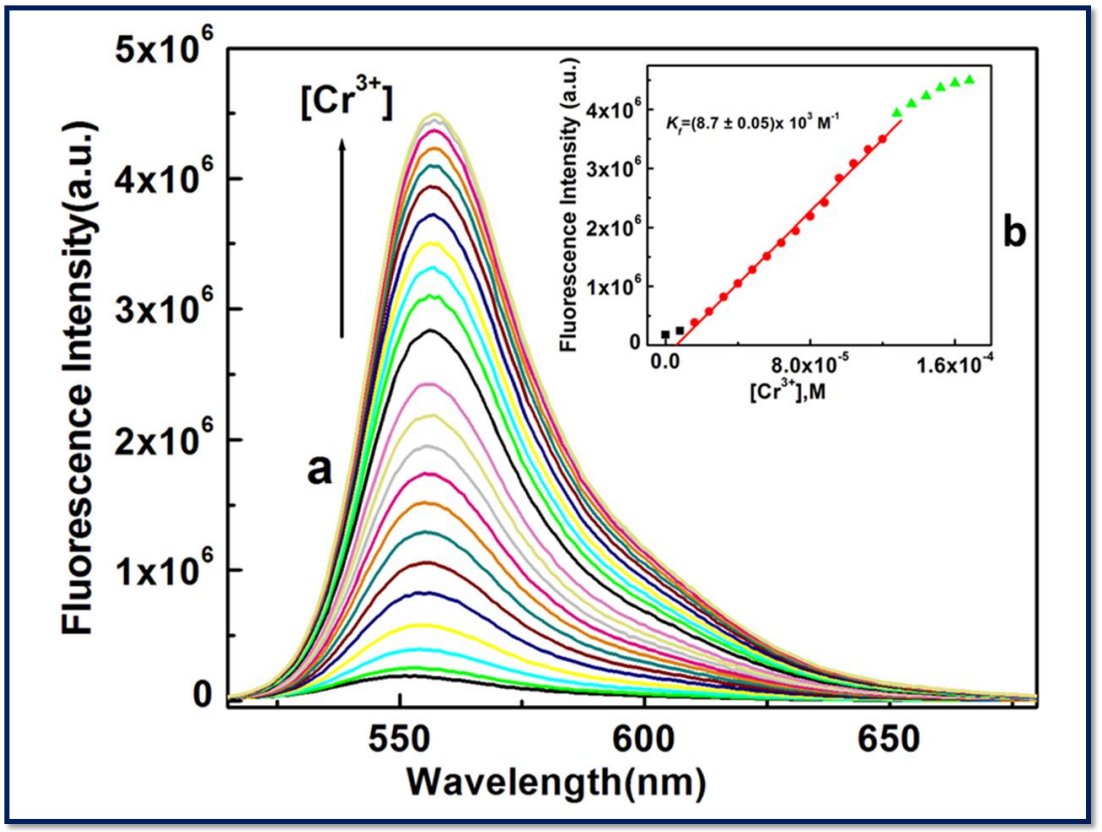

Figure-2.13: (a) Fluorometric titration of $\mathbf{L^1}$ (60 μM) in H_2O - MeCN-(4:1, v/v) in HEPES buffer at pH 7.2 by the gradual addition of Cr^{3+} (0-130 μM). Inset (b), linear curve-fit of F.I vs. [Cr^{3+}] plot. λ_{ex}= 502 nm, λ_{em}=558nm

Plots of FI vs. [M^{3+}] give linear curves. Linear curve. Fitting of the titration data according to eqn (1) (where a, b and c have the usual meaning) gave an apparent association constant K_f = (0.94 ± 0.01) × 10^4 M^{-1} for Fe^{3+} under the conditions 1 ≫ c × x with n = 1. Similarly, binding constants for Al^{3+} and Cr^{3+} were calculated and found to be (1.34 ± 0.1) × 10^4 M^{-1}, K_f = (0.87 ± 0.01) × 10^4 M^{-1}, respectively (**Figure-2.14**). There was an excellent agreement between the values of K_f obtained from the absorption and fluorescence titration data, manifesting the self-consistency of our results. Using these fluorescence data, the detection limits of the probe $\mathbf{L^1}$ for Fe^{3+}, Al^{3+} and Cr^{3+} were calculated to be 1.28, 1.34 and 2.28 μM, respectively (**Figure-2.15a-c**). These results strongly indicate that this probe $\mathbf{L^1}$ is sensitive enough to detect trace levels of Fe^{3+}, Al^{3+} and Cr^{3+}. In this context, we must highlight that the quantum yield of the ligand ($\mathbf{L^1}$) was very less. The

quantum yields of $\mathbf{L^1}$ and [$\mathbf{L^1}$–Fe^{3+}], [$\mathbf{L^1}$–Al^{3+}] and [$\mathbf{L^1}$–Cr^{3+}] complexes in H_2O/CH_3CN (4: 1, v/v, pH 7.2) were found to be 0.012, 0.489, 0.376, 0.310 respectively using rhodamine-6G as a standard. The comparatively higher values of quantum yield for complexes compared to the free ligands indicate the higher stability of the complexes in the excited states.

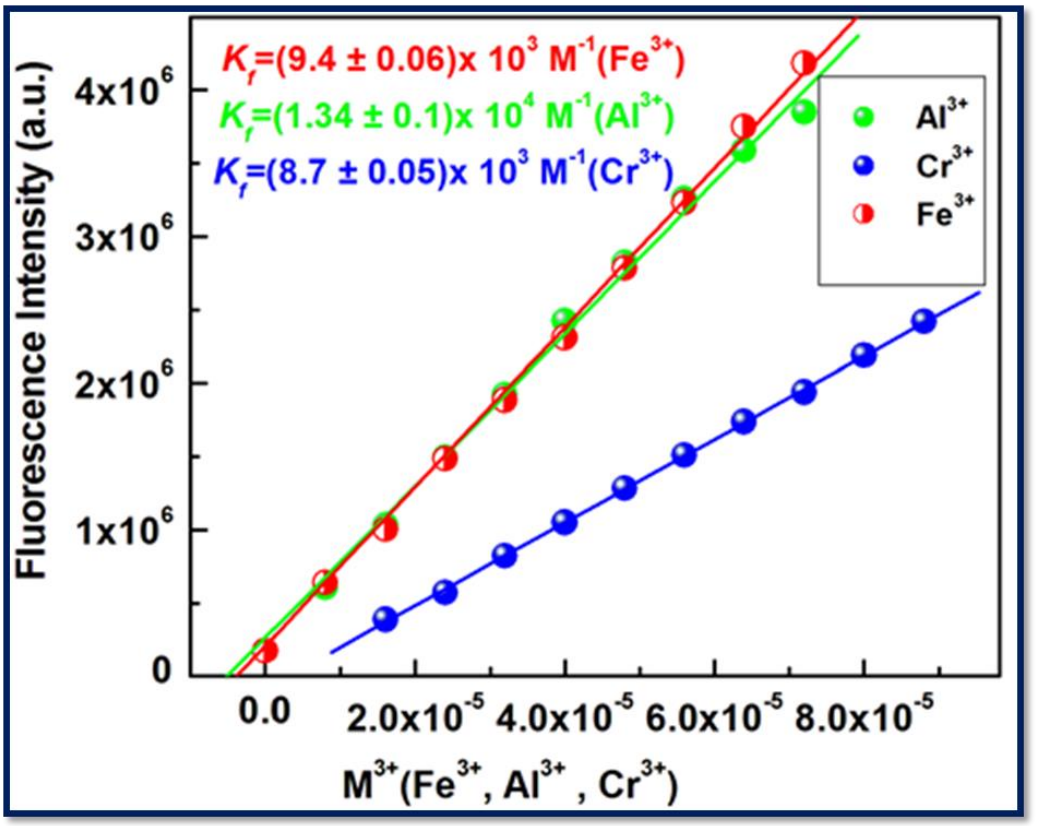

Figure-2.14: Linear fitting of fluorescence titration curves for Fe^{3+}, Al^{3+} and Cr^{3+} with K_f values.

Job's method was again employed to determine the composition of the complex, which was found to be 1:1 (**Figure-2.16a-c**) and was further supported by the mass spectrometric analysis results (m/z = 724.18 $[Fe(L^1)\ (NO_3^-)_2(CH_3CN)]^+$); (m/z = 198.06 $[Al(L^1)(MeOH)_2]^{3+}$); 721.52 $[Cr(\mathbf{L^1})(NO_3^-)_2(CH_3CN)]^+$ (**Figure-2.17-2.19).**

Moreover, a conspicuous reddish-orange fluorescence response of the probe upon interaction with M^{3+} (**Figure-2.20a**) provides the scope for naked eye detection. The possibility of using the chemosensor $\mathbf{L^1}$ in the development of paper test strips was examined and it was found that the

turn-on fluorescence response of $\mathbf{L^1}$ towards M^{3+} is also visually detectable in test paper strips (**Figure-2.20 b**).

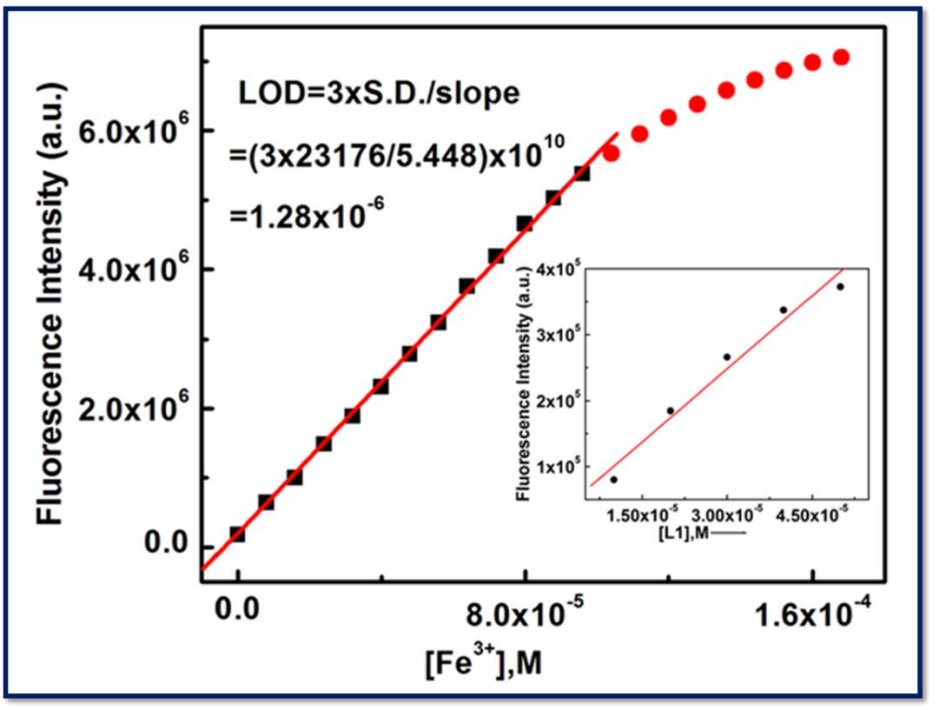

Figure-2.15a : LOD determination for Fe^{3+} by 3σ method with λ_{ex} = 502 nm, λ_{em} = 558 nm.

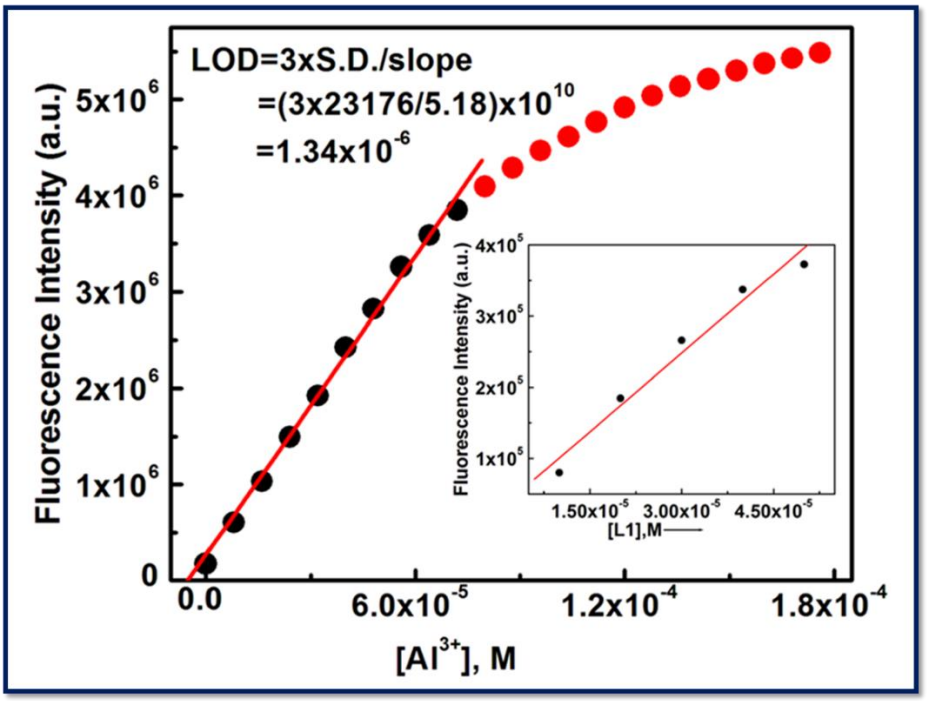

Figure-2.15b : LOD determination for Al^{3+} by 3σ method with λ_{ex} = 502 nm, λ_{em} = 558 nm.

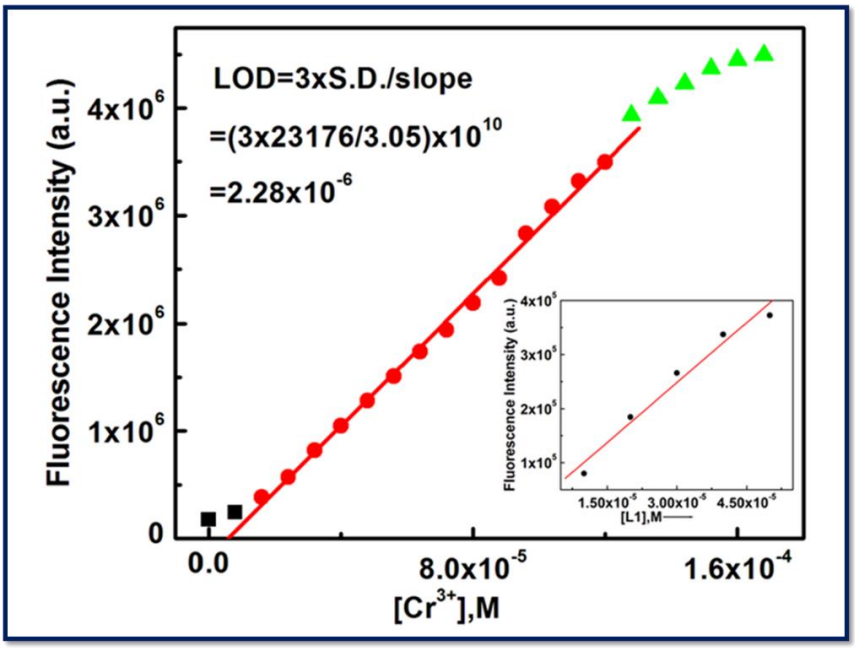

Figure-2.15c : LOD determination for Cr^{3+} by 3σ method with λ_{ex} = 502 nm, λ_{em} = 558 nm.

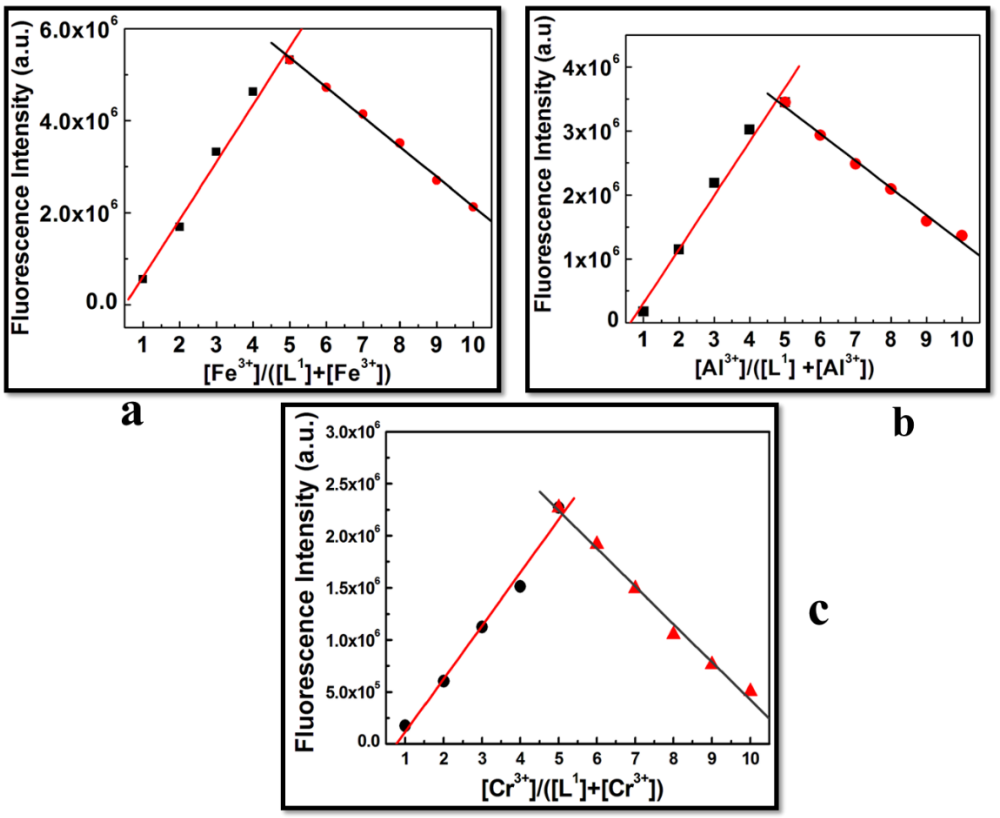

Figure-2.16: **a)** Job's plot between $\mathbf{L^1}$ and Fe^{3+} for the confirmation of (1:1) binding. **b**) Job's plot between $\mathbf{L^1}$ and Al^{3+} for the confirmation of (1:1) binding. **c**) Job's plot between $\mathbf{L^1}$ and Cr^{3+} for the confirmation of (1:1) binding.

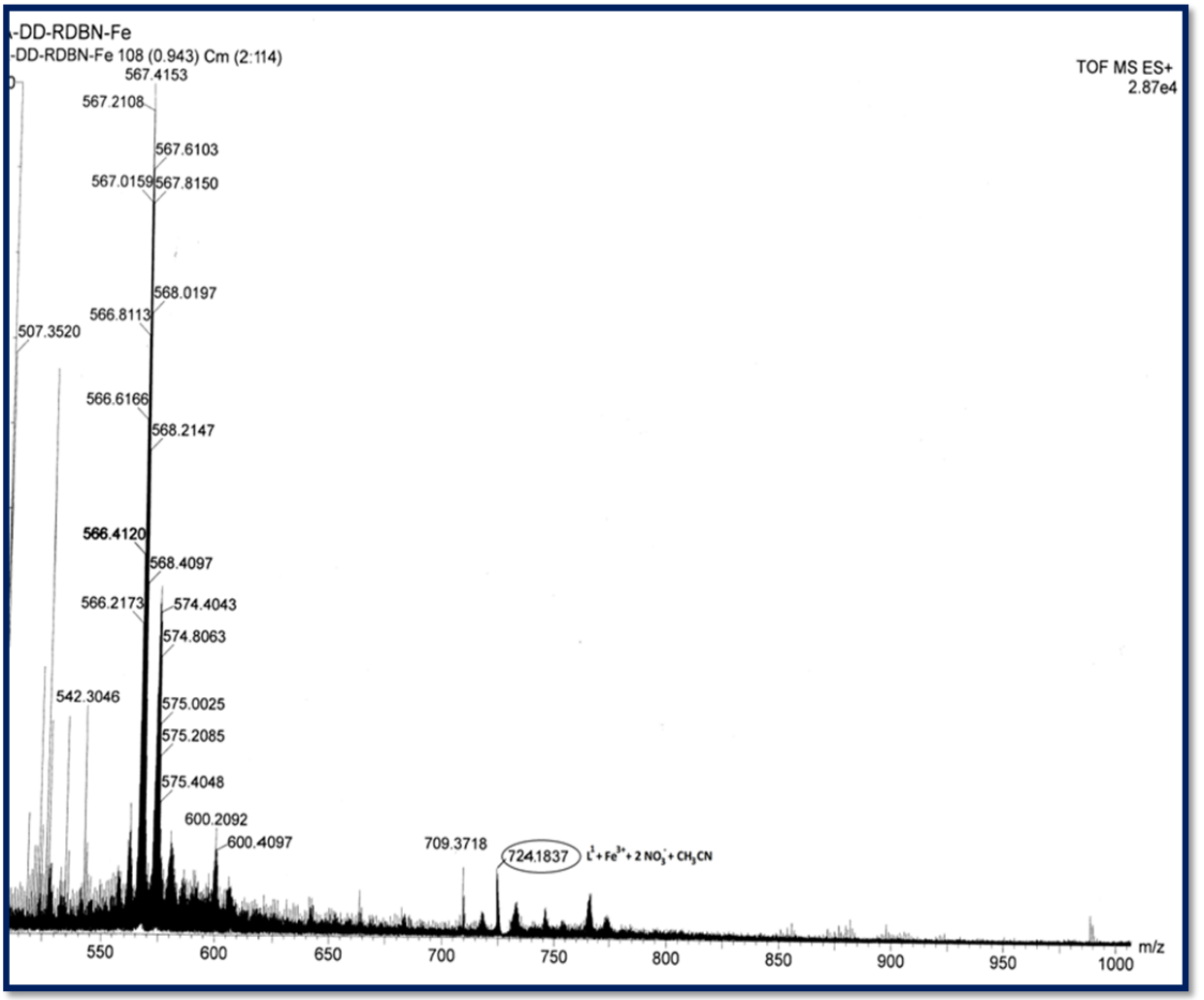

Figure-2.17: Mass spectroscopy of [$\mathbf{L^1}$-Fe^{3+}] complex in CH_3CN.

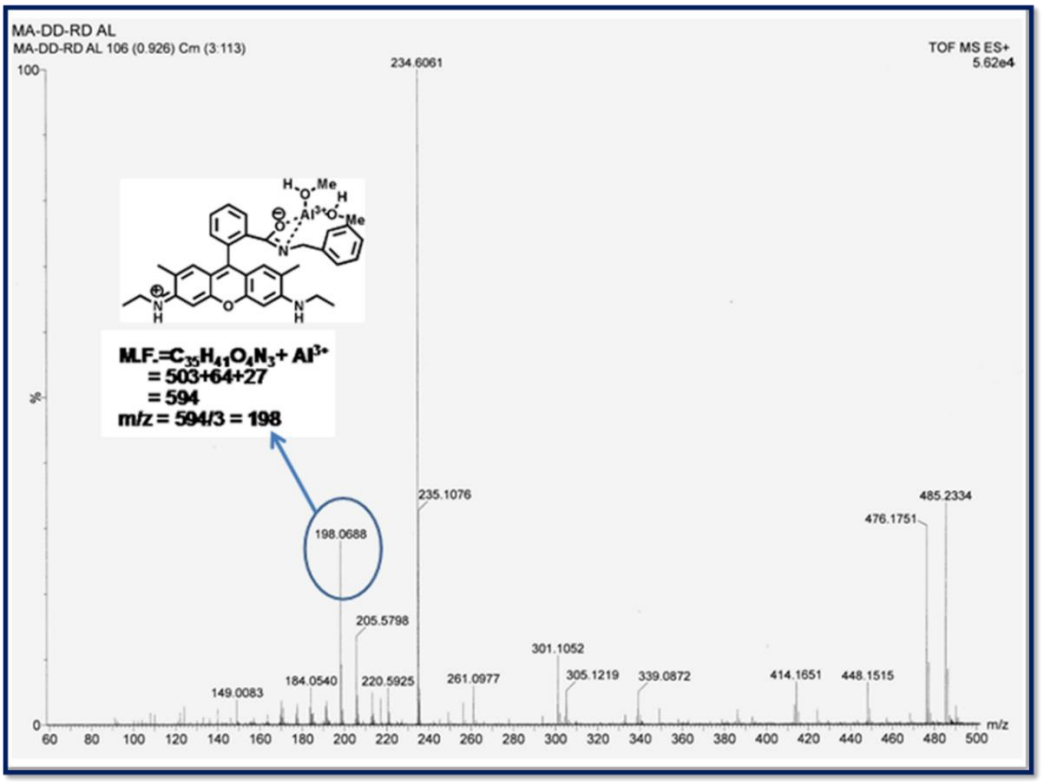

Figure-2.18: Mass spectroscopy of [L^1-Al^{3+}] complex in MeOH.

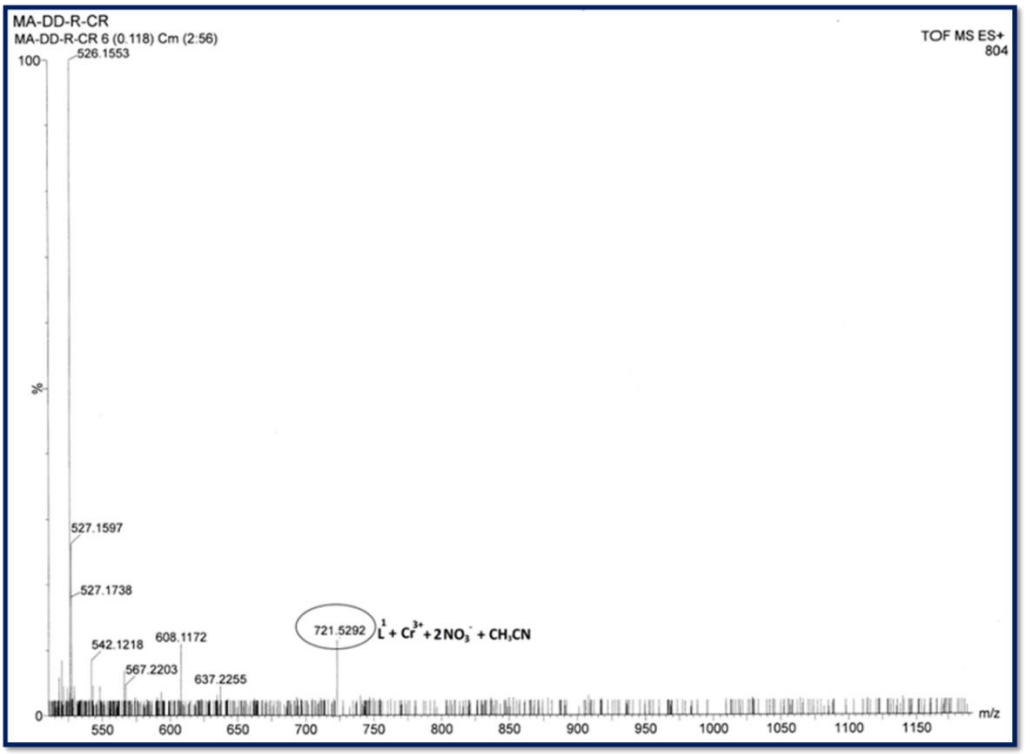

Figure-2.19: Mass spectroscopy of [$\mathbf{L^1}$-Cr^{3+}] complex in CH_3CN.

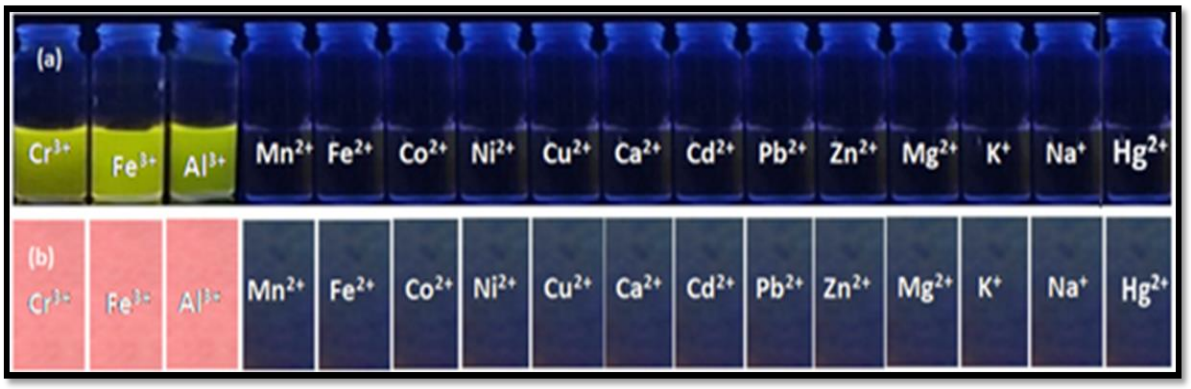

Figure-2.20: (a) Visual fluorescent response of $\mathbf{L^1}$ towards Fe^{3+}, Al^{3+} and Cr^{3+} (under 365 nm UV light). (b) Paper strip for the fluorescent sensing of Fe^{3+}, Al^{3+} and Cr^{3+}towards the probe $\mathbf{L^1}$.

2.3.4 Selectivity studies

Selectivity is an important and essential requirement for an excellent chemosensor. Selectivity experiments were carried out by taking 60 μM of probe $\mathbf{L^1}$ in a cuvette containing 2.5 mL of 20 mM buffer solution and then different metal ion solutions of about 5 equivalents were added separately. Surprisingly, $\mathbf{L^1}$ could selectively recognize the trivalent metal ions Cr^{3+}, Fe^{3+} and Al^{3+} in a mixed aqueous medium over other biologically abundant divalent 3d transition metal cations, like Mn^{2+}, Fe^{2+}, Co^{2+}, Ni^{2+}, Cu^{2+} and Zn^{2+}, hazardous heavy metal ions, like Pb^{2+}, Cd^{2+} and Hg^{2+}, alkali and alkaline earth metal ions, like Na^+, K^+, Ca^{2+}, Mg^{2+} (**Figure-2.21, Figure-2.23-2.25**) and also in the presence of Ga(III), Y(III), Sm(III), Dy(III), Au(III), Ru(III), Co(III) and Cr(VI) ions (**Figure-2.26**), which were taken in 5 equivalent with respect to the probe (1 : 5 ratio).

It was also found that not a single anionic species among OAc^-, HCO_3^-, CO_3^{2-}, $S_2O_3^{2-}$, SCN^-, N_3^-, NO_3^-, NO_2^-, $H_2PO_4^-$, SO_4^{2-}, ClO_4^-, F^-, Cl^-, Br^-, I^-, PO_4^{3-} and CN^- could enhance the fluorescence intensity of the probe $\mathbf{L^1}$ (**Figure-2.22**) when taken in 5 equivalent with respect to the probe (1:5 ratio). However, the fluorescence intensity of the [$\mathbf{L^1}$–M^{3+}] complex was found to be selectively quenched in the presence CN^- ions (**Figure-2.27 - 2.29** and **Figure-2.30 – 2.32**). An excellent reversible fluorescence ON–OFF property of $\mathbf{L^1}$ was observed through fluorescence study with the sequential addition of M^{3+} and CN^- ions in 20 mM HEPES buffer in H_2O/CH_3CN (4:1) (pH 7.2) solution at room temperature (**Figure-2.33**). The addition of cyanide ions to the solution containing L^1–M^{3+} complex quenched the emission of the probe with the disappearance of the orange-red colour of the solution. The fluorescence quenching of the complexes was

characterized by a linear Stern–Volmer (SV) plot and analyzed using the classical Stern–Volmer (SV) eqn (**7**) [65]

$$\frac{F_0}{F} = 1 + K_{SV}[Q] \qquad (7)$$

where F_0 and F are the steady state fluorescence intensities at the maximum wavelength in the absence and presence of a quencher (Q), respectively, [Q] is the quencher concentration and K_{SV} is the Stern–Volmer constant. The Stern-Volmer quenching constant (K_{SV}) of [$\mathbf{L^1}$–Fe^{3+}], [$\mathbf{L^1}$–Al^{3+}] and [$\mathbf{L^1}$–Cr^{3+}] complexes with CN^- ion were calculated and found to be (5.60 ± 0.20) × 10^2 M^{-1}, (2.42 ± 0.24) × 10^2 M^{-1} and (1.88 ±0.11) × 10^2 M^{-1}, respectively (**Figure-2.34a-c**). The reason behind this observation is that the interaction of M^{3+} with the probe results in opening of the spirolactam ring, thereby producing strong fluorescence. Then treatment with CN^- results in the abstraction of a metal ion and regeneration of the spirolactam ring, leading to quenching of the emission. The mechanism between $\mathbf{L^1}$–M^{3+} with CN^- ion sensing was confirmed by the HRMS study (**Figure-2.35a-c**). It is clear from the HRMS study that the ligand is in a ring-closed structure exactly the same with the $\mathbf{L^1}$. This reversibility test suggests the reusability of this chemosensor.

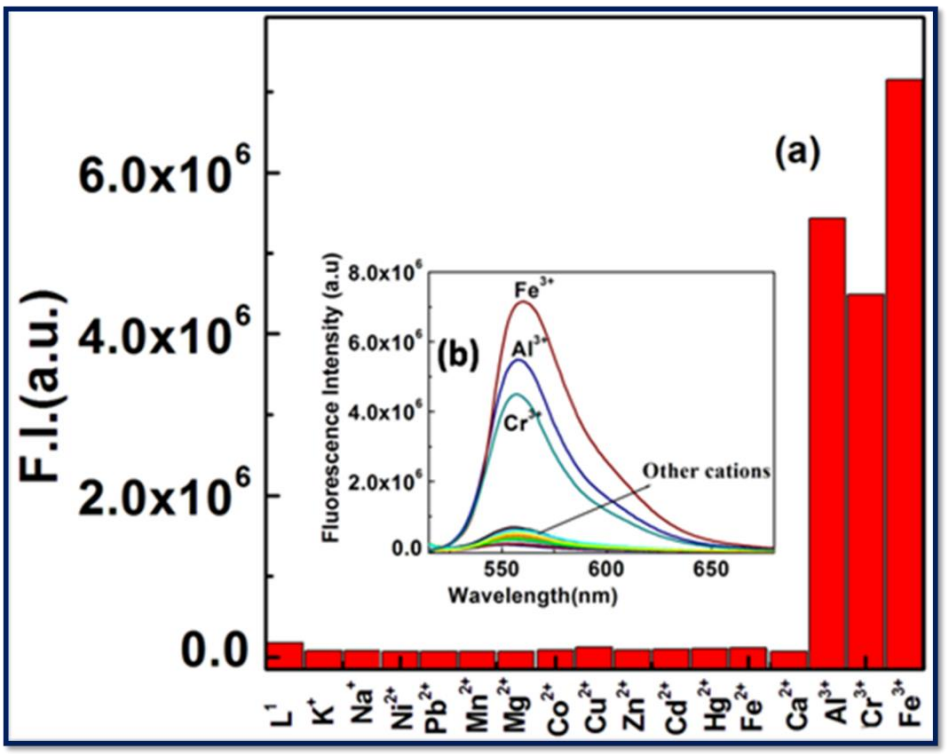

Figure-2.21: (a) Fluorescence bar diagram for the selective response of $\mathbf{L^1}$ (60 μM) towards M^{3+} (M = Fe, Al, Cr) over other di and monovalent metal ions (5 equivalent) in H_2O/CH_3CN (4:1, v/v,

pH 7.2, 20 mM HEPES buffer), λ_{ex} = 502 nm, λ_{em} = 558 nm); (b) Fluorescence response of **L**^{1} (60 μM) upon addition of 3.0 equivalent Fe^{3+}, Al^{3+}, Cr^{3+}.

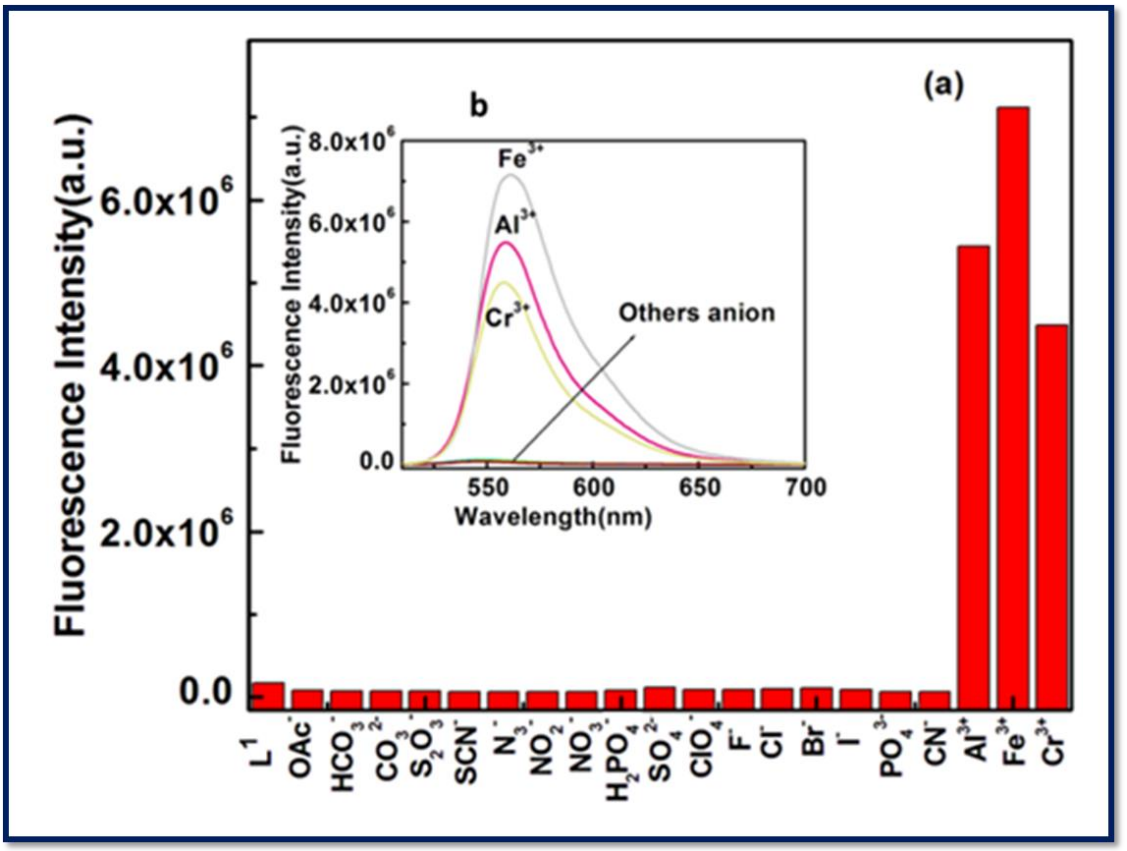

Figure-2.22 : (a) Histogram of the fluorescence responses of different anions (5 equivalent) towards **L**^{1} (60 μM) in 4:1 v/v,water/ MeCN in HEPES buffer at pH 7.2with λ_{ex} = 502 nm, λ_{em} = 558 nm. (b) The fluorescence response of **L**^{1} towards Fe^{3+}, Al^{3+}, Cr^{3+} with respect to different anions (300 μM)

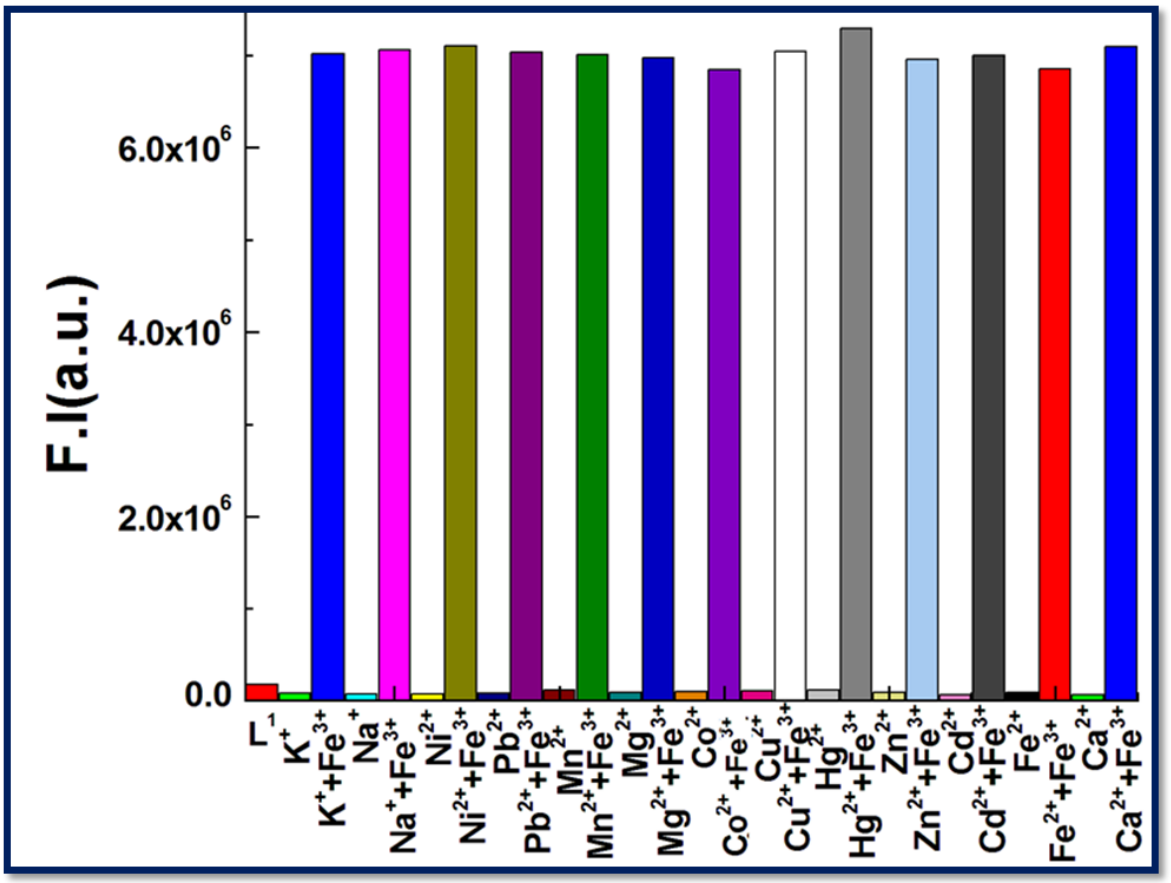

Figure-2.23: Fluorescence bar diagram for the selective response of **L[1]** (60 μM) towards M^{3+} (M = Fe) over other metal ions(5 equivalent with respect to **L[1])** in 4 : 1 v/v, water / MeCN in HEPES buffer at pH 7.2 with λ_{ex} = 502 nm, λ_{em} = 558 nm.

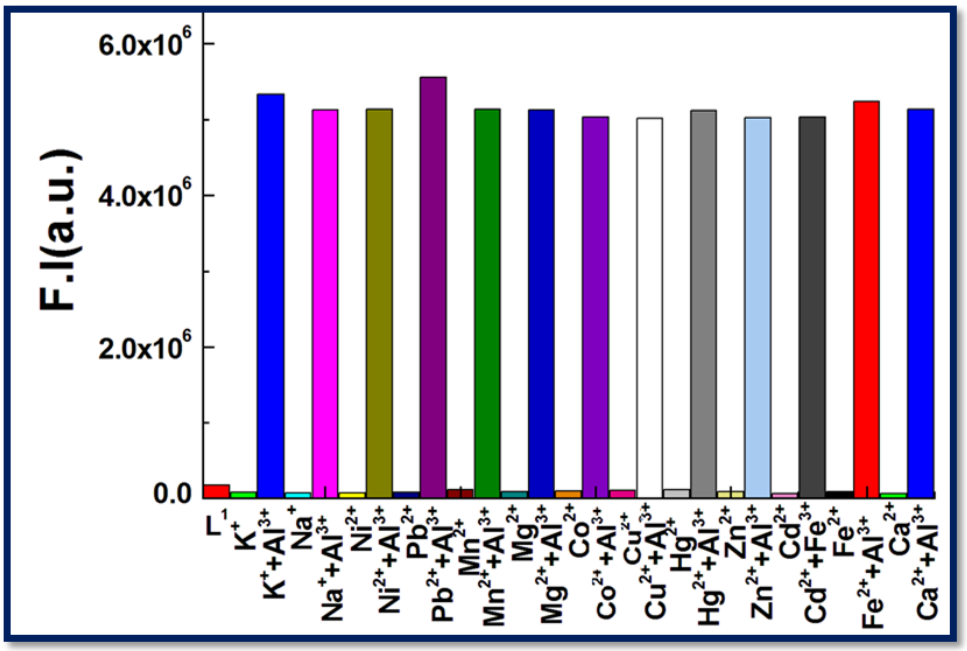

Figure-2.24 : Fluorescence bar diagram for the selective response of $\mathbf{L^1}$ (60 μM) towards M^{3+} (M = Al) over other metal ions(5 equivalent with respect to L^1) in 4 : 1 v/v, water / MeCN in HEPES buffer at pH 7.2 with λ_{ex} = 502 nm, λ_{em} = 558 nm.

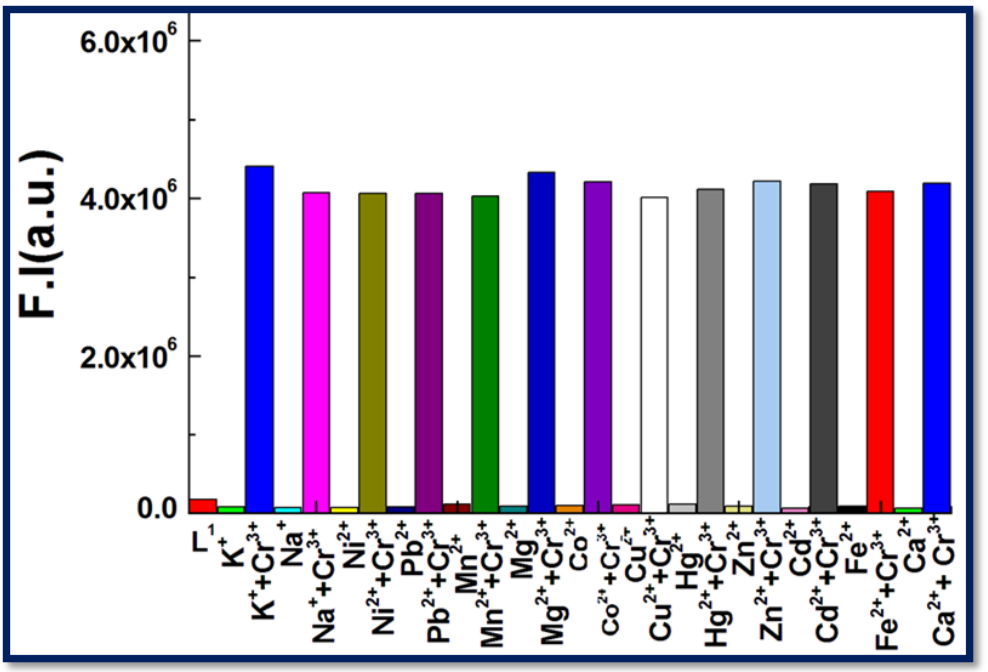

Figure-2.25 : Fluorescence bar diagram for the selective response of $\mathbf{L^1}$ (60 μM) towards M^{3+} (M = Cr) over other metal ions(5 equivalent with respect to $\mathbf{L^1}$) in 4 : 1 v/v, water / MeCN in HEPES buffer at pH 7.2 with λ_{ex} = 502 nm, λ_{em} = 558 nm.

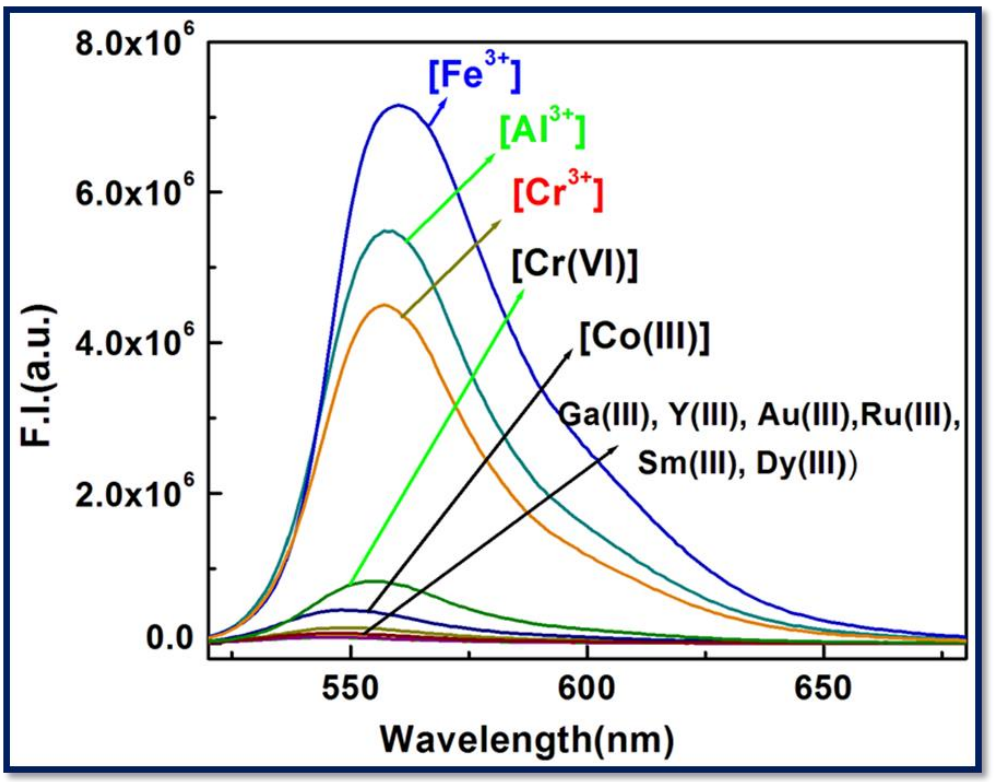

Figure-2.26: Fluorescence selective response of $\mathbf{L^1}$ (60 μM) towards M^{3+} (M = Fe, Al, Cr) over Ga(III), Y(III), Sm(III), Dy(III), Au(III), Ru(III), Co(III) and Cr(VI) ions which are taken in 5 equivalents with respect to the probe(1:5 ratio) in H_2O/CH_3CN (4:1, v/v, pH 7.2, 20 mM HEPES buffer), λ_{ex} = 502 nm, λ_{em}=558 nm.

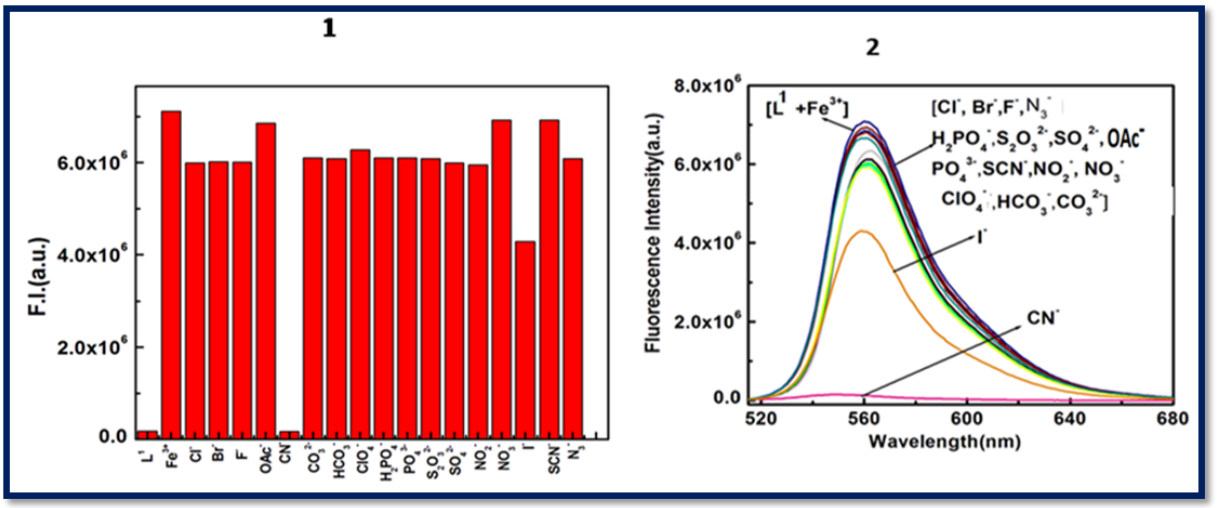

Figure-2.27 : (1) Histogram of the fluorescence quenching of [$\mathbf{L^1}$-Fe^{3+}]complex towards CN^- (100 μM) in 4 : 1 v/v, water / MeCN in HEPES buffer at pH 7.2 with λ_{ex} = 502 nm, λ_{em} = 558 nm. (2)

Selective fluorescence quenching of [$\mathbf{L^1}$–Fe^{3+}]complex towards CN^- with respect to different anions (5 equivalent with respect to [$\mathbf{L^1}$-Fe^{3+}] complex) in 4:1 v/v, water / MeCN in HEPES buffer at pH 7.2 with λ_{ex} = 502 nm, λ_{em} = 558 nm.

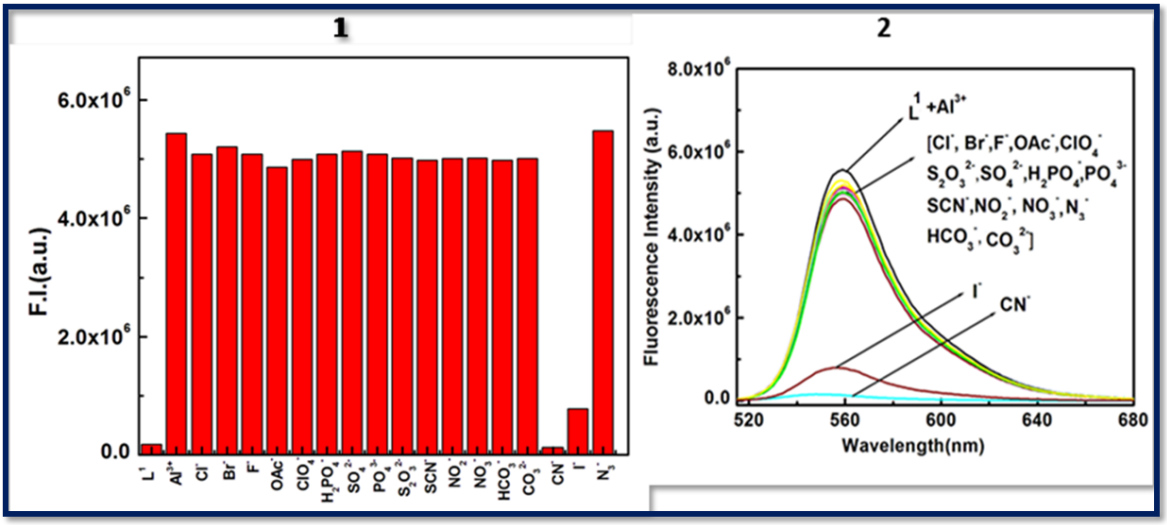

Figure-2.28 :(1) Histogram of the fluorescence quenching [$\mathbf{L^1}$-Al^{3+}]complex towards CN^- (100 μM) in 4:1 v/v, water / MeCN in HEPES buffer at pH 7.2 with λ_{ex} = 502 nm, λ_{em} = 558 nm. (2) Selective fluorescence quenching of [$\mathbf{L^1}$-Al^{3+}]complex towards CN^- with respect to different anions (5 equivalent with respect to [L^1–Al^{3+}]complex) in 4:1 v/v, water / MeCN in HEPES buffer at pH 7.2 with λ_{ex} = 502 nm, λ_{em} = 558 nm.

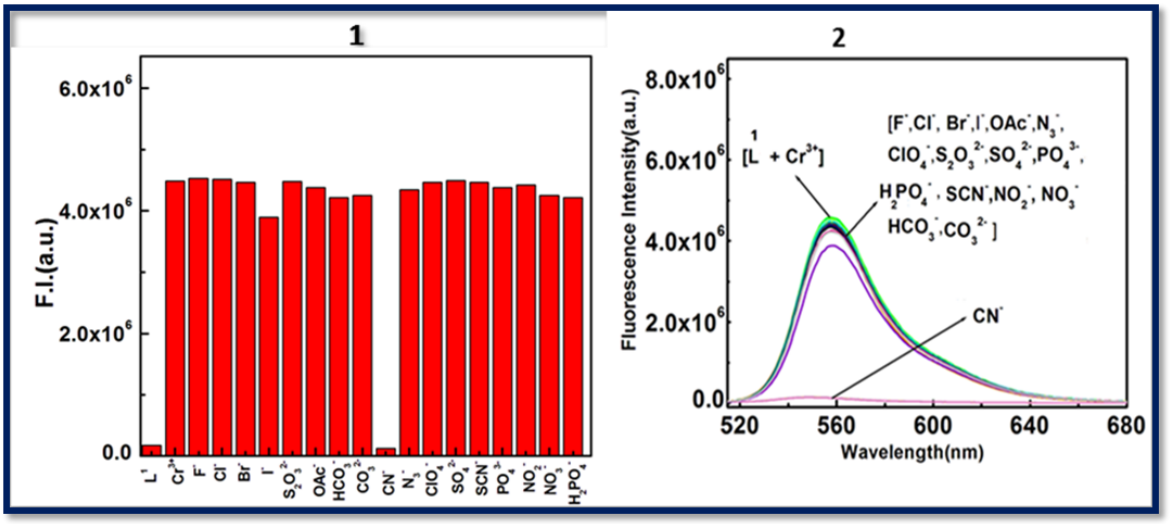

Figure-2.29 :(1) Histogram of the fluorescence quenching [$\mathbf{L^1}$-Cr^{3+}]complex towards CN^- (100 μM) in 4 : 1 v/v, water / MeCN in HEPES buffer at pH 7.2 with λ_{ex} = 502 nm, λ_{em} = 558 nm. Inset

(2) Selective fluorescence quenching of [$\mathbf{L^1}$–Cr^{3+}] complex towards CN^- with respect to different anions (5 equivalent with respect to [L^1–Cr^{3+}]complex) in 4 : 1 v/v, water / MeCN in HEPES buffer at pH 7.2 with λ_{ex} = 502 nm, λ_{em} = 558 nm.

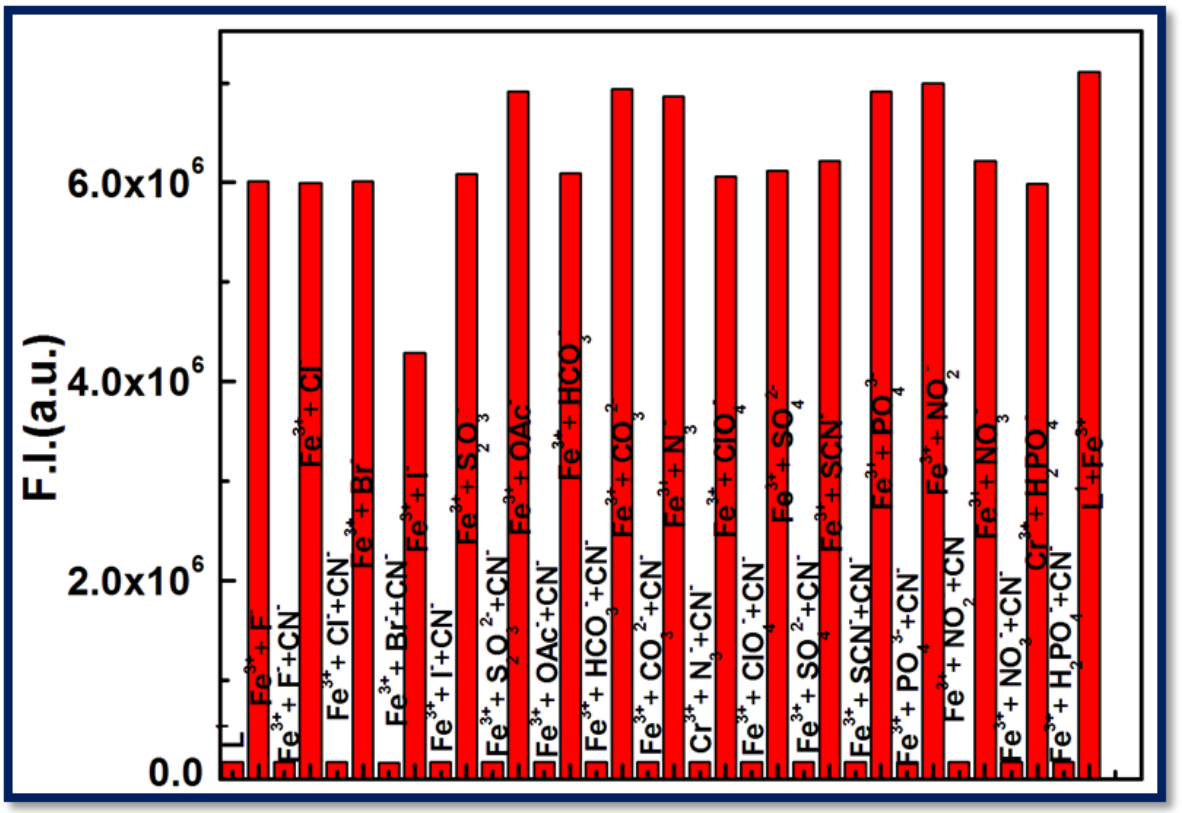

Figure-2.30 : Histogram of the selective fluorescence quenching [$\mathbf{L^1}$-Fe^{3+}] complex by CN^- (100 μM) in 4 : 1 v/v, water / MeCN in HEPES buffer at pH 7.2 in presence of different anions (5 equivalent with respect to [$\mathbf{L^1}$–Fe^{3+}] complex (λ_{ex} = 502 nm, λ_{em} = 558 nm).

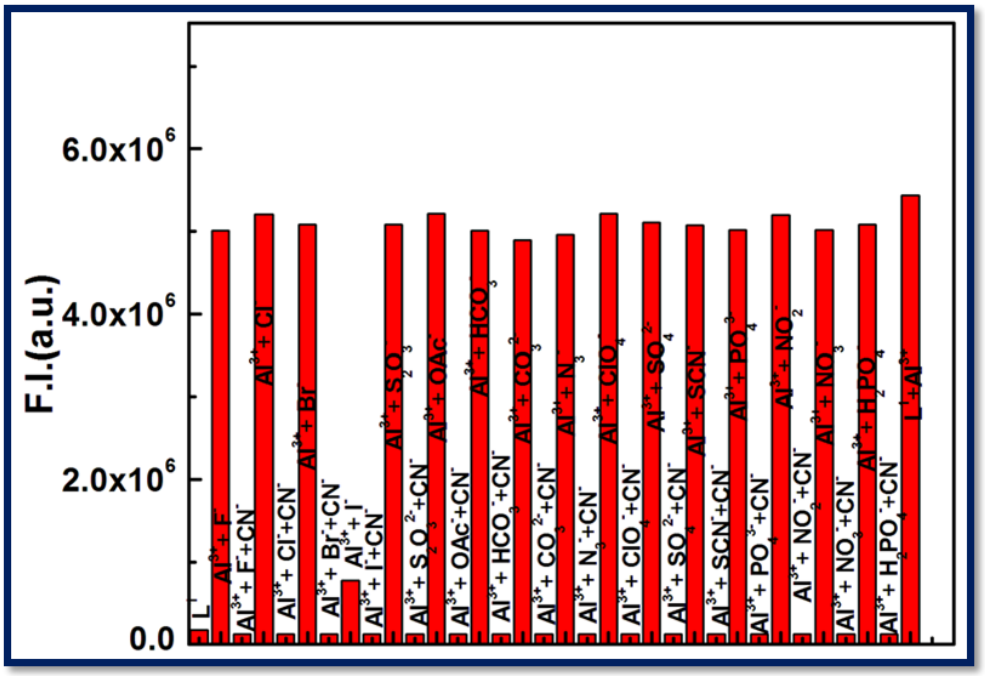

Figure-2.31: Histogram of the selective fluorescence quenching [$\mathbf{L^1}$-Al^{3+}] complex by CN^- (100 μM) in 4 : 1 v/v, water / MeCN in HEPES buffer at pH 7.2 in presence of different anions (5 equivalent with respect to [$\mathbf{L^1}Al^{3+}$] complex) (λ_{ex} = 502 nm, λ_{em} = 558 nm).

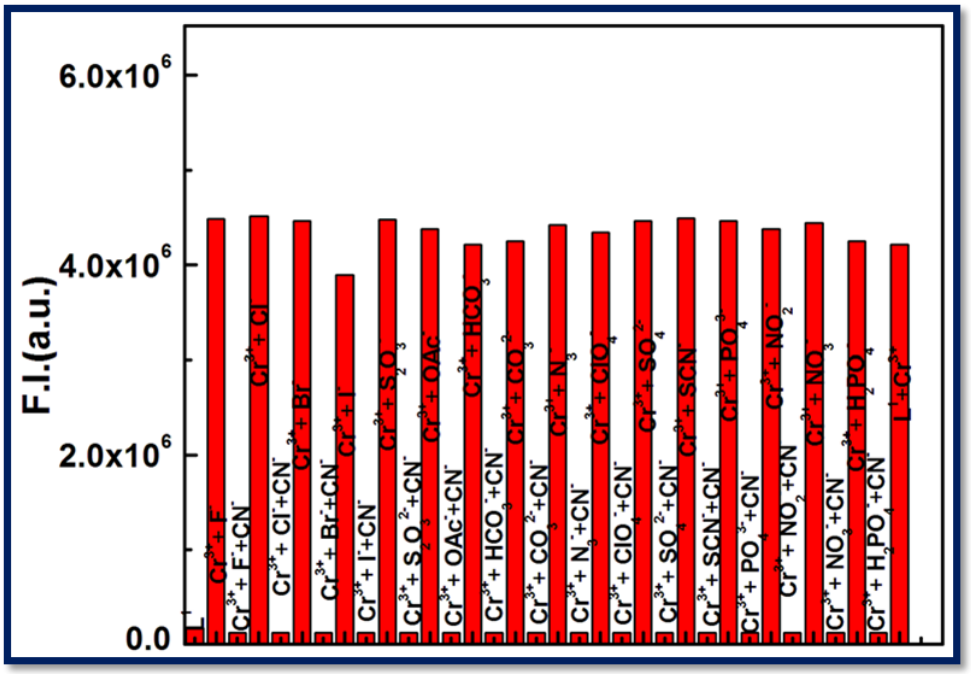

Figure-2.32: Histogram of the selective fluorescence quenching [$\mathbf{L^1}Cr^{3+}$]complex by CN^- (100 μM) in 4 : 1 v/v, water / MeCN in HEPES buffer at pH 7.2 in presence of different anions (5 equivalent with respect to [L^1Cr^{3+}]complex) (λ_{ex} = 502 nm, λ_{em} = 558 nm).

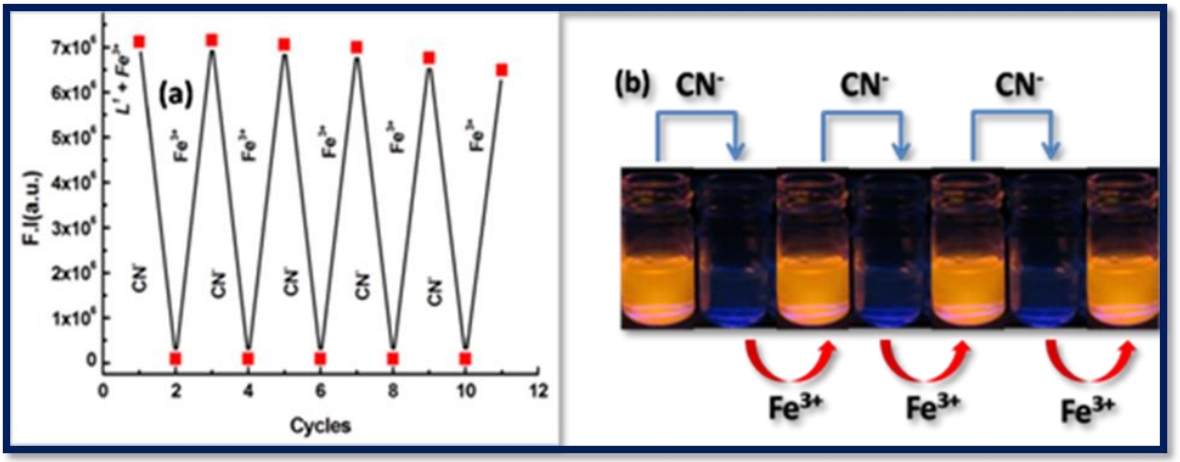

Figure-2.33: Fluorescence experiment to show the reversibility and reusability of the receptor for sensing Fe^{3+} by alternate addition of CN^-. (a) Fluorescence intensity obtained during the titration of $\mathbf{L^1}$–Fe^{3+} with CN– followed by the addition of Fe^{3+}. (b) Visual fluorescent color changes after each addition of CN^- and Fe^{3+} sequentially.

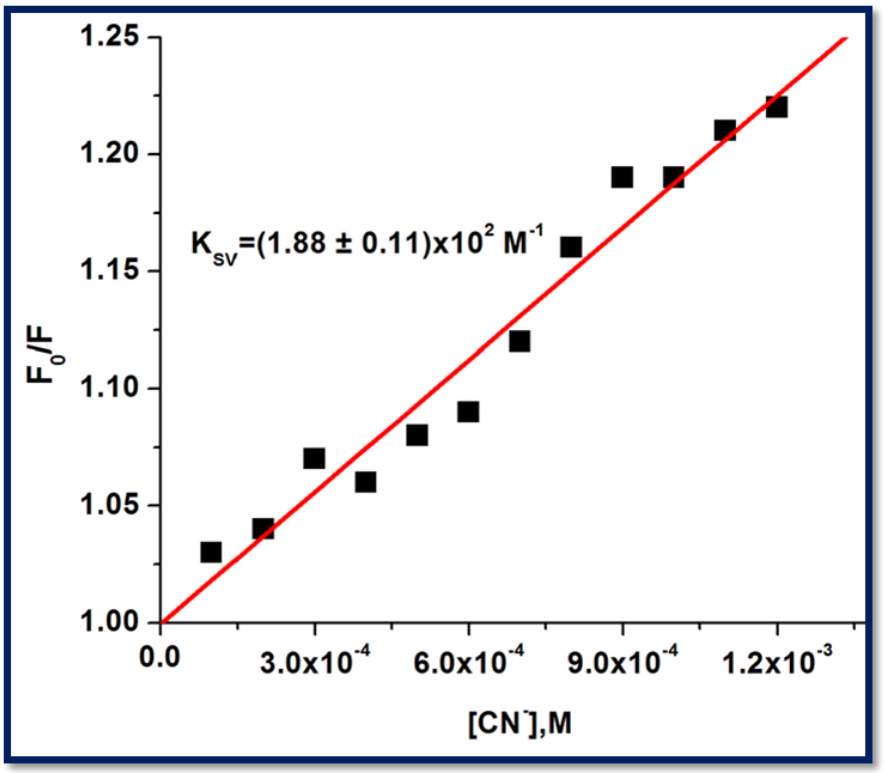

Figure-2.34a: Linear Stern–Volmer plot for the titration of [$\mathbf{L^1}$—Cr^{3+}] complex with CN^- ion.

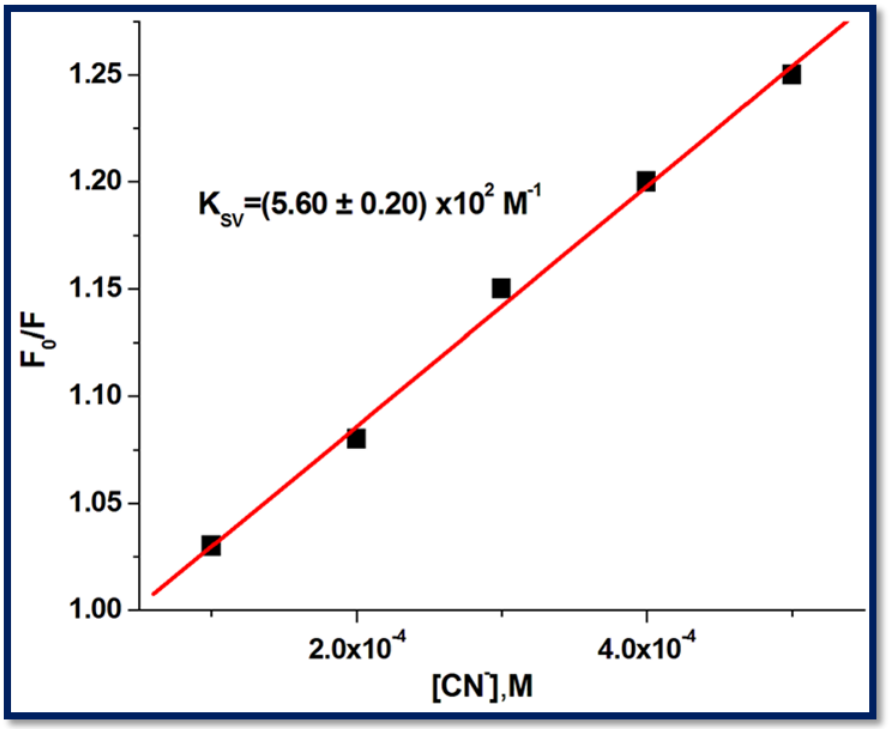

Figure-2.34b: Linear Stern–Volmer plot for the titration of [$\mathbf{L^1}$–Fe^{3+}] complex with CN^-ion.

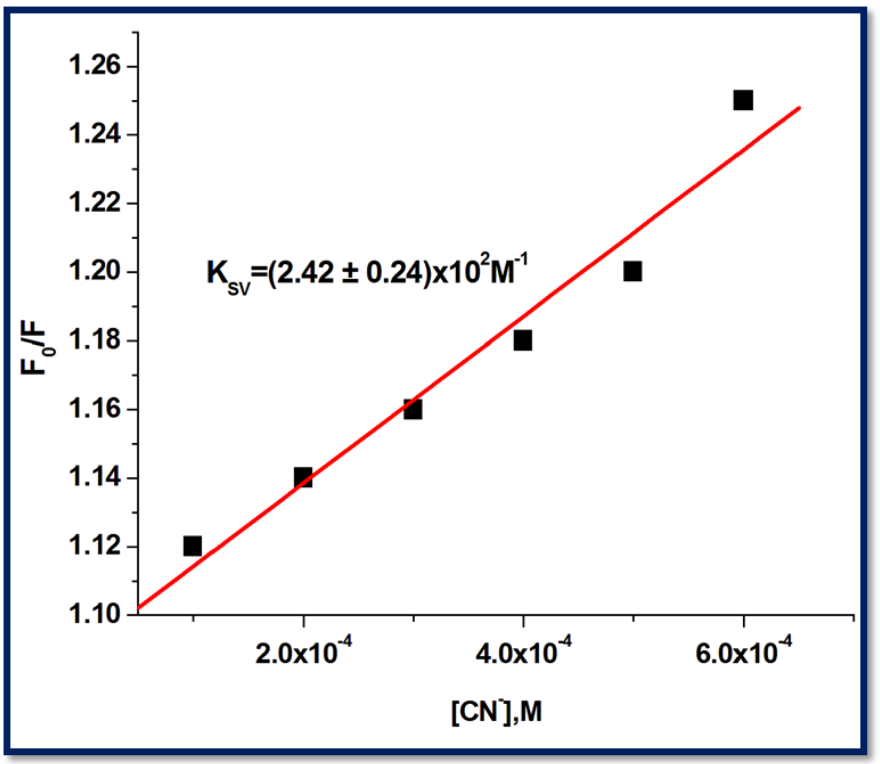

Figure-2.34c: Linear Stern–Volmer plot for the titration of [$\mathbf{L^1}$—Al^{3+}] complex with CN^- ion.

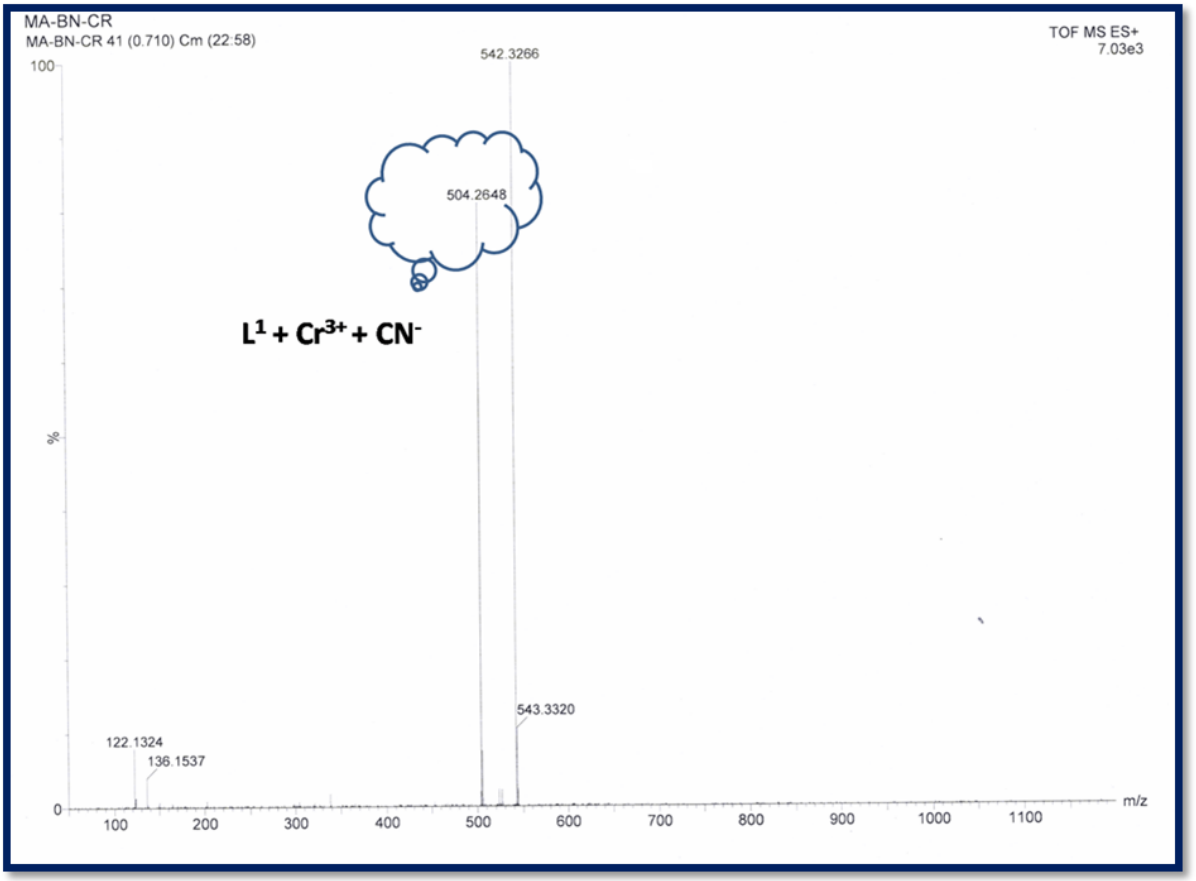

Figure- 2.35a: Mass spectroscopy of [$\mathbf{L^1}$-Cr^{3+} + CN^-] in CH_3CN.

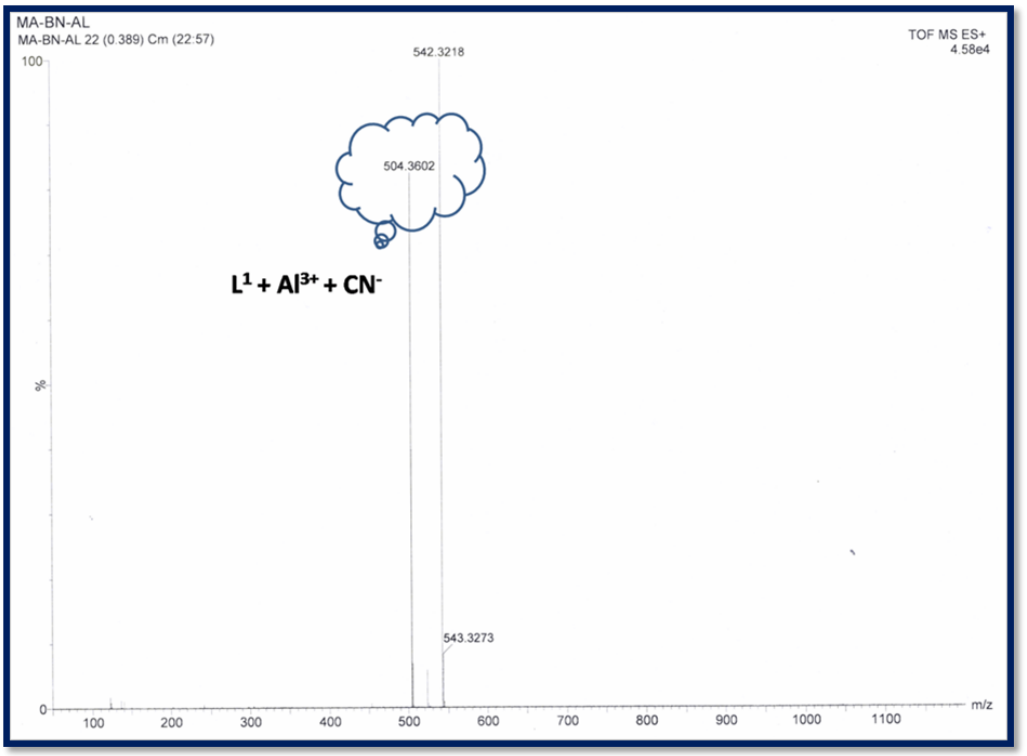

Figure-2.35b: Mass spectroscopy of [$\mathbf{L^1}$-Al^{3+} + CN^-] in CH_3CN.

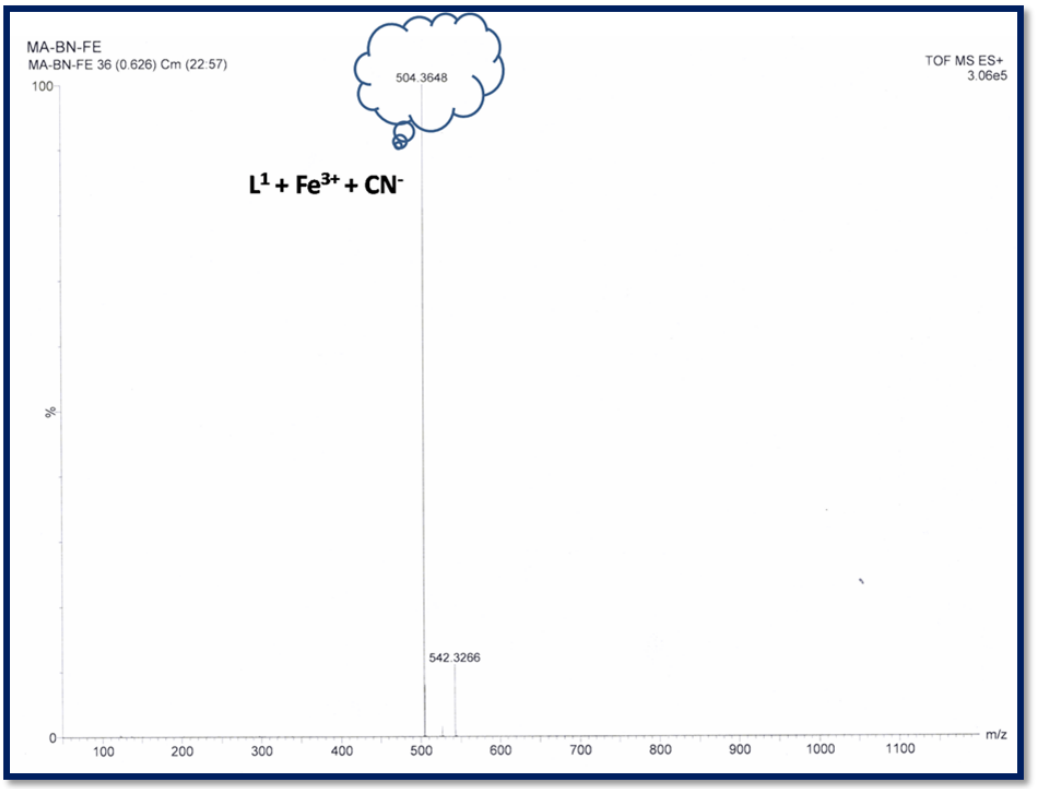

Figure-2.35c: Mass spectroscopy of [$\mathbf{L^1}$-Fe^{3+} + CN^-] in CH_3CN.

2.3.5 pH studies

For practical application, the appropriate pH condition for the sensor was evaluated. At pH > .0, no obvious ring opening of the probe was observed, thereby satisfying the usefulness of the probe in biological systems over a wide pH range (4–8) for the detection of Fe^{3+} (**Figure-2.36**), Al^{3+} and Cr^{3+} (**Figure-2.37** and **Figure-2.38**). However, upon the addition of 3.0 equivalent of Fe^{3+}, the FI jumps to a very high value and remains almost unchanged in the range pH 3–7, but then on a further increase in pH, the FI gradually falls. At pH > 8, no FI was observed in the case of Fe^{3+}, Al^{3+} and Cr^{3+} due to the precipitation of hydroxides of these metal ions.

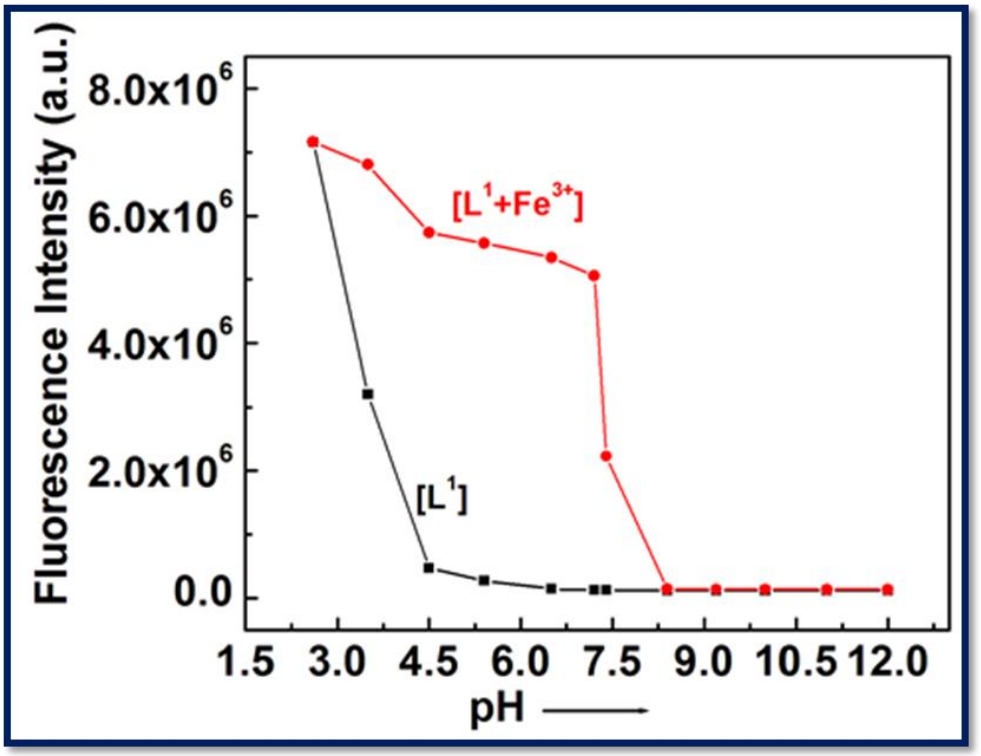

Figure-2.36 : pH dependence of fluorescence responses of $\mathbf{L^1}$ and its $\mathbf{[L^1–Fe^{3+}]}$ complex in H_2O /CH_3CN (4:1,v/v) with λ_{ex} = 502 nm, λ_{em} = 558 nm.

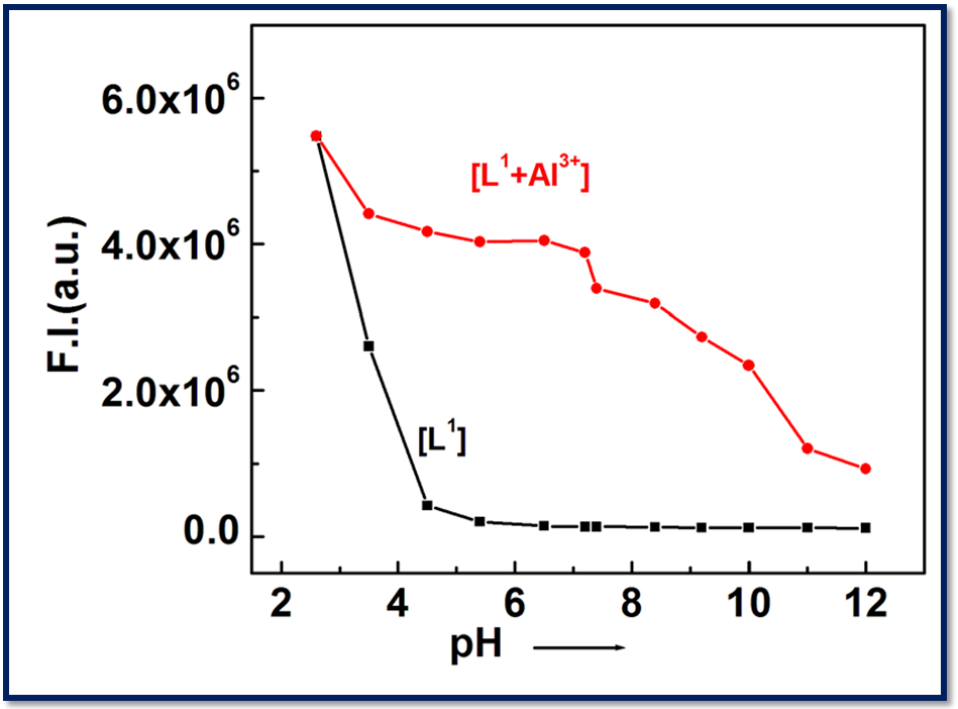

Figure-2.37: Fluorescence intensity observed at different pH for $\mathbf{L^1}$ and $[\mathbf{L^1}+Al]^{3+}$ (60 μM) in H_2O /CH_3CN (4:1,v/v) with λ_{ex} = 502 nm, λ_{em} = 558 nm.

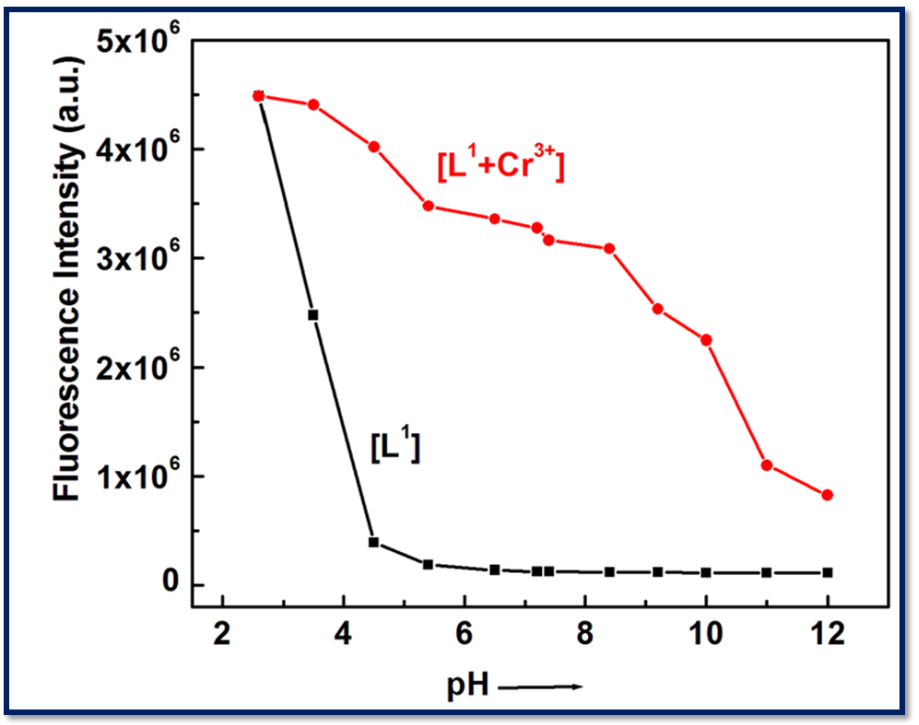

Figure-2.38 : Fluorescence intensity observed at different pH for $\mathbf{L^1}$ and $[\mathbf{L^1}+Cr]^{3+}$ (60 μM) in H_2O /CH_3CN (4:1,v/v) with λ_{ex} = 502 nm, λ_{em} = 558 nm.

2.3.6 Spectral studies

The mechanistic pathway proposed for the formation of the $\mathbf{L^1}$–M^{3+} complex by the opening of the spirolactam ring was established through IR and 1H-NMR studies. The IR studies revealed that the characteristic stretching vibrational frequencies of the amidic 'C=O' of the rhodamine moiety at 1684 cm^{-1} and azomethine group (C=N) at 1636 cm^{-1} were shifted to lower wavenumbers 1636, 1637, 1635 cm^{-1} and 1605, 1604, 1604 cm^{-1} in the presence of 3.0 equivalent of Fe^{3+}, Al^{3+} and Cr^{3+} respectively (**Figure-2.39** and **Figure-2.40**). These large shifts in IR frequencies signify a strong polarization of the C=O and C=N bonds upon efficient binding to the M^{3+} (M = Al, Fe and Cr) ion. The coordination mode of $\mathbf{L^1}$ towards Al^{3+} was supported by 1H-NMR studies (**Figure-2.41**) which showed a downfield shift of azomethine proton in $\mathbf{L^1}$ and also of the protons on the benzene ring of the benzylamine moiety in the L^1–Al^{3+} complex. The broadening of the –NH proton at 4.9 was due to opening of the spirolactam ring and it bearing a positive charge on it. HRMS study (**Figure-2.17-2.19**) also confirmed the formation of a complex with M^{3+} (M = Al, Fe and Cr).

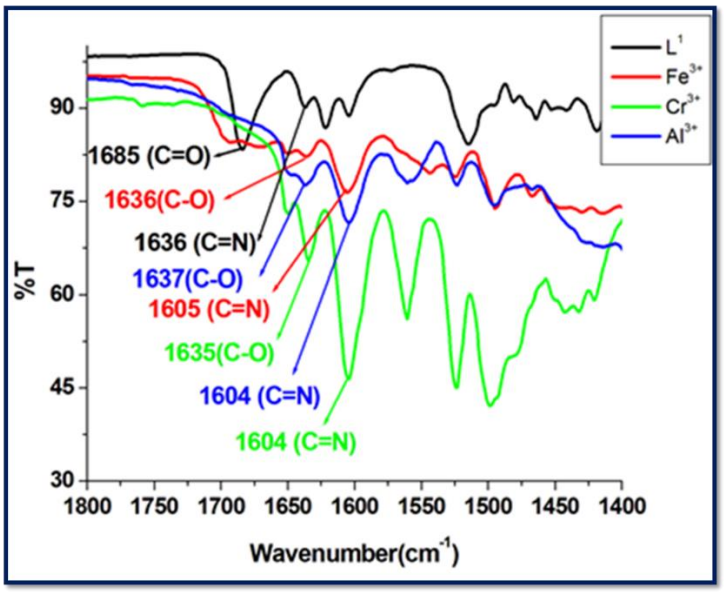

Figure-2.39: IR spectra of **($\mathbf{L^1}$),** [$\mathbf{L^1 + Fe^{3+}}$], **[$\mathbf{L^1 + Al^{3+}}$]** and**[$\mathbf{L^1 + Cr^{3+}}$]** complex in MeOH.

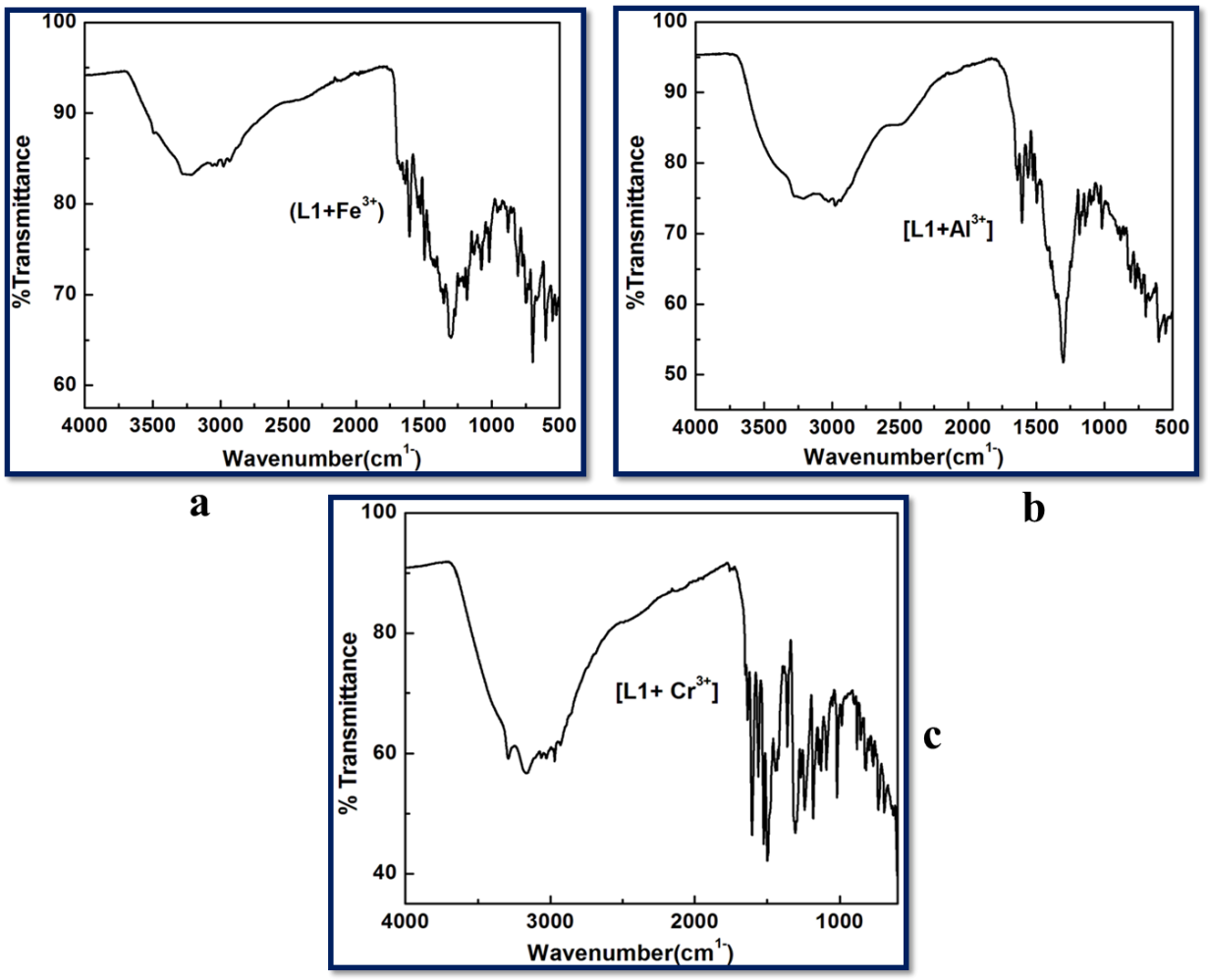

Figure-2.40: (a) FT-IR spectrumof [$\mathbf{L^1}$–Fe^{3+}] Complex. (b) FT-IR spectrum of [$\mathbf{L^1}$–Al^{3+}] Complex. (c) FT-IR spectrum of [$\mathbf{L^1}$–Cr^{3+}] Complex.

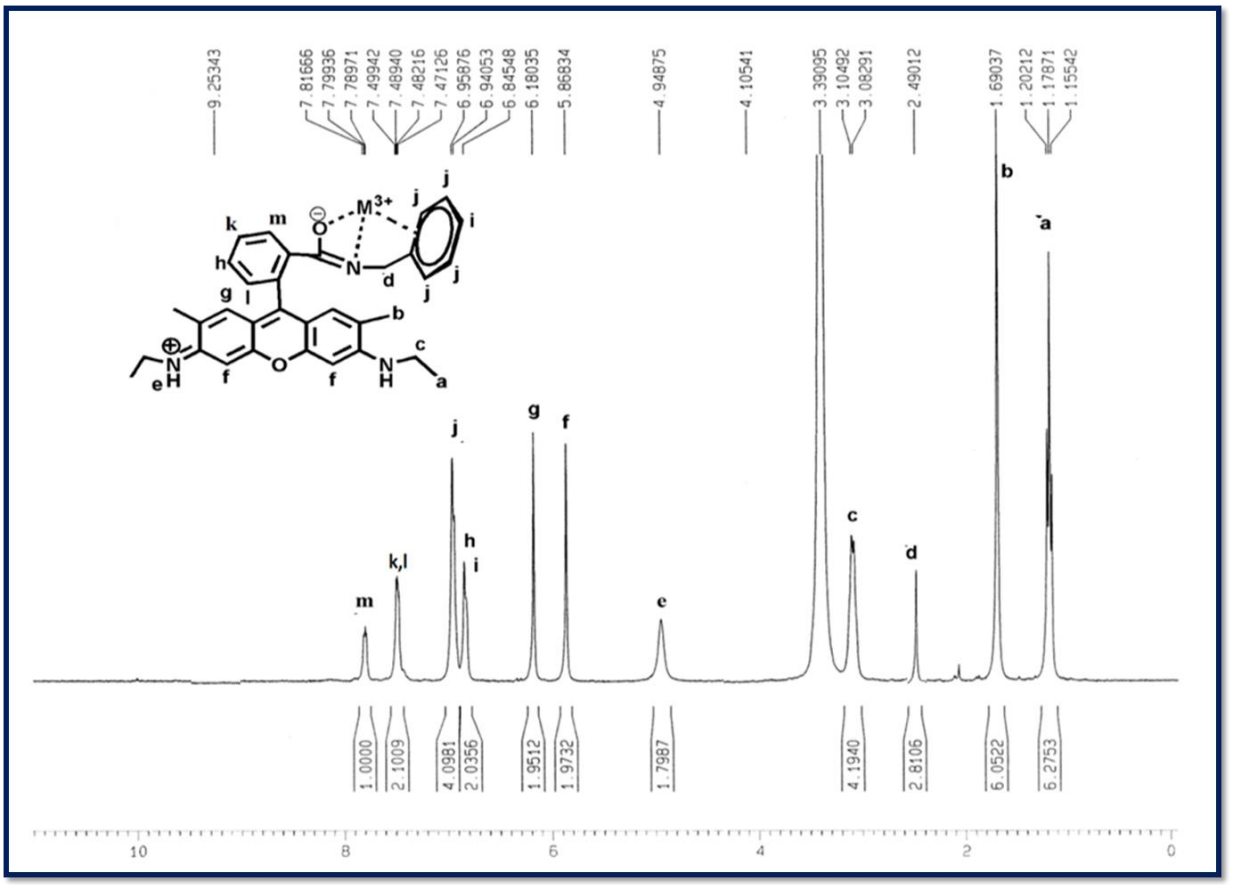

Figure-2.41: ^{1}H NMR spectrum of [$\mathbf{L^1}$–Al^{3+}] in DMSO-d_6 solvent.

2.3.7 Selective sensing of Fe^{3+}, Al^{3+} and Cr^{3+}

It is desirable for the probe to be selective towards one trivalent metal ion over the other two. The probe was sensitive towards all the three trivalent metal ions, but in the presence of ppi (inorganic pyrophosphate), the fluorescence of $\mathbf{L^1}$–Al^{3+} and $\mathbf{L^1}$–Cr^{3+} were quenched significantly while the fluorescence of $\mathbf{L^1}$–Fe^{3+} remained almost unchanged, making $\mathbf{L^1}$ selective towards Fe^{3+} in the presence of ppi (**Figure-2.42**). Again in the presence of I^-, the fluorescence of $\mathbf{L^1}$–Fe^{3+} and $\mathbf{L^1}$–Al^{3+} undergoes quenching, while that of L^1–Cr^{3+} remains unchanged, making $\mathbf{L^1}$ selective towards Cr^{3+} in the presence of I^- (**Figure-2.43**). Now if $\mathbf{L^1}$ is fluorescent towards an unknown solution, but remains non-fluorescent in the presence of both ppi and I^-, then the initial fluorescence is due to the presence of Al^{3+}. Thus, $\mathbf{L^1}$ can be made selective towards Fe^{3+}, Al^{3+} or Cr^{3+} in an unknown solution.

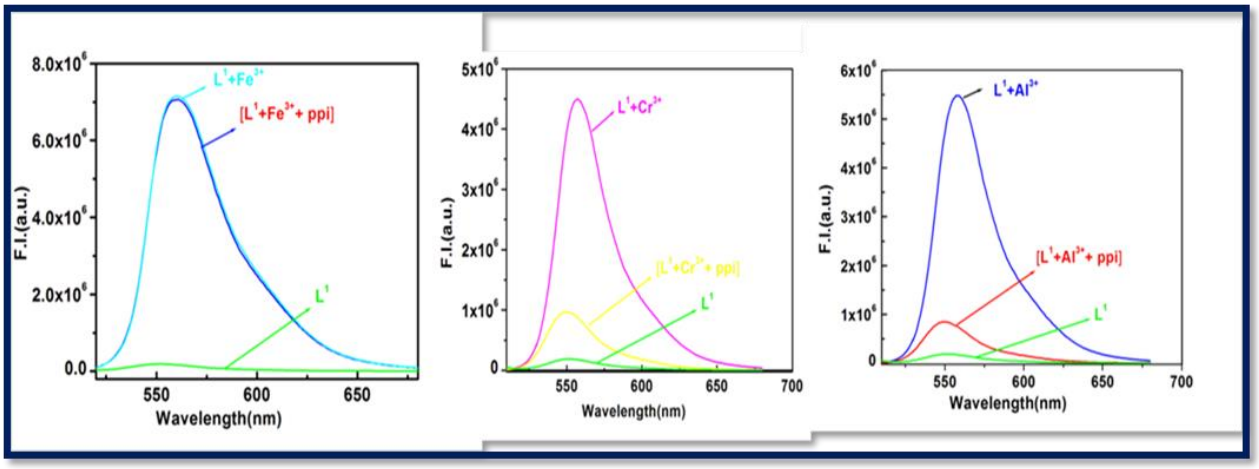

Figure-2.42: Fluorescence response of the probe (**L^1**) towards Fe^{3+}, Al^{3+} and Cr^{3+} in presence of excess (10 equivalent) ppi (Pyrophosphate).

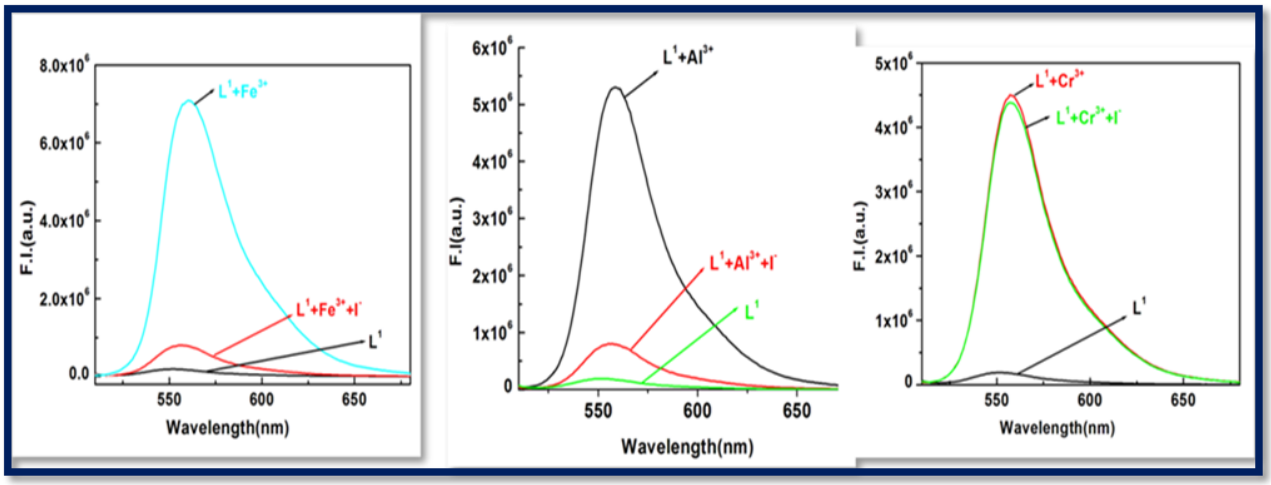

Figure-2.43: Fluorescence response of the probe (**L^1**) towards Fe^{3+}, Al^{3+} and Cr^{3+} in the presence of excess (10 equivalent) I^-.

2.3.8 Molecular logic operations

The spectroscopic properties of the probe **L^1** encouraged us to apply it for multiple logic operations with the sequential addition of inputs like cations, such as Al^{3+}, Fe^{3+}, Cr^{3+}, and CN^- anions and to then monitor their emission as the output. An INHIBIT logic gate was constructed with a particular combination of logic operations, like NOT and AND functions, which was important due to its

non-commutative behaviour, i.e. its output signal is inhibited by only one type of input. To demonstrate this INHIBIT logic function, first we chose two inputs, namely Fe^{3+} (Input 1) and CN^{-} (Input 2), and used its emission intensity at 558 nm as the output. A high value of emission intensity ($>5 \times 10^5$ at 558 nm) has been designated as 1 (ON) and a low value ($\leq 5 \times 10^5$) as 0 (OFF). In the absence of both the 1st input (Fe^{3+}) and 2nd input (CN^{-}), the emission intensity was low, indicating the OFF state; whereas when only input 1 was present, then a significant enhancement of the emission (at 558 nm) took place, indicating the 1 (ON) state, while, on the other hand, in the presence of input 2, the output emission value became very weak indicating the OFF state. Therefore, it was necessary to apply NOT gate with Input 2. Additionally, it is noteworthy that **L^1** displayed the emission output signal in such a way that it seemed to understand the requirements of the AND operation. In the presence of both inputs, the output emission value was again low, indicating the OFF state, in accordance with the truth table (**Figure-2.44**). Thus, by the sequential addition of these two inputs, an INHIBIT function logic gate could be achieved.

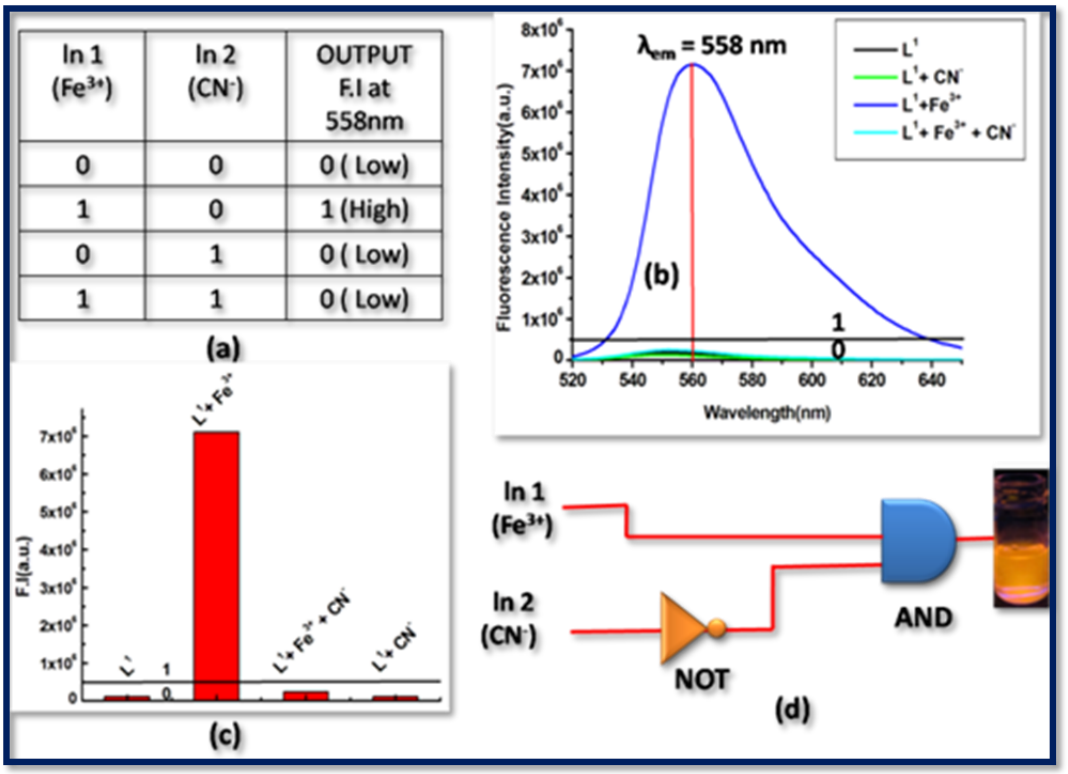

Figure-2.44: (a) Corresponding Truth Table of the logic gate. (b) Output signals (at 558 nm) of the logic gate in the presence of different inputs. (c) Corresponding bar diagram at 558 nm in the presence of different inputs (d) General representation of an INHIBIT logic gate based circuit.

2.3.9 Advanced level OR-INHIBIT gate based 4 input logic gate

A combination of OR and INHIBIT logic functions was used for the construction of the 4 inputs 1 output logic circuit. Now to imitate an OR logic gate function, the emission intensity at 558 nm was used as the output response similar to the earlier 2 input logic gate, and the inputs were Al^{3+}, Fe^{3+}, Cr^{3+} and CN^{-} (**Figure-2.45**). When the 1st (Al^{3+}) and 2nd (Fe^{3+}) inputs were both absent, the output response, i.e. the emission intensity, was very low, indicating the 0 (OFF) state. However, when only any one of the two inputs was present, the output signal was high, indicating the 1 (ON) state. Again in the presence of both the input Al^{3+} and Fe^{3+}, the output response was 1 (ON). Thus, according to its truth table (**Figure-2.46a**), an OR function logic gate could be contracted by the sequential addition of these two inputs. Then we verified the nature of the output signal in the presence of a 3rd ionic input (Cr^{3+}) in the presence of the first two ionic inputs. Here, any one of these three inputs or the presence of two of these three inputs caused a high intensity emissionoutput indicating the ON state (1). Thus, the probe behaved like an OR logic function. On the other hand, when only a 4th input (CN^{-}) was present or in the presence of all other inputs (Al^{3+}, Fe^{3+} and Cr^{3+}) in the system, the output emission was very weak, indicating the 0 (OFF) state. Therefore, we applied a NOT logic function with a 4th input. As the probe functions parallel with the output signal, so we could apply another AND logic function. Thus, from an INHIBIT logical function and following its corresponding truth table, an advanced level 4 input logic gate circuit could be constructed (**Figure-2.46b**).

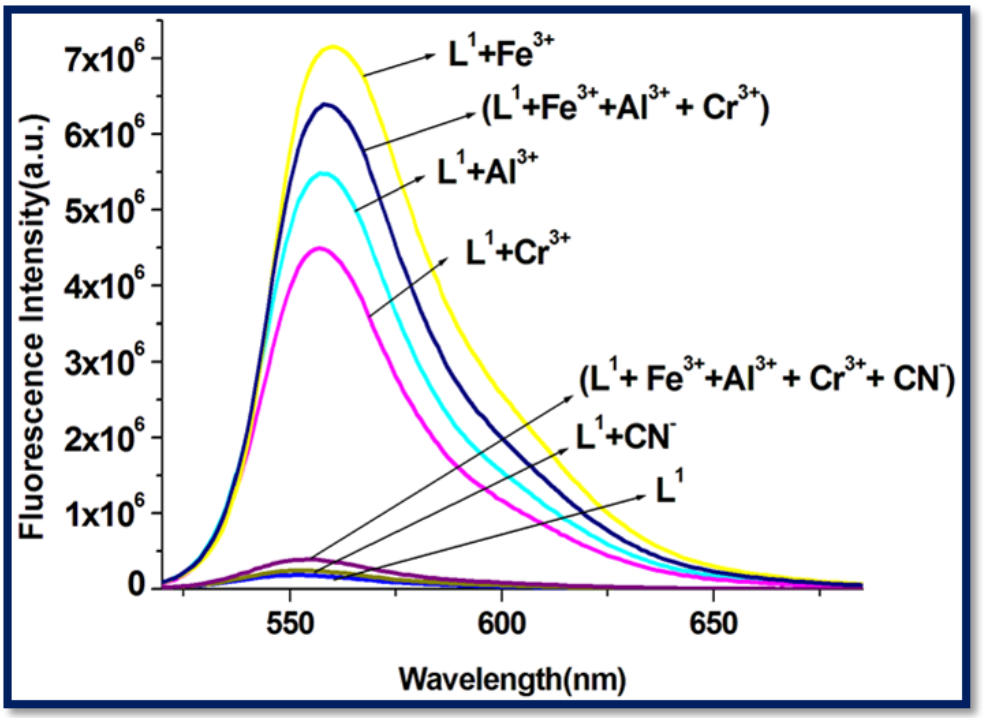

Figure-2.45: Four-input OR-INHIBIT logic gate representation of the emission of $\mathbf{L^1}$ with different input when monitoring the emission at 558 nm.

In 1 (Al^{3+})	In 2 (Fe^{3+})	In 3 (Cr^{3+})	In 4 (CN^-)	OUTPUT F.I At 558nm
0	0	0	0	0(Low)
0	0	0	1	0(Low)
0	0	1	0	1(High)
0	1	0	0	1(High)
0	1	0	1	0(Low)
0	0	1	1	0(Low)
0	1	0	1	0(Low)
0	1	1	0	1(High)
0	1	1	1	0(Low)
1	0	0	0	1(High)
1	1	0	0	1(High)
1	0	1	0	1(High)
1	1	1	0	1(High)
1	0	0	1	0(Low)
1	1	1	1	0(Low)

(a)

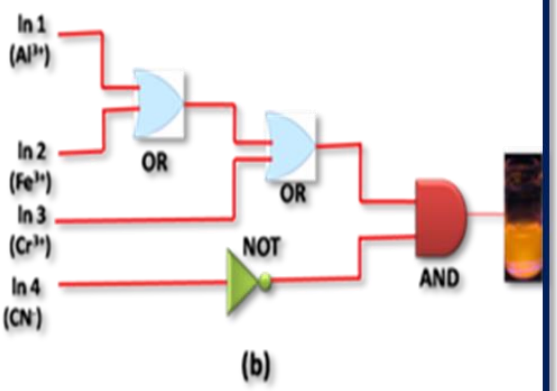

(b)

Figure-2.46: (a) Truth table of an advanced level 4 input logic gate (b) Schematic representation of a combined logic circuit of INHIBIT and OR logic gates.

2.3.10 Molecular memory device

Molecular memory devices are used for data storage technologies that use molecular species as the data storage element and can be constructed by sequential logic circuits. One of the output signals acts as the input of the memory device and it is memorized as a "memory element". So by using binary logic function, we developed a sequential logic circuit showing a "write–read–erase–read" property. For our system, we chose a strong emission output at 558 nm as the ON state (1) and a weak emission output as the OFF state (0). Now to construct this memory device, we chose two inputs, namely Fe^{3+} and CN^{-}, for the SET and RESET processes, respectively. In this memory function, the system writes when it gets input A (Fe^{3+}), i.e. a high emission value, and it memorizes the binary number 1. However, in the presence of input B (CN^{-}), which is a reset input, it erases the data and then memorizes the binary number 0 (**Figure-2.47**). The properties of the material allow for a much greater capacitance per unit area than with conventional DRAM (dynamic random-access memory), thus potentially leading to smaller and cheaper integrated circuits. The most important thing is that this write–erase–write cycle could be repeated many times using the same concentration of the system without any significant change in emission intensity.

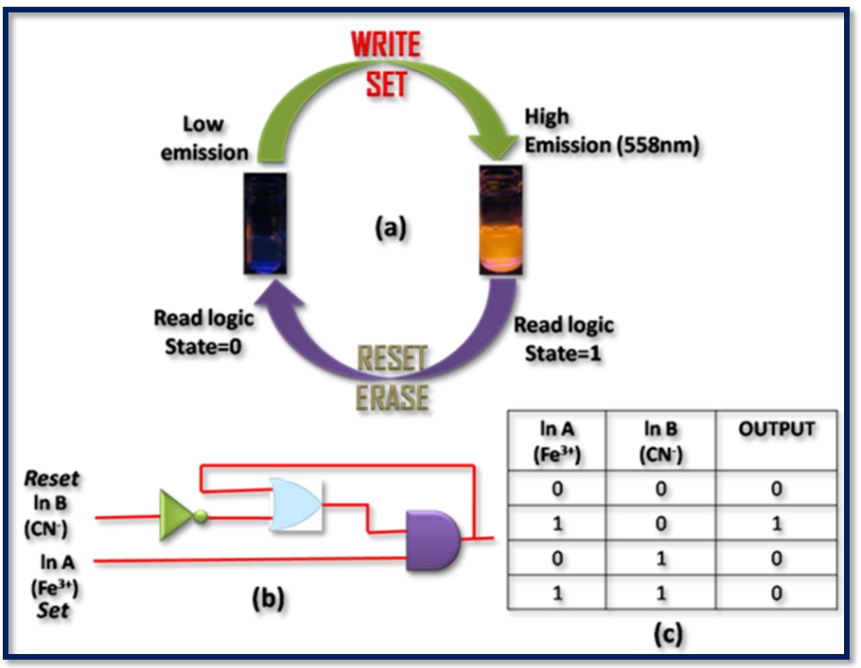

In A (Fe^{3+})	In B (CN^{-})	OUTPUT
0	0	0
1	0	1
0	1	0
1	1	0

Figure-2.47: (a)Schematic demonstration of the reversible logic operation for the memory element with "write−read−erase−read" kind of behaviour. (b) Sequential logic circuit showing memory unit with two inputs (In A and In B) and one output and (c) corresponding truth table.

2.3.11 Cell-imaging studies

As **L**^{1} showed extensive selective complex formation with trivalent metal ions (namely Fe^{3+}, Cr^{3+}, Al^{3+} ions), it was further checked for its ion-sensing ability in living cells. A cell viability assay using MTT66–68 was done to find out whether **L**^{1} had cytotoxic effects, with calculating the % cell viability on HepG2 cells (**Figure-2.48**). As found from the result, no significant decrease in formazan production occurred up to 40 μM concentration of **L**^{1}, thus reflecting that a below 40 μM ligand concentration for **L**^{1} would be much more effective for the analysis of its complex formation with trivalent metal ions in vitro. More than 95% cell viability was observed for **L**^{1} at 10 μM, after which the viability of the HepG2 cells decreases slightly. Hence, further experiments were carried out with 10 μM for **L**^{1} for treatment. Upon incubation with 10 μM of the ligand **L**^{1} for 1 h, it exhibited weak intracellular fluorescence on HepG2 cells due to the presence of intracellular Fe^{3+} (**Figure-2.49**). However, a distinct red fluorescence was observed inside the cells when the HepG2 cells were incubated with 10 μM of the trivalent metal ions for 1 h at 37 °C, washed twice with PBS buffer and then reincubated with 10 μM of the ligand **L**^{1} for 30 min at 37 °C. At 10 μM concentration of the Fe^{3+} ions, the ligand **L**^{1} showed more intense fluorescence emission than Al^{3+} and Cr^{3+} ions. Keeping the ligand **L**^{1} concentration constant (10 μM) and increasing the concentration of metal ions (from 10 μM, to 20 μM, 40 μM) showed a concentration-dependent increase in the intracellular red fluorescence, caused by the formation of the complex of **L**^{1} with either of the trivalent metal ions. Highly enhanced fluorescence was observed due to complex formation between the ligand **L**^{1} and the metal ions nearly at 40 μM of metal ion concentration. These results suggest that the ligand **L**^{1} with low cytotoxicity and biocompatibility has a high potential for in vitro application as an ion sensor of trivalent Fe^{3+}, Cr^{3+}, Al^{3+} ions as well as for live cell imaging for their detection in biological samples.

Figure-2.50 represents some trivalent sensors reported so far and **Table-2.2** displays some important parameters. A closer inspection of **Table-2.2** reveals that our probe is superior to all the probes listed here in the sense that it provides higher excitation wavelength (502 nm). There is one report (probe 6) where CH_3OH/H_2O (6: 4, v/v) was used, but the serious drawback of this system was that the excitation wavelength was in
UV region (330 nm), which is not desirable for bio imaging applications.

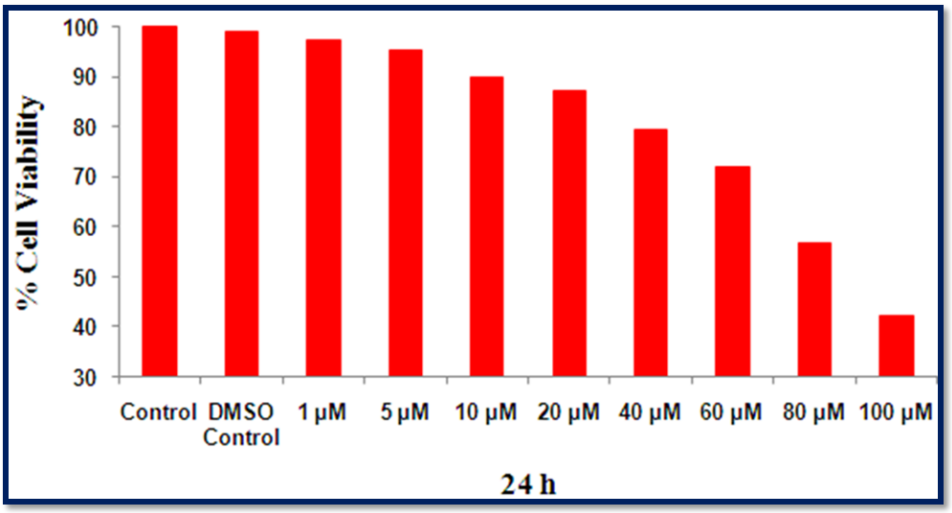

Figure-2.48: Cell viability assay performed by using ligand $\mathbf{L^1}$

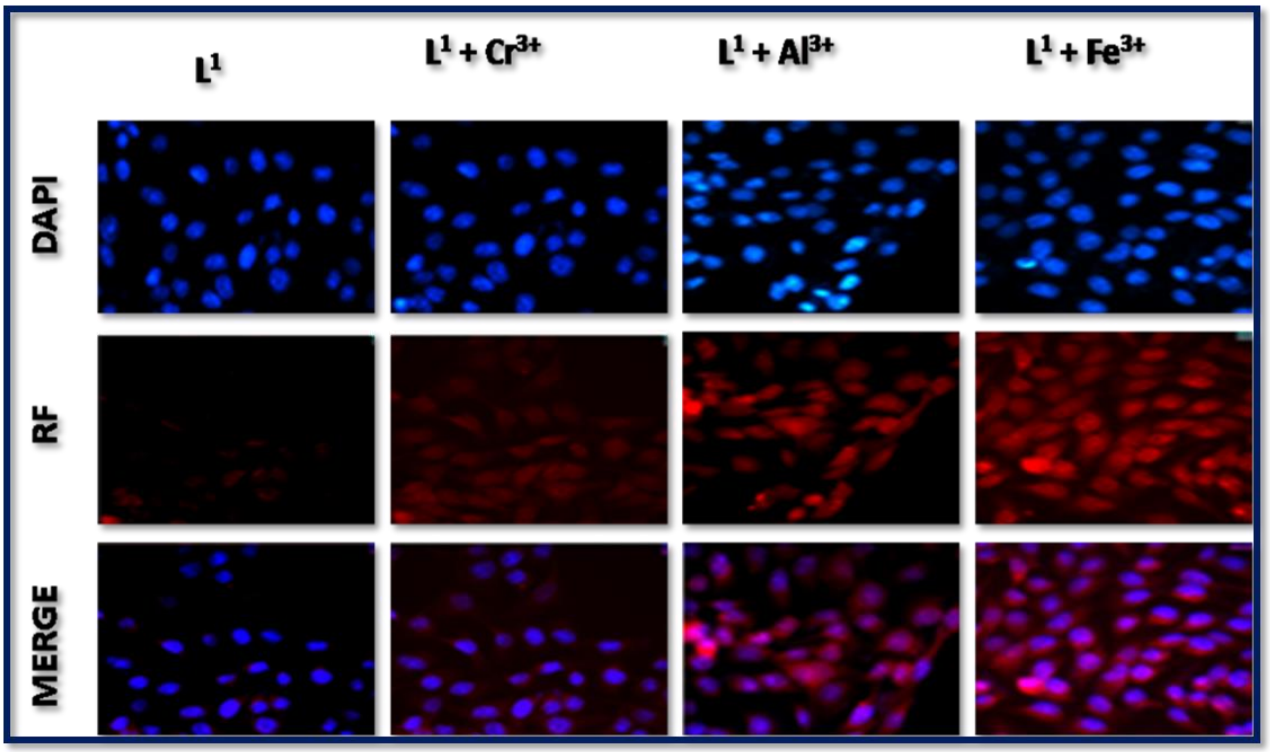

Figure-2.49: The phase contrast and fluorescence images of HepG2 cells were captured (40X) after cells were incubated with $\mathbf{L^1}$ for 30 min at 37°C and pre incubated with Al^{3+}, Cr^{3+} and Fe^{3+} for 30 min at 37°C followed washing with 1X PBS and treatment with $\mathbf{L^1}$ for 30 min at 37°C. The cytoplasmic complex formation was confirmed by nuclear stain DAPI.

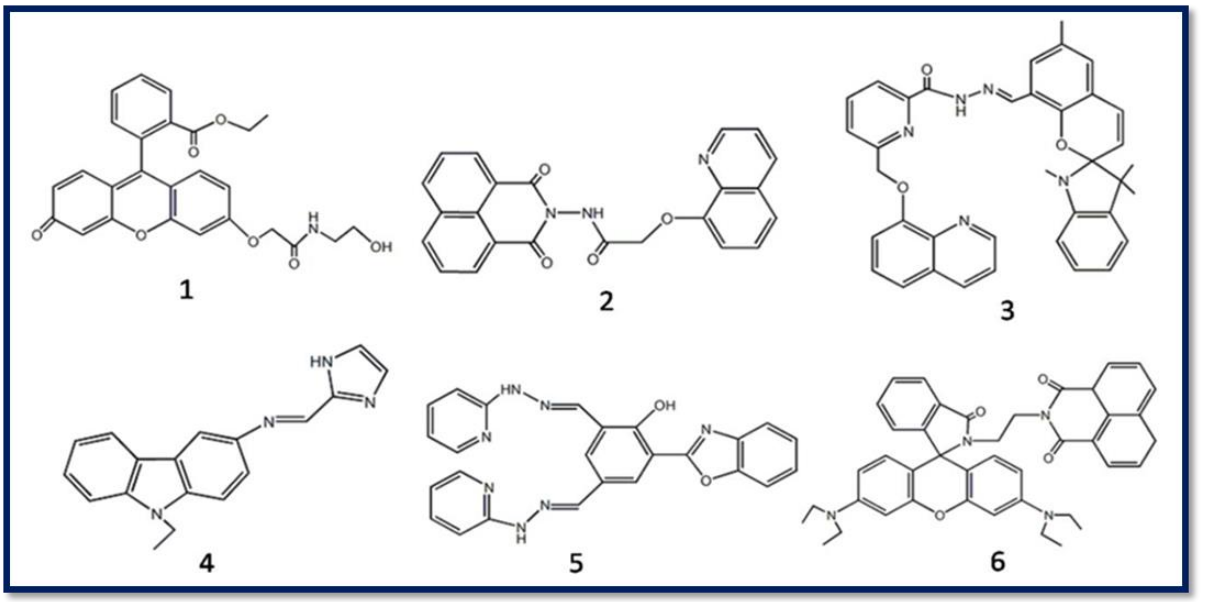

Figure-2.50: Some representative trivalent sensors.

Probe	Solvent	λ_{ex} (λ_{em})/ nm	LOD	$K_f(M^{-1})$	Ref no.
1	Pure CH_3CN	437(475)	0.5μM (Cr^{3+}) 0.3μM(Al^{3+}) 0.2μM(Fe^{3+})	1.58 x $10^4 M^{-1}$ (Cr^{3+}); 6.46 x 10^9 M^{-2} (Al^{3+}) 1.26 x 10^5 M^{-1} (Fe^{3+});	1
2	CH_3CN–HEPES buffer solution (40/60, v/v, pH = 7.4)	342(484)	25μM(Cr^{3+}) 23μM(Al^{3+}) 20μM(Fe^{3+})	1.0852 x 10^4 M^{-1}(Fe^{3+}) 8.770 x 10^3 M^{-1} (Al^{3+}) 5.676 x 10^3 M^{-1}(Cr^{3+})	2
3	CH_3CN–HEPES buffer solution (1:1, pH = 7.4)	460 (675)	93 nM(Cr^{3+}) 32 nM (Al^{3+}) 90 nM(Fe^{3+})	Not determined	3
4	THF–H_2O (8:2) mixture	330 (430)	0.36 nM (Cr^{3+}) 0.38 nM (Fe^{3+}) 0.38 nM (Al^{3+})	Not determined	4
5	H_2O:EtOH = 8:2	390(563) 390(527)	0.20μM(Cr^{3+}) 0.50μM(Al^{3+})	5.50 x 10^4 M^{-1} (Cr^{3+})	

				2.00x 10^4 M^{-1} (Al^{3+});	5
6	$CH_3OH–H_2O$ (6: 4, v/v)	330(582)	1.74 nM (Al^{3+}) 2.36 μM (Cr^{3+}) 2.90 μM (Fe^{3+})	1 x 10^4 M^{-1} (Al^{3+}); 2.6 x 10^2 M^{-1} (Cr^{3+}) 1.2 x 10^2 M^{-1} (Fe^{3+});	6
7	CH_3CN	Colorimetric	2.16 × 10^{-6} M(Al^{3+}) 1.27 × 10^{-8} M(Cr^{3+})5.03 × 10^{-8}M(Fe^{3+})	3.451 × 10^3M^{-1}(Al^{3+}) 3.751 × 10^6 M^{-1}(Cr^{3+}) 6.078 × 10^6 M^{-1}(Fe^{3+})	7
8	Methanol:water (7:3, v/v)	500(552)	1.18nM(Al^{3+}) 1.80nM(Cr^{3+}) 4.04 nM(Fe^{3+})	6.92 ± 0.18μM (Al^{3+}) 4.90 ± 0.67 μM (Fe^{3+}) 6.79 ± 0.34 μM (Cr^{3+})	8
9	1:1 methanol–water	365(509)	1.6×10^{-6} M(Al^{3+}) 2.66×10^{-6}M(Cr^{3+}) 7.99×10^{-7}M(Fe^{3+})	Not determined	9
10	CH_3CN	365(465)	1.06 × 10^{-7}M(Fe^{3+}) 1.11 × 10^{-7}M(Cr^{3+}) 1.17 × 10^{-7}M(Al^{3+})	2.25 × 106M^{-2}(Fe^{3+}) 2.24 × 106M^{-2}(Cr^{3+}) 2.26 × 106M^{-2}(Al^{3+})	10
11	H_2O/CH_3CN (4:1, v/v, pH 7.2, 20 mM HEPES buffer	502(558)	1.28 μM (Fe^{3+}) 1.34 μM(Al^{3+}) 2.28 μM(Cr^{3+})	9.4 x 10^3 M^{-1} (Fe^{3+}) 1.34 x 10^4 M^{-1}(Al^{3+}) 8.7 x 10^3 M^{-1}(Cr^{3+})	In this work

Table-2.2: A list of trivalent sensors along with some important parameters

2.4 Conclusion

In summary, we reported herein a new rhodamine-6G based fluorogenic probe, which showed a selective colorimetric as well as "turn-on" fluorescence response towards trivalent metal ions M^{3+} (M = Al, Fe and Cr) over mono- and divalent metal ions. A large enhancement of fluorescence intensity of **L^1** [Fe^{3+} (41-fold), Al^{3+} (31-fold) and Cr^{3+} (26-fold)] was observed upon the addition of 3.0 equivalent of these metal ions in H_2O/CH_3CN (4: 1, v/v, pH 7.2), which clearly indicate the feasibility of the naked eye detection of these metal ions. Take-off values were evaluated from the fluorescence titration data at variable concentrations of metal ions and a fixed concentration of ligand and were found to be $9.4 \times 10^3\ M^{-1}$ (Fe^{3+}); $8.7 \times 10^3\ M^{-1}$ (Cr^{3+}) and $13.4 \times 10^3\ M^{-1}$ (Al^{3+}). The higher values of quantum yields (0.489, 0.376, 0.310 for [L^1–Fe^{3+}], [L^1–Al^{3+}] and [L^1–Cr^{3+}], respectively) over the free ligand (0.012) indicate the higher stability of the complexes in the excited states. An excellent reversible fluorescence ON–OFF property of L^1 was observed through fluorescence study with the sequential addition of M^{3+} and CN^- ions at room temperature, which suggests the reusability of this chemosensor. The very low detection limit for Fe^{3+}, Al^{3+} and Cr^{3+} were 1.28 μM, 1.34 μM and 2.28 μM, respectively, which could make it have a potential application in real water samples for trivalent ion detection. Advanced level molecular logic devices using different inputs (2 and 4 inputs) in advanced level logic gates and memory device were constructed. A suitably large increase in fluorescence intensity of **L^1** upon complexation with M^{3+} suggests the probe may be used for bio imaging applications in living cells.

References

1. M. Wang, F. Wang, Y. Wang, W. Zhang and X. Chen, Dyes Pigm., **2015**, 120, 307.
2. X. Xing, H. Yang, M. Tao and W. Zhang, J. Hazard. Mater., **2015**, 297, 207.
3. P. Wang, J. Wu, L. Liu, P. Zhou, Y. Ge, D. Liu, W. Liu and Y. Tang, Dalton Trans., **2015**, 44, 18057.
4. Z. Xu, K.-H. Baek, H. N. Kim, J. Cui, X. Qian, D. R. Spring, I. Shin and J. Yoon, J. Am. Chem. Soc., **2009**, 132, 601.
5. L. Tang, X. Dai, K. Zhong, X. Wen and D. Wu, J. Fluoresc., **2014**, 24, 1487.
6. M. Idrees, M. Silva, A. F. Silva, L. M. Zimmermann, J. Bruch, C. O. Mendonça, G. I. Almerindo, R. A. Nome, T. D. Z. Atvars, H. D. Fiedler and F. Nome, J. Phys. Chem. C, **2012**, 116, 3517.
7. S. Maiti, Z. Aydin, Y. Zhang and M. Guo, Dalton Trans., **2015**, 44, 8942.
8. S. B. Maity and P. K. Bharadwaj, Inorg. Chem., **2013**, 52, 1161.
9. S. Sarma, P. K. Bhattacharyya and D. K. Das, J. Fluoresc., **2015**, 25, 1537.
10. Mercury Study Report to Congress, United States Environmental Protection Agency, Volume V: Health Effects of Mercury and Mercury Compounds, EPA-452/R-97-007 December (**1997**).
11. Y. Upadhyay, S. Bothra, R. Kumar and S. K. Sahoo, ChemistrySelect, **2018**, 3, 6892.
12. T. Anand, S. K. A. Kumar and S. K. Sahoo, Spectrochim. Acta, Part A, **2018**, 204, 105.
13. Y. Upadhyay, T. Anand, L. T. Babu, P. Paira, S. K. A. Kumar, R. Kumar and S. K. Sahoo, J. Photochem. Photobiol., A, **2018**, 361, 34.
14. S. K. Sahoo, D. Sharma, R. K. Bera, G. Crisponi and J. F. Callan, Chem. Soc. Rev., **2012**, 41, 7195.
15. S. Samanta, S. Goswami, A. Ramesh and G. Das, Sens. Actuators, B, **2014**, 194, 120.
16. S. Dey, S. Sarkar, D. Maity and P. Roy, Sens. Actuators, B, **2017**, 246, 518.
17. X. Chen, X. Y. Shen, E. Guan, Y. Liu, A. Qin, J. Z. Sun and B. Z. Tang, Chem. Commun., **2013**, 49, 1503.
18. N. R. Chereddy, P. Nagaraju, M. V. NiladriRaju, V. R. Krishnaswamy, P. S. Korrapati, P. R. Bangal and V. J. Rao, Biosens. Bioelectron., **2015**, 68, 749.

19. A. Barba-Bon, A. M. Costero, S. Gil, M. Parra, J. Soto, R. M. Máñez and F. Sancenón, Chem. Commun., **2012**, 48, 3000.
20. T. Simona, M. Shellaiah, V. Srinivasadesikan, C.-C. Lina, F.-H. Koa, K. W. Sun and M.-C. Lin, Sens. Actuators, B, **2016**, 231, 18.
21. A. Singh, R. Singh, M. Shellaiah, E. C. Prakash, H.-C. Chang, P. Raghunath, M.-C. Lin and H.-C. Lin, Sens. Actuators, B, **2015**, 207, 338.
22. P. N. Borase, P. B. Thale, S. K. Sahoo and G. S. Shankarling, Sens. Actuators, B, **2015**, 215, 451.
23. M. Shellaiah, T. Simon, V. Srinivasadesikan, C.-M. Lin, K. W. Sun, F.-H. Ko, M.-C. Lin and H.-C. Lin, J. Mater. Chem. C, **2016**, 4, 2056.
24. S. Tao, Y. Wei, C. Wang, Z. Wang, P. Fan, D. Shi, B. Ding and J. Qiu, RSC Adv., **2014**, 4, 46955.
25. B. L. Su, N. Moniotte, N. Nivarlet, L. H. Chen, Z. Y. Fu, J. Desmet and J. Li, J. Colloid Interface Sci., **2011**, 358, 136.
26. T. Hirayama, K. Okuda and H. Nagasawa, Chem. Sci., **2013**,4, 1250.
27. J. Xu, Z. Jia, M. D. Knutson and C. Leeuwenburgh, Int. J. Mol. Sci., **2012**, 13, 2368.
28. D. J. Bonda, H. Lee, J. A. Blair, X. Zhu, G. Perry and M. A. Smith, Metallomics, 2011, 3, 267.
29. S. Toyokuni, Cancer Sci., **2009**, 100, 9.
30. K. V. Kowdley, Gastroenterology, **2004**, 127, S79.
31. F. Molina-Holgado, R. Hider, A. Gaeta, R. Williams and P. Francis, BioMetals, **2007**, 20, 639.
32. Z. Zhou, M. Yu, H. Yang, K. Huang, F. Li, T. Yi and C. Huang, Chem. Commun., **2008**, 29, 3387.
33. J. B. Vincent, Nutr. Rev., **2000**, 58, 67.
34. M. Zhang, Z. Chen, Q. Chen, H. Zou, J. Lou and J. He, Mutat. Res., Genet. Toxicol. Environ. Mutagen., **2008**, 654, 45.
35. B. Vincent, Nutr. Rev., **2000**, 58, 67.
36. H. X. Jiang, L. S. Chen, J. G. Zheng, S. Han, N. Tang and B. R. Smith, Tree Physiol., **200**8, 28, 1863.
37. G. Berthon, Coord. Chem. Rev., **1996**, 149, 241.

38. S. M. Candura, L. Manzo and L. G. Costa, Role of occupational neurotoxicants in psychiatric and neurodegenerative disorders, in Occupational Neurotoxicology, ed.L. G. Costa and L. Manzo, CRC Press, Boca Raton, **1998**, p. 131.
39. R. J. P. Williams, Coord. Chem. Rev., **1992**, 149, 1.
40. G. R. Rout, S. S. Roy and P. Das, Agronomie, **2001**, 21, 3.
41. (a) J. Barcelo and C. Poschenrieder, Environ. Exp. Bot.,**2002**, 48, 75; (b) B. Valeur and I. Leray, Coord. Chem. Rev.,**2000**, 205, 3; (c) Z. Krejpcio and R. W. P. Wojciak, Int. J. Environ. Stud., **2002**, 11, 251.
42. M. R. Wills, C. D. Hewitt, B. C. Sturgill, J. Savory and M. M. Herman, Ann. Clin. Lab. Sci., **1993**, 23, 1.
43. G. Sahin, I. Varol and A. Temizer, Biol. Trace Elem. Res.,**1994**, 41, 129.
44. A. C. Alfrey, NeuroToxicology, **1980**, 1, 43.
45. (a) G. D. Fasman, Coord. Chem. Rev., 1996, 149, 125;(b) P. Nayak, Environ. Res., **2002**, 89, 111; (c) C. S. Cronan, W. J. Walker and P. R. Bloom, Nature, **1986**, 324, 140; (d) G. Berthon, Coord. Chem. Rev., **2002**, 228, 319; (e) D. R. Burwen, S. M. Olsen, L. A. Bland, M. J. Arduino, M. H. Reid and W. R. Jarvis, Kidney Int., **1995**, 48, 469.
46. S. G. Lambert, J. A. M. Taylor, K. L. Wegener, S. L. Woodhouse, S. F. Lincoln and A. D. Ward, New J. Chem., **2000**, 24, 541.
47. D. Maity and T. Govindaraju, Chem. Commun., **2010**, 46, 4499.
48. Y. S. Jang, B. Yoon and J. M. Kim, Macromol. Res., **2011**, 19, 97.
49. A. M. Zayed and N. Terrey, Plant Soil, **2003**, 249, 139.
50. W. Fresenius, K. E. Quentin and W. Schneider, Water Analysis, Springer, Berlin, **1988**.
51. X.-d. Wang and O. S. Wolfbeis, Chem. Soc. Rev., **2014**, 43, 3666.
52. B. Gibson, S. Carter, A. S. Fisher, S. Lancaster, J. Marshall and I. Whiteside, J. Anal. At. Spectrom., **2014**, 29, 1969.
53. J. Wang, Y. Li, N. G. Patel, G. Zhang, D. Zhouand and Y. Pang, Chem. Commun., **2014**, 50, 12258.
54. S. Goswami, K. Aich, S. Das, A. K. Das, D. Sarkar, S. Panja, T. K. Mondal and S. Mukhopadhyay, Chem. Commun., **2013**, 49, 10739.
55. M. Venkateswarulu, T. Mukherjee, S. Mukherjee and R. R. Koner, Dalton Trans., **2014**, 43, 5269.

56. J. Miao, L. Wang, W. Dou, X. L. Tang, Y. Yan and W. S. Liu, Org. Lett., **2007**, 9, 4567.
57. E. Delhaize and P. R. Ryan, Plant Physiol., **1995**, 107, 315.
58. S. Goswami, A. K. Das, A. K. Maity, A. Manna, K. Aich, S. Maity, P. Saha and T. K. Mandal, Dalton Trans., **2014**, 43, 231.
59. S. Fakih, M. Podinovskaia, X. Kong, H. L. Collins, V. E. Schoible and R. C. J. Hider, Med. Chem., **2008**, 51, 4539.
60. S. Kim, J. Y. Noh, K. Y. Kim, J. H. Kim, H. K. Kang, S. W. Nam, S. H. Kim, S. Park, C. Kim and J. H. Kim, Inorg. Chem., **2012**, 51, 3597.
61. S. Paul, A. Manna and S. Goswami, Dalton Trans., **2015**, 44, 11805.
62. R. Alam, R. Bhowmick, A. S. M. Islam, A. Katarkar, K. Chaudhuri and M. Ali, New J. Chem., **2017**, 41, 8359.
63. R. Alam, T. Mistri, R. Bhowmick, A. Katarkar, K. Chaudhuri and M. Ali, RSC Adv., **2016**, 6, 1268.
64. H. A. Molla, R. Bhowmick, A. Katarkar, K. Chaudhuri, S. Gangopadhyay and M. Ali, Anal. Methods, **2015**, 7, 5149.
65. Y. Liu, K. Ai, X. Cheng, L. Huo and L. Lu, Adv. Funct. Mater., **2010**, 20, 951.
66. R. Alam, T. Mistri, R. Bhowmick, A. Katarkar, K. Chaudhuri and M. Ali, RSC Adv., **2015**, 5, 53940.
67. R. Alam, T. Mistri, A. Katarkar, K. Chaudhuri, S. K. Mandal, A. R. Khuda-Bukhsh, K. K. Das and M. Ali, Analyst, **2014**, 139, 4022.
68. R. Alam, T. Mistri, P. Mondal, D. Das, S. K. Mandal, A. R. Khuda-Bukhsh and M. Ali, Dalton Trans., **2014**, 43, 2566.

A rhodamine-based fluorescent sensor for rapid detection of Hg^{2+} exhibiting aggregation induced enhancement of emission (AIEE) in aqueous surfactant medium

Abstract

An easily synthesizable rhodamine-based chemosensor, **L^2**, selectively recognizes Hg^{2+} and Al^{3+} ions in the presence of all biologically relevant and toxic heavy metal ions. Very low detection limit (47 nM for Hg^{2+}) along with cell permeability and negligible cytotoxicity provides a good opportunity towards cell imaging of Hg^{2+}. SEM studies reveal rod-like microstructure for **L^2** in water, which changes to a porous microstructure in the presence of Hg^{2+}. It was interesting to note that the presence of SDS solubilized the otherwise insoluble probe in pure aqueous medium. In case of Al^{3+} it was astonishingly observed a fluorescence quenching on increasing the SDS concentration, while a ~33-fold enhancement of fluorescence intensity of [L^2-Hg^{2+}] complex was observed compared to that in the presence of SDS, making the prove selective towards Hg^{2+} over Al^{3+} in the aqueous SDS medium. In SDS/water system, there is a steep rise in FI, reaches a maximum at ~7 mM of SDS and then fluorescence intensity decreases gradually with the increase in [SDS] up to 28 mM. These observations clearly signify the SDS-assisted formation of polymer aggregates of the complex on the surface of monolayer of SDS formed in pre-micellar concentrations with higher fluorescence intensity, which is converted to the monomer being trapped inside the micellar cavity beyond the critical micellar concentration (CMC) with comparatively lower fluorescence intensity, indicating an interesting AIEE phenomenon. This proposition is further supported by the dependence of fluorescence anisotropy (*r*) on [SDS].

3.1 Introduction

The fabrication of appealing supramolecular assemblies are achieved through bottom-up approach by an elegant use of noncovalent interactions like electrostatic, hydrophobic, van der Waals, hydrogen bonding etc.[1–4] Out of these, ionic self-assembly by various combinations between peptides, polyelectrolytes, surfactants and extended rigid organic scaffolds has attracted considerable attention of the researchers due to its application towards the fabrication of optical materials and advanced nano-devices. Another interesting feature of these supramolecular assemblies is their different behaviour in solution and solid state exhibiting either aggregation induced emission enhancement (AIEE) or aggregation caused quenching (ACQ)[5–9]**.** Till date, the AIEE mechanism has been observed in silole derivative[10], 1,1,2,2-tetraphenylethene (TPE)[11–13], 1-cyano-*trans*-1,2-bis-(4-methylphenyl) ethylene (CN-MBE) etc..[14,15]

The amphiphilic nature of surfactants readily produces various supramolecular aggregates like micelles and vesicles in aqueous solution.[16,17] It could be used as a coupling unit to induce structural changes by ionic self-assembly. Recently surfactants have been suitably exploited to generate AIEE.[18–20] Heavy metals like mercury, lead, cadmium and semimetal arsenic[21] are widely distributed, extensively used, and highly toxic, and pose the greatest environmental threat; as soils and sediments are the ultimate sink for them. The water-soluble Hg^{2+} ion is highly toxic and can damage the brain, nervous system, kidneys, and endocrine system.[22,23] Again, due to very high thiophilicity, Hg^{2+} can deactivate many thiol-containing enzymes, thereby stopping or altering the metabolic processes.[24–26] Over the past decade, increasing attention has been paid to the development of efficient chromo and fluorogenic sensors for Hg^{2+} ions for real-time monitoring of environmental, biological and industrial samples.[27–35]

Here, a rhodamine-6G based probe with potential NO_3 donor atoms have been synthesized and used successfully for the selective and rapid recognition of toxic Hg^{2+} ion (**Scheme-3.1**) exhibiting chromo and fluorogenic metal-induced "OFF-ON" responses through the opening of the spirolactam ring. In addition, although the current probe is poorly soluble in 100% aqueous medium, the presence of SDS makes it soluble in this medium, thereby making it useful for monitoring Hg^{2+} ion in the purely aqueous medium in the presence of SDS with enhanced sensitivity and selectivity, even in the presence of Al^{3+} which otherwise gives fluorescence response with the probe in the absence of SDS.[19,20]

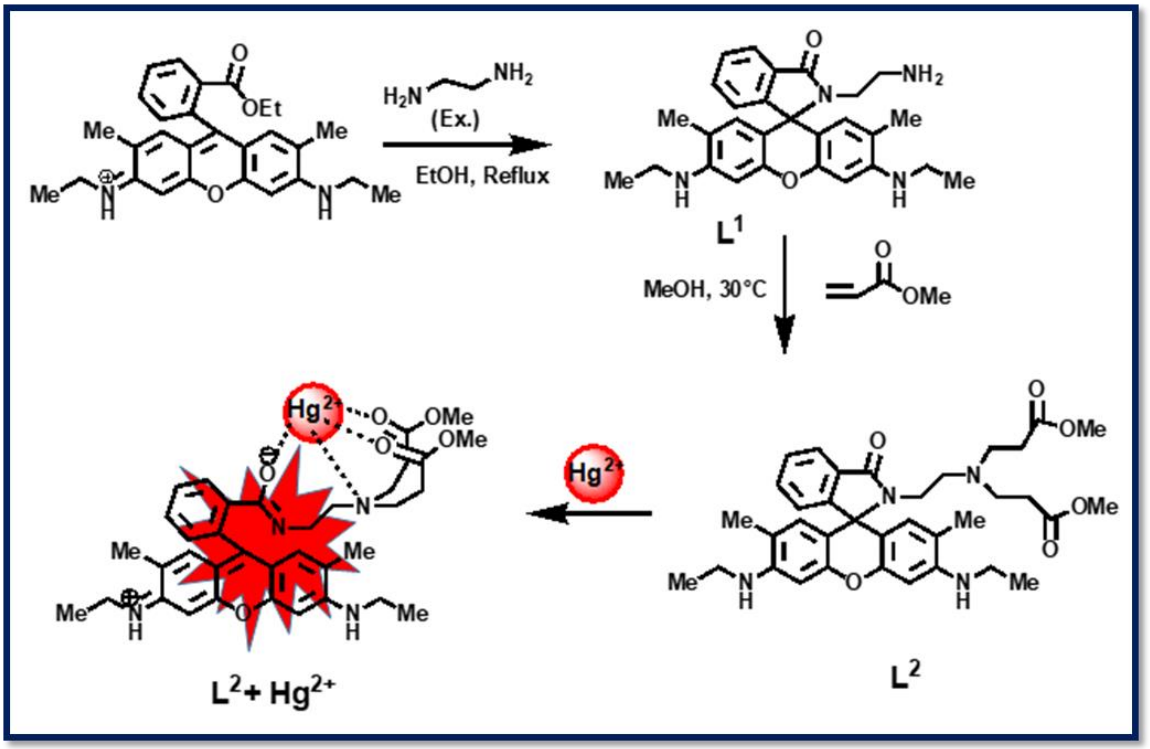

Scheme-3.1: Synthetic steps leading the formation of [$\mathbf{L^2}$-$\mathbf{Hg^{2+}}$] complex.

3.2 Experimental Section

3.2.1 Materials and reagents

All solvents used for the synthetic purposes were of reagent grade (Merck). For spectroscopic (UV/Vis and fluorescence) studies double-distilled water and HPLC-grade MeCN were used. Rhodamine 6G hydrochloride, ethylene diamine, methyl acrylate and perchlorate salts of Na^+, K^+, Ca^{2+}, Ni^{2+}, Zn^{2+}, Pb^{2+}, Cd^{2+}, Fe^{2+}, Co^{2+}, Hg^{2+} and Cu^{2+} were purchased from Sigma-Aldrich and used as received. Sodium salts of anions like SO_4^{2-}, NO_3^-, PO_4^{3-}, S_2^-, Cl^-, F^-, Br^-, I^-, OAc^-, $H_2AsO_4^-$ and N_3^- were of reagent grade and used as received.

3.2.2 Physical measurements

UV/Vis absorption spectra were recorded with an Agilent 8453 diode array spectrophotometer. Steady-state fluorescence studies were carried out with a PTI (QM-40) spectrofluorimeter. Bruker NMR spectrometers of 300 and 500 MHz were used for ^1H and ^{13}C NMR studies. The ESI-MS+

spectra were recorded on a Waters HRMS spectrometers (Model: QTOF Micro YA263 and Model: XEVO-G2QTOF#YCA351).

3.2.3 Synthesis

3.2.3.1 Synthesis of rhodamine 6G hydrazide (L^1)

Rhodamine 6G (5.0 mmol) and ethylenediamine (10.0 mmol) were dissolved in EtOH and refluxed for 4 hours with continuous stirring whereupon a white crystalline solid of the probe (**L^1**) was deposited. The solid was filtered and washed several times with water and dried in air (83% yield). The crude product was crystallised from ethanol.

3.2.3.2 Synthesis of rhodamine 6G based probe (L^2)

To a suspension of 30 mL ice-cooled (0 ºC) methanolic solution of L^1 (0.456 g, 1.0 mM), a 4 mL methanol solution of methylacrylate (0.36 mL, 10 mmol) was added dropwise over a period of 30 min. The reaction mixture was allowed to warm slowly to room temperature at which it was stirred for 3 days. The final product was obtained after evaporation of methylacrylate and methanol under vacuum as white crystals (yield 0.55 g, 88%) with m.p. 134–136 ºC, R_f = 0.66 in a toluene/ethanol = 2: 1 solvent system.

^{1}H NMR (DMSO-*d*6, 500 MHz), δ ppm: 7.75– 7.77 (1H, t, -Ar-H), 7.48–7.53 (2H, m, Ph-H), 6.98–7.00 (1H, t, -Ar-H), 6.25 (2H, s, Ph-H), 6.03 (2H, s, -Ar-H), 5.0 (2H, t, $ArNHCH_2$), 3.33 (6H, s, $-COOCH_3$), 3.09–3.17 (4H, m, $ArNHCH_2$), 2.89–2.92 (2H, t, $-CH_2NCOAr$), 2.42–2.44 (4H, t, $-CH_2-$ CH_2COOMe), 2.11–2.14 (4H, t, $-CH_2-COOMe$), 2.01–2.05 (2H, t, $-CH_2-N$), 1.88 (6H, s, $-ArCH_3$), 1.18–1.20 (6H, t, $-CH_2CH_3$) [**Figure-3.1**]; ^{13}C NMR (DMSO-*d*6, 500 MHz), δ ppm:14.70,17.54,32.47,37.97,38.06,49.40,50.91,51.70,64.95,96.15,105.2,118.84,122.82,124.24,128.92,131.58,133.21,148.33,151.86,153.64,167.67,172.72 **[Figure-3.2]**.ES+ MS = 629.3890 [L^2+H+] [**Figure-3.3**]. FT-IR (KBr) cm–1: 3324 (-NH); 2942, 2896 (-CH); 1723 (-C=O); 1670 (-COOMe); 1622, 1518 and 1450 (-ArCH). [**Figure-3.4**]

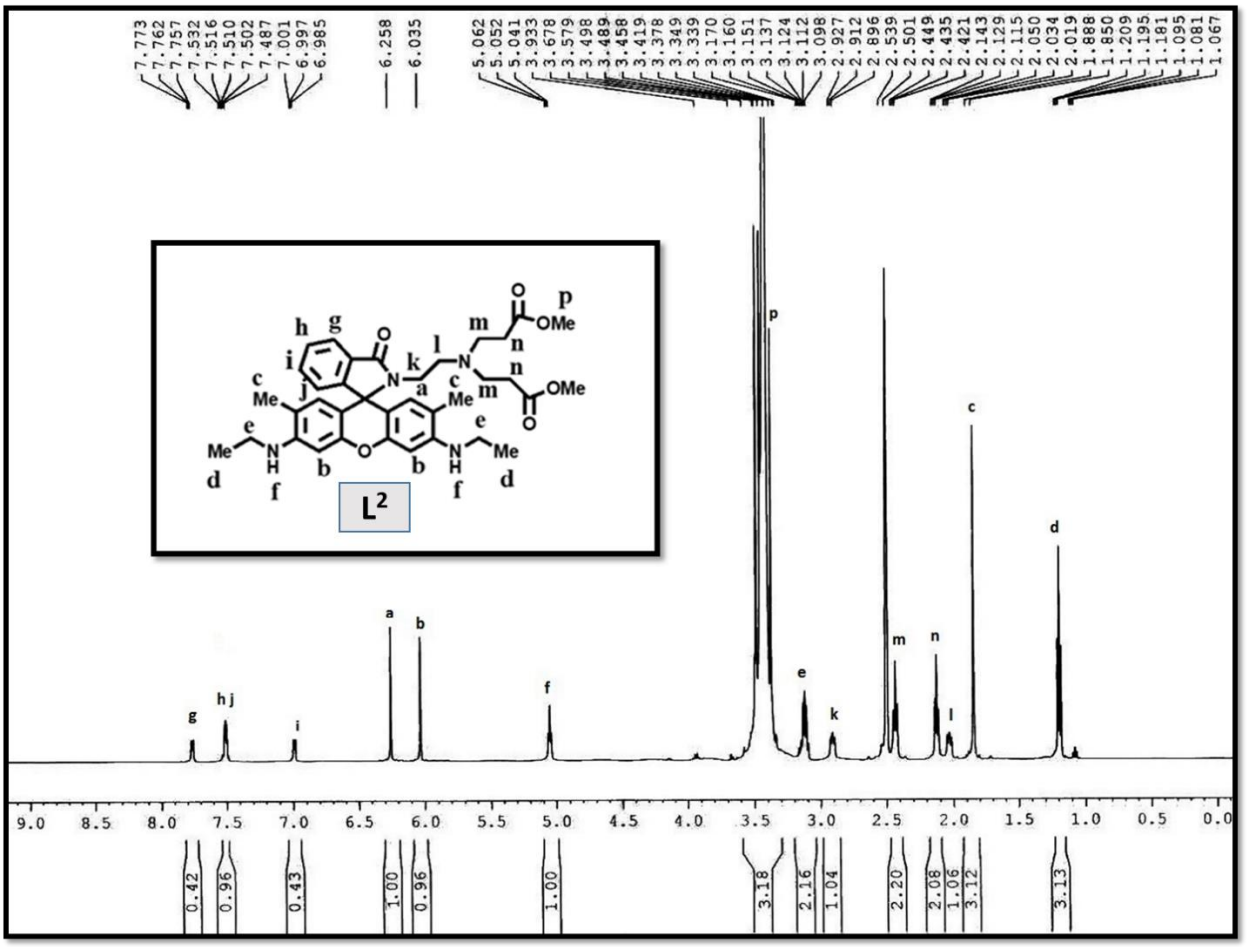

Figure-3.1: ^{1}H NMR spectrum of **L**^{2} in DMSO-d_6, in Bruker 500 MHz instrument.

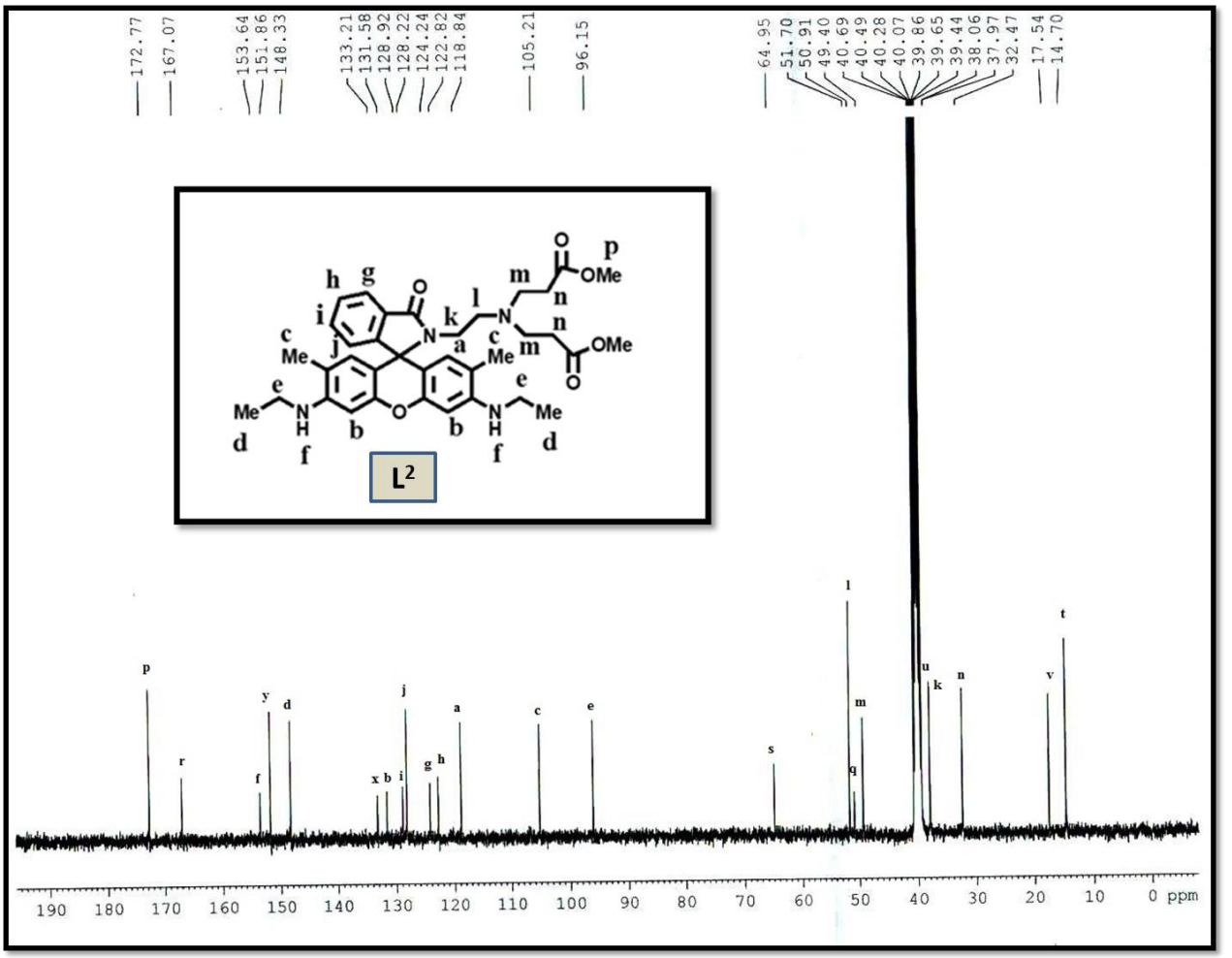

Figure-3.2: ^{1}H NMR spectrum of **L^{2}** in DMSO-d_6, in Bruker 500 MHz instrument.

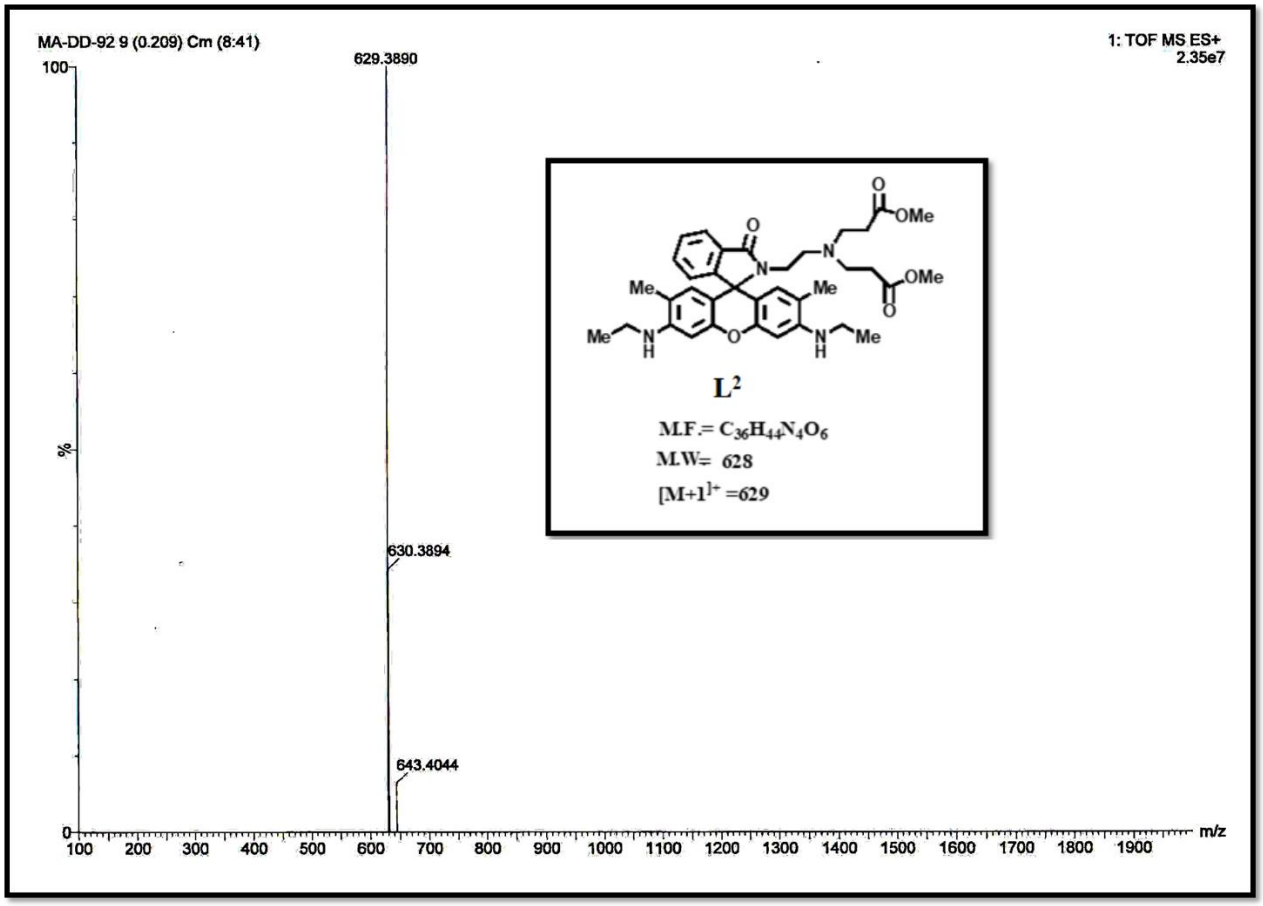

Figure-3.3: Mass spectrum of $\mathbf{L^2}$ in MeOH

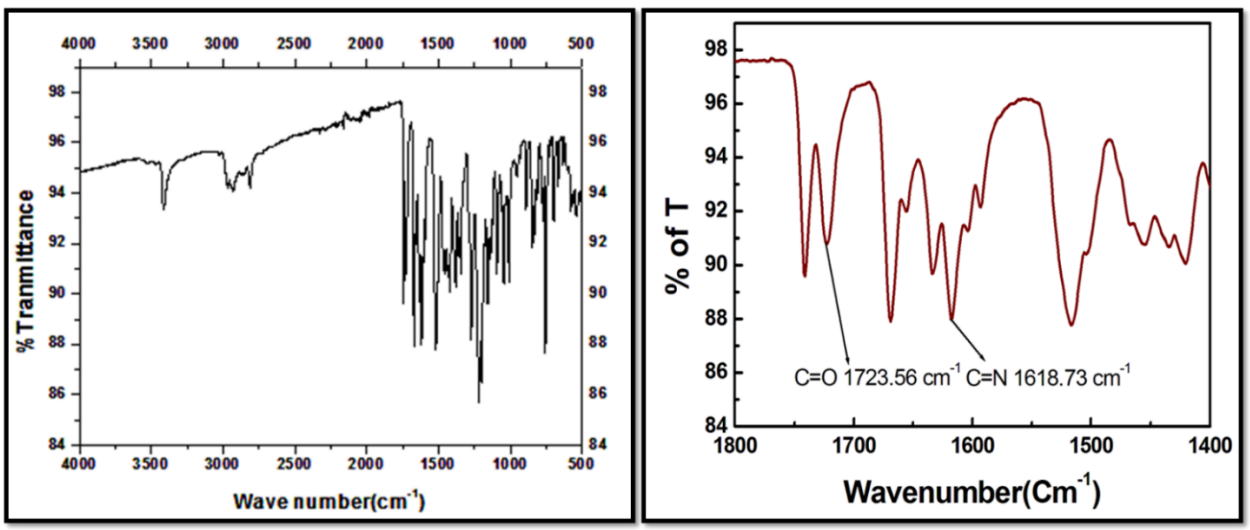

Figure-3.4: FT-IR spectrum of $\mathbf{L^2}$ in KBr pellet.

3.2.4 Methods of characterization

A scanning electron microscope (SEM) (ZEOLSM 8360) operating at an accelerating voltage of 5 kV was used for the study of morphologies of the free probe (**L^2**) in aqueous medium and also in the presence of Hg^{2+} (L^2-Hg^{2+}). Before SEM, the samples were vacuum dried and then gold coated to minimize the sample charging. Fluorescence anisotropies (*r*), defined by eq. (**3**), were measured on a PTI QM-40 spectrofluorimeter.

$$r = (I_{VV} - G \cdot I_{VH})/ (I_{VV} + 2G \cdot I_{VH}) \ldots\ldots\ldots\ldots \quad (\mathbf{3})$$

where, I_{VV} and I_{VH} indicate the emission intensities with the excitation polarizer oriented vertically and emission polarizer oriented vertically and horizontally, respectively, and corresponding *G* factor is calculated as in eq. (**4**)[19];

$$G = I_{HV}/I_{HH} \quad (\mathbf{4})$$

where, I_{HV} and I_{HH} refer to the intensities corresponding to the vertical and horizontal positions of the emission polarizer, with the excitation polarizer being horizontal.

3.2.5 Cell culture and cell cytotoxicity assay

HepG2 (Human hepatocellular liver carcinoma) cell lines (NCCS, Pune, India) grown in DMEM was supplemented with 10% FBS and antibiotics (penicillin –100 µg/ml; streptomycin – 50 µg/ml). Conditions for the culture of cells are: 37 ºC in 95% air, 5% CO_2 incubator. To test the cytotoxicity of **L^2**, the 3-(4,5-di-methylthiazol-2-yl)-2,5-diphenyl-tetrazolium bromide (MTT) assay was performed. The cytotoxicity effects of **L^2** determined by MMT assay for HepG2 cells up to 60 µM (<30% cytotoxicity) of **L^2** following the procedure described previously[36–39].

Cell imaging studies - Cell imaging study of Hg^{2+} ions with **L^2**. The fluorescence images of HepG2 cells were captured (40X and 100X) after incubating with 10 µM of **L^2** for 30 min at 37 °C, also in pre-incubated 10 µM of Hg^{2+} for 3 h at 37°C followed by washing twice with 1X PBS and, subsequent incubation with 1µM, 5µM and 10µM of ligand **L^2** for 30 min at 37^0C.

3.3 Results and Discussion

A simple reaction between $\mathbf{L^1}$ and methyl acrylate in methanol leads to the formation of $\mathbf{L^2}$ in quantitative yield (**Scheme-3.1**) which was thoroughly characterized by ^{1}H NMR (**Figure-3.1**), ^{13}C NMR (**Figure-3.2**), ESI-MS$^+$ (**Figure-3.3**) and IR studies (**Figure-3.4**). Formation of metal complex, **[$\mathbf{L^2}$-$\mathbf{Hg^{2+}}$]** followed by Spiro lactam ring opening also characterised by ^{1}H NMR **(**Figure-3.5), FTIR (**Figure-3.6**) and ESI-MS$^+$(**Figure-3.7**) studies.

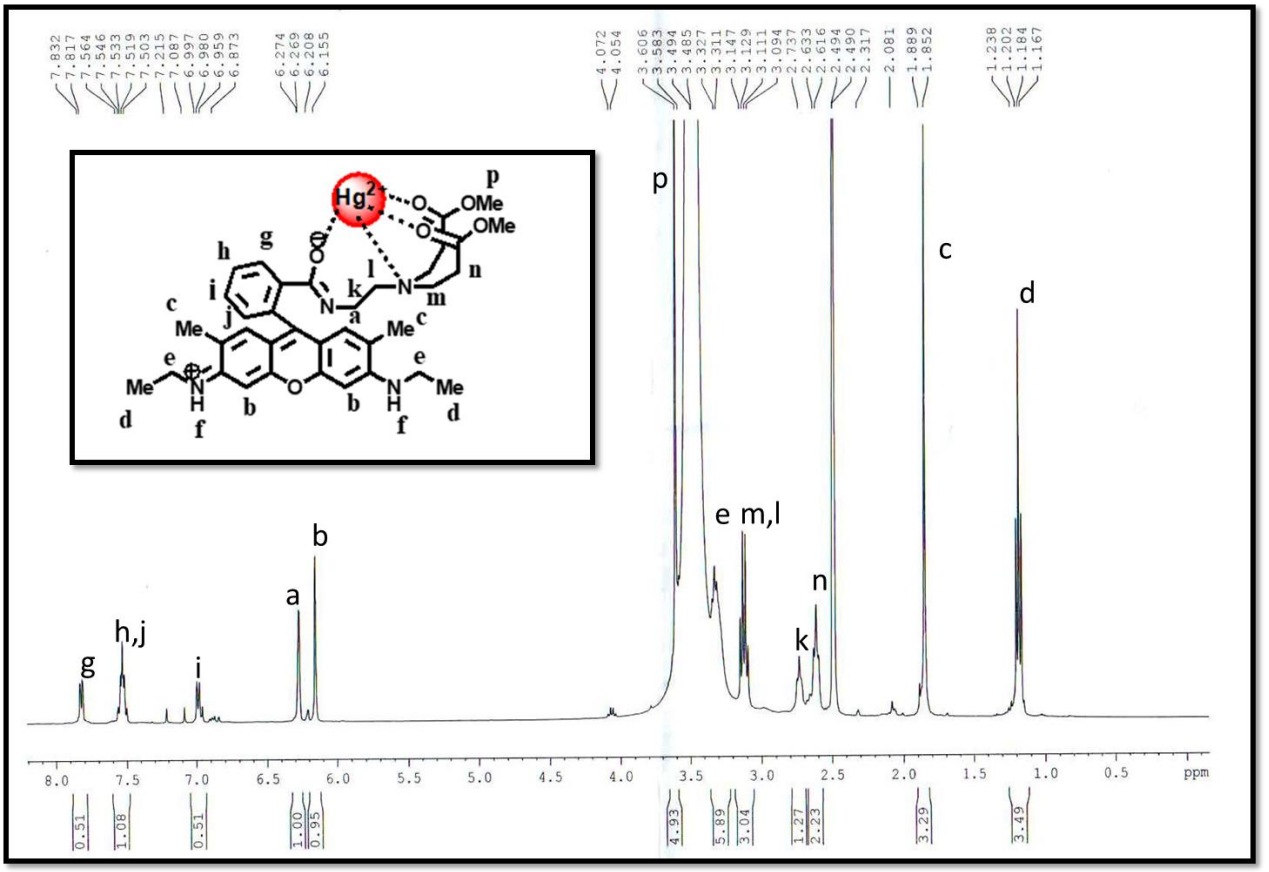

Figure-3.5: ^{1}H NMR spectrum of [$\mathbf{L^2}$+$\mathbf{Hg^{2+}}$] in DMSO-d_6, in Bruker 500 MHz instrument.

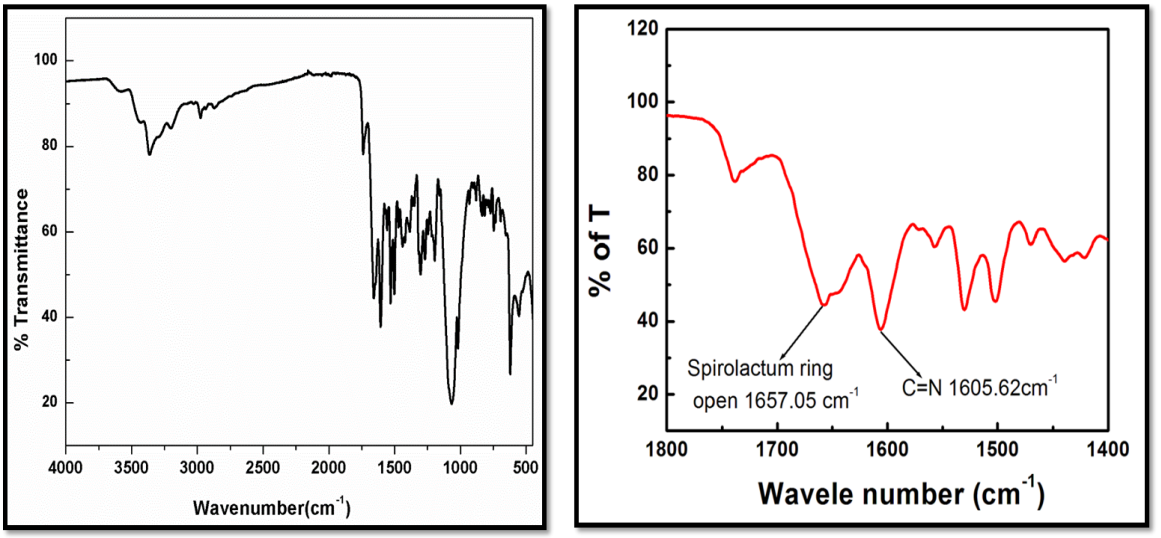

Figure-3.6: FT-IR spectrum of [$\mathbf{L^2}$-$\mathbf{Hg^{2+}}$] complex.

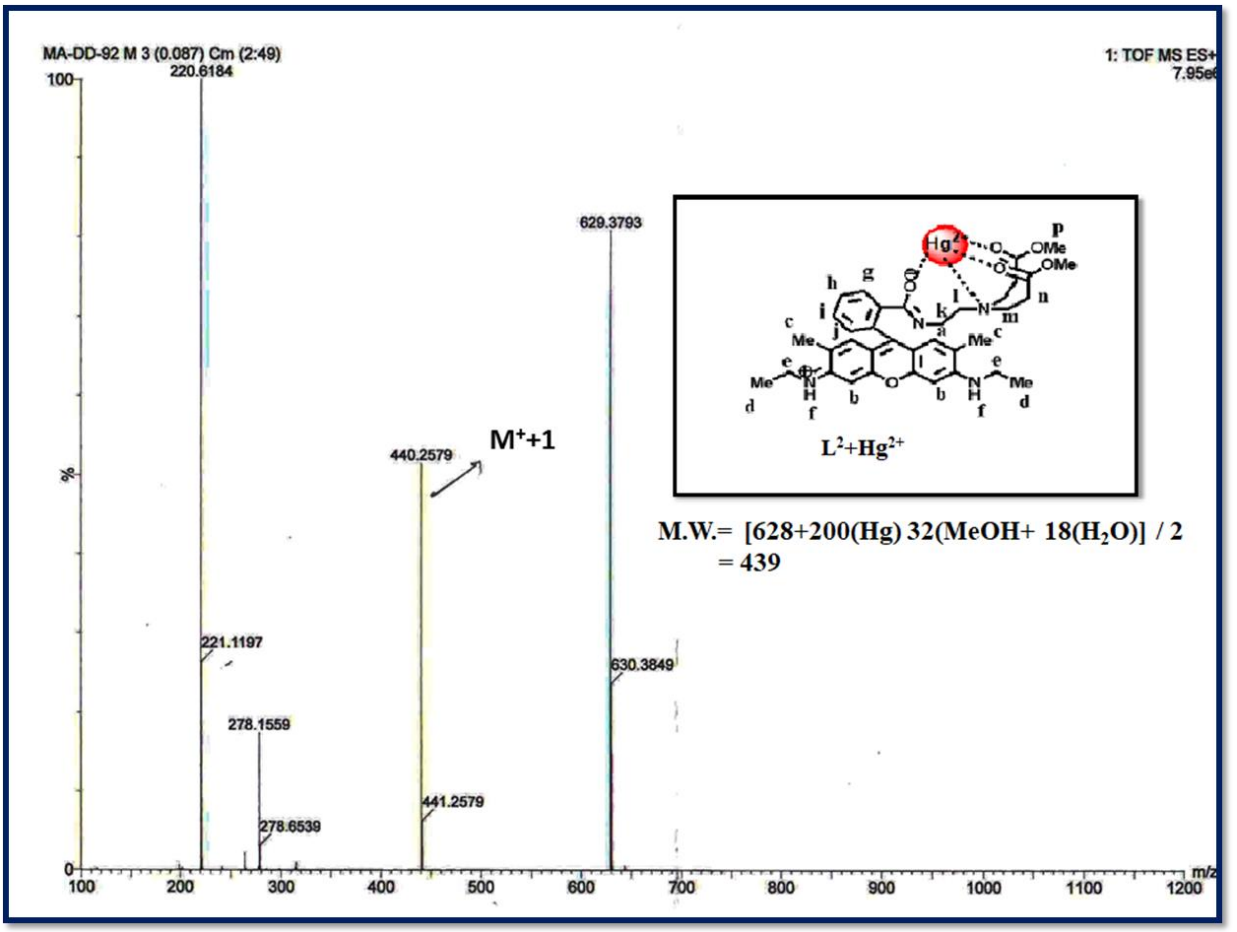

Figure-3.7: Mass spectrum of [$\mathbf{L^2}$+$\mathbf{Hg^{2+}}$] in MeOH.

3.3.1 Steady-state absorption and emission studies

The UV-Vis titrations reveals that on gradual addition of Hg^{2+} to a 50 μM solution of $\mathbf{L^2}$ there occurs a gradual growing of two peaks at 350 nm and 528 nm (**Figure-2.8**) clearly manifesting the chelation induced opening of the spirolactam ring of the probe. The probable coordination mode of $\mathbf{L^2}$ towards Hg^{2+} is demonstrated in **Scheme-2.1**. When absorbances were plotted against [Hg^{2+}] it gives a non-linear curve of decreasing slope. Eq. (**5**)[19] was employed to solve such dependence with *a* and *b* as the absorbance in the absence and presence of excess metal ions, *c* (= K_f) is the apparent formation constant and *n* is the stoichiometry of the reaction. The evaluated apparent association constant K_f is (3.08±0.53) $\times 10^3$ M^{-1} with *n* =1.0.

$$y = a+bx^n / 1+cx^n \quad \text{.....(5)}$$

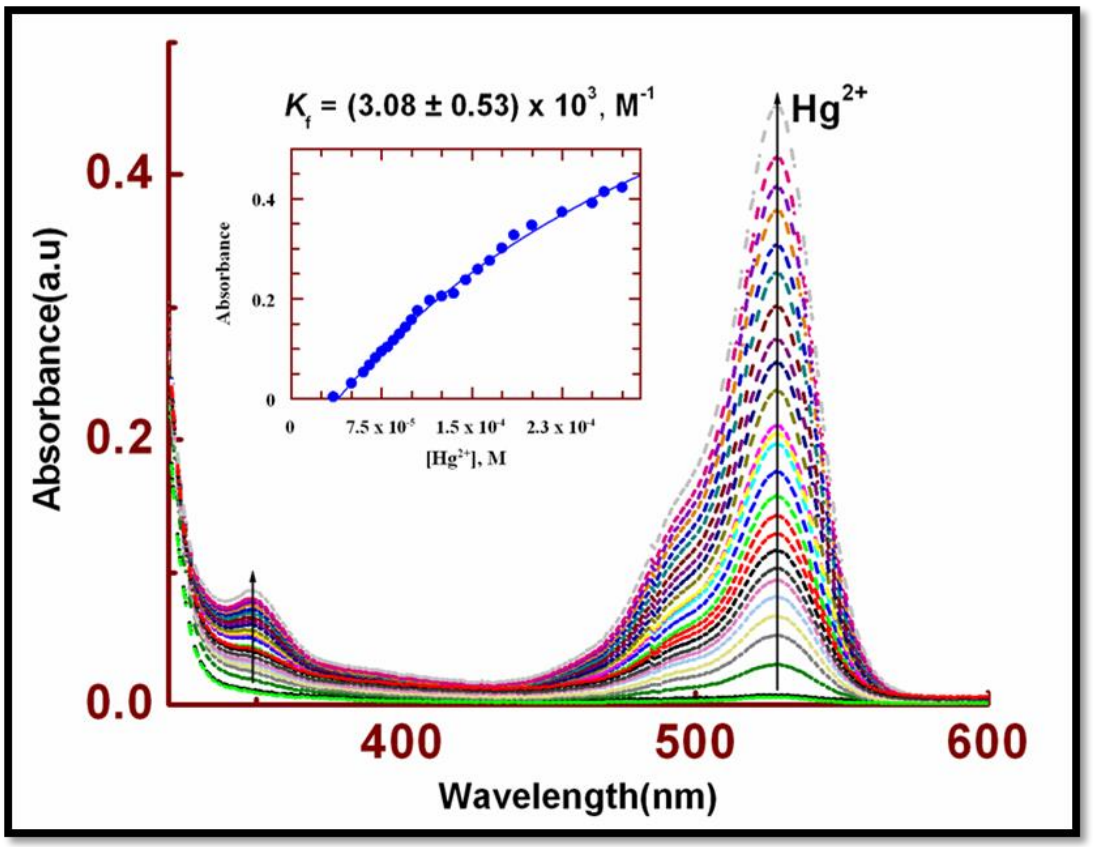

Figure-3.8: (a) UV-Vis titration of $\mathbf{L^2}$ (50 μM) in MeCN-H_2O (1:1, v/v) in HEPES buffer at pH 7.2 by the gradual addition of Hg^{2+} (0-130 μM). Inset (D), non-linear curve-fit of F.I vs. [Hg^{2+}] plot.

Job's method was used to determine the composition of the metal-ligand complex composition.Fluorescence intensity was measured at different mole fraction of the ligand and metal in MeCN-H_2O(1:1,v/v).Then the fluorescence intensity was plotted against mole fraction of the metal ion solution and it give maximum fluorescence intensity at 0.5 mole fraction and hence confirms 1:1 (**Figure-3.9**) complexation between $\mathbf{L^2}$ and Hg^{2+} which was further supported by mass spectrometric analysis (*m*/*z* = 440.2579) $[Hg(L^2)\ (MeOH)\ (H_2O)]^{2+}$ **(Figure-3.7**). The fluorescence titration was carried out by gradual addition of Hg^{2+} (0–130 μM) to a fixed concentration of $\mathbf{L^2}$ (20 μM) in MeCN /water (1: 1, v/v, HEPES buffer, pH 7.2**)** which yielded ~126-fold enhancement in fluorescence intensity at 558 nm on excitation at 502 nm (**Figure-3.10**). The titration data were again solved by employing eq. (**5**) under the condition $1>>cx^n$, with $n = 1$ prevailing a linear form. A linear least-square fitting of data gives the apparent association constant $K_f = (1.01\pm0.01) \times 10^4\ M^{-1}$ (see **Figure-3.10** inset).

Al^{3+} also induces an opening of Spiro lactam ring of the probe leading to enhancement of fluorescence intensity **(Figure- 3.11)**. So, analogously the fluorescence titration data for $\mathbf{L^2}$-$\mathbf{Al^{3+}}$ complexation was solved and the apparent formation constant was calculated to be (1.45± 0.02) $\times 10^4\ M^{-1}$(**Figure- 3.11** inset)

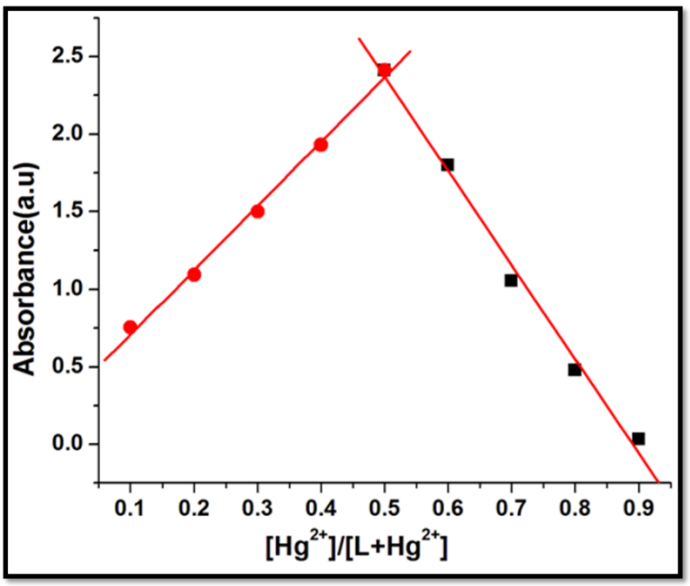

Figure-3.9: Job's plot between $\mathbf{L^2}$ and Hg^{2+} for the confirmation of 1:1 binding.

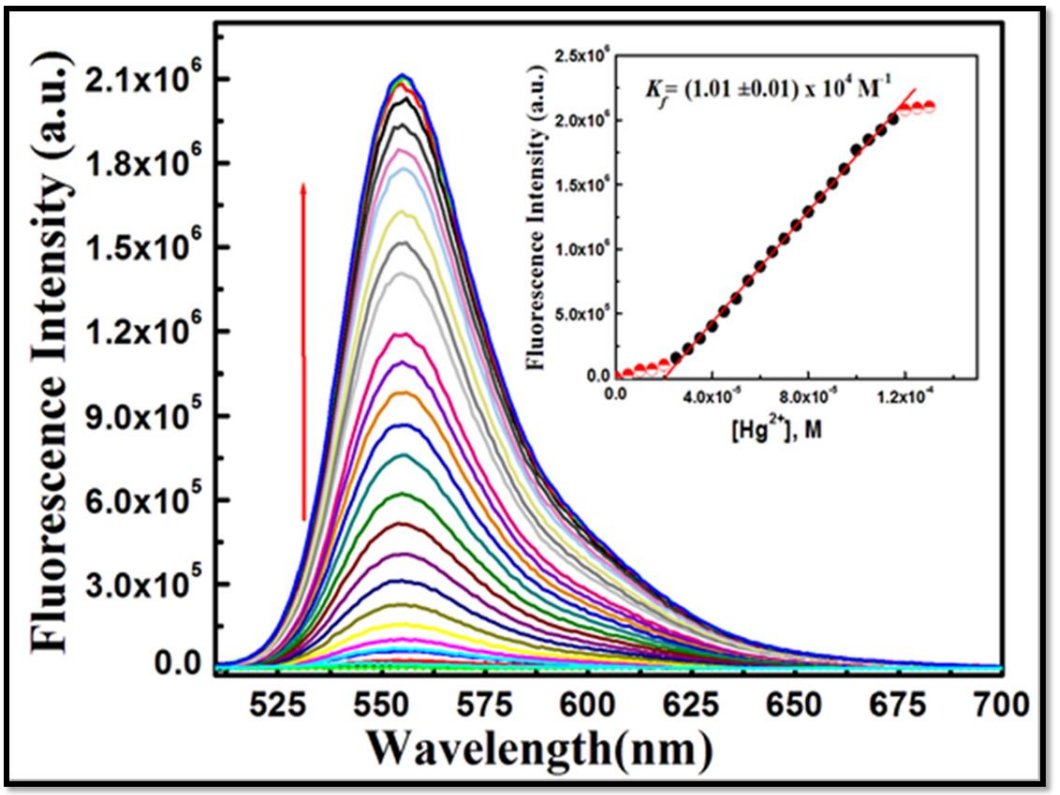

Figure-3.10: Fluorescence titration of $\mathbf{L^2}$ (20 μM) in MeCN-H_2O (1: 1, v/v) in HEPES buffer at pH 7.2 by the gradual addition of Hg^{2+} (0–130 μM) with λex = 502 nm. Inset: linear curve-fit of FI vs [Hg^{2+}] plot.

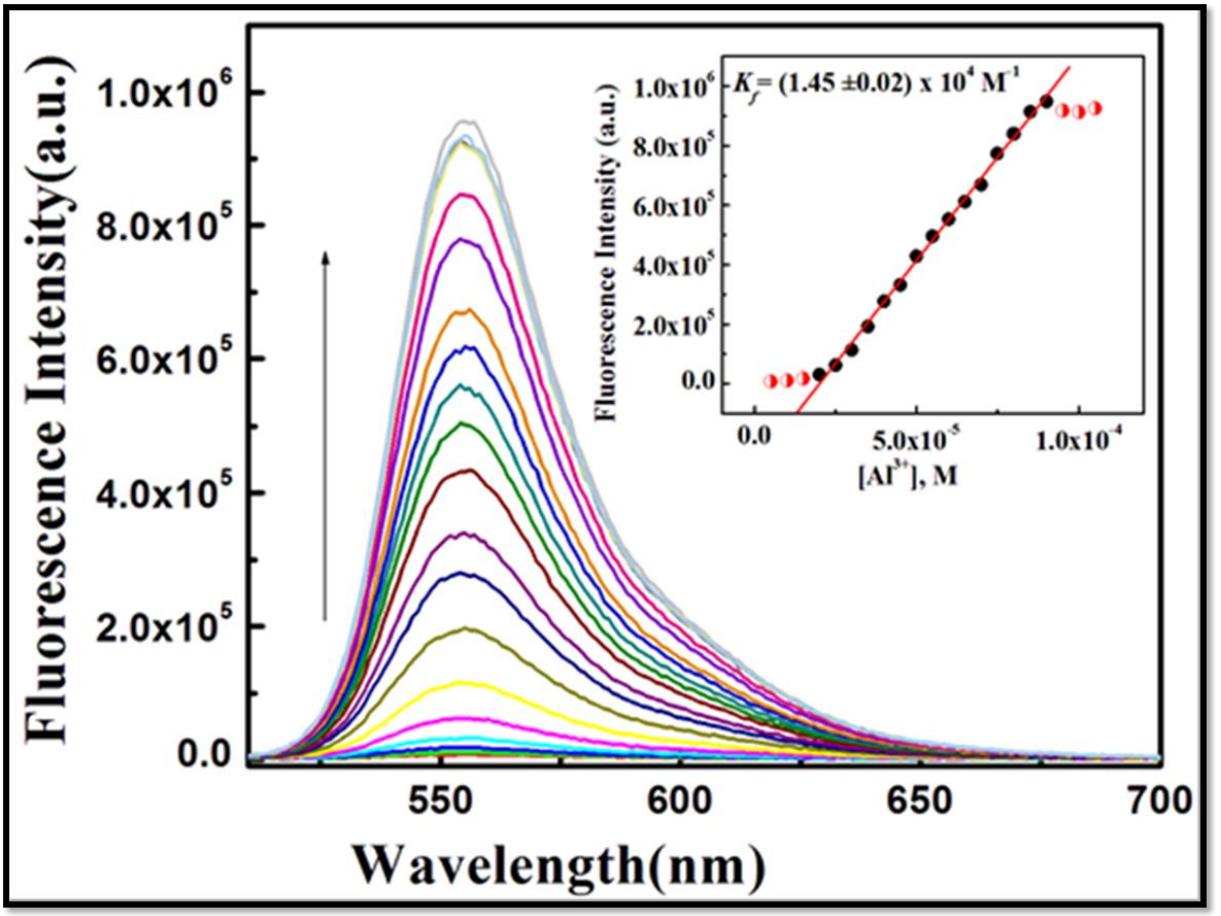

Figure-3.11: Fluorescence titration of $\mathbf{L^2}$ (20 μM) in MeCN-H_2O (1:1, v/v) in HEPES buffer at pH 7.2 by the gradual addition of Al^{3+} (0–130 μM) with λ_{ex} = 502 nm. Inset: linear curve-fit of FI vs [Al^{3+}] plot.

3.3.2 Selectivity of the probe

The probe was found to be sensitive towards Hg^{2+}, but interfered by the presence of Al^{3+}. However, in the presence of SDS in aqueous medium the fluorescence of $\mathbf{L^2}$-Al^{3+} was completely quenched, but not the $\mathbf{L^2}$-Hg^{2+} complex, instead there was an increase in FI (*vide infra*). In case of $\mathbf{L^2}$-Al^{3+} complexation the quenching of fluorescence intensity may arise due to abstraction of Al^{3+} from the [$\mathbf{L^2}$-Al^{3+}] complex by SDS arising out of strong hard-hard interaction between Sulfonic-O and Al^{3+} ion; which is absent for $\mathbf{L^2}$-Hg^{2+} complex. Again, the detection of Hg^{2+} was not perturbed by 5

equivalents of metal ions like Na^{+}, K^{+}, Ca^{2+}, Mg^{2+}, Fe^{3+}, Co^{2+}, Cu^{2+}, Cr^{3+}, Mn^{2+}, Fe^{2+}, Ni^{2+}, Zn^{2+}, Cd^{2+} and Pb^{2+} (**Figure-3.12**) under the identical reaction conditions. Also, the introduction of 5 equivalents of anions like SO_4^{2-}, NO_3^{-}, PO_4^{3-}, S_2^{-}, CN^{-}, Cl^{-}, F^{-}, Br^{-}, I^{-}, OAc^{-}, $H_2AsO_4^{-}$ and N_3^{-}into the solution of $\mathbf{L^2}$ (**Figure-3.13**) did not show any appreciable fluorescence change. However, I^{-} has a strong affinity towards Hg^{2+}. As a result, I^{-} abstracts Hg^{2+} ion from the [$\mathbf{L^2}$-Hg^{2+}] complex resulting the disappearance of emission band at 558 nm through the re-establishment of the spirolactam ring **(**Figure-3.14**)**.

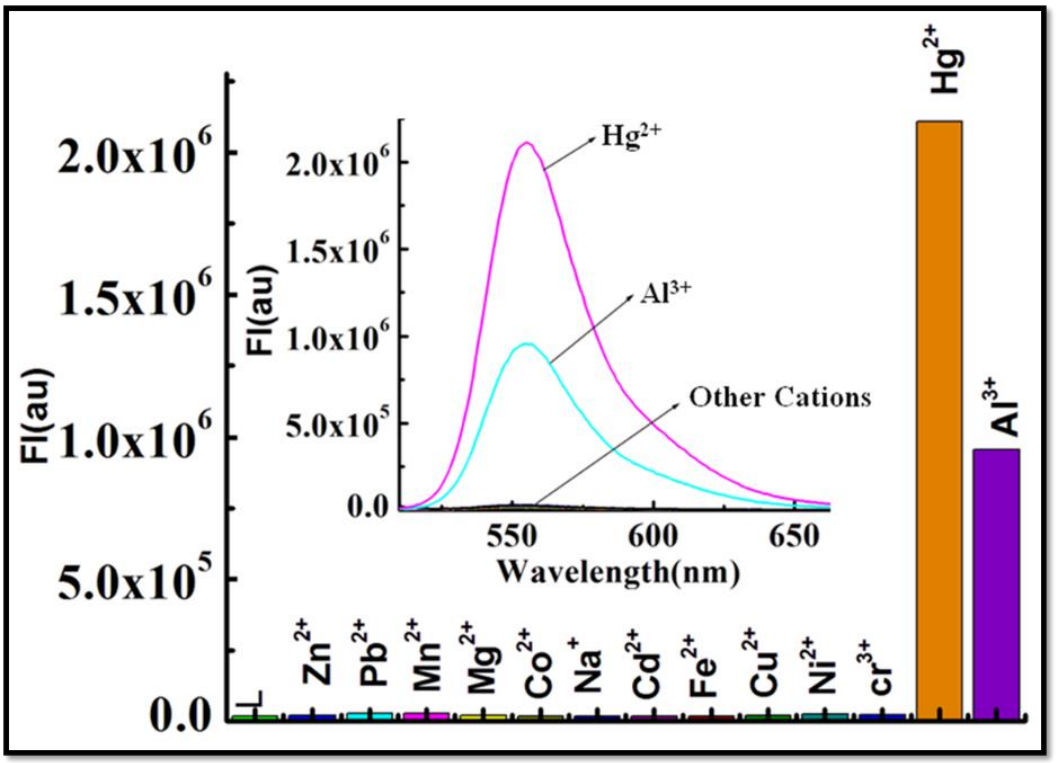

Figure-3.12: (a) Histogram of the fluorescence responses of different metal ions (100 mM) towards $\mathbf{L^2}$ (20 mM) in 1 : 1 v/v MeCN/water in HEPES buffer at pH 7.2 with λ_{ex} = 502 nm, λ_{em} = 558 nm, (b) Histogram of the fluorescence responses of different anions (100 mM) towards $\mathbf{L^2}$ (20 mM) in 1 : 1 v/v MeCN/water in HEPES buffer at pH 7.2.

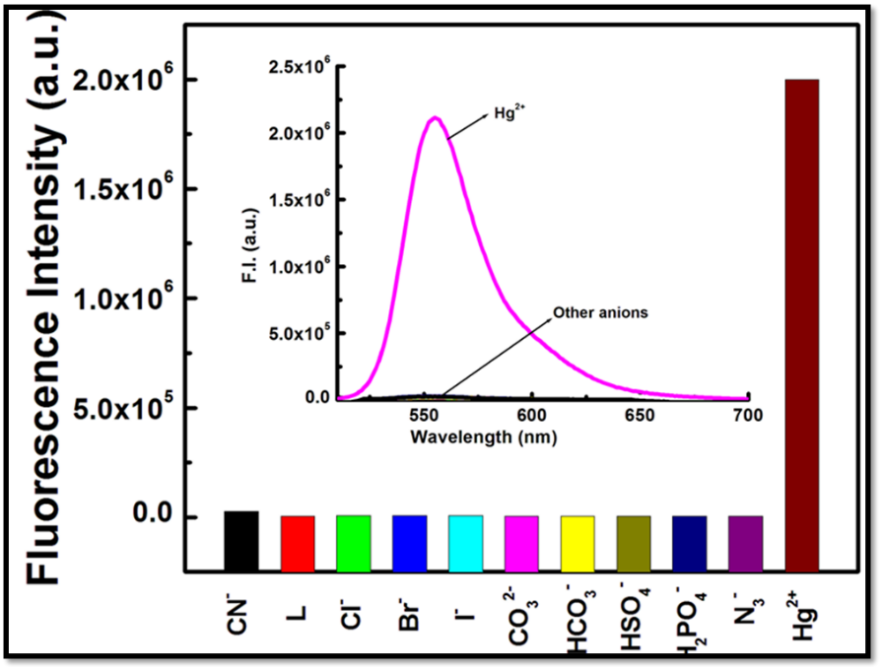

Figure-3.13: Histogram of the fluorescence responses of different anions (100 μM) towards $\mathbf{L^2}$ (20 μM) in 1 : 1 v/v MeCN /water in HEPES buffer at pH 7.2 with λ_{ex} = 502 nm, λ_{em} = 558 nm.

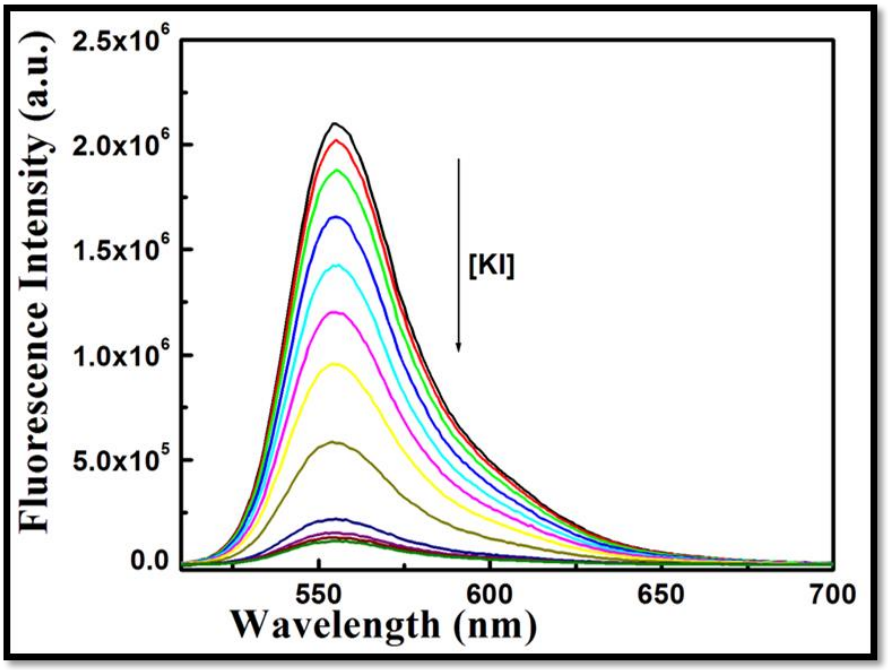

Figure-3.14: Fluorometric titration of [$\mathbf{L^2}$-$\mathbf{Hg^{2+}}$] complex with KI in CH_3CN/H_2O (1:1, v/v) in HEPES buffer pH 7.2.

The quantum yield (ϕ) of the [$\mathbf{L^2}$-$\mathbf{Hg^{2+}}$] complex and ligand were determined to be 0.8609 and 0.011 respectively (rhodamine-6G as a standard). The limits of detection (LOD) of Hg^{2+} and Al^{3+} were found to be as low as 47 and 73 nM, respectively (**Figure-3.15**) as delineated by 3σ method. The increased quantum yield (ϕ) and lifetime (τ) of [$\mathbf{L^2}$-$\mathbf{Hg^{2+}}$] over the free ligand $\mathbf{L^2}$ clearly indicate the enhanced stability of the formed complex in the excited state. pH-stability of the probe was checked over a wide range of pH (2–12). There is no obvious fluorescence emission of $\mathbf{L^2}$ in the range of pH 4–12, establishing the fact that the spirolactam form of $\mathbf{L^2}$ is stable over this wide pH range **(Figure-3.16)**. However, the presence Hg^{2+} ion induces the opening of spirolactam ring at pH 7.0 resulting a fluorescence enhancement and hence seems to be compatible for biological applications under physiological conditions. IR studies showed a characteristic amidic "C=O" stretching frequency of the rhodamine moiety at 1723 cm^{-1} which is shifted to a lower wave number (1657 cm^{-1}) in the presence of 1.2 equivalent of Hg^{2+} **(Figure-3.6)**. Thus, a strong binding of $\mathbf{L^2}$ to the Hg^{2+} ion and the cleavage of N-C bond in spirolactam ring is apparent. The ^1H NMR spectra showed the ring proton "b" (**Figure-3.17**) of the rhodamine moiety is shifted downfield in the presence of 1.2 equivalents of Hg^{2+} ions. The "f" proton of -NH^+ group vanishes as this group possesses a positive charge due to ring opening upon binding with Hg^{2+} ion. The "a" proton also shows a down-field shift. The down-field shift of "a" and "b" protons in the presence of Hg^{2+} arises mainly due to decrease in electron density on opening of the spirolactam ring. The signal pattern of the other aromatic protons in [$\mathbf{L^2}$-$\mathbf{Hg^{2+}}$] also indicates the involvement of the receptor unit of $\mathbf{L^2}$ in the binding to Hg^{2+}.

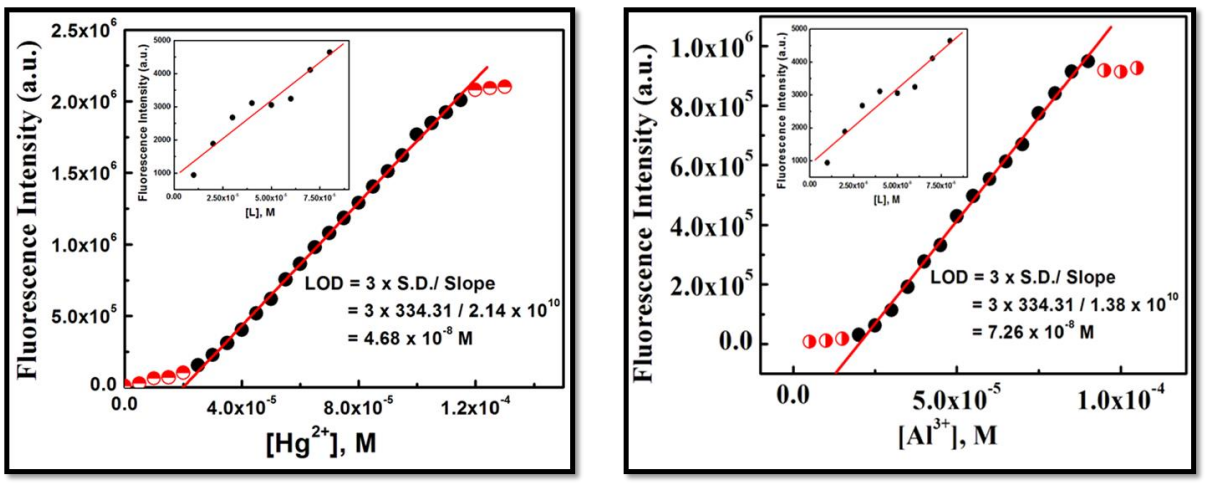

Figure-3.15: LOD determination by 3σ method with λ_{ex} = 502 nm, λ_{em} = 558 nm.

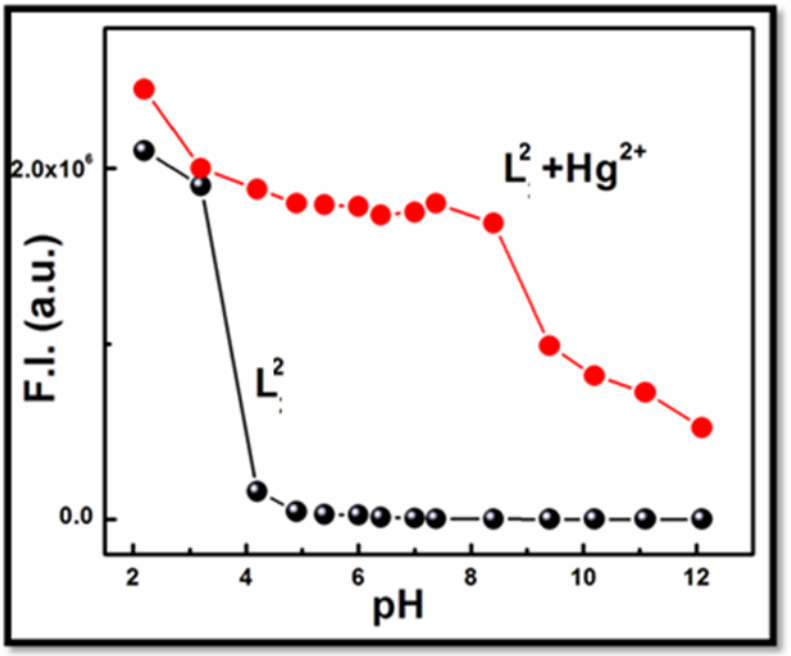

Figure-3.16: Fluorescence intensity observed at different pH for $\mathbf{L^2}$ and [$\mathbf{L^2}$+$\mathbf{Hg^{2+}}$] (20 μM) in CH_3CN/H_2O (1:1,v/v) with λ_{ex} = 502 nm, λ_{em} = 558 nm.

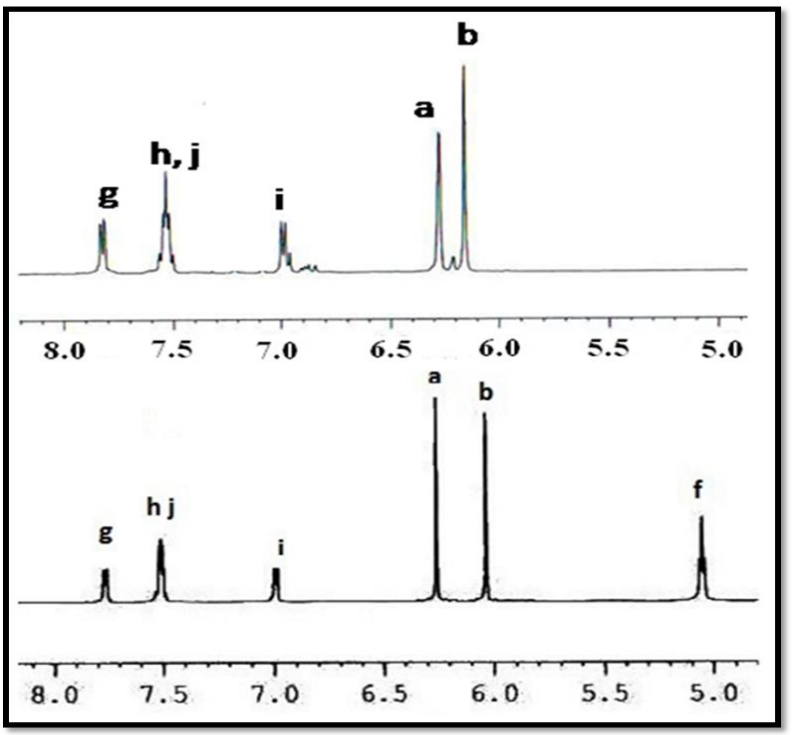

Figure-3.17: ^{1}H-NMR spectra of (a) $\mathbf{L^2}$ and (b) $\mathbf{L^2}$ in presence of 1.2 equivalent of Hg^{2+}. Both spectra were recorded on a Bruker 500 MHz spectrometer in DMSO-d_6.

3.3.3 Time resolved fluorescence studies

The fluorescence decay behaviour of the **L²** and [**L²**-Hg^{2+}] were studied in aqueous medium (**Figure-3.18**) both in the absence and presence of SDS. The bi exponential decay of **L²** resulted life times of 1.53 ns (τ_1) and 6.11 ns (τ_2). But in the presence of SDS it prevails a mono-exponential decay with τ = 3.63 ns. In the presence of Hg^{2+} the decay processes are mono-exponential both in the absence and presence of SDS with respective τ values of 4.47 and 5.44 ns (**Figure-3.18**). Bi-exponential decay of free ligand may arise due to $\pi\ldots\pi^*$ stacking interactions between the probe and molecules. The enhanced life time of **L²** and [**L²**-Hg^{2+}] complex in the presence of SDS may arise due to enhanced stability of the probe and its complex in the excited state in the presence of SDS. Thus, this observation clearly indicates the fact that SDS imposes more restriction on the movement of the probe in micro-heterogeneous environments through the formation polymeric aggregates.

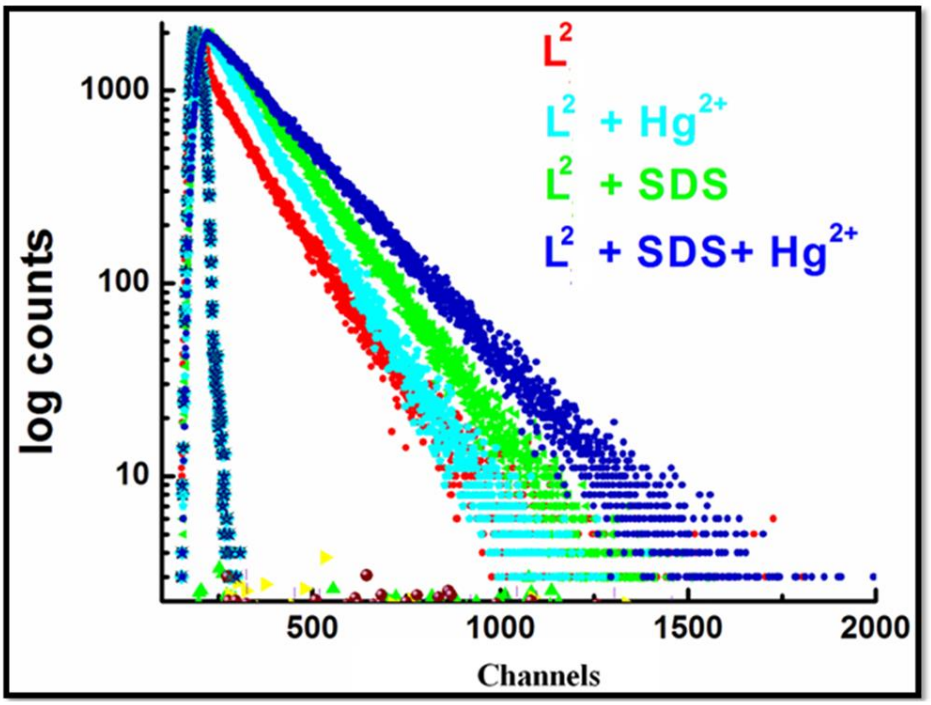

Figure-3.18: Fluorescence decay curves of free **L²** ligand (20 μM) and in the presence of Hg^{2+} (130 μM) in 1:1 (MeCN: H_2O, v/v) at 25 °C, λ_{em} = 554 nm. While in the presence of SDS pure aqueous medium was used.

3.3.4 Steady-state fluorescence studies in aqueous SDS

In pure aqueous solution the $\mathbf{L^2}$-Hg^{2+} complex is weakly fluorescent, however, in the presence of SDS enhanced fluorescence was observed. Thus, steady state fluorescence studies were also carried out in the presence of SDS in two separate experiments. In one case, the SDS concentration was kept fixed at 7 mM and [Hg^{2+}] was varied in the range 0–40 mM giving a non-linear curve of decreasing slope which was solved by adopting eq. (**5**) (**Figure-3.19**) and evaluated apparent formation constant K_f = (1.00±0 0.02) ×10^5 M^{-1} was found to be an order of magnitude higher than that obtained in the absence of SDS. This enhanced stability constant value may be due to the restricted movement of the doubly positively charged $\mathbf{L^2}$-Hg^{2+} complex, which were held fixed in position by the strong electrostatic interaction with the negatively charged sulphonic acid head groups of SDS in the form of layer structure. This causes the formation of aggregates of $\mathbf{L^2}$-Hg^{2+} complex through strong cooperative π…..π* interactions among the complexes held sidewise.

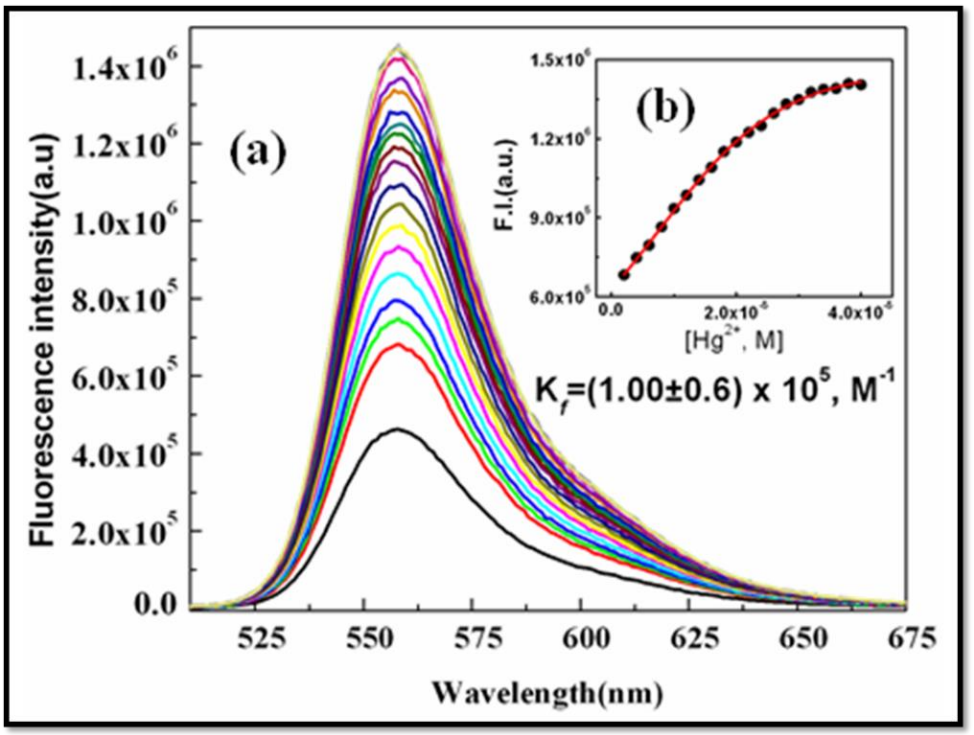

Figure-3.19: (a) Florescence titration of $\mathbf{L^2}$ (20 µM) by Hg^{2+} (0-40 µM) in the presence of [SDS] = 7 mM with λ_{ex} = 502 nm, (b) Plot of Fluorescence Intensity as a function of [SDS].

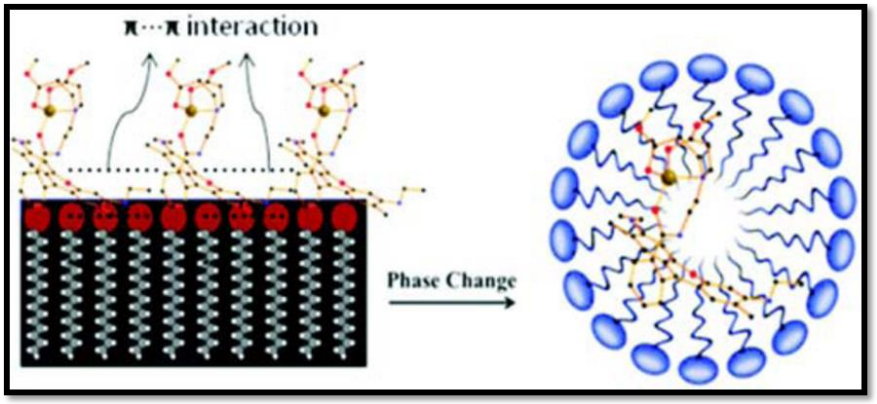

Scheme 3.2: Schematic presentation of the formation of polymeric aggregates and monomer in presences of SDS before and after the cmc. Adopted from http:// www.ecoboss.com.au/img/micelle.jpg.

In another experiment both [$\mathbf{L^2}$] and [$\mathbf{Hg^{2+}}$] was kept fixed at 20 and 150 µM, respectively and [SDS] was varied between 0–28 mM. A plot of FI vs [SDS] showed a gradual increase in FI with the increase in [SDS], reaches a maximum at ~7 mM and then gradually decreases with the increase in [SDS] (**Figure-3.20**). The fluorescence maximum at [SDS] ~7 mM clearly points out a critical micellar concentration (CMC) of SDS as ~7 mM under the experimental conditions. The decrease in FI with [SDS] beyond 7 mM may be attributed to a change in polymeric aggregates of the complex to a monomer arising due to the formation of spherical micelle on increasing the [SDS] (**Scheme 3.2**) in which the complex is trapped. The increase in FI with [SDS] manifests the fact of aggregation induced enhancement (AIE) of fluorescence. In the case of Al^{3+} ion, fluorescence quenching was observed on increasing the concentration of SDS (**Figure-3.21**) and may be explained by considering the fact that sulphonic acid group abstract Al^{3+} ion from [$\mathbf{L^2}$-Al^{3+}] complex by strong electrostatic interaction. So, in aqueous SDS the probe becomes more selective towards Hg^{2+}. The fluorescence quenching experiment by iodide ion in the presence of [SDS] = 7 mM was carried out to verify the reversibility and reusability of the probe (**Figure-3.22, a**). The formation constant for this quenching phenomenon found to be, $K_f = (5.606+0.067) \times 10^4$ **(Figure-3.22, c)** and K_{SV} was evaluated to be 5.69×10^6 **(Figure-3.22b)** indicating an easy accessibility of the [$\mathbf{L^2}$-$\mathbf{Hg^{2+}}$] complex located on the laminar surface of the SDS to I^- ion to form HgI_2.

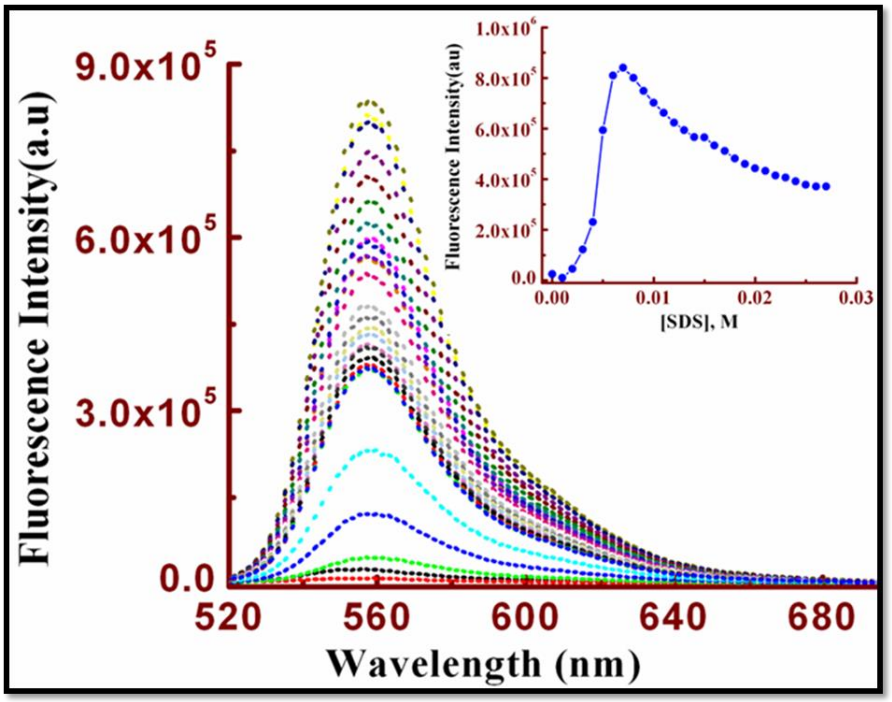

Figure-3.20: (a) Florescence titration of $\mathbf{L^2}$ (20 µM) by SDS in presence of [Hg^{2+}] (130 µM) with λ_{ex} = 502 nm,; (b) Plot of Fluorescence Intensity as a function of [SDS].

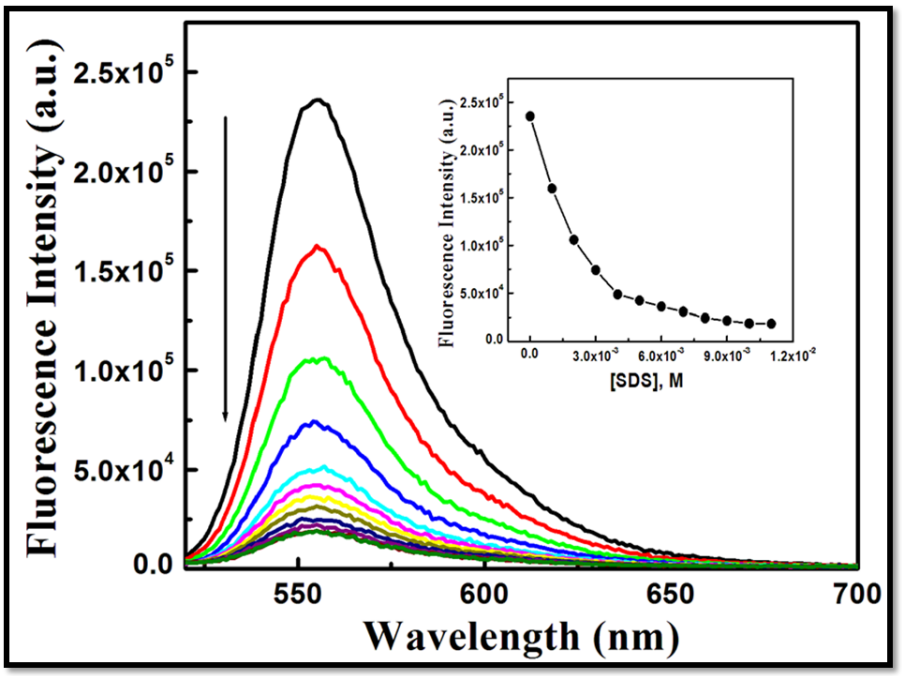

Figure-3.21:(a) Florescence titration of $\mathbf{L^2}$ (20 µM) by SDS in presence of [Al^{3+}] (130 µM) with λ_{ex} = 502 nm,; (b) Plot of Fluorescence Intensity as a function of [SDS].

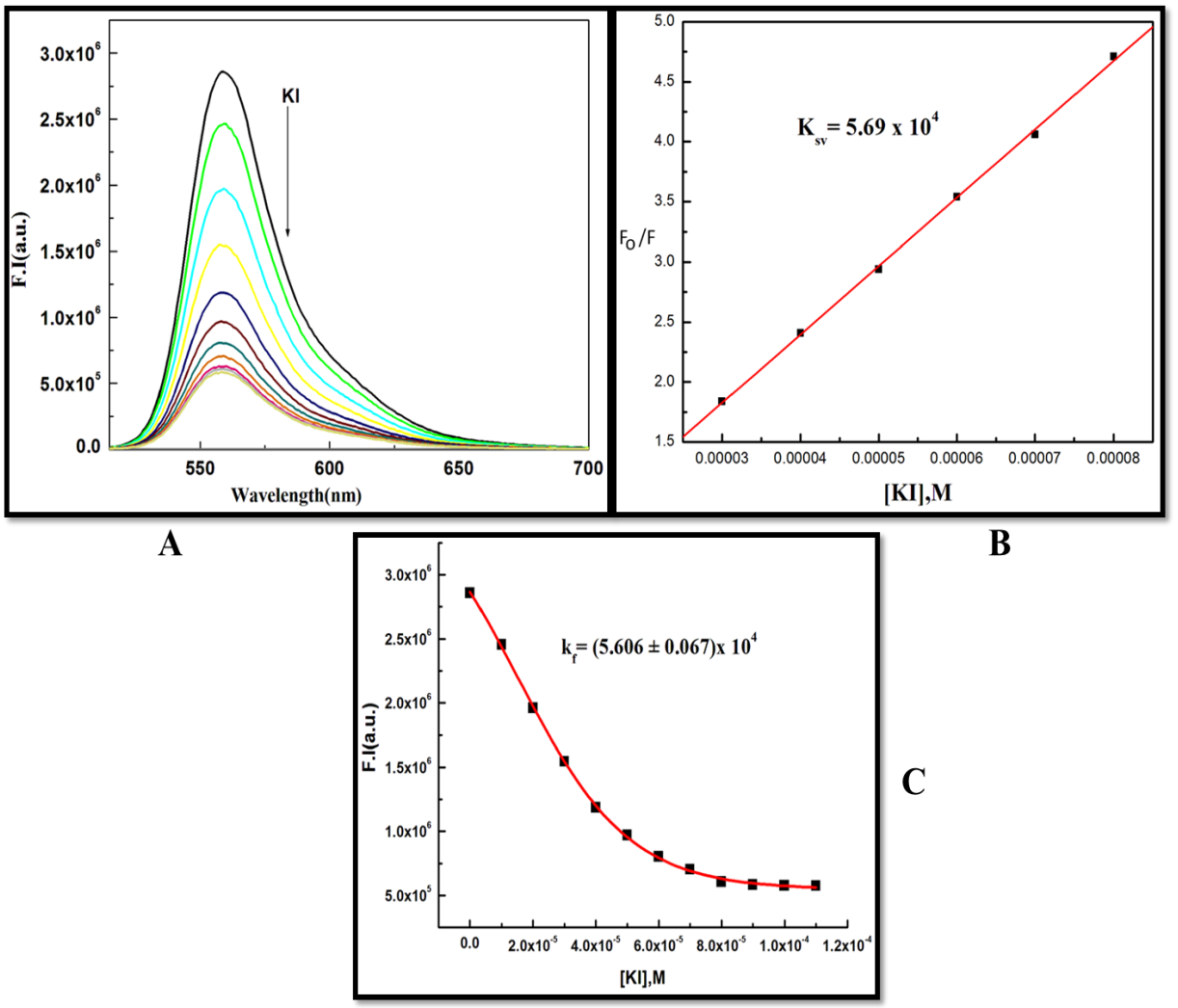

Figure-3.22: (a) Fluorometric titration of $[\mathbf{L^2}\text{-Hg}]^{2+}$ complex (prepared from 20 µM $\mathbf{L^2}$ and 130 µM Hg^{2+}) with KI in aqueous SDS medium with λ_{ex} = 502 nm (diagram A). (b) Determination of K_{sv} from the titration of $\mathbf{[L^2}\text{-Hg}]^{2+}$ complex by KI (diagram B). (c) Non-linear fitting of FI vs. [KI] curve (diagram C).

3.3.5 Determination of steady-state fluorescence anisotropy

Steady-state fluorescence anisotropy is usually taken as a measure of the extent of restriction imposed by the micro heterogeneous environments on the dynamic properties of the probe. An increase in rigidity of the fluorophore results in an increase in the fluorescence anisotropy[19]. We have monitored the fluorescence anisotropy as a function of SDS concentration at a fixed

concentration of $\mathbf{L^2}$ and Hg^{2+} (20 and 150 μM, respectively) at 558 nm which showed a marked increase in anisotropy on increasing SDS concentration up to 3.5 mM, then gradually decreases with SDS concentration reaches a plateau at ~5 mM and maintains steady value up to 12 mM. In the range 1–3.5 mM concentration, the SDS arranges them in a layered fashion. Now, the doubly charged [$\mathbf{L^2}$-Hg^{2+}] complexes are held firmly by the strong electrostatic interactionsbetween negatively charged sulfonic acid head groups and doubly positively charged complexes; which are again held together by strong π…π* interactions thereby restricting their free movement. As a result, there occurs a sharp increase in anisotropy in the [SDS] ~1–3.5 mM. Further increase in the SDS concentration, a phase transition occurs through the formation of micelle. The slight drop in ***r*** values with [SDS] beyond 3.5 mM may be rationalized by considering the formation of a monomer of [$\mathbf{L^2}$-Hg^{2+}] complex which is again trapped inside the cavity of the micelle. The higher values of *r* in case of polymeric aggregates arise due to cooperative interactions among the [$\mathbf{L^2}$-Hg^{2+}] complexes which is absent in monomer trapped inside the cavity of the micelle. The variation of fluorescence anisotropy (*r*) as a function of SDS concentration is presented in (**Figure-3.23**).

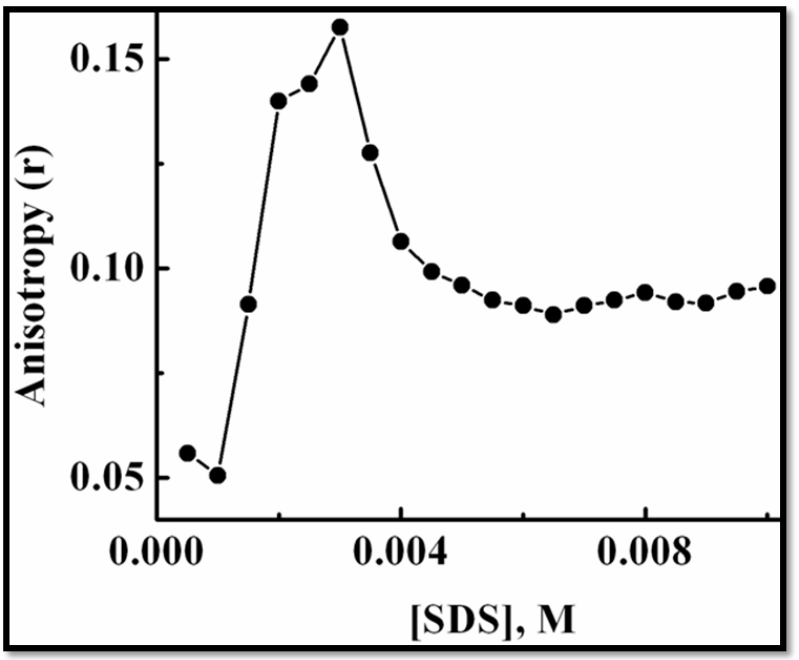

Figure-3.23: Plot of fluorescence anisotropy (r) as a function of [SDS] in purely aqueous medium at 25 °C and [$\mathbf{L^2}$] = [Hg^{2+}] = 20 μM, λ_{ex} = 502 nm, λ_{em} = 558 nm.

3.3.6 SEM study

The SEM micrographs of **L²** (0.50 mM) prevails rod-like microstructures which interestingly changes to porous like architecture in presence of Hg^{2+} (0.50 mM) (**Figure-3.24**). In case of pure ligand in water the structures are similar to the hexagonal prisms that arises due to the presence of two different polar ends (xanthine moiety and carboxylic ester moiety) favouring the stacking of **L²** one over another. However, in presence of Hg^{2+} these stacking interactions are disrupted leading to the formation of porous microstructures centring Hg^{2+} with the ligands at the periphery.

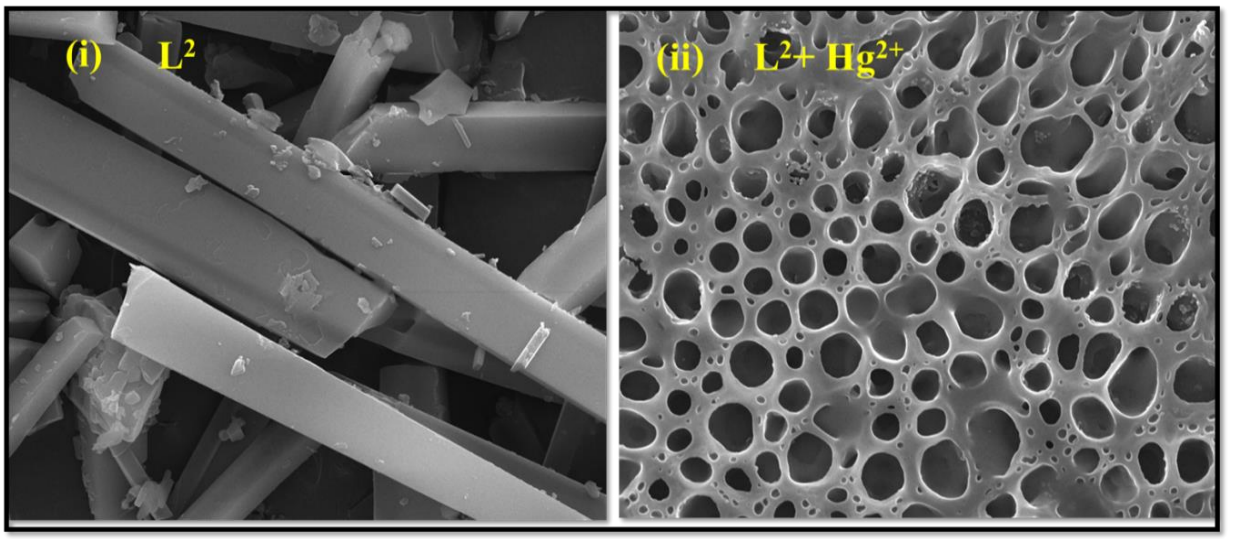

Figure-3.24: SEM images of microstructures. Conditions: (i) **L²** (0.5 mM) and (ii) (0.5 mM each) in aqueous medium.

3.3.7 Cell imaging applications

Hg^{2+} capturing capability of **L²** was assessed by performing the fluorescence imaging of **L²** with Hg^{2+} into the live HepG2 cells (**Figure-3.26**). The cytotoxicity effects of **L²** determined by MMT assay indicate no significant cell cytotoxicity for HepG2 cells up to 60 µM (<30% cytotoxicity) of **L²** (**Figure-3.25**). Interestingly, up to 10 µM of **L²** there was more than 90% of cell viability and fluorescence imaging were carried out at 1 µM, 5 µM and 10 µM of **L²**. Significantly, an excellent red intracellular cytoplasmic fluorescence was observed inside the live HepG2 cells pre-incubated

with 10 µM of Hg^{2+} followed by washing with 1X PBS and subsequent incubation with 1 µM, 5 µM and 10 µM of **L²**. Interestingly, we observed that **L²** has excellent Hg^{2+} capturing capability even at low concentration likely at 1 µM and 5µM at cytoplasmic level of Hg^{2+} ions (**Figure-3.26**). Moreover, the concentration dependent binding of the **L²** with Hg^{2+} ions was observed. Parallel staining of cells was carried out with DAPI and superimposed with the correspondingly treated cells with Hg^{2+} (10 µM) followed by **L²** (10, 1, 5, 10 µM) to show the cytoplasmic staining of **L²** with HepG2 cells.

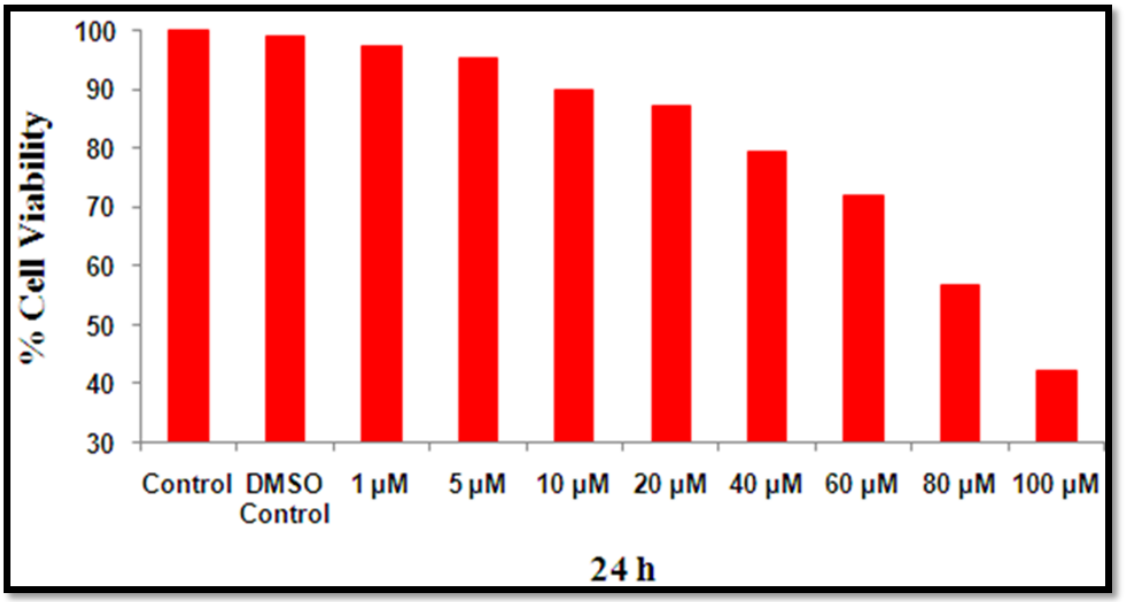

Figure-3.25: Cell viability assay performed by using ligand **L²**.

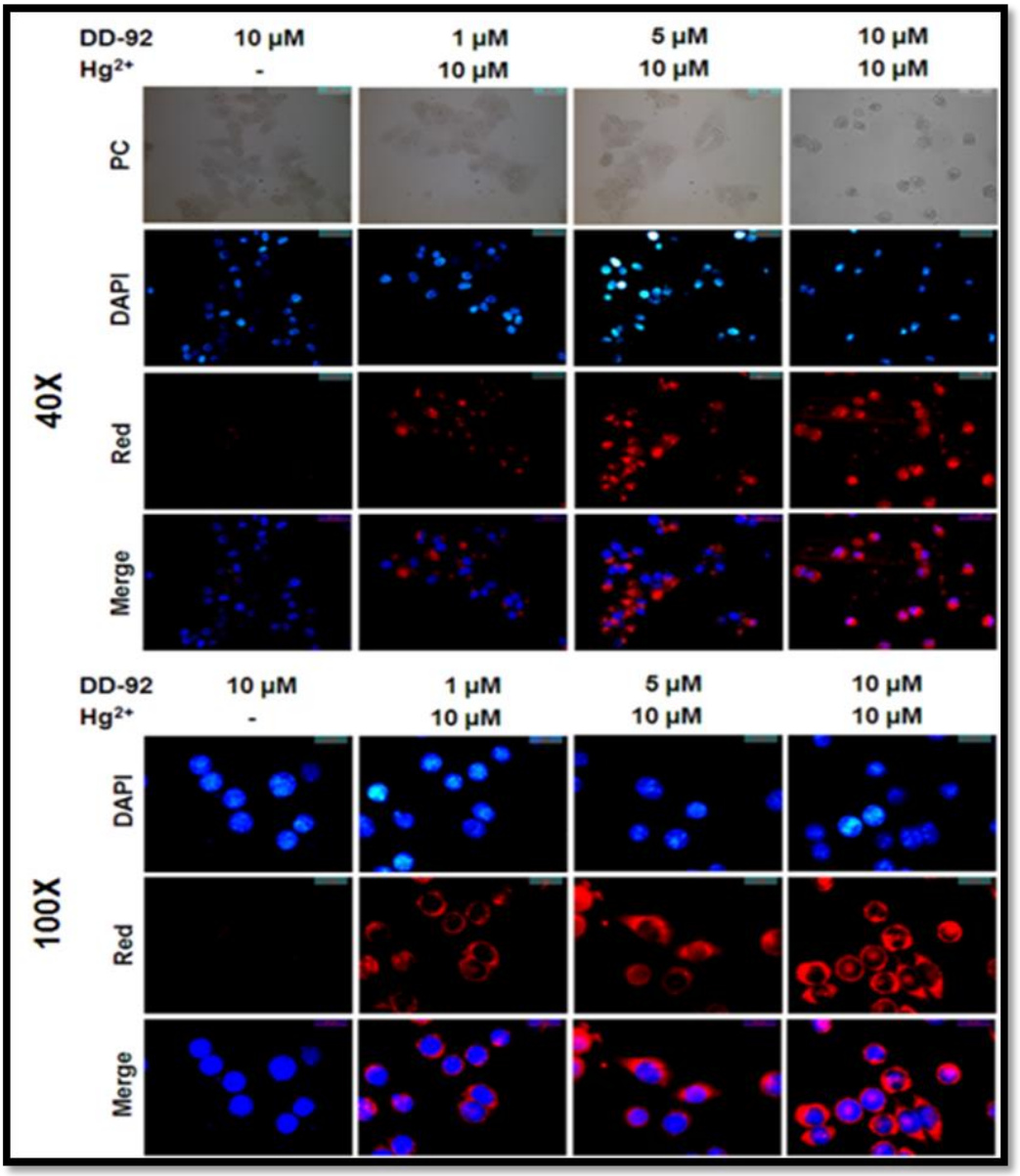

Figure-3.26: Cell imaging study of Hg^{2+} ions with $\mathbf{L^2}$. The fluorescence images of HepG2 cells were captured (40X and 100X) after incubating with 10 µM of $\mathbf{L^2}$ for 30 min at 37 °C, also in pre-incubated 10 µM of Hg^{2+} for 3 h at 37°C followed by washing twice with 1X PBS and, subsequent incubation with 1µM, 5µM and 10µM of ligand $\mathbf{L^2}$ for 30 min at 37^0C. The imaging study shows the strong red florescence when $\mathbf{L^2}$ binds with cytoplasmic Hg^{2+} ions. The merge images show the cytoplasmic $\mathbf{Hg^{2+}}$-$\mathbf{L^2}$ fluorescence.

3.4 Conclusion

In summary, we present herein a rhodamine-6G based chemosensor with potential NO_3 donor atoms for the selective and rapid recognition of toxic Hg^{2+} ions. The binding stoichiometry of the sensor with Hg^{2+} was established by the combined Job's and HRMS (*m/ z*) methods. All biologically relevant as well as toxic heavy metal ions did not interfere with the detection of Hg^{2+} ion. The detection limit of Hg^{2+} calculated by 3σ method gives a value of 1.52 nM. Its exhibits live cell imaging application of Hg^{2+} with no or negligible cytotoxicity. SEM studies reveal a rod-like microstructure for $\mathbf{L^2}$ which changes to a porous microstructure in presence of Hg^{2+} (0.50 mM). The presence of SDS causes enhanced quantum yield (ϕ), life time (τ), and stability constant (K_f) by an order of magnitude compared to those in the absence of SDS. Again, the FI of [$\mathbf{L^2}$-Hg^{2+}] complex is enhanced by 33-fold in the presence of 7 mM SDS to that in the absence of SDS. In SDS/water system, there is a steep rise in FI with the increase in [SDS], reaches a maximum at ~7 mM and then FI decreases gradually with the increase in [SDS] up to 28 mM, indicating the formation of polymeric aggregates of [$\mathbf{L^2}$-Hg^{2+}] complex on layers of the SDS at pre-micellar concentrations with higher FI values – a phenomenon reminiscent with the aggregation induced emission enhancement (AIEE). However, it turns into monomer and trapped inside the cavity of the micelle beyond CMC with comparatively lower FI. This proposition is further supported by the dependence of fluorescence anisotropy (*r*) with [SDS].

References

1. F. J. M. Hoeben, P. L. Jonkheijm, E. W. Meijer and A. P. H. J. Schenning, Chem. Rev., **2005**,105, 1491.
2. T. L. Greaves and C. J. Drummond, Chem. Soc. Rev., **2008**, 37, 1709.
3. T. H. Rehm and C. Schmuck, Chem. Soc. Rev., **2010**, 39, 3597.
4. T. L. Greaves and C. J. Drummond, Chem. Soc. Rev., **2013**, 42, 1096.
5. B. K. An, J. Gierschner and S. Y. Park, Acc. Chem. Res., **2012**, 45, 544.
6. X. Luo, J. Li, C. Li, L. Heng, Y. Q. Dong, Z. Liu, Z. Bo and B. Z. Tang, Adv. Mater., **2011**, 23, 3261.
7. K. Dhara, Y. Hori, R. Baba and K. Kikuchi, Chem. Commun., **2012**, 48, 11534.
8. Y. Ren and T. Baumgartner, Inorg. Chem., **2012,** 51, 2669.
9. C. Shi, Z. Guo, Y. Yan, S. Zhu, Y. Xie, Y. S. Zhao, W. Zhu and H. Tian, ACS Appl. Mater. Interfaces, **2013**, 5, 192.
10. J. Luo, Z. Xie, J. W. Y. Lam, L. Cheng, H. Chen, C. Qiu, H. S. Kwok, X. Zhan, Y. Liu, D. Zhu and B. Z. Tang, Chem. Commun., **2001**, 1740.
11. X. Huang, X. Gu, G. Zhang and D. Zhang, Chem. Commun., **2012**, 48, 12195.
12. S. Li, S. M. Langenegger and R. Haner, Chem. Commun., **2013**, 49, 5835.
13. W. Wu, S. Ye, R. Tang, L. Huang, Q. Li, G. Yu, Y. Liu, J. Qin and Z. Li, Polymer, **2012**, 53, 3163.
14. B. K. An, S. K. Kwon, S. D. Jung and S. Y. Park, J. Am. Chem. Soc., **2002**, 124, 14410.
15. S. J. Li, B. K. An, S. D. Jung, M. A. Chung and S. Y. Park, Angew. Chem., Int. Ed., **2004**, 43, 6346.
16. M. Rosoff, Ed. Vesicles, Dekker, New York, **1996**.

17. A. M. Carmona-Ribeiro, *Chem. Soc. Rev.*, **1992**, 21, 209.

18. S. Dutta Choudhury, A. C. Bhasikuttan, H. Pal and J. Mohanty, Langmuir, **2011**, 27, 12312.

19. R. Bhowmick, R. Alam, T. Mistri, D. Bhattacharya, P. Karmakar and M. Ali, *Appl*. Mater. Interfaces, **2015**, 7, 7476.

20. R. Bhowmick, A. S. M. Islam, A. Katarkar, K. Chaudhuri and M. Ali, Analyst, **2016**, 141, 225.

21. H. N. Kim, W. X. Ren, J. S. Kim and J. Yoon, Chem. Soc. Rev., **2012**, 4, 3210.

22. D. G. He, X. X. He, K. M. Wang, Y. X. Zhao and Z. Zou, Langmuir, **2013**, 29, 5896.

23. Y. C. Shih, C. Y. Ke, C. J. Yu, C. Y. Lu and W. L. Tseng, ACS Appl. Mater. Interfaces, **2014**, 6, 17437.

24. P. B. Tchounwou, W. K. Ayensu, N. Ninashvili and D. Sutton, Environ. Toxicol., **2003**, 18, 149.

25. A. C. Bittner (Jr.), D. Echeverria, J. S. Woods, H. Vasken. Aposhian, C. Naleway, M. D. Martin, R. K. Mahurin, N. J. Heyer and M. Cianciola, J. Indian Chem. Soc., Vol. 94, July 2017, 828 Neurotoxicol. Teratol., **1998**, 20, 429.

26. Mercury Study Report to Congress, United States Environmental Protection Agency, Volume V: Health Effects of Mercury and Mercury Compounds, EPA-452/R-97-007 December 1997.

27. M. Suresh, A. Ghosh and A. Das, Chem. Commun., **2008**, 3906.

28. O. A. Bozdemir, R. Guliyev, O. Buyukcakir, S. Selcuk, S. Kolemen, G. Gulseren, T. Nalbantoglu, H. Boyaci and E. U. Akkaya, J. Am. Chem. Soc.,**2010**, 132, 8029.

29. A. Thakur, S. Sardar and S. Ghosh, Inorg. Chem., **2011**, 50, 7066.

30. J. R. Lakowicz, "Principles of Fluorescence Spectroscopy", 3rd. ed., Springer, New York, **2006**,67.

31. R. P. Haugland, "The Handbook: A Guide to Fuorescent Probes and Labeling Technologies", 10th ed., Invitrogen Corp., Karlsbad, CA, **2005**.

32. H. Y. Lee, K. M. K. Swamy, J. Y. Jung, G. Kim and J. Yoon, Sens. Actuators *(B)*, **2013**, 182, 530. 33. X. Chen, T. Pradhan, F. Wang, J. S. Kim and J. Yoon, Chem. Rev., **2012**, 112, 1910.

34. K. Bera, A. K. Das, M. Nag and S. Basak, Anal. Chem., **2014**, 86, 2740.

35. V. Dujols, F. Ford and A. W. Czarnik, J. Am. Chem. Soc., **1997**, 119, 7386.

36. J. S. Wu, I. C. Hwang, K. S. Kim and J. S. Kim, Org. Lett., **2007**, 9, 907.

37. R. Alam, T. Mistri, P. Mondal, D. Das, S. K. Mandal, A. R. Khuda-Bukhsh and M. Ali, Dalton Trans., **2014**, 43, 2566.

38. R. Alam, T. Mistri, A. Katarkar, K. Chaudhuri, S. K. Mandal, A. R. Khuda-Bukhsh, K. K. Das and M. Ali, Analyst, **2014**, 139, 4022.

39. R. Bhowmick, M. Dolai, R. Alam, T. Mistri, A. Katarkar, K. Chaudhuri and M. Ali, RSC Adv., **2014**, 4, 41784.

Rhodamine 6G-based efficient chemosensor for trivalent metal ions (Al^{3+}, Cr^{3+} and Fe^{3+}) upon single excitation with applications in combinational logic circuits and memory devices

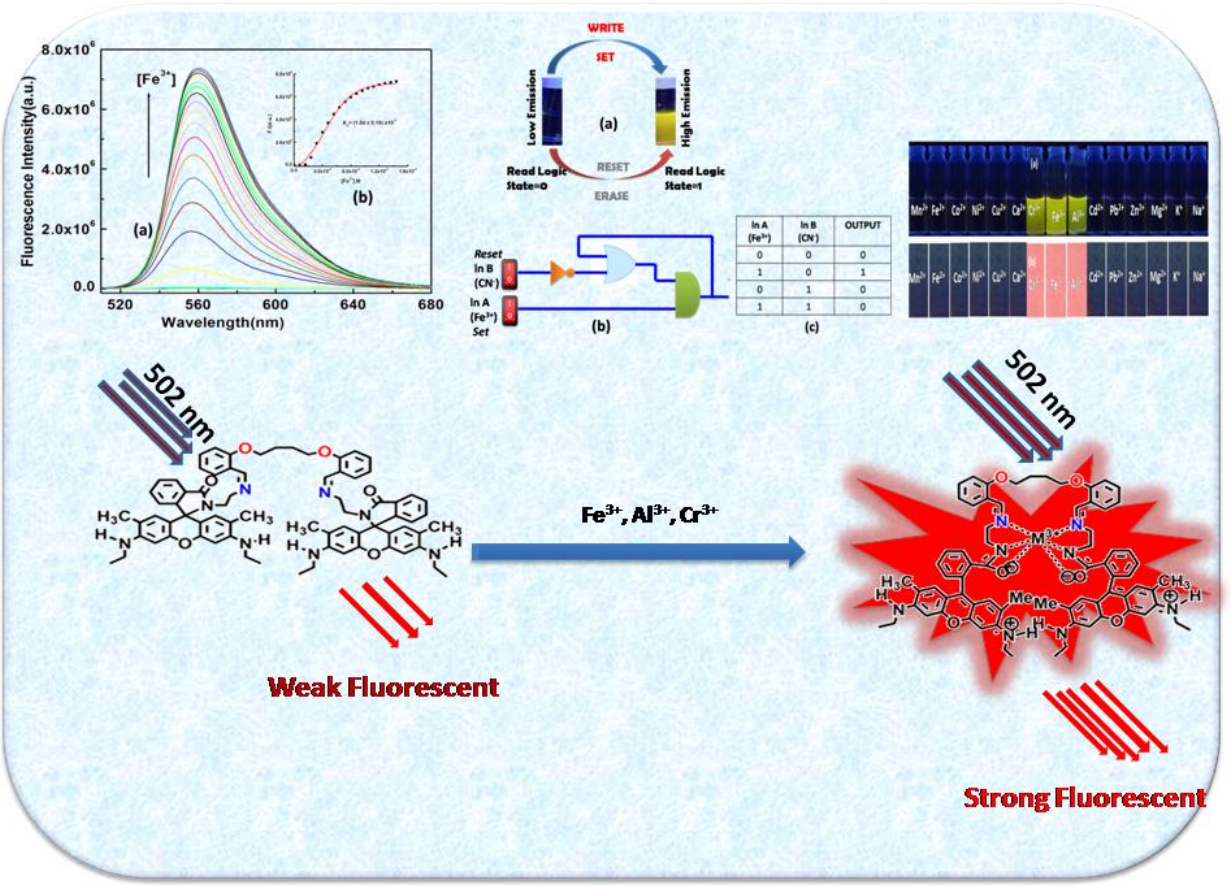

Abstract

A new rhodamine 6G-based chemosensor, **L³**, was synthesized and characterized by ^{1}H, ^{13}C, IR and mass spectroscopy studies. It exhibited an excellent selective and sensitive CHEF-based recognition of trivalent metal ions M^{3+} (M = Fe, Al and Cr) over mono and di-valent and other trivalent metal ions with prominent enhancement in the absorption and fluorescence intensity for Fe^{3+} (669-fold), Al^{3+} (653-fold) and Cr^{3+} (667-fold) upon the addition of 2.6 equivalent of these metal ions in the probe in H_2O/CH_3CN (7:3, v/v, pH 7.2). The corresponding K_d values were evaluated to be 1.94 × 10−5 (Fe3+), 3.15 × 10−5 (Al3+) and 2.26 × 10 −5 M (Cr^{3+}). The quantum yields of **L³**, [**L³**–Fe^{3+}], [**L³**–Al^{3+}] and [**L³**–Cr^{3+}] complexes in H_2O/CH_3CN (7:3, v/v, pH 7.2) were found to be 0.0005, 0.335, 0.327 and 0.333, respectively, using rhodamine-6G as the standard. The LODs for Fe^{3+}, Al^{3+} and Cr^{3+} were determined by 3σ methods and found to be 2.57, 0.78 and 0.47 μM, respectively. The cyanide ion snatched Fe^{3+} from the [Fe^{3+}– **L³**] complex and quenched its fluorescence via its ring-closed spirolactam form. Advanced level molecular logic devices using different inputs (2 and 4 input) and a memory devices were constructed.

4.1 Introduction

Due to biological and environmental importance the selective and sensitive detection of transition metal ions through the design of suitable fluorescent chemosensors have attracted profound attention of chemists and biologists.[1,2] Excess or deficiency of a metal ion in living system may lead to several diseases. Although, chemosensors for single analyte detection are plenty, chemosensors corresponding to multiple metal ion detection have been less explored[3], even though a number of trivalent metal ions like Fe^{3+}, Al^{3+} and Cr^{3+} are important both biologically and environmentally. As for example, Cr^{3+}, an essential trace element, displays a huge impact on the metabolism of carbohydrates, fats, proteins and nucleic acids through activation of certain enzymes and stabilization of proteins and nucleic acids.[4,5] It also plays an important role in the maintenance of normal levels of glucose, triglyceride and total cholesterol.[6–11] While overdose of

Cr^{3+} inflicts a negative effect on normal enzymatic activities, cellular structure and function causing a disturbance in glucose levels and lipid metabolism, its deficiency would lead to a variety of diseases, including the risk of diabetes, cardiovascular diseases, and nervous system disorders.[12]

The Cr^{3+} ion, present in the cytoplasm, may lead to mutation and cancer due to non-specific binding to DNA at elevated levels affecting the cellular structures and damaging the cellular components.[13] Moreover, Cr^{6+}, the oxidized form of Cr^{3+}, is extremely toxic and carcinogenic as it can easily penetrate cell membranes causing cancers through oxidation of DNA and some proteins.[14–17]

Aluminium (Al^{3+}), the third most prevalent element, is wildely present in the Earth's crust and in most kind of the animal and plant tissues and natural waters.[18-2] It finds wide applications in the food, textile and paper industries and also in the manufacture of household utensils. According to the World Health Organization (WHO), aluminum is a food pollutant and prescribed a safe Al concentrations of 200 mg L^{-1} in drinking water.[23] It accumulates in various mammalian tissues such as brain, bone, liver, and kidney[24,25] which causes renal failure[26] which is associated with age.[27] Aluminium toxicity damages the central nervous system resulting neurodegenerative Alzheim er and Parkinson diseases.[28]

Among these trivalent metal ions, Fe^{3+} is an essential element in living organisms and plays a vital role in the life process of organisms[29] and many biological activities of organisms, such as muscle contraction, nerve conduction, and enzyme catalysis.[30] On the other hand, excess accumulation of Fe^{3+} can lead to a variety of diseases, such as cell damage and organ dysfunction through the abnormal production of reactive oxygen species (ROS)[31,32] leading to Alzheimer's, Huntington's, Parkinson's, etc diseases.[33]

Over the past few decades, traditional techniques like atomic absorption spectroscopy (AAS), inductively coupled plasma atomic emission spectroscopy (ICP-AES) voltammetry, X-Ray photoelectron Spectrometry (XPS) have been used for heavy metal ion detection.[34-37] Compared with these complicated methods, optical probes are simple, low cost, highly sensitive, selective and finds finest way of detection.

So, there is an urgent need to design a single fluorogenic probe, displaying changes in optical properties through a ''turn-on'' response towards Fe^{3+}, Al^{3+} and Cr^{3+} simultaneously, in the

presence of a large number of mono-, di- or other trivalent metal cations in biological and environmental samples.

The trivalent metal cations e.g., Fe^{3+}, Cr^{3+}, Al^{3+} are environmentally and biologicaly important and involved directly in many cellular functions. Al^{3+} is diamagnetic while Fe^{3+} and Cr^{3+} are paramagnetic. As a consequence, the later two ions are expected to show turn-off sensing. But our probe, $\mathbf{L^3}$ is so designed that all thses cations show turn-on sensing property together or in the presence of any of them. Very few turn on Rhodamine-6G based sensors for Cr^{3+} and Fe^{3+} have been reported.[39-40]

Due to its strong hydration in aquous medium Al^{3+} exhibits turn-on fluorescent response towards a very few number of probes.[28] As a result, most of the reported dye-based Al^{3+} sensors require organic solvents.[41] The excellent optical properties such as a high molar extinction coefficient, good light stability, high fluorescence quantum yield, large excitation and visible emission wavelengths (>500 nm), and insensitivity towards pH make Rhodamine-6G derivatives suitable fluorescent probes towards different metal ions.[42]

We have reported a rhodamine-6G based probe $\mathbf{L^3}$ (**Scheme-4.1**) and its synthetic flow chart given in **Scheme-4.2** which was characterized by ^{1}H NMR (**Figure- 4.1**), ^{13}C NMR (**Figure-4.2**), Mass spectrophotometry (**Figure-4.3**) and IR (**Figure-4.4**) study, for the selective detection of trivalent cations like Fe^{3+}, Al^{3+} and Cr^{3+} in mixed aqueous medium (7:3, H_2O:CH_3CN, v/v) with very high fluorescence enhancement over monovalent, divalent and other trivalent metal ions.

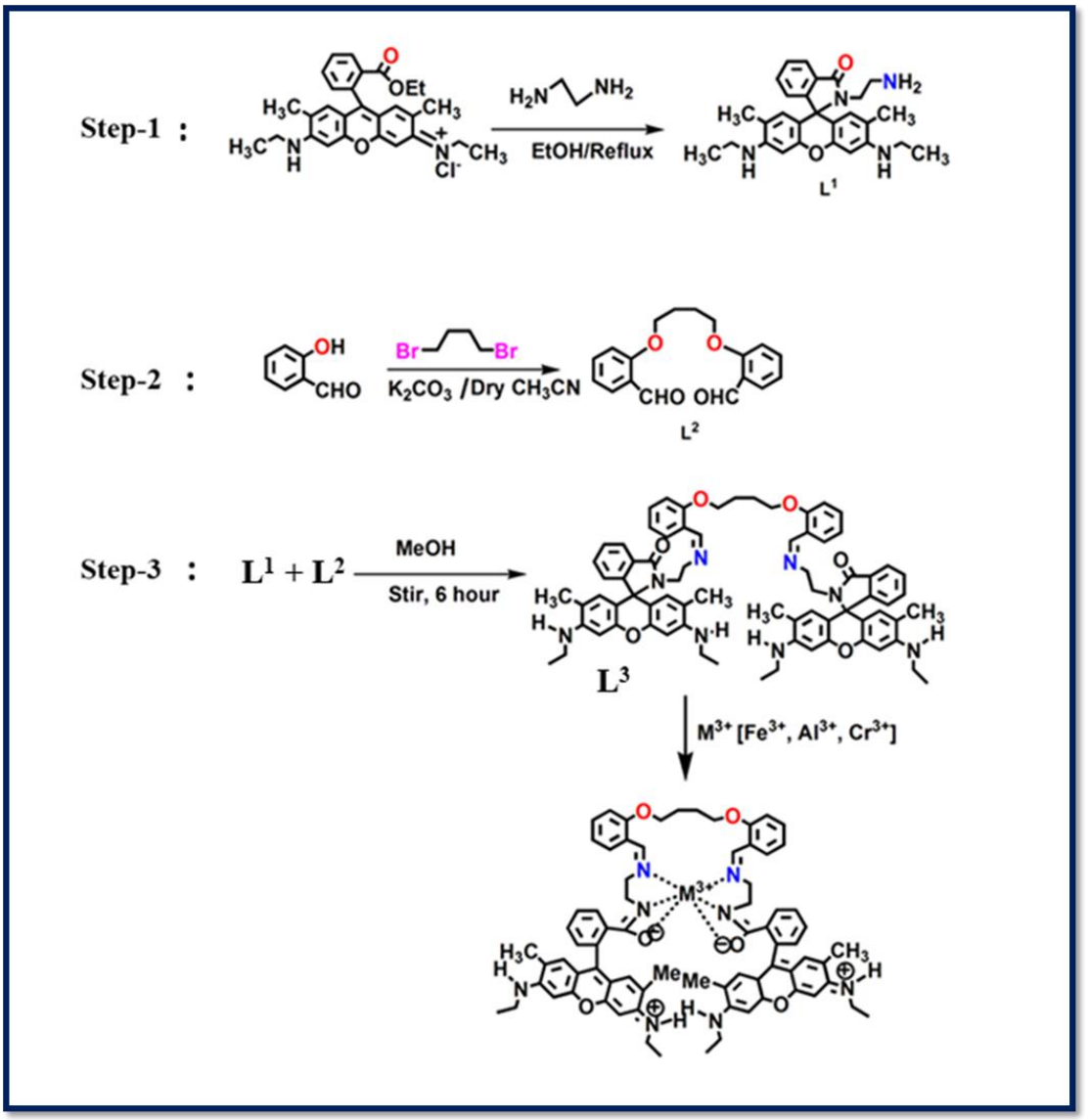

Scheme 4.1: Synthetic routes to chemosensor $\mathbf{L^3}$ and its tentative binding mode of $\mathbf{L^3}$ with M^{3+}.

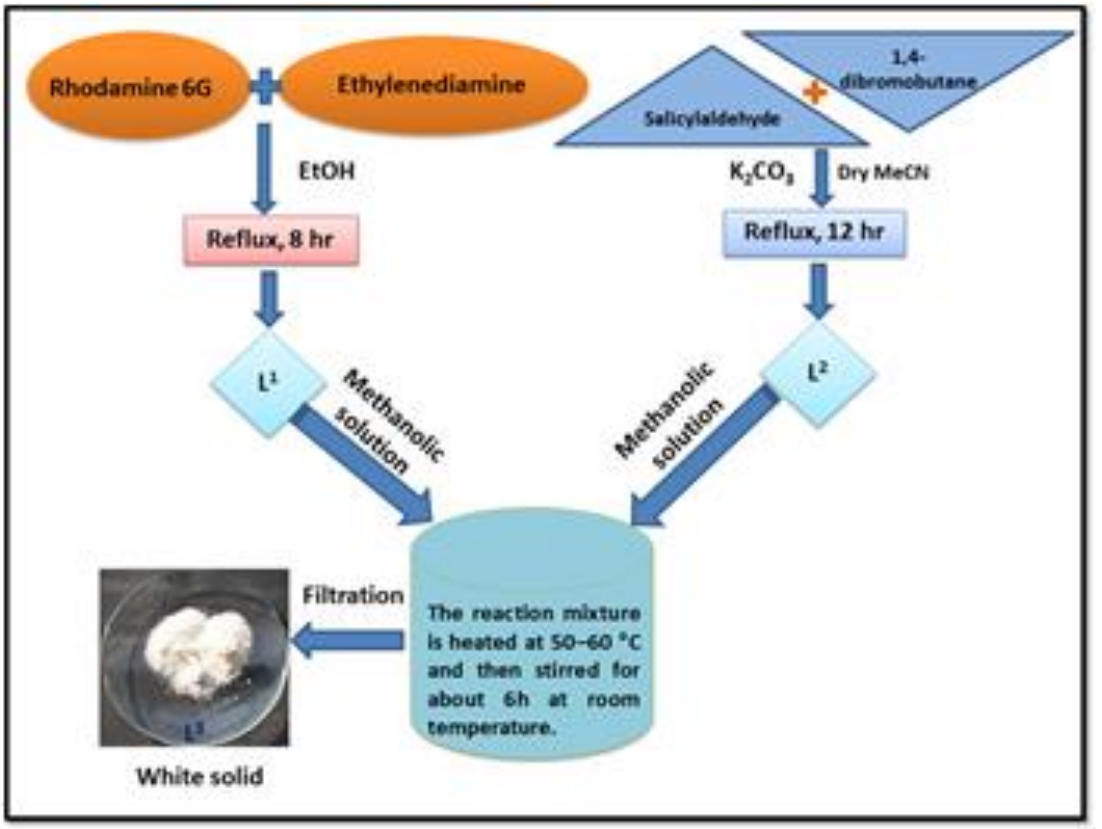

Scheme 4.2: Flow chart of Synthetic routes to chemosensor $\mathbf{L^3}$.

4.2 Experimental Section

4.2.1 Materials and Methods

All solvents used for synthesis were of reagent-grade (Merck). For spectroscopic (UV/Vis and fluorescence) studies HPLC-grade MeCN (Acetonitrile) and double-distilled water was used. Rhodamine 6G hydrochloride and metal salts such as perchlorates of Na^+, Fe^{2+}, Co^{2+}, Ni^{2+}, Zn^{2+}, Pb^{2+}, Cd^{2+}, Hg^{2+}, Cu^{2+}, $Al(NO_3)_3.9H_2O$, $CrCl_3.6H_2O$, $Fe(NO_3)_3.9H_2O$ were purchased either from Sigma–Aldrich or Merck and used as received. All other compounds were purchased from commercial sources and used without further purification.

4.2.2 Physical measurements

^{1}H-NMR spectra were recorded in $CDCl_3$, on a Bruker 300 MHz NMR spectrometer using tetramethylsilane (δ =0) as an internal standard. Infrared spectra (400–4000 cm^{-1}) were recorded

in liquid state in a Nickolet Magna IR 750 series-II FTIR spectrometer. ESI-MS$^+$ (m/z) of the ligand and complexes were recorded on a Waters' HRMS spectrometer (Model: XEVO G2QTof). UV-Vis spectra were recorded on an Agilent diode-array spectrophotometer (Model, Agilent 8453). Steady-state fluorescence measurements were performed on a PTI QM-40 spectrofluorometer. The pH of the solutions was recorded in a digital pH meter 335, calibrated using pH 4, 7 and 10 buffers in the range pH 2-12.

4.2.3 Synthesis

4.2.3.1 Preparation of L^1: Rhodamine 6G (5.0 mmol) and ethylenediamine (10.0 mmol) were dissolved in EtOH and refluxed for 4 hours with continuous stirring whereupon a white crystalline solid of the probe ($\mathbf{L^1}$) was deposited (**Scheme 4.1**). The solid was filtered and washed several times with water and dried in air (83% yield). The crude product was crytallised from ethanol.[43]

4.2.3.2 Preparation of L^2: $\mathbf{L^2}$ was prepared by a modification of a literature procedure.[44] Salicylaldehyde (10 mmol, 1.23 g) and K_2CO_3 (18 mmol, 2.52 g) were added to dry MeCN (60 mL), and the mixture was refluxed for 40 min. then 1,4-dibromobutane (5 mmol, 1.08 g) was then added to the above reaction mixture, which was then again refluxed for 12 hr. Then the mixture was cooled and filtered. The filtrate was evaporated to one-third of its initial volume and diluted with water (40 mL). Then the pH of the solution was adjusted to 4.0 by the addition of 1 M HCl and extracted with dichloromethane (DCM; 2x40 mL). The pH of the aqueous solution was then adjusted to 8 by the addition of 4.0 M Na_2CO_3 solution and extracted with DCM (3x40 mL). Then the combined organic phase after drying with anhydrous Na_2SO_4 was evaporated to dryness under reduced pressure to give a yellowish-brown solid residue. The crude solid product was recrystallized in MeOH to give the desired pure product as an off-white crystalline solid (66% yield). MS (ES$^+$): m/z = 321.112 [$\mathbf{L^2}$ + Na]$^+$ (**Figure-4.5**). $C_{18}H_{18}O_4$ (298.33): calcd. C 72.47, H 6.08; found C 72.46, H 6.09.

4.2.3.3 Preparation of the probe L^3: $\mathbf{L^2}$ (1 mmol, 0.2983 g) in MeOH (10 mL) was added dropwise over 30 min to a methanol solution (30 mL) of $\mathbf{L^1}$ (1 mmol, 0.456 g) under hot (50–60 °C) condition. Then the reaction mixture was stirred for around 6 h at room temperature. A white

precipitate was formed, which was collected by filtration. The residue was washed thoroughly with cold methanol and purified by crystallization to isolate **L^3** in pure form in 84% yield.

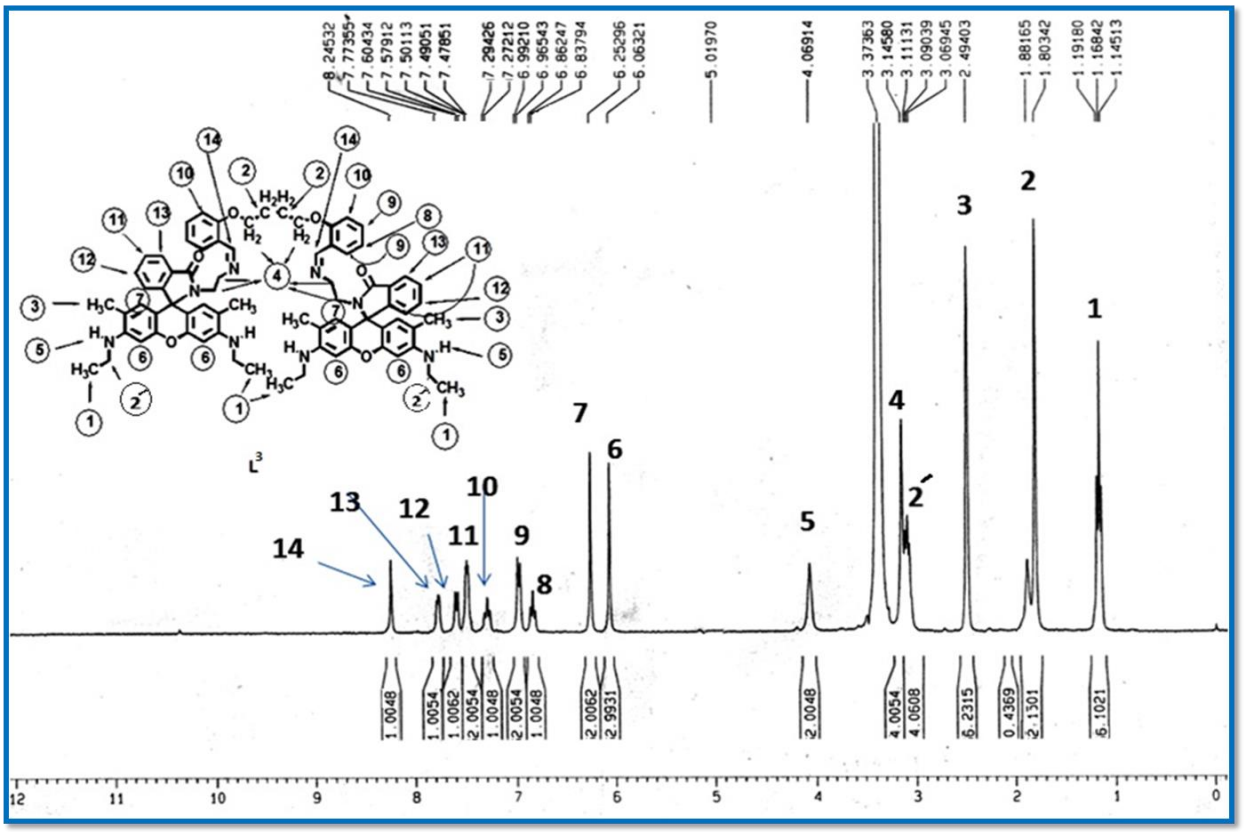

Figure-4.1: ^{1}H NMR spectrum of **L^3** in DMSO-d_6, in Bruker 300 MHz instrument.

^{1}H NMR ($CDCl_3$): δ = 1.16 (12H, t, -CH3), 1.88 (4H, m, -CH_2), 2.49 (12H, s, -CH3), 3.08 (4H, m, -CH2), 3.14 (8H, m, -CH_2), 4.06 (4H, s, -NH), 6.06 (4H, s, -Ar-H), 6.25 (4H, s, -Ar-H), 6.84 (2H, d, -Ar-H), 6.97 (4H, d, -Ar-H), 7.28 (2H, d, Ar-H), 7.48 (4H, m, -Ar-H), 7.58 (d, 2H, Ar-H), 7.77 (2H, d, -Ar-H), 8.24(2H, s) (**Figure-4.1**). ^{13}CNMR: 14.57, 17.40, 25.80, 31.15, 37.95, 59.07, 64.78, 68.05, 79.41, 96.02, 105.15, 112.88, 118.74, 120.80, 122.75, 124.20, 127.16, 128.09, 128.73, 131.04, 132.43, 133.15, 148.15, 151.58, 153.83, 157.38, 158.02, 167.34 (**Figure-4.2**).$C_{74}H_{78}N_8O_6$ (1175.46): calcd. C 75.61, H 6.69, N 9.53; found C75.57, H 6.68, N 9.54. ESI-MS$^+$ (m/z): 1175.61 (**L^3** + H$^+$) (**Figure-4.3**). IR spectrum: 1699cm^{-1}(-C=O), 1378cm^{-1}(–C-N), 1637 cm^{-1}(C=N) (**Figure-4.4**).

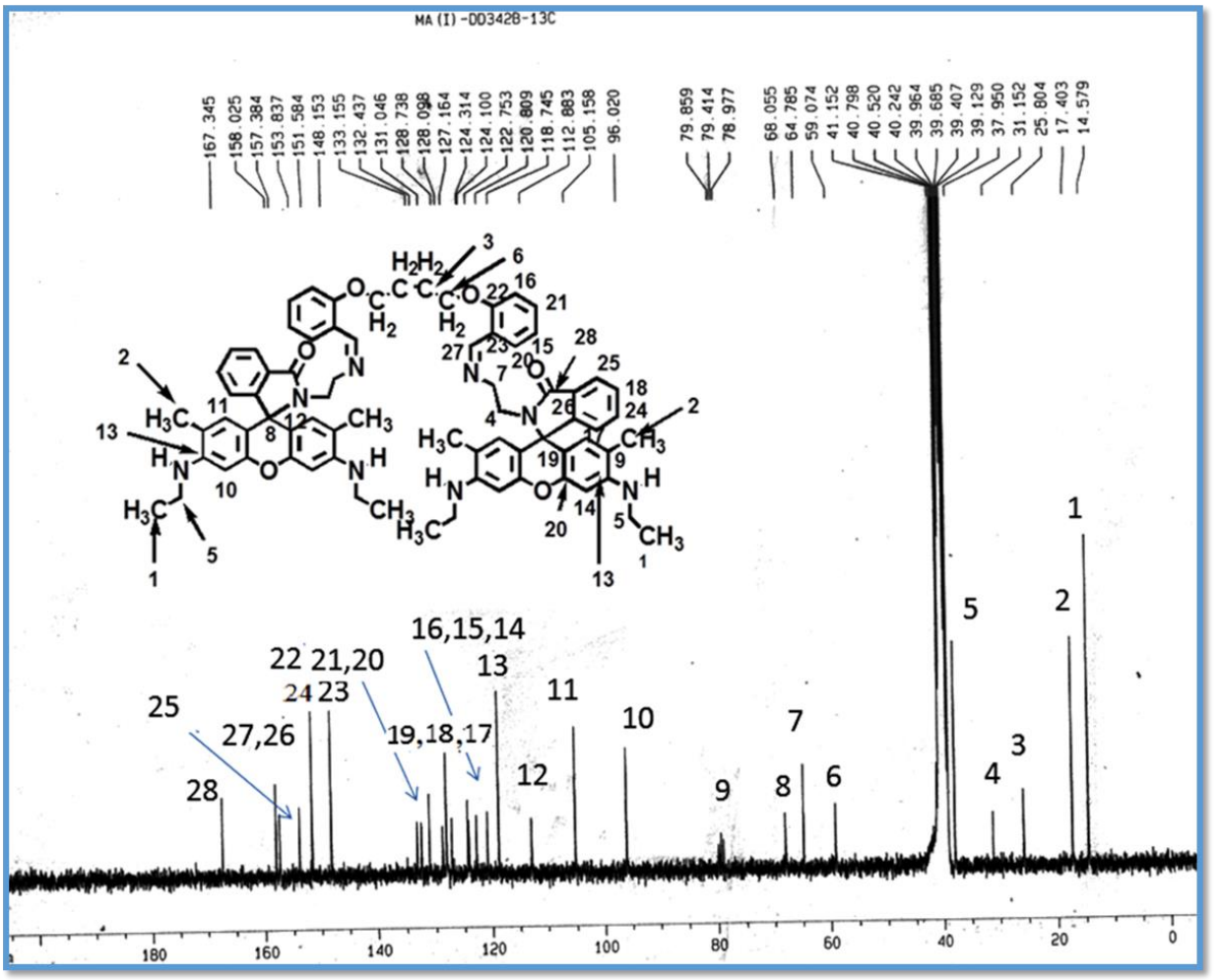

Figure-4.2: ^{13}C NMR spectrum of $\mathbf{L^3}$ in DMSO-$d_{6,}$ in Bruker 300 MHz instrument.

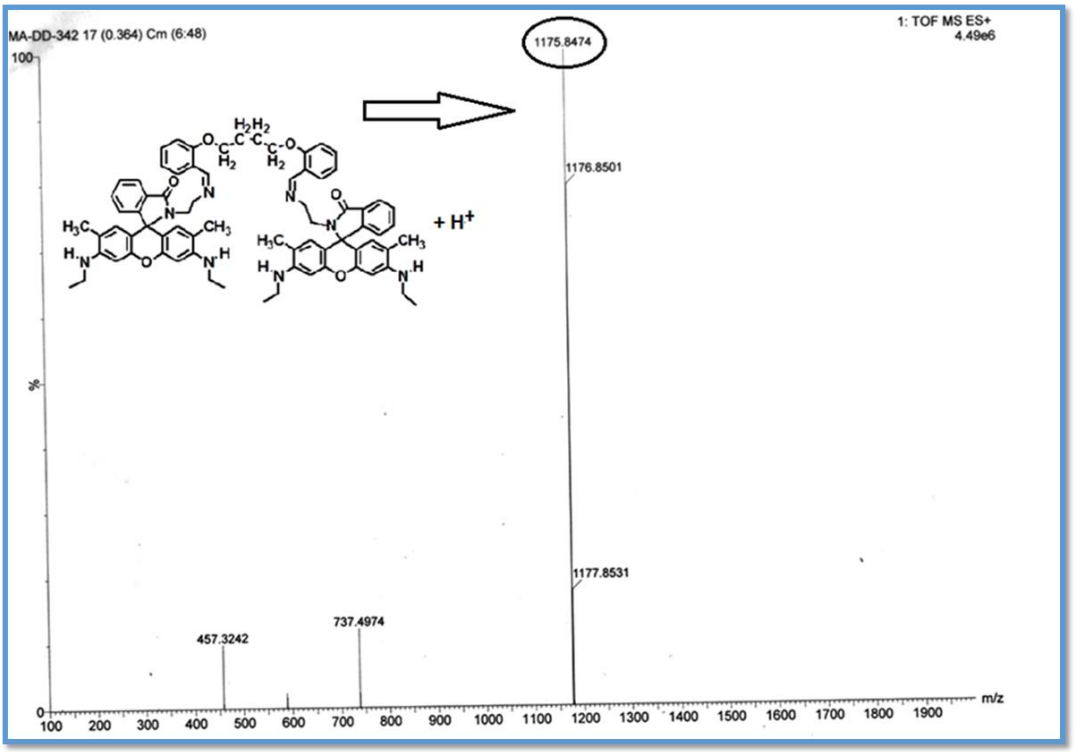

Figure-4.3: Mass spectroscopy of $\mathbf{L^3}$ in MeCN.

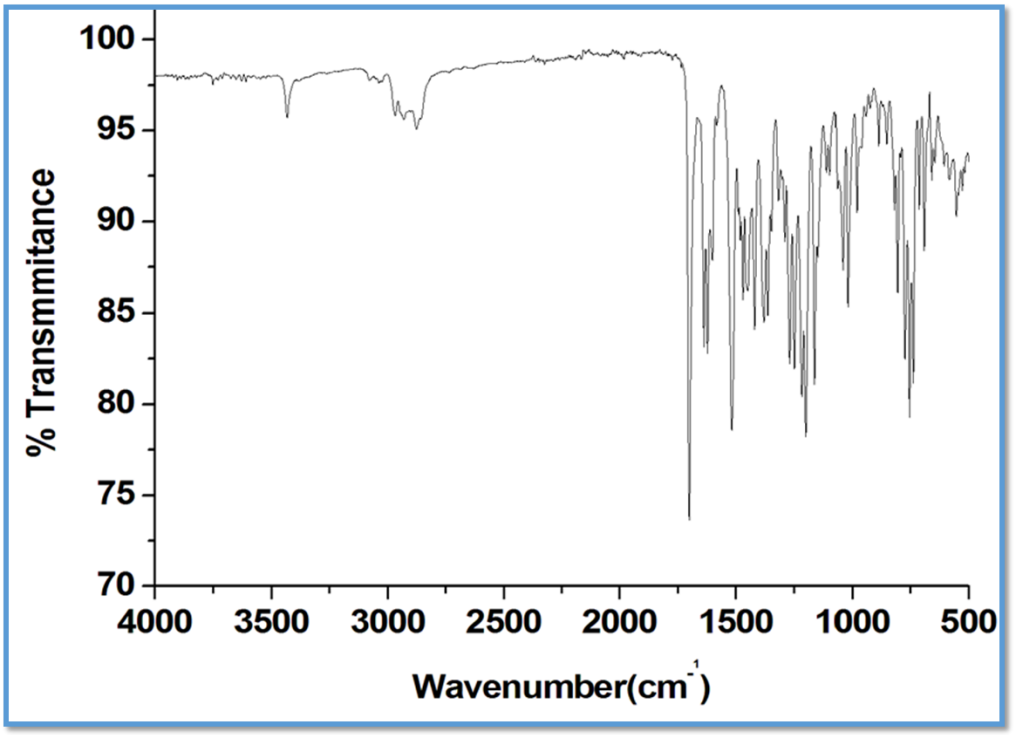

Figure-4.4: FT-IR spectrum of $\mathbf{L^3}$

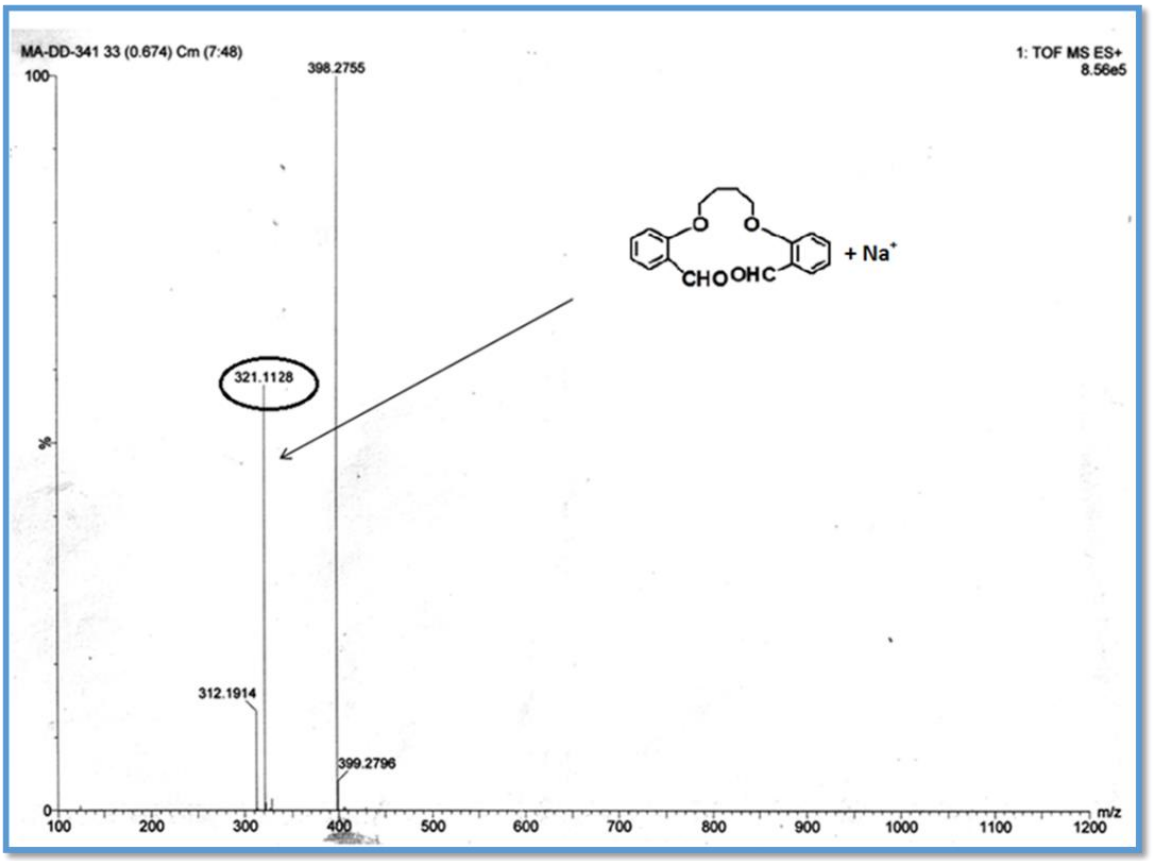

Figure-4.5: Mass spectroscopy of $\mathbf{L^2}$ in MeCN.

4.2.4 Solution preparation for UV-Vis and fluorescence studies

For both UV-Vis and fluorescence titrations, a stock solution of 1.0 x 10^{-3} M of the probe $\mathbf{L^3}$ was prepared by dissolving it in 25 mL CH_3CN. Analogously, 1.0 x 10^{-3} M stock solutions of Fe^{3+}, Al^{3+}, Cr^{3+} were prepared in MeOH. A solution of 20 mM HEPES buffer (7:3, H_2O:CH_3CN) was prepared and *p*H was adjusted to 7.2 by using HCl and NaOH. For UV-Vis spectra 60 µM probe was taken in cuvette containing 2.5 mL of buffer solution and Fe^{3+} salt solution was added incrementally starting from 0 to 336 µM in a regular interval of time and absorption spectra were recorded. Similar experiments were performed for Al^{3+} and Cr^{3+}. Again 2.5 ml of this buffer solution was pipetted out into a cuvette to which 60 µM of the probe ($\mathbf{L^3}$) solution was added and Fe^{3+} salt solution was added incrementally starting from 0 to 160 µM in a regular interval of time (3 minutes) and fluorescence spectra were recorded setting the excitation wavelength at 502 nm. Similar titrations were conducted with Al^{3+} and Cr^{3+}. Path lengths of the cells used for absorption

and emission studies were 1 cm. Fluorescence measurements were performed using 2 nm x 2 nm slit width.

4.2.5 Job's Plot

This method is based on the measurement of fluorescence of a series of solutions in which molar concentrations of the probe (**L^3**) and M^{3+} vary but their sum remains constant. The fluorescence of each solution was measured at 558 nm and plotted against the mole fraction of M^{3+}. A maximum of fluorescence occurs at the mole ratio corresponding to the combining ratio of the two components. The composition of the complex was determined by Job's method and found to be (1:1) with respect to **L^3** for Fe^{3+}, Al^{3+} and Cr^{3+} complexes.

4.2.6 Calculation of LOD

The analytical detection limit was obtained by performing fluorescence titration of **L^3** with M^{3+} by adding aliquots in a micromolar concentration of M^{3+} to 20 μM solution of **L^3** in 2.5 mL buffer and the LOD was calculated by the 3σ method[47,48]. LOD = 3 x S_d/S, where S_d is the standard deviation of the intercept of the blank (**L^3** only) obtained from a plot of fluorescence intensity (FI) versus [**L^3**], and S is the slope obtained from the linear part of the plot of FI versus [M^{3+}].

4.3 Results and Discussion

2As depicted in **Scheme-4.1**, receptor **L^3** was synthesized from the reaction between **L^1** and **L^2** in MeOH in stirring condition for 6h. The final crystallized product (**L^3**) was well characterized by ^{1}H NMR (**Figure-4.1**), ^{13}C NMR (**Figure-4.2**) IR (**Figure-4.4**) and Mass spectrophotometry (**Figure-4.3**) study. The receptor **L^3** was found to be very sensitive and highly selective colorimetric and fluorogenic chemosensor for trivalent metal ions, M^{3+}(M^{3+}=Fe^{3+}, $Al^{3+}$and Cr^{3+}) while in the absence of M^{3+}, the solution of **L^3** is colourless and non-fluorescent.

4.3.1 UV-Vis absorption studies

The UV-Vis spectrum recorded in mixed aqueous solvent, H_2O/CH_3CN (7:3, v/v, pH 7.2, 20 mM HEPES buffer). The UV-Vis titration reveals that with the gradual addition of Fe^{3+}, Al^{3+} and Cr^{3+} separately to **L^3** (60 μM) solution an absorption band appeared at 528 nm (**Figure-4.6**, **Figure-4.7**

and **Figure-4.8)** with the sharp visual colour change of the representative solution from colorless to orange-red whereas no such peak appeared in the presence of other monovalent and divalent metal ion solutions. The appearance of this peak clearly manifests the opening of the spirolactam ring through the chelation of M^{3+} (Fe^{3+}, Al^{3+} and Cr^{3+}) with the probe. The probable coordination mode of $\mathbf{L^3}$ towards M^{3+} is demonstrated in **Scheme-4.1**. UV-Vis titrations were carried out by varying trivalent metal-ion concentrations (0–336 μM), keeping the probe concentration fixed at 60 μM at a pH of 7.2 (20 mM HEPES buffer, H_2O/CH_3CN (7:3, v/v). Plots of absorbance vs. [$\mathbf{M^{3+}}$] yielded non-linear curves which were analyzed by adopting non-linear curve-fitting methods[45,46], and the evaluated K_d values are 6.32 x 10^{-5} M^{-1} (Fe^{3+}); 3.48 x 10^{-5} M^{-1}(Al^{3+}) and 9.48 x 10^{-5} M^{-1}(Cr^{3+}) (inset **Figure-4.6**, **Figure-4.7** and **Figure-4.8**).

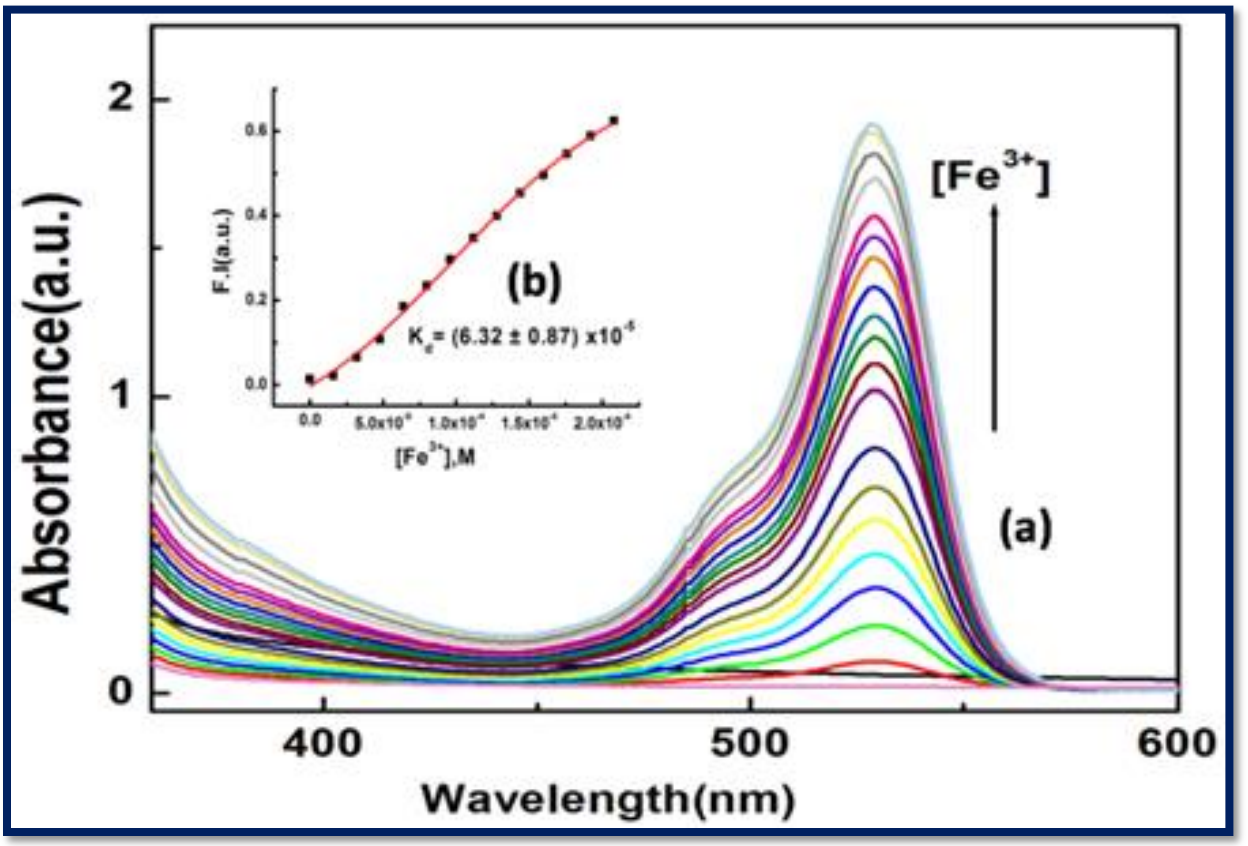

Figure-4.6: (a) UV-Vis absorption spectra of $\mathbf{L^3}$ (60μM) in H_2O/CH_3CN(7:3, v/v, pH 7.2, 20 mM HEPES buffer) solutions with the increase in concentration of Fe^{3+} solution (0-336μM); (b) linear fit of absorbance vs. [Fe^{3+}] plot.

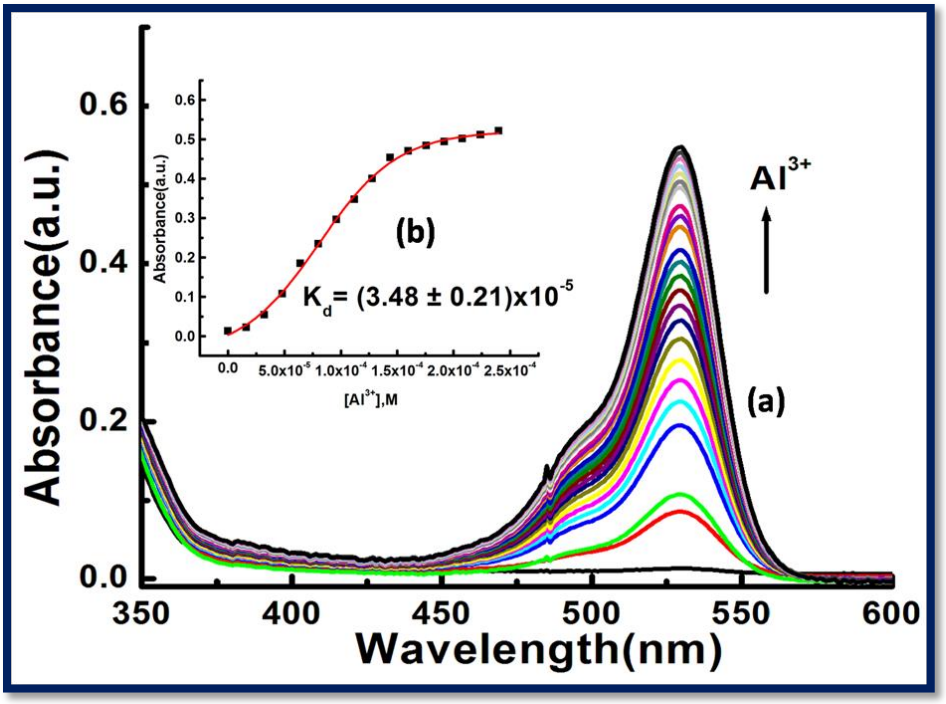

Figure-4.7: (a) UV-VIS titration of $\mathbf{L^3}$(60 μM) in H_2O- MeCN-(7:3, v/v) in HEPES buffer at pH 7.2 by the gradual addition of Al^{3+} (0-336 μM). Inset (b) Nonlinear curve-fit of F.I vs. [Al^{3+}] plot.

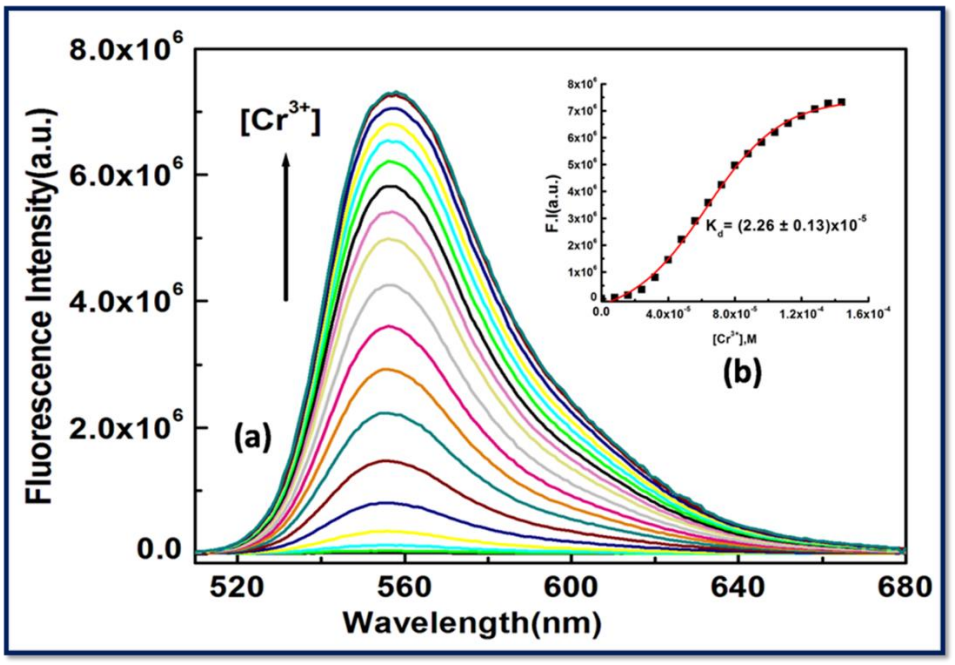

Figure-4.8: (a) UV-VIS titration of $\mathbf{L^3}$(60 μM) in H_2O- MeCN-(7:3, v/v) in HEPES buffer at pH 7.2 by the gradual addition of Cr^{3+} (0-336 μM). Inset (b)Nonlinear curve-fit of F.I vs. [Cr^{3+}] plot.

4.3.2 Fluorescence studies

The emission spectra of L^3 and its fluorescence titration with M^{3+} (Fe^{3+}, Al^{3+} and Cr^{3+}) were performed in H_2O/CH_3CN (7:3, v/v, pH 7.2, 20 mM HEPES buffer) with the fixed concentration of L^3 at 60 μM. A significant turn on fluorescence emission were observed in presence of Fe^{3+}, Al^{3+} and Cr^{3+} with a maximum fluorescence intensity at 558 nm. As for example, on gradual addition of Fe^{3+} (0-2.6 equivalent) to the non-fluorescent solution of **L^3**, a 669-fold enhancement in fluorescence intensity at 558 nm was observed following excitation at 502 nm, which also suggests the opening of the spirolactam ring in **L^3** on coordination to the Fe^{3+} ion[47,48] (**Figure-4.9**). Similarly, 653 fold and 667fold enhancement of fluorescence intensity was observed during the titration of **L^3** with Al^{3+} and Cr^{3+}respectively (**Figure-4.10** and **4.11**).

Likewise, plots of FI vs. [M^{3+}] give nonlinear curves which were analysed by the nonlinear curve-fitting method giving K_d = 1.94 x 10^{-5} M^{-1}; 3.15 x 10^{-5} M^{-1} and 2.26 x 10^{-5} M^{-1} for Fe^{3+}, Al^{3+} and Cr^{3+} respectively (**Figure-4.12**). There are excellent agree ments between the K_d values obtained from the absorbance and fluorescence titration data suggesting the self-consistency of our results.

Using these fluorescence data detection limit of Fe^{3+}, Al^{3+} and Cr^{3+} by the probe **L^3** were calculated to be 2.57, 0.78 and 0.47 μM respectively (**Figure-4.13a-c**)**.** These results strongly indicate that this probe **L^3** is sensitive enough to detect the trace level of Fe^{3+}, Al^{3+} and Cr^{3+}. Quantum yields of **L^3, [L^3—Fe^{3+}], [L^3—Al^{3+}]** and **[L^3—Cr^{3+}]** complexes in H_2O/CH_3CN (7:3, v/v, pH 7.2) are found to be 0.0005, 0.335, 0.327, 0.333 respectively using Rhodamine-6G as standard. The comparatively higher values of quantum yield for complexes compare to free ligand indicate the higher stability of the complexes in the excited states.

Job's method was again employed to determine the composition of the complex, which was found to be 1:1 (**Figure-4.14a-c**) and was further supported by mass spectrometric analysis (m/z =410.18 [Fe(**L^3**)]$^{3+}$; (m/z = 400.53 [Al(**L^3**)]$^{3+}$; 408.85 [Cr(**L^3**)]$^{3+}$ (**Figure-4.24a-c**)

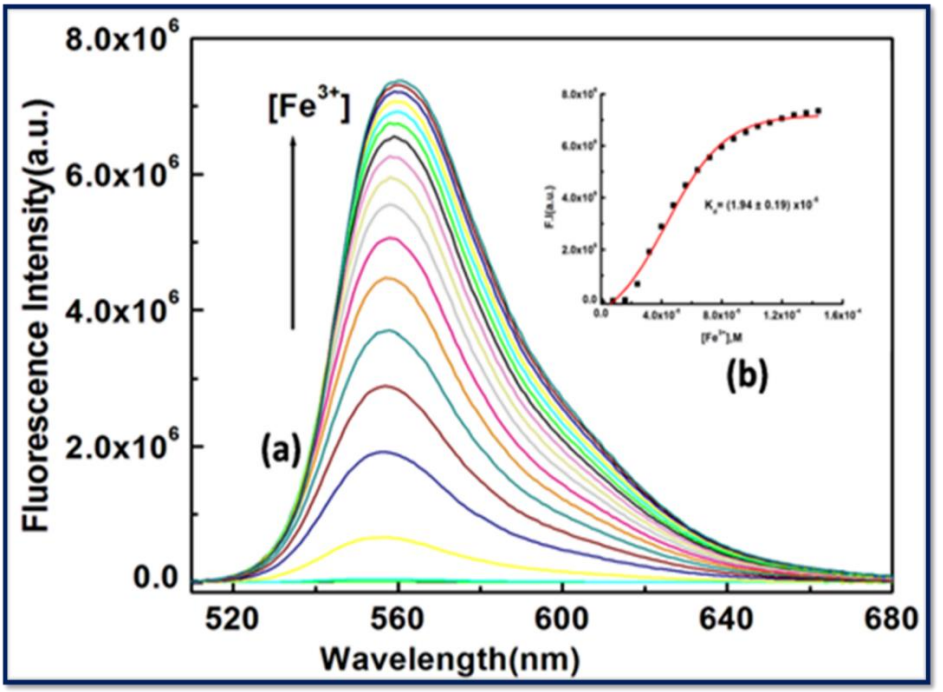

Figure-4.9: (a) Fluorescence spectra of **L^3** (60 μM) in H_2O/CH_3CN (7:3, v/v, pH 7.2, 20 mM HEPES buffer) solutions upon addition of Fe^{3+}(160 μM), each spectrum was taken after 3-minute interval of Fe^{3+} addition, λ_{ex}= 502 nm, λ_{em}=558nm; (b) Non-linear curve fitting of titration curves with K_d values.

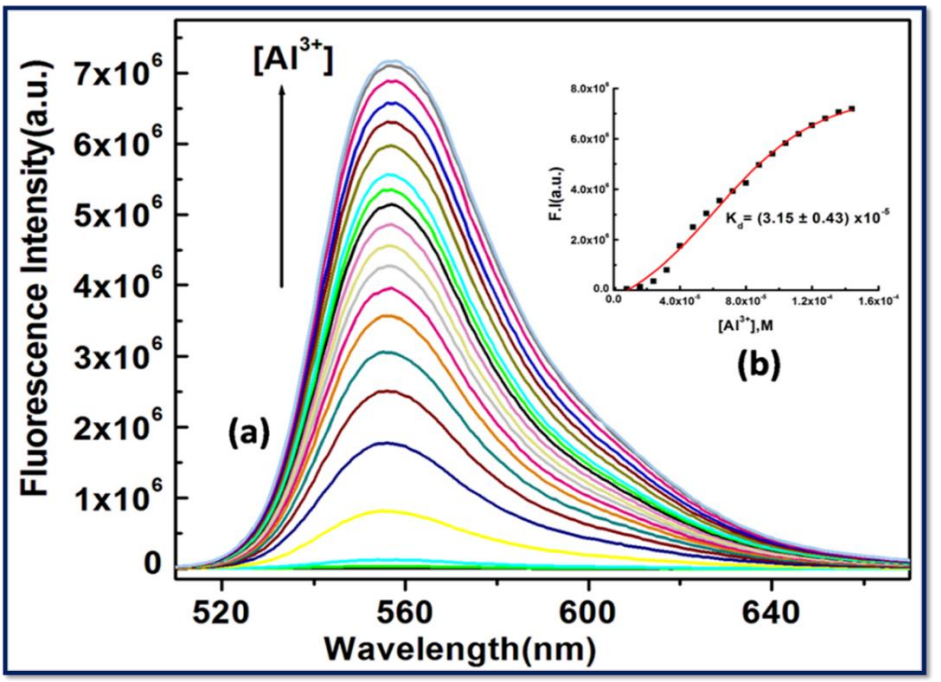

Figure-4.10: (a) Fluorescence titration of **L**^{3}(60 μM) in H_2O- MeCN-(7:3, v/v) in HEPES buffer at pH 7.2 by the gradual addition of Al^{3+} (0-160 μM). Inset (b) Nonlinear curve-fit of F.I vs. [Al^{3+}] plot.

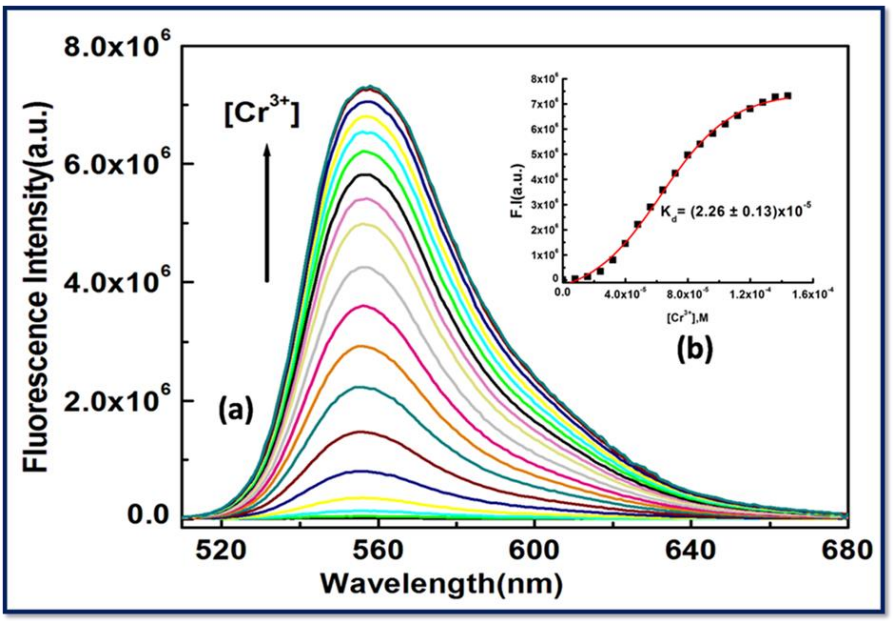

Figure-4.11: (a) Fluorometric titration of **L**^{3} (60 μM) in H_2O- MeCN-(7:3, v/v) in HEPES buffer at pH 7.2 by the gradual addition of Cr^{3+} (0-160 μM). Inset (b) Nonlinear curve-fit of F.I vs. [Cr^{3+}] plot.

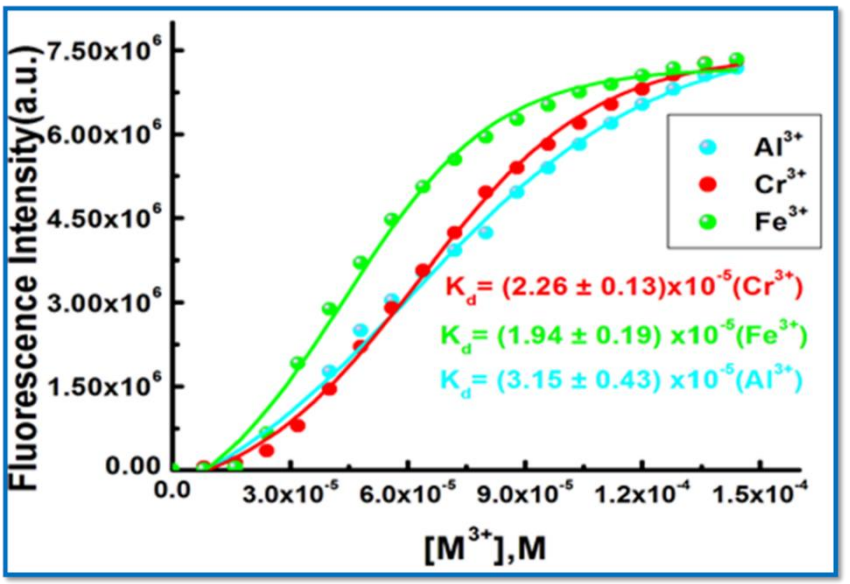

Figure-4.12: Non-linear fitting of fluorescence titration curves for Fe^{3+}, Al^{3+} and Cr^{3+} with K_d values.

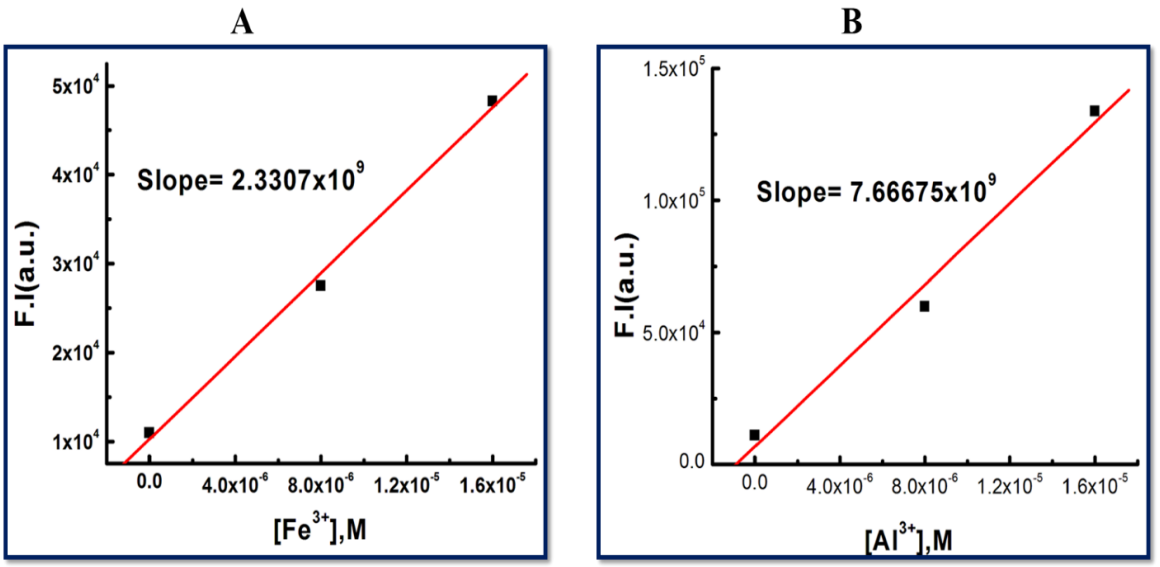

$LOD\ (Fe^{3+}) = 3 \times S.D/Slope$
$= (3 \times 2001.751 / 2.3307 \times 10^{9}$
$= 2.57\ \mu M$

$LOD[Al^{3+}] = 3 \times S.D/Slope$
$= (3 \times 2001.751 / 7.66675 \times 10^{9}$
$= 0.78\ \mu M$

Figure-4.13: a) Linear dyanamic plot of FI (at 558nm) vs [Fe^{3+}] for the determination of S (slope), diagram A. **b)** Linear dyanamic plot of FI (at 558nm) vs [Al^{3+}] for the determination of S (slope), diagram B.

C

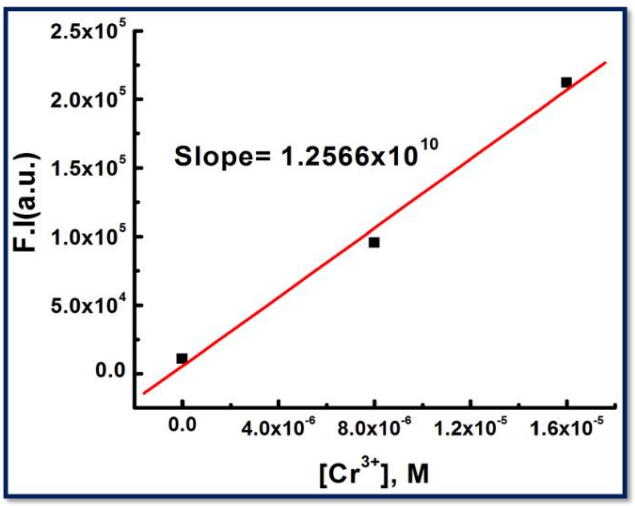

$LOD\ (Cr^{3+}) = 3 \times S.D/Slope$
$= (3 \times 2001.751 / 1.2566 \times 10^{10}$
$= 0.47\ \mu M$

Figure-4.13: c) Linear dyanamic plot of FI (at 558nm) vs [Cr^{3+}] for the determination of S (slope), diagram C.

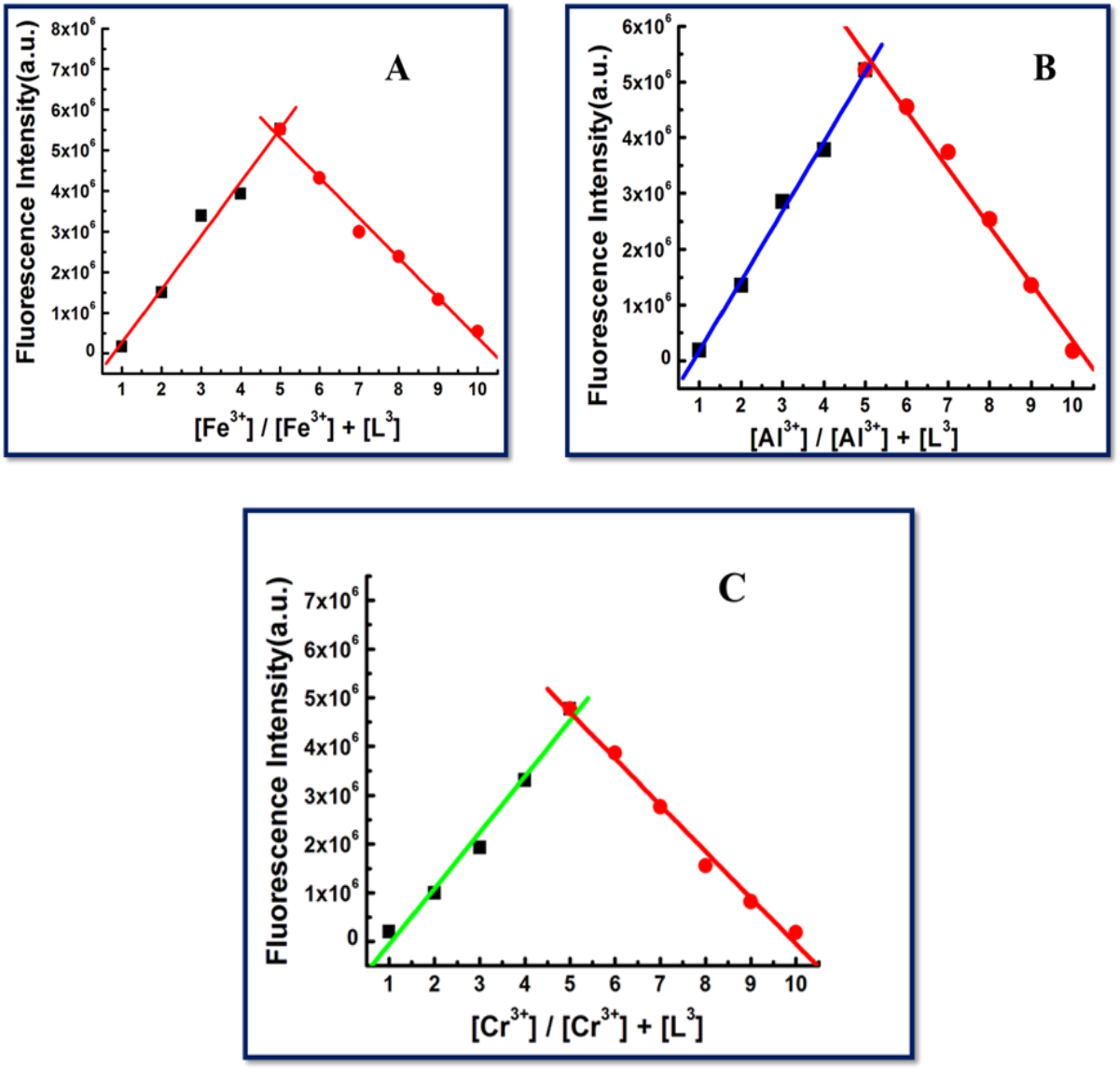

Figure-4.14: a) Job's plot between $\mathbf{L^3}$ and Fe^{3+} for the confirmation of (1:1) binding (diagram A). b) Job's plot between $\mathbf{L^3}$ and Al^{3+} for the confirmation of (1:1) binding (diagram B). c) Job's plot between $\mathbf{L^3}$ and Cr^{3+} for the confirmation of (1:1) binding (diagram C).

Moreover, a conspicuous display of reddish–orange fluorescence response of the probe upon interaction with M^{3+}(**Figure-4.15a**) provides the scope for naked eye detection. The possibility of using chemosensor $\mathbf{L^3}$ in the development of paper test strips was examined and found that the turn-on fluorescence responseof $\mathbf{L^3}$ towards M^{3+} is also visually detectable in test paper strips (**Figure-4.15b**).

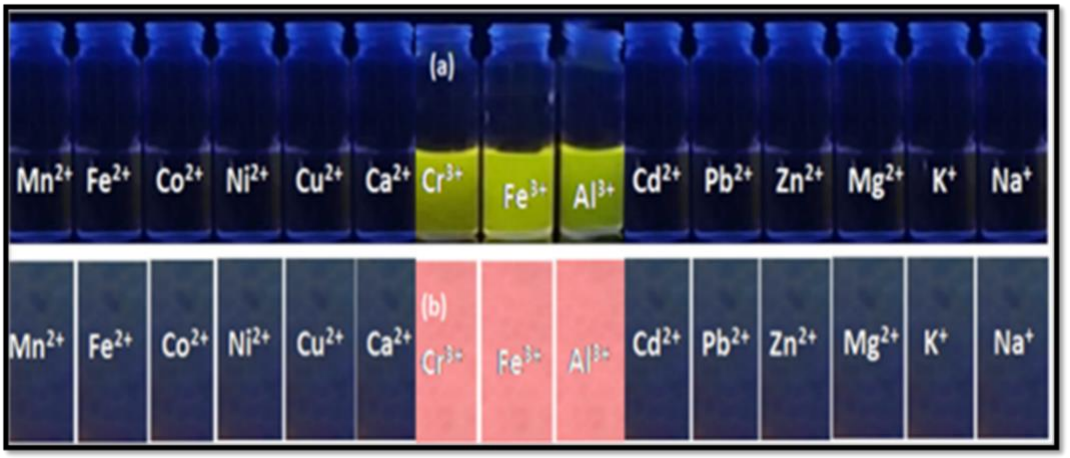

Figure-4.15: (a) Visual fluorescent response of **L^3** towards Fe^{3+}, Al^{3+} and Cr^{3+} (under 365 nm UV light). (b) Paper strip experiment for the fluorescent sensing of Fe^{3+}, Al^{3+} and Cr^{3+} toward the probe **L^3**

4.3.3 Selectivity studies

Selectivity is an important and essential requirement for an excellent chemosensor. Selectivity experiment was carried out by taking 60 μM of probe **L^3** in a cuvette containing 2.5 mL of 20 mM HEPES buffer solution and then different metal ion solutions of about 5 equivalents were added separately. Surprisingly, **L^3** could selectively recognize only Cr^{3+}, Fe^{3+} and Al^{3+} in mixed aqueous medium over other biologically abundant divalent 3d transition metal cations like Mn^{2+}, Fe^{2+}, Co^{2+}, Co^{3+}, Ni^{2+}, Cu^{2+}, Cu^{+} and Zn^{2+}, hazardous heavy metal ions like Pb^{2+}, Pd^{2+}, Cd^{2+} and Hg^{2+}, alkali and alkaline earth metal ions like Na^{+}, K^{+}, $Ca^{2+}$and Mg^{2+}(**Figure-4.16**). The presence of 5 equivalents of other trivalent metal ions like Ga (III), Y (III), Sm(III), Dy(III), Au(III), Ru(III) and Co(III) does not interfere with the detection of Cr^{3+}, Fe^{3+} and Al^{3+} ions (**Figure-4.16a**).

When the sample containing probe **L^3**, comes in contact with trivalent cation (Fe^{3+}, Cr^{3+}, Al^{3+}), donor atoms (oxygen and nitrogen of the amidic linkage) of the two separate spirolactam ring, the imine nitrogen atom and the oxygen atom of the unit derived from salicyldehyde coordinate with the trivalent metal cation. The coordination from the amidic linkage increases ring opening probability. Mesomeric effect of the secondary nitrogen atom which is joined to the xanthene ring pushes the electron density to the amidic linkage through the xanthene ring resulting the opening of the spirolactam ring. After cleavage of the spirolactam ring amidic moiety forms an ionic bond with the metal ion but remaining donor atoms still maintains coordinate bonds in the metal

complex. So, metal ion assisted ring opening facilitates the formation of complex and exhibits enhancement of fluorescence intensity and generation of the orange–red colour in naked eye (**Scheme 4.3**).

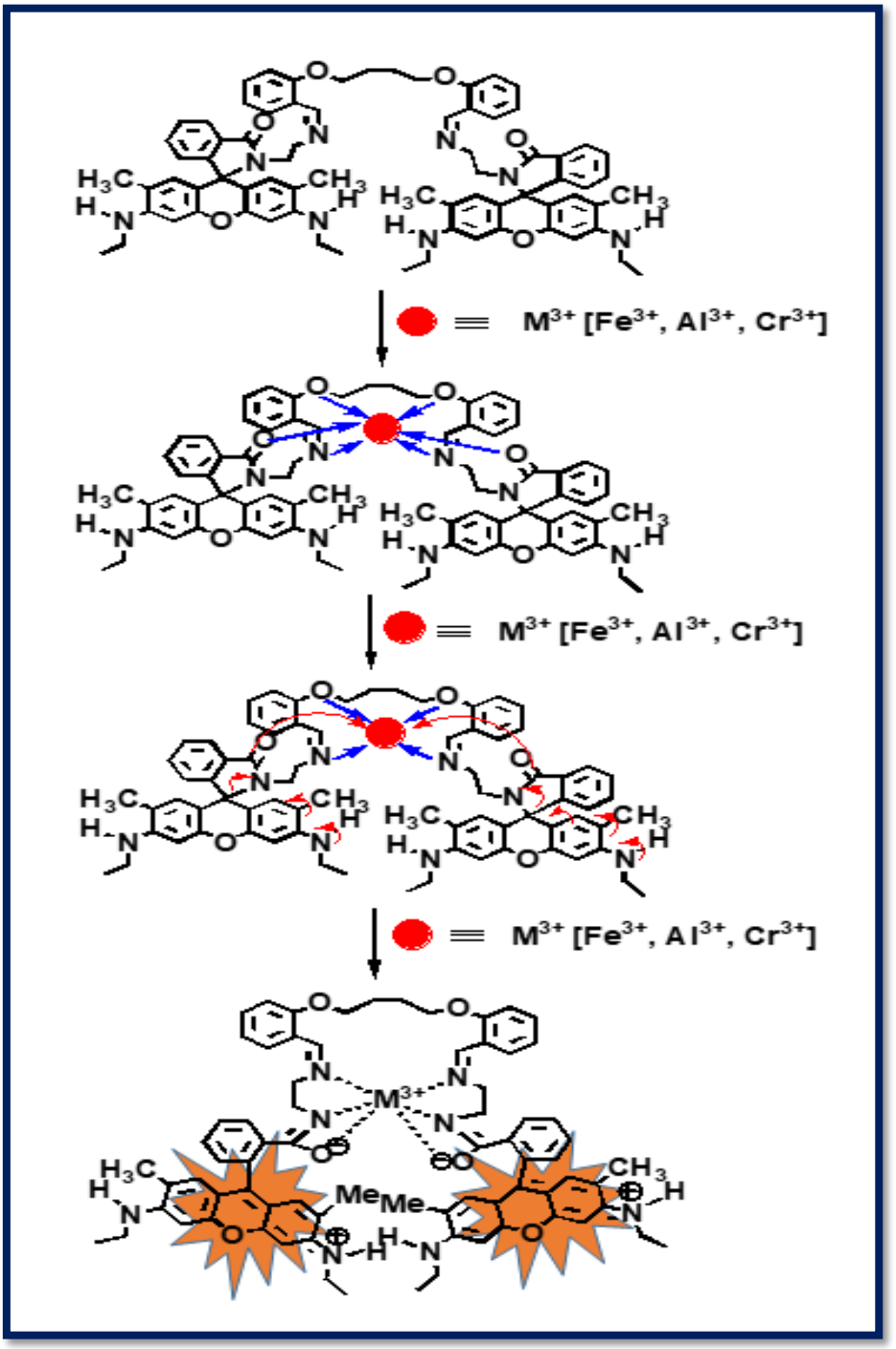

Scheme 4.3: Mechanism of spirolactum ring opening in the presence of M^{3+} (M=Fe, Cr, Al).

It was also found that not a single anionic species among $S_2O_3^{2-}$, $S_2O_4^{2-}$, N_3^-, NO_2^-, SCN^-, NO_3, $H_2PO_4^-$, PO_4^{3-}, SO_4^{2-}, ClO_4^- , F^-, Cl^-, Br^-, I^-, HSO_4^- and CN^- could enhance the fluorescence intensity of the probe **L**^{3} (**Figure-4.17**) but the fluorescence intensity of [**L**^{3}-M^{3+}] complex was found to be quenched in the presence CN^- ion (**Figure-4.18a-c**). An excellent reversible fluorescence OFF-ON property of **L**^{3} has been observed through fluorescence study with the sequential addition of M^{3+} and CN^- ions in 20 mM HEPES buffer in H_2O/CH_3CN (7:3) (pH 7.2) solution at room temperature (**Figure-4.19**). Addition of cyanide ion to the solution containing [**L**^{3}-M^{3+}] complex quenches the emission of the probe with the disappearance of the pink color of the solution. The reason behind this observation is that the interaction of M^{3+} with probe results in opening of spirolactam ring thereby producing a strong fluorescence. Then treatment with CN^- results in the abstraction of metal ion and regeneration of the spirolactam ring, leading to the quenching of emission. This reversibility test suggests the reusability of this chemosensor.

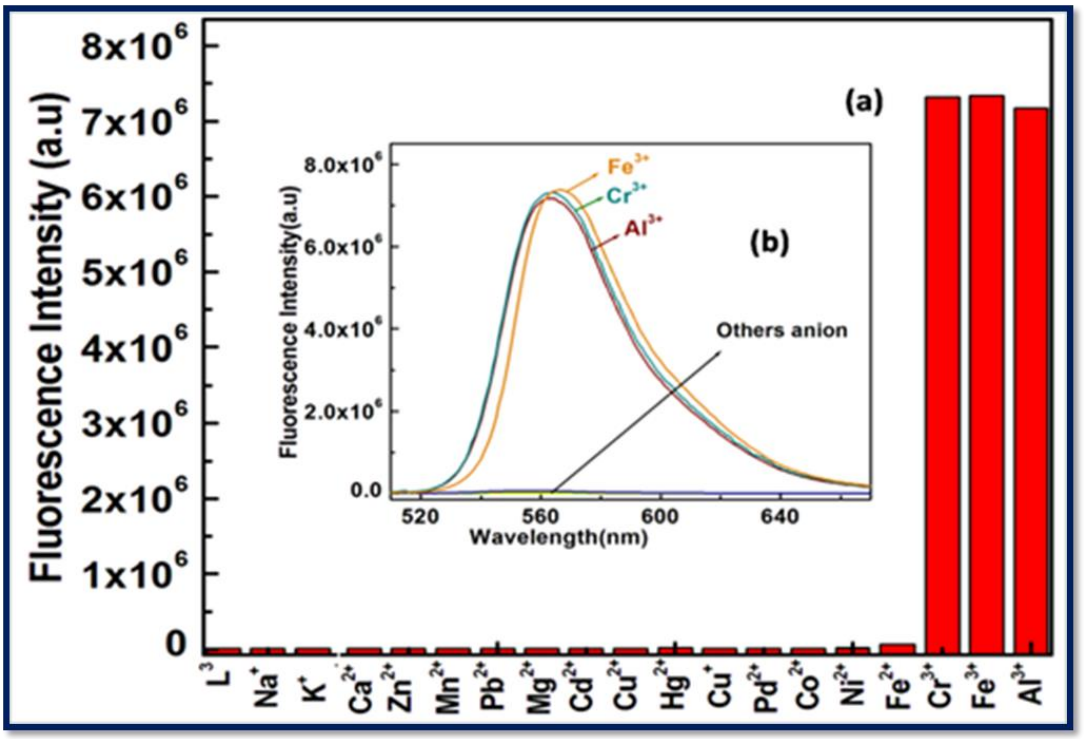

Figure-4.16: (a) Fluorescence bar diagram for the selective response of **L**^{3} (60μM) towards M^{3+}(M=Fe, Al, Cr) in H_2O/CH_3CN (7:3, v/v, pH 7.2, 20 mM HEPES buffer), λ_{ex} = 502 nm, λ_{em} =558 nm); (b) Fluorescence responce of **L**^{3} (60 μM) upon addition of 2.6 equivalent Fe^{3+}, Al^{3+}, Cr^{3+}.

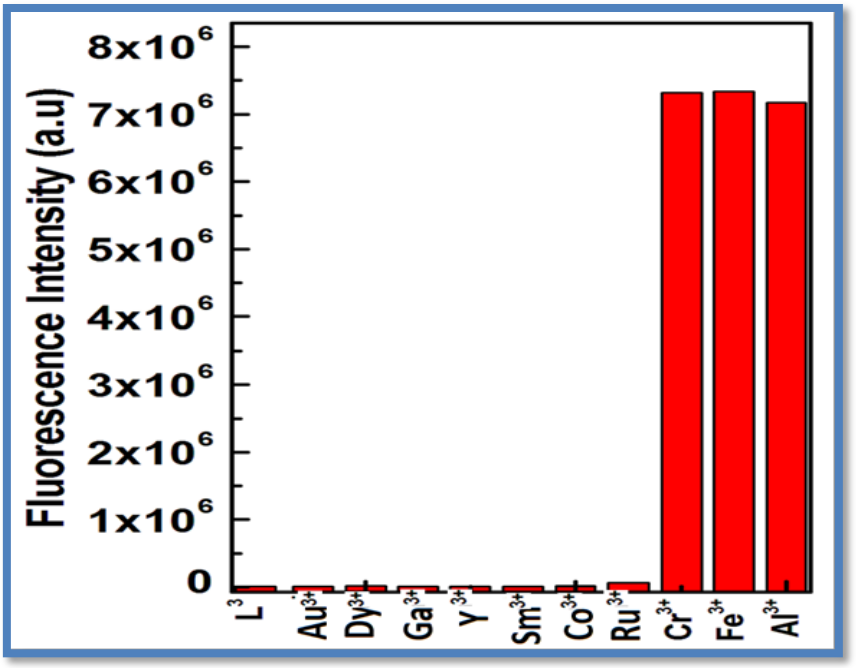

Figure-4.16a: Fluorescence response of the probe $\mathbf{L^3}$ in the presence of Au(III), Dy(III), Ga(III), Y(III), Sm(III), Ru(III) and Co(III) with respect to Fe^{3+}, Al^{3+} and Cr^{3+}

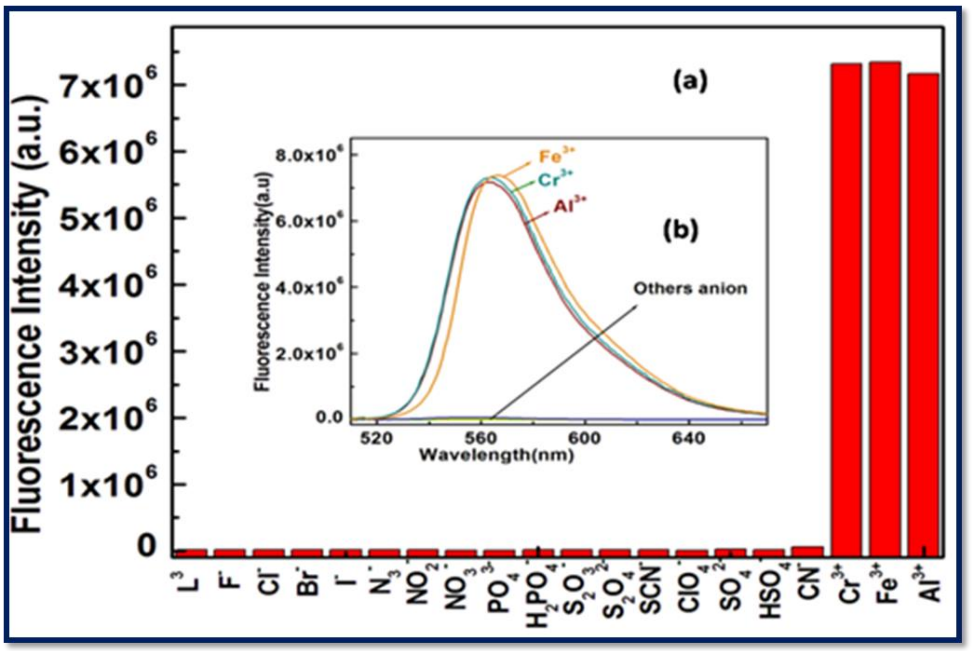

Figure-4.17: (a) Histogram of the fluorescence responses of different anions (100 μM) towards $\mathbf{L^3}$ (60 μM) in 7:3 v/v, water/ MeCN in HEPES buffer at pH 7.2 with λ_{ex} = 502 nm, λ_{em} = 558 nm. (b) Fluorescence response of $\mathbf{L^3}$ towards Fe^{3+}, Al^{3+}, Cr^{3+} with respect to different anions (100 μM).

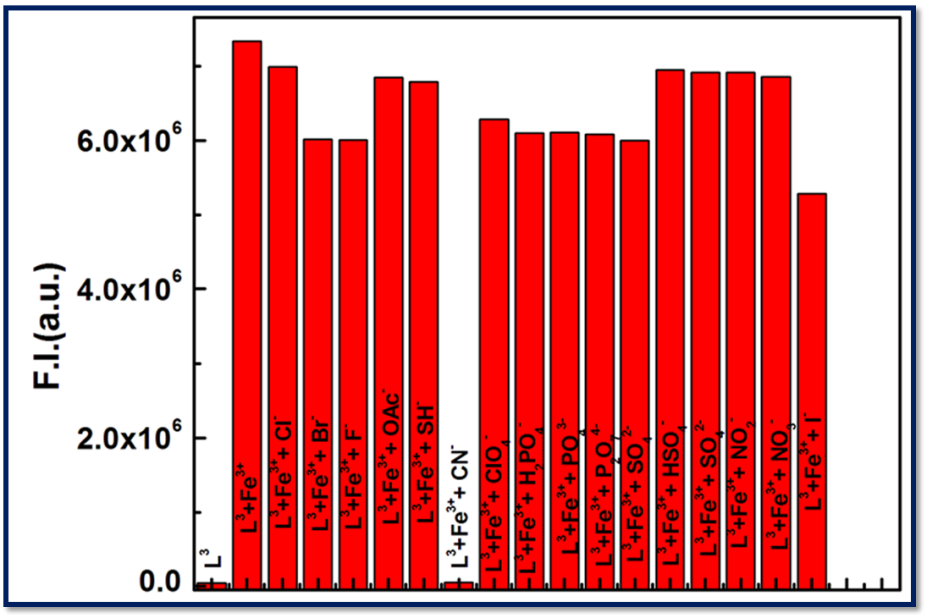

Figure-4.18a: Histogram of the fluorescence quenching [$\mathbf{L^3}$-Fe^{3+}] complex by CN^- (100 μM) towards $\mathbf{L^3}$ (60 μM) in H_2O- MeCN-(7:3, v/v) in presence of different anions(100 μM) in HEPES buffer at pH 7.2 with λ_{ex} = 502 nm, λ_{em} = 558 nm.

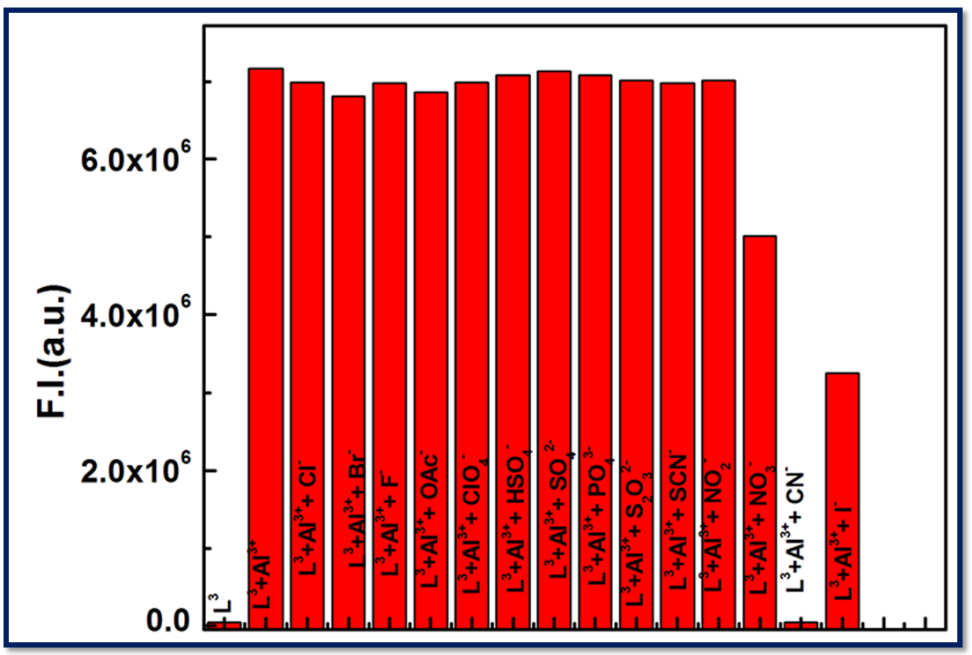

Figure-4.18b : Histogram of the fluorescence quenching [$\mathbf{L^3}$-Al^{3+}] complex by CN^- (100 μM) towards $\mathbf{L^3}$ (60 μM) in H_2O- MeCN-(7:3, v/v) in presence of different anions(100 μM) in HEPES buffer at pH 7.2 with λ_{ex} = 502 nm, λ_{em} = 558 nm.

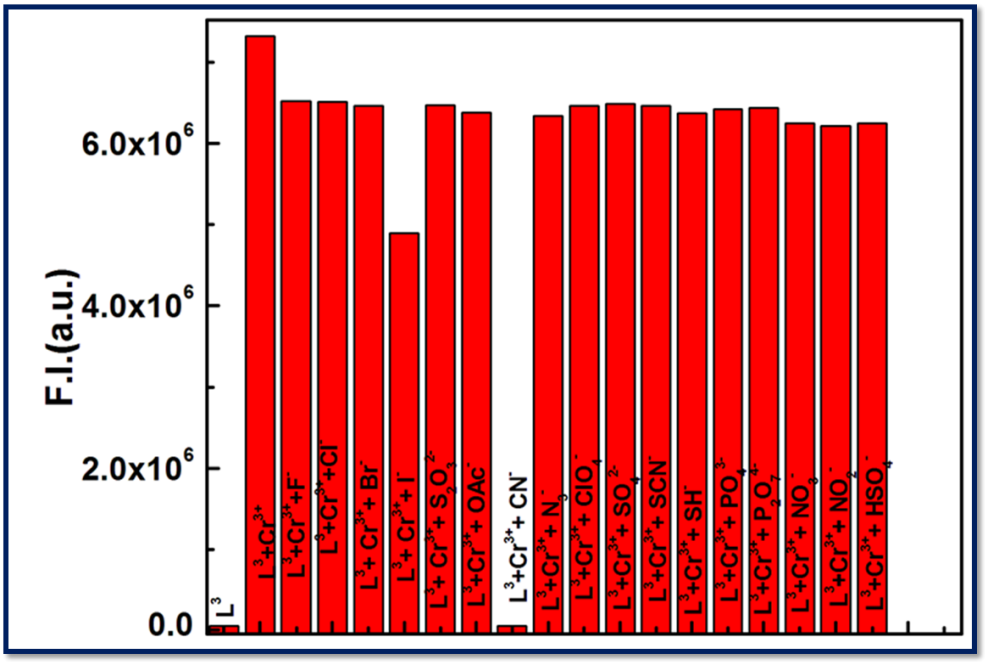

Figure-4.18c : Histogram of the fluorescence quenching [$\mathbf{L^3}$-Cr^{3+}]complex by CN^- (100 μM) towards $\mathbf{L^3}$ (60 μM) in H_2O- MeCN-(7:3, v/v) in presence of different anions(100 μM) in HEPES buffer at pH 7.2 with λ_{ex} = 502 nm, λ_{em} = 558 nm.

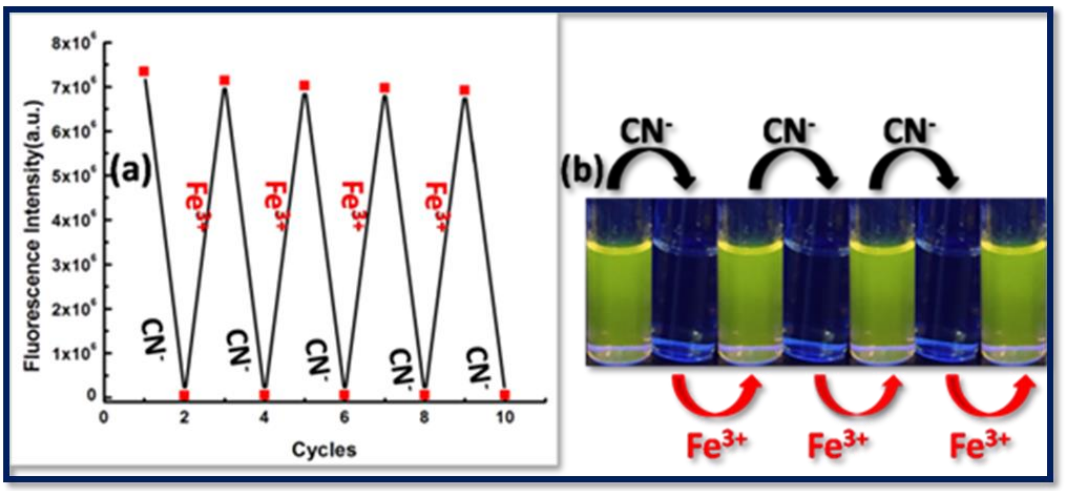

Figure-4.19: Fluorescence experiment to show the reversibility and reusability of the receptor for sensing Fe^{3+} by alternate addition of CN^-. (a) Fluorescence intensity obtained during the titration of $\mathbf{L^3}$-Fe^{3+} with CN^- followed by the addition of Fe^{3+}. (b) Fluorescent color changes after each addition of CN^- and Fe^{3+} sequentially.

4.3.4 pH Studies

For practical application, the appropriate pH condition for the sensor was evaluated. At pH > 4.0, no obvious ring opening of the probe was observed thereby satisfying the usefulness of the probe in biological system over a wide pH range (4.5-8) for the detection of Fe^{3+} (**Figure-4.20**), Al^{3+} and Cr^{3+} (**Figure-4.21a** and **Figure-4.21b**). However, upon addition of 3.0 equivalents of Fe^{3+} the FI jumps to very high value and remains almost unchanged in the range pH 3.2-7.25 but on further increase in pH the FI gradually falls. At pH > 8 no FI is observed in case of Fe^{3+}, Al^{3+} and Cr^{3+} due to the precipitation of hydroxides of these metal ions.

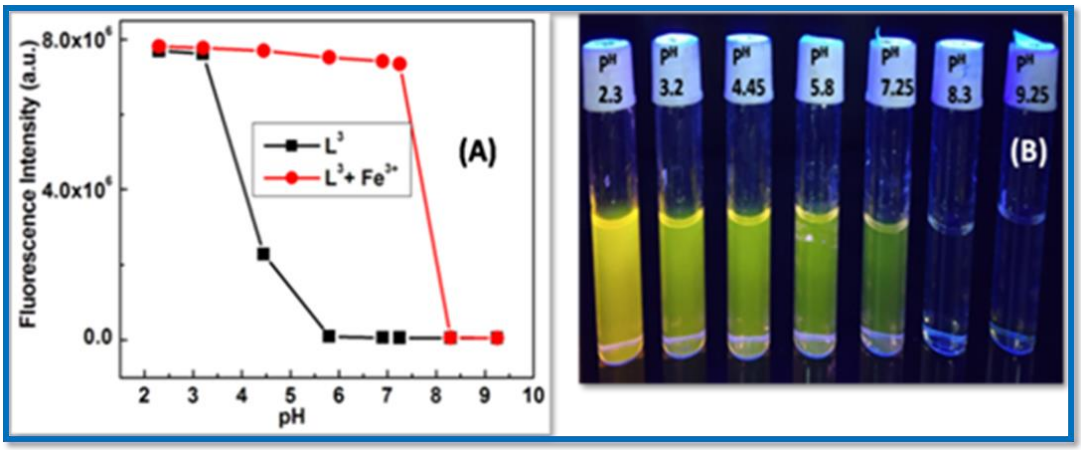

Figure-4.20: (A) pH dependence of fluorescence responses of $\mathbf{L^3}$ and its $\mathbf{[L^3\text{-}Fe^{3+}]}$ complex; (B) Fluorescent response of $\mathbf{L^3}$ towards Fe^{3+} at different pH.

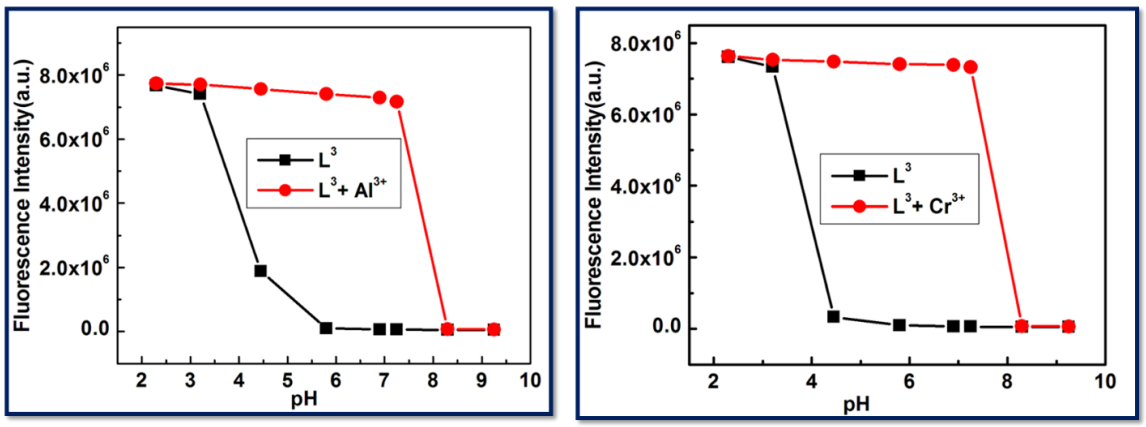

Figure-4.21 : a) Fluorescence intensity observed at different pH for $\mathbf{L^3}$ and $[\mathbf{L^3}+Al]^{3+}$ (60 μM) in H_2O /CH_3CN (7:3,v/v) with λ_{ex} = 502 nm, λ_{em} = 558 nm. **b**) Fluorescence intensity observed at

different pH for $\mathbf{L^3}$ and $[\mathbf{L^3}+Cr]^{3+}$ (60 μM) in H_2O /CH_3CN (7:3,v/v) with λ_{ex} = 502 nm, λ_{em} = 558 nm.

4.3.5 Spectral studies

The mechanistic pathway proposed for the formation of the $\mathbf{L^3}$– M^{3+} complex by opening of the spirolactam ring was established through IR and ^{1}H-NMR studies. The IR studies revealed that the characteristic stretching vibrational frequencies of the amidic 'C=O' of the rhodamine moiety at 1699 cm^{-1} and azomethine group (C=N) at 1637 cm^{-1} were shifted to lower wave numbers 1646 cm^{-1}, 1600 cm^{-1} and 1599, 1500 cm^{-1} in the presence of 3.0 equivalent of Al^{3+} and Cr^{3+} respectively (**Figure-4.22**).

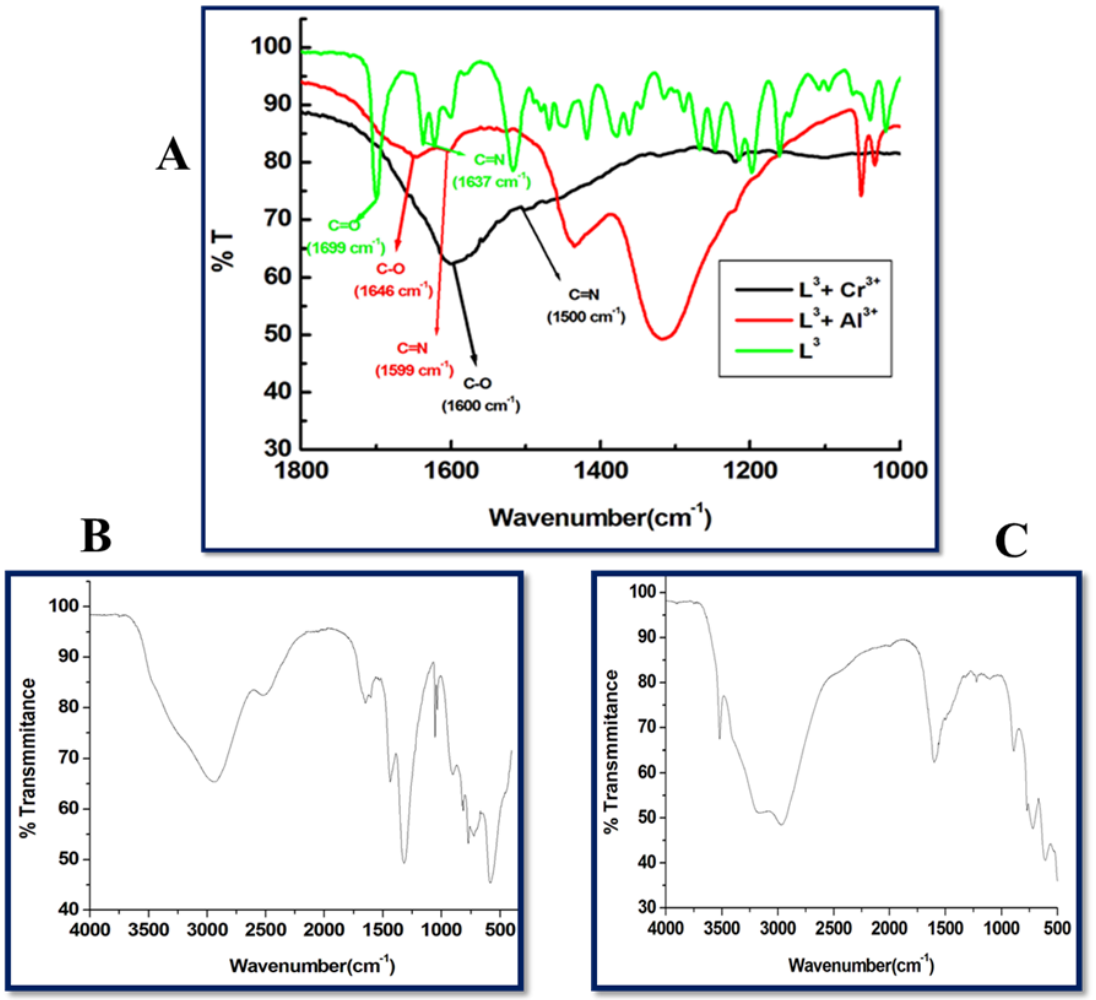

Figure-4.22: a) Comparative IR spectra of **(L^3), [L^3 +Al^{3+}]** and **[L^3 +Cr^{3+}]** complex in MeCN (diagram A). b) IR spectra of **[L^3 +Al^{3+}]** complex in MeCN (diagram B). c) IR spectra of **[L^3 +Cr^{3+}]** complex in MeCN (diagram C).

Also These large shifts in IR frequencies signifies a strong polarization of the C=O bond upon efficient binding to the M^{3+} ion. The coordination mode of **L^3** towards Al^{3+} was supported by ^{1}H-NMR studies (**Figure-4.23**) which shows that a down field shift of azomethine proton (from δ =8.24 to 10.35) in **L^3** and also the protons on benzene ring of L^3 moiety in **L^3**–Al^{3+} complex. Broadening of the –NH proton from 4.06 to 4.20 is due to opening of the spirolactam ring and bearing a positive charge on it. HRMS study (**Figure-4.24a, Figure-4.24b, Figure-4.24c**) also confirms the formation of complex with M^{3+} (M= Al, Fe and Cr).

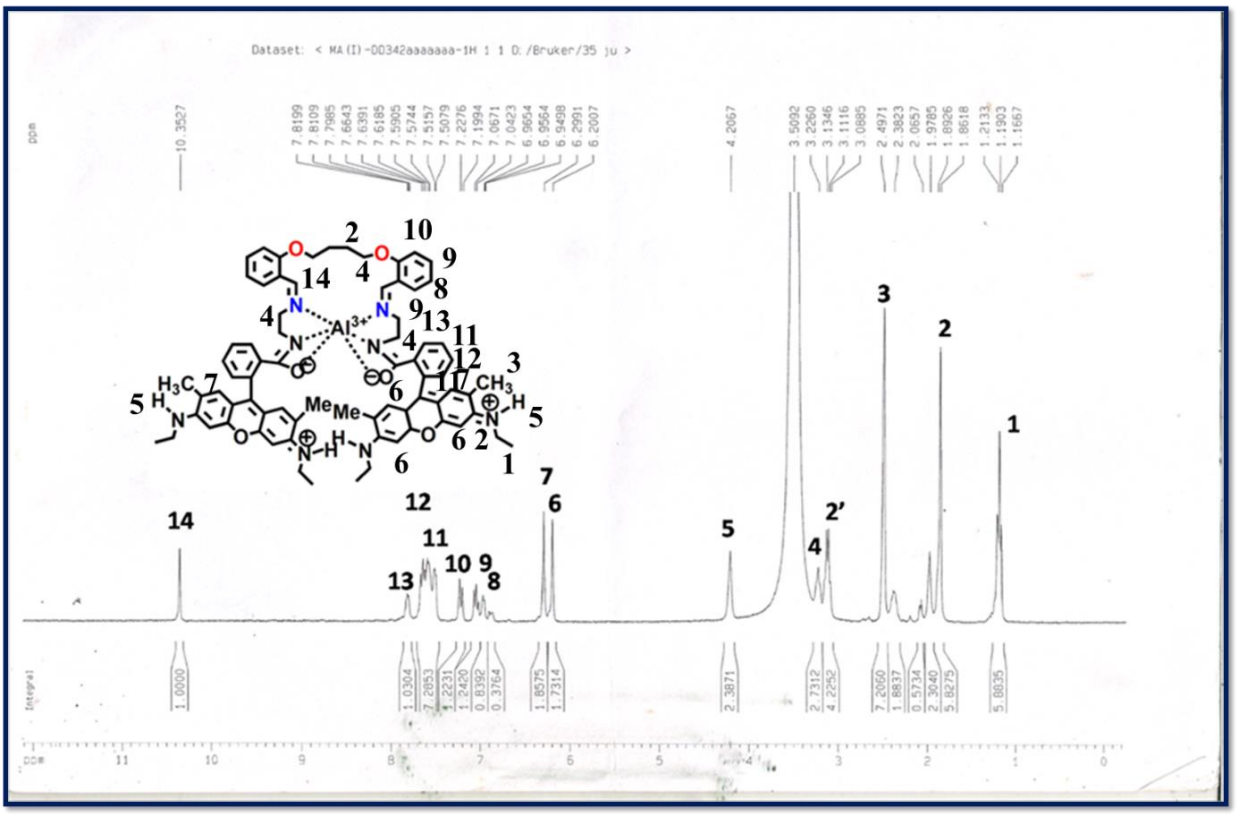

Figure-4.23: ^{1}H NMR spectrum of [**L^3**+Al]$^{3+}$ complex in DMSO-d_6, in Bruker 300 MHz instrument

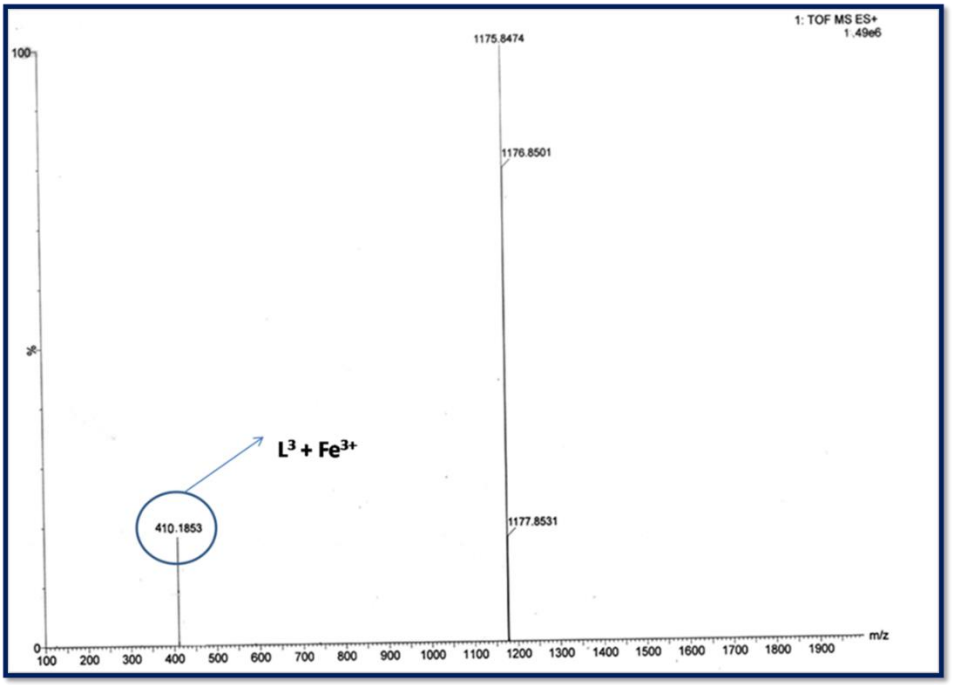

Figure-4.24a: Mass spectroscopy of [L^3 + Fe^{3+}] in MeCN.

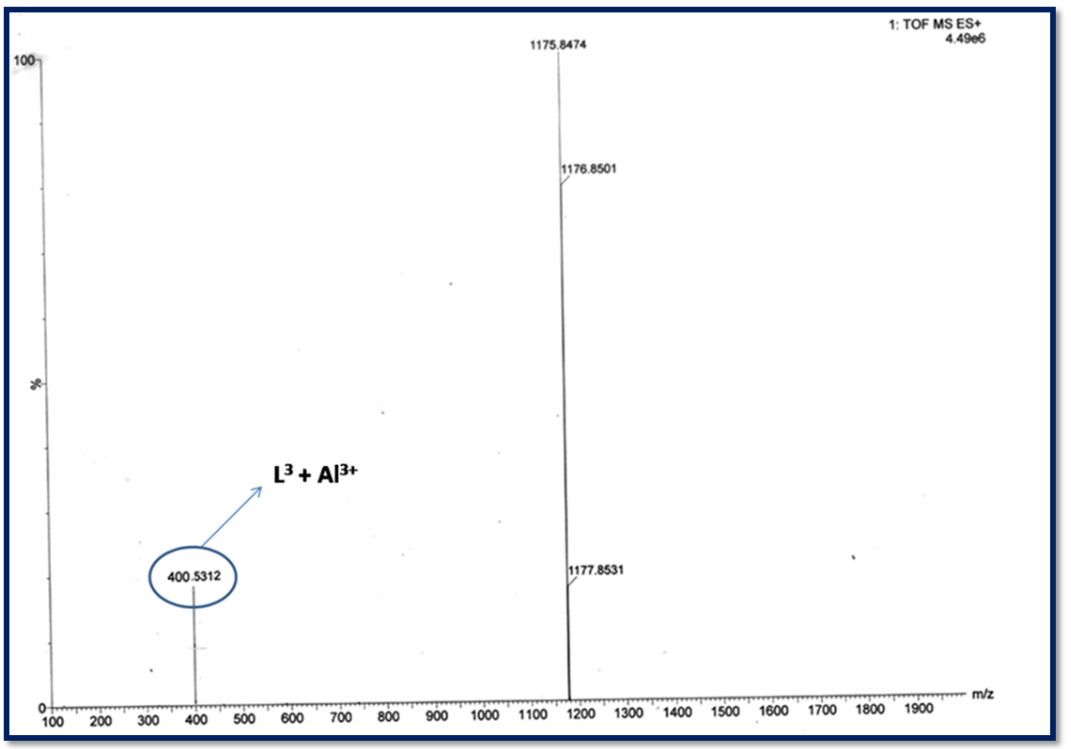

Figure-4.24b: Mass spectroscopy of [L^3 + Al^{3+}] in MeCN.

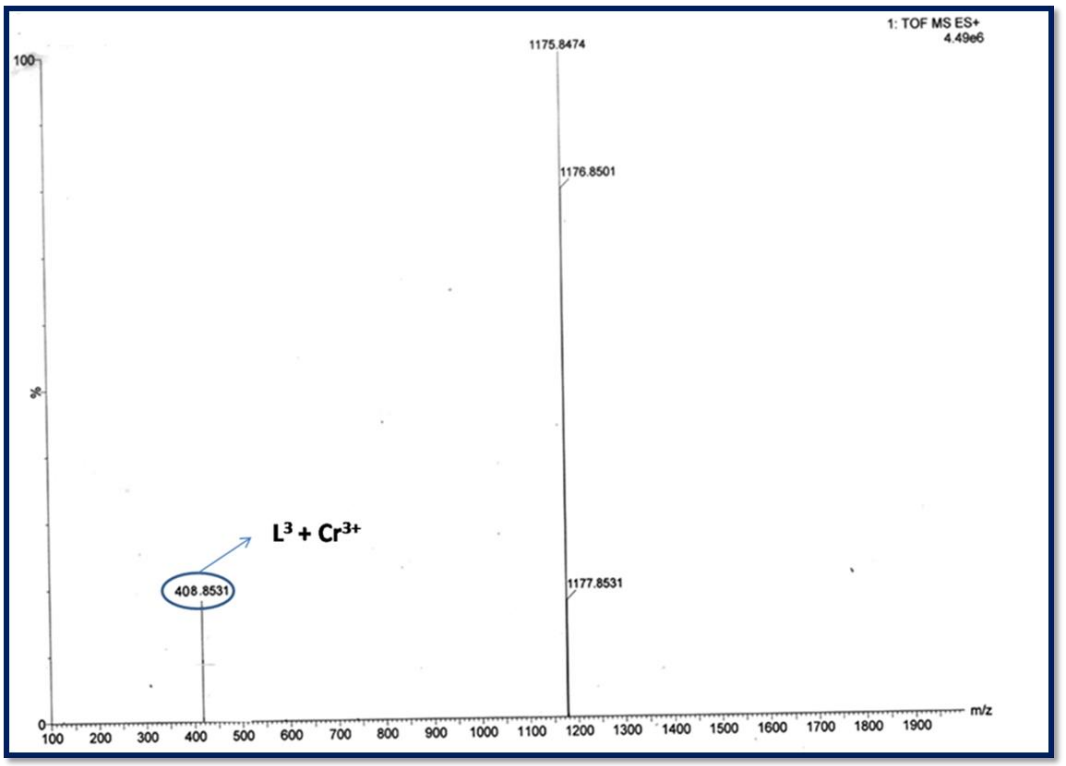

Figure-4.24c: Mass spectroscopy of [L^3 + Cr^{3+}] in MeCN

4.3.6 Molecular logic operations

Based on the investigation the fluorescence ‘‘OFF’- ON” states of **L^3** through controlled experiments some interesting chemistry related to multiple logic operations can be achieved with the sequential addition of inputs like cations such as Al^{3+}, Fe^{3+}, Cr^{3+} and CN^- anion and monitoring their emission as the output. An INHIBIT logic gate is constructed with a particular combination of the logic operation like NOT and AND functions, and it is important due to its non-commutative behaviour i.e. its output signal is inhibited by only one type of input. For the demonstration of this INHIBIT logic function, first we chose two inputs namely Fe^{3+} as input 1 and CN^- as input 2 and use its emission intensity at 558 nm as the output. The high value of emission intensity (>5 x 10^4, at 558 nm) has been designated as 1 (ON) and the low value (≤ 5 x 10^4) has been designated as 0 (OFF). In the absence of both the 1st input (Fe^{3+}) and 2nd input (CN^-), the emission intensity is low which indicates the OFF state. Whereas when only input 1 is present, then a significant enhancement of emission (at 558 nm) occours, indicating the 1 (ON) state, while, on the other

hand, in the presence of input 2 the output emission value becomes very weak designating OFF state. Therefore, it is necessary to apply NOT gate with Input 2. Additionally, it is interesting that $\mathbf{L^3}$ displays the emission output signal in such a way that it seems to understand the requirements of AND operation. In the presence of both inputs the output emission value is again low designating OFF state, in agrees with the truth table **[Figure-4.25(a)].** Thus, by sequential addition of these two inputs INHIBIT function logic gate can be achieved.

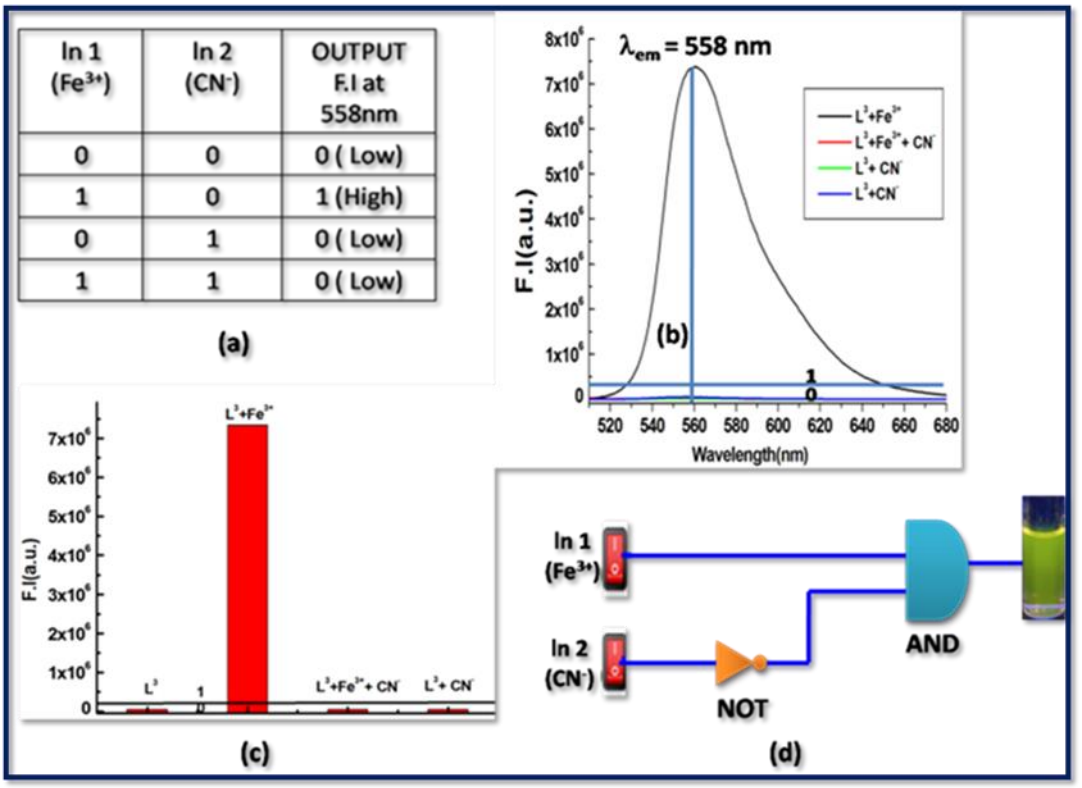

Figure-4.25: (a) Corresponding Truth Table of the logic gate. (b) Output signals (at 558 nm) of the logic gate in the presence of different inputs. (c) Corresponding bar diagram at 558 nm in presence of different inputs. (d) General representation of an INHIBIT logic gate based circuit.

4.3.7 Advanced level OR-INHIBIT gate based 4 input logic gate

A combination of OR and INHIBIT logic functions has been used for the construction of the 4 inputs 1 output logic gate circuit. Now to emulate an OR logic gate function, the emission intensity at 558 nm has been used as the output response similar to the earlier 2 input logic gate and the inputs are Al^{3+}, Fe^{3+}, Cr^{3+} and CN^- (**Figure-4.26**). When 1st (Al^{3+}) and 2nd (Fe^{3+}) input both are

absent the output response i.e. emission intensity is very low, designating 0 (OFF) state. However, when only any one of the two inputs is present, the output signal is high designating 1 (ON) state. Again in the presence of both the input Al^{3+} and Fe^{3+}, the output response is 1 (ON). Thus, according to its truth table (**Figure-4.27a**) an OR function logic gate can be contracted by sequential addition of these two inputs. Then we verify the nature of the output signal in the presence of 3rd ionic input (Cr^{3+}) in the presence of the first two ionic inputs. As any one of these three inputs or presence of two of these three inputs causes high intensity emission output indicating ON state (1). Thus, the probe behaves like an OR logic functions. On the other hand, when only 4th input (CN^-) is present or in the presence of all other inputs (Al^{3+}, Fe^{3+} and Cr^{3+}) in the system, the output emission is very weak indicating the 0 (OFF) state. Therefore, we apply NOT logic function with 4th input. As the probe functions parallel with the output signal, so we can apply another AND logic function. Thus, from an INHIBIT logical function and following its corresponding truth table an advanced level 4 input logic gate circuit can be constructed (**Figure-4.27**).

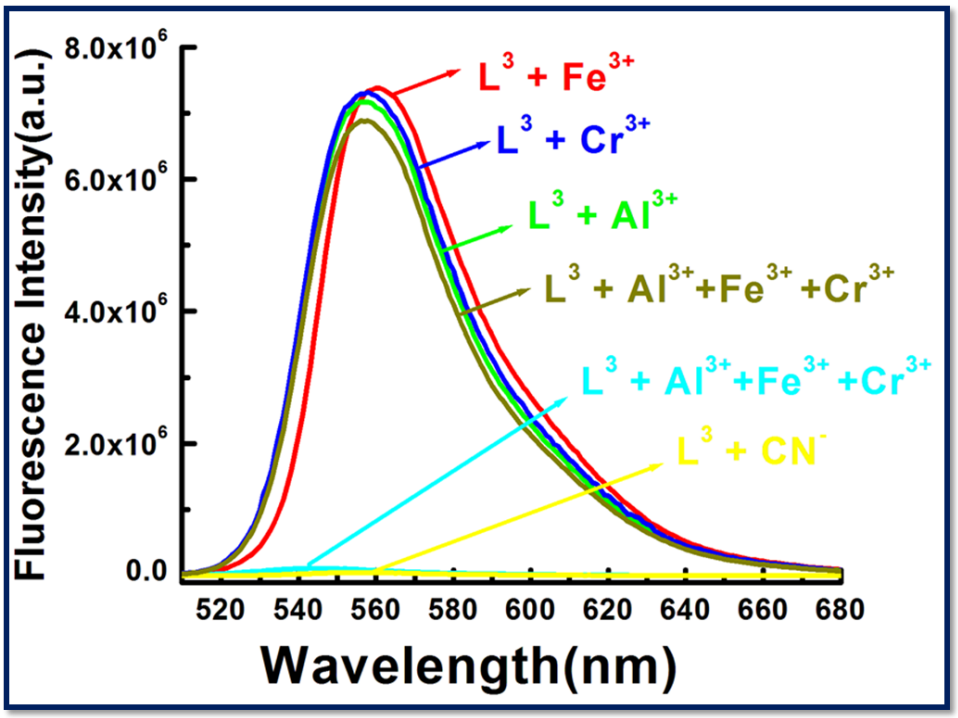

Figure-4.26: Four-input OR-INHIBIT logic gate representation of the emission of $\mathbf{L^3}$ with different input when monitoring the emission at 558 nm.

In 1 (Al^{3+})	In 2 (Fe^{3+})	In 3 (Cr^{3+})	In 4 (CN^-)	OUTPUT F.I At 558nm
0	0	0	0	0(Low)
0	0	0	1	0(Low)
0	0	1	0	1(High)
0	1	0	0	1(High)
0	1	0	1	0(Low)
0	0	1	1	0(Low)
0	1	0	1	0(Low)
0	1	1	0	1(High)
0	1	1	1	0(Low)
1	0	0	0	1(High)
1	1	0	0	1(High)
1	0	1	0	1(High)
1	1	1	0	1(High)
1	0	0	1	0(Low)
1	1	1	1	0(Low)

(a)

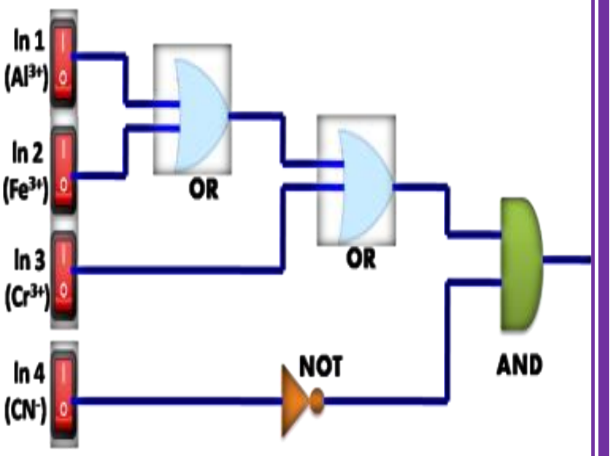

(b)

Figure-4.27: (a) Truth table of an advanced level 4 input logic gate (b) Schematic representation of a combined logic circuit of INHIBIT and OR logic gates.

4.3.8 Molecular memory device

Molecular memory devices are the data storage technologies that use molecular species as the data storage element and can be constructed by sequential logic circuits. One of the output signal acts as the input of the memory device and it is memorized as a "memory element". So by using binary logic function we have developed a sequential logic circuit which shows "Write –Read – Erase−Read" property. For our system, we have chosen strong emission output at 558 nm as **ON** state (1) and weak emission output as **OFF** state (0). Now to construct this memory device, we have chosen two inputs Fe^{3+} and CN^- for the SET and RESET processes, respectively. In this memory function, the system writes when it gets input A (Fe^{3+}) i.e. high emission value and it memorizes binary number 1. But in the presence of input B (CN^-), which is a reset input, erases the data and then memorize the binary number 0 (**Figure-4.28**). The properties of the material allow for a much greater capacitance per unit area than with conventional DRAM(Dynamic random-access memory), thus potentially leading to smaller and cheaper integrated circuits. The

most important thing is that this write-erase-write cycles could be repeated many times (**Figure-4.19**) using the same concentration of the system with negligible change in emission intensity.

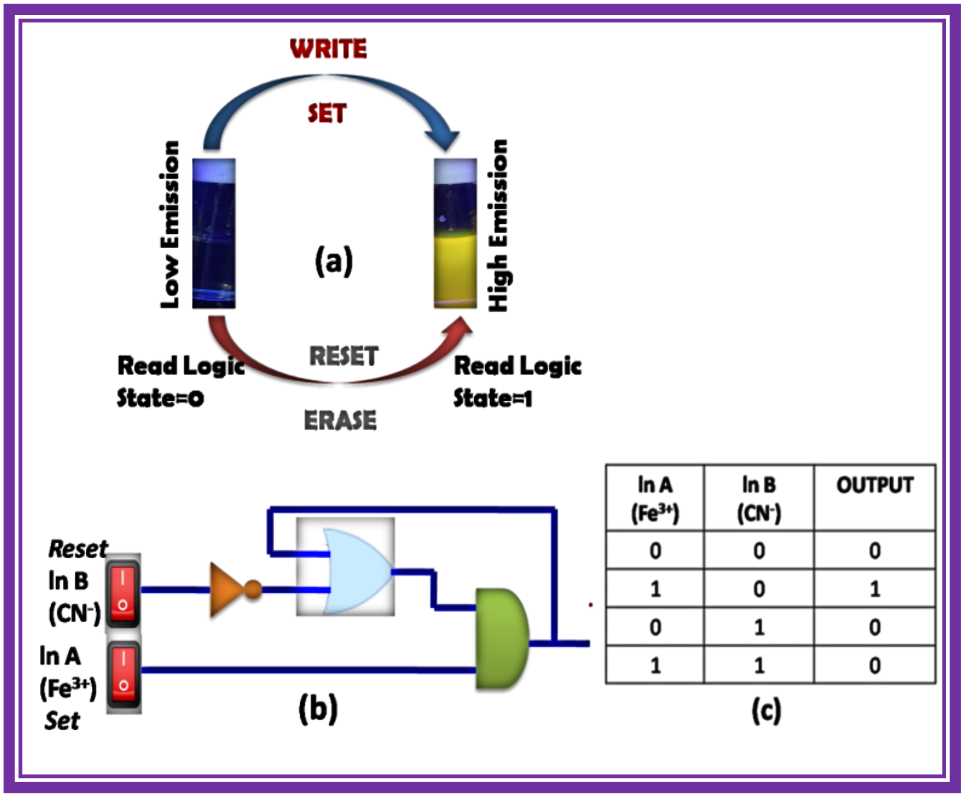

Figure-4.28: (a) Schematic demonstration of the reversible logic operation for the memory element with "write−read−erase−read" kind of behaviour. (b) Sequential logic circuit showing memory unit with two inputs (In A and In B) and one output and (c) corresponding truth table.

4.4 Conclusion

In summary, we reported herein a new rhodamine-6G based chemosensor(**L**^{3}) which showed a selective colorometric as well as "turn-on" fluorescence response towards trivalent metal ions M^{3+} (M= Al, Fe and Cr) over mono and divalent metal ions. A large enhancement of fluorescence intensity of **L**^{3} with Fe^{3+} (669 fold), Al^{3+} (653 fold) and Cr^{3+} (667 fold) was observed upon addition of 3.0 equivalent of these metal ions in H_2O/CH_3CN (7:3, v/v, pH 7.2) which clearly indicate the feasibility of naked eye detection of these metal ions. The K_d values were evaluated from the fluorescence titration data at variable concentration of metal ions and fixed concentration of ligand

and found to be 1.94 x 10^{-5} M^{-1} (Fe^{3+}); 3.15 x 10^{-5} M^{-1}(Al^{3+}) and 2.26 x 10^{-5} M^{-1}(Cr^{3+}). The higher values of quantum yields (0.335, 0.327, 0.333) for [$\mathbf{L^3}$—Fe^{3+}], [$\mathbf{L^3}$—Al^{3+}] and [$\mathbf{L^3}$— Cr^{3+}] respectively over the free ligand (0.0005) indicate the higher stability of the complexes in the excited states. An excellent reversible fluorescence "OFF-ON" property of $\mathbf{L^3}$ has been observed through fluorescence study with the sequential addition of M^{3+} and CN^- ions at room temperature which suggests the reusability of this chemosensor. The very low detection limit for Fe^{3+}, Al^{3+} and Cr^{3+} are 2.57, 0.78 and 0.47 μM respectively which could make it have a potential application in real water samples for trivalent ion detection. Advanced level molecular logic devices using different inputs (2 and 4 input) an advanced level logic gates and memory device have been constructed.

Some trivalent sensors were reported so far (**Figure-4.29**) and some important parameters of these ligands are reported in **Table-4.1**. A closer inspection of **Table-4.1** reveals that there is one report (probe 6) where CH_3OH–H_2O (6 : 4, v/v) was used, but the serious drawback of this system was that the excitation wavelength was in UV region (330 nm), which is not desirable for bioimaging applications. Our probe is superior with respect to all the previously reported probes listed in the table in the sense that $\mathbf{L^3}$ provides higher excitation wavelength (502 nm).

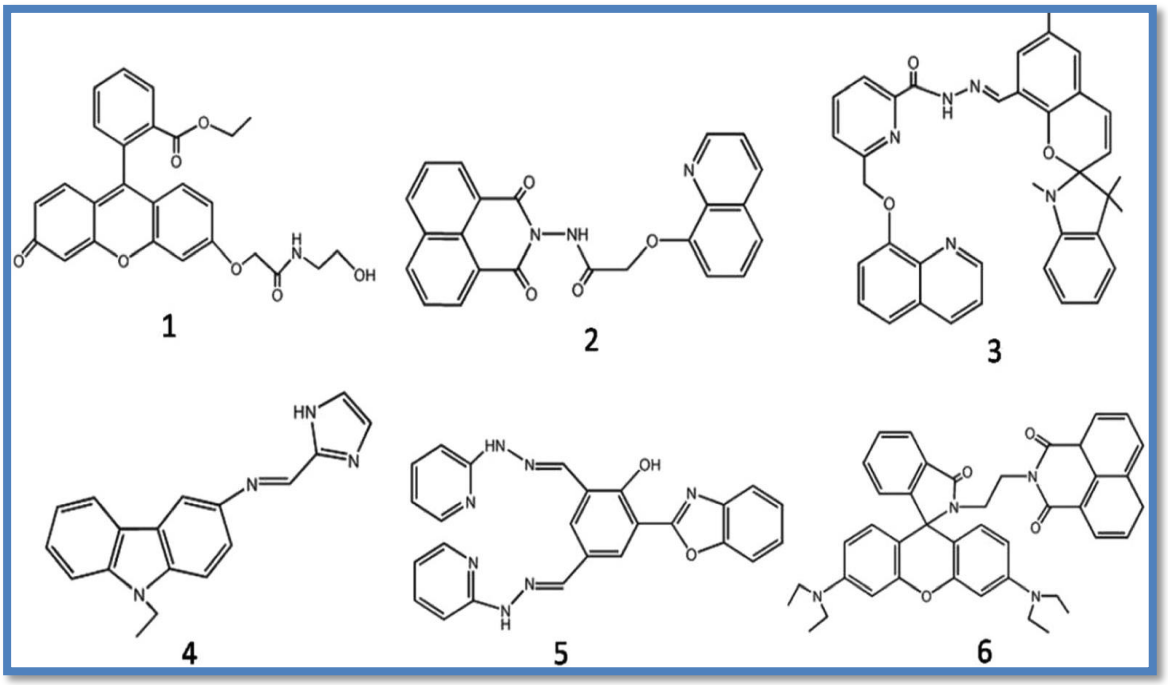

Figure-4.29: Some previously representative trivalent sensors.

Probe	Solvent	λ_{ex} (λ_{em})/ nm	LOD	$K_f(M^{-1})$	Ref no.
1	Pure CH_3CN	437 (475)	0.5nM (Cr^{3+}) 0.3nM(Al^{3+}) 0.2nM(Fe^{3+})	1.58 x $10^4 M^{-1}$ (Cr^{3+}); 6.46 x 10^9 M^{-2} (Al^{3+}) 1.26 x 10^5 M^{-1} (Fe^{3+});	1
2	CH_3CN–HEPES buffer solution (40/60, v/v, pH =7.4)	342 (484)	25nM(Cr^{3+}) 23nM(Al^{3+}) 20nM(Fe^{3+})	1.0852 x 10^4 M^{-1}(Fe^{3+}) 8.770 x 10^3 M^{-1} (Al^{3+}) 5.676 x 10^3 M^{-1}(Cr^{3+})	2
3	CH_3CN–HEPES buffer solution (1:1 , pH = 7.4)	460 (675)	93 nM(Cr^{3+}) 32 nM (Al^{3+}) 90 nM (Fe^{3+})	Not determined	3
4	THF–H_2O (8:2) mixture	330 (430)	0.36 nM (Cr^{3+}) 0.38 nM (Fe^{3+}) 0.38 nM (Al^{3+})	Not determined	4
5	H_2O:EtOH = 8:2	390 (563) 390 (527)	0.20μM(Cr^{3+}) 0.50μM(Al^{3+})	5.50 x 10^4 M^{-1} (Cr^{3+}) 2.00x 10^4 M^{-1} (Al^{3+});	5
6	CH_3OH–H_2O (6 : 4, v/v)	330 (582)	1.74 nM (Al^{3+}) 2.36 μM (Cr^{3+}) 2.90 μM (Fe^{3+})	1 x 10^4 M^{-1} (Al^{3+}); 2.6 x 10^2 M^{-1} (Cr^{3+}) 1.2 x 10^2 M^{-1} (Fe^{3+});	6
7	CH_3CN	Colorimetric	2.16 × 10^{-6} M (Al^{3+}) 1.27 × 10^{-8} M (Cr^{3+}) 55.03 x 10^{-8} (Fe^{3+})	3.451 × $10^3 M^{-1}$(Al^{3+}) 3.751 × 10^6 M^{-1}(Cr^{3+}) 6.078 x 10^6 M^{-1}(Fe^{3+})	7
8	Methanol:water (7:3, v/v)	500(552)	1.18nM(Al^{3+}) 1.80nM(Cr^{3+}) 4.04 nm (Fe^{3+})	6.92 ± 0.18μM (Al^{3+}) 4.90 ± 0.67 μM (Fe^{3+}) 6.79 ± 0.34 μM (Cr^{3+})	8
9	1:1 methanol–water	365(509)	1.6×10^{-6} M(Al^{3+}) 2.66×10^{-6}M(Cr^{3+}) 7.99×10^{-7}M(Fe^{3+})	Not determined	9
10	CH_3CN	365(465)	1.06 × 10^{-7}M(Fe^{3+})	2.25 × $10^6 M^{-2}$(Fe^{3+})	10

			1.11×10^{-7}M(Cr^{3+}) 1.17×10^{-7}M(Al^{3+})	$2.24 \times 10^{6}M^{-2}$(Cr^{3+}) $2.26 \times 10^{6}M^{-2}$(Al^{3+})	
11	H_2O/CH_3CN (7:3, v/v, pH 7.2, 20 mM HEPES buffer	502(558)	2.57μM (Fe^{3+}) 0.78 μM(Al^{3+}) 0.47 μM(Cr^{3+})	$5.15x10^4$ M^{-1} (Fe^{3+}) 3.17 x 10^4 M^{-1}(Al^{3+}) 4.42 x 10^5 M^{-1}(Cr^{3+})	This work

Table 4.1: A list of trivalent sensors along with some important parameters

In our recent report, the rhodamine 6G-benzylamine-based trivalent chemosensor has been found to display enhancement in fluorescence intensity as: 41-fold for Fe^{3+}, 31-fold for Al^{3+} and 26-fold for Cr^{3+}; but in our current work a prominent enhancement in fluorescence intensity was observed. As for example, a 669 fold enhancement for Fe^{3+}, 653 fold for Al^{3+} and 667 fold for Cr^{3+} upon addition of 2.6 equivalent of these metal ions into the probe. Not only that LODs for Al^{3+} and Cr^{3+} determined by 3σ methods were found to be 0.78 and 0.47 μM respectively which are far below than the LODs determined in our previous work (1.34 μM for Al^{3+} and 2.28 μM for Cr^{3+}). Again, K_f values evaluated to be 5.15×10^4 M^{-1} (Fe^{3+}), 3.17×10^4 M^{-1} (Al^{3+}) and 4.42×10^4 M^{-1} (Cr^{3+}) are far improved compared to our previous probe which were found to be 9.4×10^3 M^{-1} for Fe^{3+}, 1.34×10^4 M^{-1} for Al^{3+} and 8.7×10^3 M^{-1} for Cr^{3+}. All these observations lead us to conclude that our current probe L^3 is superior to our previous probe in the analytical point of view.

References

1. S. Chan, Q. Li, H. Tse, A. W. M. Lee, N. K. Mak, H. L. Lung and W. -H. Chan, RSC Adv., **2016**, 6, 74389.

2. (a)T. Rasheed, C. Li, F. Nabeel, W. Huang and Y. Zhou, Chem. Eng. J., 2019, 358, 101; (b) T. Rasheed and F. Nabeel, Coord. Chem. Rev., **2019**, 401, 213065; (c) T. Rasheed, F. Nabeel, M. Adeel, K. Rizwan, M. Bilal and H. M. N. Iqbal, J. Mol. Liq., **2019**, 292, 111425; (d) T. Rasheed, F. Nabeel, C. Li and M. Bilal, J. Lumin., **2019**, 208, 519; (e) T. Rasheed, F. Nabeel, C. Li and Y. Zhang, J. Mol. Liq., **2019**, 274, 461; (f) T. Rasheed, F. Nabeel and S. Shafi, J. Mol. Liq., **2019**, 282, 489; (g) T. Rasheed, F. Nabeel, S. Shafi, M. Bilal and K. Rizwan, J. Mol. Liq., **2019**, 296, 111966; (h) T. Rasheed, M. Bilal, F. Nabeel, H. M. N. Iqbal, C. Li and Y. Zhou, Sci. Total Environ., **2018**, 615, 476; (i) T. Rasheed, C. Li, M. Bilal, C. Yu and H. M. N. Iqbal, Sci. Total Environ., **2018**, 640, 174; (j) T. Rasheed, C. Li, L. Fu, F. Nabeel, C. Yu, L. Gong and Y. Zhou, J. Mol. Liq., **2018**, 272, 440; (k) T. Rasheed, C. Li, F. Nabeel, M. Qi, Y. Zhang and C. Yu, New J. Chem., **2018**, 42, 10940; (l) T. Rasheed, C. Li, Y. Zhang, F. Nabeel, J. Peng, J. Qi, L. Gong and C. Yu, Sens. Actuators, B, **2018,** 258, 115.

3. (a)Y. Li, J. Wu, X. Jin, J. Wang, S. Han, W. Wu, J. Xu, W. Liu, X. Yao and Y. Tang, Dalton Trans., **2014**, 43, 1881; (b) Z. Zhanga, S. Lu, C. Sha and D. Xu, Sens. Actuators, B, **2015**, 208, 258; (c) J. M. Junga, S. Y. Lee and C. Kim, Sens. Actuators, B, **2017**, 251, 291; (d) T. G. Jo, J. M. Jung, J. Han, M. H. Lim and C. Kim, RSC Adv., **2017**, 7, 28723.

4. H. Arakawa, R. Ahmad, M. Naoui and H. A. Tajmir-Riahi, J. Biol. Chem., **2000**, 275, 10150.

5. X. Chen, X. Y. Shen, E. Guan, Y. Liu, A. Qin, J. Z. Sun and B. Z. Tang, Chem. Commun., **2013**, 49, 1503.

6. A. Pechova and L. Pavlata, Vet. Med., **2007**, 52, 1.

7. H. G. Seiler, H. Sigel and A. Sigel, Handbook on Toxicity of Inorganic Compounds, Marcel Dekker Inc., New York, USA, **1988**, 239.

8. A. K. Singh, V. Gupta and B. Gupta, Anal. Chim. Acta, **2007**, 585, 171.

9. M. Sperling, S. Xu and B. Welz, Anal. Chem., **1992**, 64, 3101.

10. J. B. Vincent, Nutr. Rev., **2000**, 58, 67.

11. A. Zhitkovich, G. Quievryn, J. Messer and Z. Motylevich, Environ. Health Perspect., **2002**, 110, 729.

12. J. B. Vincent, Nutr. Rev., **2000**, 58, 67. 2.

13. M. Zhang, Z. Chen, Q. Chen, H. Zou, J. Lou and J. He, Mutat. Res., Genet. Toxicol. Environ. Mutagen, **2008**, 654, 45.

14. M. Costa and C. B. Klein, CRC Crit. Rev. Toxicol., **2006**, 36, 155.

15. R. Dai, C. Yu, J. Liu, Y. Lan and B. Deng, Environ. Sci. Technol., **2010**, 44, 6959.

16. T. O'Brien, H. G. Mandel, D. E. Pritchard and S. R. Patierno, Biochemistry, **2002**, 41, 12529.

17. V. Bravo, S. Gil, A. M. Costero, M. N. Kneeteman, U. Llaosa, P. M. Mancini, L. E. Ochando and M. Parra, Tetrahedron, **2012**, 68, 4882.

18. T. Shoda, K. Kikuchi, H. Kojima, Y. Urano, H. Komatsu, K. Suzukic and T. Nagano, Analyst, **2003**, 128, 719.

19. H. X. Jiang, L. S. Chen, J. G. Zheng, S. Han, N. Tang and B. R. Smith, Tree Physiol., **2008**, 28, 1863.

20. G. Berthon, Coord. Chem. Rev., **1996**, 149, 241

21. S. M. Candura, L. Manzo and L. G. Costa, Role of occupational neurotoxicants in psychiatric and neurodegenerative disorders, in Occupational Neurotoxicology, ed., L. G. Costa and L. Manzo, CRC Press, Boca Raton, **1998**, 131.

22. R. J. P. Williams, Coord. Chem. Rev., **1992**, 149, 1.

23. T. Han, X. Feng, B. Tong, J. Shi, L. Chen, J. Zhi and Y. Dong, Chem. Commun., **2012**, 48, 416.

24. G. R. Rout, S. S. Roy and P. Das, Agronomie, **2001**, 21, 3.

25. (a) J. Barcelo and C. Poschenrieder, Environ. Exp. Bot., 2002, 48, 75; (b) B. Valeur and I. Leray, Coord. Chem. Rev., **2000**, 205, 3; (c) Z. Krejpcio and R. W. P. Wojciak, Int. J. Environ. Stud., **2002**, 11, 251.

26. M. R. Wills, C. D. Hewitt, B. C. Sturgill, J. Savory and M. M. Herman, Ann. Clin. Lab. Sci., **1993**, 23, 1.

27. G. Sahin, I. Varol and A. Temizer, Biol. Trace Elem. Res., **1994**, 41, 129.

28. (a) T. P. Flaten, Brain Res. Bull., 2001, 55, 187. (b) J. R. Walton, NeuroToxicology, **2006**, 27, 385.

29. B. L. Su, N. Moniotte, N. Nivarlet, L. H. Chen, Z. Y. Fu, J. Desmet and J. Li, J. Colloid Interface Sci., **2011**, 358,136.

30. (a) P. Aisen, M. Wessling-Resnick and E. A. Leibold, Curr. Opin. Chem. Biol., 1999, 3, 200; (b) R. S. Eisenstein, Annu. Rev. Nutr., **2000**, 20, 627; (c) T. A. Rouault, Nat. Chem. Biol., 2006, 2, 406.

31. T. Hirayama, K. Okuda and H. Nagasawa, Chem. Sci., **2013**, 4, 1250.

32. J. Xu, Z. Jia, M. D. Knutson and C. Leeuwenburgh, Int.J. Mol. Sci., **2012**, 13, 2368.

33. D. J. Bonda, H. Lee, J. A. Blair, X. Zhu, G. Perry and M. A. Smith, Metallomics., **2011**, 3, 267.

34. Y. Li, J. Wu, X. Jin, J. Wang, S. Han, W. Wu, J. Xu, W. Liu, X. Yao and Y. Tang, Dalton Trans., **2014**, 43, 1881;

35. Z. Zhanga, S. Lu, C. Sha and D. Xu, Sens. Actuators B, **2015**, 208, 258;

36. J. M. Junga, S. Y. Lee and C. Kim, Sens. Actuators B, **2017**, 251, 291.

37. T. G. Jo, J. M. Jung, J. Han, M. H. Lim and C. Kim, RSC Adv., **2017**, 7, 28723.

38. J. Miao, L. Wang, W. Dou, X. L. Tang, Y. Yan and W. S. Liu, Org. Lett., **2007**, 9, 4567

39. S. Goswami, A. K. Das, A. K. Maity, A. Manna, K. Aich, S. Maity, P. Saha and T. K. Mandal, Dalton Trans., **2014**, 43, 231.

40. S. Fakih, M. Podinovskaia, X. Kong, H. L. Collins, V. E. Schoible and R. C. Hider, J. Med. Chem., **2008**, 51, 4539.

41. S. K. Sahoo, D. Sharma, R. K. Bera, G. Crisponi and J. F. Callan, Chem. Soc. Rev., **2012**, 41, 7195.

42. (a)R. Alam, R. Bhowmick, A. S. M. Islam, A. katarkar, K. Chaudhuri and M. Ali, New J. Chem., **2017**, 41, 8359;(b) T. Mistri , R. Alam, R. Bhowmick, A. Katarkar, K. Chaudhuri and M. Ali, New J. Chem., **2016**, 40, 330; c) D.Das, R. Alam, A. Katarkar and M. Ali, Photochem.Photobiol.Sci.,**2019**, 18, 242; (d) T. Mistri, R. Alam, M. Dolai, S. K. Mandal, P.Guha, A. R. Khuda-Bukhsh, and M. Ali, EJIC, **2013**, 34, 5854.

43. J. -S. Wu, I. -C. Hwang, K. S. Kim and J. S. Kim, Org. Lett., **2007**, 9, 907.

44. D. F. Perkins, L. F. Lindoy, A. McAuley, G. V. Meehan, P. Turner, Proc. Natl. Acad. Sci. USA **2006**, 103, 532.

45. Q. Liu, M.-R. Gao, Y. Liu, J. S. Okasinski, Y. Ren and Y. Sun, Nano Lett., **2016**, 16(1), 715.

46. S. Ozkar and R. G. Finke, J. Phys. Chem. C, **2017,** 121, 27643.

47. H. A. Molla, R. Bhowmick, A. Katarkar, K. Chaudhuri, S. Gangopadhyay and M. Ali, Anal. Methods, **2015**, 7, 5149.

48. Y. Xiang and A. Tong, Org. Lett., **2006**, 8, 1549.

A novel and highly selective "turn-on" rhodamine-6G based chromo and fluorogenic sensor for the detection of Fe^{3+} in aqueous medium with potential applications for INHIBIT logic gate and memory devices

Abstract

A novel rhodamine-6G based fluorogenic and chromogenic "OFF-ON" biocompatible chemosensor **L^4** having amide moiety in its receptor part has been synthesized using Michael addition reaction and this probe **L^4** has been characterised by IR, NMR and HRMS spectroscopic studies. It exhibits an excellent selectivity and high sensitivity for the detection of Fe^{3+} in absolute aqueous medium over mono and di-valent and other trivalent metal ions. Enhancement of fluorescence intensity of the probe **L^4** was found to be 14 fold upon addition of the Fe^{3+} metal ions to the aqueous solution (pH 7.2, 10 mM HEPES buffer) of the probe exhibiting a shape change in colour from colourless to reddish yellow establishing the suitablity of the probe for naked eye detection of Fe^{3+} in water. The corresponding K_f values were evaluated to be (1.16 ± 0.04) x 10^4 M^{-1} for 1:1 stoichiometric binding between **L^4** and Fe^{3+}. Quantum yields of **L^4** and [**L^4**–Fe^{3+}] complex in H_2O (pH 7.2, 10 mM HEPES buffer) were found to be 0.013, 0.523 respectively, using Rhodamine-6G as standard. LOD of Fe^{3+} in aqueous medium by **L^4** determined by 3σ method was found to be 4.184 μM. Cyanide ion scavanges Fe^{3+} from [**Fe^{3+}– L^4**] complex and quenches its fluorescence emission with the reattainment of the non-fluorescent spirolactam ring form of the probe. As the sensing phenomenon is reversible, the sensor beautifully mimics INHIBIT logic gate which helps to construct a memory device.

5.1 Introduction

"All people, whatever their stage of development and their social and economic conditions, have the right to have access to an adequate supply of safe drinking water." – WHO. In recent decades, heavy metal pollution in the environment has become a serious problem for living organism and the extent of pollutants has increased many folds due to both natural and anthropogenic sources. Again, more and more industrialization increases ionic pollutant in water, which increases toxic effect in day to day life.

Iron is the second most abundant metal in the earth's crust, of which it accounts for about 5%. Iron mainly exist in the form of oxides, hydroxides, carbonates, and sulphides.[1,2] Aeration of iron-containing layers in the soil can affect the quality of both ground water and surface water. Dissolution of iron can occur as a result of oxidation and causes decrease in pH. Iron deficiency causes chlorosis which is a wide spread agricultural problem that affects the development of corps and decreases the yield in calcareous and alkaline soils.[3]

Iron is an essential element for almost all organisms on Earth and nutritionally trace element in biological system. Iron is a central component of electron chains and a co-factor of many vital enzymes. Only a few bacteria are able to substitute iron with other metals, making it an essential element for virtually all life forms. In plants, iron is also required for photosynthesis and chlorophyll synthesis. It has an important role such as respiration, transport and storage of oxygen in mammals, electron transfer support in a variety of iron sulphur protein or cytochrome reactions.[4] It acts as cofactor in different enzymes in our body and it imparts a crucial role in cellular metabolism and both DNA and RNA synthesis.[5-10] Indeed, both deficiency and excess of iron can induce biological disorders in the human body. Disorder of iron metabolism are among the most common diseases of humans and encompasses a broad spectrum disease with diverse clinical manifestation ranging from anemia, hypo immunity, low blood pressure to tiredness, noticeable heartbeats, headaches and dizziness, feeling short of breath to neurodegenerative diseases such as Parkinson's disease and Alzheimer's disease.[11,12]

Determination of iron content in water, biological samples and the removal of this kind of toxic species from water is important for the whole world. Traditional methods for the detection of heavy metal ions includes Flame Atomic Absorption Spectrometry, Atomic Absorbtion Spectroscopy (AAS), X-ray Photoelectron Spectrometry (XPS),[13] Atomic Fluorescence Spectroscopy (AFS),[14]

Inductively-Coupled Plasma Mass Spectroscopy (ICP-MS),[15] Inductively-Coupled Plasma Optical Emission Spectroscopy (ICP-OES),[16] and Graphite Furnace Atomic Absorption Spectroscopy (GFAAS).[17] In comparison to these methods, chemo sensing method is less expensive, non-destructive and rapid. So the use of sensors in this field is rapidly growing because these are simple, fast, accurate and highly sensitive.

Though human body can regulate iron to some extent, detection and analysis of bioactive iron is an important healthcare challenge for the chemist. So, there is an urgent need to develope various chemical devices through design and synthesis of fluorescent molecules for the detection of various metal ions, specially for the detection of iron (II/III) in the environmental and biological samples in the presence of other metal ions in a complicated aqueous environment at physiological pH.[18,19]

Numerous excellent works focusing on the selective and sensitive detection of iron (III) have been reported.[20-24] Most of the known Fe^{3+} sensors are fluorescence quencher due to its paramagnetic nature.[28-31]Despite its importance in many biochemical processes at the cellular level[25-27] only few Fe^{3+}chemosensors based on fluorescence enhancement are reported. So development of highly sensitive chemosensor with fluorescence enhancement signal upon binding with Fe^{3+} is a difficult challenge. The most fundamental route is the rhodamine scaffold, an ideal template chromophore for the construction of such chemosensors. Its excellent photophysical properties with excellent quantum yields, large molar extinction coefficient, great photostability and long emission wavelengths make it as an ideal choice.[32-34] It is colourless and non-fluorescent in its ring closed spirolactam form, whereas in its ring opened amide form both chromogenic and fluorogenic response facilitates an OFF/ ON type fluorescence detection.[35,36]

A remarkable progress has been achieved in recent times in the development of molecular systems which are capable of performing logic operations and molecular devices which are very demanding in information technology.[37] Logic systems is consist of chemically encoded information as input and a fluorescence signal as output which have received considerable attention and functions such as AND, NAND, OR, NOR, XOR, XNOR and INHIBIT have been widely explored.[38] In all molecular logic gates, the molecule demonstrates “ON” or “OFF” switching of the fluorescence signal, which symbolized as an output “1” or “0”, respectively, in response to the addition “1” or no addition “0” of the input chemicals. Such devices operate in wireless mode and have the

potential for computation on a molecular level over silicon-based devices. Hence, these have possible applications in the development of electronic and photonic devices.

Focousing our interest in developing new chemosensors herein, we are going to report synthesis and characterisation of a new rhodamine-based turn-on fluorescent chemosensor **L^4** (**Scheme 5.1**) for the selective and sensitive detection of Fe^{3+}. Fluorescent sensor **L^4** is colourless and non-fluorescent in the absence of Fe^{3+}, but it shows reddish-pink colour in naked eyes and it exhibits a high fluorescent intensity in the presence of Fe^{3+} over other metal ions with a 14-fold enhancement in fluorescence intensity in aqueous medium in 10 mM HEPES buffer.

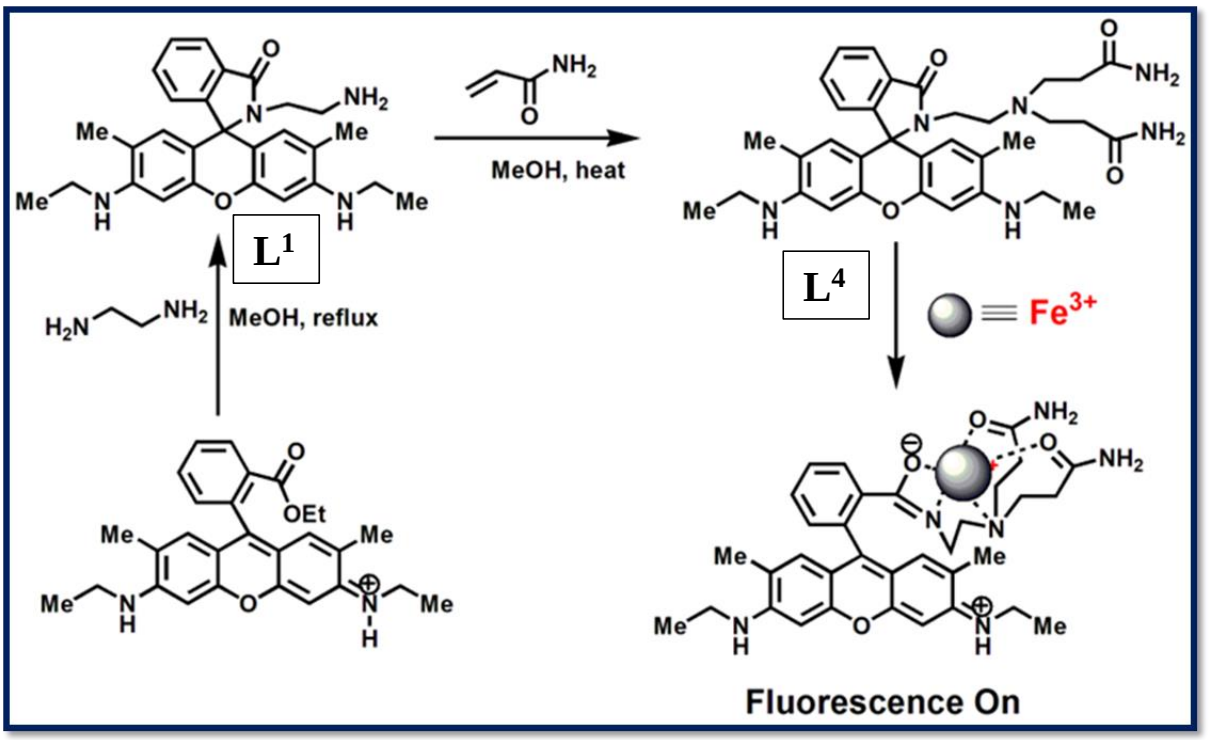

Scheme 5.1: Tentative binding mode of **L^4** with Fe^{3+}.

5.2 Experimental Section

5.2.1 Materials and Methods

All solvents used for synthesis were of reagent grade purchased from Merck. For the UV/Vis and fluorescence studies HPLC-grade MeCN and double-distilled water were used. Rhodamine-6G hydrochloride and metal salts, such as chloride salt of Na^+, K^+, nitrate salt of Co^{2+}, Ni^{2+}, Fe^{2+}, Zn^{2+},

Pb^{2+}, Cd^{2+}, Hg^{2+}, Cu^{2+}, Al^{3+} Cr^{3+} and Fe^{3+} were purchased either from Sigma–Aldrich or Merck and used as received. All other chemicals were purchased from commercial sources and used without further purification.

5.2.2 Physical measurements

^{1}H-NMR spectra were recorded in $CDCl_3$ and DMSO-d_6, on a Bruker300 MHz NMR spectrometer using tetramethylsilane (δ =0) as an internal standard. Infrared spectra (400–4000 cm^{-1}) were recorded in liquid state in a Nickolet Magna IR 750 series-II FTIR spectrometer. ESI-MS^+ (m/z) of the ligand and its iron (III) complex were recorded on a Waters' HRMS spectrometer (Model: XEVO G2QTof). UV-Vis spectra were recorded on an Agilent diode-array spectrophotometer (Model, Agilent 8453). Steady-state fluorescence measurements were performed on a PTI QM-40 spectrofluorometer. Lifetime is measured in Horiba Jobin–Yvon Hamamatsu MCP photomultiplier (R3809) and data were analyzed by using IBH DAS6 software. The pH of the solutions was recorded in a digital pH meter 335 (Cystronics, India), which was calibrated using pH 4, 7 and 10 buffers in the range pH 2-12.

5.2.3 Synthesis of Rhodamine 6G conjugate (L^4)

5.2.3.1 Synthesis of rhodamine 6G hydrazide (L^1)

Rhodamine 6G (5.0 mmol) and ethylenediamine (10.0 mmol) were dissolved in EtOH and refluxed for 4 hours with continuous stirring whereupon a white crystalline solid of the probe (**L^1**) was deposited (**Scheme 5.1**). The solid was filtered and washed several times with water and dried in air (83% yield). The crude product was crytallised from ethanol.

5.2.3.2 Synthesis of rhodamine 6G based probe (L^4)

To a suspension of 40 mL ice-cooled (0 ºC) ethanolic solution of **L^1** (0.456 g, 1.0 mM), a 5 mL aqueous ethanoic solution of acrylamide (0.3655g, 5 mmol) was added dropwise over a period of 20 min. The reaction mixture was allowed to warm slowly at which it was stirred for 20 h. The

final product, our target fluorescent probe **L^4** (**Scheme 5.1**) was obtained as an off-white precipitate after stirring. The product collected after washing with little amount of water was dried and stored as off-white powder (yield recorded 62%).

^{1}H NMR (300 MHz, DMSO-d_6) (ppm): 1.20 (t, J = 6.0 Hz, 6H (-CH_3)), 1.85 (s, 6H (-Ar-CH_3)), 1.93 (t, J=7.2Hz, 4H, (NH-CH_2)), 2.40 (t, J=7.2Hz,2H, (-CH_2)), 2.49 (t, J= 1.8Hz, 4H, (CH_2-)), 2,97 (t, J=6.9, 2H, (CH_2)), 3.11 (t, J=.9Hz, 4H, (CH_2)), 5.04 (t, J = 5.4 Hz, 4H (N-H)), 6.04 (s, 2H, (-Ar-H)), 6.27 (s, 2H, (Ar-H)), 6.66 (s, 2H, (NH_2)), 6.98(m,J=3.0Hz,1H(Ar-H)), 7.11(s,2H, NH_2),7.50(m,J=2.4,1H,Ar-H),7.75(t,1H,Ar-H)(**Figure-5.1**).^{13}CNMR: 14.84,16.87,33.59,38.53,50.49,50.76,96.71,105.85,118.22,122.68,124.13,128.57,131.44,132.81,147.74,152.04,175.13 (**Figure-5.2**).ESI-MS$^+$ (m/z): 599.313 (**L^4** + H$^+$) (**Figure-5.3**). IR spectrum: 3342cm^{-1}(-N-H), 1691cm^{-1}(C=O), 1619cm-^{1} (C=O, Amide-I), 1514cm-^{1}(NH_2, Amide-II) (**Figure-5.4**).

5.2.4 Solution preparation for UV-Vis and fluorescence studies

A stock solution of 1.0 x 10^{-2} M of the probe **L^4** was prepared by dissolving 0.059g **L^4** in 10 mL CH_3CN which was then diluted quantitatively to prepare the ligand solution of 1.0x10^{-3}M for UV-Vis and fluorescence study. Analogously, 1.0 x 10^{-3} M stock solutions of Fe^{3+} was prepared in MeOH. A solution of 10 mM HEPES buffer in water was prepared by addition of 0.595g of HEPES in 250 mL of HPLC water and *p*H was adjusted to 7.2 by using HCl and NaOH. For UV-Vis spectra 20 µM probe was taken in cuvette containing 2.5 mL of HEPES buffer 100% aqueous solution and Fe^{3+} salt solution was added incrementally starting from 0 to 430 µM in a regular interval of time and concentration and absorption spectra were recorded. Again 2.5 ml of this buffer solution was pipetted out into a cuvette to which 20 µM of the probe (**L^4**) solution was added and Fe^{3+}salt solution was added incrementally starting from 0 to 208 µM in a regular interval of time and concentration and fluorescence spectra were recorded setting the excitation wavelength at 510 nm. Path lengths of the cells used for absorption and emission studies were 1 cm. Fluorescence measurements were performed using 2 nm x 2 nm slit width.

5.2.5 Job's Plot

This method is based on the measurement of fluorescence of a series of solutions in which molar concentrations of the probe (**L^4**) and Fe^{3+} vary but their sum remains constant. The fluorescence of each solution was measured at 551 nm and plotted against the mole fraction of Fe^{3+}. A maximum fluorescence intensity was observed at the mole ratio corresponding to the combining ratio of the two components which was found to be 1:1.

5.2.6 Calculation of LOD

The analytical detection limit was obtained by performing fluorescence titration of **L^4** with M^{3+} by adding aliquots in a micromolar concentration of Fe^{3+} to 20 μM **L^4** in 2.5 mL buffer and the LOD was calculated by the 3σ method [39,40] with LOD = 3 x S_d/S, where S_d is the standard deviation of the intercept of the blank (**L^4** only) obtained from a plot of fluorescence intensity (FI) versus [**L^4**], and S is the slope obtained from the linear part of the plot of FI versus [Fe^{3+}].

5.3 Results and Discussion

As depicted in **Scheme-5.1**, **L$_1$** was synthesized from the reaction of rhodamine-6G with ethylenediamine in EtOH under reflux condition for 4 h. The receptor **L^4** was synthesized from **L^1** after reaction with acrylamide under warm and stirring condition for about 20 h in ethanol-water. The final product (**L^4**) was well characterized by ^{1}H NMR (**Figure-5.1**), ^{13}C NMR (**Figure-5.2**), HRMS (**Figure-5.3**), IR (**Figure-5.4**) spectroscopic studies. The receptor **L^4** was found to be very sensitive and highly selective colorimetric and fluorogenic chemosensor for trivalent metal ion, Fe^{3+}, while in the absence of Fe^{3+}, the solution of **L^4** is colorless and non-fluorescent.

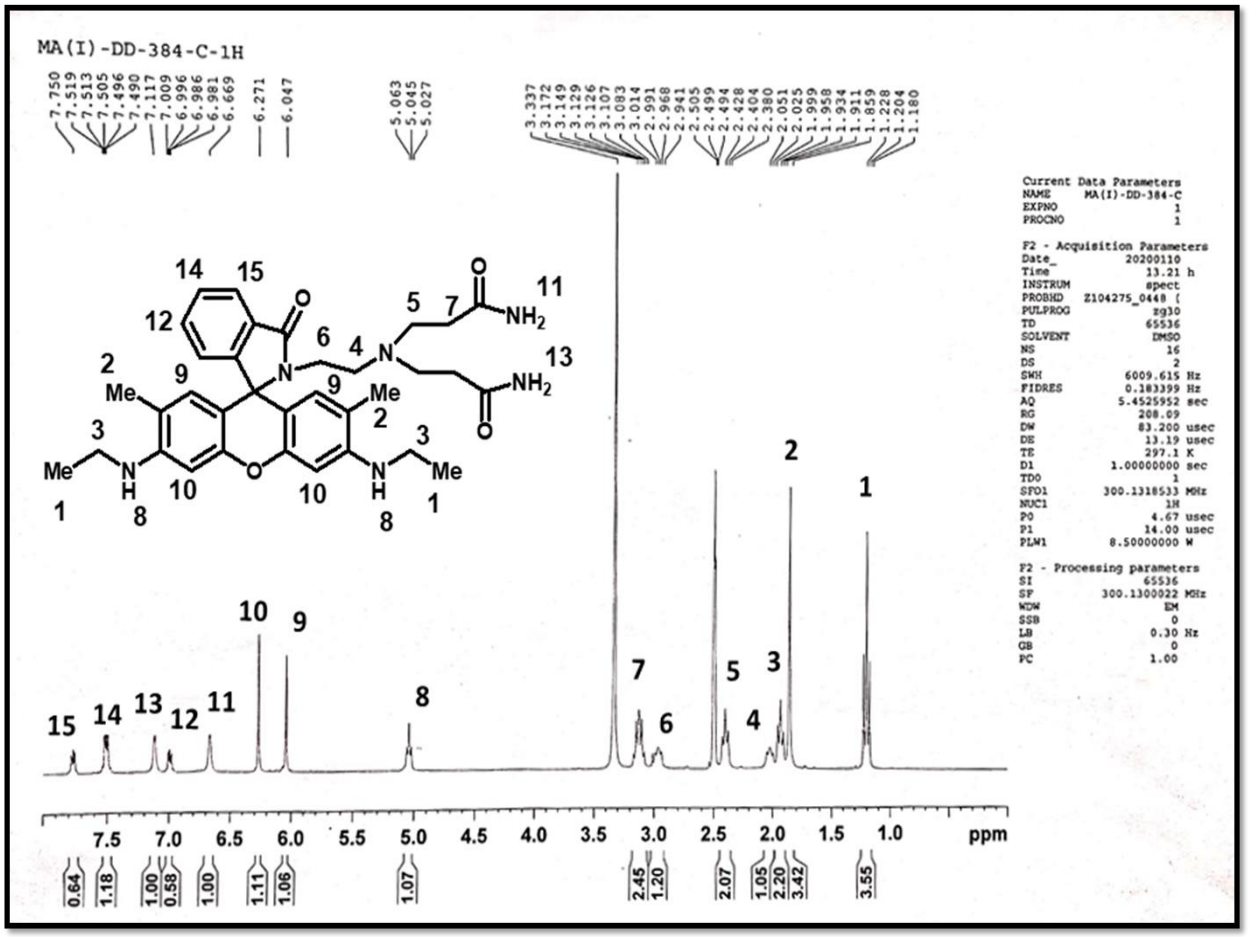

Figure-5.1: ^{1}H NMR spectrum of $\mathbf{L^4}$ in DMSO-d_6, in Bruker 300 MHz instrument.

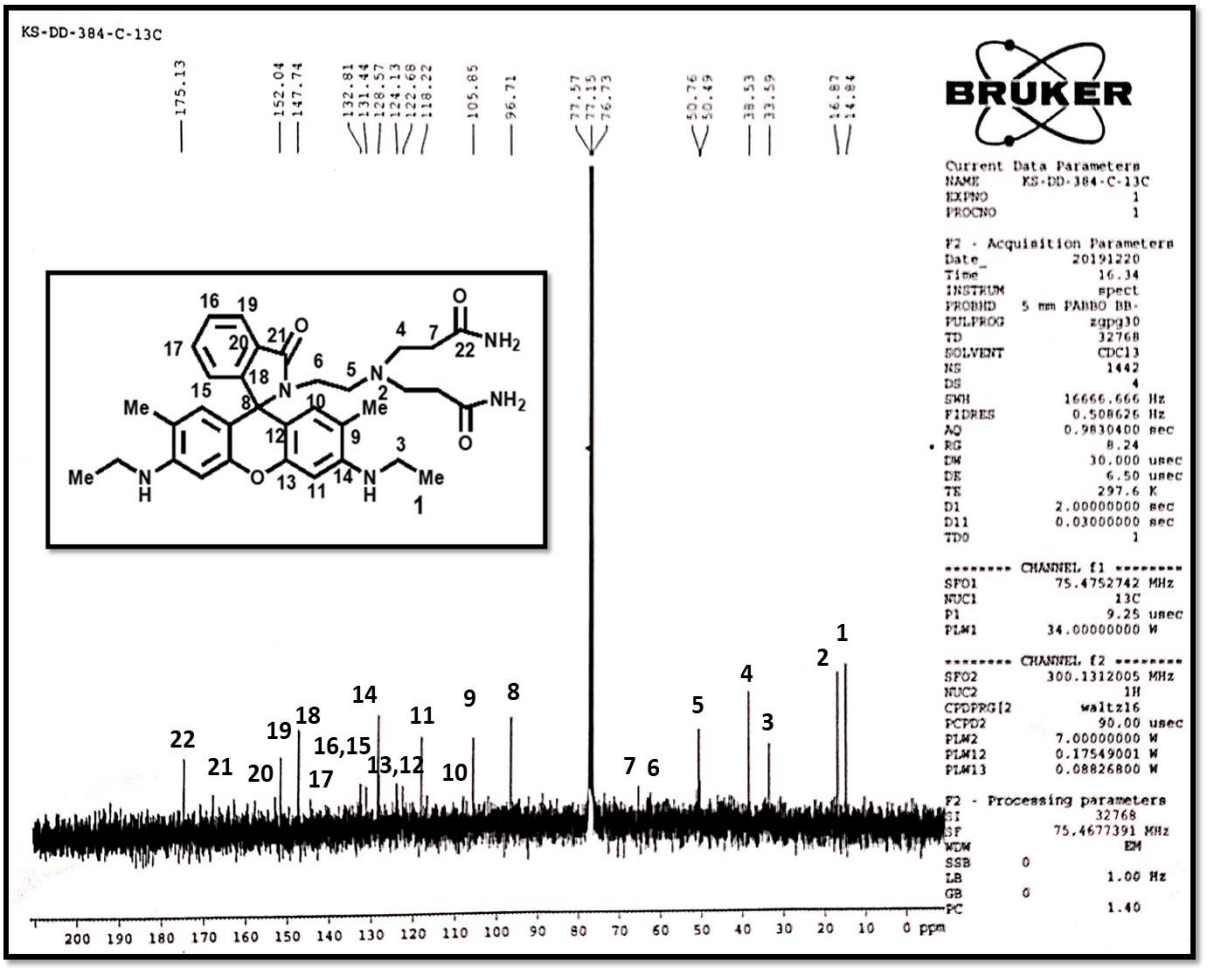

Figure-5.2: ^{13}C NMR spectrum of **L^4** in DMSO-d_6, in Bruker 300 MHz instrument.

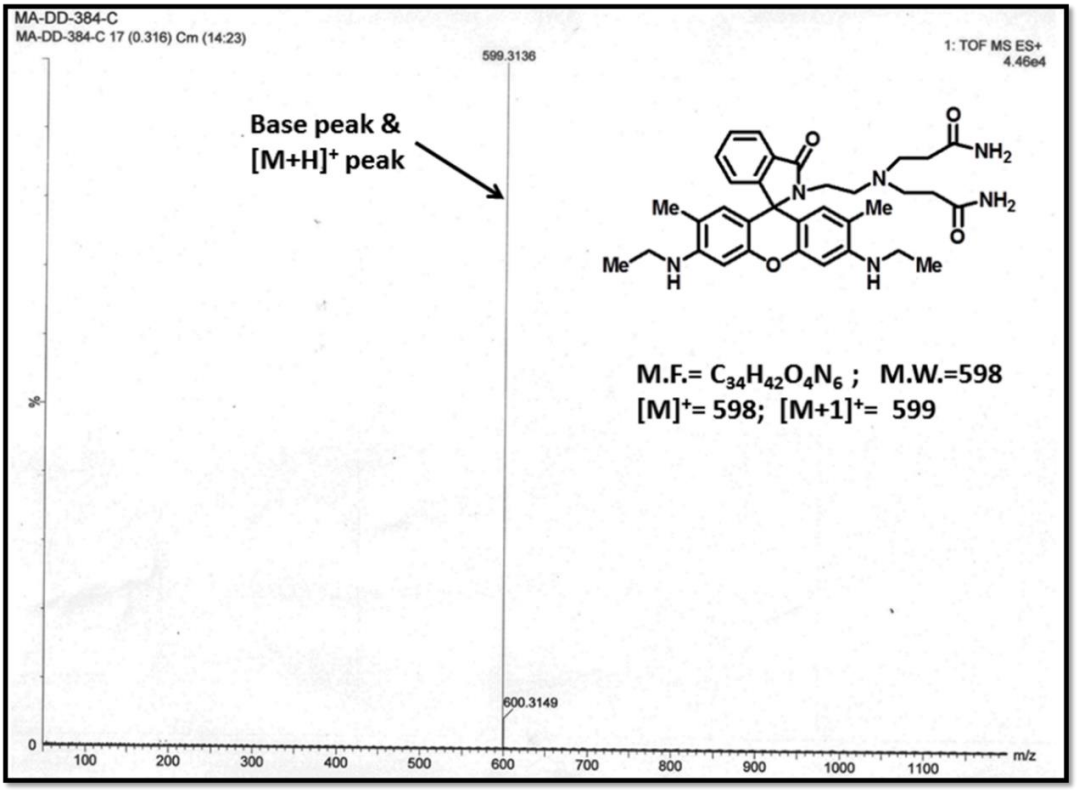

Figure-5.3: Mass spectrum of $\mathbf{L^4}$ in MeOH.

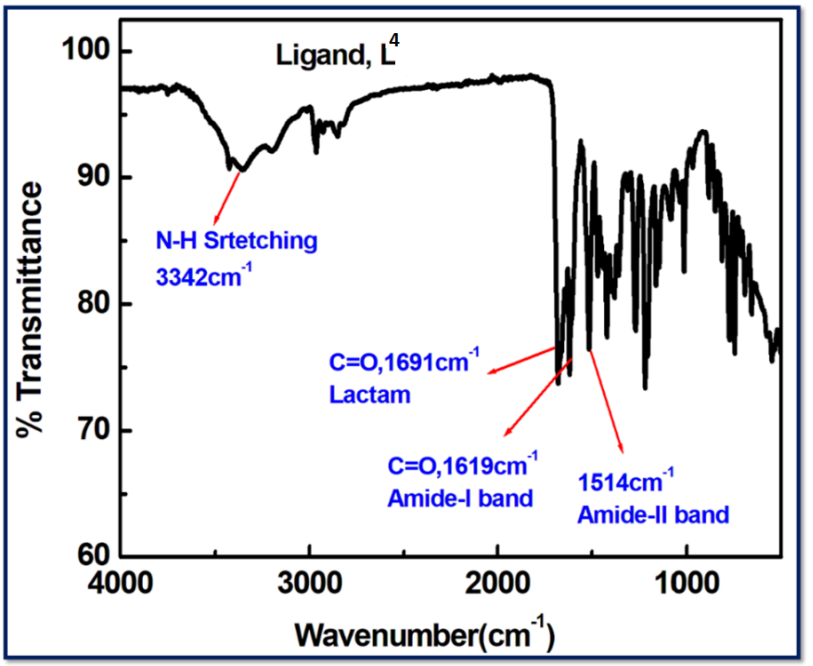

Figure-5.4: FT-IR spectrum of $\mathbf{L^4}$

5.3.1 UV-Vis Absorption studies

The UV-Vis spectrum of **L^4** (20 μM) recorded in completely aqueous solution (pH 7.2, 10 mM HEPES buffer) **L^4** showed a very weak band near 350 nm. Gradual addition of Fe^{3+} to a solution of **L^4** reveals that there was a development of two absorption peaks; one at 350 nm and enhancement of a more intense peak in the visible region at 530 nm (**Figure-5.5**) with the sharp visual colour change of the representative solution from colorless to reddish yellow indicating that closed spirolactam ring in absence of Fe^{3+} ion is now opened by the presence of Fe^{3+} which leads to the increase of chromophoric path length. In the presence of other trivalent metal ions like Al^{3+} and Cr^{3+} change of absorbance of the **L^4** solution was very insignificant as compared to Fe^{3+}. Whereas no such band appeared in the presence of other monovalent and divalent metal ion solutions. The appearance of this band clearly manifests the opening of spirolactam ring due to coordination of Fe^{3+} with **L^4**. The probable coordination mode of **L^4** towards Fe^{3+} is demonstrated in **Scheme 5.1**. UV-vis titration was carried out by varying trivalent metal ion, Fe^{3+}, concentration (0-230 μM) keeping the probe concentration fixed at 20 μM in H_2O, pH 7.2, 10 mM HEPES buffer. Plot of absorbance vs. [Fe^{3+}] (**Figure-5.5(b) inset**) yielded linear curve which was analyzed by linear curve-fitting of titration data according to Eqn. (1) (where a, b and c have usual meaning) under the conditions 1>> c*x with n = 1 giving linear relationship indicating 1:1 binding between **L^4** and Fe^{3+} with apparent association constant K_f values as (8.3±0.019) x $10^3 M^{-1}$ for Fe^{3+}.

$$\mathbf{y = (\mathit{a}+\mathit{b}*c*x^n)/(1+\mathit{c}*x^n),\ (1)}$$

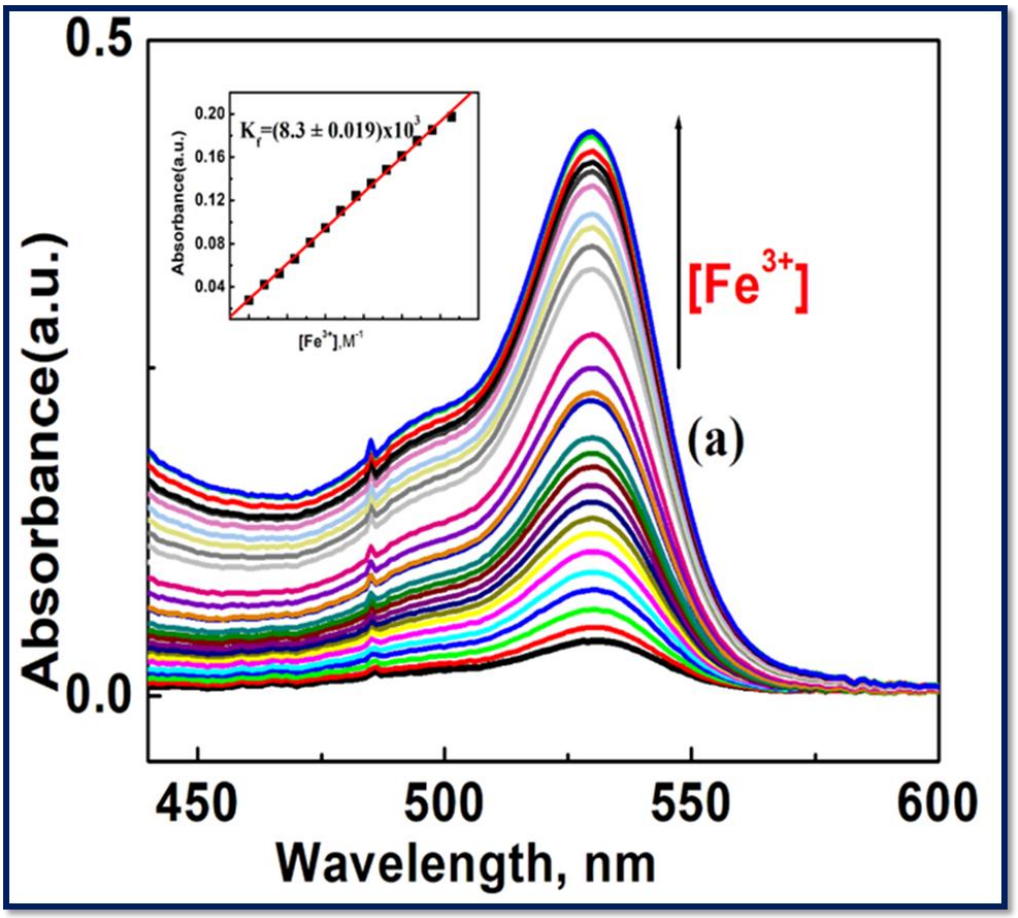

Figure-5.5: (a) UV-Vis absorption spectra of **L^4** (20 μM) in H_2O pH 7.2,10 mM HEPES buffer) solutions with the increase in concentration of Fe^{3+} solution (0-430 μM); (b) a linear fit of absorbance vs. [Fe^{3+}] plot.

5.3.2 Fluorescence studies

The emission spectra of **L^4** and its fluorescence titration with Fe^{3+} was performed in purely aqueous medium (pH 7.2, 10 mM HEPES buffer) with 20 μM fixed concentration of **L^4** at. A significant turn on fluorescence response was observed in the presence of Fe^{3+} and gradual enhancement of a maximum fluorescence intensity culminated at 551 nm. As for example, on gradual addition of Fe^{3+} (0-11.5 equivalent) to the non-fluorescent solution of **L^4**, a 14-fold enhancement in fluorescence intensity at 551 nm was noticed following excitation at 510 nm and the increase in fluorescence intensity attributed to the increase of conjugation in the xanthene moiety of the **L^4** which also suggests the opening of the spirolactam ring in **L^4** on coordination to the Fe^{3+} ion[50]

(**Figure-5.6**). A significant turn on fluorescence response was observed in the presence of Fe^{3+} and gradual enhancement of a maximum fluorescence intensity culminated at 551 nm. Same type of fluorescence titration of **L**^{4} with Al^{3+} and Cr^{3+} were carried out in purely aqueous medium (pH 7.2, 10 mM HEPES buffer) with the fixed concentration of **L**^{4} at 20 μM but no significant enhancement of fluorescence intensity was observed (**Figure-5.7** and **Figure-5.8**). Fascinatingly, this change was also accompanied with a naked-eye colour change from colorless to reddish-yellow after addition of Fe^{3+} indicating that the probe **L**^{4} is a highly sensitive colorimetric chemosensor for this trivalent metal cation (Fe^{3+}).

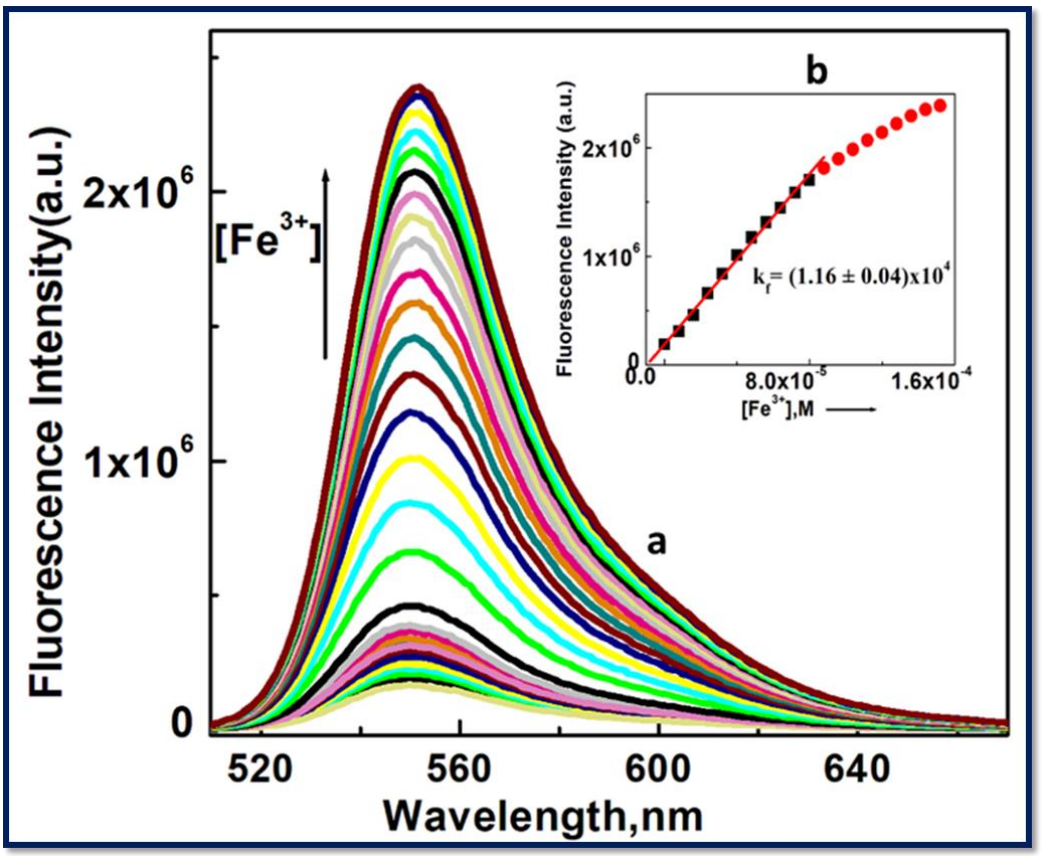

Figure-5.6: (a) Fluorescence spectra of **L**^{4} (20 μM) in H_2O (pH 7.2, 10 mM HEPES buffer) solution upon addition of Fe^{3+} (0-11.5 equivalent), each spectrum was taken after 3-4 minutes' interval of Fe^{3+}addition, λ_{ex}= 510nm, λ_{em}=551nm;(b) Linear curve fitting of titration curves with K_f values.

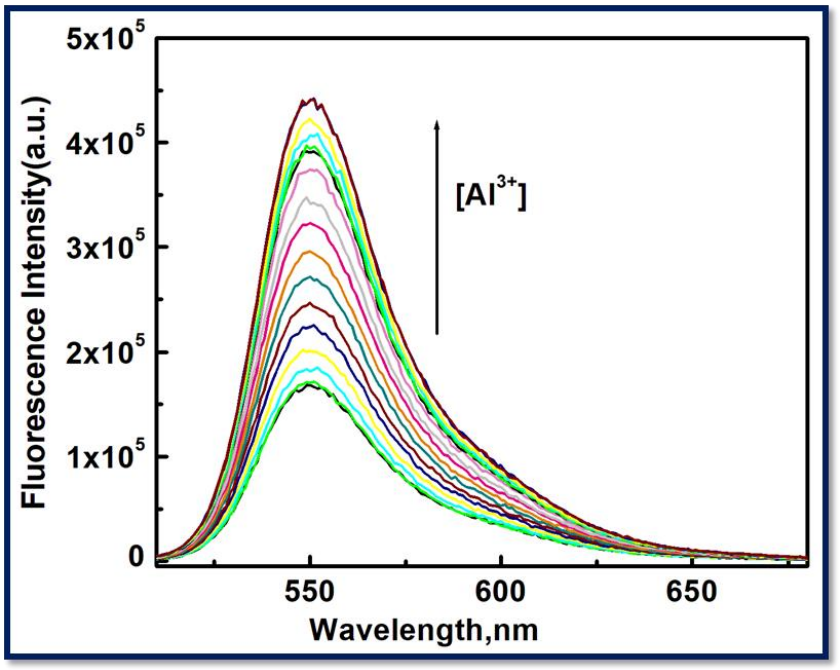

Figure-5.7: (a) Fluorescence spectra of $\mathbf{L^4}$ (20 μM) in H_2O (pH 7.2, 10 mM HEPES buffer) solution upon addition of Al^{3+} (0-6 equivalent), each spectrum was taken after 3-4-minute interval of Al^{3+}addition, λ_{ex}= 510nm, λ_{em}=551nm.

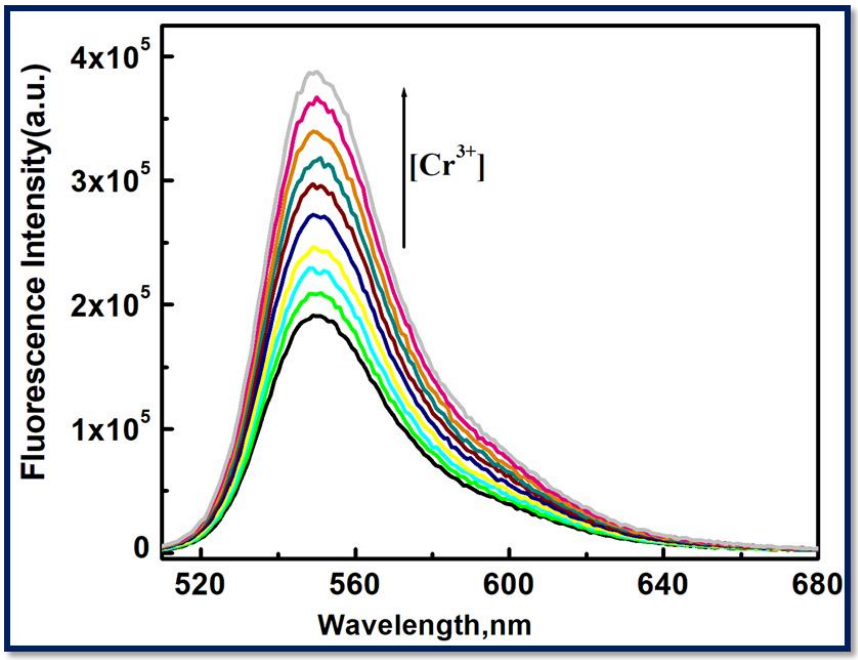

Figure-5.8: Fluorescence spectra of $\mathbf{L^4}$ (20 μM) in H_2O (pH 7.2, 10 mM HEPES buffer) solution upon addition of Cr^{3+} (0-4.0 equivalent), each spectrum was taken after 3-4-minutes interval of Cr^{3+}addition, λ_{ex}= 510 nm, λ_{em}=551nm.

Plots of **FI** vs. **[Fe^{3+}]** gives liner curve and linear curve-fitting of titration data according to Eqn. (1) (where a, b and c have usual meaning) gives apparent association constant K_f= (1.16 ± 0.04) x 10^4 M^{-1} for Fe^{3+}under the conditions 1>> c*x with n = 1 (Fig. 3 inset). There is an excellent agreement between the value of K_f obtained from absorption and fluorescence titration data manifesting the self-consistency of our results.

From the fluorescence data detection limit of the probe **L^4** for **Fe^{3+}** was evaluated to be 4.184 μM (**Figure-5.9**). These results surely reveals that the probe **L^4** is very much sensitive to detect a trace amount of Fe^{3+} in aqueous solution. In this context, we must highlight that quantum yield of the ligand (**L^4**) was very less. Quantum yields of **L^4**, [**L^4–Fe^{3+}**] complex in H_2O (pH 7.2 10 mM HEPES buffer) was found to be 0.013, 0.532 using Rhodamine-6G as standard. The higher value of quantum yields for the complex as compared to the free ligand **L^4** indicates that the stability of the complex in the excited states is higher.

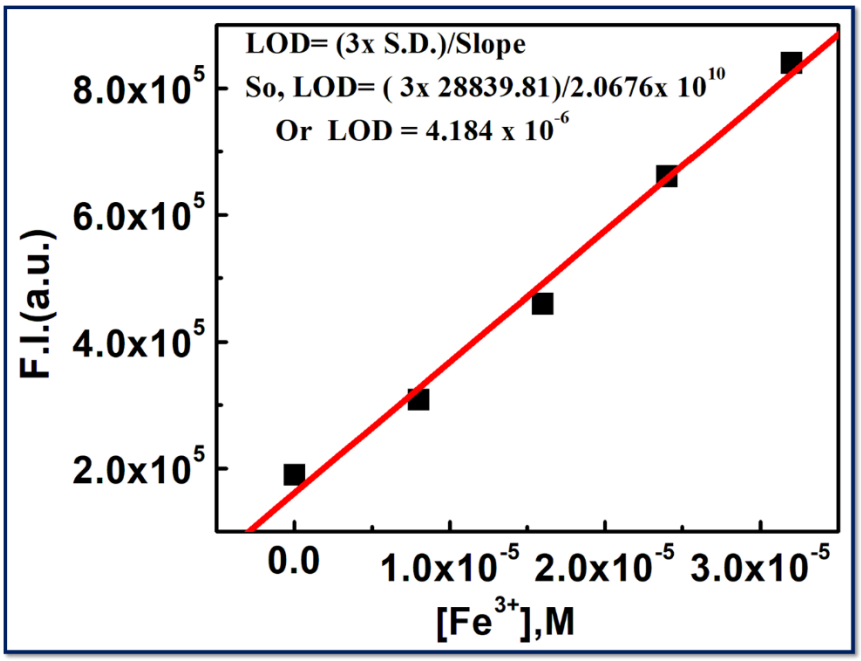

Figure-5.9: Linear dyanamic plot of FI (at 551nm) vs [Fe^{3+}] for the determination of S (slope) and LOD calculation.

The composition of the complex was supported by mass spectrometric analysis (m/z =413.09 [Fe(**L^4**) $(NO_3^-)_2(CH_3CN)_2$ (MeOH) $(H_2O)_2]^{2+}$); (**Figure-5.10**) and Job's method was again employed to determine the composition of the complex, which was found to be 1:1 (**Figure-5.11**)

Moreover, a conspicuous display of reddish–yellow fluorescence response of the probe upon interaction with Fe^{3+} provides the scope for naked eye detection of Fe^{3+} (**Figure-5.12 a**). The possibility of using chemosensor $\mathbf{L^4}$ in the development of paper test strips was examined and found that the turn-on fluorescence response of $\mathbf{L^4}$ towards Fe^{3+} is also visually detectable in test paper strips (**Figure-5.12b**).

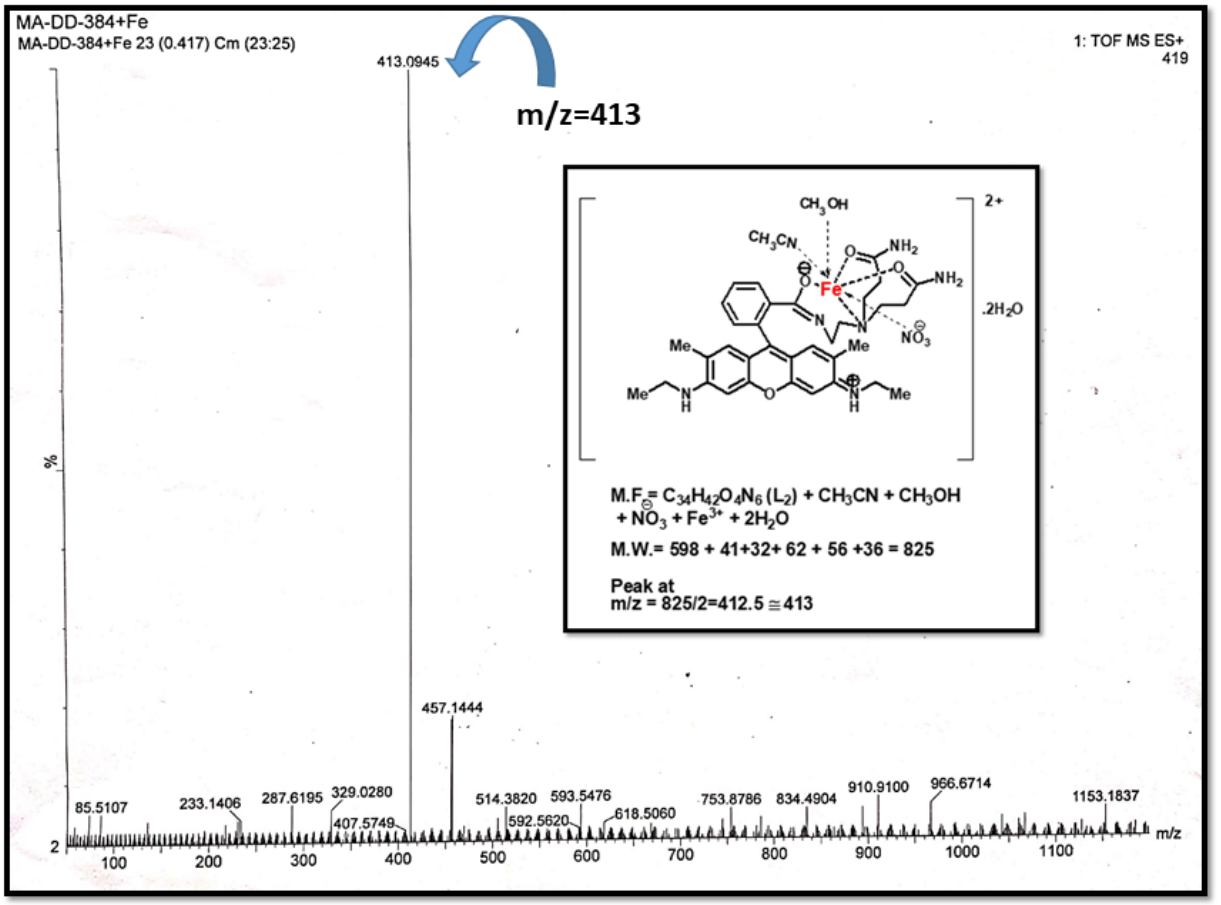

Figure-5.10: Mass spectroscopy of [$\mathbf{L^4}$ + Fe^{3+}] in mixed MeOH and MeCN.

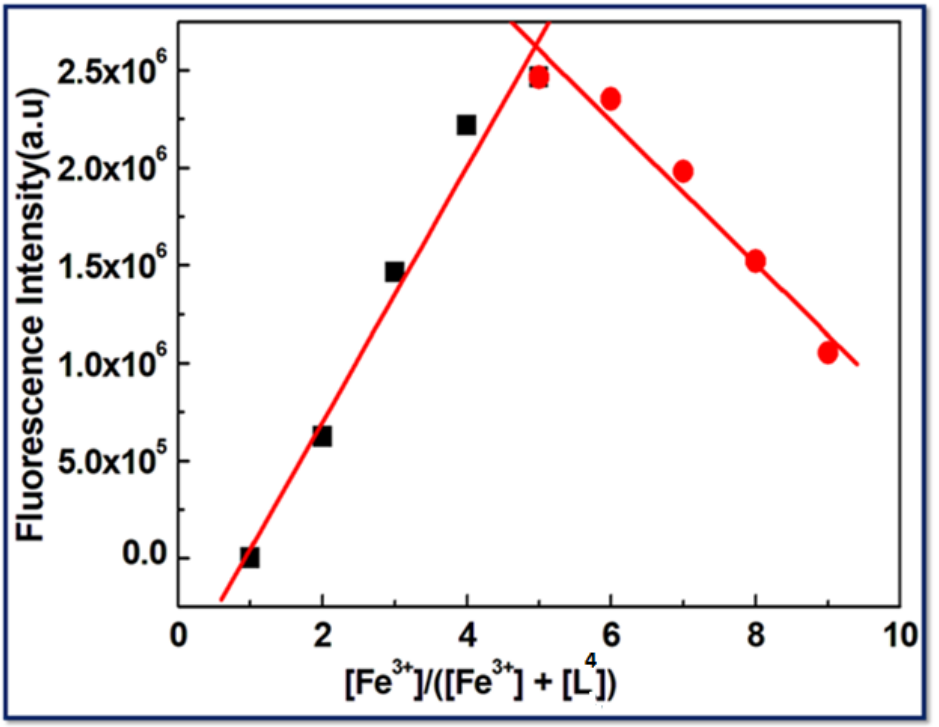

Figure-5.11: Job's plot between $\mathbf{L^4}$ and Fe^{3+} for the confirmation of (1:1) binding

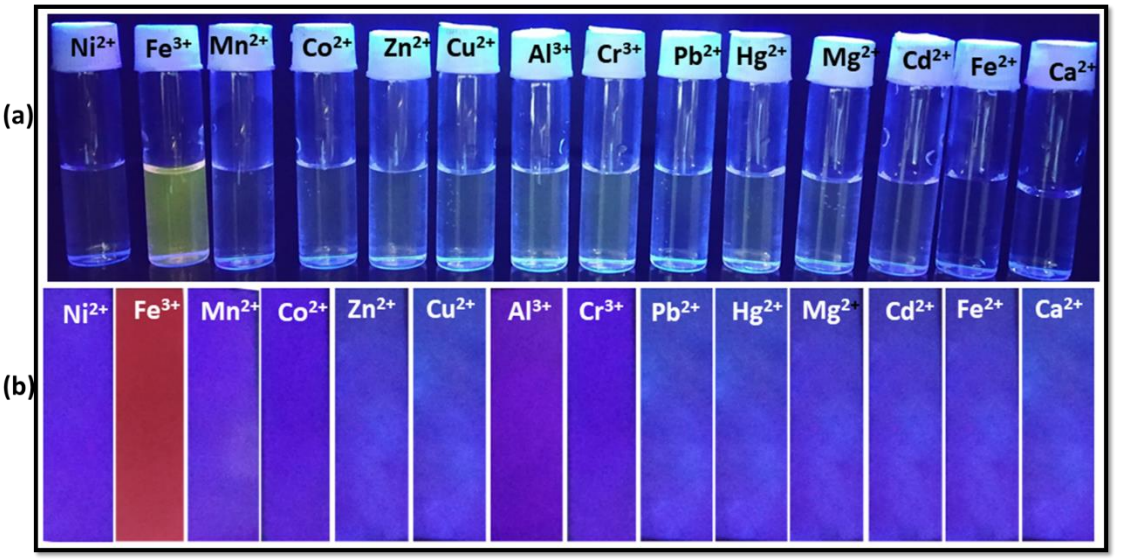

Figure-5.12: (a) Visual fluorescent response of $\mathbf{L^4}$ towards Fe^{3+} (under 365 nm UV light); (b) Paper strip for the fluorescent sensing of Fe^{3+} toward the probe $\mathbf{L^4}$.

5.3.3 Selectivity studies

To be excellent chemosensor selectivity for that chemosensor towards a particular cation is the most important and absolutely essential criteria. Experimental work for selectivity was performed in aqueous medium by taking 20 μM of probe **L^4** in a cuvette containing 2.5 mL of 10 mM buffer solution and then a particular metal ion solution of about 5.0 equivalent was added and then after allowing some time absorbance and fluorescence intensity was recorded for each solution. Similarly, experiment was done for many divalent and trivalent metal ions. Surprisingly, **L^4** could selectively recognize only a trivalent metal ion, Fe^{3+}, in aqueous medium over other biologically abundant divalent metal cations like Mn^{2+}, Fe^{2+}, Co^{2+}, Ni^{2+}, $Cu^{2+}$and Zn^{2+}, hazardous heavy metal ions like Pb^{2+}, Cd^{2+} and Hg^{2+}, alkali and alkaline earth metal ions like Na^{+}, K^{+}, Ca^{2+} and Mg^{2+}(**Figure-5.13**).

It was also found that not even a single anionic species among OAc^{-},HCO_3^{-}, CO_3^{2-}, $S_2O_3^{2-}$, SCN^{-}, N_3^{-}, NO_3^{-}, NO_2^{-}, $H_2PO_4^{-}$, SO_4^{2-},ClO_4^{-}, F^{-}, Cl^{-}, Br^{-}, I^{-}, PO_4^{3-} and CN^{-} could be able to enhance the fluorescence intensity of the probe **L^4** (**Figure-5.14**) but the fluorescence intensity of **[L^4 -** Fe^{3+}] complex was found to be selectively quenched in the presence CN^{-} ion (**Figure-5.15**).The excellent reversibility in OFF-ON fluorescence property of this probe **L^4** has been established through fluorescence study with the sequential addition of Fe^{3+} and CN^{-} ions into the solution of **L^4** containing 10 mM HEPES buffer in H_2O (pH 7.2) at room temperature (**Figure-5.16**). Addition of cyanide ion to the solution containing [**L^4**–Fe^{3+}] complex quenches the fluorescence emission of the probe with the disappearance of the fluorescent reddish -yellow color of the solution. The main reason for this kind of observation is that the interaction of Fe^{3+} with probe results in opening of spirolactam ring of the rhodamine 6G moiety of **L^4** and thereby causes a strong fluorescence. But after the addition of CN^{-} to that resulted fluorescent Fe^{3+} complex the fluoresce emission was found to quenched and the solution becomes colourless. This type of observation was witnessed after sequential addition of Fe^{3+} and CN- ion to the same soluton of **L^4**. This indicates that CN^{-} binds with the Fe^{3+} ion and due to strong affinity between them Fe^{3+} was forced to be removed from that complex. As a result, the spirolactam ring was reestablished that leads to the quenching of fluorescence. So it can be safely said that this probe **L^4** works in a reversible manner. The fluorescence quenching phenomenon of the [**L^4**-Fe^{3+}] complex with CN^{-} ion was confirmed by using HRMS study (**Figure-5.17**). From HRMS study it is confirmed that the ligand in its

regenerated ring closed structure after addition of CN- ion exactly same as that with the **L**^{4}. This reversibility test suggests the reusability of this chemosensor.

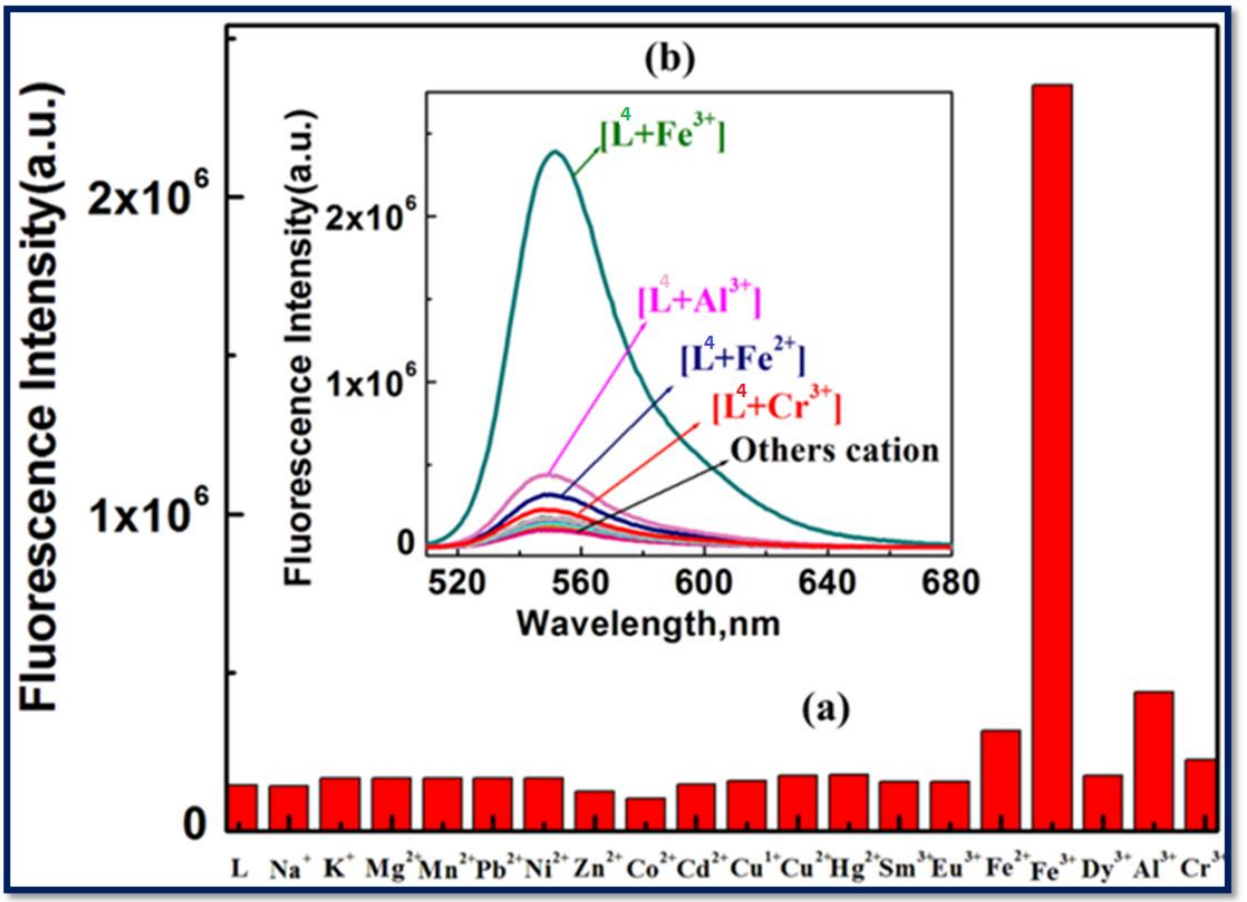

Figure-5.13: (a) Fluorescence bar diagram for the selective response of **L**^{4} (20 μM) towards Fe^{3+} over other mono and divalent metal ions in aqueous medium (pH=7.2, 10 mM HEPES buffer),λ_{ex} = 510 nm,λ_{em}=551 nm); (b) Fluorescence responce of **L**^{4} (20 μM) upon addition of 11.0 equivalent of Fe^{3+}.

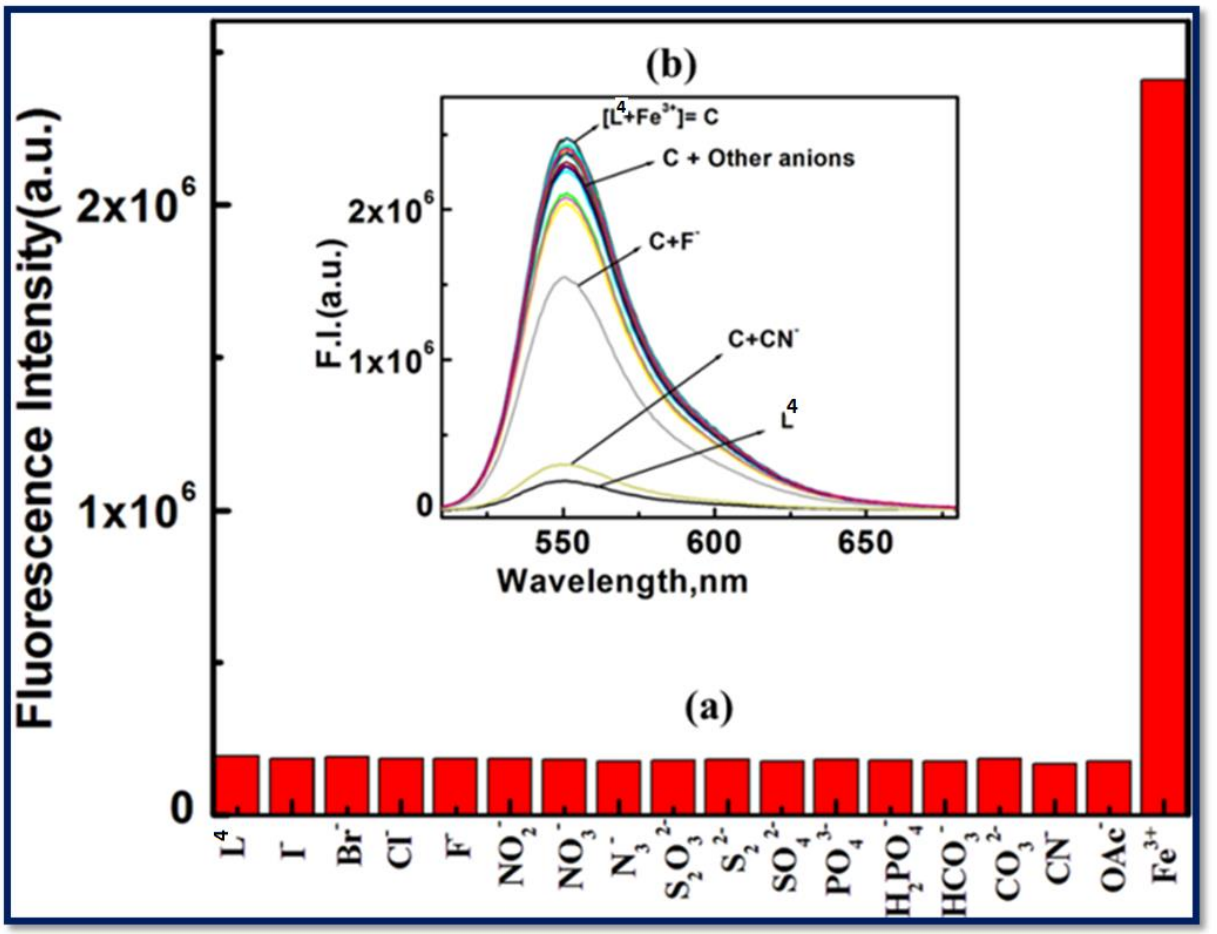

Figure-5.14: (a) Histogram of the fluorescence responses of different anions (100 μM) towards **L**^{4} (20 μM) in HEPES buffer at pH 7.2 with λ_{ex} = 510 nm, λ_{em} = 551 nm. (b) Fluorescence response of **L**^{4} towards Fe^{3+} with respect to different anions (100 μM).

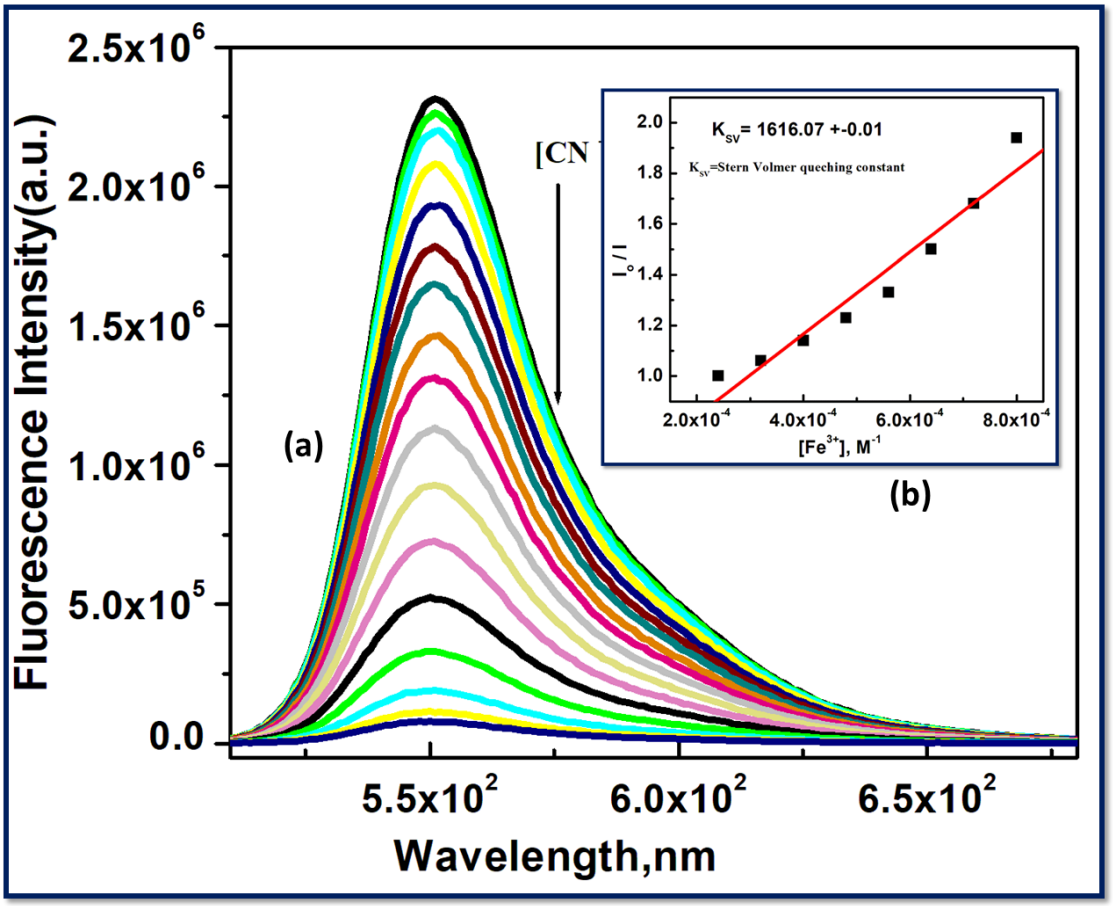

Figure-5.15: (a) Fluorescence quenching spectra of (**L^4–Fe^{3+}**) complex (20 μM) **L^4** in H_2O (pH 7.2, 10 mM HEPES buffer) and 11.5 eqivalents of Fe^{3+}] solution upon addition of CN^-, each spectrum was taken after 3-4 minutes' interval of CN^- addition, λ_{ex}= 510 nm, λ_{em}=551nm; (b) Linear Stern–Volmer plot for the titration of [**L^4–Fe^{3+}**] complexes with CN^-ion.

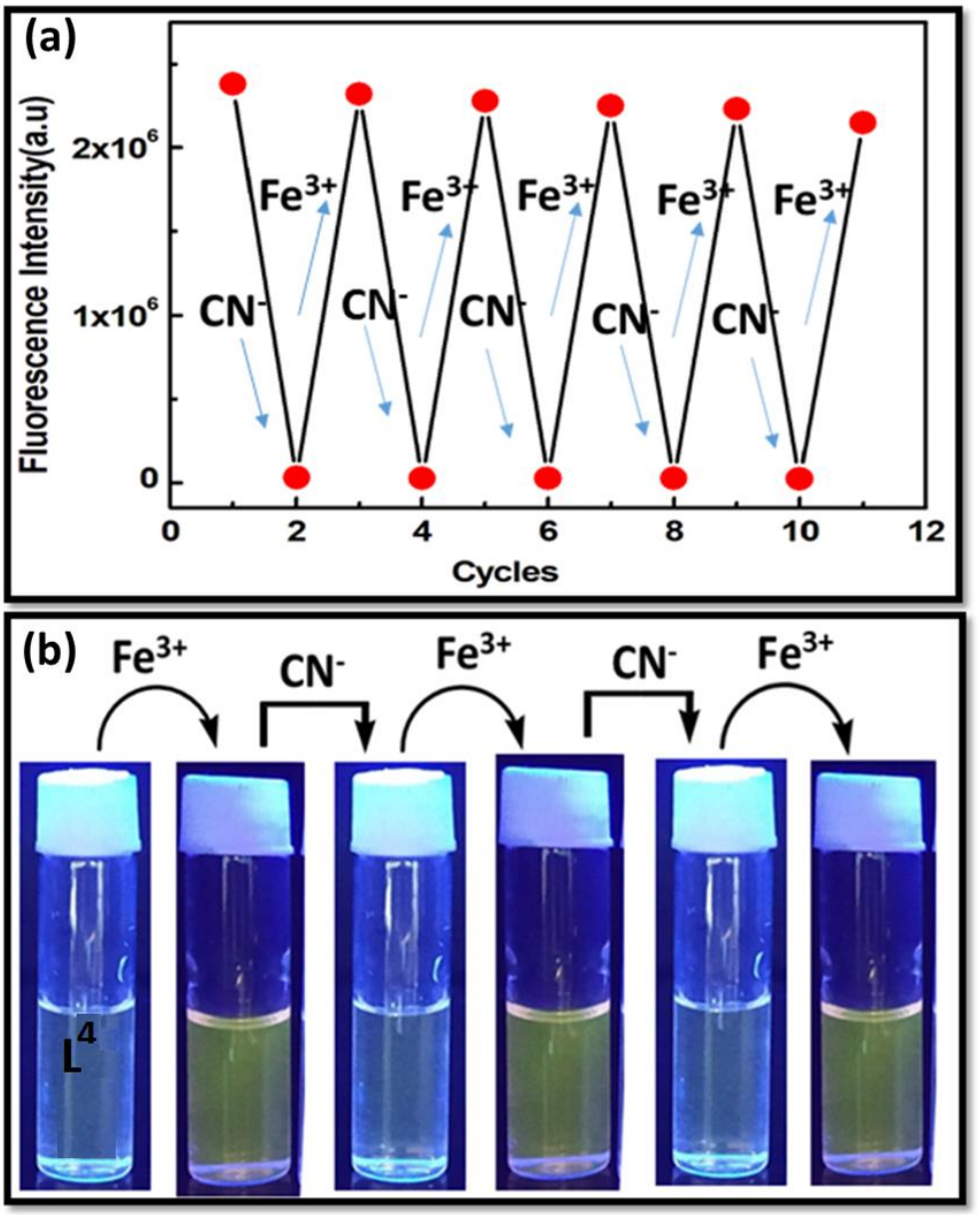

Figure-5.16: Fluorescence experiment to show the reversibility and reusability of the receptor for sensing Fe^{3+} by alternate addition of Fe^{3+} and CN^-. (a) Fluorescence intensity obtained during the titration of $\mathbf{L^4}$–Fe^{3+} with CN^- followed by the addition of Fe^{3+}. (b) Visual fluorescent color changes after each addition of CN^- and Fe^{3+} sequentially.

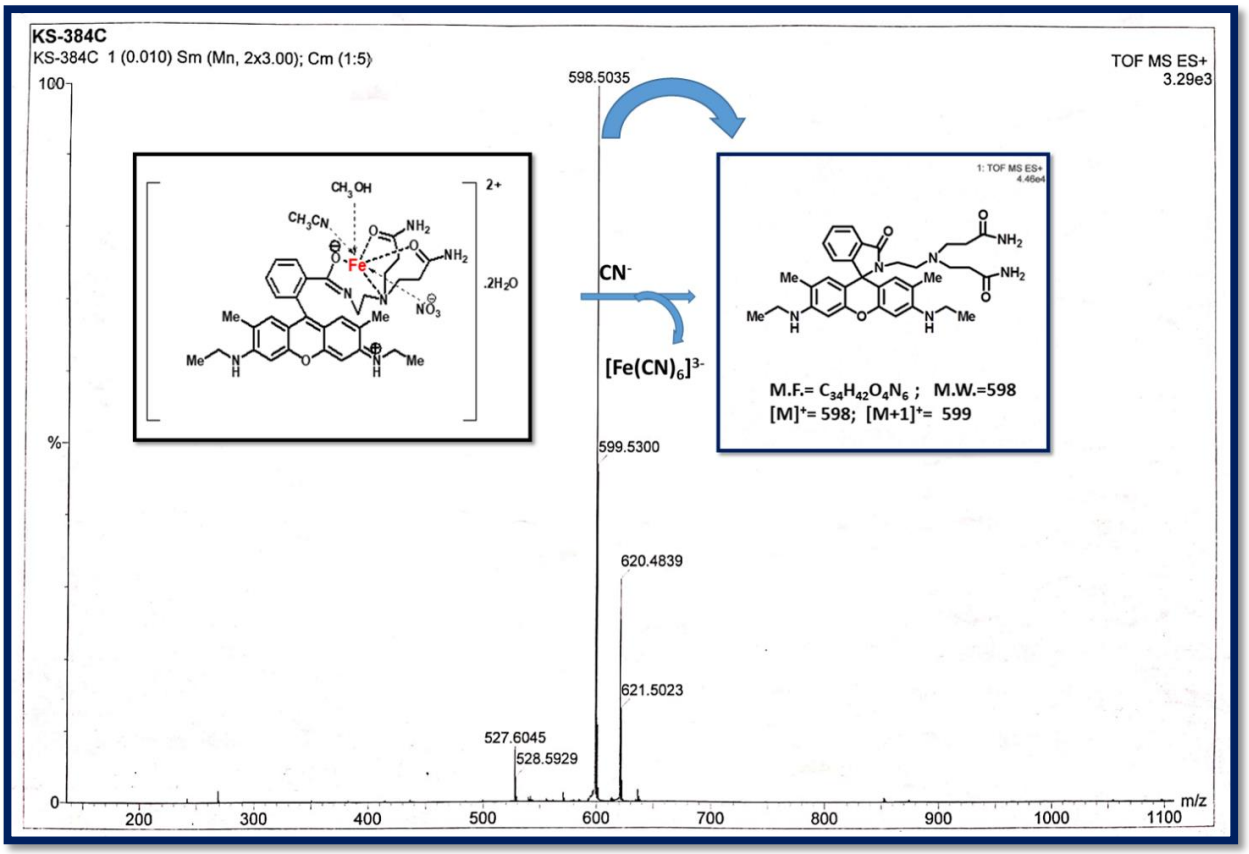

Figure-5.17: Mass spectrum of the [$\mathbf{L^4}$–Fe^{3+}] complex with cyanide in mixed MeOH and MeCN.

5.3.4 pH Studies

For practical application, the appropriate pH condition for the sensor was evaluated. At pH > 6.5 there is no fluorescence and the probe $\mathbf{L^4}$ solution is colourless. This suggests that probe is insensitive to pH higher than 6.5 and so spirolactam form of the probe prefers under such condition thereby satisfying the usefulness of the probe in physiological conditions over a wide pH range (6.5-8) for the detection of Fe^{3+} (**Figure-5.18**), However, on addition of 11.0 equivalents of Fe^{3+} at pH 3.0 the fluorescence intensity jumps to highest value and emission intensity of the complex gradually decreases on changing the pH from 3 to 6 but on further increase in pH the FI gradually falls sharply. At pH > 8 no fluorescence emission was found for the Fe^{3+} complex and that is due to the removal of Fe^{3+} may be through precipitation in the hydroxide form of this metal. So, this probe could act as very selective and sensitive fluorescent probe under biological condition.

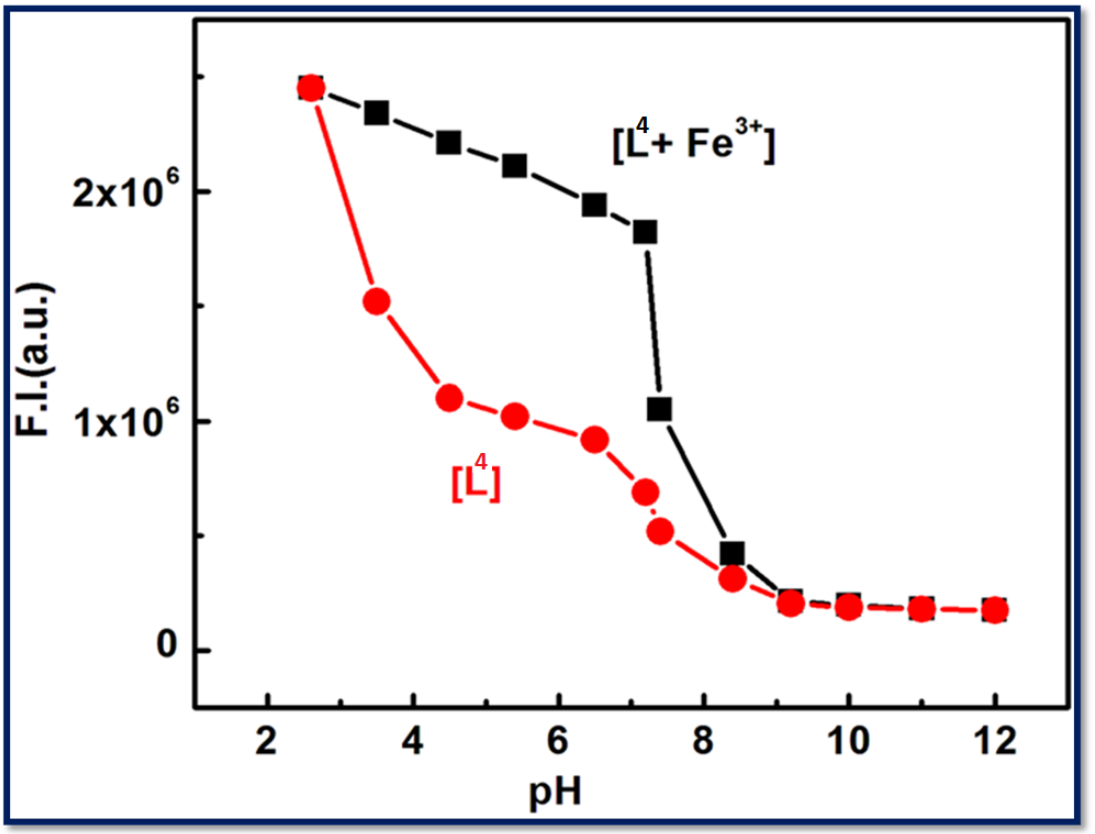

Figure-5.18: pH dependence of fluorescence responses of $\mathbf{L^4}$ and its $\mathbf{[L^4\text{-}Fe^{3+}]}$ complex.

5.3.5 Spectral studies

The main reason for showing fluorescent behavior by $\mathbf{L^4}$ in the presence of Fe^{3+} is Fe^{3+} the assisted spirolactam ring opening. The mechanistic route proposed for the formation of the $\mathbf{L^4}$–Fe^{3+} complex followed by the opening of spirolactam ring of the rhodamine moiety was established through IR and ^{1}H-NMR studies (**Figure-5.19**). The IR studies revealed that the characteristic stretching vibrational frequency of the aromatic N-H group of $\mathbf{L^4}$ showed at 3342 cm^{-1} and this IR band shifted to 3197cm^{-1} after the formation of Fe^{3+} complex. Broadening of the IR band for aromatic N-H group after complexation with Fe^{3+} also suggest that N-H proton becomes more exchangeable and N-H bond strength fluctuates constantly due to possession of positive charge on nitrogen atom and that proves the ring opening phenomenon. The IR peak at 1691cm^{-1} for the lactam amidic 'C=O' of the rhodamine moiety shifted to lower wavenumber, 1647cm^{-1}. This also

indicates weakening of the C=O bond strength and gets almost single bond character when ring opens up. The characteristic IR bands of an amide moiety are that Amide-I and Amide-II bands that appeared at at 1619 cm^{-1} and 1514 cm^{-1}. These two bands are shifted to 1606 cm^{-1} and 1288 cm^{-1} respectively with the broadening of the amide–II band upon binding with Fe^{3+}. These large shifts in IR frequencies signifies a strong polarization of the C=O and N-H bond upon efficient binding to the Fe^{3+} ion (**Figure-5.20**). The coordination mode of $\mathbf{L^4}$ towards Fe^{3+} was supported by HRMS studies (**Figure-5.11**). ^{1}H-NMR studies (**Figure-5.19**) also show that a down field shift of azomethine proton in $\mathbf{L^4}$, and broadening and shifting of the of the –NH proton from δ5.02 to δ5.34 arrises due to opening of the spirolactam ring and bearing a positive charge on it also confirms the formation of complex with Fe^{3+}.

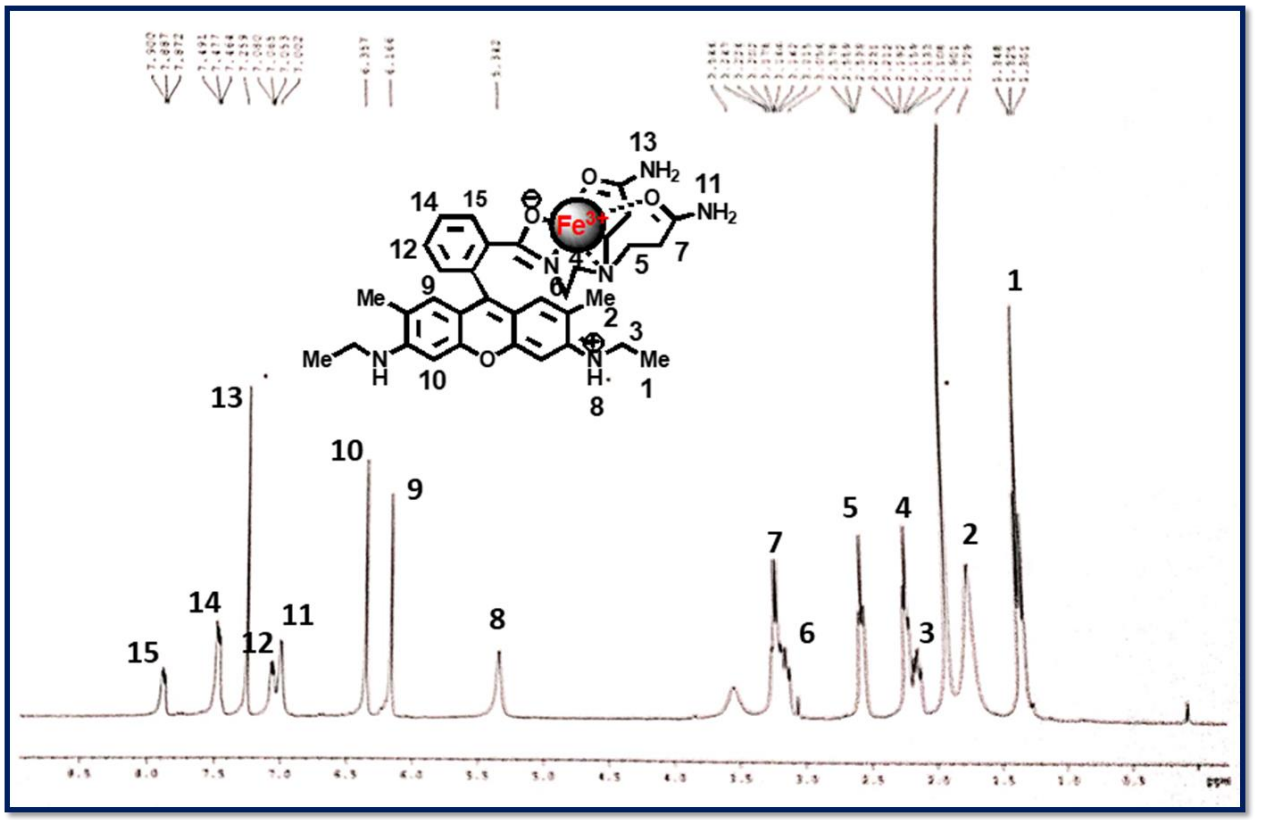

Figure-5.19: ^{1}H NMR spectrum of [$\mathbf{L^4}$ –$\mathbf{Fe^{3+}}$] complex in DMSO-d_6 solvent.

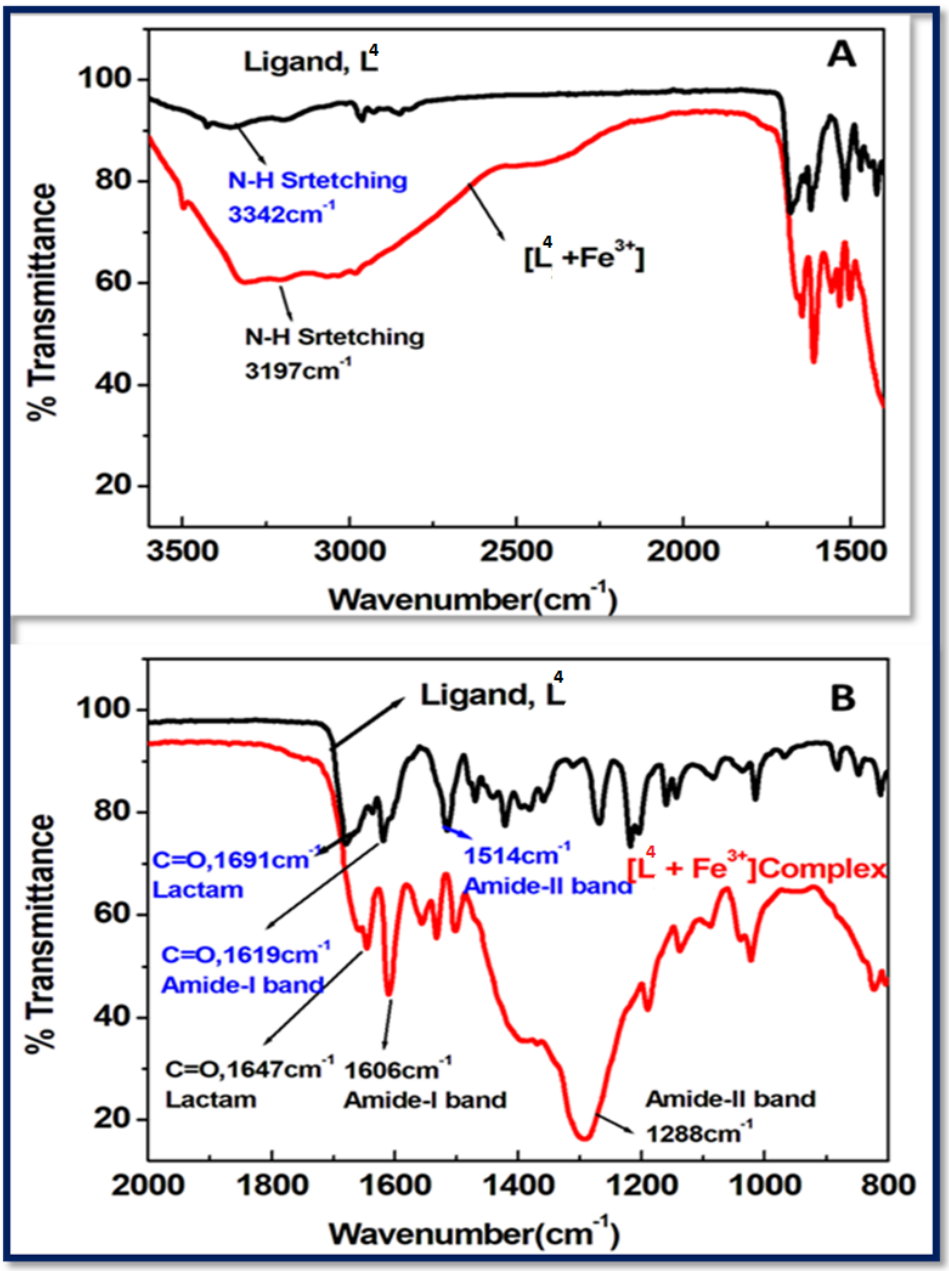

Figure-5.20: IR spectra of **(L^4) and** [L^4 **–**Fe^{3+}] complex in MeOH. (A) Shift of N-H band and (B) shift of Amide-I and Amide-II band on complexation.

5.3.6 Molecular logic operations

Based on the investigation the fluorescence ‘‘OFF’-ON” states of L^4 through controlled experiments some interesting chemistry related to multiple logic operations can be achieved with the sequential addition of inputs like Fe^{3+} and CN^- anion. The INHIBIT logic gate involves a particular combination of the LOGIC functions AND and NOT. For our system we can make a

correlation by taking two input signals, namely input 1 (Fe^{3+}) and input 2 (CN^-), along with fluorescence signal of the probe **L^4** (20 μm) at 551 nm as the output. The high value of emission intensity (>3.2 x 10^5, at 551 nm) has been designated as 1 (ON) and the low value (≤ 2 x 10^5) has been designated as 0 (OFF). In the absence of both the 1st input (Fe^{3+}) and 2nd input (CN^-), the emission intensity is low which indicates the OFF state. Whereas when only input 1 is present, then a significant enhancement of emission (at 551 nm) occours, indicating the 1 (ON) state, while, in the presence of input 2 only, the output emission value becomes very weak indicating OFF state. Therefore, it is necessary to apply NOT gate with Input 2. Additionally, it is interesting that **L^4** displays the emission output signal in such a way that it seems to understand the requirements of AND operation. In the presence of both inputs the output emission value is again low designating OFF state, in agreement with the Truth Table (**Figure-5.20(a)**). Thus, by sequential addition of these two inputs INHIBIT function logic gate can be achieved.

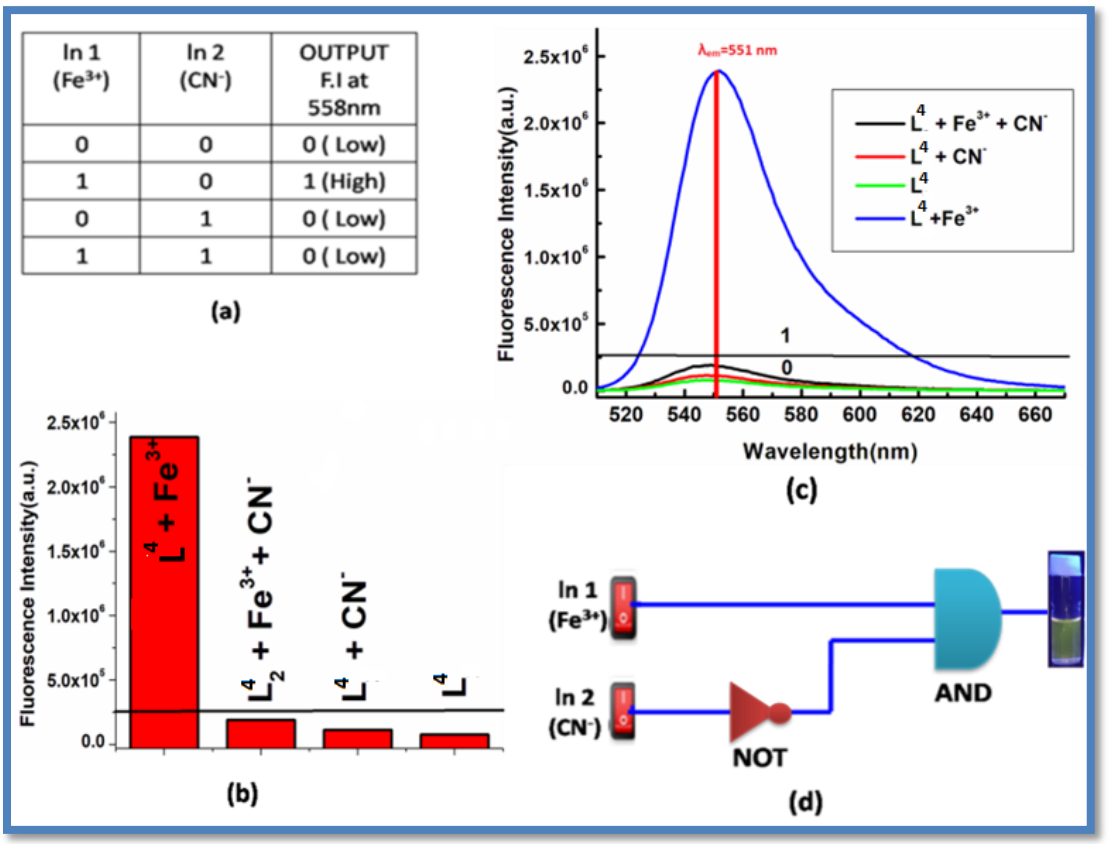

Figure-5.20: (a) Corresponding Truth Table of the logic gate; (b) corresponding bar diagram at 551 nm in the presence of different input; (c) output signals (at 551 nm) of the logic gate in the presence of different inputs; (d) general representation of an INHIBIT logic gate based circuit.

5.3.7 Molecular memory devices

Molecular memory devices are the data storage technologies that use molecular species as the data storage element and can be constructed by sequential logic circuits. One of the output signal acts as the input of the memory device and it is memorized as a "memory element". So by using binary logic function we have developed a sequential logic circuit which shows "Write –Read –Erase−Read" property. For our system, we have chosen strong emission output at 551 nm as ON state (1) and weak emission output as OFF state (0). Now to construct this memory device, we have chosen two inputs Fe^{3+} and $CN^{-}$for the SET and RESET processes, respectively. In this memory function, the system writes when it gets input A (Fe^{3+}) i.e. high emission value and it memorizes binary number 1. But in the presence of input B (CN^{-}), which is a reset input, erases the data and then memorize the binary number 0 (**Figure-5.21**). The properties of the material allow for a much greater capacitance per unit area than with conventional DRAM (Dynamic random-access memory), thus potentially leading to smaller and cheaper integrated circuits. The most important thing is that this write-erase-write cycles could be repeated many times (**Figure-5.16(a)**) using the same concentration of the system with negligible change in emission intensity.

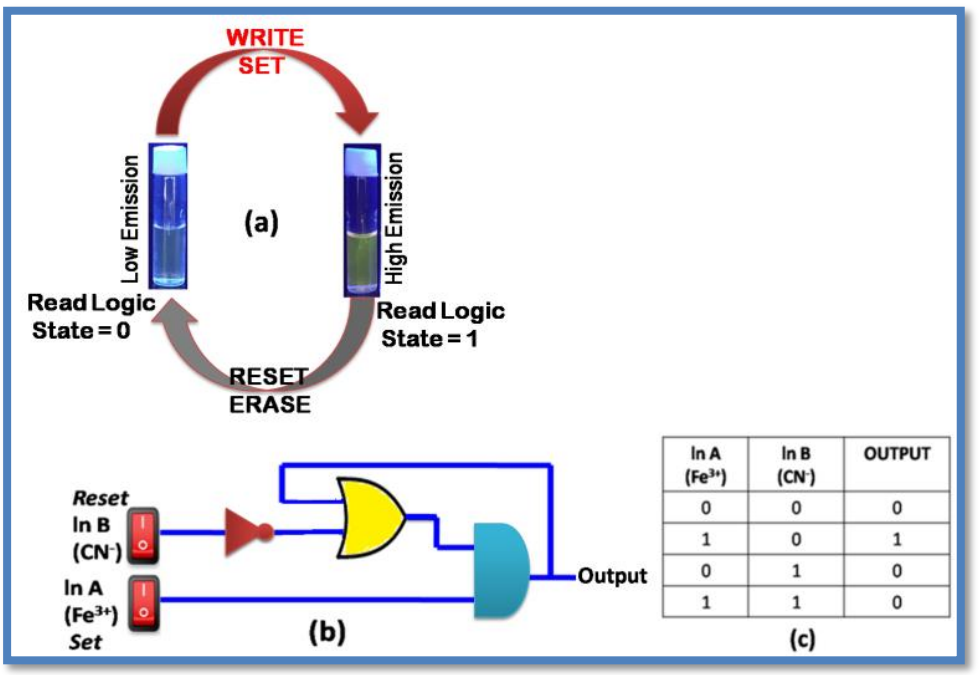

Figure-5.21: (a) Schematic demonstration of the reversible logic operation for the memory element with "write−read−erase−read" kind of behaviour. (b) Sequential logic circuit showing memory unit with two inputs (In A and In B) and one output and (c) corresponding truth table.

5.4 Conclusion

In summary, we have successfully synthesized a new biocompatible chromogenic and fluorogenic probe **L^4** derived from rhodamine-6G which showed a selective colorometric as well as "turn-on" fluorescence response towards Fe^{3+} ion over mono, divalent and other trivalent metal ions. Complete aquea friendliness of this probe has drawn special attention over other rhodamine 6G based chemosensors. A large enhancement of fluorescence intensity of **L^4** (14 fold) was found to be observed in the presence of Fe^{3+} in aqueous medium (HEPES buffer at pH 7.2) with the development of reddish yellow colour which clearly indicate that this probe **L^4** can be used for the detection of Fe^{3+} through naked eye. The`K_f value was evaluated to be (1.16 ± 0.04) x 10^4 M^{-1} from the fluorescence titration data at systematic increasing concentration of metal ions and fixed concentration of ligand, 20 μM. The higher values of quantum yields (0.523) for [**L^4**–Fe^{3+}] over the free ligand (0.013) indicate the higher stability of the complex in the excited states. Job's plot confirms 1:1 stoichiometric complexation Fe^{3+} with **L^4**. An excellent reversible fluorescence 'OFF-ON' property of **L^4** has been observed through fluorescence study with the alternate addition of Fe^{3+} and CN^- ions at room temperature which suggests the reusability of this chemosensor. The detection limit of **L^4** for Fe^{3+} evaluated to be 4.184 μM and this make the probe to have potential application in real water samples for Fe^{3+} ion detection. Suitably large increase in fluorescence intensity of **L^4** upon complexation with Fe^{3+}.

References

1. M. Ghaedi, A. Shokrollahi, R. Mehrnoosh, O. Hossaini, M. Soylak, Cent. Eur. J. Chem., **2008**,6, 488.
2. S. Bae, J. Tae, Tetrahedron Lett., **2007**, 48, 5389.
3 Y. Chen, P. Barak, Adv. Agron., **1982**,35, 217.
4. R. Crichton, and J.R. Boelaert. Inorganic biochemistry of iron metabolism: from molecular mechanisms to clinical consequences. John Wiley & Sons, **2001**.
5. K. P. Carter, A. M. Young and A. E. Palmer, Chem. Rev., **2014**,114, 4564.

6. X. Chen, T. Pradhan, F. Wang, J. S. Kim and J. Yoon, Chem. Rev., **2012**, 112, 1910.
7. J. Du, M. Hu, J. Fan and X. Peng, Chem. Soc. Rev., **2012**, 41,4511.
8. Papanikolaou and K. Pantopoulos, Toxicol. Appl. Pharmacol., **2005**, 202, 199.
9. T. A. Rouault and W. H. Tong, Trends Genet., **2008**, 24, 398.
10. M. Andjelkovic, J. Vancamp, B. Demeulenaer, G. Depaemelaere, C. Socaciu, M. Verloo and R. Verhe, Food Chem., **2006**, 98, 23.
11. T. Ganz, Blood, **2003**, 102, 783.
12. K. D. Welch, T. Z. Davis and S. D. Aust, Arch. Biochem. Biophys., **2002**, 397, 360.
13. S. Ray, A. G. Shard, Quantitative Analysis of Adsorbed Proteins by X-ray Photoelectron Spectroscopy. Analytical Chemistry, **2011**, 83(22), 8659.
14. J. R. Lakowicz, Principles of Fluorescence Spectroscopy. Kluwer Academic / Plenum Publishers,**1999**.
15. R.J.C. Brown, M.J.T. Milton, Trends in Analytical Chemistry, **2005**, 24, 266.
16. M. Bıngöl, G. Yentür, Er B, A.B. Öktem, Czech Journal of Food Sciences **2010**, 28, 213.
17. S. Gupta, P. Pandotra, A.P. Gupta, J.K. Dhar, G.R. Sharma, Y.S. Bedi, Food Chem Toxicol, **2012**,48, 2966.
18. D.A. Leigh, M.A.F. Morales, E.M. Perez, J.K.Y. Wong, C.G. Saiz, A.M.Z. Slawin, A.J. Carmichael, D.M. Haddleton, A.M. Brouwer, W.J. Buma, W.H. Wurpel, S. Leon, F. Zerbetto, Angew. Chem. Int. Ed. **2005**, 117, 3122.
19. A.P. de Silva, H.Q.N. Gunaratne, T. Gunnlaugsson, A.J.M. Huxley, C.P. McCoy, J.T. Rademacher, T.E. Rice, Chem. Rev.**1997**,97, 1515.
20. T. Gunnlaugsson, J. P Leonard. &, N. S. Murray. Org. Lett.**2004**, 6, 1557.
21. M. Royzen, Z. Dai, J. W. Canary, J. Am. Chem. Soc. **2005**,127, 1612.
22. R. Krämer, Angew. Chem., Int. Ed. **1998**,37, 772.
23. P. J. Jiang. & Z. J. Guo, Coord. Chem. Rev., **2004**, 248, 205.
24. L Zeng. E. W. Miller, A. Pralle, E. Y. Isacoff. &, C. J. Chang, J. Am. Chem. Soc. **2006**,128, 10.
25. Y. Xiang. &, A. Tong, Org. Lett. **2006**, 8, 1549.

26. J. L Bricks, et al. J. Am. Chem. Soc. **2005**,127, 13522.
27. M. Zhang. et. al. Tetrahedron Lett. **2007**, 48, 3709.
28. J. L Bricks. et al. J. Am. Chem. Soc. ,**2005**,127, 13522.
29. G. E. Tumambac, C. M Rosencrance. & C. Wolf, Tetrahedron, **2004**, 60, 11293.
30. Ma, L., Luo, W., Quinn, P. J., Liu, Z. & Hider, R. C. J. Med. Chem., **2004**, 47, 6349.
31. H. Weizman. et al. J. Am. Chem. Soc.,**1996**, 118, 12368.
32. H.N. Kim, M.H. Lee, H.J. Kim, J.S. Kim, J.Y. Yoon Chem Soc Rev., **2008**, 37, 1465.
33. M. Beija, C.A.M. Afonso, J.M.G. Martinho, Chem Soc Rev., **2009**, **38**, 2410.
34. X.Q. Chen, T. Pradhan, F. Wang, J.S. Kim, J.Y. Yoon, Chem Rev., **2012**, 112, 3, 1910.
35. S.K. Ko, Y.K. Yang, J. Tae, I. Shin, J Am Chem Soc., **2006**, 128, 43, 14150.
36. A. Chatterjee, M, Santra, N. Won, S. Kim, J.K. Kim, S.B. Kim, K.H. Ahn, J Am Chem Soc.,**2009**, 131(6):2040.
37. a) V. Balzani, A. Credi, F. M. Raymo and J. F. Stoddart, Angew. Chem., 39(19):3348. b) J. Andrasson and U. Pischel, Chem. Soc. Rev., 2010,**39**, 174; c) K. Szacilowski, Chem. Rev., 2008, 108, 9, 3481; d) D. Margulies, G. Melman and A. Shanzer, J. Am. Chem. Soc., **2006**, 128, 14, 4865.
38. a) A. P. de Silva, H. Q. N. Gunaratne and C. P. McCoy, Nature, **1993**, 364, 42; b) M. N. Stojanovic, T. E. Mitchell and D. Stefanovic, J. Am. Chem. Soc., **2002**, 124, 14, 3555; c) X. Guo, D. Zhang, T. Wang and D. Zhu, Chem. Commun., **2003**, 914-915; d) D. Zhang, J. Su, X. Ma and H. Tian, Tetrahedron, **2008**, 64, 8515;e) M. Kumar, R. Kumar and V. Bhalla, Tetrahedron Lett., **2010**, 51: 5559; f) M. Kumar, R. Kumar and V. Bhalla, Chem. Commun., **2009**, 7384; g) M. Kumar, A. Dhir and V. Bhalla, Org. Lett., 2009, 11, 2567; h) X. Meng, W. Zhu, Q. Zhang, Y. Feng, W. Tan and H. Tian, J. Phys. Chem. B, **2008**, 112, 15636; i) Z. Dong, X. Tian, Y. Chen, J. Hou and J. Ma, RSC Adv., **2013**, **3**, 2227.
39. H. A. Molla, R. Bhowmick, A. Katarkar, K. Chaudhuri, S. Gangopadhyay and M. Ali, Anal. Methods, **2015**, 7,5149.
40. Y. Xiang and A. Tong, Org. Lett., **2006**, 8, 1549.

Highlights of The Thesis

The research work presented in the thesis entitled **''Design and Synthesis of Rhodamine-6G Based Highly Selective Fluorescent Probes for The Metal Ion Sensing"**

I have incorporated my research work in this thesis. I have developed and reported some new and simple fluorescent molecular probes (**L^1, L^2, L^3 and L^4**) which are extremely sensitive, highly selective, bio-compatible and reusable with minimum toxicity for the recognition of cations in mixed organo- aqueous medium and sometimes in pure aqueous medium. Different spectroscopic techniques like ^{1}H NMR, Mass, UV−Vis, FTIR have been utilized to characterize the probes and their metal complexes.

Thesis consists of five chapters which are summarized below-

Chapter-1 focuses on brief introduction of chemosensing method and its need for the detection of biologically important and toxic metal ions fluorometrically over conventional methods. Discussion on different chemosensing pathways with mechanism through diagrammatic presentation are given here. Designing and development strategies of a suitable and efficient chemosensor are also explained in this chapter. Literature survey on different molecular probes for the recognition of metal ions like Chromium, Iron, Aluminium, Zinc, Mercury, Lead and Cupper based on Rhodamine -6G moiety as a core part of the chemosensing ligands are reported briefly. A very brief overview of the present work is highlighted in this chapter.

Chapter-2 presents development of a new rhodamine 6G based chemosensor (**L^1**), which is characterized through spectroscopic studies and by single-crystal X-ray crystallographic study. Excellent selectivity and sensitivity of **L^1** for Fe^{3+}, Al^{3+} and Cr^{3+} having absorption at 530 nm and emission at 558nm with large enhancement of the fluorescence intensity for Fe^{3+} (41-fold), Al^{3+} (31-fold) and Cr^{3+} (26-fold) upon the addition of 3.0 equivalent of these metal ions into the probe in H_2O/CH_3CN (4: 1, v/v, pH 7.2) along with naked eyes colour change from colourless to orange-

red colour are explained graphically. The K_f -values are evaluated and reported as- 9.4×10^3 M^{-1} (Fe^{3+}), 1.34×10^4 M^{-1} (Al^{3+}) and 8.7×10^3 M^{-1} (Cr^{3+}). Quantum yields of $\mathbf{L^1}$, [$\mathbf{L^1}$–Fe^{3+}], [$\mathbf{L^1}$–Al^{3+}] and [$\mathbf{L^1}$–Cr^{3+}] complexes (0.012, 0.489, 0.376 and 0.310) in H_2O/CH_3CN (4: 1, v/v, pH 7.2) using rhodamine-6G as standard are given. LODs for Fe^{3+}, Al^{3+} and Cr^{3+} are determined by 3σ methods and found to be 1.28, 1.34 and 2.28 μM, respectively. Cyanide ion scavenges Fe^{3+} from the [Fe^{3+}–$\mathbf{L^1}$] complex and quenches its fluorescence via its ring-closed spirolactam form. Advanced level molecular logic devices using different inputs (2 and 4 inputs) as advanced level logic gates and memory devices have been constructed.

Chapter-3 describes synthesis, characterisation and photophysical studies of rhodamine-6G based chemosensor, $\mathbf{L^2}$. This probe, $\mathbf{L^2}$ selectively recognizes Hg^{2+} and Al^{3+} ions in presence of all other biologically relevant and toxic heavy metal ions. This probe shows maximum absorption at 528nm and emission at 558nm with 126-fold enhancement of fluorescence intensity. Formation constant are reported as- $K_f = (1.01\pm0.01) \times 10^4$ M^{-1} for Hg^{2+} and $K_f = (1.45\pm 0.02) \times 10^4$ M^{-1} for Al^{3+}.This probe shows low detection limit (47 nM) for Hg^{2+} along with cell permeability and negligible cytotoxicity. SEM study reveals rod-like microstructure of $\mathbf{L^2}$ in water, which changes to a porous microstructure in the presence of Hg^{2+}. In this chapter it is shown that fluorescence quenching of Al^{3+} complex occurs on increasing the SDS concentration, while a ~33-fold enhancement of fluorescence intensity of [$\mathbf{L^2}$-$\mathbf{Hg^{2+}}$] complex was observed in presence of SDS, making the prove selective towards Hg^{2+} over Al^{3+} in the aqueous SDS medium. In SDS/water system, fluorescence intensity increases and reaches to maximum at ~7 mM of SDS and then fluorescence intensity decreases gradually with increase in [SDS] up to 28 mM.

Chapter-4 presents synthesis, characterisation and photophysical studies of rhodamine-6G based chemosensor, $\mathbf{L^3}$. It's excellent selectivity and sensitivity through **CHEF** based recognition of trivalent metal ions M^{3+} (M= Fe, Al, and Cr) over mono-valent, di-valent and other trivalent metal ions are presented graphically. It ($\mathbf{L^3}$) shows prominent enhancement in absorption at 528nm and fluorescence emission at 558nm for Fe^{3+} (669 fold), Al^{3+} (653 fold) and Cr^{3+} (667 fold) upon addition of 2.6 equivalent of these metal ions into the probe in H_2O/CH_3CN (7:3, v/v, pH 7.2). The corresponding K_d values of the complexes are reported as- 1.94×10^{-5} M^{-1} (Fe^{3+}); 3.15×10^{-5} M^{-1}(Al^{3+}) and 2.26×10^{-5} M^{-1}(Cr^{3+}). Quantum yields of $\mathbf{L^3}$, [$\mathbf{L^3}$—Fe^{3+}], [$\mathbf{L^3}$—Al^{3+}] and [$\mathbf{L^3}$—Cr^{3+}] complexes in H_2O/CH_3CN (7:3, v/v, pH 7.2) are calculated and given as 0.0005, 0.335, 0.327,

0.333 respectively using Rhodamine-6G as standard. LOD's for Fe^{3+}, Al^{3+} and Cr^{3+} are found to be 2.57, 0.78 and 0.47 μM respectively. Cyanide ion snatches Fe^{3+} from [Fe^{3+}-**L^3**] complex and quenches its fluorescence via its ring closed spirolactam form. Advanced level molecular logic devices using different inputs (2 and 4 input) and memory device have been constructed.

Chapter-5 presents synthesis and characterisation of a novel rhodamine-6G based chromo and fluorogenic "OFF-ON" biocompatible chemosensor **L^4.** It exhibits an excellent selectivity and high sensitivity for the detection of Fe^{3+} in absolute aqueous medium over and other metal ions. Enhancement of fluorescence intensity of the probe **L^4** is found to be 14 fold at 551nm upon addition of the Fe^{3+} into the probe in H_2O (pH 7.2, 10 mM HEPES buffer) with colour change from colourless to reddish yellow which makes it suitable for naked eyes detection. The corresponding K_f values are evaluated to be (1.16 ± 0.04) x 10^4 M^{-1} for the 1:1 stoichiometric binding between **L^4** and Fe^{3+}.Quantum yields of **L^4** and [**L^4**—Fe^{3+}] complex in H_2O (pH 7.2, 10 mM HEPES buffer) are found to be 0.013, 0.523 respectively using Rhodamine-6G as standard. LOD of **L^4** for Fe^{3+} in aqueous medium was calculated and reported as 4.184 μM. Cyanide ion scavanges Fe^{3+} ion from [**Fe^{3+}-L^4**] complex and quenches its fluorescence emission with the re-attainment of the non-fluorescent spirolactam ring form of the probe is shown.

List of Publications

1. **A novel copper(II) complex as a nitric oxide turn-on fluorosensor: intracellular applications and DFT calculation.**

   Rabiul Alam, Tarun Mistri, Pallab Mondal, **Dipankar Das**, Sushil Kumar Mandal, Anisur Rahman Khuda-Bukhsh and Mahammad Ali, Dalton Trans., **2014**, 43, 2566.

2. **A rhodamine-based fluorescent sensor for rapid detection of Hg^{2+} exhibiting aggregation induced enhancement of emission (AIEE) in aqueous surfactant medium.**

   Dipankar Das, Rahul Bhowmick, Atul Katarkar, Keya Chaudhuri and Mahammad Ali, J. Indian Chem. Soc., Vol. 94, July **2017**, pp. 819-828.

3. **A differentially selective probe for trivalent chemosensor upon single excitation with cell imaging application: potential applications in combinatorial logic circuit and memory devices**.

   Dipankar Das, Rabiul Alam, Atul Katarkar and Mahammad Ali, Photochem. Photobiol. Sci., **2019**, 18, 242.

4. **Rhodamine 6G-based efficient chemosensor for trivalent metal ions (Al^{3+}, Cr^{3+} and Fe^{3+}) upon single excitation with applications in combinational logic circuits and memory devices.**

   Dipankar Das, Rabiul Alam and Mahammad Ali, Analyst, **2022**, 147, 471

Photochemical & Photobiological Sciences

PAPER

View Article Online
View Journal | View Issue

Cite this: *Photochem. Photobiol. Sci.*, 2019, **18**, 242

A differentially selective probe for trivalent chemosensor upon single excitation with cell imaging application: potential applications in combinatorial logic circuit and memory devices†

Dipankar Das,[a] Rabiul Alam,[a] Atul Katarkar[b] and Mahammad Ali *[a,c]

Received 25th August 2018,
Accepted 31st October 2018

DOI: 10.1039/c8pp00381e

rsc.li/pps

A new rhodamine 6G-benzylamine-based sensor (**L^1**), having only hydrocarbon skeletons in the extended part, was synthesized and characterized by single-crystal X-ray crystallographic study. It exhibited excellent selective and sensitive recognition of trivalent metal ions M^{3+} (M = Fe, Al and Cr) over mono- and divalent and other trivalent metal ions. A large enhancement of the fluorescence intensity for Fe^{3+} (41-fold), Al^{3+} (31-fold) and Cr^{3+} (26-fold) was observed upon the addition of 3.0 equivalent of these metal ions into the probe in H_2O/CH_3CN (4 : 1, v/v, pH 7.2) with naked eye detection. The corresponding K_f values were evaluated to be 9.4×10^3 M^{-1} (Fe^{3+}), 1.34×10^4 M^{-1} (Al^{3+}) and 8.7×10^3 M^{-1} (Cr^{3+}). Quantum yields of the **L^1**, [**L^1**–Fe^{3+}], [**L^1**–Al^{3+}] and [**L^1**–Cr^{3+}] complexes in H_2O/CH_3CN (4 : 1, v/v, pH 7.2) were found to be 0.012, 0.489, 0.376 and 0.310, respectively, using rhodamine-6G as standard. LODs for Fe^{3+}, Al^{3+} and Cr^{3+} were determined by 3σ methods and found to be 1.28, 1.34 and 2.28 μM, respectively. Cyanide ion scavenged Fe^{3+} from the [Fe^{3+}–**L^1**] complex and quenched its fluorescence *via* its ring-closed spirolactam form. Advanced level molecular logic devices using different inputs (2 and 4 inputs) as advanced level logic gates and memory devices were constructed. The large enhancement in fluorescence emission of **L^1** upon complexation with M^{3+} metal ions makes the probe suitable for the bio-imaging of M^{3+} (M = Fe, Al and Cr) in living cells.

Introduction

With the increase in urbanization and socioeconomic activities, unlike other pollutants like petroleum hydrocarbons and domestic and municipal litter, which may visibly build up in the environment, the traces of heavy metal ions increase the toxicity level to a higher extent in the environment and also cause harmful effects on human health. Nowadays, contamination by toxic metal ions is increasing due to leather tanning, electroplating, pigments, emissions from vehicular traffic gas exhausts, energy and fuel production, intensive agriculture and sludge dumping and from mining industries.

As a result, drinking water and food, especially in developing countries, with metal contamination is very much unsafe. So many researchers have tried to detect toxic metal ions, such as iron,[1] chromium,[2] aluminium,[3,4] lead,[5] silver,[6] cadmium,[7] zinc[8,9] and mercury,[10] in water and foods.

Among these trivalent metal ions, Fe^{3+}, $Al^{3+}$and Cr^{3+} have biological as well as environmental importance.[11–24] Fe^{3+} is not only the most abundant transition metal in cellular systems but also plays an important role in many metabolic pathways, such as oxygen transport processes in tissues, nerves signal conduction, cellular growth and tissue formation.[25] On the other hand, the excess accumulation of Fe^{3+} can lead to a variety of diseases, such as cell damage and organ dysfunction through the abnormal production of reactive oxygen species (ROS),[26,27] leading to Alzheimer's, Huntington's, Parkinson's *etc*. diseases.[28] Moreover, disruption of iron homeostasis can lead to a number of disease, such as cancer,[29] hepatitis[30] and neurodegenerative diseases.[31]

Cr^{3+} is an effective nutrient and gives immunity power to the human body. Cr^{3+} overdose is known to inflict a negative effect on normal enzymatic activities, and the cellular structure and function causing a disturbance in glucose levels and lipid metabolism, while a deficiency of Cr^{3+} in humans can cause maturity-onset diabetes and cardiovascular disease and nervous system disorders.[32,33] The Cr^{3+} ion, present in the

[a]*Department of Chemistry Jadavpur University, Kolkata 700 032, India. E-mail: m_ali2062@yahoo.com; Fax: +91-33-2414-6223*
[b]*Department of Molecular & Human Genetics Division, CSIR-Indian Institute of Chemical Biology, 4 Raja S.C. Mullick Road, Kolkata-700032, India*
[c]*Vice-Chancellor, Aliah University, IIA/27, New Town, Kolkata 700160, India*

†Electronic supplementary information (ESI) available. CCDC 1836133. For ESI and crystallographic data in CIF or other electronic format see DOI: 10.1039/c8pp00381e

cytoplasm, is known to bind non-specifically to DNA at an elevated level, affecting the cellular structures and damaging the cellular components, which can lead to mutation and cancer.[34] Chromium deficiency can cause a risk of diabetes, cardiovascular diseases and nervous system disorders.[35]

Al^{3+} is the third most abundant metal in the Earth's crust and also one of the most common species of metal cations that are mostly found in the +3 oxidation state in most kinds of animal and plant tissues and in natural waters everywhere.[36–40] It has been found that aluminium accumulates in various mammalian tissues, such as the brain, bone, liver and kidney,[41,42] which causes renal failure[43] and problems associated with age.[44] Aluminium toxicity damages the central nervous system and it is surmised to play a role in neurodegenerative Alzheimer's and Parkinson's diseases. It is also responsible for intoxication in haemodialysis patients.[45] Moreover, aluminium toxicity may cause gastrointestinal problems and interference with Ca^{2+} metabolism.[46–48] Again, increasing free Al^{3+} due to acid rain and human activities in the environment and surface water is detrimental to growing plants.[49]

Various methods, such as inductively coupled plasma emission spectrometery (ICP),[50] X-ray photoelectron spectrometry (XPS) and atomic fluorescence spectroscopy (AFS) have been used for heavy metal ion detection.[51,52] Compared with these complicated methods, optical probes are inexpensive, simple and rapid.

Thus, there is an urgent need to design single fluorogenic probes, displaying changes in optical properties through a "turn-on" response that are capable of detecting the presence of Fe^{3+}, Al^{3+} and Cr^{3+} ions simultaneously and in the presence of large number of monovalent, divalent and other trivalent metal cations[53–55] in biological samples.

As Cr^{3+} and Fe^{3+} are paramagnetic in nature, they function as fluorescent quenchers,[56] which makes it a challenging task to develop a turn-on fluorescent sensor for these ions. Very few turn-on sensors for Cr^{3+} and Fe^{3+} have been reported with cell-imaging applications.[57–59]

Although, Al^{3+} functions as a turn-on fluorescent sensor, due to its strong hydration in water, most of the reported dye-based Al^{3+} sensors require organic solvents or mixed solvents, with very few being suitable for Al^{3+}-imaging applications.[60]

Given our interest in developing new chemosensors, we report herein a rhodamine 6G-based probe (Scheme 1), characterized by X-ray single-crystal diffraction analysis (Fig. 1) and by other common spectroscopic analysis, for the detection of trivalent cations, like Fe^{3+}, Al^{3+} and Cr^{3+}, in an aqueous medium over monovalent, divalent and other trivalent metal ions. Though there are a few[61,62] reports on trivalent sensors, where in all cases external coordinating atom(s) are present along with the basic amidic moiety of rhodamine, however, in our reported probe it is absent. Herein, we disclose a benzylamine-rhodamine-6G ($\mathbf{L^1}$) conjugate (Scheme 1) that selectively senses these trivalent metal ions in a mostly aqueous medium (4 : 1, H_2O : CH_3CN, v/v) with very high fluorescence enhancement.

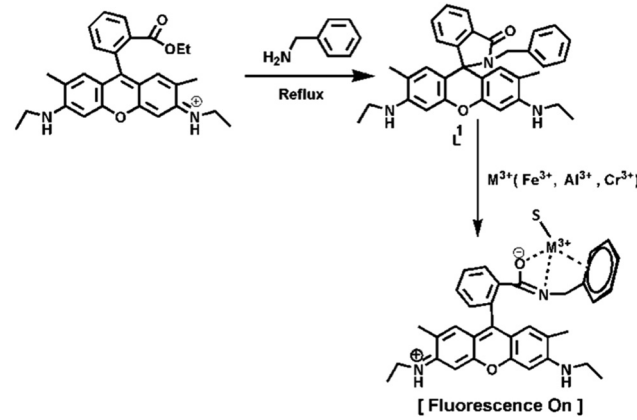

Scheme 1 Tentative binding mode of L^1 with M^{3+}.

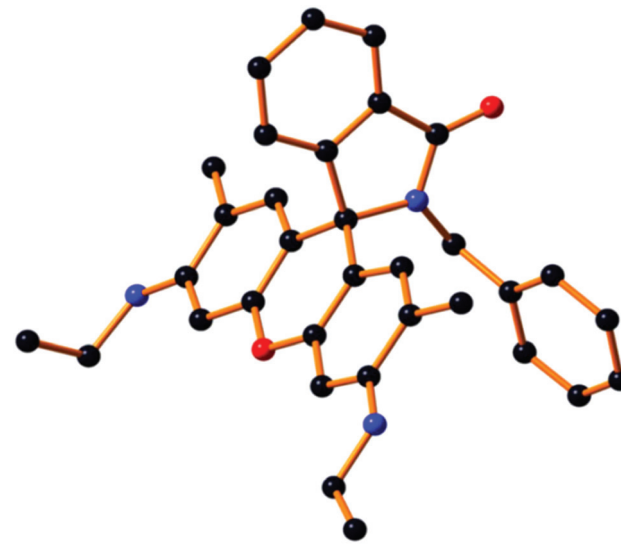

Fig. 1 The molecular view of ligand L^1. All H-atoms are omitted for clarity.

Experimental section

Materials and methods

All solvents used for synthesis were of reagent grade (Merck). For the spectroscopic (UV/Vis and fluorescence) studies, HPLC-grade MeCN and double-distilled water were used. Rhodamine 6G hydrochloride and metal salts, such as perchlorates of Na^+, Fe^{2+}, Co^{2+}, Ni^{2+}, Zn^{2+}, Pb^{2+}, Cd^{2+}, Hg^{2+}, Cu^{2+}, $Al(NO_3)_3{\cdot}9H_2O$, $Cr(NO_3)_3{\cdot}9H_2O$, $Fe(NO_3)_3{\cdot}9H_2O$ were purchased either from Sigma–Aldrich or Merck and used as received. All other compounds were purchased from commercial sources and used without further purification.

Physical measurements

^{1}H-NMR spectra were recorded in $CDCl_3$ and DMSO-d_6, on a Bruker 300 MHz NMR spectrometer using tetramethylsilane (δ = 0) as an internal standard. Infrared spectra

(400–4000 cm^{-1}) were recorded in the liquid state using a Nickolet Magna IR 750 series-II FTIR spectrometer. ESI-MS^+ (m/z) of the ligand and complexes were recorded on a Waters' HRMS spectrometer (Model: XEVO G2QTof). UV-Vis spectra were recorded on an Agilent diode-array spectrophotometer (Model, Agilent 8453). Steady-state fluorescence measurements were performed on a PTI QM-40 spectrofluorometer. Lifetimes were measured using an Horiba Jobin–Yvon Hamamatsu MCP photomultiplier (R3809) and data were analyzed using IBH DAS6 software. The pH of the solutions were recorded using a digital pH meter 335, calibrated using pH 4, 7 and 10 buffers in the range pH 2–12.

Synthesis of rhodamine 6G conjugate (L^1)

Rhodamine 6G (5.0 mmol) and benzylamine (10.0 mmol) were dissolved in EtOH and refluxed for 10 h with continuous stirring, whereupon a white crystalline solid of the probe (L^1) was deposited (Scheme 1). The solid was filtered and washed several times with ethanol and dried in air (75% yield). The compound (L^1), was dissolved in MeOH and refluxed for 2 h with constant stirring and filtered. After 2 days, single crystals suitable for X-ray diffraction studies were obtained. ^1H NMR (300 MHz, DMSO-d_6) (ppm): 1.18 (t, J = 6.8 Hz, 6H (–CH3)), 1.69 (s, 6H (–Ar–CH_3)), 2.49 (s, 2H, (–CH2)), 3.09 (t, J = 6.3 Hz, 4H (–Ar–CH2)), 4.96 (s, 2H, (–NH)), 5.87 (s, 2H, (–Ar–H)), 6.18 (s, 2H, (–Ar–H)), 6.85 (s, 2H, (–Ar–H)), 6.95 (d, J = 5.4 Hz, 4H (–Ar–H)), 7.48 (m, 1H,(–Ar–H)), 7.50 (m, 1H, (Ar–H)), 7.80 (m, 1H, (–Ar–H)) (Fig. S1†). ^{13}C NMR: 14.63, 17.32, 37.90, 43.69, 65.08, 95.90, 104.76, 118.44, 122.84, 124.09, 126.53, 127.75, 128.39, 128.68, 130.92, 133.16, 138.07, 147.90, 151.54, 153.95, 167.38 (Fig. S2†). ESI-MS^+ (m/z): 504.26 (L^1 + H^+) (Fig. S3†). IR spectrum: 1684 cm^{-1} (–C═O), 1378 cm^{-1} (–C–N) (Fig. S4†).

Solution preparation for UV-Vis and fluorescence studies

For both the UV-Vis and fluorescence titrations, a stock solution of 1.0×10^{-3} M of the probe L^1 was prepared by dissolving 12.58 mg in 25 mL CH_3CN. Analogously, 1.0×10^{-3} M stock solutions of Fe^{3+}, Al^{3+} and Cr^{3+} were prepared in MeOH. A solution of 20 mM HEPES buffer (4 : 1, H_2O : CH_3CN) was prepared and the pH was adjusted to 7.2 by using HCl and NaOH. For the UV-Vis spectra, a 60 μM probe was taken in a cuvette containing 2.5 mL of buffer solution and then Fe^{3+} salt solution was added incrementally starting from 0 to 240 μM in a regular interval of time, and the absorption spectra were recorded. Similar experiments were performed for Al^{3+} and Cr^{3+}. Again 2.5 ml of this buffer solution was pipetted into a cuvette to which 60 μM of the probe (L^1) solution was added and Fe^{3+} salt solution was then added incrementally starting from 0 to 140 μM in a regular interval of time, and the fluorescence spectra were recorded, setting the excitation wavelength at 502 nm. Similar titrations were conducted with Al^{3+} and Cr^{3+}. Path lengths of the cells used for absorption and emission studies were 1 cm. Fluorescence measurements were performed using a 2 nm × 2 nm slit width.

Cell culture

Human hepatocellular liver carcinoma (HepG2) cell lines (NCCS, Pune, India), were grown in DMEM supplemented with 10% FBS and antibiotics (penicillin, 100 μg ml^{-1}; streptomycin, 50 μg ml^{-1}). Cells were cultured at 37 °C in a 95% air/5% CO_2 incubator.

Cell cytotoxicity assay

To assess if there was any cytotoxic effect of the ligand (L^1), a cell viability assay was performed using 3-(4,5-dimethylthiazol-2-yl)-2,5-diphenyltetra-zolium bromide (MTT).[63] HepG2 cells (1×10^5 cells per well) were cultured in a 96-well plate with incubating at 37 °C, and were treated with increasing concentrations of L^1 (1, 10, 20, 40, 60, 80 and 100 μM) for 24 h. After the incubation, 10 μl of MTT solution [5 mg ml^{-1}, dissolved in 1× phosphate-buffered saline (PBS)] was added to each well of the 96-well culture plate, and then incubated at 37 °C for 4 h. Media were decanted from the wells and 100 μL of 0.04 N acidic isopropyl alcohol was added into each well to solubilize the intracellular formazan crystals (blue-violet) formed, and the absorbance of the solutions was measured at 595 nm wavelength (EMax Precision Micro Plate Reader, Molecular Devices, USA). Values were calculated as the mean ± standard errors of three independent experiments. The cell viability was expressed as the optical density ratio of the treatment to control.

Cell-imaging study by fluorescence microscopy

HepG2 cells were cultured in a 35 × 10 mm culture dish on a coverslip for 24 h at 37 °C. The cells were treated with 10 μm solutions of L^1, prepared by dissolving L^1 into the mixed solvent DMSO : water = 1 : 9 (v/v) and incubated for 1 h at 37 °C. To study the complex formation of L^1 with the three metal ions (Fe^{3+}, Cr^{3+}, Al^{3+}), HepG2 cells were pre-incubated separately with 10 μM, 20 μM and 40 μM of each of the metal ions for 60 min at 37 °C, followed by washing them twice with 1× PBS and subsequent incubation with 10 μM L^1 for 60 min at 37 °C. Fluorescence images of HepG2 cells were taken using a fluorescence microscope (Leica DM3000, Germany) with an objective lens of 40× magnification.

Job's plot

This method is based on the measurement of the fluorescence of a series of solutions in which molar concentrations of the probe (L^1) and M^{3+} vary but their sum remains constant. Here, the fluorescence of each solution was measured at 558 nm and plotted against the mole fraction of M^{3+}. The maximum fluorescence occurred at the mole ratio corresponding to the combined ratio of the two components. The composition of the complex was determined by Job's method and found to be 1 : 1 with respect to L^1 for the Fe^{3+}, Al^{3+} and Cr^{3+} complexes.

Results and discussion

As depicted in Scheme 1, receptor L^1 was synthesized from the reaction of rhodamine-6G with benzylamine in EtOH in reflux

conditions for 10 h. The final crystallized product ($\mathbf{L^1}$) was well characterized by ^{1}H NMR (Fig. S1†), ^{13}C NMR (Fig. S2†), HRMS (Fig. S3†), IR (Fig. S4†) and a single-crystal X-ray diffraction method (Fig. 1). The receptor $\mathbf{L^1}$ was found to be a very sensitive and highly selective colorimetric and fluorogenic chemosensor for trivalent metal ions, M^{3+} (M^{3+} = Fe^{3+}, Al^{3+} and Cr^{3+}), while in the absence of M^{3+}, the solution of $\mathbf{L^1}$ was colourless and very weakly fluorescent.

X-ray crystallography study

Single-crystal X-ray diffraction studies revealed that the compound $\mathbf{L^1}$ crystallizes in a triclinic system of space group $P\bar{1}$ (no. 2). The crystallographic details are depicted in Table 1. A molecular view of $\mathbf{L^1}$ is shown in Fig. 1, with H atoms are removed to get better clarity.

UV-Vis absorption studies

The UV-Vis spectrum of $\mathbf{L^1}$ (60 μM) was recorded in a mixed aqueous solvent of H_2O/CH_3CN (4 : 1, v/v, pH 7.2, 20 mM HEPES buffer). The gradual addition of Fe^{3+}, Al^{3+} and Cr^{3+} separately to a solution of $\mathbf{L^1}$ revealed that there was a development of two absorption peaks at 350 nm and 530 nm (Fig. 2 and Fig. S5, S5a†), with a sharp visual colour change of the representative solution from colourless to orange-red, whereas no such peaks appeared in the presence of other monovalent, divalent or trivalent metal ion solutions (Fig. S5b†). Between these two peaks, the second one is very important as it exhibits a greater increase in absorbance. The appearance of this peak clearly manifested the opening of the spirolactam ring due to the coordination of Fe^{3+}, Al^{3+} and Cr^{3+} with the probe $\mathbf{L^1}$. The probable coordination mode of $\mathbf{L^1}$ towards M^{3+} (Fe^{3+}, Al^{3+} and Cr^{3+}) is demonstrated in Scheme 1. UV-Vis titrations were carried out by varying the trivalent metal ion Fe^{3+}, Al^{3+} and Cr^{3+} concentration (0–240 μM) keeping the probe concentration fixed at 60 μM in H_2O/CH_3CN (4 : 1, v/v, pH 7.2, 20 mM HEPES buffer). Plots of absorbance *vs.* [M^{3+}] yielded linear curves, which were analyzed by linear curve-fitting of the titration data according to eqn (1) (where a, b and c have the usual meaning) under the conditions $1 \gg c \times x$ with $n = 1$, giving apparent association constant K_f values as 1.19×10^4 M^{-1}, 1.09×10^4 M^{-1} and 1.04×10^4 M^{-1} for Fe^{3+}, Al^{3+} and Cr^{3+}, respectively.

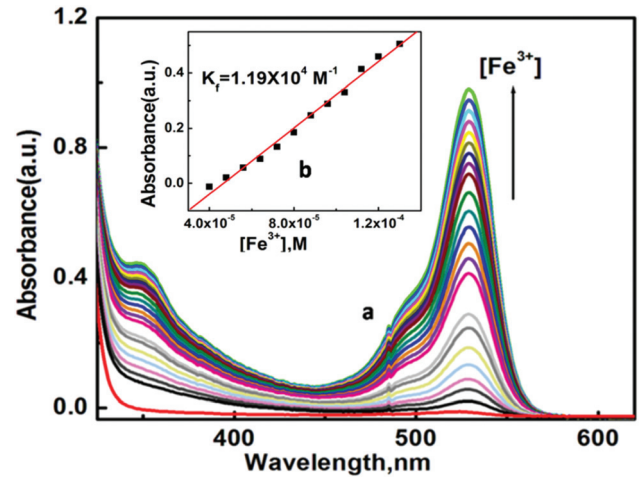

Fig. 2 (a) UV-Vis absorption spectra of $\mathbf{L^1}$ (60 μM) in H_2O/CH_3CN (4 : 1, v/v, pH 7.2, 20 mM HEPES buffer) solutions with the increase in concentration of Fe^{3+} solution (0–240 μM); (b) linear fit of absorbance *vs.* [Fe^{3+}] plot.

$$y = (a + b \times c \times x^n)/(1 + c \times x^n) \quad (1)$$

The absorbance intensity of the [$\mathbf{L^1}$–$\mathbf{Fe^{3+}}$] complex was found to be selectively quenched in the presence CN^- ion (Fig. S6†).

Fluorescence studies

The emission spectra of $\mathbf{L^1}$ and its fluorescence titration with M^{3+} (Fe^{3+}, Al^{3+} and Cr^{3+}) were performed in H_2O/CH_3CN (4 : 1, v/v, pH 7.2, 20 mM HEPES buffer) with the fixed concentration of $\mathbf{L^1}$ at 60 μM. A significant turn-on fluorescence response was observed in the presence of Fe^{3+}, Al^{3+} and Cr^{3+} with a fluorescent maximum at 558 nm. For example, upon the gradual addition of Fe^{3+} (0–3 equivalent) to the non-fluorescent solution of $\mathbf{L^1}$, a 41-fold enhancement in fluorescence intensity at 558 nm was observed following excitation at 502 nm, which also suggests the opening of the spirolactam ring in $\mathbf{L^1}$ upon coordination to the Fe^{3+} ion[64] (Fig. 3). A 31-fold and 26-fold enhancement of fluorescence intensity was observed during the titration of $\mathbf{L^1}$ with Al^{3+} and Cr^{3+} respectively (Fig. S7 and S7a†). Fascinatingly, this change was also accompanied with a naked-eye colour change from colourless to orange-red after the addition of Fe^{3+}, Al^{3+} and Cr^{3+}, indicating that the probe $\mathbf{L^1}$ is a highly sensitive colorimetric chemosensor for these trivalent metal cations.

Plots of FI *vs.* [M^{3+}] give linear curves. Linear curve-fitting of the titration data according to eqn (1) (where a, b and c have

Table 1 Crystallographic data and details of the structure determination

Molecular formula	$C_{33}H_{33}N_3O_2$
Formula weight	503.62
Crystal system	Triclinic
Space group	$P\bar{1}$ (no. 2)
a/Å	9.0397(8)
b/Å	12.5823(11)
c/Å	12.8196(11)
α/°	86.214(2)
β/°	73.428(2)
γ/°	72.357(2)
V/Å^3	1331.5(2)
Z	2
D(calc)/g cm^{-3}	1.256
μ(MoK$_\alpha$)/mm^{-1}	0.079
F(000)	536
T/K	273
θ min, max/°	2.3, 27.5
Dataset	−11: 11; −16: 16; −16: 16
Tot., Uniq. data, R(int)	13 172, 6036, 0.023
Observed data [$I > 2\sigma(I)$]	4637
N_{ref}, N_{par}	6036, 356
R, wR_2, S	0.0527, 0.1522, 1.05

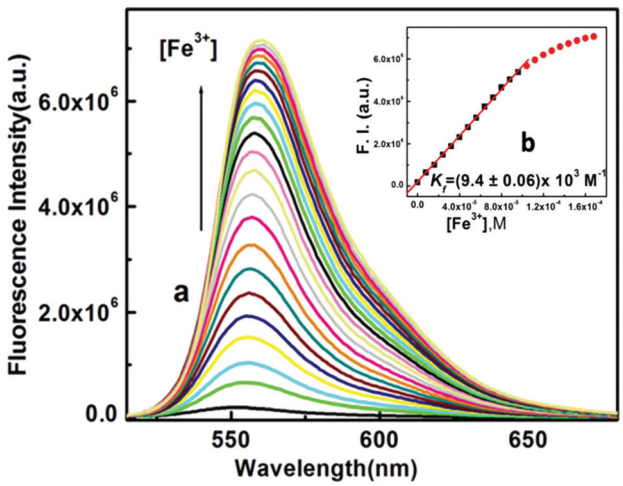

Fig. 3 (a) Fluorescence spectra of L^1 (60 μM) in H_2O/CH_3CN (4 : 1, v/v, pH 7.2, 20 mM HEPES buffer) solutions upon the addition of Fe^{3+} (0–3.0 equivalent), each spectrum was taken after 3 min of Fe^{3+} addition; λ_{ex} = 502 nm, λ_{em} = 558 nm; (b) linear curve fitting of the titration curves with K_f values.

the usual meaning) gave an apparent association constant K_f = (0.94 ± 0.01) × 10^4 M^{-1} for Fe^{3+} under the conditions $1 \gg c \times x$ with n = 1. Similarly, binding constants for Al^{3+} and Cr^{3+} were calculated and found to be (1.34 ± 0.1) × 10^4 M^{-1}, K_f = (0.87 ± 0.01) × 10^4 M^{-1}, respectively (Fig. 4). There was an excellent agreement between the values of K_f obtained from the absorption and fluorescence titration data, manifesting the self-consistency of our results. Using these fluorescence data, the detection limits of the probe L^1 for Fe^{3+}, Al^{3+} and Cr^{3+} were calculated to be 1.28, 1.34 and 2.28 μM, respectively (Fig. S8, S8a and S8b†). These results strongly indicate that this probe L^1 is sensitive enough to detect trace levels of Fe^{3+}, Al^{3+} and Cr^{3+}. In this context, we must highlight that the quantum yield of the ligand (L^1) was very less. The quantum yields of L^1 and

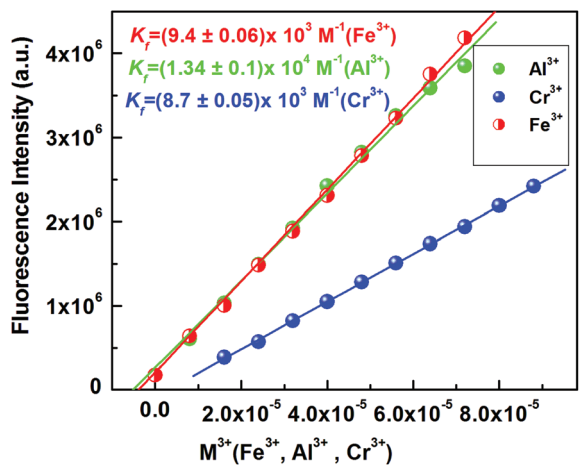

Fig. 4 Linear fitting of the fluorescence titration curves for Fe^{3+}, Al^{3+} and Cr^{3+} with K_f values.

[L^1–Fe^{3+}], [L^1–Al^{3+}] and [L^1–Cr^{3+}] complexes in H_2O/CH_3CN (4 : 1, v/v, pH 7.2) were found to be 0.012, 0.489, 0.376, 0.310 respectively using rhodamine-6G as a standard. The comparatively higher values of quantum yields for complexes compared to the free ligands indicate the higher stability of the complexes in the excited states.

Job's method was again employed to determine the composition of the complex, which was found to be 1 : 1 (Fig. S9†) and was further supported by the mass spectrometric analysis results (m/z = 724.18 $[Fe(L^1)(NO_3^-)_2(CH_3CN)]^+$); ($m/z$ = 198.06 $[Al(L^1)(MeOH)_2]^{3+}$); 721.52 $[Cr(L^1)(NO_3^-)_2(CH_3CN)]^+$ (Fig. S3a and S3b†).

Moreover, a conspicuous reddish-orange fluorescence response of the probe upon interaction with M^{3+} (Fig. 5a) provides the scope for naked eye detection. The possibility of using the chemosensor L^1 in the development of paper test strips was examined and it was found that the turn-on fluorescence response of L^1 towards M^{3+} is also visually detectable in test paper strips (Fig. 5b).

Selectivity studies

Selectivity is an important and essential requirement for an excellent chemosensor. Selectivity experiments were carried out by taking 60 μM of probe L^1 in a cuvette containing 2.5 mL of 20 mM buffer solution and then different metal ion solutions of about 5 equivalent were added separately. Surprisingly, L^1 could selectively recognize the trivalent metal ions Cr^{3+}, Fe^{3+} and Al^{3+} in a mixed aqueous medium over other biologically abundant divalent 3d transition metal cations, like Mn^{2+}, Fe^{2+}, Co^{2+}, Ni^{2+}, Cu^{2+} and Zn^{2+}, hazardous heavy metal ions, like Pb^{2+}, Cd^{2+} and Hg^{2+}, alkali and alkaline earth metal ions, like Na^+, K^+, Ca^{2+}, Mg^{2+} (Fig. 6 and Fig. S10†) and also in the presence of Ga(III), Y(III), Sm(III), Dy(III), Au(III), Ru(III), Co(III) and Cr(VI) ions (Fig. S17†), which were taken in 5 equivalent with respect to the probe (1 : 5 ratio).

It was also found that not a single anionic species among OAc^-, HCO_3^-, CO_3^{2-}, $S_2O_3^{2-}$, SCN^-, N_3^-, NO_3^-, NO_2^-, $H_2PO_4^-$, SO_4^{2-}, ClO_4^-, F^-, Cl^-, Br^-, I^-, PO_4^{3-} and CN^- could enhance the fluorescence intensity of the probe L^1 (Fig. 7) when taken in 5 equivalent with respect to the probe (1 : 5 ratio). However, the fluorescence intensity of the [L^1–M^{3+}] complex was found to be selectively quenched in the presence CN^- ions (Fig. S11 and S12†). An excellent reversible fluorescence ON–OFF property of L^1 was observed through fluorescence study with the

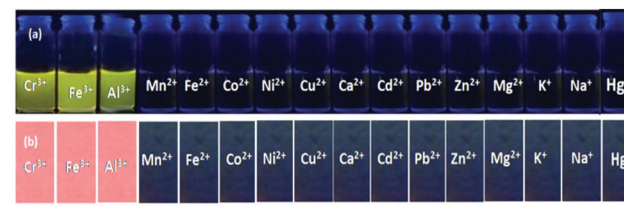

Fig. 5 (a) Visual fluorescent response of L^1 towards Fe^{3+}, Al^{3+} and Cr^{3+} (under 365 nm UV light). (b) Paper strip for the fluorescent sensing of Fe^{3+}, Al^{3+} and Cr^{3+} towards the probe L^1.

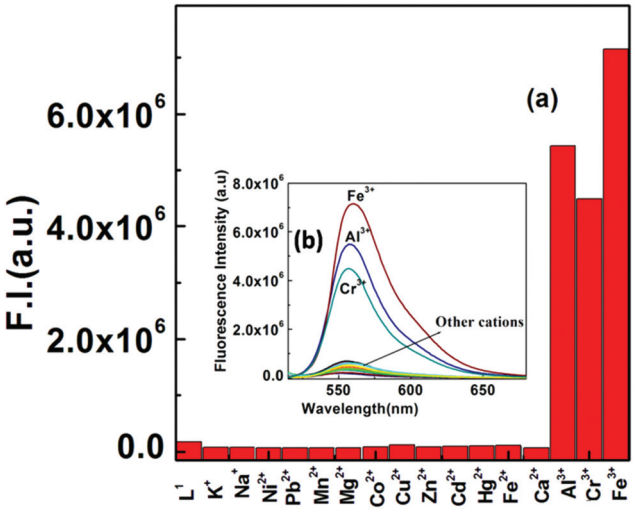

Fig. 6 (a) Fluorescence bar diagram for the selective response of $\mathbf{L^1}$ (60 μM) towards M^{3+} (M = Fe, Al, Cr) over other di- and monovalent metal ions (5 equivalent) in H_2O/CH_3CN (4 : 1, v/v, pH 7.2, 20 mM HEPES buffer), λ_{ex} = 502 nm, λ_{em} = 558 (nm); (b) fluorescence response of $\mathbf{L^1}$ (60 μM) upon the addition of 3.0 equivalent of Fe^{3+}, Al^{3+}, Cr^{3+}.

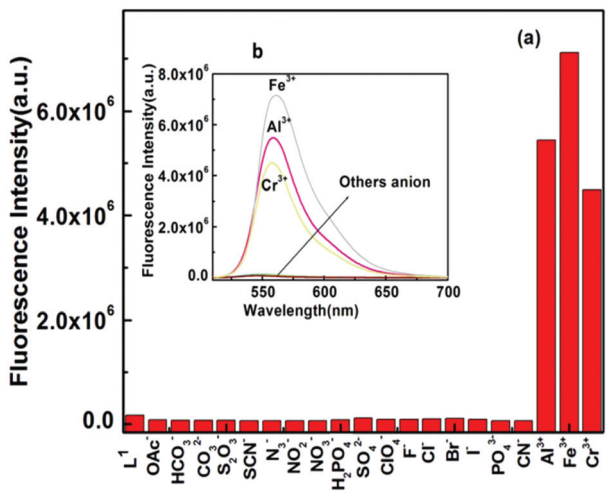

Fig. 7 (a) Histogram of the fluorescence responses of different anions (5 equivalent) towards $\mathbf{L^1}$ (60 μM) in 4 : 1 v/v, water/MeCN in HEPES buffer at pH 7.2 with λ_{ex} = 502 nm, λ_{em} = 558 nm. (b) The fluorescence response of $\mathbf{L^1}$ towards Fe^{3+}, Al^{3+}, Cr^{3+} with respect to different anions (300 μM).

sequential addition of M^{3+} and CN^- ions in 20 mM HEPES buffer in H_2O/CH_3CN (4 : 1) (pH 7.2) solution at room temperature (Fig. 8). The addition of cyanide ions to the solution containing $\mathbf{L^1}$–M^{3+} complex quenched the emission of the probe with the disappearance of the orange-red colour of the solution. The fluorescence quenching of the complexes was characterized by a linear Stern–Volmer (SV) plot and analyzed using the classical Stern–Volmer (SV) eqn (2) [65]

$$\frac{F_0}{F} = 1 + K_{SV}[Q] \quad (2)$$

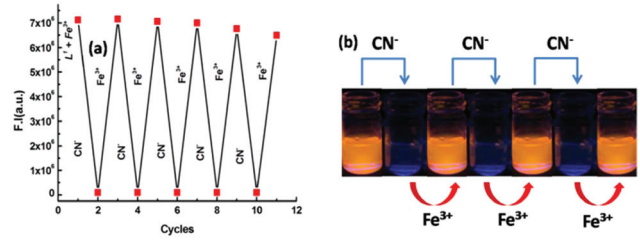

Fig. 8 Fluorescence experiment to show the reversibility and reusability of the receptor for sensing Fe^{3+} by the alternate addition of CN^-: (a) Fluorescence intensity obtained during the titration of $\mathbf{L^1}$–Fe^{3+} with CN^- followed by the addition of Fe^{3+}. (b) Visual fluorescent colour changes after each addition of CN^- and Fe^{3+} sequentially.

where F_0 and F are the steady state fluorescence intensities at the maximum wavelength in the absence and presence of a quencher (Q), respectively, [Q] is the quencher concentration and K_{SV} is the Stern–Volmer constant. The Stern–Volmer quenching constant (K_{SV}) of [$\mathbf{L^1}$–Fe^{3+}], [$\mathbf{L^1}$–Al^{3+}] and [$\mathbf{L^1}$–Cr^{3+}] complexes with CN^- ion were calculated and found to be (5.60 ± 0.20) × 10^2 M^{-1}, (2.42 ± 0.24) × 10^2 M^{-1} and (1.88 ± 0.11) × 10^2 M^{-1}, respectively (Fig. S18†). The reason behind this observation is that the interaction of M^{3+} with the probe results in opening of the spirolactam ring, thereby producing strong fluorescence. Then treatment with CN^- results in the abstraction of a metal ion and regeneration of the spirolactam ring, leading to quenching of the emission. The mechanism between $\mathbf{L^1}$–M^{3+} with CN^- ion sensing was confirmed by the HRMS study (Fig. S13†). It is clear from the HRMS study that the ligand is in a ring-closed structure exactly the same with the $\mathbf{L^1}$. This reversibility test suggests the reusability of this chemosensor.

pH studies

For practical application, the appropriate pH condition for the sensor was evaluated. At pH > 4.0, no obvious ring opening of the probe was observed, thereby satisfying the usefulness of the probe in biological systems over a wide pH range (4–8) for the detection of Fe^{3+} (Fig. 9), Al^{3+} and Cr^{3+} (Fig. S14†). However, upon the addition of 3.0 equivalent of Fe^{3+}, the FI jumps to a very high value and remains almost unchanged in the range pH 3–7, but then on a further increase in pH, the FI gradually falls. At pH > 8, no FI was observed in the case of Fe^{3+}, Al^{3+} and Cr^{3+} due to the precipitation of hydroxides of these metal ions.

Spectral studies

The mechanistic pathway proposed for the formation of the $\mathbf{L^1}$–M^{3+} complex by the opening of the spirolactam ring was established through IR and ^{1}H-NMR studies. The IR studies revealed that the characteristic stretching vibrational frequencies of the amidic 'C=O' of the rhodamine moiety at 1684 cm^{-1} and azomethine group (C=N) at 1636 cm^{-1} were shifted to lower wavenumbers 1636, 1637, 1635 cm^{-1} and 1605, 1604, 1604 cm^{-1} in the presence of 3.0 equivalent of

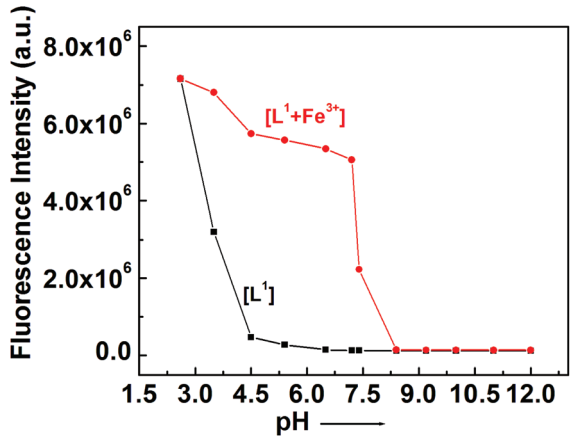

Fig. 9 pH dependence of fluorescence responses of L^1 and its $[L^1–Fe^{3+}]$ complex.

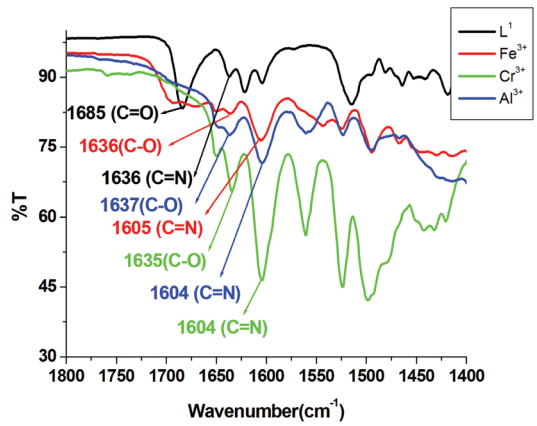

Fig. 10 IR spectra of (L^1), [L^1 + Fe^{3+}], [L^1 + Al^{3+}] and [L^1 + Cr^{3+}] complexes in MeOH.

Fe^{3+}, Al^{3+} and Cr^{3+}, respectively (Fig. 10). These large shifts in IR frequencies signify a strong polarization of the C=O and C=N bonds upon efficient binding to the M^{3+} (M = Al, Fe and Cr) ion. The coordination mode of $\mathbf{L^1}$ towards Al^{3+} was supported by ^{1}H-NMR studies (Fig. S1a†), which showed a downfield shift of azomethine proton in $\mathbf{L^1}$ and also of the protons on the benzene ring of the benzylamine moiety in the $\mathbf{L^1}$–Al^{3+} complex. The broadening of the –NH proton at 4.9 was due to opening of the spirolactam ring and it bearing a positive charge on it. HRMS study (Fig. S1a†) also confirmed the formation of a complex with M^{3+} (M = Al, Fe and Cr).

Selective sensing of Fe^{3+}, Al^{3+} or Cr^{3+}

It is desirable for the probe to be selective towards one trivalent metal ion over the other two. The probe was sensitive towards all the three trivalent metal ions, but in the presence of ppi (inorganic pyrophosphate), the fluorescence of $\mathbf{L^1}$–Al^{3+} and $\mathbf{L^1}$–Cr^{3+} were quenched significantly while the fluorescence of $\mathbf{L^1}$–Fe^{3+} remained almost unchanged, making $\mathbf{L^1}$ selective towards Fe^{3+} in the presence of ppi (Fig. S19†). Again in the presence of I^-, the fluorescence of $\mathbf{L^1}$–Fe^{3+} and $\mathbf{L^1}$–Al^{3+} undergoes quenching, while that of $\mathbf{L^1}$–Cr^{3+} remains unchanged, making $\mathbf{L^1}$ selective towards Cr^{3+} in the presence of I^- (Fig. S20†). Now if $\mathbf{L^1}$ is fluorescent towards an unknown solution, but remains non-fluorescent in the presence of both ppi and I^-, then the initial fluorescence is due to the presence of Al^{3+}. Thus, $\mathbf{L^1}$ can be made selective towards Fe^{3+}, Cr^{3+} or Al^{3+} in an unknown solution.

Molecular logic operations

The spectroscopic properties of the probe $\mathbf{L^1}$ encouraged us to apply it for multiple logic operations with the sequential addition of inputs like cations, such as Al^{3+}, Fe^{3+}, Cr^{3+}, and CN^- anions and to then monitor their emission as the output. An INHIBIT logic gate was constructed with a particular combination of logic operations, like NOT and AND functions, which was important due to its non-commutative behaviour, *i.e.* its output signal is inhibited by only one type of input. To demonstrate this INHIBIT logic function, first we chose two inputs, namely Fe^{3+} (Input 1) and CN^- (Input 2), and used its emission intensity at 558 nm as the output. A high value of emission intensity (>5 × 10^5 at 558 nm) has been designated as 1 (ON) and a low value (≤5 × 10^5) as 0 (OFF). In the absence of both the 1st input (Fe^{3+}) and 2nd input (CN^-), the emission intensity was low, indicating the OFF state; whereas when only input 1 was present, then a significant enhancement of the emission (at 558 nm) took place, indicating the 1 (ON) state, while, on the other hand, in the presence of input 2, the output emission value became very weak indicating the OFF state. Therefore, it was necessary to apply NOT gate with Input 2. Additionally, it is noteworthy that $\mathbf{L^1}$ displayed the emission output signal in such a way that it seemed to understand the requirements of the AND operation. In the presence of both inputs, the output emission value was again low, indicating the OFF state, in accordance with the truth table (Fig. 11(a)). Thus, by the sequential addition of these two inputs, an INHIBIT function logic gate could be achieved.

Advanced level OR-INHIBIT gate based 4 input logic gate

A combination of OR and INHIBIT logic functions was used for the construction of the 4 inputs 1 output logic circuit. Now to imitate an OR logic gate function, the emission intensity at 558 nm was used as the output response similar to the earlier 2 input logic gate, and the inputs were Al^{3+}, Fe^{3+}, Cr^{3+} and CN^- (Fig. S15†). When the 1st (Al^{3+}) and 2nd (Fe^{3+}) inputs were both absent, the output response, *i.e.* the emission intensity, was very low, indicating the 0 (OFF) state. However, when only any one of the two inputs was present, the output signal was high, indicating the 1 (ON) state. Again in the presence of both the input Al^{3+} and Fe^{3+}, the output response was 1 (ON). Thus, according to its truth table (Fig. 12a), an OR function logic gate could be contracted by the sequential addition of these two inputs. Then we verified the nature of the output signal in the presence of a 3rd ionic input (Cr^{3+}) in the presence of the first two ionic inputs. Here, any one of these three inputs or the presence of two of these three inputs caused a high inten-

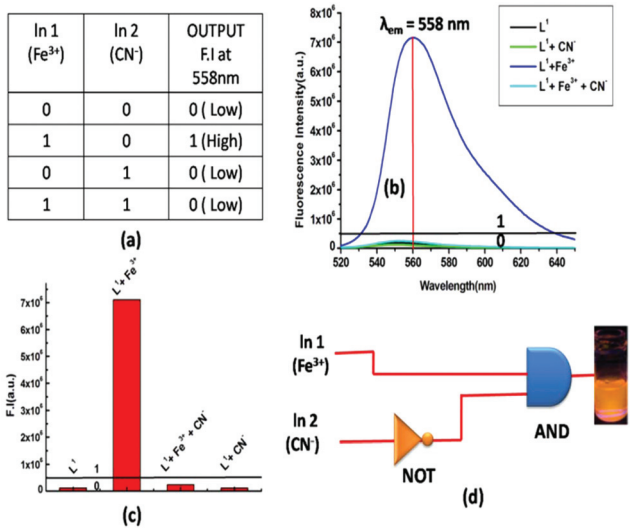

Fig. 11 (a) Corresponding truth table of the logic gate. (b) Output signals (at 558 nm) of the logic gate in the presence of different inputs. (c) Corresponding bar diagram at 558 nm in the presence of different inputs. (d) General representation of an INHIBIT logic gate-based circuit.

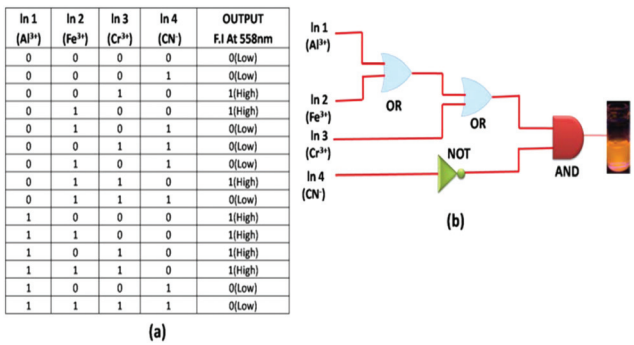

Fig. 12 (a) Truth table of an advanced level 4 input logic gate. (b) Schematic representation of a combined logic circuit of INHIBIT and OR logic gates.

sity emission, output indicating the ON state (1). Thus, the probe behaved like an OR logic function. On the other hand, when only a 4th input (CN^-) was present or in the presence of all other inputs (Al^{3+}, Fe^{3+} and Cr^{3+}) in the system, the output emission was very weak, indicating the 0 (OFF) state. Therefore, we applied a NOT logic function with a 4th input. As the probe functions parallel with the output signal, so we could imply another AND logic function. Thus, from an INHIBIT logical function and following its corresponding truth table, an advanced level 4 input logic gate circuit could be constructed (Fig. 12b).

Molecular memory device

Molecular memory devices are used for data storage technologies that use molecular species as the data storage element and can be constructed by sequential logic circuits. One of the output signals acts as the input of the memory device and it is memorized as a "memory element". So by using binary logic function, we developed a sequential logic circuit showing a "write–read–erase–read" property. For our system, we chose a strong emission output at 558 nm as the ON state (1) and a weak emission output as the OFF state (0). Now to construct this memory device, we chose two inputs, namely Fe^{3+} and CN^-, for the SET and RESET processes, respectively. In this memory function, the system writes when it gets input A (Fe^{3+}), *i.e.* a high emission value, and it memorizes the binary number 1. However, in the presence of input B (CN^-), which is a reset input, it erases the data and then memorizes the binary number 0 (Fig. 13). The properties of the material allow for a much greater capacitance per unit area than with conventional DRAM (dynamic random-access memory), thus potentially leading to smaller and cheaper integrated circuits.

The most important thing is that this write–erase–write cycle could be repeated many times (Fig. 8) using the same concentration of the system without any significant change in emission intensity.

Cell-imaging studies

As $\mathbf{L^1}$ showed extensive selective complex formation with trivalent metal ions (namely Fe^{3+}, Cr^{3+}, Al^{3+} ions), it was further checked for its ion-sensing ability in living cells (Fig. 14). A cell viability assay using MTT[66–68] was done to find out whether $\mathbf{L^1}$ had cytotoxic effects, with calculating the % cell viability on HepG2 cells (Fig. S16†). As found from the result, no significant decrease in formazan production occurred up to 40 μM concentration of $\mathbf{L^1}$, thus reflecting that a below 40 μM ligand concentration for $\mathbf{L^1}$ would be much more effective for the analysis of its complex formation with trivalent metal ions *in vitro*. More than 95% cell viability was observed for $\mathbf{L^1}$ at 10 μM, after which the viability of the HepG2 cells decreases slightly. Hence, further experiments were carried out with 10 μM for $\mathbf{L^1}$ for treatment.

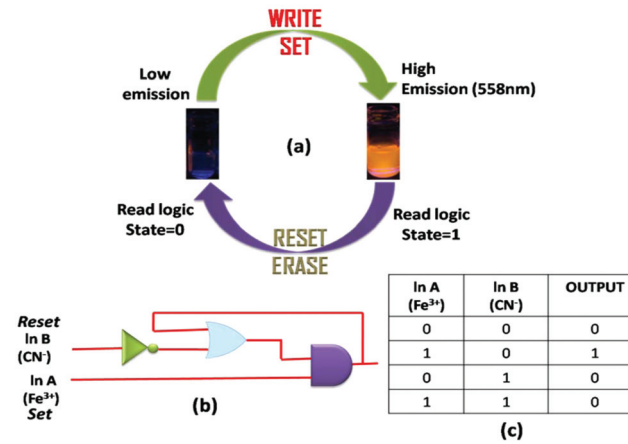

Fig. 13 (a) Schematic demonstration of the reversible logic operation for the memory element with a "write–read–erase–read" kind of behaviour. (b) Sequential logic circuit showing a memory unit with two inputs (In A and In B) and one output, and (c) the corresponding truth table.

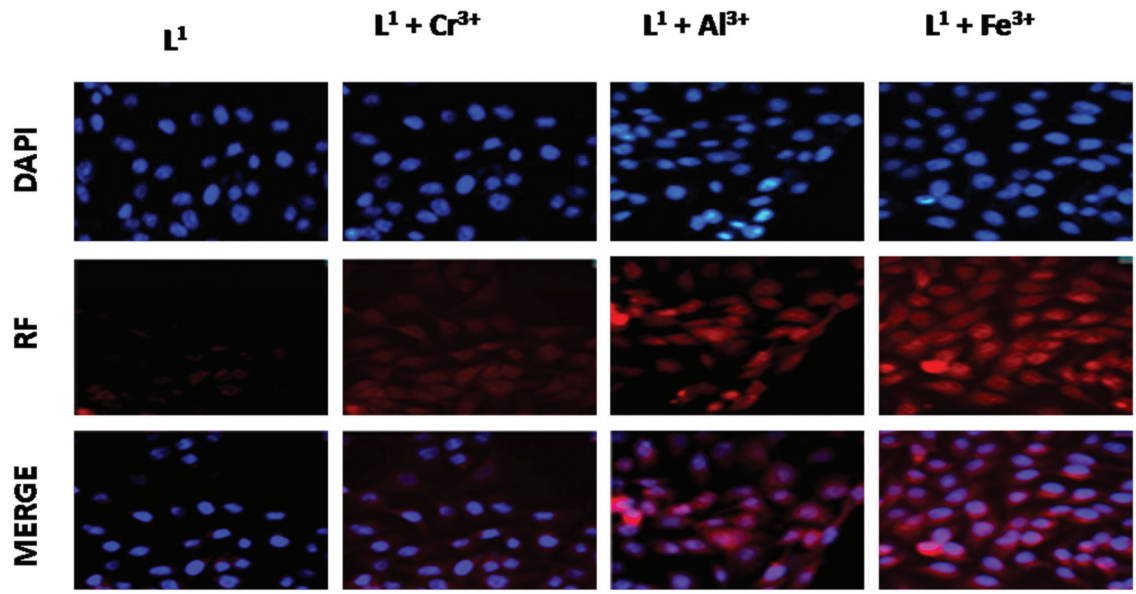

Fig. 14 Phase contrast and fluorescence images of HepG2 cells captured (40×) after cells were incubated with $\mathbf{L^1}$ for 30 min at 37 °C and pre-incubated with Al^{3+}, Cr^{3+} and Fe^{3+} for 30 min at 37 °C, followed by washing with 1× PBS and treatment with $\mathbf{L^1}$ for 30 min at 37 °C. The cytoplasmic complex formation was confirmed by nuclear stain DAPI.

Upon incubation with 10 μM of the ligand $\mathbf{L^1}$ for 1 h, it exhibited weak intracellular fluorescence on HepG2 cells due to the presence of intracellular Fe^{3+} (Fig. 14). However, a distinct red fluorescence was observed inside the cells when the HepG2 cells were incubated with 10 μM of the trivalent metal ions for 1 h at 37 °C, washed twice with PBS buffer and then reincubated with 10 μM of the ligand $\mathbf{L^1}$ for 30 min at 37 °C. At 10 μM concentration of the Fe^{3+} ions, the ligand $\mathbf{L^1}$ showed more intense fluorescence emission than Al^{3+} and Cr^{3+} ions.

Keeping the ligand $\mathbf{L^1}$ concentration constant (10 μM) and increasing the concentration of metal ions (from 10 μM, to 20 μM, 40 μM) showed a concentration-dependent increase in the intracellular red fluorescence, caused by the formation of the complex of $\mathbf{L^1}$ with either of the trivalent metal ions. Highly enhanced fluorescence was observed due to complex formation between the ligand $\mathbf{L^1}$ and the metal ions nearly at 40 μM of metal ion concentration. These results suggest that the ligand $\mathbf{L^1}$ with low cytotoxicity and biocompatibility has a high potential for *in vitro* application as an ion sensor of trivalent Fe^{3+}, Cr^{3+}, Al^{3+} ions as well as for live cell imaging for their detection in biological samples.

Fig. 15 represents some trivalent sensors reported so far and Table S1† displays some important parameters. A closer inspection of Table S1† reveals that our probe is superior to all the probes listed here in the sense that it provides higher excitation wavelength (502 nm). There is one report (probe 6)

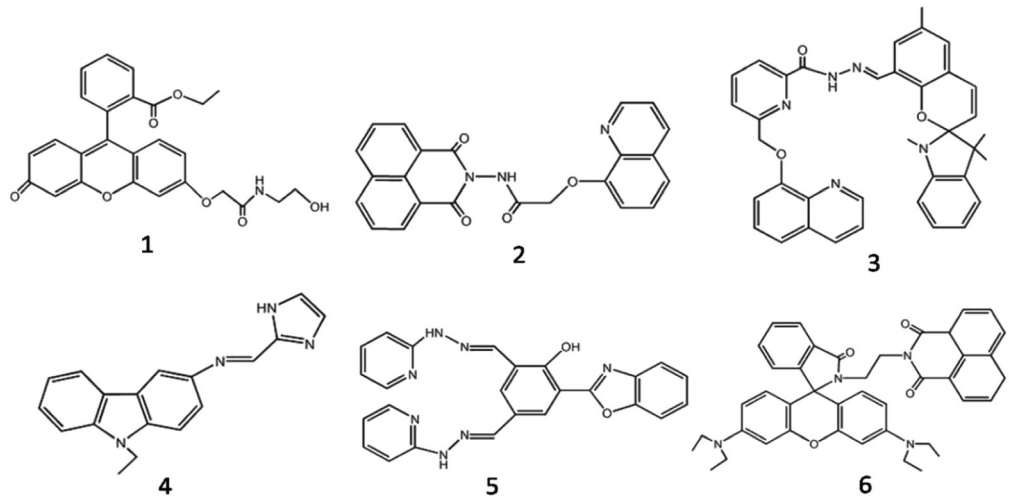

Fig. 15 Some representative trivalent sensors.

where CH_3OH–H_2O (6 : 4, v/v) was used, but the serious drawback of this system was that the excitation wavelength was in UV region (330 nm), which is not desirable for bioimaging applications.

Conclusion

In summary, we reported herein a new rhodamine-6G based fluorogenic probe, which showed a selective colorimetric as well as "turn-on" fluorescence response towards trivalent metal ions M^{3+} (M = Al, Fe and Cr) over mono- and divalent metal ions. A large enhancement of fluorescence intensity of $\mathbf{L^1}$ [Fe^{3+} (41-fold), Al^{3+} (31-fold) and Cr^{3+} (26-fold)] was observed upon the addition of 3.0 equivalent of these metal ions in H_2O/CH_3CN (4 : 1, v/v, pH 7.2), which clearly indicate the feasibility of the naked eye detection of these metal ions. Take-off values were evaluated from the fluorescence titration data at variable concentrations of metal ions and a fixed concentration of ligand and were found to be 9.4×10^3 M^{-1} (Fe^{3+}); 8.7×10^3 M^{-1} (Cr^{3+}) and 13.4×10^3 M^{-1} (Al^{3+}). The higher values of quantum yields (0.489, 0.376, 0.310 for [$\mathbf{L^1}$–Fe^{3+}], [$\mathbf{L^1}$–Al^{3+}] and [$\mathbf{L^1}$–Cr^{3+}], respectively) over the free ligand (0.012) indicate the higher stability of the complexes in the excited states. An excellent reversible fluorescence ON–OFF property of $\mathbf{L^1}$ was observed through fluorescence study with the sequential addition of M^{3+} and CN^- ions at room temperature, which suggests the reusability of this chemosensor. The very low detection limit for Fe^{3+}, Al^{3+} and Cr^{3+} were 1.28 μM, 1.34 μM and 2.28 μM, respectively, which could make it have a potential application in real water samples for trivalent ion detection. Advanced level molecular logic devices using different inputs (2 and 4 inputs) in advanced level logic gates and memory device were constructed. A suitably large increase in fluorescence intensity of $\mathbf{L^1}$ upon complexation with M^{3+} suggests the probe may be used for bioimaging applications in living cells.

Conflicts of interest

There are no conflicts to declare.

Acknowledgements

Financial supports from DST (Ref. SR/S1/IC-20/2012) New Delhi are gratefully acknowledged.

References

1 M. Wang, F. Wang, Y. Wang, W. Zhang and X. Chen, *Dyes Pigm.*, 2015, **120**, 307.
2 X. Xing, H. Yang, M. Tao and W. Zhang, *J. Hazard. Mater.*, 2015, **297**, 207.
3 P. Wang, J. Wu, L. Liu, P. Zhou, Y. Ge, D. Liu, W. Liu and Y. Tang, *Dalton Trans.*, 2015, **44**, 18057.
4 Z. Xu, K.-H. Baek, H. N. Kim, J. Cui, X. Qian, D. R. Spring, I. Shin and J. Yoon, *J. Am. Chem. Soc.*, 2009, **132**, 601.
5 L. Tang, X. Dai, K. Zhong, X. Wen and D. Wu, *J. Fluoresc.*, 2014, **24**, 1487.
6 M. Idrees, M. Silva, A. F. Silva, L. M. Zimmermann, J. Bruch, C. O. Mendonça, G. I. Almerindo, R. A. Nome, T. D. Z. Atvars, H. D. Fiedler and F. Nome, *J. Phys. Chem. C*, 2012, **116**, 3517.
7 S. Maiti, Z. Aydin, Y. Zhang and M. Guo, *Dalton Trans.*, 2015, **44**, 8942.
8 S. B. Maity and P. K. Bharadwaj, *Inorg. Chem.*, 2013, **52**, 1161.
9 S. Sarma, P. K. Bhattacharyya and D. K. Das, *J. Fluoresc.*, 2015, **25**, 1537.
10 Mercury Study Report to Congress, United States Environmental Protection Agency, Volume V: Health Effects of Mercury and Mercury Compounds, EPA-452/R-97-007 December (1997).
11 Y. Upadhyay, S. Bothra, R. Kumar and S. K. Sahoo, *ChemistrySelect*, 2018, **3**, 6892.
12 T. Anand, S. K. A. Kumar and S. K. Sahoo, *Spectrochim. Acta, Part A*, 2018, **204**, 105.
13 Y. Upadhyay, T. Anand, L. T. Babu, P. Paira, S. K. A. Kumar, R. Kumar and S. K. Sahoo, *J. Photochem. Photobiol., A*, 2018, **361**, 34.
14 S. K. Sahoo, D. Sharma, R. K. Bera, G. Crisponi and J. F. Callan, *Chem. Soc. Rev.*, 2012, **41**, 7195.
15 S. Samanta, S. Goswami, A. Ramesh and G. Das, *Sens. Actuators, B*, 2014, **194**, 120.
16 S. Dey, S. Sarkar, D. Maity and P. Roy, *Sens. Actuators, B*, 2017, **246**, 518.
17 X. Chen, X. Y. Shen, E. Guan, Y. Liu, A. Qin, J. Z. Sun and B. Z. Tang, *Chem. Commun.*, 2013, **49**, 1503.
18 N. R. Chereddy, P. Nagaraju, M. V. NiladriRaju, V. R. Krishnaswamy, P. S. Korrapati, P. R. Bangal and V. J. Rao, *Biosens. Bioelectron.*, 2015, **68**, 749.
19 A. Barba-Bon, A. M. Costero, S. Gil, M. Parra, J. Soto, R. M. Máñez and F. Sancenón, *Chem. Commun.*, 2012, **48**, 3000.
20 T. Simona, M. Shellaiah, V. Srinivasadesikan, C.-C. Lina, F.-H. Koa, K. W. Sun and M.-C. Lin, *Sens. Actuators, B*, 2016, **231**, 18.
21 A. Singh, R. Singh, M. Shellaiah, E. C. Prakash, H.-C. Chang, P. Raghunath, M.-C. Lin and H.-C. Lin, *Sens. Actuators, B*, 2015, **207**, 338.
22 P. N. Borase, P. B. Thale, S. K. Sahoo and G. S. Shankarling, *Sens. Actuators, B*, 2015, **215**, 451.
23 M. Shellaiah, T. Simon, V. Srinivasadesikan, C.-M. Lin, K. W. Sun, F.-H. Ko, M.-C. Lin and H.-C. Lin, *J. Mater. Chem. C*, 2016, **4**, 2056.
24 S. Tao, Y. Wei, C. Wang, Z. Wang, P. Fan, D. Shi, B. Ding and J. Qiu, *RSC Adv.*, 2014, **4**, 46955.
25 B. L. Su, N. Moniotte, N. Nivarlet, L. H. Chen, Z. Y. Fu, J. Desmet and J. Li, *J. Colloid Interface Sci.*, 2011, **358**, 136.

26 T. Hirayama, K. Okuda and H. Nagasawa, *Chem. Sci.*, 2013, **4**, 1250.
27 J. Xu, Z. Jia, M. D. Knutson and C. Leeuwenburgh, *Int. J. Mol. Sci.*, 2012, **13**, 2368.
28 D. J. Bonda, H. Lee, J. A. Blair, X. Zhu, G. Perry and M. A. Smith, *Metallomics*, 2011, **3**, 267.
29 S. Toyokuni, *Cancer Sci.*, 2009, **100**, 9.
30 K. V. Kowdley, *Gastroenterology*, 2004, **127**, S79–S86.
31 F. Molina-Holgado, R. Hider, A. Gaeta, R. Williams and P. Francis, *BioMetals*, 2007, **20**, 639.
32 Z. Zhou, M. Yu, H. Yang, K. Huang, F. Li, T. Yi and C. Huang, *Chem. Commun.*, 2008, **29**, 3387.
33 J. B. Vincent, *Nutr. Rev.*, 2000, **58**, 67.
34 M. Zhang, Z. Chen, Q. Chen, H. Zou, J. Lou and J. He, *Mutat. Res., Genet. Toxicol. Environ. Mutagen.*, 2008, **654**, 45.
35 B. Vincent, *Nutr. Rev.*, 2000, **58**, 67.
36 H. X. Jiang, L. S. Chen, J. G. Zheng, S. Han, N. Tang and B. R. Smith, *Tree Physiol.*, 2008, **28**, 1863.
37 G. Berthon, *Coord. Chem. Rev.*, 1996, **149**, 241.
38 S. M. Candura, L. Manzo and L. G. Costa, Role of occupational neurotoxicants in psychiatric and neurodegenerative disorders, in *Occupational Neurotoxicology*, ed. L. G. Costa and L. Manzo, CRC Press, Boca Raton, 1998, p. 131.
39 R. J. P. Williams, *Coord. Chem. Rev.*, 1992, **149**, 1.
40 G. R. Rout, S. S. Roy and P. Das, *Agronomie*, 2001, **21**, 3.
41 (*a*) J. Barcelo and C. Poschenrieder, *Environ. Exp. Bot.*, 2002, **48**, 75; (*b*) B. Valeur and I. Leray, *Coord. Chem. Rev.*, 2000, **205**, 3; (*c*) Z. Krejpcio and R. W. P. Wojciak, *Int. J. Environ. Stud.*, 2002, **11**, 251.
42 M. R. Wills, C. D. Hewitt, B. C. Sturgill, J. Savory and M. M. Herman, *Ann. Clin. Lab. Sci.*, 1993, **23**, 1.
43 G. Sahin, I. Varol and A. Temizer, *Biol. Trace Elem. Res.*, 1994, **41**, 129.
44 A. C. Alfrey, *NeuroToxicology*, 1980, **1**, 43.
45 (*a*) G. D. Fasman, *Coord. Chem. Rev.*, 1996, **149**, 125; (*b*) P. Nayak, *Environ. Res.*, 2002, **89**, 111; (*c*) C. S. Cronan, W. J. Walker and P. R. Bloom, *Nature*, 1986, **324**, 140; (*d*) G. Berthon, *Coord. Chem. Rev.*, 2002, **228**, 319; (*e*) D. R. Burwen, S. M. Olsen, L. A. Bland, M. J. Arduino, M. H. Reid and W. R. Jarvis, *Kidney Int.*, 1995, **48**, 469.
46 S. G. Lambert, J. A. M. Taylor, K. L. Wegener, S. L. Woodhouse, S. F. Lincoln and A. D. Ward, *New J. Chem.*, 2000, **24**, 541.
47 D. Maity and T. Govindaraju, *Chem. Commun.*, 2010, **46**, 4499.
48 Y. S. Jang, B. Yoon and J. M. Kim, *Macromol. Res.*, 2011, **19**, 97.
49 A. M. Zayed and N. Terrey, *Plant Soil*, 2003, **249**, 139.
50 W. Fresenius, K. E. Quentin and W. Schneider, *Water Analysis*, Springer, Berlin, 1988.
51 X.-d. Wang and O. S. Wolfbeis, *Chem. Soc. Rev.*, 2014, **43**, 3666.
52 B. Gibson, S. Carter, A. S. Fisher, S. Lancaster, J. Marshall and I. Whiteside, *J. Anal. At. Spectrom.*, 2014, **29**, 1969.
53 J. Wang, Y. Li, N. G. Patel, G. Zhang, D. Zhouand and Y. Pang, *Chem. Commun.*, 2014, **50**, 12258.
54 S. Goswami, K. Aich, S. Das, A. K. Das, D. Sarkar, S. Panja, T. K. Mondal and S. Mukhopadhyay, *Chem. Commun.*, 2013, **49**, 10739.
55 M. Venkateswarulu, T. Mukherjee, S. Mukherjee and R. R. Koner, *Dalton Trans.*, 2014, **43**, 5269.
56 J. Miao, L. Wang, W. Dou, X. L. Tang, Y. Yan and W. S. Liu, *Org. Lett.*, 2007, **9**, 4567.
57 E. Delhaize and P. R. Ryan, *Plant Physiol.*, 1995, **107**, 315.
58 S. Goswami, A. K. Das, A. K. Maity, A. Manna, K. Aich, S. Maity, P. Saha and T. K. Mandal, *Dalton Trans.*, 2014, **43**, 231.
59 S. Fakih, M. Podinovskaia, X. Kong, H. L. Collins, V. E. Schoible and R. C. J. Hider, *Med. Chem.*, 2008, **51**, 4539.
60 S. Kim, J. Y. Noh, K. Y. Kim, J. H. Kim, H. K. Kang, S. W. Nam, S. H. Kim, S. Park, C. Kim and J. H. Kim, *Inorg. Chem.*, 2012, **51**, 3597.
61 S. Paul, A. Manna and S. Goswami, *Dalton Trans.*, 2015, **44**, 11805.
62 R. Alam, R. Bhowmick, A. S. M. Islam, A. Katarkar, K. Chaudhuri and M. Ali, *New J. Chem.*, 2017, **41**, 8359.
63 R. Alam, T. Mistri, R. Bhowmick, A. Katarkar, K. Chaudhuri and M. Ali, *RSC Adv.*, 2016, **6**, 1268.
64 H. A. Molla, R. Bhowmick, A. Katarkar, K. Chaudhuri, S. Gangopadhyay and M. Ali, *Anal. Methods*, 2015, **7**, 5149.
65 Y. Liu, K. Ai, X. Cheng, L. Huo and L. Lu, *Adv. Funct. Mater.*, 2010, **20**, 951.
66 R. Alam, T. Mistri, R. Bhowmick, A. Katarkar, K. Chaudhuri and M. Ali, *RSC Adv.*, 2015, **5**, 53940.
67 R. Alam, T. Mistri, A. Katarkar, K. Chaudhuri, S. K. Mandal, A. R. Khuda-Bukhsh, K. K. Das and M. Ali, *Analyst*, 2014, **139**, 4022.
68 R. Alam, T. Mistri, P. Mondal, D. Das, S. K. Mandal, A. R. Khuda-Bukhsh and M. Ali, *Dalton Trans.*, 2014, **43**, 2566.

J. Indian Chem. Soc.,
Vol. 94, July 2017, pp. 819-828

A rhodamine-based fluorescent sensor for rapid detection of Hg^{2+} exhibiting aggregation induced enhancement of emission (AIEE) in aqueous surfactant medium

Dipankar Das[a], Rahul Bhowmick[a], Atul Katarkar[b], Keya Chaudhuri[b] and Mahammad Ali*[a]

[a]Department of Chemistry, Jadavpur University, Jadavpur, Kolkata-700 032, India

E-mail : m_ali2062@yahoo.com *Fax* : 91-33-24146223

[b]Department of Molecular & Human Genetics Division, CSIR-Indian Institute of Chemical Biology, 4, Raja S. C. Mallick Road, Kolkata-700 032, India

Manuscript received 20 June 2017, accepted 25 June 2017

Abstract : An easily synthesizable rhodamine-based chemosensor, L_2, selectively recognizes Hg^{2+} and Al^{3+} ions in the presence of all biologically relevant and toxic heavy metal ions. Very low detection limit (47 nM for Hg^{2+}) along with cell permeability and negligible cytotoxicity provides a good opportunity towards cell imaging of Hg^{2+}. SEM studies reveal rod-like microstructure for L_2 in water, which changes to a porous microstructure in the presence of Hg^{2+}. It was interesting to note that the presence of SDS solubilized the otherwise insoluble probe in pure aqueous medium. In case of Al^{3+} it was astonishingly observed a fluorescence quenching on increasing the SDS concentration, while a ~33-fold enhancement of FI of [L_2-Hg^{2+}] complex was observed compared to that in the absence of SDS, making the prove selective towards Hg^{2+} over Al^{3+} in the aqueous SDS medium. In SDS/water system, there is a steep rise in FI, reaches a maximum at ~7 mM of SDS and then fluorescence intensity decreases gradually with the increase in [SDS] up to 28 mM. These observations clearly signify the SDS-assisted formation of polymer aggregates of the complex on the surface of monolayer of SDS formed in pre-micellar concentrations with higher FI, which is converted to the monomer being trapped inside the micellar cavity beyond the critical micellar concentration (cmc) with comparatively lower FI, indicating an interesting AIEE phenomenon. This proposition is further supported by the dependence of fluorescence anisotropy (*r*) on [SDS].

Keywords : Rhodamine-based turn-on Hg^{2+} sensor, aggregation induced enhancement of emission (AIEE), fluorescence anisotropy (*r*), microstructure formation, live cell imaging.

Introduction

The fabrication of appealing supramolecular assemblies are achieved through bottom-up approach by an elegant use of noncovalent interactions like electrostatic, hydrophobic, van der Waals, hydrogen bonding etc.[1–4]. Out of these, ionic self-assembly by various combinations between peptides, polyelectrolytes, surfactants and extended rigid organic scaffolds has attracted considerable attention of the researchers due to its application towards the fabrication of optical materials and advanced nano-devices. Another interesting feature of these supramolecular assemblies is their different behaviour in solution and solid state exhibiting either aggregation induced emission enhancement (AIEE) or aggregation caused quenching (ACQ)[5–9]. Till date, the AIEE mechanism has been observed in silole derivative[10], 1,1,2,2-tetraphenylethene (TPE)[11–13], 1-cyano-*trans*-1,2-bis-(4-methylphenyl)ethylene (CN-MBE) etc.[14,15].

The amphiphilic nature of surfactants readily produces various supramolecular aggregates like micelles and vesicles in aqueous solution[16,17]. It could be used as a coupling unit to induce structural changes by ionic self-assembly. Recently surfactants have been suitably exploited to generate AIEE[18–20].

Heavy metals like mercury, lead, cadmium and

semimetal arsenic[21] are widely distributed, extensively used, and highly toxic, and pose the greatest environmental threat; as soils and sediments are the ultimate sink for them. The water-soluble Hg^{2+} ion is highly toxic and can damage the brain, nervous system, kidneys, and endocrine system[22,23]. Again, due to very high thiophilicity Hg^{2+} can deactivate many thiol-containing enzymes, thereby stopping or altering the metabolic processes[24–26]. Over the past decade, increasing attention has been paid to the development of efficient chromo- and fluorogenic sensors for Hg^{2+} ions for real-time monitoring of environmental, biological and industrial samples[27–35].

Here, a rhodamine-based probe with potential NO_3 donor atoms have been synthesized and used successfully for the selective and rapid recognition of toxic Hg^{2+} ion (Scheme 1) exhibiting chromo- and fluorogenic metal-induced OFF-ON responses through the opening of the spirolactam ring.

In addition, although the current probe is poorly soluble in 100% aqueous medium, the presence of SDS makes it soluble in this medium, thereby making it useful for monitoring Hg^{2+} ion in the purely aqueous medium in the presence of SDS with enhanced sensitivity and selectivity, even in the presence of Al^{3+} which otherwise gives fluorescence response with the probe in the absence of SDS[19,20].

Experimental

Materials and reagents :

All solvents used for the synthetic purposes were of reagent grade (Merck). For spectroscopic (UV/Vis and fluorescence) studies double-distilled water and HPLC-grade MeCN were used. Rhodamine 6G hydrochloride, ethylene diamine, methyl acrylate and perchlorate salts of Na^+, K^+, Ca^{2+}, Ni^{2+}, Zn^{2+}, Pb^{2+}, Cd^{2+}, Fe^{2+}, Co^{2+}, Hg^{2+} and Cu^{2+} were purchased from Sigma-Aldrich and used as received. Sodium salts of anions like SO_4^{2-}, NO_3^-, PO_4^{3-}, S^{2-}, Cl^-, F^-, Br^-, I^-, OAc^-, $H_2AsO_4^-$ and N_3^- were of reagent grade and used as received.

Steady-state fluorescence studies were carried out with a PTI (QM-40) spectrofluorimeter. UV/Vis absorption spectra were recorded with an Agilent 8453 diode array spectrophotometer. Bruker spectrometers of 300 and 500 MHz were used for ^1H and ^{13}C NMR

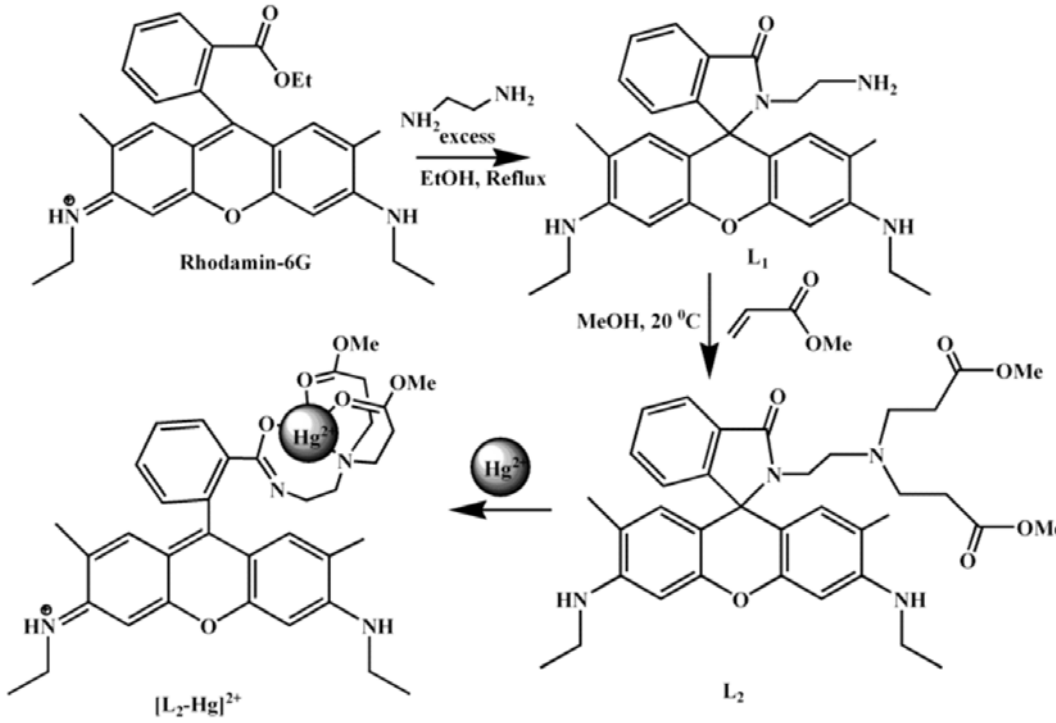

Scheme 1. Synthetic steps leading the formation of $[L_2\text{-}Hg^{2+}]$ complex.

studies. The ESI-MS^+ spectra were recorded on a Waters XEVO G2QTof (Micro YA263) mass spectrometer.

Synthesis of rhodamine 6G hydrazide (L_1) :

It was synthesized by the literature method[36].

Synthesis of rhodamine 6G probe (L_2) :

To a suspension of 30 mL ice-cooled (0 °C) methanolic solution of L_1 (0.456 g, 1.0 mM), a 4 mL methanol solution of methylacrylate (0.36 mL, 10 mmol) was added dropwise over a period of 30 min. The reaction mixture was allowed to warm slowly to room temperature at which it was stirred for 3 days. The final product was obtained after evaporation of methylacrylate and methanol under vacuum as white crystals (yield 0.55 g, 88%) with m.p. 134–136 °C, $R_f = 0.66$ in a toluene/ethanol = 2 : 1 solvent system.

FT-IR (KBr) cm^{-1} : 3324 (-NH); 2942, 2896 (-CH); 1723 (-C=O); 1670 (-COOMe); 1622, 1518 and 1450 (-ArCH).

^1H NMR (DMSO-d_6, 500 MHz), δ ppm : 7.75–7.77 (1H, t, -Ar-H), 7.48–7.53 (2H, m, Ph-H), 6.98–7.00 (1H, t, -Ar-H), 6.25 (2H, s, Ph-H), 6.03 (2H, s, -Ar-H), 5.0 (2H, t, $ArNHCH_2$), 3.33 (6H, s, $-COOCH_3$), 3.09–3.17 (4H, m, $ArNHCH_2$), 2.89–2.92 (2H, t, $-CH_2NCOAr$), 2.42–2.44 (4H, t, $-CH_2-CH_2COOMe$), 2.11–2.14 (4H, t, $-CH_2-COOMe$), 2.01–2.05 (2H, t, $-CH_2-N$), 1.88 (6H, s, $-ArCH_3$), 1.18–1.20 (6H, t, $-CH_2CH_3$); ES^+ MS = 629.3890 [L_2+H^+].

Methods of characterization :

A scanning electron microscope (SEM) (ZEOL, JSM 8360) operating at an accelerating voltage of 5 kV was used for the study of morphologies of the free probe (L_2) in aqueous medium and also in the presence of Hg^{2+} (L_2-Hg^{2+}). Before SEM, the samples were vacuum dried and then gold coated to minimize the sample charging.

Fluorescence anisotropies (r), defined by eq. (1), were measured on a PTI QM-40 spectrofluorometer.

$$r = (I_{VV} - G \cdot I_{VH})/(I_{VV} + 2G \cdot I_{VH}) \quad (1)$$

where, I_{VV} and I_{VH} indicate the emission intensities with the excitation polarizer oriented vertically and emission polarizer oriented vertically and horizontally, respectively, and corresponding G factor is calculated as in eq. (2)[19];

$$G = I_{HV}/I_{HH} \quad (2)$$

where, I_{HV} and I_{HH} refer to the intensities corresponding to the vertical and horizontal positions of the emission polarizer, with the excitation polarizer being horizontal.

Cell culture and cell cytotoxicity assay :

HepG2 (Human hepatocellular liver carcinoma) cell lines (NCCS, Pune, India) grown in DMEM was supplemented with 10% FBS and antibiotics (penicillin –100 μg/ml; streptomycin – 50 μg/ml). Conditions for the culture of cells are : 37 °C in 95% air, 5% CO_2 incubator. To test the cytotoxicity of L_2, the 3-(4,5-di-methylthiazol-2-yl)-2,5-diphenyl-tetrazolium bromide (MTT) assay was performed following the procedure described previously[36–39].

Cell imaging studies :

Cell imaging studies were performed by using the protocol as described previously[36–39].

Results and discussion

A simple reaction between L_1 and methyl acrylate in methanol leads to the formation of L_2 in quantitative yield (Scheme 1) which was thoroughly characterized by ^1H NMR (Fig. S1), ^{13}C NMR (Fig. S2), ESI-MS^+ (Fig. S3) and IR studies (Fig. S4a).

Steady-state absorption and emission studies :

The UV-Vis titrations reveals that on gradual addition of Hg^{2+} to a 50 μM solution of L_2 there occurs a gradual growing of two peaks at 350 nm and 528 nm (Fig. S5) clearly manifesting the chelation induced opening of the spirolactam ring of the probe. The probable coordination mode of L_2 towards Hg^{2+} is demonstrated in Scheme 1. When absorbances were plotted against [Hg^{2+}] it gives a non-linear curve of decreasing slope (Fig. S5). Eq. (3)[19] was employed to solve such dependence with a and b as the absorbance in the absence and presence of excess metal ions, c (= K_f) is the apparent formation constant and n is the stoichio-

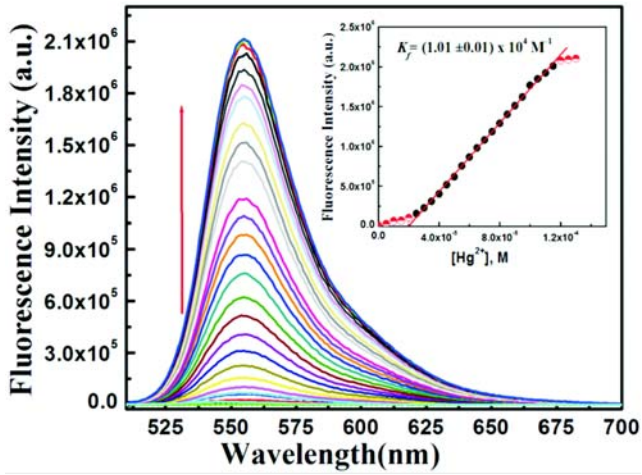

Fig. 1. Fluorescence titration of L_2 (20 μM) in MeCN-H_2O (1 : 1, v/v) in HEPES buffer at pH 7.2 by the gradual addition of Hg^{2+} (0–130 μM) with λ_{ex} = 502 nm. Inset : linear curve-fit of FI vs [Hg^{2+}] plot.

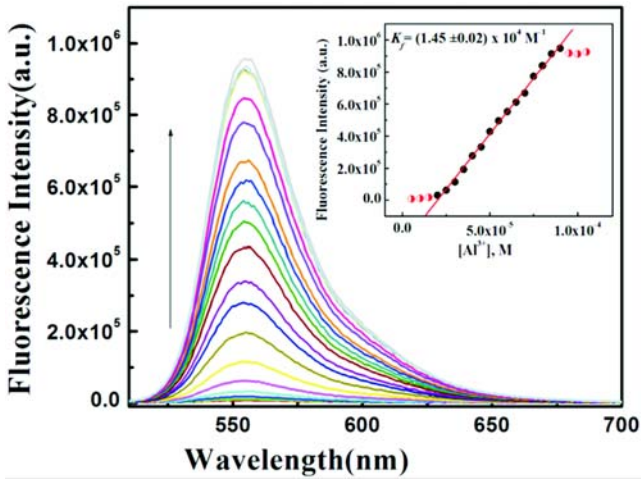

Fig. 2. Fluorescence titration of L_2 (20 μM) in MeCN-H_2O (1 : 1, v/v) in HEPES buffer at pH 7.2 by the gradual addition of Al^{3+} (0–130 μM) with λ_{ex} = 502 nm. Inset : linear curve-fit of FI vs [Al^{3+}] plot.

metry of the reaction. The evaluated apparent association constant K_f is $(3.08\pm0.53)\times10^3$ M^{-1} with n = 1.0.

$$y = \frac{a+bx^n}{1+cx^n} \qquad (3)$$

Job's method also gives 1 : 1 (Fig. S6) complexation between L_2 and Hg^{2+} which was further supported by mass spectrometric analysis (m/z = 440.2579) $[Hg(L_2)(MeOH)(H_2O)]^{2+}$ (see Fig. S3a in the Supporting Information).

The fluorescence titration was carried out by gradual addition of Hg^{2+} (0–130 μM) to a fixed concentration of L_2 (20 μM) in MeCN/water (1 : 1, v/v, HEPES buffer, pH 7.2) which yielded ~126-fold enhancement in fluorescence intensity at 558 nm on excitation at 502 nm (Fig. 1). The titration data were again solved by employing eq. (3) under the condition $1 >> c\times x^n$ with n = 1 prevailing a linear form. A linear least-square fitting of data gives the apparent association constant $K_f = (1.01\pm0.01)\times10^4$ M^{-1} (see Fig. 1 inset). Al^{3+} also induces an opening of spirolactam ring of the probe leading to enhancement of fluorescence intensity. So, analogously the fluorescence titration data for L_2-Al^{3+} complexation was solved and the apparent formation constant was calculated to be $(1.45\pm0.02)\times10^4$ M^{-1}(Fig. 2 inset)

Selectivity of the probe :

The probe was found to be sensitive towards Hg^{2+}, but interfered by the presence of Al^{3+}. However, in the presence of SDS in aqueous medium the fluorescence of L_2-Al^{3+} was completely quenched, but not the L_2-Hg^{2+} complex, instead there was an increase in FI (*vide infra*). In case of L_2-Al^{3+} complexation the quenching of fluorescence intensity may arise due to abstraction of Al^{3+} from the [L_2-Al^{3+}] complex by SDS arising out of strong hard-hard interaction between sulfonic-O and Al^{3+} ion; which is absent for L_2-Hg^{2+} complex. Again, the detection of Hg^{2+} was not perturbed by 5 equivalents of metal ions like Na^+, K^+, Ca^{2+}, Mg^{2+}, Fe^{3+}, Co^{2+}, Cu^{2+}, Cr^{3+}, Mn^{2+}, Fe^{2+}, Ni^{2+}, Zn^{2+}, Cd^{2+} and Pb^{2+} (Fig. 3) under the identical reaction conditions. Also, the introduction of 5 equivalents of anions like SO_4^{2-}, NO_3^-, PO_4^{3-}, S^{2-}, CN^-, Cl^-, F^-, Br^-, I^-, OAc^-, $H_2AsO_4^-$ and N_3^- into the solution of L_2 (Fig. S7) did not show any appreciable fluorescence change. However, I^- has a strong affinity towards Hg^{2+}. As a result I^- abstracts Hg^{2+} ion from the [L_2-Hg^{2+}] complex resulting the disappearance of emission band at 558 nm through the re-establishment of the spirolactam ring (Fig. S8). The quantum yield (ϕ) of the [L_2-Hg^{2+}] complex and ligand were determined to be 0.8609 and

0.011 respectively (rhodamine 6G as a standard). The limits of detection (LOD) of Hg^{2+} and Al^{3+} were found to be as low as 47 and 73 nM, respectively (Fig. S9) as delineated by 3σ method. The increased quantum yield (ϕ) and lifetime (τ) of [L_2-Hg^{2+}] over the free ligand L_2 clearly indicate the enhanced stability of the formed complex in the excited state.

pH-stability of the probe was checked over a wide range of pH (2–12). There is no obvious fluorescence emission of L_2 in the range of pH 4–12, establishing the fact that the spirolactam form of L_2 is stable over this wide pH range (Fig. S10). However, the presence Hg^{2+} ion induces the opening of spirolactam ring at pH ≥ 7.0 resulting a fluorescence enhancement and hence seems to be compatible for biological applications under physiological conditions.

IR studies showed a characteristic amidic "C=O" stretching frequency of the rhodamine moiety at 1723 cm^{-1} which is shifted to a lower wave number (1657 cm^{-1}) in the presence of 1.2 equivalent of Hg^{2+} (Fig. S4b). Thus a strong binding of L_2 to the Hg^{2+} ion and the cleavage of N-C bond in spirolactam ring is apparent. The ^1H NMR spectra showed the ring proton "b" (Fig. 4 and Fig. S1) of the rhodamine moiety is shifted downfield in the presence of 1.2 equivalents of Hg^{2+} ions. The "f" proton of -NH^+ group vanishes as

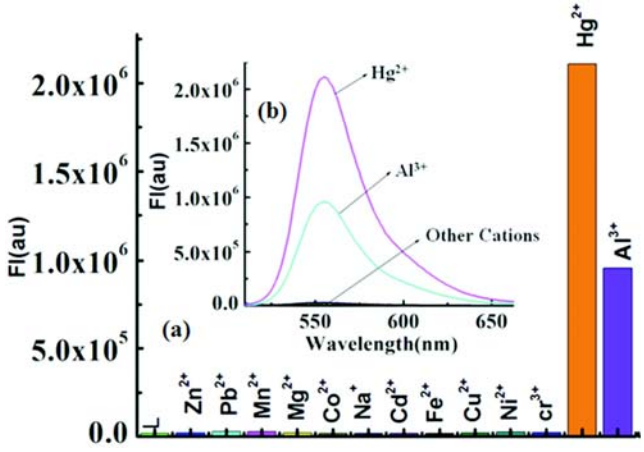

Fig. 3. (a) Histogram of the fluorescence responses of different metal ions (100 mM) towards L_2 (20 mM) in 1 : 1 v/v MeCN/water in HEPES buffer at pH 7.2 with λ_{ex} = 502 nm, λ_{em} = 558 nm. (b) Fluorescence responses of different cations (100 mM) towards L_2 (20 mM) in 1 : 1 v/v MeCN/water in HEPES buffer at pH 7.2.

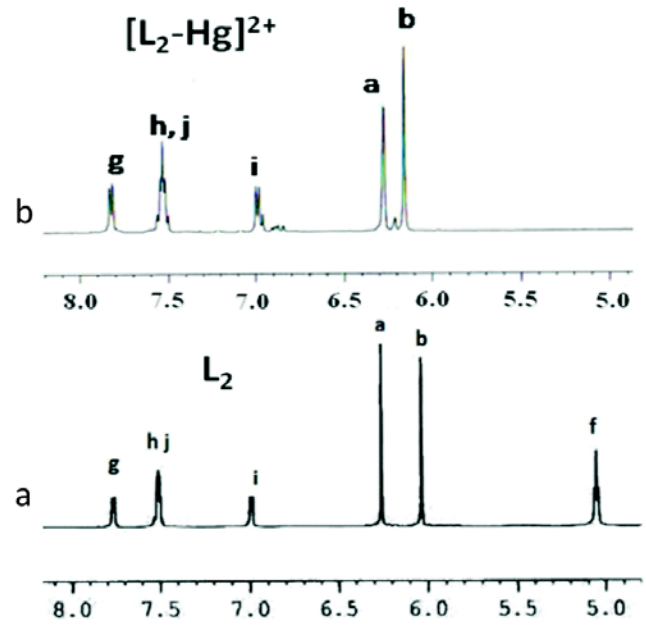

Fig. 4. ^1H NMR spectra of (a) L_2 and (b) L_2 in presence of 1.2 equivalent of Hg^{2+}. Both spectra were recorded on a Bruker 500 MHz spectrometer in DMSO-d_6 (For atom numbering, please see Fig. S1).

this group possesses a positive charge due to ring opening upon binding with Hg^{2+} ion. The "a" proton also shows a down-field shift. The down-field shift of "a" and "b" protons in the presence of Hg^{2+} arises mainly due to decrease in electron density on opening of the spirolactam ring. The signal pattern of the other aromatic protons in [L_2-Hg^{2+}] also indicates the involvement of the receptor unit of L_2 in the binding to Hg^{2+}.

Time resolved fluorescence studies :

The fluorescence decay behaviour of the L_2 and [L_2-Hg^{2+}] were studied in aqueous medium (Fig. S11) both in the absence and presence of SDS. The bi-exponential decay of L_2 resulted life times of 1.53 ns (τ_1) and 6.11 ns (τ_2). But in the presence of SDS it prevails a mono-exponential decay with τ = 3.63 ns. In the presence of Hg^{2+} the decay processes are mono-exponential both in the absence and presence of SDS with respective τ values of 4.47 and 5.44 ns (Fig. S11). Bi-exponential decay of free ligand may arise due to π···π stacking interactions between the probe molecules. The enhanced life time of L_2 and [L_2-Hg^{2+}] complex in the presence of SDS may arise due to enhanced stability of the probe and its complex in the

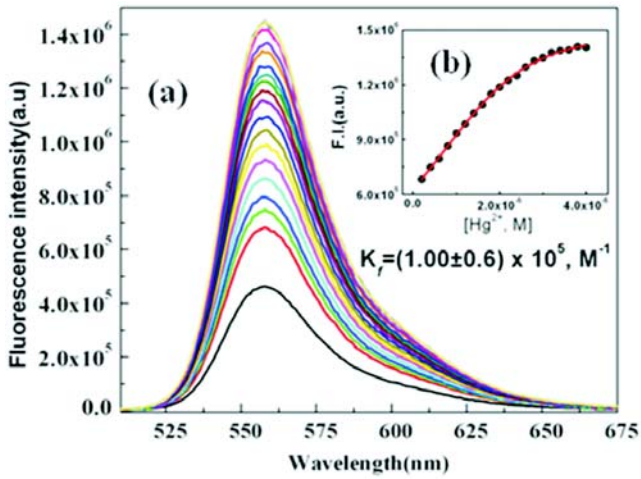

Fig. 5. (a) Florescence titration of L_2 (20 μM) by Hg^{2+} (0–40 μM) in presence of [SDS] = 7 mM with λ_{ex} = 502 nm. (b) Plot of fluorescence intensity as a function of [SDS].

excited state in the presence of SDS. Thus this observation clearly indicates the fact that SDS imposes more restriction on the movement of the probe in microheterogeneous environments through the formation polymeric aggregates.

Steady-state fluorescence studies in aqueous SDS:

In purely aqueous solution the L_2-Hg^{2+} complex is weakly fluorescent, however, in the presence of SDS enhanced fluorescence was observed. Thus, steady state fluorescence studies were also carried out in the presence of SDS in two separate experiments. In one case, the SDS concentration was kept fixed at 7 mM and [Hg^{2+}] was varied in the range 0–40 μM giving a non-linear curve of decreasing slope which was solved by adopting eq. (3) (Fig. 5b) and evaluated apparent formation constant $K_f = (1.00 \pm 0\ 0.02) \times 10^5\ M^{-1}$ was found to be an order of magnitude higher than that obtained in the absence of SDS. This enhanced stability constant value may be due to the restricted movement of the doubly positively charged L_2-Hg^{2+} complex, which were held fixed in position by the strong electrostatic interaction with the negatively charged sulphonic acid head groups of SDS in the form of layer structure. This causes the formation of aggregates of L_2-Hg^{2+} complex through strong cooperative

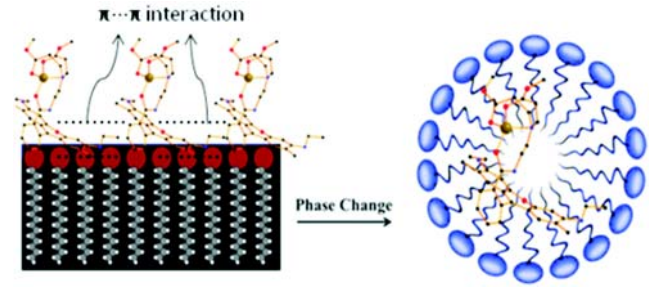

Scheme 2. Schematic presentation of the formation of polymeric aggregates and monomer in presences of SDS before and after the cmc. Adopted from http://www.ecoboss.com.au/img/micelle.jpg.

π···π interactions among the complexes held sidewise (Scheme 2).

In another experiment both [L_2] and [Hg^{2+}] was kept fixed at 20 and 150 μM, respectively and [SDS] was varied between 0–28 mM. A plot of FI vs [SDS] showed a gradual increase in FI with the increase in [SDS], reaches a maximum at ~7 mM and then gradually decreases with the increase in [SDS] (Fig. 6b). The fluorescence maximum at [SDS] ~7 mM clearly points out a critical micellar concentration (CMC) of SDS as ~7 mM under the experimental conditions. The decrease in FI with [SDS] beyond 7 mM may be attributed to a change in polymeric aggregates of the complex to a monomer arising due to the formation of spherical micelle on increasing the [SDS] (Scheme 2) in which the complex is trapped. The increase in FI with [SDS] manifests the fact of aggregation induced enhancement (AIE) of fluorescence. In the case of Al^{3+} ion, fluorescence quenching was observed on increasing the concentration of SDS (Fig. 6c) and may be explained by considering the fact that sulphonic acid group abstract Al^{3+} ion from [L_2-Al^{3+}] complex by strong electrostatic interaction. So in aqueous SDS the probe becomes more selective towards Hg^{2+}. The fluorescence quenching experiment by iodide ion in the presence of [SDS] = 7 mM was carried out to verify such a proposition and was evaluated to be $K_{SV} = (7.23 \pm 4.3) \times 10^6$ indicating an easy accessibility of the [L_2-Hg^{2+}] complex located on the laminar surface of the SDS to I^- ion to form HgI_2.

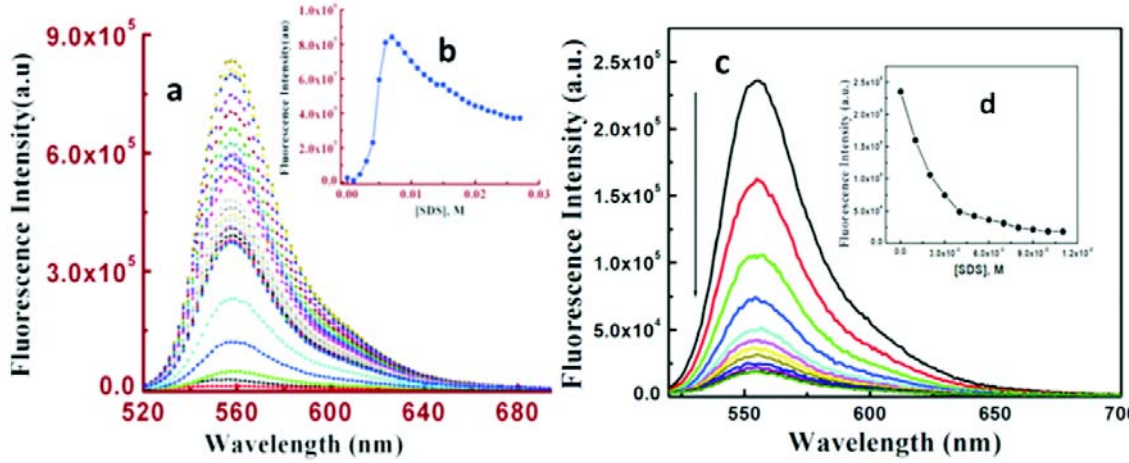

Fig. 6. (a) Fluorescence titration of L_2 (20 μM) by [SDS] in presence of [Hg^{2+}] (130 μM) with λ_{ex} = 502 nm; (b) plot of fluorescence intensity as a function of [SDS]; (c) fluorescence titration of L_2 (20 μM) by [SDS] in presence of [Al^{3+}] (130 μM) with λ_{ex} = 502 nm; (d) plot of fluorescence intensity as a function of [SDS].

Determination of steady-state fluorescence anisotropy :

Steady-state fluorescence anisotropy is usually taken as a measure of the extent of restriction imposed by the micro heterogeneous environments on the dynamic properties of the probe. An increase in rigidity of the fluorophore results in an increase in the fluorescence anisotropy[19]. We have monitored the fluorescence anisotropy as a function of SDS concentration at a fixed concentration of L_2 and Hg^{2+} (20 and 150 μM, respectively) at 558 nm which showed a marked increase in anisotropy on increasing SDS concentration up to 3.5 mM, then gradually decreases with SDS concentration reaches a plateau at ~5 mM and maintains steady value up to 12 mM. In the range 1–3.5 mm concentration, the SDS arranges them in a layered fashion. Now, the doubly charged [L_2-Hg^{2+}] complexes are held firmly by the strong electrostatic interactions between negatively charged sulfonic acid head groups and doubly positively charged complexes; which are again held together by strong π···π interactions thereby restricting their free movement. As a result, there occurs a sharp increase in anisotropy in the [SDS] ~1–3.5 mM. Further increase in the SDS concentration, a phase transition occurs through the formation of micelle. The slight drop in *r* values with [SDS] beyond 3.5 mM may be rationalized by considering the formation of a monomer of [L_2-Hg^{2+}] complex which is again trapped inside the cavity of the micelle. The higher values of *r* in case of polymeric aggregates arise due to cooperative interactions among the [L_2-Hg^{2+}] complexes which is absent in monomer trapped inside the cavity of the micelle. The variation of fluorescence anisotropy (*r*) as a function of SDS concentration is presented in Fig. 7.

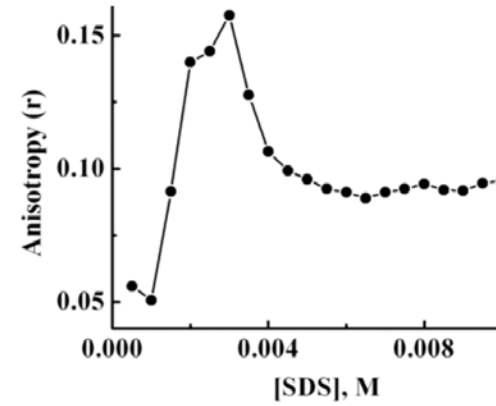

Fig. 7. Plot of fluorescence anisotropy (*r*) as a function of [SDS] in purely aqueous medium at 25 °C and [L_2] = [Hg^{2+}] = 20 μM, λ_{ex} = 502 nm, λ_{em} = 558 nm.

SEM study :

The SEM micrographs of L_2 (0.50 mM) prevails rod-like microstructures which interestingly changes to porous like architecture in presence of Hg^{2+} (0.50 mM) (Fig. 8). In case of pure ligand in water the

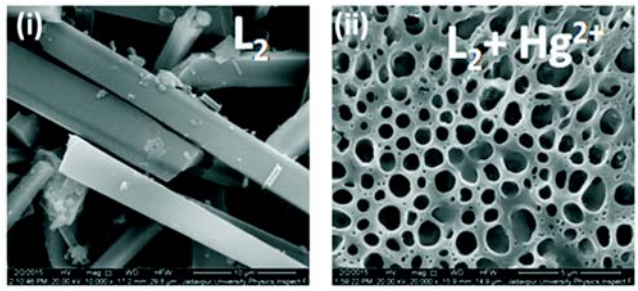

Fig. 8. SEM images of microstructures conditions : (i) L_2 0.5 mM and (ii) L_2+Hg^{2+} (0.5 mM each) in aqueous medium.

structures are similar to the hexagonal prisms that arises due to the presence of two different polar ends (xanthine moiety and carboxylic ester moiety) favoring the stacking of L_2 one over another. However, in presence of Hg^{2+} these stacking interactions are disrupted leading to the formation of porous microstructures centering Hg^{2+} with the ligands at the periphery.

Cell imaging applications :

Hg^{2+} capturing capability of L_2 was assessed by performing the fluorescence imaging of L_2 with Hg^{2+} into the live HepG2 cells (Fig. 9). The cytotoxicity effects of L_2 determined by MMT assay indicate no significant cell cytotoxicity for HepG2 cells up to 60 μM (<30% cytotoxicity) of L_2 (Fig. S13). Interestingly, up to 10 μM of L_2 there was more than 90% of cell viability and fluorescence imaging were carried out at 1 μM, 5 μM and 10 μm of L_2. Significantly, an excellent red intracellular cytoplasmic fluorescence was observed inside the live HepG2 cells pre-incubated with 10 μM of Hg^{2+} followed by washing with 1X PBS and subsequent incubation with 1 μM, 5 μM and 10 μM of L_2. Interestingly, we observed that L_2 has excellent Hg^{2+} capturing capability even at low concentration likely at 1 μM and 5 μM at cytoplasmic level of Hg^{2+} ions (Fig. 9). Moreover, the concentration dependent binding of the L_2 with Hg^{2+} ions was observed (Fig. 9). Parallel staining of cells were carried out with DAPI and superimposed with the correspondingly treated cells with Hg^{2+} (10 μM) followed by L_2 (10, 1, 5, 10 μM) to show the cytoplasmic staining of L_2 with HepG2 cells.

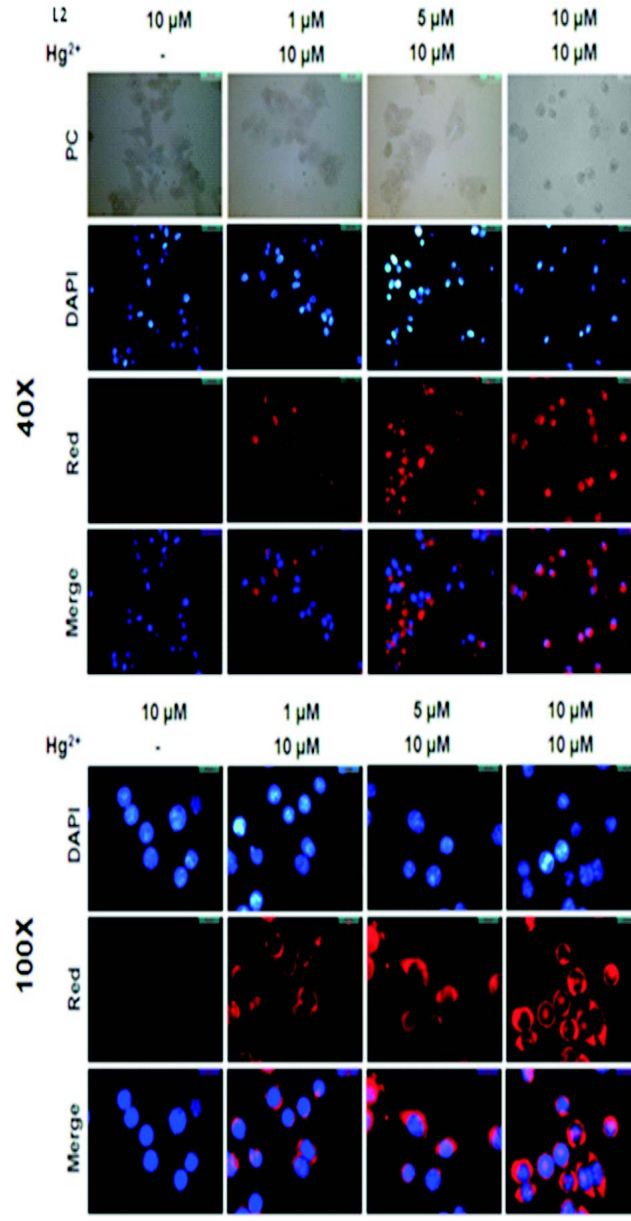

Fig. 9. Cell imaging study of Hg^{2+} ions with L_2. The fluorescence images of HepG2 cells were captured (40X and 100X) after incubated with 10 μM of L_2 for 30 min at 37 °C, also in pre-incubated 10 μM of Hg^{2+} for 3 h at 37 °C followed by washing twice with 1X PBS and, subsequent incubation with 1 μM, 5 μM and 10 μM of ligand L_2 for 30 min at 37 °C. The imaging studies showed the strong red fluorescence when L_2 binds with cytoplasmic Hg^{2+} ions. The merge images show the cytoplasmic Hg^{2+}-L_2 fluorescence.

Conclusions

In summary, we present herein a rhodamine-based chemosensor with potential NO_3 donor atoms for the selective and rapid recognition of toxic Hg^{2+} ions. The binding stoichiometry of the sensor with Hg^{2+} was established by the combined Job's and HRMS (*m/z*) methods. All biologically relevant as well as toxic heavy metal ions did not interfere with the detection of Hg^{2+} ion. The detection limit of Hg^{2+} calculated by 3σ method gives a value of 1.52 nM. Its exhibits live cell imaging application of Hg^{2+} with no or negligible cytotoxicity. SEM studies reveal a rod-like microstructure for L_2 which changes to a porous microstructure in presence of Hg^{2+} (0.50 mM). The presence of SDS causes enhanced quantum yield (θ), life time (τ), and stability constant (K_f) by an order of magnitude compared to those in the absence of SDS. Again, the FI of [L_2-Hg^{2+}] complex is enhanced by 33-fold in the presence of 7 mM SDS to that in the absence of SDS. In SDS/water system, there is a steep rise in FI with the increase in [SDS], reaches a maximum at ~7 mM and then FI decreases gradually with the increase in [SDS] up to 28 mM, indicating the formation of polymeric aggregates of [L_2-Hg^{2+}] complex on layers of the SDS at pre-miceller concentrations with higher FI values – a phenomenon reminiscent with the aggregation induced emission enhancement (AIEE). However, it turns into monomer and trapped inside the cavity of the micelle beyond CMC with comparatively lower FI. This proposition is further supported by the dependence of fluorescence anisotropy (*r*) with [SDS].

Acknowledgement

Financial supports from DST, New Delhi (Ref. SR/S1/IC-20/2012) and UGC CAS-II are gratefully acknowledged.

References

1. F. J. M. Hoeben, P. L. Jonkheijm, E. W. Meijer and A. P. H. J. Schenning, *Chem. Rev.*, 2005, **105**, 1491.
2. T. L. Greaves and C. J. Drummond, *Chem. Soc. Rev.*, 2008, **37**, 1709.
3. T. H. Rehm and C. Schmuck, *Chem. Soc. Rev.*, 2010, **39**, 3597.
4. T. L. Greaves and C. J. Drummond, *Chem. Soc. Rev.,* 2013, **42**, 1096.
5. B. K. An, J. Gierschner and S. Y. Park, *Acc. Chem. Res.*, 2012, **45**, 544.
6. X. Luo, J. Li, C. Li, L. Heng, Y. Q. Dong, Z. Liu, Z. Bo and B. Z. Tang, *Adv. Mater.,* 2011, **23**, 3261.
7. K. Dhara, Y. Hori, R. Baba and K. Kikuchi, *Chem. Commun.*, 2012, **48**, 11534.
8. Y. Ren and T. Baumgartner, *Inorg. Chem.*, 2012**, 51**, 2669.
9. C. Shi, Z. Guo, Y. Yan, S. Zhu, Y. Xie, Y. S. Zhao, W. Zhu and H. Tian, *ACS Appl. Mater. Interfaces*, 2013, **5**, 192.
10. J. Luo, Z. Xie, J. W. Y. Lam, L. Cheng, H. Chen, C. Qiu, H. S. Kwok, X. Zhan, Y. Liu, D. Zhu and B. Z. Tang, *Chem. Commun.*, 2001, 1740.
11. X. Huang, X. Gu, G. Zhang and D. Zhang, *Chem. Commun.,* 2012, **48**, 12195.
12. S. Li, S. M. Langenegger and R. Haner, *Chem. Commun.,* 2013, **49**, 5835.
13. W. Wu, S. Ye, R. Tang, L. Huang, Q. Li, G. Yu, Y. Liu, J. Qin and Z. Li, *Polymer,* 2012, **53**, 3163.
14. B. K. An, S. K. Kwon, S. D. Jung and S. Y. Park, *J. Am. Chem. Soc.*, 2002, **124**, 14410.
15. S. J. Li, B. K. An, S. D. Jung, M. A. Chung and S. Y. Park, *Angew. Chem., Int. Ed.*, 2004, **43**, 6346.
16. M. Rosoff, Ed. Vesicles, Dekker, New York, 1996.
17. A. M. Carmona-Ribeiro, *Chem. Soc. Rev.*, 1992, **21**, 209.
18. S. Dutta Choudhury, A. C. Bhasikuttan, H. Pal and J. Mohanty, *Langmuir,* 2011, **27**, 12312.
19. R. Bhowmick, R. Alam, T. Mistri, D. Bhattacharya, P. Karmakar and M. Ali, *Appl. Mater. Interfaces,* 2015, **7**, 7476.
20. R. Bhowmick, A. S. M. Islam, A. Katarkar, K. Chaudhuri and M. Ali, *Analyst*, 2016, **141**, 225.
21. H. N. Kim, W. X. Ren, J. S. Kim and J. Yoon, *Chem. Soc. Rev.,* 2012, **4**, 3210.
22. D. G. He, X. X. He, K. M. Wang, Y. X. Zhao and Z. Zou, *Langmuir,* 2013, **29**, 5896.
23. Y. C. Shih, C. Y. Ke, C. J. Yu, C. Y. Lu and W. L. Tseng, *ACS Appl. Mater. Interfaces,* 2014, **6**, 17437.
24. P. B. Tchounwou, W. K. Ayensu, N. Ninashvili and D. Sutton, *Environ. Toxicol.,* 2003, **18**, 149.
25. A. C. Bittner (Jr.), D. Echeverria, J. S. Woods, H. Vasken. Aposhian, C. Naleway, M. D. Martin, R. K. Mahurin, N. J. Heyer and M. Cianciola,

Neurotoxicol. Teratol., 1998, **20**, 429.

26. Mercury Study Report to Congress, United States Environmental Protection Agency, Volume V : Health Effects of Mercury and Mercury Compounds, EPA-452/R-97-007 December 1997.
27. M. Suresh, A. Ghosh and A. Das, *Chem. Commun.,* 2008, 3906.
28. O. A. Bozdemir, R. Guliyev, O. Buyukcakir, S. Selcuk, S. Kolemen, G. Gulseren, T. Nalbantoglu, H. Boyaci and E. U. Akkaya, *J. Am. Chem. Soc.,* 2010, **132**, 8029.
29. A. Thakur, S. Sardar and S. Ghosh, *Inorg. Chem.,* 2011, **50**, 7066.
30. J. R. Lakowicz, "Principles of Fluorescence Spectroscopy", 3rd. ed., Springer, New York, 2006, **67**.
31. R. P. Haugland, "The Handbook : A Guide to Fuorescent Probes and Labeling Technologies", 10th ed., Invitrogen Corp., Karlsbad, CA, 2005.
32. H. Y. Lee, K. M. K. Swamy, J. Y. Jung, G. Kim and J. Yoon, *Sens. Actuators (B)*, 2013, **182**, 530.
33. X. Chen, T. Pradhan, F. Wang, J. S. Kim and J. Yoon, *Chem. Rev.*, 2012, **112**, 1910.
34. K. Bera, A. K. Das, M. Nag and S. Basak, *Anal. Chem.*, 2014, **86**, 2740.
35. V. Dujols, F. Ford and A. W. Czarnik, *J. Am. Chem. Soc.*, 1997, **119**, 7386.
36. J. S. Wu, I. C. Hwang, K. S. Kim and J. S. Kim, *Org. Lett.*, 2007, **9**, 907.
37. R. Alam, T. Mistri, P. Mondal, D. Das, S. K. Mandal, A. R. Khuda-Bukhsh and M. Ali, *Dalton Trans.,* 2014, **43**, 2566.
38. R. Alam, T. Mistri, A. Katarkar, K. Chaudhuri, S. K. Mandal, A. R. Khuda-Bukhsh, K. K. Das and M. Ali, *Analyst,* 2014, **139**, 4022.
39. R. Bhowmick, M. Dolai, R. Alam, T. Mistri, A. Katarkar, K. Chaudhuri and M. Ali, *RSC Adv.,* 2014, **4**, 41784.

Analyst

ROYAL SOCIETY OF CHEMISTRY

PAPER

View Article Online
View Journal | View Issue

Cite this: *Analyst*, 2022, **147**, 471

Rhodamine 6G-based efficient chemosensor for trivalent metal ions (Al^{3+}, Cr^{3+} and Fe^{3+}) upon single excitation with applications in combinational logic circuits and memory devices†

Dipankar Das,[a] Rabiul Alam [a] and Mahammad Ali *[a,b]

A new rhodamine 6G-based chemosensor (**L**^{3}) was synthesized and characterized by ^{1}H, ^{13}C, IR and mass spectroscopy studies. It exhibited an excellent selective and sensitive **CHEF**-based recognition of trivalent metal ions M^{3+} (M = Fe, Al and Cr) over mono and di-valent and other trivalent metal ions with prominent enhancement in the absorption and fluorescence intensity for Fe^{3+} (669-fold), Al^{3+} (653-fold) and Cr^{3+} (667-fold) upon the addition of 2.6 equivalent of these metal ions in the probe in H_2O/CH_3CN (7 : 3, v/v, pH 7.2). The corresponding K_d values were evaluated to be 1.94×10^{-5} (Fe^{3+}), 3.15×10^{-5} (Al^{3+}) and 2.26×10^{-5} M (Cr^{3+}). The quantum yields of **L**^{3}, [**L**^{3}–Fe^{3+}], [**L**^{3}–Al^{3+}] and [**L**^{3}–Cr^{3+}] complexes in H_2O/CH_3CN (7 : 3, v/v, pH 7.2) were found to be 0.0005, 0.335, 0.327 and 0.333, respectively, using rhodamine-6G as the standard. The LODs for Fe^{3+}, Al^{3+} and Cr^{3+} were determined by 3σ methods and found to be 2.57, 0.78 and 0.47 μM, respectively. The cyanide ion snatched Fe^{3+} from the [Fe^{3+}–**L**^{3}] complex and quenched its fluorescence *via* its ring-closed spirolactam form. Advanced level molecular logic devices using different inputs (2 and 4 input) and a memory device were constructed.

Received 2nd October 2021,
Accepted 9th December 2021

DOI: 10.1039/d1an01788h

rsc.li/analyst

1. Introduction

Due to their biological and environmental importance, the selective and sensitive detection of transition metal ions through the design of suitable fluorescent chemosensors has attracted the deep attention of chemists and biologists.[1,2] The excess or deficiency of a metal ion in a living system can lead to several diseases. Although, chemosensors for single analyte detection are plentiful, chemosensors corresponding to multiple metal-ion detection have been less explored,[3] even though a number of trivalent metal ions, like Fe^{3+}, Al^{3+} and Cr^{3+}, are important both biologically and environmentally. As for example, Cr^{3+}, an essential trace element, displays a huge impact on the metabolism of carbohydrates, fats, proteins and nucleic acids through the activation of certain enzymes and by the stabilization of proteins and nucleic acids.[4,5] It also plays an important role in the maintenance of normal levels of glucose, triglycerides and total cholesterol.[6–11] While an overdose of Cr^{3+} inflicts a negative effect on normal enzymatic activities, and cellular structure and function, causing a disturbance in glucose levels and lipid metabolism, its deficiency would lead to a variety of diseases, including the risk of diabetes, cardiovascular diseases and nervous system disorders.[12]

The Cr^{3+} ion, present in the cytoplasm, can lead to mutation and cancer due to non-specific binding to DNA at elevated levels affecting the cellular structures and damaging the cellular components.[13] Moreover, Cr^{6+}, the oxidized form of Cr^{3+}, is extremely toxic and carcinogenic as it can easily penetrate cell membranes, causing cancers through the oxidation of DNA and some proteins.[14–17]

Aluminium (Al^{3+}), the third most prevalent element on Earth, is widely present in the Earth's crust and in most kind of animal and plant tissues and natural waters.[18–22] It has found wide applications in the food, textile and paper industries and also in the manufacture of household utensils. According to the World Health Organization (WHO), aluminium is a food pollutant and the WHO prescribed a safe Al concentration of 200 mg L^{-1} in drinking water.[23] It accumulates in various mammalian tissues, such as the brain, bone, liver and kidney,[24,25] where it causes renal failure,[26] which is associated with age.[27] Aluminium toxicity damages the central nervous system, resulting in neurodegenerative Alzheimer and Parkinson diseases.[28]

Among these trivalent metal ions, Fe^{3+} is an essential element in living organisms and plays a vital role in the life process of organisms[29] and in many biological activities of organisms, such as muscle contraction, nerve conduction and

[a]*Department of Chemistry, Jadavpur University, Kolkata 700 032, India. E-mail: mali2062@yahoo.com; Fax: +91-33-2414-6223*
[b]*Vice-Chancellor, Aliah University, IIA/27 New Town, Kolkata 700160, India*
†Electronic supplementary information (ESI) available. See DOI: 10.1039/d1an01788h

enzyme catalysis.[30] On the other hand, the excess accumulation of Fe^{3+} can lead to a variety of diseases, such as cell damage and organ dysfunction through the abnormal production of reactive oxygen species (ROS),[31,32] leading to Alzheimer's, Huntington's, Parkinson's diseases, *etc.*[33]

Over the past few decades, traditional techniques, like atomic absorption spectroscopy (AAS), inductively coupled plasma atomic emission spectroscopy (ICP-AES) voltammetry and X-ray photoelectron spectrometry (XPS), have been used for heavy-metal-ion detection.[34–37] Compared with these complicated methods, optical probes are simple, low cost, highly sensitive and selective and one of the finest way of performing detection.

So, there is an urgent need to design a single fluorogenic probe, displaying changes in optical properties through a "turn-on" response towards Fe^{3+}, Al^{3+} and Cr^{3+} simultaneously and in the presence of a large number of mono-, di- or other trivalent metal cations in biological and environmental samples.

The trivalent metal cations, *e.g.* Fe^{3+}, Cr^{3+} and Al^{3+}, are environmentally and biologically important and are involved directly in many cellular functions. Al^{3+} is diamagnetic while Fe^{3+} and Cr^{3+} are paramagnetic. As a consequence, the latter two ions are expected to show turn-off sensing. However, our probe, $\mathbf{L^3}$, was so designed that all these cations would show a turn-on sensing property together or in the presence of any of them. Very few turn-on rhodamine-6G-based sensors for Cr^{3+} and Fe^{3+} have been reported to date.[38–40]

Due to its strong hydration in aqueous medium, Al^{3+} exhibits a turn-on fluorescent response towards a very few number of probes.[28] As a result, most of the reported dye-based Al^{3+} sensors require organic solvents.[41] The excellent optical properties, such as a high molar extinction coefficient, good light stability, high fluorescence quantum yield, large excitation and visible emission wavelengths (>500 nm), and insensitivity towards pH make rhodamine-6G derivatives suitable fluorescent probes towards different metal ions.[42]

We report herein a rhodamine-6G-based probe $\mathbf{L^3}$ (Schemes 1 and 2), which was characterized by ^{1}H NMR (Fig. S1†), ^{13}C NMR (Fig. S2†), mass spectrophotometry (Fig. S3†) and IR (Fig. S4†) studies. It displays the capability for the selective detection of trivalent cations, like Fe^{3+}, Al^{3+} and Cr^{3+}, in mixed aqueous medium (7 : 3, H_2O : CH_3CN, v/v) with a very high fluorescence enhancement over mono-, di- and other trivalent metal ions with a low limit of detection (LOD).

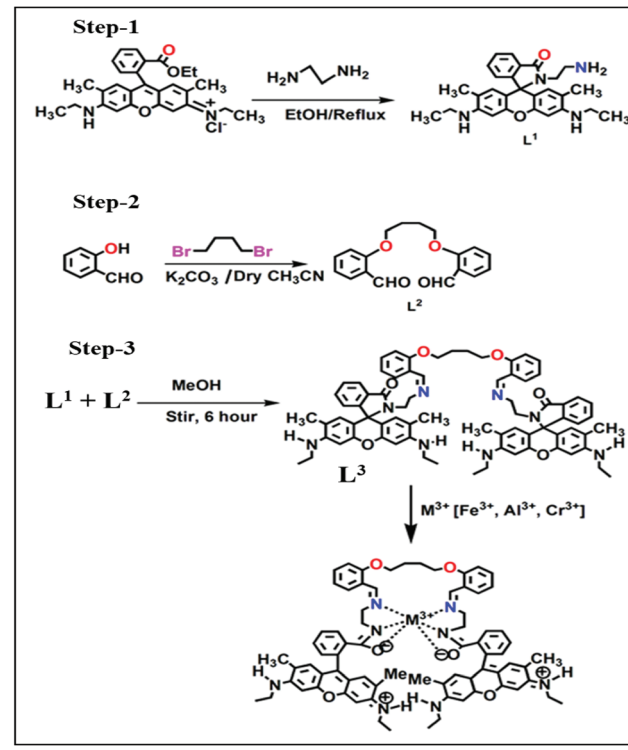

Scheme 1 Synthetic route to the chemosensor $\mathbf{L^3}$ and its tentative binding mode with M^{3+}.

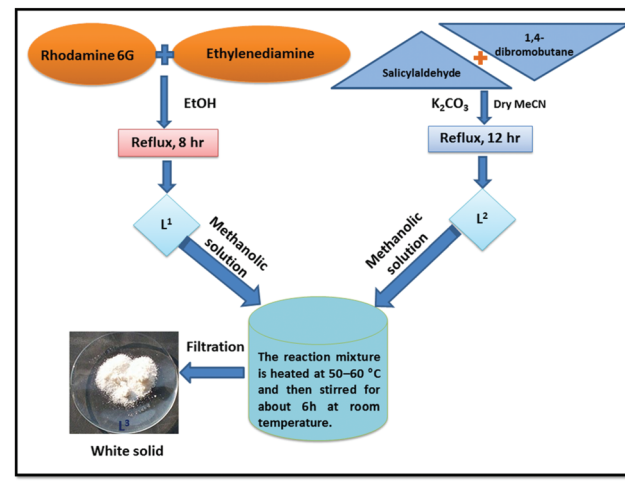

Scheme 2 Flow chart showing the synthetic route to the chemosensor $\mathbf{L^3}$.

Experimental section

Materials and methods

All the solvents used in the synthetic works were reagent-grade (Merck). For the spectroscopic (UV/Vis and fluorescence) studies, HPLC-grade MeCN and double-distilled water were used. Rhodamine 6G hydrochloride and metal salts, such as perchlorates of Na^+, Fe^{2+}, Co_2^+, Ni^{2+}, Zn^{2+}, Pb^{2+}, Cd^{2+}, Hg^{2+}, Cu^{2+}, $Al(NO_3)_3{\cdot}9H_2O$, $CrCl_3{\cdot}6H_2O$ and $Fe(NO_3)_3{\cdot}9H_2O$, were purchased either from Sigma-Aldrich or Merck and used as received. All the other compounds were purchased from commercial sources and used without further purification.

Physical measurements

The ^{1}H-NMR spectra were recorded in $CDCl_3$, on a Bruker 300 MHz NMR spectrometer using tetramethylsilane (δ = 0)

as an internal standard. The infrared spectra (400–4000 cm^{-1}) were recorded in the liquid state in a Nickolet Magna IR 750 series-II FTIR spectrometer. ESI-MS^+ (m/z) of the ligand and complexes were recorded on a Waters' HRMS spectrometer (Model: XEVO G2QTof). UV-Vis spectra were recorded on an Agilent diode-array spectrophotometer (Model, Agilent 8453). Steady-state fluorescence measurements were performed on a PTI QM-40 spectrofluorometer. The pH of the solutions were recorded by a digital pH meter 335, calibrated using pH 4, 7 and 10 buffers in the range pH 2–12.

Preparation of the probe L^3

Rhodamine-6G ethylenediamine ($\mathbf{L^1}$) was prepared according to a literature method (Scheme 2).[43]

Preparation ($\mathbf{L^2}$). $\mathbf{L^2}$ was prepared by a slight modification of the literature procedure.[44] Salicylaldehyde (10 mmol, 1.23 g) and K_2CO_3 (18 mmol, 2.52 g) were added to dry MeCN (60 mL), and the mixture was refluxed for 40 min. Then, 1,4-dibromobutane (5 mmol, 1.08 g) was added to the above reaction mixture, which was further refluxed for 12 h. Then the mixture was cooled and filtered. The filtrate was evaporated to one-third of its initial volume and diluted with water (40 mL). Then the pH of the solution was adjusted to 4.0 by the addition of 1 M HCl and extracted with dichloromethane (DCM; 2 × 40 mL). The pH of the aqueous solution was then adjusted to 8 by the addition of 4.0 M Na_2CO_3 solution and extracted with DCM (3 × 40 mL). Then the combined organic phases, after drying with anhydrous Na_2SO_4, was evaporated to dryness under reduced pressure to give a yellowish-brown solid residue. The crude solid product was recrystallized in MeOH to give the desired pure product as an off-white crystalline solid (66% yield) (Scheme 2). MS (ES^+): m/z = 321.112 [$\mathbf{L^2}$ + $Na]^+$(Fig. S3†). $C_{18}H_{18}O_4$ (298.33): calcd C 72.47, H 6.08; found C 72.46, H 6.09.

Preparation of the probe $\mathbf{L^3}$. $\mathbf{L^2}$ (1 mmol, 0.2983 g) in MeOH (10 mL) was added dropwise over a period of 30 min to a methanolic solution (30 mL) of $\mathbf{L^1}$ (1 mmol, 0.456 g) under hot conditions (*ca.* 50–60 °C). Then the reaction mixture was stirred for around 6 h at room temperature. A white precipitate was formed, which was collected by filtration. The residue was washed thoroughly with cold methanol and purified by crystallization to isolate $\mathbf{L^3}$ in a pure form in 84% yield (Scheme 2). ^{1}H NMR ($CDCl_3$): δ = 1.16 (12H, t, –CH3), 1.88 (4H, m, $–CH_2$), 2.49 (12H, s, –CH3), 3.08 (4H, m, –CH2), 3.14 (8H, m, $–CH_2$), 4.06 (4H, s, –NH), 6.06 (4H, s, –Ar-H), 6.25 (4H, s, –Ar-H), 6.84 (2H, d, –Ar-H), 6.97 (4H, d, –Ar-H), 7.28 (2H, d, Ar-H), 7.48 (4H, m,-Ar-H), 7.58 (d, 2H, Ar-H), 7.77 (2H, d, –Ar-H), 8.24 (2H, s) (Fig. S1†). ^{13}C NMR: 14.57, 17.40, 25.80, 31.15, 37.95, 59.07, 64.78, 68.05, 79.41, 96.02, 105.15, 112.88, 118.74, 120.80, 122.75, 124.10, 124.20, 127.16, 128.09, 128.73, 131.04, 132.43, 133.15, 148.15, 151.58, 153.83, 157.38, 158.02, 167.34 (Fig. S2†). $C_{74}H_{78}N_8O_6$ (1175.46): calcd C 75.61, H 6.69, N 9.53; found C 75.57, H 6.68, N 9.54. ESI-MS^+ (m/z): 1175.61 ($\mathbf{L^3}$ + H^+) (Fig. S3a†). IR spectrum: 1699 cm^{-1} (–C═O), 1378 cm^{-1} (–C–N), 1637 cm^{-1} (C═N) (Fig. S4†).

Solution preparation for the UV-Vis and fluorescence studies

For both the UV-Vis and fluorescence titrations, a stock solution of 1.0×10^{-3} M of probe $\mathbf{L^3}$ was prepared by dissolving it in 25 mL CH_3CN. Analogously, 1.0×10^{-3} M stock solutions of Fe^{3+}, Al^{3+} and Cr^{3+} were prepared in MeOH. A solution of 20 mM HEPES buffer (7 : 3, H_2O : CH_3CN) was prepared and the pH was adjusted to 7.2 by using HCl and NaOH. For the UV-Vis spectra, 60 μM probe was taken in a cuvette containing 2.5 mL of buffer solution, and Fe^{3+} salt solution was added incrementally starting from 0 to 336 μM in a regular interval of time and the absorption spectra were recorded. Similar experiments were performed for Al^{3+} and Cr^{3+}. Again 2.5 mL of this buffer solution was pipetted into a cuvette to which 60 μM of the probe ($\mathbf{L^3}$) solution was added and Fe^{3+} salt solution was added incrementally starting from 0 to 160 μM in a regular interval of time (3 min) and the fluorescence spectra were recorded setting the excitation wavelength at 502 nm. Similar titrations were conducted with Al^{3+} and Cr^{3+}. The path lengths of the cells used for the absorption and emission studies were 1 cm. Fluorescence measurements were performed using a 2 nm × 2 nm slit width.

Job's plot

The Job's method is based on the measurement of the fluorescence of a series of solutions in which the molar concentrations of the probe ($\mathbf{L^3}$) and M^{3+} were varied but their sum remained constant. The fluorescence of each solution was measured at 558 nm and plotted against the mole fraction of M^{3+}. A maximum fluorescence occurred at the mole ratio corresponding to the combining ratio of the two components. The composition of the complex was determined by Job's method and found to be (1 : 1) with respect to $\mathbf{L^3}$ for Fe^{3+}, Al^{3+} and Cr^{3+} complexes.

Calculation of LOD

The analytical detection limit was obtained by performing the fluorescence titration of $\mathbf{L^3}$ with M^{3+} by adding aliquots in a micromolar concentration of M^{3+} to 20 μM solution of $\mathbf{L^3}$ in 2.5 mL buffer and the LOD was calculated by the 3σ method.[47,48] LOD = $3 \times S_d/S$, where S_d is the standard deviation of the intercept of the blank ($\mathbf{L^3}$ only) obtained from a plot of the fluorescence intensity (FI) *versus* [$\mathbf{L^3}$], and S is the slope obtained from the linear part of the plot of FI *versus* [M^{3+}].

Results and discussion

As depicted in Scheme 1, receptor $\mathbf{L^3}$ was synthesized from the reaction between $\mathbf{L^1}$ and $\mathbf{L^2}$ in MeOH under stirring for 6 h. The final crystallized product ($\mathbf{L^3}$) was well characterized by ^{1}H NMR (Fig. S1†), ^{13}C NMR (Fig. S2†), IR (Fig. S4†) and mass spectrophotometry (Fig. S3†) studies. The receptor $\mathbf{L^3}$ was found to be very sensitive as a selective colorimetric and fluorogenic chemosensor for trivalent metal ions, M^{3+} (M^{3+} = Fe^{3+}, Al^{3+} and Cr^{3+}), while in the absence of M^{3+}, the solution of $\mathbf{L^3}$ was colourless and non-fluorescent.

UV-Vis absorption studies

The UV-Vis spectra were recorded in the mixed aqueous solvent H_2O/CH_3CN (7 : 3, v/v, pH 7.2, 20 mM HEPES buffer). The UV-Vis titration revealed that with the gradual addition of Fe^{3+}, Al^{3+} or Cr^{3+} separately to the $\mathbf{L^3}$ (60 μM) solution, an absorption band appeared at 528 nm [Fig. 1(a), Fig. S5 and S5a, ESI†] with a sharp visual colour change of the representative solution from colourless to orange-red, whereas no such peak appeared in the presence of mono-, di- or other trivalent metal ions in solution. The appearance of this peak clearly manifested the opening of the spirolactam ring through the chelation of M^{3+} (Fe^{3+}, Al^{3+} and Cr^{3+}) with the probe. The probable coordination mode of $\mathbf{L^3}$ towards M^{3+} is demonstrated in Scheme 1. UV-Vis titrations were carried out by varying the trivalent metal-ion concentrations (0–336 μM), while keeping the probe concentration fixed at 60 μM at a pH of 7.2 (20 mM HEPES buffer, H_2O/CH_3CN (7 : 3, v/v). Plots of the absorbance *vs.* $[M^{3+}]$ yielded non-linear curves, which were analyzed by adopting non-linear curve-fitting methods,[45,46] and the evaluated K_d values were 6.32×10^{-5} (Fe^{3+}); 3.48×10^{-5} (Al^{3+}) and 9.48×10^{-5} M (Cr^{3+}).

Fluorescence studies

The emission spectra of $\mathbf{L^3}$ and its fluorescence titration with M^{3+} (Fe^{3+}, Al^{3+} and Cr^{3+}) were performed in H_2O/CH_3CN (7 : 3, v/v, pH 7.2, 20 mM HEPES buffer) keeping concentration of $\mathbf{L^3}$ fixed at 60 μM. A significant turn-on fluorescence emission was observed in the presence of Fe^{3+}, Al^{3+} and Cr^{3+} with a maximum fluorescence intensity at 558 nm. For example, upon the gradual addition of Fe^{3+} (0–2.6 equivalent) to the non-fluorescent solution of $\mathbf{L^3}$, a 669-fold enhancement in fluorescence intensity at 558 nm was observed following excitation at 502 nm, which also suggested the opening of the spirolactam ring in $\mathbf{L^3}$ on coordination to the Fe^{3+} ion[47] (Fig. 2). Similarly, 653-fold and 667-fold enhancements in fluorescence intensity were observed during the titration of $\mathbf{L^3}$ with Al^{3+} and Cr^{3+}, respectively (Fig. S6 and S6a†).

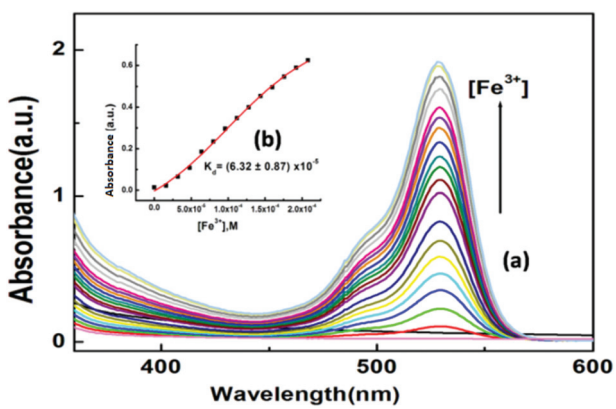

Fig. 1 (a) UV-Vis absorption spectra of $\mathbf{L^3}$ (60 μM) in H_2O/CH_3CN (7 : 3, v/v, pH 7.2, 20 mM HEPES buffer) with the incremental addition of Fe^{3+} (0–336 μM); (b) Non-linear curve-fitting of the absorbance *vs.* $[Fe^{3+}]$ plot.

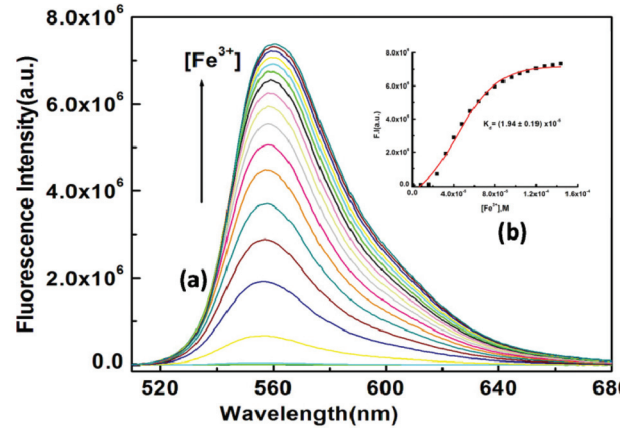

Fig. 2 (a) Fluorescence spectra of $\mathbf{L^3}$ (60 μM) in H_2O/CH_3CN (7 : 3, v/v, pH 7.2, 20 mM HEPES buffer) solutions upon the addition of Fe^{3+} (160 μM), each spectrum was taken in 3 min time interval after addition of Fe^{3+}, λ_{ex} = 502 nm, λ_{em} = 558 nm; (b) non-linear fitting of the titration curve with the K_d values.

Likewise, plots of FI *vs.* $[M^{3+}]$ gave non-linear curves, which were analyzed by the non-linear curve-fitting method, giving $K_d = 1.94 \times 10^{-5}$, 3.15×10^{-5} and 2.26×10^{-5} M for Fe^{3+}, Al^{3+} and Cr^{3+}, respectively (Fig. S6b†). There was thus excellent agreement between the K_d values obtained from the absorbance and fluorescence titration data, suggesting the self-consistency of our results.

Using these fluorescence data, the detection limit of Fe^{3+}, Al^{3+} and Cr^{3+} by $\mathbf{L^3}$ were calculated to be 2.57, 0.78 and 0.47 μM, respectively (Fig. S8, S8a and S8b†). These results strongly indicate that the probe $\mathbf{L^3}$ is sensitive enough to detect trace levels of Fe^{3+}, Al^{3+} and Cr^{3+}. The quantum yields of $\mathbf{L^3}$, [$\mathbf{L^3}$–Fe^{3+}], [$\mathbf{L^3}$–Al^{3+}] and [$\mathbf{L^3}$–Cr^{3+}] complexes in H_2O/CH_3CN (7 : 3, v/v, pH 7.2) were found to be 0.0005, 0.335, 0.327 and 0.333, respectively, using rhodamine-6G as the standard. The comparatively higher values of quantum yields for the complexes compared to the free ligand indicate the higher stability of the complexes in the excited states.

Job's method was again employed to determine the composition of the complex, which was found to be 1 : 1 (Fig. S9†) and this was further supported by mass spectrometric analysis (m/z = 410.18 [Fe($\mathbf{L^3}$)]$^{3+}$; (m/z = 400.53 [Al($\mathbf{L^3}$)]$^{3+}$; 408.85 [Cr($\mathbf{L^3}$)]$^{3+}$ (Fig. S3b–d†)

Moreover, the conspicuous reddish-orange fluorescence response of the probe upon interaction with M^{3+} (Fig. 3a) provides a scope for naked-eye detection of these metal ions. The possibility of using the chemosensor $\mathbf{L^3}$ in the development of paper test strips was examined and it was found that the turn-on fluorescence response of $\mathbf{L^3}$ towards M^{3+} was also visually detectable with the test paper strips (Fig. 3b).

Selectivity studies

Selectivity is an important and essential requirement for an excellent chemosensor. Selectivity experiments were thus carried out by taking 60 μM of probe $\mathbf{L^3}$ in a cuvette containing

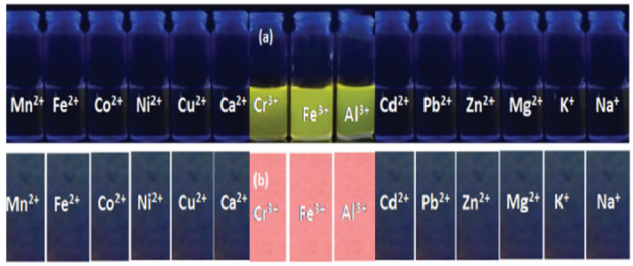

Fig. 3 (a) Visual fluorescent response of L^3 towards Fe^{3+}, Al^{3+} and Cr^{3+} (under 365 nm UV light); (b) paper strip experiments for the fluorescent sensing of Fe^{3+}, Al^{3+} and Cr^{3+} towards the probe L^3.

2.5 mL of 20 mM HEPES buffer solution and then different metal-ion solutions of about 5 equivalent were added separately. Surprisingly, L^3 could selectively recognize only Cr^{3+}, Fe^{3+} and Al^{3+} in mixed aqueous medium over other biologically abundant divalent 3d transition metal cations, like Mn^{2+}, Fe^{2+}, Co_2^{+}, Co^{3+}, Ni^{2+}, Cu^{2+}, Cu^{+} and Zn^{2+}, hazardous heavy metal ions, like Pb^{2+}, Pd^{2+}, Cd^{2+} and Hg^{2+}, and alkali and alkaline earth metal ions, like Na^{+}, K^{+}, Ca^{2+} and Mg^{2+} (Fig. 4). The presence of 5 equivalents of other trivalent metal ions, like Ga(III), Y(III), Sm(III), Dy(III), Au(III), Ru(III) and Co(III), did not interfere with the detection of Cr^{3+}, Fe^{3+} and Al^{3+} ions (Fig. S13†).

When the sample containing probe L^3 came in to contact with trivalent cation (Fe^{3+}, Cr^{3+}, Al^{3+}), the donor atoms (oxygen and nitrogen of the amidic linkage) of the two separate spirolactam rings, the imine nitrogen atom and the oxygen atom of the unit derived from salicyldehyde coordinated with the trivalent metal cation. The coordination from the amidic linkage increased the ring opening probability. The mesomeric effect of the secondary nitrogen atom joined to the xanthene ring pushed the electron density to the amidic linkage through the xanthene ring, resulting in the opening of the spirolactam ring. After cleavage of the spirolactam ring, the amidic moiety formed an ionic bond with the metal ion, but the remaining donor atoms still maintained coordinate bonds in the metal complex. So, the metal-ion-assisted ring opening facilitated the formation of the complex and exhibited an enhancement in the fluorescence intensity and generation of the orange-red colour that was visible to the naked eye (Scheme S1†).

It was also found that not a single anionic species among $S_2O_3^{2-}$, $S_2O_4^{2-}$, N_3^{-}, NO_2^{-}, SCN^{-}, NO_3^{-}, $H_2PO_4^{-}$, PO_4^{3-}, SO_4^{2-}, ClO_4^{-}, F^{-}, Cl^{-}, Br^{-}, I^{-} and HSO_4^{-} could enhance the fluorescence intensity of the probe L^3 (Fig. 5) or interfere with the detection of M^{3+}, but the fluorescence intensity of [L^3–Fe^{3+}], [L^3–Al^{3+}] and [L^3–Cr^{3+}] complexes was found to be quenched in the presence CN^{-} ions (Fig. S10, S10a and S10b†). An excellent reversible fluorescence OFF–ON property of L^3 was observed through the fluorescence study with the sequential addition of Fe^{3+} and CN^{-} ions in to 20 mM HEPES buffer in H_2O/CH_3CN (7 : 3) (pH 7.2) solution at room temperature (Fig. S10c†). The addition of cyanide ions to the solution containing the [L^3–M^{3+}] complex quenched the emission of the probe with the disappearance of the pink colour of the solution. The reason behind this observation is that the interaction of M^{3+} with the probe results in opening of the spirolactam ring, thereby producing a strong fluorescence. Then, treatment with CN^{-} results in the abstraction of metal ion and regeneration of the spirolactam ring, leading to the quenching of emission. This reversibility test suggests the reusability of this chemosensor.

pH studies

For practical application, the appropriate pH condition for the sensor was evaluated. At pH > 4.0, no obvious ring opening of the probe was observed, thereby satisfying the usefulness of the probe in biological systems over a wide pH range (pH 4.5–8) for the detection of Fe^{3+} (Fig. S11†), Al^{3+} and Cr^{3+} (Fig. S11a and b†). However, upon the addition of 3.0 equivalents of Fe^{3+}, the FI jumped to a very high value and remained almost unchanged in the range pH 3.2–7.25, but on further increasing the pH, the FI gradually fell. At pH > 8, no FI was

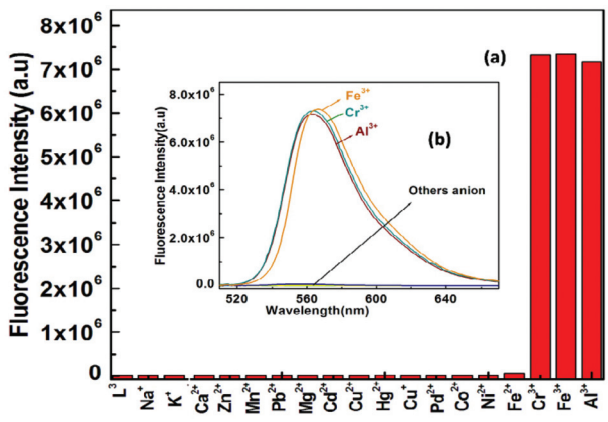

Fig. 4 (a) Fluorescence bar diagram for the selective response of L^3 (60 μM) towards M^{3+} (M = Fe, Al, Cr) over other mono- and divalent metal ions in H_2O/CH_3CN (7 : 3, v/v, pH 7.2, 20 mM HEPES buffer), λ_{ex} = 502 nm, λ_{em} = 558 nm; (b) fluorescence response of L^3 (60 μM) upon the addition of 2.6 equivalent of Fe^{3+}, Al^{3+} or Cr^{3+}.

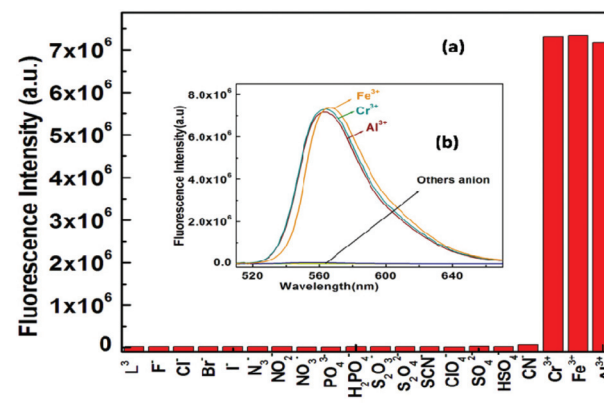

Fig. 5 (a) Histogram of the fluorescence responses of different anions (100 μM) towards L^3 (60 μM) in 7 : 3 v/v, water/MeCN in HEPES buffer at pH 7.2 with λ_{ex} = 502 nm, λ_{em} = 558 nm. (b) Fluorescence response of L^3 towards Fe^{3+}, Al^{3+} or Cr^{3+} with respect to different anions (100 μM).

observed in the case of Fe^{3+}, Al^{3+} and Cr^{3+} due to precipitation of hydroxides of these metal ions.

Spectral studies

The mechanistic pathway proposed for the formation of the $\mathbf{L^3}$–M^{3+} complex by opening of the spirolactam ring was established through IR and ^{1}H-NMR studies. The IR studies revealed that the characteristic stretching vibrational frequencies of the amidic 'C=O' of the rhodamine moiety at 1699 cm^{-1} and azomethine group (C=N) at 1637 cm^{-1} shifted to lower wavenumbers 1646, 1600 and 1599, 1500 cm^{-1} in the presence of 3.0 equivalent of Al^{3+} and Cr^{3+}, respectively (Fig. S4c†). Also, these large shifts in IR frequencies signified a strong polarization of the C=O bond upon efficient binding to the M^{3+} ion. The coordination mode of $\mathbf{L^3}$ towards Al^{3+} was supported by the ^{1}H-NMR studies (Fig. S1a†), which showed a downfield shift of the azomethine proton (from δ = 8.24 to 10.35) in $\mathbf{L^3}$ and also the protons on the benzene ring of the $\mathbf{L^3}$ moiety in the $\mathbf{L^3}$–Al^{3+} complex. A broadening as well as shifting of the –NH proton signal from 4.06 to 4.20 in the delta scale was also observed due to the opening of the spirolactam ring and bore a positive charge on it. HRMS studies (Fig. S3b–d†) also confirmed the formation of the complex with M^{3+} (M = Al, Fe and Cr).

Molecular logic operations

Based on the investigation of the fluorescence "OFF–ON" states of $\mathbf{L^3}$ through controlled experiments, some interesting chemistry related to multiple logic operation could be achieved with the sequential addition of inputs, like cations, such as Al^{3+}, Fe^{3+} or Cr^{3+}, and the CN^- anion and with monitoring their emission as the output. An INHIBIT logic gate was constructed with a particular combination of logic operations, like NOT and AND functions, and this was important due to its non-commutative behaviour, *i.e.* its output signal was inhibited by only one type of input. For the demonstration of this INHIBIT logic function, first we chose two inputs, namely Fe^{3+} as input 1 and CN^- as input 2, and used its emission intensity at 558 nm as the output.

The high value of emission intensity (>5 × 10^4, at 558 nm) was designated as 1 (ON) and the low value (≤5 × 10^4) was designated as 0 (OFF). In the absence of both the 1st input (Fe^{3+}) and 2nd input (CN^-), the emission intensity was low, which indicated the OFF state. Whereas when only input 1 was present, then a significant enhancement of emission (at 558 nm) occurred, indicating the 1 (ON) state; while on the other hand, in the presence of input 2, the output emission value became very weak, designating the OFF state. Therefore, it was necessary to apply a NOT gate with input 2. Additionally, it was interesting that $\mathbf{L^3}$ displayed the emission output signal in such a way that it seemed to understand the requirements of the AND operation. In the presence of both inputs, the output emission value was again low, designating the OFF state, in agreement with the truth table (Fig. 6(a)). Thus, by the sequential addition of these two inputs, an INHIBIT function logic gate could be achieved.

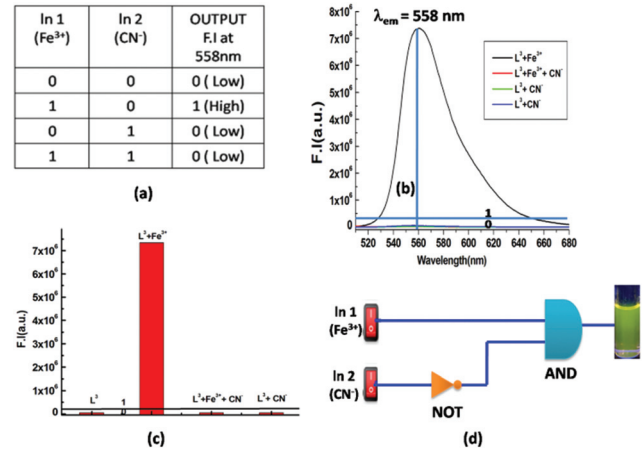

Fig. 6 (a) Corresponding truth table of the logic gate. (b) Output signals (at 558 nm) of the logic gate in the presence of different inputs. (c) Corresponding bar diagram at 558 nm in the presence of different inputs. (d) General representation of an INHIBIT logic gate-based circuit.

Advanced level OR–INHIBIT gate based on a 4-input logic gate

A combination of OR and INHIBIT logic functions was used for the construction of a 4-inputs 1-output logic gate circuit. Next, to emulate an OR logic gate function, the emission intensity at 558 nm was used as the output response, similar to the earlier 2-input logic gate, and the inputs were Al^{3+}, Fe^{3+}, Cr^{3+} and CN^- (Fig. S12†). When the 1st (Al^{3+}) and 2nd (Fe^{3+}) inputs were both absent, the output response, *i.e.* emission intensity, was very low, designating the 0 (OFF) state. However, when only any one of the two inputs was present, the output signal was high, designating the 1 (ON) state. Again in the presence of both the input Al^{3+} and Fe^{3+}, the output response was 1 (ON). Thus, according to its truth table (Fig. 7a), an OR function logic gate could be contracted by the sequential addition of these two inputs. Next, we verified the nature of the output signal in the presence of a 3rd ionic input (Cr^{3+}) in the presence of the first two ionic inputs. As any one of these three inputs or the presence of two of these three inputs causes a high intensity emission output indicating the ON state (1), thus, the probe behaved like an OR logic function. On the other hand, when only the 4th input (CN^-) was present or in the presence of all the other inputs (Al^{3+}, Fe^{3+} and Cr^{3+}) in the system, the output emission was very weak, indicating the 0

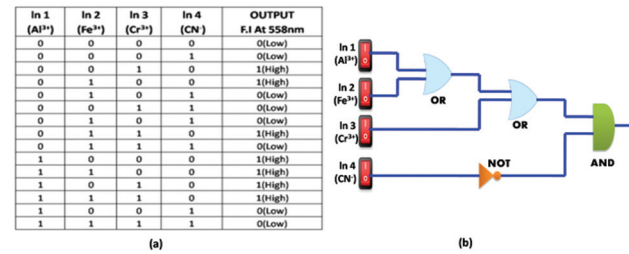

Fig. 7 (a) Truth table of an advanced level 4-input logic gate, (b) schematic representation of a combined logic circuit of INHIBIT and OR logic gates.

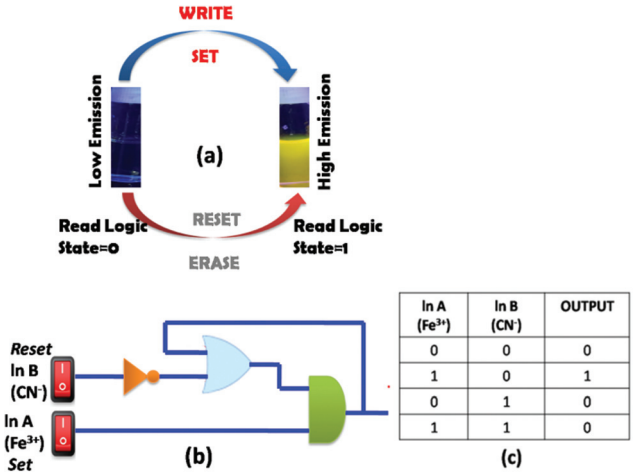

Fig. 8 (a) Schematic demonstration of the reversible logic operation for the memory element with "write–read–erase–read" kind of behaviour. (b) Sequential logic circuit showing the memory unit with two inputs (In A and In B) and one output, and (c) corresponding truth table.

(OFF) state. Therefore, we applied the NOT logic function with the 4th input. As the probe functioned in parallel with the output signal, so we can imply another AND logic function. Thus, from an INHIBIT logical function and following its corresponding truth table, an advanced level 4-input logic gate circuit could be constructed (Fig. 7b).

Molecular memory device

Molecular memory devices are data storage technologies that use molecular species as the data storage element and can be constructed by sequential logic circuits. One of the output signals acts as the input of the memory device and it is memorized as a "memory element". So by using a binary logic function, we developed a sequential logic circuit that showed a "write–read–erase–read" property. For our system, we chose a strong emission output at 558 nm as the ON state (1) and a weak emission output as the OFF state (0). Next to construct this memory device, we chose two inputs, namely Fe^{3+} (A) and CN^- (B), for the SET and RESET processes, respectively. In this memory function, the system writes when it gets input A (Fe^{3+}), *i.e.* a high emission value, and it memorizes the binary number 1. However in the presence of input B (CN^-), which is a reset input, it erases the data and then memorizes the binary number 0 (Fig. 8). The properties of the material allow for a much greater capacitance per unit area than with conventional DRAM (dynamic random-access memory), thus potentially leading to smaller and cheaper integrated circuits. The most important thing is that the write–erase–write cycles could be repeated many times (Fig. S10c†) using the same concentration of the system with a negligible change in emission intensity.

Conclusion

In summary, we reported herein a new rhodamine-6G-based chemosensor ($\mathbf{L^3}$), which showed a selective colorimetric response as well as a "turn-on" fluorescence response towards trivalent metal ions M^{3+} (M = Fe, Al and Cr) over mono and divalent metal ions. Large enhancement of the fluorescence intensity of $\mathbf{L^3}$ with Fe^{3+} (669-fold), Al^{3+} (653-fold) and Cr^{3+} (667-fold) were observed upon the addition of around 3.0 equivalent of these metal ions in H_2O/CH_3CN (7 : 3, v/v, pH 7.2), which clearly indicated the feasibility of the naked-eye detection of these metal ions. The K_d values evaluated from the fluorescence titration data at variable concentrations of metal ions and a fixed concentration of ligand were found to be 1.94×10^{-5} M for Fe^{3+}, 3.15×10^{-5} M for Al^{3+} and 2.26×10^{-5} M for Cr^{3+}. The higher values of quantum yields (0.335, 0.327, 0.333) for [$\mathbf{L^3}$–Fe^{3+}], [$\mathbf{L^3}$–Al^{3+}] and [$\mathbf{L^3}$–Cr^{3+}], respectively, over the free ligand (0.0005) indicated the higher stability of the complexes in the excited states. An excellent reversible fluorescence "OFF–ON" property of $\mathbf{L^3}$ was observed through the fluorescence study with the sequential addition of M^{3+} and CN^- ions at room temperature, which suggests the reusability of this chemosensor. The very low detection limits for Fe^{3+}, Al^{3+} and Cr^{3+} (2.57, 0.78 and 0.47 μM, respectively), could make it suitable for the detection of these metal ions in real water samples. Advanced level molecular logic devices using different inputs (2 and 4 inputs) along with logic gates and memory devices were constructed.

Some trivalent sensors have already been reported so far (Fig. S14†) and some important parameters of these ligands are reported in Table S1.† A closer inspection of Table S1† reveals that there is one report (probe 6) where CH_3OH–H_2O (6 : 4, v/v) was used, but the serious drawback of this system was that the excitation wavelength was in the UV region (330 nm), which is not desirable for bioimaging applications. Our probe is superior with respect to all the previously reported probes listed in the table in the sense that $\mathbf{L^3}$ provides a higher excitation wavelength (502 nm). We also included a detailed comparison of our trivalent probe with previously reported rhodamine-based trivalent sensors as outlined in Table S2 and Fig. S16.† The real-time application of our probe for monitoring Fe^{3+}, Cr^{3+} and Al^{3+} ions was investigated with real water samples collected from different parts of West Bengal. The $Fe^{3+}/Cr^{3+}/Al^{3+}$ content was found to be very low and below the detection limit of the probe and no fluorescence enhancement was observed with the water samples. However, upon the addition of Fe^{3+} externally an enhancement in fluorescence intensity (Fig. S15 and Table S3†) was noticed.

In our recent report, the rhodamine 6G-benzylamine-based trivalent chemosensor[42] was found to display an enhancement in fluorescence intensity by: 41-fold for Fe^{3+}, 31-fold for Al^{3+} and 26-fold for Cr^{3+}; but in our current work, a prominent enhancement in fluorescence intensity was observed; for example, a 669-fold enhancement for Fe^{3+}, 653-fold for Al^{3+} and 667-fold for Cr^{3+} upon the addition of 2.6 equivalent of these metal ions in the probe. Not only that, but the LODs for Al^{3+} and Cr^{3+} determined by 3σ methods were found to be 0.78 and 0.47 μM, respectively, which are far below the LODs determined in our previous work (1.34 μM for Al^{3+} and 2.28 μM for Cr^{3+}). Again, the K_f values were evaluated to be 5.15×10^4 M^{-1}

(Fe^{3+}), 3.17×10^4 M^{-1} (Al^{3+}) and 4.42×10^4 M^{-1} (Cr^{3+}), which were far improved compared to our previous probe, which were found to be 9.4×10^3 M^{-1} for Fe^{3+}, 1.34×10^4 M^{-1} for Al^{3+} and 8.7×10^3 M^{-1} for Cr^{3+}. All these observations lead us to conclude that our current probe $\mathbf{L^3}$ is superior to our previous probe from an analytical point of view.

Conflicts of interest

There are no conflicts to declare.

Acknowledgements

Financial supports from the DST (Ref. No. 809(Sanc)/ST/P/S&T4G-9/2104), West Bengal and the CSIR (Ref. 01(2896)/17/EMR-II), New Delhi, India are gratefully acknowledged.

References

1 S. Chan, Q. Li, H. Tse, A. W. M. Lee, N. K. Mak, H. L. Lung and W.-H. Chan, *RSC Adv.*, 2016, **6**, 74389.
2 (*a*) T. Rasheed, C. Li, F. Nabeel, W. Huang and Y. Zhou, *Chem. Eng. J.*, 2019, **358**, 101; (*b*) T. Rasheed and F. Nabeel, *Coord. Chem. Rev.*, 2019, **401**, 213065; (*c*) T. Rasheed, F. Nabeel, M. Adeel, K. Rizwan, M. Bilal and H. M. N. Iqbal, *J. Mol. Liq.*, 2019, **292**, 111425; (*d*) T. Rasheed, F. Nabeel, C. Li and M. Bilal, *J. Lumin.*, 2019, **208**, 519; (*e*) T. Rasheed, F. Nabeel, C. Li and Y. Zhang, *J. Mol. Liq.*, 2019, **274**, 461; (*f*) T. Rasheed, F. Nabeel and S. Shafi, *J. Mol. Liq.*, 2019, **282**, 489; (*g*) T. Rasheed, F. Nabeel, S. Shafi, M. Bilal and K. Rizwan, *J. Mol. Liq.*, 2019, **296**, 111966; (*h*) T. Rasheed, M. Bilal, F. Nabeel, H. M. N. Iqbal, C. Li and Y. Zhou, *Sci. Total Environ.*, 2018, **615**, 476; (*i*) T. Rasheed, C. Li, M. Bilal, C. Yu and H. M. N. Iqbal, *Sci. Total Environ.*, 2018, **640**, 174; (*j*) T. Rasheed, C. Li, L. Fu, F. Nabeel, C. Yu, L. Gong and Y. Zhou, *J. Mol. Liq.*, 2018, **272**, 440; (*k*) T. Rasheed, C. Li, F. Nabeel, M. Qi, Y. Zhang and C. Yu, *New J. Chem.*, 2018, **42**, 10940; (*l*) T. Rasheed, C. Li, Y. Zhang, F. Nabeel, J. Peng, J. Qi, L. Gong and C. Yu, *Sens. Actuators, B*, 2018, **258**, 115.
3 (*a*) Y. Li, J. Wu, X. Jin, J. Wang, S. Han, W. Wu, J. Xu, W. Liu, X. Yao and Y. Tang, *Dalton Trans.*, 2014, **43**, 1881; (*b*) Z. Zhanga, S. Lu, C. Sha and D. Xu, *Sens. Actuators, B*, 2015, **208**, 258; (*c*) J. M. Junga, S. Y. Lee and C. Kim, *Sens. Actuators, B*, 2017, **251**, 291; (*d*) T. G. Jo, J. M. Jung, J. Han, M. H. Lim and C. Kim, *RSC Adv.*, 2017, **7**, 28723.
4 H. Arakawa, R. Ahmad, M. Naoui and H. A. Tajmir-Riahi, *J. Biol. Chem.*, 2000, **275**, 10150.
5 X. Chen, X. Y. Shen, E. Guan, Y. Liu, A. Qin, J. Z. Sun and B. Z. Tang, *Chem. Commun.*, 2013, **49**, 1503.
6 A. Pechova and L. Pavlata, *Vet. Med.*, 2007, **52**, 1.
7 H. G. Seiler, H. Sigel and A. Sigel, *Handbook on Toxicity of Inorganic Compounds*, Marcel Dekker Inc., New York, USA, 1988, pp. 239–250.
8 A. K. Singh, V. Gupta and B. Gupta, *Anal. Chim. Acta*, 2007, **585**, 171–178.
9 M. Sperling, S. Xu and B. Welz, *Anal. Chem.*, 1992, **64**, 3101.
10 J. B. Vincent, *Nutr. Rev.*, 2000, **58**, 67.
11 A. Zhitkovich, G. Quievryn, J. Messer and Z. Motylevich, *Environ. Health Perspect*, 2002, **110**, 729.
12 J. B. Vincent, *Nutr. Rev.*, 2000, **58**, 67–72.
13 M. Zhang, Z. Chen, Q. Chen, H. Zou, J. Lou and J. He, *Mutat. Res., Genet. Toxicol. Environ. Mutagen.*, 2008, **654**, 45.
14 M. Costa and C. B. Klein, *CRC Crit. Rev. Toxicol.*, 2006, **36**, 155.
15 R. Dai, C. Yu, J. Liu, Y. Lan and B. Deng, *Environ. Sci. Technol.*, 2010, **44**, 6959.
16 T. O'Brien, H. G. Mandel, D. E. Pritchard and S. R. Patierno, *Biochemistry*, 2002, **41**, 12529.
17 V. Bravo, S. Gil, A. M. Costero, M. N. Kneeteman, U. Llaosa, P. M. Mancini, L. E. Ochando and M. Parra, *Tetrahedron*, 2012, **68**, 4882.
18 T. Shoda, K. Kikuchi, H. Kojima, Y. Urano, H. Komatsu, K. Suzukic and T. Nagano, *Analyst*, 2003, **128**, 719.
19 H. X. Jiang, L. S. Chen, J. G. Zheng, S. Han, N. Tang and B. R. Smith, *Tree Physiol.*, 2008, **28**, 1863.
20 G. Berthon, *Coord. Chem. Rev.*, 1996, **149**, 241.
21 S. M. Candura, L. Manzo and L. G. Costa, Role of occupational neurotoxicants in psychiatric and neurodegenerative disorders, in *Occupational Neurotoxicology*, ed. L. G. Costa and L. Manzo, CRC Press, Boca Raton, 1998, p 131.
22 R. J. P. Williams, *Coord. Chem. Rev.*, 1992, **149**, 1.
23 T. Han, X. Feng, B. Tong, J. Shi, L. Chen, J. Zhi and Y. Dong, *Chem. Commun.*, 2012, **48**, 416.
24 G. R. Rout, S. S. Roy and P. Das, *Agronomie*, 2001, **21**, 3.
25 (*a*) J. Barcelo and C. Poschenrieder, *Environ. Exp. Bot.*, 2002, **48**, 75; (*b*) B. Valeur and I. Leray, *Coord. Chem. Rev.*, 2000, **205**, 3; (*c*) Z. Krejpcio and R. W. P. Wojciak, *Int. J. Environ. Stud.*, 2002, **11**, 251.
26 M. R. Wills, C. D. Hewitt, B. C. Sturgill, J. Savory and M. M. Herman, *Ann. Clin. Lab. Sci.*, 1993, **23**, 1.
27 G. Sahin, I. Varol and A. Temizer, *Biol. Trace Elem. Res.*, 1994, **41**, 129.
28 (*a*) T. P. Flaten, *Brain Res. Bull.*, 2001, **55**, 187; (*b*) J. R. Walton, *Neurotoxicology*, 2006, **27**, 385.
29 B. L. Su, N. Moniotte, N. Nivarlet, L. H. Chen, Z. Y. Fu, J. Desmet and J. Li, *J. Colloid Interface Sci.*, 2011, **358**, 136.
30 (*a*) P. Aisen, M. Wessling-Resnick and E. A. Leibold, *Curr. Opin. Chem. Biol.*, 1999, **3**, 200; (*b*) R. S. Eisenstein, *Annu. Rev. Nutr.*, 2000, **20**, 627; (*c*) T. A. Rouault, *Nat. Chem. Biol.*, 2006, **2**, 406.
31 T. Hirayama, K. Okuda and H. Nagasawa, *Chem. Sci.*, 2013, **4**, 1250.
32 J. Xu, Z. Jia, M. D. Knutson and C. Leeuwenburgh, *Int. J. Mol. Sci.*, 2012, **13**, 2368.
33 D. J. Bonda, H. Lee, J. A. Blair, X. Zhu, G. Perry and M. A. Smith, *Metallomics*, 2011, **3**, 267.
34 Y. Li, J. Wu, X. Jin, J. Wang, S. Han, W. Wu, J. Xu, W. Liu, X. Yao and Y. Tang, *Dalton Trans.*, 2014, **43**, 1881.

35 Z. Zhanga, S. Lu, C. Sha and D. Xu, *Sens. Actuators, B*, 2015, **208**, 258.
36 J. M. Junga, S. Y. Lee and C. Kim, *Sens. Actuators, B*, 2017, **251**, 291.
37 T. G. Jo, J. M. Jung, J. Han, M. H. Lim and C. Kim, *RSC Adv.*, 2017, **7**, 28723.
38 J. Miao, L. Wang, W. Dou, X. L. Tang, Y. Yan and W. S. Liu, *Org. Lett.*, 2007, **9**, 4567.
39 S. Goswami, A. K. Das, A. K. Maity, A. Manna, K. Aich, S. Maity, P. Saha and T. K. Mandal, *Dalton Trans.*, 2014, **43**, 231.
40 S. Fakih, M. Podinovskaia, X. Kong, H. L. Collins, V. E. Schoible and R. C. Hider, *J. Med. Chem.*, 2008, **51**, 4539.
41 S. K. Sahoo, D. Sharma, R. K. Bera, G. Crisponi and J. F. Callan, *Chem. Soc. Rev.*, 2012, **41**, 7195.
42 (*a*) R. Alam, R. Bhowmick, A. S. M. Islam, A. Katarkar, K. Chaudhuri and M. Ali, *New J. Chem.*, 2017, **41**, 8359; (*b*) T. Mistri, R. Alam, R. Bhowmick, A. Katarkar, K. Chaudhuri and M. Ali, *New J. Chem.*, 2016, **40**, 330; (*c*) D. Das, R. Alam, A. Katarkar and M. Ali, *Photochem. Photobiol. Sci.*, 2019, **18**, 242; (*d*) T. Mistri, R. Alam, M. Dolai, S. K. Mandal, P. Guha, A. R. Khuda-Bukhsh and M. Ali, *Eur. J. Org. Chem.*, 2013, 5854.
43 J.-S. Wu, I.-C. Hwang, K. S. Kim and J. S. Kim, *Org. Lett.*, 2007, **9**, 907.
44 D. F. Perkins, L. F. Lindoy, A. McAuley, G. V. Meehan and P. Turner, *Proc. Natl. Acad. Sci. U. S. A.*, 2006, **103**, 532.
45 Q. Liu, M.-R. Gao, Y. Liu, J. S. Okasinski, Y. Ren and Y. Sun, *Nano Lett.*, 2016, **16**(1), 715.
46 S. Ozkar and R. G. Finke, *J. Phys. Chem. C*, 2017, **121**, 27643.
47 H. A. Molla, R. Bhowmick, A. Katarkar, K. Chaudhuri, S. Gangopadhyay and M. Ali, *Anal. Methods*, 2015, **7**, 5149.
48 Y. Xiang and A. Tong, *Org. Lett.*, 2006, **8**, 1549.

Dipankar Das.
28/03/2022